Novel Approaches to Targeted Drug Delivery via Endogenous Enzyme Activation

Trinity College Dublin
Coláiste na Tríonóide, Baile Átha Cliath
The University of Dublin

Connor O'Leary

Trinity College Dublin, The University of Dublin

Based on research carried out under the supervision of Prof. Joanna McGouran

A thesis submitted to the School of Chemistry for the degree of Doctor of Philosophy.

January 2025

Declaration

I declare that this thesis has not been submitted as an exercise for a degree at this or any other university and it is entirely my own work.

I agree to deposit this thesis in the University's open access institutional repository or allow the library to do so on my behalf, subject to Irish Copyright Legislation and Trinity College Library conditions of use and acknowledgement.

Signed: 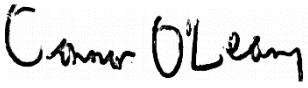 Date: 31 October 2024

Abstract

Current treatments used in cancer chemotherapy are limited due to their narrow therapeutic window, dose-limiting toxicity and low cancer-cell specificity, making the development of targeted drug delivery strategies an urgent research challenge. The overexpression of certain enzymes in cancer cells has been exploited for the specific activation of prodrugs in the tumour microenvironment, facilitating significantly improved selectivity of the active drug and reduced off-target effects.

Innovative strategies applied to polymeric systems for responsive applications, depolymerisation and drug delivery systems are being developed. Such systems which are activated in response to endogenous stimuli in the tumour microenvironment represent an underexplored field in chemical biology and materials science. In addition, examples of enzyme-responsive systems generated by lithographic polymerisation techniques are very limited.

In this work, the synthesis of a suite of glycomonomer conjugates and their subsequent polymerisation to form glycopolymers is presented, designed to be specifically activated by endogenous glycosidases as well as recognised by lectin and boronic acid substrates. Furthermore, the design and synthesis of various advanced self-immolative crosslinkers is reported, which are designed to be activated by endogenous β-galactosidase, applying a previously reported prodrug activation strategy to a polymeric system. Efforts to polymerise these crosslinkers via two-photon polymerisation and bulk methods are described, aiming to generate polymer networks that would depolymerise upon enzymatic activation.

Cyclic peptides such as somatostatin are attracting growing attention as therapeutics due to their favourable pharmacological characteristics, with increased metabolic stability and binding affinity as a result of their limited conformational flexibility. Both β-galactosidase and somatostatin receptors are overexpressed in a range of tumour types. Somatostatin and its analogues have a well-defined pharmacophore which is constituted by the Phe-Trp-Lys-Thr residues of the β-turn; modifying this sequence would be expected to generate an inactive analogue of the active peptide.

Here, analogues of essential amino acids in the pharmacophore of therapeutic peptide somatostatin which bear enzyme-activated galactoside and bioreductive groups are presented. Unnatural threonine amino acid analogues are successfully synthesised and an example of a glycopeptide somatostatin prodrug analogue is reported, with preliminary biological results presented. This represents the development of a new, dual-targeted prodrug strategy which exploits the overexpression of both β-galactosidase and somatostatin receptors in certain tumour types, for targeted delivery of a peptide therapeutic.

Explanatory note

Carbohydrates are numbered according to standard convention as shown below.

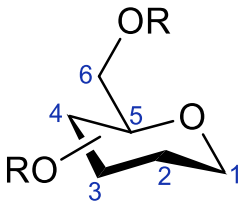

Abbreviations

Ac	Acetyl
AcOH	Acetic acid
ADEPT	Antibody-directed enzyme prodrug therapy
ADMET	Absorption, distribution, metabolism, excretion and toxicity
Ala, A	Alanine
app.	Apparent
aq.	Aqueous
Boc	*tert*-butyloxycarbonyl
Boc	*Tert*-Butoxycarbonyl
br	Broad
BSA	Bovine serum albumin
CAZy	Carbohydrate-active enzymes
Cbz	Benzyloxycarbonyl
CDI	1,1′-Carbonyldiimidazole
CE	Carboxylesterase
Cit	Citrulline
CRD	Carbohydrate-recognition domain
CuAAC	Cu(I)-catalysed alkyne-azide cycloaddition
CYP004	Cytochrome P450 family 4
Cys, C	Cysteine
d	Doublet
DALY	Disability-adjusted life-year
DBU	1,8-Diazabicyclo[5.4. 0]undec-7-ene
DCA	Dichloroacetic acid
DCM	Dichloromethane
DEATC	7-Diethylamino-3-thenoylcoumarin
DKP	Diketopiperazine
DLW	Direct laser writing

DMF	Dimethylformamide
DMSO	Dimethyl sulfoxide
DNA	Deoxyribonucleic acid
DPTA	Diethylenetriaminopentaacetic acid
DTC	Dithiocarbamate
DT-diaphorase	NAD(P)H dehydrogenase (quinone)
EPR	Enhanced permeability and retention
ESI	Electrospray ionisation
EtOAc	Ethyl acetate
FA	Folic acid
FDA	Food and Drug Administration
Fmoc	Fluorenylmethoxycarbonyl
FOLR1	Folate receptor α
GGT	γ-glutamyltranspeptidase
GH	Growth hormone
GLOBOCAN	Global Cancer Observatory
GLUT1	Glucose transporter 1
Gly, G	Glycine
GPCR	G-protein coupled receptor
GSH	Glutathione
h	Hour
HAP	Hypoxia-activated prodrug
HAS	Human serum albumin
HDAC	Histone deacetylase
HER2	Human epidermal growth factor receptor 2
HOBt	Hydroxy benzotriazole
Hof	Homophenylalanine
Hz	Hertz
IARC	International Agency for Research on Cancer

IC_{50}	Half-maximal inhibitory concentration
IEDDA	Inverse electron-demand Diels-Alder
J	Coupling constant
KDAC	Lysine deacetylase
LAP	Lithium phenyl(2,4,6-trimethylbenzoyl)phosphinate
LCST	Lower critical solution temperature
Leu, L	Leucine
Lys, K	Lysine
M	Molar, mol dm^{-3}
MDO	2-methylene-1,3-dioxepane
min	Minute
MMP	Matrix metalloproteinase
mp	Melting point
MS	Mass spectrometry
Nal	Naphthylalanine
NB	Nitrobenzyl
NI	Nitroimidazole
NIR	Near-infrared
NMR	Nuclear magnetic resonance
NQO1	NAD(P)H quinone dehydrogenase 1
NT	Nitrothiophene
p	Pentet
Pano	Panobinostat
PDC	Peptide-drug conjugate
PEG	Polyethylene glycol
PEGDMA	poly(ethylene glycol) dimethacrylate
PET	positron emission tomography
PETA	Pentaerythritol tetraacrylate
PGA	Penicillin amidase

Phe, F	Phenylalanine
PMBCl	*para*-methoxybenzyl chloride
PMT	Prodrug monotherapy
pNIPAAM	poly(N-isopropylacrylamide)
PPI	Protein-protein interaction
Pro, P	Proline
PRRT	Peptide receptor radionuclide therapy
q	Quartet
ROMP	Ring-opening metathesis polymerisation
ROS	Reactive oxygen species
RP-HPLC	Reverse-phase-high performance liquid chromatography
s	Singlet
sat.	Saturated
Ser, S	Serine
SIP	Self-immolative polymer
SN-38	7-Ethyl-10-hydroxycamptothecin
SPAAC	Strain-promoted alkyne-azide cycloaddition
SPECT	Single-Photon Emission Computed Tomography
SPPS	Solid-phase peptide synthesis
SPS	Solution-phase peptide synthesis
SST	Somatostatin
SSTR	Somatostatin receptor
t	Triplet
TBAF	Tetrabutylammonium fluoride
TBS	*tert*-butyldimethylsilyl
^{t}Bu	*tert*-butyl
TFA	Trifluoroacetic acid
THF	Tetrahydrofuran
Thr, T	Threonine

TLC	Thin layer chromatography
TMOF	Trimethyl orthoformate
TMS	Trimethylsilyl
TPA	Two-photon absorption
TPP	Two-photon polymerisation
Trp, W	Tryptophan
Trt	Trityl
Tyr, Y	Tyrosine
UV	Ultraviolet
UV-vis	Ultraviolet-visible
Val, V	Valine

Acknowledgements

Firstly, I would like to thank my supervisor Prof. Joanna McGouran for taking a chance on me and giving me the opportunity to move to Dublin for this PhD, and for her support and guidance over the last four years. Despite the ups and downs, the past four years have been the best years of my life so far and I am truly grateful to have been given this opportunity. I'd also like to thank my MChem project supervisor Dr Kalesh Karunakaran – without your encouragement it's unlikely I would ever have sought to apply for PhD positions in the first place. It was that final-year project that sparked my interest in chemical biology.

I'd like to thank SSPC for providing the funding for my PhD and for being a supportive organisation to be part of during my time in Ireland. The numerous Molecules II meetings and other events have provided a great platform for networking and have given me opportunities to present my researchers to and meet peers from institutions across the country. From the very start I was made to feel like the management were on our side, so I would like to especially thank Sarah, Hilda, Colm, Louise and others for fostering a positive community to be part of beyond Trinity during my time here. The industry placement I had the opportunity to do at SK Pharmteco is something I am very grateful to SSPC for facilitating.

Most of the work presented in this thesis is of a collaborative nature, so I would especially like to acknowledge anyone who has carried out any experiments or assisted in any of the projects. I am grateful to the huge amount of time Dr Alexa Ennis has dedicated to all polymerisation aspects in Chapters 2 and 3, undertaking a lot of work for polymerisation cocktail development, TPP and microscopy. Alexa has been a fantastic collaborator throughout; her positivity has made the challenges encountered along the way far more manageable. I'd like to also thank Prof. Larisa Florea and Prof. Colm Delaney for their advice at all stages of these projects. For HPLC support for peptide analysis and purification in Chapter 4, I am very grateful to Prof. Eoin Scanlan for facilitating this collaboration and to Alby for leading the HPLC work required to complete this project. Thanks also goes to Ines, Conor and Nikitas for ad-hoc sample running and advice. Finally, Sara Corbezzolo and Prof. Michael Monaghan have been fantastic collaborators, carrying out the biological evaluation work for Chapter 4.

The work described in this thesis would not have been possible without the excellent technical staff in the School of Chemistry. In particular, I would like to thank Dr John O'Brien, who I

truly regard as the crown jewel in the department. His tireless dedication to the NMR service over more than three decades deserves a huge amount of recognition; John's expertise and enthusiasm have taught me so much. I would also like to thank Dr Manuel Ruether, who has always been so proactive in sorting any issues with technical equipment (and even projectors needed for group meetings and tables needed for lunch rooms), as well as Dr Gary Hessman for the running of mass spec samples. Beyond the School of Chemistry, I have to thank Derek from solvents/HMF, who was always a friendly face when popping down on a Friday morning.

For better or for worse, I have become well acquainted with the sales and customer service teams of various suppliers and vendors of the McGouran group during my time in the group. This section wouldn't be complete without extending thanks in particular to Ashleigh at Fluorochem (which quickly became the first-choice supplier of the McGouran group), who has endeavoured to ensure our stock of sturdy balloons was replenished as and when needed. One highlight has to be our care package in July 2023 with all sorts of goodies in addition to our balloon request. In addition, we like to support local family-run businesses in the McGouran group, and Derek & family at Eirglass have been a reliable glassblowing contact since I broke that first tap in December 2020..

I have been lucky to work with a great team of people in the McGouran group. Firstly, I'm very grateful to have been able to share this experience from start to finish with Valerio – you've been such a supportive presence and great friend through everything. Plus, you make an incredible carbonara. I'm also thankful to have had Ellen and Susie in the lab for most of my time here – you both always had a great way of keeping things fun and light-hearted, even in the dark early days of Covid. Your creative spirits definitely won us that Halloween party in 2022.. I'd also like to especially thank André, whose endless positivity and up-beat attitude have really kept be going in this incredibly tough final year. Thanks also to Julie who has become another positive, warm presence and best of luck with carrying the torch of the responsive materials – I hope you have better luck than me.. To all other group members since I've been here: Neil, Eva, Mark, Sean, Tomasz, and our new arrivals Ailish, Ilaria and Fayanne,

thanks for being a great group of people to work with and I wish you all the best moving forward.

Most of all, beyond the McGouran group, sharing the lab/office with the Scanlan and Connon groups has really made this experience for me. I've met some amazing people, many of whom I regard as great friends – I'd especially like to shout out Alby, Nikitas, Laura, Ines, Ian, Glenna and Lorenzo who have been here for the whole journey. Katie, Josh, Lee, Harlei, Alejandro, Conor, Lucy and Matthew – you have all been amazing people to be around. All the hikes, drinks, celebrations, Werner events and trips have been so much fun.

Moving abroad during the pandemic in 2020 was a daunting move and I am incredibly grateful to Rachel and Matei who really ensured I landed on my feet when moving to Dublin in the runup to a second Covid lockdown in September 2020. Without your support, this move would have been much harder and far more daunting. Finally, I'd like to thank my friends and family for their support over the years, and particularly my parents who have always supported and encouraged me. And a special mention to Mr Grant Duff who told me I wasn't good enough to do A-level chemistry…

Contents

Abstract ..... **ii**

Abbreviations ..... **v**

Acknowledgements ..... **ix**

Chapter 1: Introduction **2**

1.1 Current therapeutics and their limitations 2

1.2 Targeted drug delivery 3

1.2.1 Prodrugs 3

1.2.2 Bioorthogonal cleavage reactions for prodrug activation 6

1.2.3 Prodrugs targeting the tumour microenvironment 7

1.2.4 Enzyme-activatable prodrugs 10

1.3 Lectin recognition and glycopolymers 23

1.4 Peptide therapeutics 25

1.4.1 Therapeutic properties of peptides 25

1.4.2 Cyclic peptides 27

1.4.3 Somatostatin and its analogues as therapeutics in the clinic 28

1.4.4 Tumour-targeting peptides and peptide-drug conjugates 30

1.5 Responsive polymers for biotechnology and drug delivery 33

1.5.1 Polymer-based drug delivery systems 36

1.5.2 Two-photon polymerisation (TPP) 38

1.6 Work described in this thesis **45**

Chapter 2: Glycosidase Responsive Glycopolymers **47**

2.1 Introduction and Aims **47**

2.2 Results and Discussion 49

2.2.1 Synthesis 49

2.2.1 β-glucuronide monomer synthesis 49

2.2.1.1 Polymerisation and enzymatic testing of glucuronide monomers 57

2.2.2 β-Galactoside Monomer Synthesis 73

2.2.2.1 Polymerisation and Enzymatic Testing of Galactoside Monomers 76

2.3 Conclusions and Future Work 86

Chapter 3: Development of Self-Immolative Glycosidase-Responsive Crosslinkers for Degradable Polymers **90**

3.1 Introduction **90**

3.2 Aims **91**
3.3 Synthesis of carbohydrate-conjugate crosslinkers **93**
3.3.1 Crosslinker design based on ACE nucleotide protecting group 93
3.3.2 Crosslinker design based on bis-acetal-based substrates (BABS) 95
3.3.3 Crosslinker design based on glycosidase-responsive prodrugs for multidrug release 98
3.4 Polymerisation of β-galactosidase-responsive self-immolative crosslinkers 116
3.4.1 Polymerisation of difunctional styrene crosslinker 165 116
3.4.2 Polymerisation of difunctional methacrylamide crosslinker 167 120
3.5 Conclusions and Future Work **125**
Chapter 4: Development of a β-Galactosidase-Activated Glycopeptide Prodrug Analogue **127**
4.1 Introduction **127**
4.2 Results and Discussion 129
4.2.1 Glycoamino acid synthesis 130
4.2.2 Biological evaluation 145
4.3 Conclusions and Future Work 148
Chapter 5: Efforts Towards the Development of a Hypoxia-Activated Peptide Prodrug Analogue **151**
5.1 Introduction **151**
5.2 Aims **152**
5.3 Results and Discussion **153**
5.3.1 Nitrobenzyl bioreductive group 153
5.3.2 Nitroimidazole bioreductive group 156
5.3.3 Nitroquinoline bioreductive group 159
5.4 Conclusions and Future Work **161**
Chapter 6: Conclusions and Summary **165**
6 Conclusions and Summary **165**
Chapter 7: Experimental **168**
7.1 General Methods **168**
7.2 Synthetic Methods for Chapter 2 ..... **171**
7.2.2 General Polymerisation Methods 198
7.3 Synthetic Methods for Chapter 3 ..... **199**
7.4 Synthetic Methods for Chapter 4 ..... **234**

7.4.1 Standard Procedures for Solid-Phase Peptide Synthesis (SPPS)....247
7.5 Synthetic Methods for Chapter 5 257
Chapter 8: References.... 269

Chapter 1

Introduction

Chapter 1: Introduction

1.1 Current therapeutics and their limitations

Significant advances in cancer prevention, diagnosis and treatment have been made in recent decades, with Cancer Research UK estimating in excess of one million deaths avoided as a result of this progress in the UK since the mid 1980s. Specifically, the identification of distinct drug targets associated with the virulence of certain cancers and the subsequent development of therapeutics targeting these proteins, such as Herceptin which targets HER2 receptors linked to breast cancer growth promotion, have been essential to rapid improvements in patient prognosis following cancer diagnosis.[1]

Despite this progress, the multifaceted disease remains a leading cause of mortality globally, with contemporary estimates from the International Agency for Research on Cancer (IARC) suggesting over 30% of premature deaths from non-communicable diseases (those aged 30 – 69) are caused by cancer, with a total of 9.7 million deaths resulting from 20 million diagnosed cancer cases in 2022.[2] Moreover, the macroeconomic costs associated with cancer are vast and wide-ranging, with factors such as one million children becoming maternal orphans in 2020 as well as measures of disease burden such as disability-adjusted life-years (DALYs) contributing to an estimated global cost of cancer from 2020 to 2050 of $25.2 trillion, with health services under increasing stress.[3, 4] The latest IARC statistics documented in the GLOBOCAN database outline a disproportionate growing burden of cancer on developing and impoverished regions and highlight the pressing need for cancer research to be a continued priority for funding agencies and researchers across life science disciplines.[5, 6]

Much of the progress in public health outcomes following cancer diagnosis has been driven by the development of potent anticancer chemotherapeutics which are successfully used clinically.[7] These drugs include doxorubicin **1**, tamoxifen **2**, paclitaxel **3** and methotrexate **4**, approved for clinical use towards the end of the 20th century (**Fig. 1.1**). However, despite routine use of these agents in the clinic, they have a characteristically narrow therapeutic window, being associated with a range of severe side-effects as well as dose-limiting toxicity due to their lack of specificity for cancer cells, limiting patient outcomes.[8] For example, risks

associated with doxorubicin-induced toxicity include cardiotoxicity, cognitive impairment and liver injury.[9] This necessitates dose-limited administration and therefore precludes the efficacy potential of the agent against the tumour being treated.

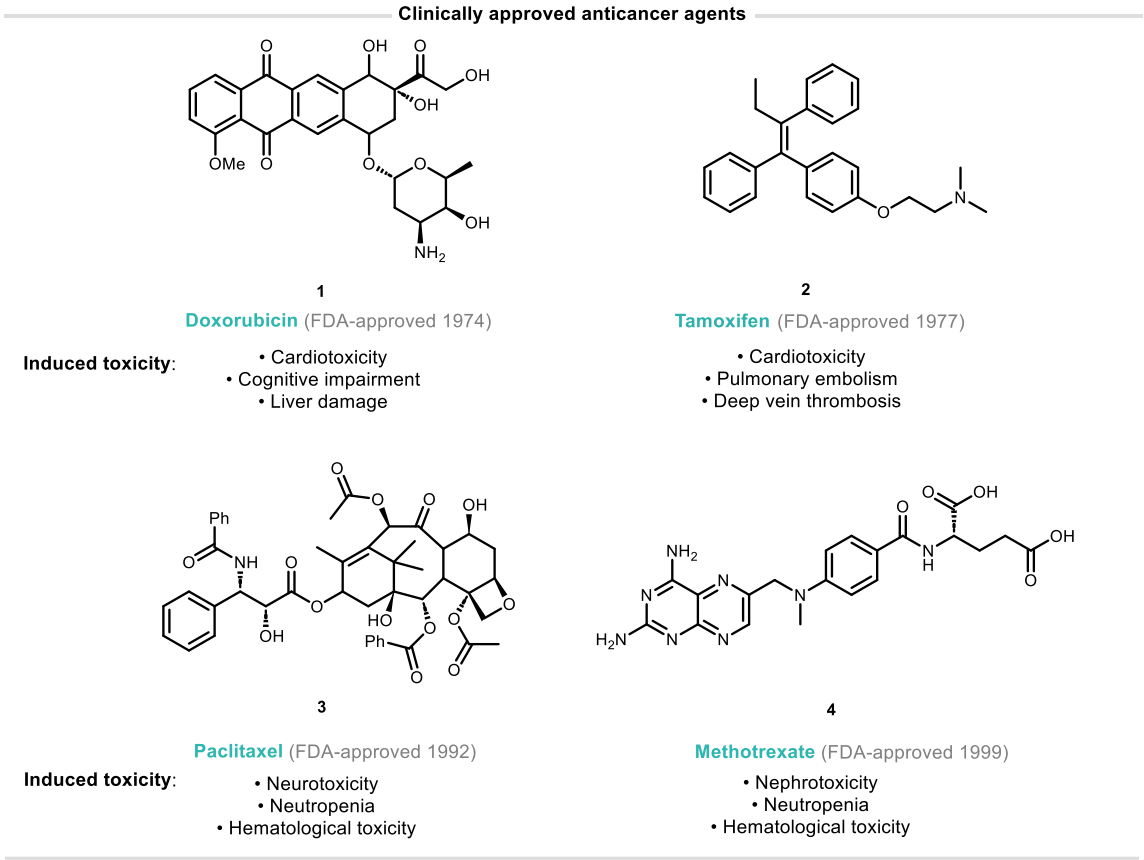

Figure 1.1 Structures, years of FDA-approval for clinical use and associated toxicities of doxorubicin, tamoxifen, paclitaxel and methotrexate anticancer agents.[9-12]

In order to effectively tackle the global cancer burden, enhance patient outcomes and minimise the adverse effects of chemotherapeutic treatments, developing new classes of anticancer agents which significantly reduce systemic effects and new delivery systems that increase their specificity represents an urgent research challenge.

1.2 Targeted drug delivery

1.2.1 Prodrugs

A common therapeutic strategy specifically designed to reduce the systemic effects of cytotoxic drugs on healthy cells in the body is prodrug therapy. Prodrugs are

pharmacologically inactive analogues of the parent drug which release the active form by enzymatic or chemical reaction *in vivo*, typically removing a masking group, or 'promoiety', rationally incorporated into the structure design.[13] Conventional prodrugs have been designed to incorporate structural modifications which improve the absorption, distribution, metabolism, excretion and toxicity (ADMET) properties of the drug. This is achieved through modifications which affect factors including hydrophobicity, hydrogen bonding, solubility, enzymatic stability and permeability. With over 30 prodrugs being approved for clinical use by the FDA over 2008 - 2017, accounting for 10% of all drug approvals, they continue to represent an important class of therapeutic routinely used by clinicians.[14]

The term 'prodrug' was defined by Albert in 1958, however the concept predates this work as far back as 1886 to pain-relievers acetanilide **5** and phenacetin **7**, both having their activity retrospectively traced to their metabolism to the pharmacologically-active acetaminophen **6** (**Fig. 1.2**).[15, 16] In 1899, the first intentionally designed prodrugs came to market. These were methenamine, which releases formaldehyde and ammonium ions in acidic urine, and aspirin **8**, which incorporates an esterase-cleavable acetyl ester to the structure, reducing irritation and releasing the active drug **9** when metabolised.[17, 18]

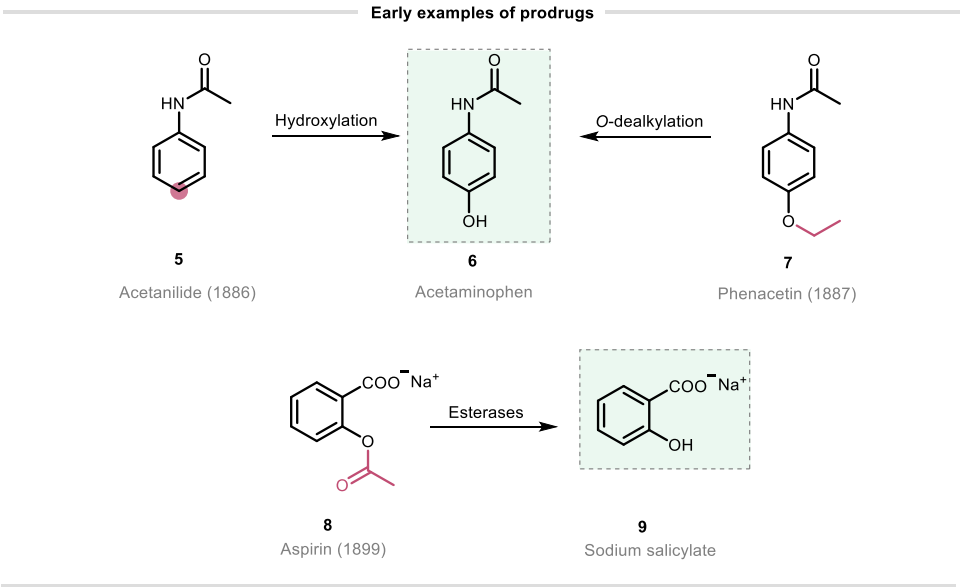

Figure 1.2 Selected early examples of prodrugs (acetanilide, phenacetin and aspirin) in the 19th century, which are converted into the active acetoaminophen and sodium salicylate forms when metabolised in the body.

The early examples of prodrugs in the late 19th and early 20th century, which were initially characterised by serendipitous elucidation of therapeutic pharmacological activity and subsequently by efforts to alleviate a medicinal chemistry shortcoming. More recently, rationally designed prodrug strategies have become an integral part of the drug discovery process, optimising structure design through conscious selection in the development stages rather than through retroactive necessity. Beyond improving the ADMET properties of a drug through generation of an inactive analogue, innovative prodrug design can facilitate significantly improved targeting of therapeutics. Modern prodrug design is diverse and increasingly innovative, targeting differential endogenous properties of the tumour microenvironment such as physiological conditions (acidic pH)[19] and site-specific enzyme overexpression,[20] as well as exogenous targeting approaches including directed enzyme prodrug therapies,[21] macromolecule-based prodrug targeting[22, 23] and drug-conjugates with a targeting antibody[24] or ligand.[25]

Prodrug design typically requires synthetic modification of a chosen functional group of an active drug with a masking promoiety to generate an inactive analogue with significantly reduced cytotoxicity. Depending on the specificity of the cleavage of the masking group to the tumour cells being targeted, a targeting moiety such as an antibody or peptide with known affinity to binding sites overexpressed on the membrane surface of tumour cells may be incorporated into the structure design to enhance specificity. The general design and mode of action of a typical modern prodrug is described in **Fig. 1.3**, whereby a masking group is removed selectively in the tumour microenvironment to release the active drug.

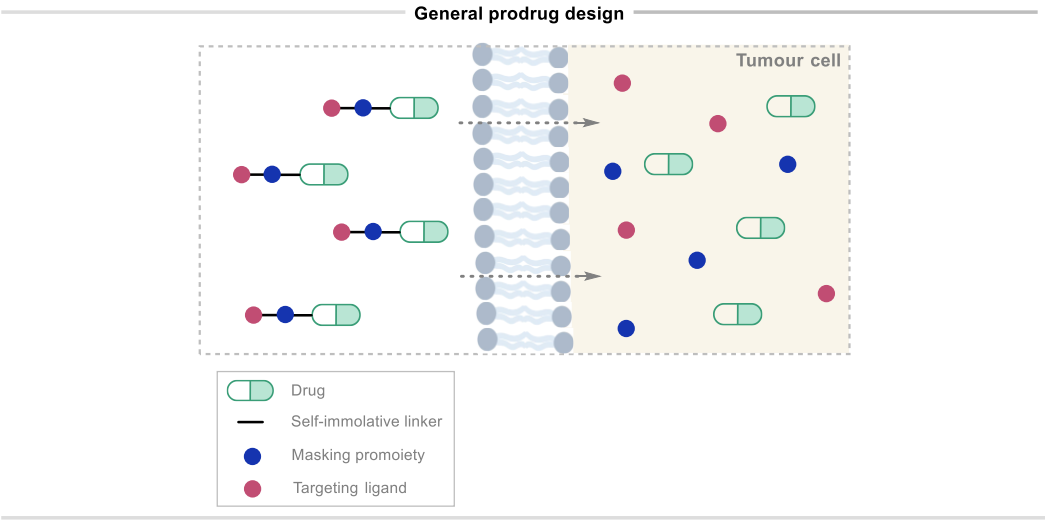

Figure 1.3 The general structure and mode of action of prodrugs, with a masking promoiety on a key functional group of the drug connected via a self-immolative linker. Some prodrugs incorporate an additional targeting ligand.

1.2.2 Bioorthogonal cleavage reactions for prodrug activation

The term 'bioorthogonal chemistry' was first coined by Hang *et al.* in 2003 to describe the utilisation of the biocompatible, chemoselective Staudinger ligation reaction between a cell-surface azidosugar and a modified triphenylphosphine-fluorophore probe.[26] Since then, the Cu(I)-catalysed alkyne-azide cycloaddition (CuAAC) has become an indispensable tool employed widely in chemical proteomics methodologies following Bertozzi and co-workers' seminal work in the early 2000s.[27] The cytotoxicity of Cu^{I} at low concentration has led to growing interest in the strain-promoted alkyne-azide cycloaddition (SPAAC) and inverse electron-demand Diels-Alder (IEDDA) reactions for application in living systems.[28]

As a strategy to reduce systemic drug release and associated adverse side-effects, inactive prodrugs which mask essential functional groups have been developed.[29] The activation of such prodrugs via bioorthogonal cleavage reactions has generated a new class of prodrug design, facilitating targeted release of the drug in a spatiotemporally controlled manner.[30] The described copper-free alternatives to the bioorthogonal CuAAC reaction have been applied to prodrug activation strategies, often labelled 'click-to-release' drug targeting (**Fig 1.4**). For example, Gamble and co-workers reported the first use of the

SPAAC reaction for prodrug activation in 2015, exploiting the hydrolysis-susceptible triazoline adduct as an efficient route to active drug release via the acid-labile aldimine in the tumour microenvironment.[31]

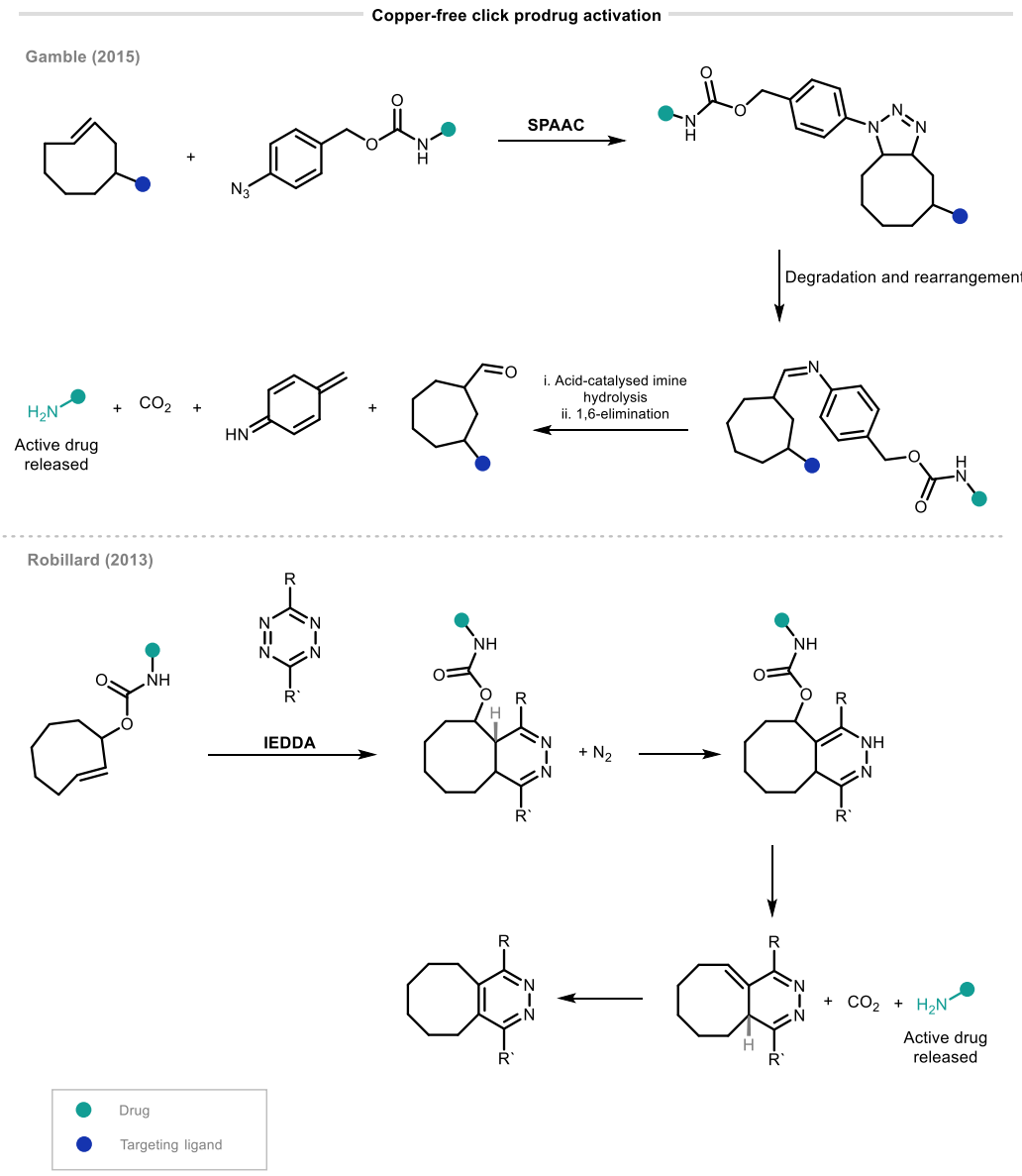

Figure 1.4 Application of copper-free click bioorthogonal reactions for prodrug activation and targeted drug release: SPAAC (Gamble and co-workers, 2015) and IEDDA (Robillard and co-workers, 2013).

1.2.3 Prodrugs targeting the tumour microenvironment

In order to develop more targeted therapeutics, the difference in properties between the tumour microenvironment and healthy cells can be exploited, including acidic extracellular

pH, elevated levels of reactive oxygen species (ROS) and high concentrations of glutathione (GSH).[19]

The acidic intra- and extracellular acidic pH characteristic of cancer cells is associated with cancer cell proliferation, metastasis, immune surveillance evasion and drug resistance. It can be exploited for the specific activation of pH-responsive prodrugs which incorporate acid-sensitive functional groups such that the active drug is released at the tumour site.[32] For this purpose, the acid-labile hydrazone functional group is the most widely used masking promoiety that has been effectively employed to conjugate a cytotoxic drug to a targeting ligand.

Warnecke and co-workers demonstrated this principle through the generation of an inactive doxorubicin analogue **10**, in which the drug is conjugated to a thiol-reactive maleimide moiety via a hydrazone linker, which reacts selectively with the Cys-34 of endogenous human serum albumin (HSA) via a Michael addition at the maleimide (**Fig. 1.5A**).[33] Zhao and co-workers have applied a similar strategy, conjugating doxorubicin to tumour-targeting decapeptide AP2H via a hydrazone bond, efficiently releasing the active drug in the pH range associated with endosomes and lysosomes and leading to translocation to the tumour cell nucleus .[34]

An imbalance of redox states is associated with cancer cells, exhibiting excessive levels of ROS compared to healthy cells including superoxide (O_2^-), hydroxyl radicals (HO^-) and hydrogen peroxide (H_2O_2), which have been linked directly to cancer cell proliferation and homeostasis.[35, 36] Research groups have exploited these high ROS levels through the development of ROS-activated prodrugs, designed to selectively release the active drug in regions of high ROS in the tumour microenvironment.

Boronic acids and boronate esters have been widely employed in ROS-activated prodrug design. In addition to enhancing targeted release to tumours, the polysaccharaides which coat the cell surface, known collectively as the glycocalyx,[37] have been specifically targeted to enhance the cellular delivery of therapeutics through use of boronic acids which form boronate esters with the 1,2- and 1,3-diols of these saccharides.[38] Lu and co-workers

presented the boronic-acid-masked prodrug derivative of SN-38, **11**, which was confirmed to be selectively activated by H_2O_2 to give **12**, liberating the active form SN-38 **14** following aryl group migration and subsequent hydrolysis of the borate ester **13** (**Fig. 1.5B**).[39]

Whilst the bulk of ROS-activated prodrugs use boron chemistry to mask essential functional groups of an active drug, these are limited to prodrugs which release alcohol and amine groups upon activation. Cohen and co-workers sought to expand the diversity of ROS-activated prodrugs, reporting a thiazolidinone-masked prodrug **15** which releases the free carboxylic acid **16** upon activation by H_2O_2.[40] Their study demonstrated high stability of the thazolidinone promoiety, little activity of the prodrug form and efficient H_2O_2-dependent release (**Fig. 1.5B**).

GSH is a tripeptide which contains a thiol functional group and represents the most abundant thiol in cells, regulating intracellular redox balance as an antioxidant.[19] GSH levels are upregulated in cancer cells, at a concentration of approximately 20 mM compared to 5 mM in healthy cells,[41] with the elevated GSH level found to contribute to tumour cell progression and drug resistance.[42] Kang and co-workers successfully exploited this reducing GSH environment of tumour cells via the introduction of a disulfide linker designed to selectively cleave by thiol-containing species such as GSH (**Fig. 1.5C**) into a prodrug analogue, **17**, of camptothecin **18**. A folic acid (FA) ligand for tumour targeting was incorporated, as the high expression of folate receptor α (FOLR1) in a range of tumour types has resulted in the use of FA as an established tumour-targeting conjugation strategy.[43-45] The amphiphilic structure facilitated self-assembly in aqueous solution followed by rapid GSH-mediated disassembly and camptothecin release.

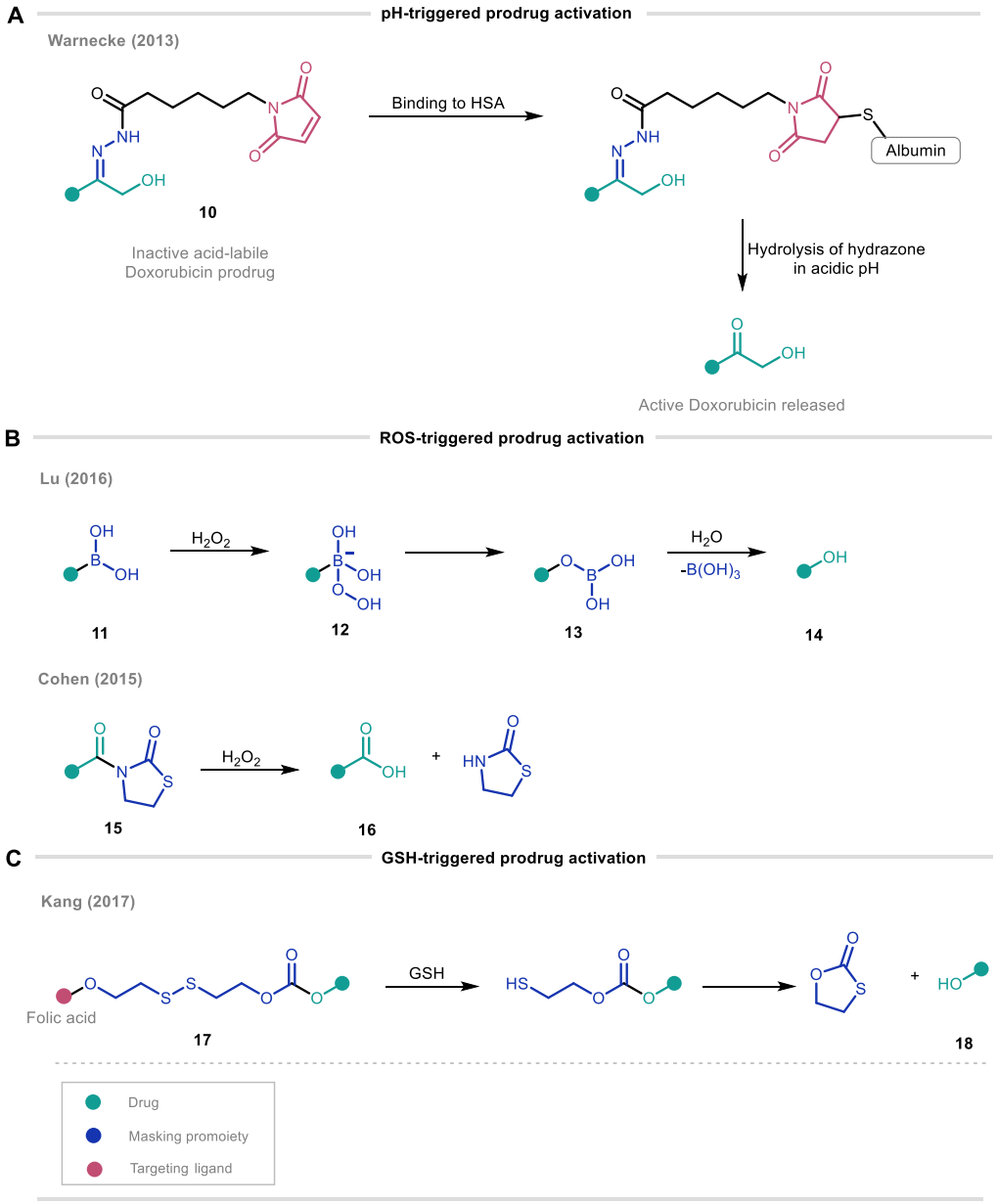

Figure 1.5 Examples of endogenous prodrug activation in response to the tumour microenvironment; A) prodrug activation via response to acidic pH; B) prodrug activation via response to elevated levels of ROS including H_2O_2; C) prodrug activation via response to elevated GSH levels.

1.2.4 Enzyme-activatable prodrugs

Elevated enzymatic activity in cancer cells has been directly implicated in a range of processes associated with cancer development and progression,[46] including immune system evasion and hijacking,[47] resistance to apoptosis signals,[48] metastasis,[49] as well as characteristic changes in the extracellular matrix and basement membrane.[50, 51] The elevated levels of particular enzymes in cancer cells has been exploited for the specific activation of prodrugs in a targeted

manner. Compared to the previously discussed (**Section 1.2.3**) endogenous conditions of the tumour microenvironment that can also be targeted, enzymatic reactions for prodrug activation are characteristically rapid, specific and mild, thereby offering an attractive mode of activation for targeted prodrugs.[20] Enzymes which have been exploited for prodrug activation include carboxylesterase (CE), matrix metalloproteinases (MMPs), esterase and caspase-3, cathepsin B, γ-glutamyltranspeptidase (GGT) and β-glycosidases.

A range of proteases are overexpressed in cancer and linked to tumour proliferation, including MMPs which are a family of over 20-dependent endopeptidases implicated in tumorigenesis and tumour progression and upregulated in almost every cancer type.[52, 53] To form a MMP prodrug **19**, Albright and co-workers coupled the C-terminus of the Pro-Cit-Gly-Hof-Tyr-Leu hexapeptide to the free amine of Doxorubicin, whilst capping the N-terminus with acetyl and succinate groups to prevent aminopeptidase degradation and to increase solubility (**Fig. 1.6A**).[54, 55] MMP cleavage by MMP-2, MMP-9 and MMP-14 in the middle of the peptide generates a tripeptide Doxorubicin conjugate **20** which is then cleaved by extracellular proteases to liberate Leu-Doxorubicin **21** which is finally converted to the free Doxorubicin **1**, with the prodrug demonstrating a significantly improved therapeutic index.

Kim and co-workers developed an esterase-responsive prodrug **22** by conjugating doxorubicin to a dichloroacetic acid mitochondrial inhibitor which has been found to aid overcoming drug resistance and a lipophilic triphenylphosphonium (TPP) mitochondrial targeting ligand, via a linker (**Fig. 1.6B**).[56] Restoration of oxidative phosphorylation over the aerobic glycolysis of the Warburg effect, which is strongly associated with tumour progression and proliferation, has the potential to enhance chemotherapeutic outcomes.[57] This prodrug seeks to overcome the dose-limiting toxicity of conventional metabolic blockers through a trifunctional mitochondrial-targeting agent that releases the active Doxorubicin **1** as well as dichloroacetic acid (DCA) **23** upon carboxylesterase-mediated amide hydrolysis, exploiting the enhanced fluorescence emission observed of free Doxorubicin at 560 nm for detection of the released drug.

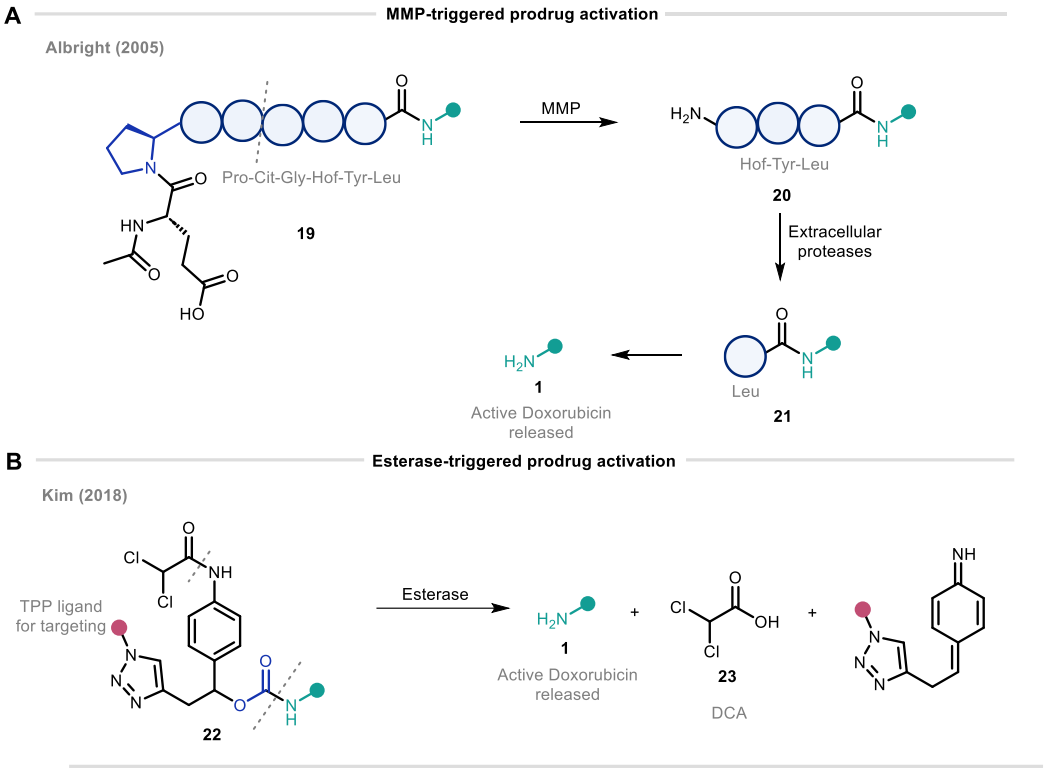

Figure 1.6 Selected protease-triggered prodrug activation. A) MMP-triggered prodrug activation (Albright and co-workers, 2005); B) trifunctional (cytotoxic Doxorubicin, DCA inhibitor, TPP ligand for mitochondrial targeting) esterase-triggered prodrug (Kim and co-workers, 2018).

Cathepsin B is a cysteine protease overexpressed and activated in a range of tumour types, with the concentration of active cathepsin B constituting up to 20% of the total lysosomal protein in tumour cells,[58] associated with tumour metastasis, growth and angiogenesis.[59] Since the discovery of cathepsin-B-labile peptide sequences, cathepsin-B-responsive systems such as those for prodrug activation have been developed.[60, 61] Originally, lysosomally cathepsin-B-cleavable peptides used by researchers centred around the Gly-Phe-Leu-Gly (GFLG) and Ala-Leu-Ala-Leu (ALAL) tetrapeptides.[62, 63] In recent years, slow payload release and aggregation of conjugates resulting from these hydrophobic sequences has led to the identification of cleavable dipeptide linkers.[64]

Bernardes and co-workers employed three of these dipeptide units (Cbz-Val-Cit, Cbz-Val-Ala, Cbz-Phe-Cit) to generate *ortho*-quinone conjugates which mask the redox activity of cytotoxic *ortho*-quinone natural products (**Fig. 1.7**).[65] Despite promising efficacy of cytotoxic *ortho*-quinones such as β-lapachone against cancers including leukaemia, breast and pancreatic cancer,[66] their NQO1-dependent redox-cycling behaviour generates ROS,[67]

resulting in systemic toxicity and precluding the progression of therapeutic candidates through clinical trials.[68, 69] The prodrug **24** utilises cathepsin-B-cleavable dipeptide linkers conjugated to a *para*-aminobenzyl linker attached at the quinone carbon as a benzyl ketol, masking its redox activity. This scaffold enables hydroquinone **25** release upon enzymatic activation and 1,6-elimination, which then spontaneously oxidises to the active cytotoxic quinone **26.**

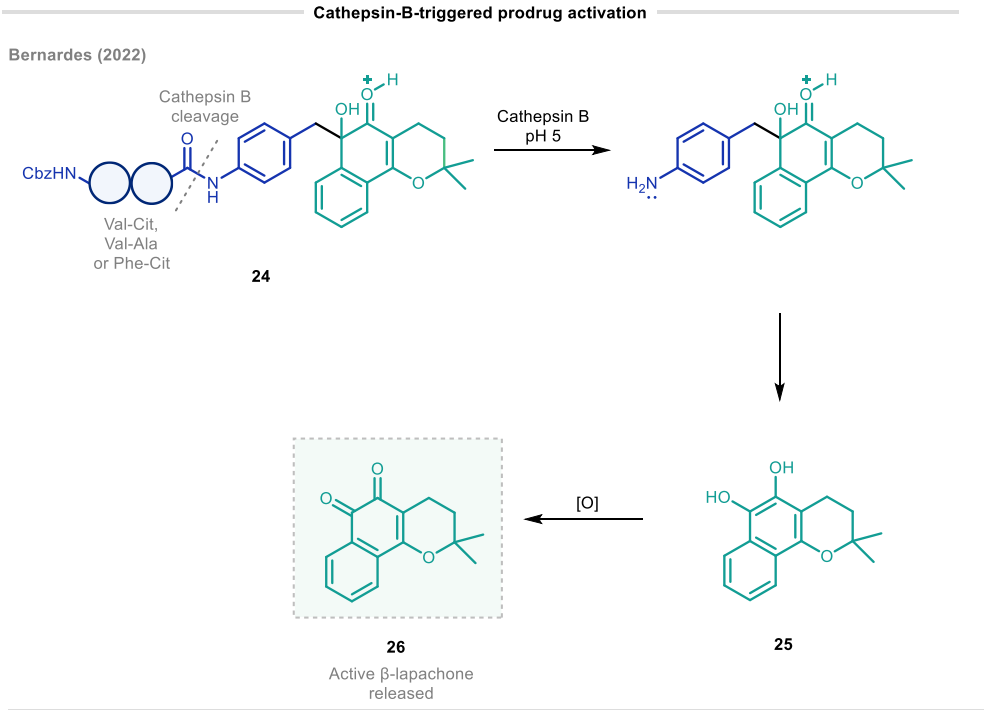

Figure 1.7 An example of a cathepsin-B triggered prodrug reported by Bernardes and co-workers in 2022, employing cleavable dipeptide units which mask the redox activity of the active β-lapachone.

γ-Glutamyltranspeptidase (GGT) is a cell-surface enzyme overexpressed in many cancer cells, associated with GSH metabolism and linked to tumour progression and chemotherapeutic resistance.[70, 71] GGT-responsive systems have been developed for fluorescent imaging applications and for drug conjugates.[72, 73] Franz and co-workers developed prochelator **27**, consisting of a γ-glutamate promoiety for tumour targeting conjugated to effective copper-chelating anticancer agent dithiocarbamate (DTC) via a *para*-aminobenzyl self-immolative linker (**Fig. 1.8**).[74] Following hydrolysis of the γ-glutamyl amide bond by GGT, 1,6-elimination of the *para*-aminobenzyl linker liberates DTC **28** which subsequently chelates Cu(II) to form the cytotoxic $Cu(DTC)_2$ complex **29.**

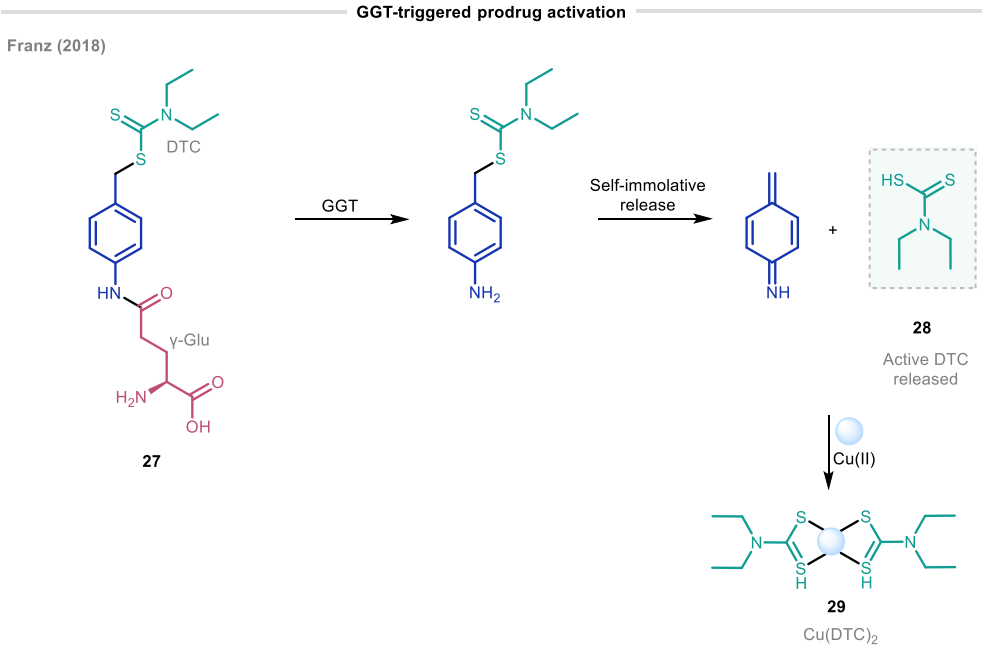

Figure 1.8 An example of a GGT-triggered prodrug reported by Franz and co-workers in 2018, forming a cytotoxic $Cu(DTC)_2$ complex.

A low concentration of oxygen, or hypoxia, is a pathological hallmark of malignant solid tumours first identified by Thomlinson and Gray in a landmark study linking tumour hypoxia to radiotherapy resistance.[75] When the tumour diameter exceeds approximately 1 mm, uncontrolled cell proliferation exceeds the ability to satisfy the oxygen demand from existing blood vessels, causing abnormal vascularisation and an insufficient oxygen supply.[76] The resulting cellular response to hypoxia, is associated with resistance to conventional cancer therapy, including chemotherapy, radiotherapy and phototherapy.[77] [78] Crucially, under hypoxic conditions, a number of intracellular reductases are overexpressed, such as nitroreductases,[79] DT-diaphorase[80] and azoreductase,[81] which can be exploited for the activation of hypoxia-activated prodrugs, including quinones,[82] *N*-oxides,[83] azoaromatics[84] and nitroaromatics.[85, 86]

In particular, in the tumour microenvironment, the nitroreductase level is correlated directly to the level of hypoxia, even being utilised quantitatively to determine the hypoxic degree of a tumour from the nitroreductase level.[87, 88] Nitroreductases readily reduce nitroaromatics to their corresponding amines, making them an attractive target for the development of hypoxia-activated prodrugs. A quantitative approach to assessing a bioreductive group's

susceptibility to reduction is the comparison of their calculated reduction potentials. The associated reduction potential for 1-methyl-5-nitropyrrole **30** and nitrobenzene **31** are the most negative at -0.56 V and -0.49 V respectively, reducing to their corresponding amine species the least readily in accordance with the thermodynamic relationship between free energy and cell potentials. The 1-methyl-2-nitroimidazole **32**, 5-nitrothiophenyl **33** and 5-nitrofuranyl **34** are more easily reduced with reduction potentials of -0.33 V, -0.39 V and -0.39 V for this series (**Fig. 1.9**).[89]

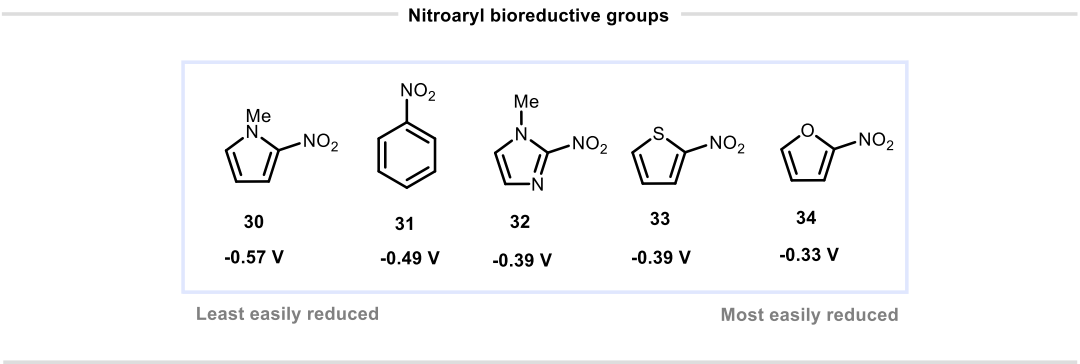

Figure 1.9 Various nitroaryl bioreductive groups and their associated reduction potentials.

Nitroreductases mediate one-electron reduction of the nitro group to a radical anion *in vivo*. In a normoxic environment this anion is rapidly oxidised by oxygen, which forms superoxide and renders this pathway unproductive.[90] However, under hypoxic conditions this radical anion instead undergoes further reduction to an amine via the nitroso and hydroxylamine intermediates (**Fig. 1.10**). This reduction step reverses the reactivity of the aromatic substituent from strongly electron-withdrawing to strongly electron-donating, triggering a self-immolative fragmentation event.

In the development of a novel lysine deacetylase (KDAC) inhibitory HAP, Conway and co-workers provided a direct comparison of analogues of their Panobinostat prodrug design bearing the nitrobenzyl (NB-Pano **36**), nitrothiophene (NT-Pano **37**), nitroimidazole (NI-Pano **35**) and nitroquinoline (NQ-Pano **38**) bioreductive groups, chosen due to the range of reduction potentials they provide, predicting a similar potential for the nitroquinoline to the nitroimidazole group (**Fig. 1.10**).[91] Incubation with NADPH-CYP reductase (CYP004) in

both normoxic and hypoxic allowed the group to determine whether or not the prodrugs underwent hypoxia-dependent reduction and fragmentation.

This analysis demonstrated no apparent Panobinostat release with the least-easily reduced NB-Pano **36** with a higher enzyme concentration required to reduce and fragment the prodrug, making the prodrug less suitable for *in vivo* studies.[92] Panobinostat was released in both normoxic and hypoxic conditions for NT-Pano **37**, making it unsuitable in the described methodology. Concentrations of NQ-Pano **38** were depleted in both normoxic and hypoxic conditions, however Panobinostat was only released in hypoxic conditions, indicating only partial reduction in the normoxic environment, therefore demonstrating potential for use as a HAP. However, NI-Pano **35** gave the most promising reduction and fragmentation profile, stable in normoxic conditions and oxygen-dependent release displayed in the hypoxic environment. Furthermore, the nitroimidazole prodrug showed no inhibition of the KDAC target in the inactive prodrug form and, crucially, significant growth delay in hypoxic tumours in an esophageal xenograft mouse model.

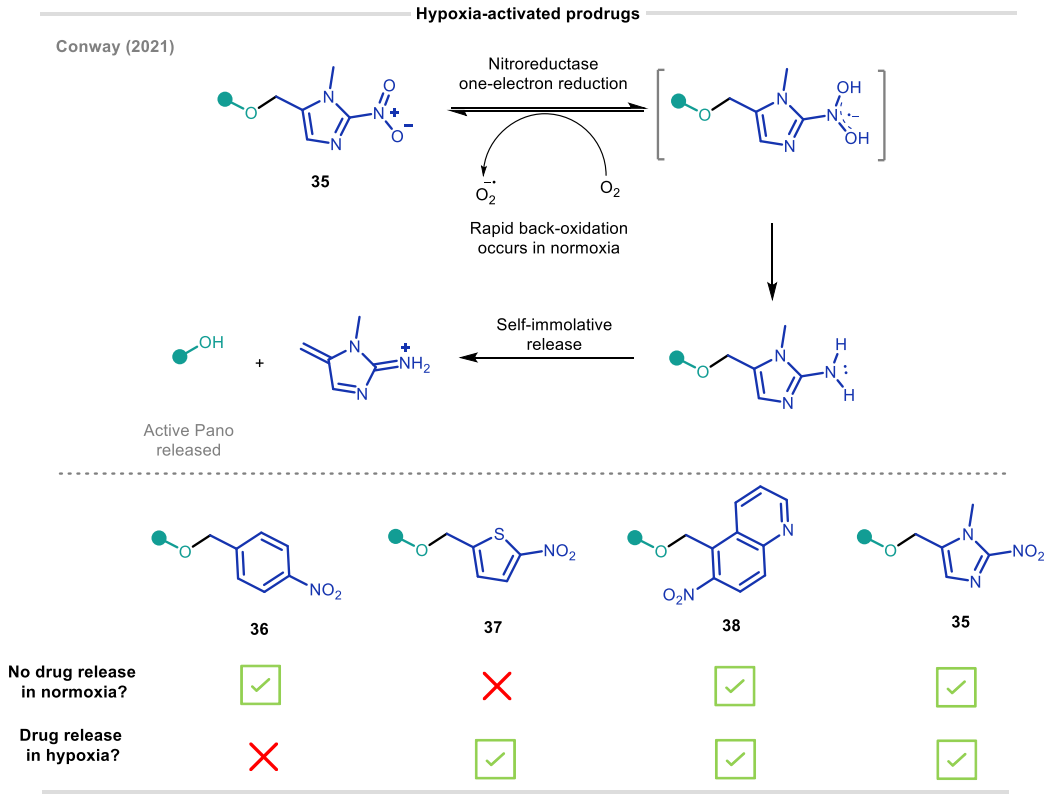

Figure 1.10 The mechanism of activation of a HAP reported by Conway and co-workers in 2021 and drug release results from nitrobenzyl, nitrothiophene, nitroquinoline and nitroimidazole hypoxia-activated protecting groups.

Glycosidases are glycoside hydrolase enzymes primarily involved in the hydrolysis or transglycosylation of glycosidic bonds in a variety of substrates including polysaccharides, glycoproteins and glycolipids, ubiquitous in living organisms.[93] These are highly efficient catalysts, providing rate enhancements of glycoside hydrolysis of more than 10^{17} (k_{cat}/k_{non}).[94] They require two catalytic amino acid residues, typically glutamic or aspartic acid, which act as a general acid or general base respectively to catalyse the hydrolysis of these bonds. First postulated by Koshland in 1953, the reaction takes place with either retention or inversion of configuration of the anomeric carbon depending on the spatial arrangement of the catalytic amino acids, with the mechanism proceeding via oxocarbenium-ion-like transition states (**Fig. 1.11**).[95] The mechanism of inverting glycosidases involves a single step S_N2 displacement with the acid/base glutamate and apartate side chains approximately 6 to 11 Å apart (**Fig. 1.11A**), whilst retaining glycosidases react via a two-step S_N2 displacement involving a glycosyl-enzyme intermediate with both acid/base assistance and nucleophilic reaction of the amino acids, 5.5 Å apart (**Fig. 1.11B**).[96]

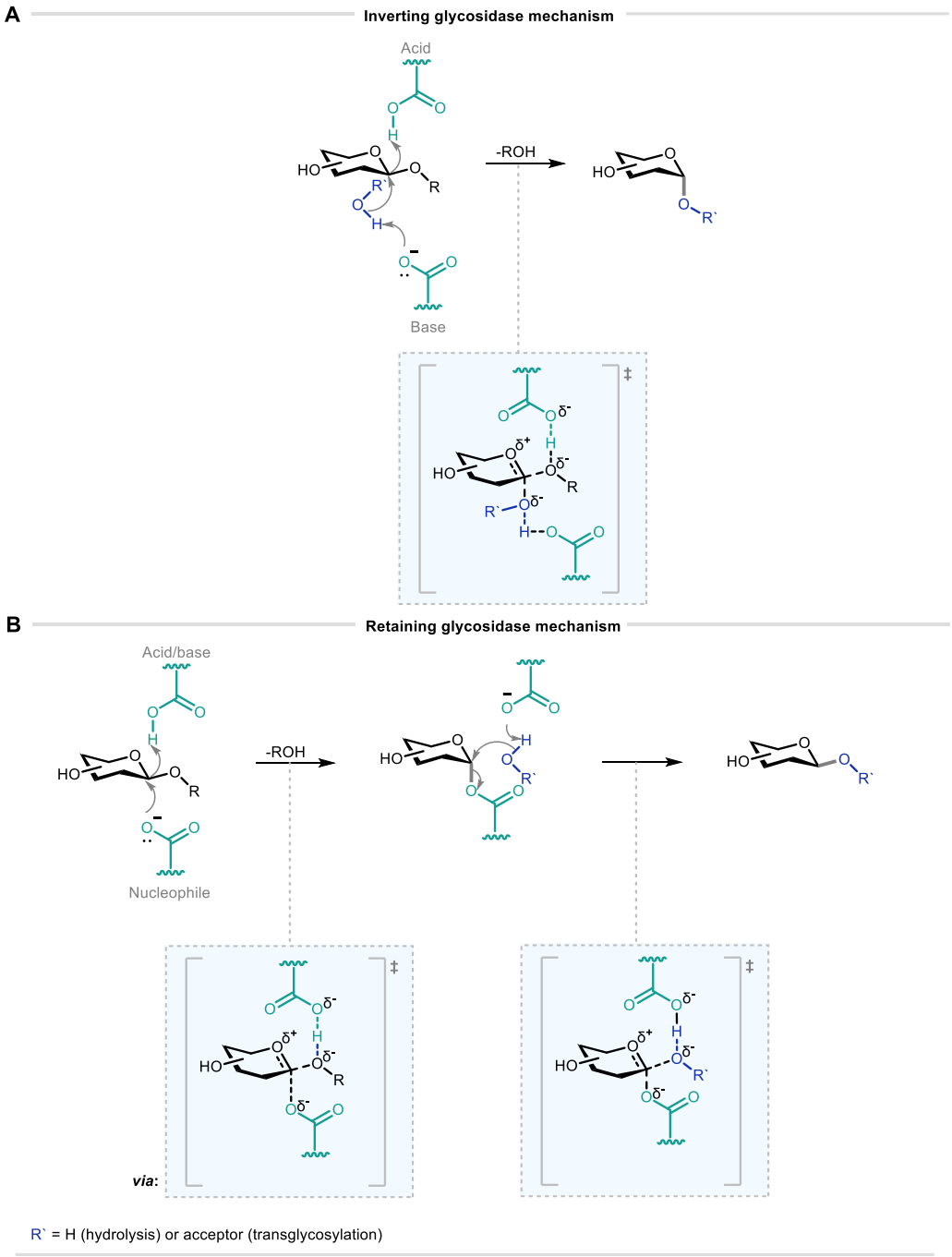

Figure 1.11 Catalytic mechanisms of glycosidases involving a glycoside and glutamic/aspartic acid residues for hydrolysis and transglycosylation; A) Retaining glycosidase mechanism involving double S_N2 displacement; B) Inverting glycosidase mechanism involving a single S_N2 displacement.

The selective hydrolysis of glycosidic bonds by glycosidases is essential to a range of cellular processes including energy uptake, cell wall expansion and degradation.[97] Encoded by approximately 1% of genomes of all organisms,[98] glycosidases are of long-standing and increasing interest due to the ubiquity of carbohydrates in nature and their biological importance.[99] There are two main types of these hydrolases: exoglycosidases which cleave the

glycosidic bond of terminal non-reducing sugar residues from glycan substrates and endoglycosidases which catalyse the cleavage of internal glycosidic linkages within sugar chains. Beyond these two main families, they represent a diverse group of enzymes, classified further into 133 families on the carbohydrate-active enzymes (CAZy) database.[100]

Carbohydrates are an essential energy source, as the human body uses glycosidases to hydrolyse digestible oligo- and disaccharides such as amylose and sucrose into their glucose and fructose monosaccharide constituents respectively, which then participate in energy-producing metabolic pathways to harness their nutritional value.[101] The bulk of this process takes place in the small intestine, where membrane-bound glycosidases in the brush border of the jejunum generate monosaccharides which are subsequently taken up by glycosyl transporters and excreted into the bloodstream.[102] Glycosidase activity is also implicated in certain diseases such as lysosomal storage disorders. These are a group of heritable metabolism defects that result from lysosomal glycosidase deficiencies whereby incomplete glycan substrate degradation accumulate in lysosomes, leading to cellular dysfunction, tissue damage and cell death.[103-106]

A variety of glycosidases including β-glucuronidase, β-galactosidase, β-glucosidase, *N*-acetyl-β-D-glucosaminidase, α-glucosidase, α-mannosidase and α-fucosidase are upregulated across a range of tumour types compared to significantly lower expression levels in healthy cells.[107] Various glycosidases and their level of activity have also been implicated throughout the cancer development stages: in early-stage cell transformation to malignant tumour cells, localised tumour growth and metastatic propagation, making them promising targets for developing enzyme-activated prodrugs.[99, 108, 109]

Early examples of carbohydrate-based prodrugs (**Fig. 1.12**) in the early 1990s were designed primarily to improve the pharmacokinetic properties of the active anticancer agents through water solubility and serum stability improvements, as well as enhancing blood-brain-barrier transport via glucose transporter 1 (GLUT1) which is overexpressed in many cancers.[110-114] Glycosylation of a number of cytotoxic anticancer agents including chlorambucil and docetaxel has achieved significant reductions in toxicity for these purposes.[115, 116] It wasn't until 1995 when Wiessler and co-workers reported glufosfamide as the first tumour-targeted

sugar-conjugate prodrug, which exploits GLUT1 overexpression and requires β-glucosidase-mediated cleavage to liberate the corresponding algycone cytotoxic ifosfamide DNA alkylating agent.[117]

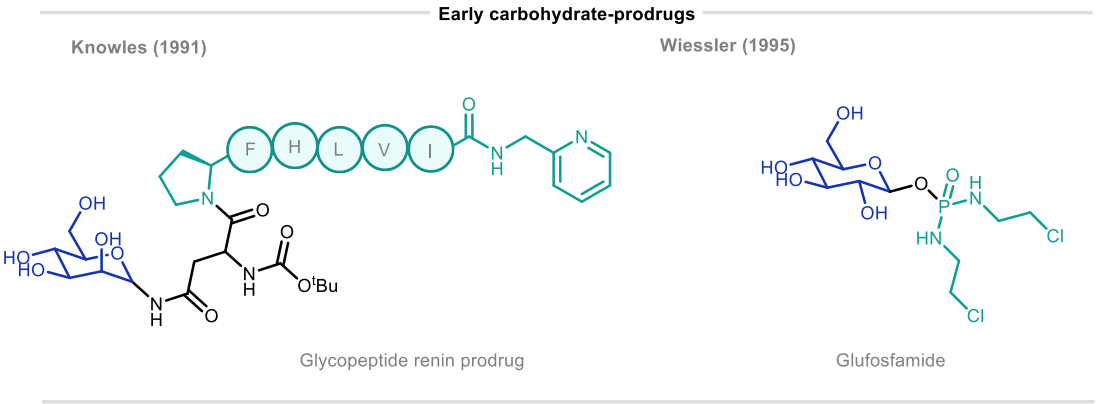

Figure 1.12 Early examples of carbohydrate-based prodrugs.

The more recent targeted carbohydrate-prodrug activation which exploits the overexpression of glycosidases in tumour cells consist of a cytotoxic anticancer drug conjugated to a sugar via a self-immolative linker, such that enzymatic cleavage of the glycosidic bond will liberate the active drug (**Fig. 1.13**). Seminal work by Katzenellenbogen and co-workers in 1981 introduced the concept of self-immolative linker design to the chemical sciences,[118] which refers to a chemical spacer which responds to a stimuli to induce a reaction cascade releasing a desired payload.[119]

Until recently, glycosidase prodrug design had been largely applied to directed enzyme prodrug therapies such as antibody-directed enzyme prodrug therapy (ADEPT), in which an enzyme-antibody conjugate is administered, which subsequently binds to antigens on the tumour cell surface and accumulates. Next, an enzyme-activatable prodrug is injected whereby the active drug is released at the tumour cell. Pioneered by Tietze and co-workers in the 2000s, a number of proof-of-concept studies employing glycosidase-responsive prodrugs which are compatible with the ADEPT delivery strategy have been developed, typically using duocarmycin and doxorubicin as model cytotoxic payloads.[120-125]

However, the implementation and advancement of ADEPT to clinical settings has been precluded, remaining challenging due to the immune response risk associated with the antibody-enzyme conjugates administered, as well as the general complexity and costs of the

therapies.[126, 127] As a result, more recent efforts to develop targeted β-glycosidase-activated therapies have focused on those which depend on the selective activation by endogenous glycosidase activity in the tumour microenvironment in prodrug monotherapy (PMT).[128] Following the proposal of developing inactive prodrugs for selective activation by β-glucuronidase by Tietze *et al.*,[129] Bosslet *et al.* published the first study to demonstrate the exploitation of the enzyme in PMT for the release of a cytotoxic payload in 1998.[130]

Selected examples of β-glycosidase-activated prodrugs based on simple glycoconjugate scaffolds designed for ADEPT are shown in **Fig. 1.13A**, including **39**, a β-glucuronide prodrug of histone deacetylase (HDAC) inhibitor Vorinostat developed by Akkinepally and co-workers. Four HDAC inhibitors have been approved for cancer treatment by the FDA including Vorinostat, although poor water solubility and dose-limiting toxicity limits its efficacy. Whilst the prodrug demonstrated a reduced inhibitory effect with an IC_{50} value of 10 μM without β-glucuronidase treatment, introduction of the enzyme reduced the IC_{50} value to that of the parent drug at 2.39 μM. The sugar moiety facilitated a significant increase in water solubility from 0.1 mg/mL to 40-45 mg/mL.[131] Most β-glycosidase-activated prodrugs since the early 2000s feature a nitro-substitution on the aromatic ring of the linker to increase the rate of self-immolation.[132]

Extensive pre-clinical studies of the early examples of glycosidase-activated prodrugs for prodrug monotherapy, most notably β-glucuronidase-activated Doxorubicin analogue **40** developed by Bosslet and co-workers, have demonstrated unsatisfactory results primarily due to an insufficient rate of turnover of β-glucuronidase in the tumour microenvironment and rapid renal clearance by the kidneys, therefore necessitating the administration of very high doses.[133] Therefore, the PMT prodrugs developed since 2010 have mostly sought to utilise ligands for tumour targeting and self-immolative dendrimers for multi-component release (**Fig. 1.13B**).[133-135]

The enhanced permeability and retention (EPR) effect is a characteristic of solid tumours a allowing macromolecules to accumulate due to the enhanced vascular permeability of solid tumours, allowing for the formation of a macromolecular drug carrier.[136] This concept was first applied to a glycosidase-activated prodrug by Papot and co-workers in 2012, generating

a dendritic analogue of glucuronide prodrug **40**, compound **41** which bears a maleimide functional group for albumin binding to form a macromolecular carrier, conjugated to the scaffold via a PEG linker.[137] The researchers were able to demonstrate the significantly improved antitumour activity of **41** compared to **40**, demonstrating similar efficacy to Doxorubicin, whilst also exhibiting a 4-fold higher IC_{50} than **40** (14 μM vs 3.5 μM) and therefore being 4-fold less toxic prior to activation.

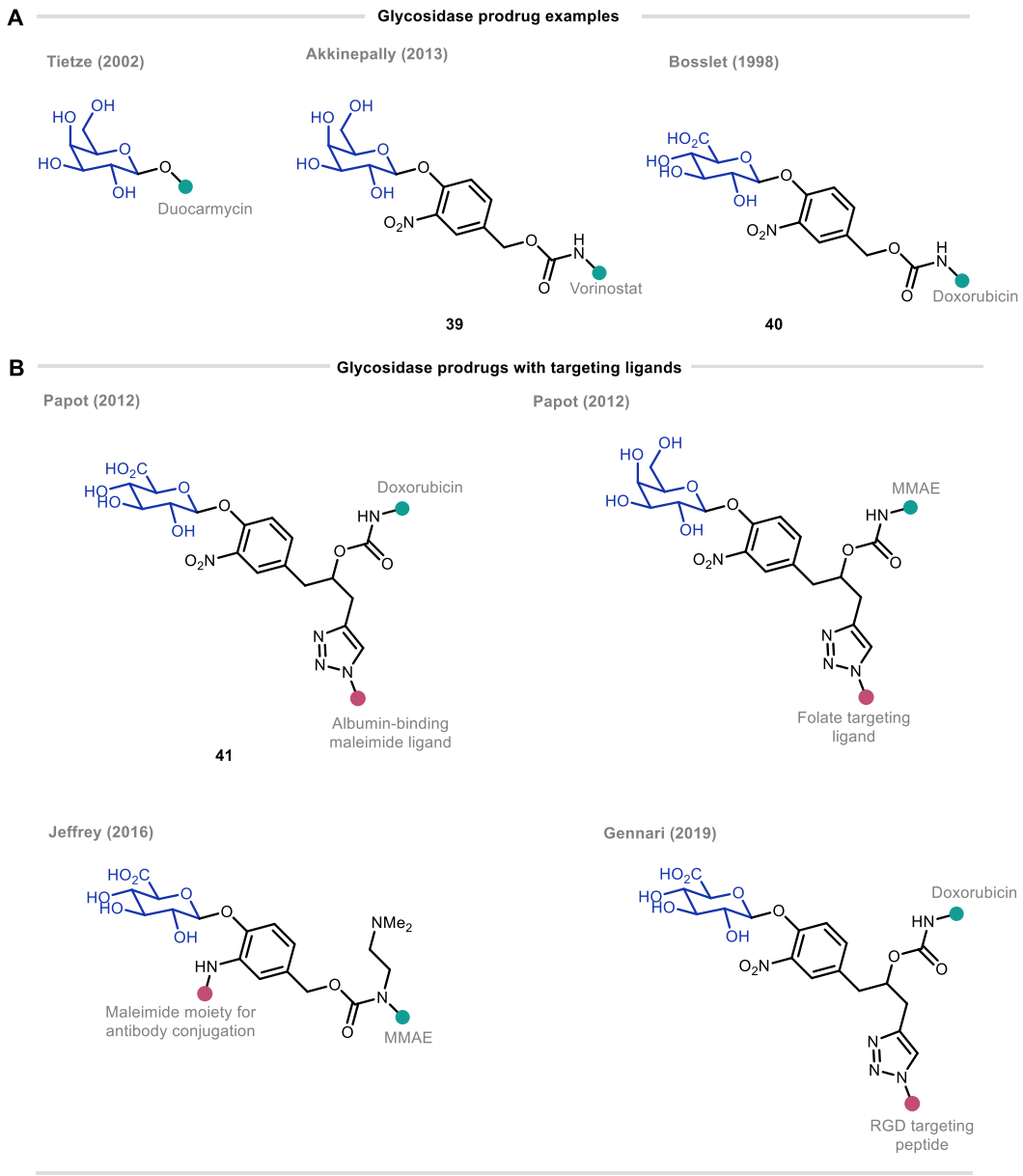

Figure 1.13 Examples of glycosidase-responsive prodrugs. A) Early and simple glycoconjugate examples; B) Examples featuring targeting ligands.

Furthermore, the continued development of self-immolative dendritic glycosidase-activated prodrugs has led to prodrugs designed for dual-release of the active drug. Papot and co-workers demonstrated both β-glucuronidase-activated prodrug **42** which releases two molecules of doxorubicin as well as extending this to β-galactosidase-responsive prodrug **43** which incorporates an additional folate targeting ligand (**Fig. 1.14**). These exhibited increased toxicity upon enzymatic activation compared to the parent drug, low toxicity prior to enzymatic activation and increased drug release in folate-receptor-positive cells for **43**.[138, 139]

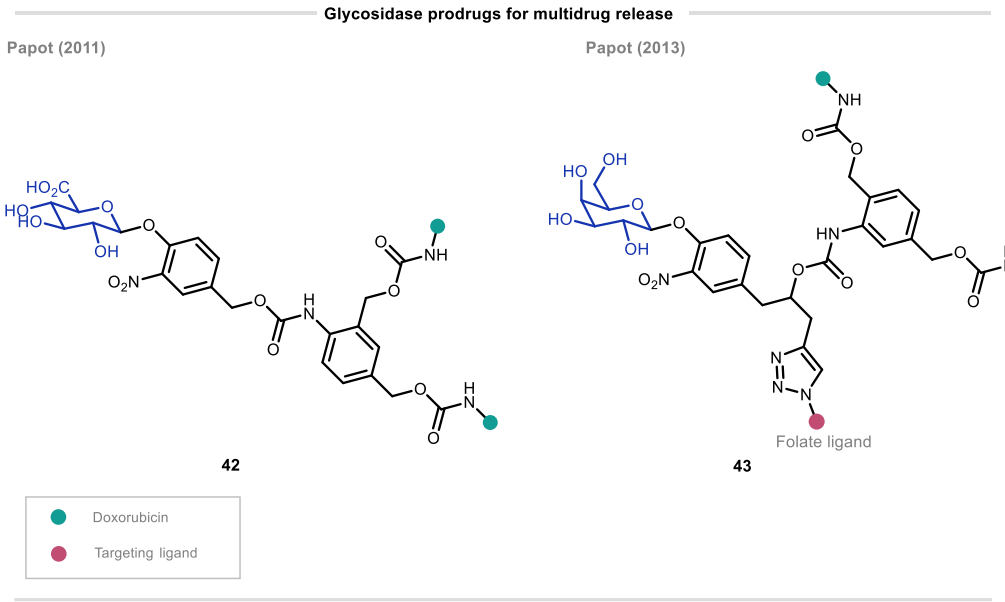

Figure 1.14 Glycosidase-responsive prodrugs designed for multidrug release.

1.3 Lectin recognition and glycopolymers

Glycans are glycoconjugates of carbohydrates with proteins and lipids, typically found on cell surfaces. Glycan recognition modulates important biological processes including cell adhesion, immunological responses and disease progression.[37] Lectins are a type of glycan binding proteins which recognise terminal groups on glycan ligands which fit into carbohydrate-recognition domains (CRDs).[140]

Since their initial discovery in the electric organ of the electric eel by Resheff and co-workers in 1975,[141] followed by galectin isolation in the laboratory in 1976,[142] the physiological functions of galectins which bind to β-galactosides have been steadily elucidated over the

ensuing decades.[143] They are known to be the only glycan-binding proteins which can be excreted into the extracellular space and also located in the cytoplasm and nucleus, involved in homeostasis, cell adhesion and immunity, modulating immune cells through binding to glycans on their surface or intracellularly via intracellular protein interactions.[144, 145]

Glycopolymers may be defined as polymers bearing pendant saccharide groups, which exhibit multivalent interactions and large amplification effects in molecular recognition; these molecular recognition amplification effects are sometimes referred to as the glycoside cluster effect.[146, 147] Applications of glycopolymers include lectin and cell recognition, including those produced by Kiessling and co-workers in 2000 using ring-opening metathesis polymerisation (ROMP) to generate polymers carrying β-galactose pendant moieties which demonstrated a strong affinity with *E. coli* due to the multivalent effect with galectins on the cell surface.[148] The glycopolymer induced clustering of lectins and of other receptors which do not bind galactose through inter-receptor communications, resulting in lectin crosslinking and chemotaxis.

Provided the saccharide-lectin interaction is sufficiently strong, glycopolymers may offer alternatives to antibodies for molecular recognition applications in sensing and diagnostics.[149] As the saccharides provide a molecular recognition element, biosensors typically include an additional sensing part which is often a gold, semiconductor or metal nanoparticle substrate which may be used in surface plasmon resonance, quartz crystal microbalance and electrochemical techniques.[146]

In addition, by generating block copolymers of glycopolymers with hydrophobic polymers, polymeric micelles and vesicles may be prepared for the encapsulation of hydrophobic small molecule drugs such as doxorubicin. For example, the Armes group demonstrated a variety of self-assembled block glycopolymers featuring variations in the ratio of glycosylated and hydrophobic sections, generating polymeric micelles and vesicles with affinity to galectins which enabled the delivery to human dermal fibroblast cells.[150]

1.4 Peptide therapeutics

First isolated by Banting in 1921, followed swiftly by breakthrough results from its first clinical use at Toronto General Hospital in 1922, commercial availability in early 1923 and the awarding of the Nobel Prize in Medicine in October 1923, the discovery of 51-amino-acid peptide hormone insulin represents one of the leading triumphs in medical research of the 20th century, revolutionising the treatment of diabetes.[151] Peptide isolation was subsequently limited to natural sources until breakthroughs in amine protecting group chemistry in the 1930s starting with the carbobenoxyl (Cbz) group by Bergmann and Zervas in 1932,[152] leading to the first synthetically produced naturally occurring small peptides carnosine and glutathione in 1935,[153, 154] followed 18 years later by the first syntheses of peptide hormones, oxytocin and vasopressin.[155, 156]

However, the limitations of solution-phase peptide synthesis (SPS) precluded notable progress in peptide therapeutic development until the advent of solid-phase peptide synthesis (SPPS) in 1963[157] and the development of purification methods such as high-performance liquid chromatography (HPLC) in 1976.[158] Since then, 80 peptide therapeutics have been approved for use in the clinic, with 30 receiving authorisation in the last two decades alone, more than 150 undergoing clinical trials and a further 400-600 in pre-clinical development.[159] From a commercial perspective, peptide drugs account for approximately 5% of the global pharmaceutical market with revenue exceeding $50 billion in 2019, with clinical approvals steadily rising over recent decades.[160]

1.4.1 Therapeutic properties of peptides

Peptide therapeutics are recognised to occupy a unique chemical space in pharmaceutical development between conventional small-molecule inhibitors and biologics. Biologics such as antibodies exhibit exceptional target specificity,[161] however their use has been limited by their lack of membrane permeability and their associated immunogenicity, inducing anti-drug antibody responses which can significantly reduce the efficacy of the drug and causing adverse immune reactions in the clinic.[162, 163] Small molecules have traditionally dominated pharmaceutical development, typically conforming to Lipinski's rule of five to demonstrate favourable pharmacokinetic properties such as good membrane permeability, as well as being

associated with low cost and suitable for oral administration. However, they can access more limited defined targets and in recent years the rate of clinical approval has reduced.[164] Therefore, peptides occupy a 'Goldilocks zone' with the potential to develop therapeutics with favourable properties of biologics, high potency and specificity, and small molecules, increased bioavailability and membrane permeability.[165]

Peptide drugs are known to be capable of inhibiting intracellular protein-protein interactions (PPIs), a well-established class of drug targets that are often deemed an 'undruggable' space for small molecules.[166] PPIs control many essential cellular processes implicated in disease, demonstrating recognised potential as a significant class of drug targets with only 1% of PPIs in the human body being studied to date.[167] Whilst the targets to which small molecule inhibitors bind typically have contact areas in the region of 300 – 1,000 $Å^2$, this rises to 1,500-3,000 $Å^2$ for PPI interfaces, distributed over a collection of small binding pockets referred to as 'hot spots'.[168, 169] In contrast to small molecules, the large contact surfaces of therapeutic peptides make them viable candidates to inhibit PPI targets. Following the continued development of therapeutic peptide PPI inhibitors, over 60 peptide drugs targeting PPIs have been clinically approved and marketed.[170]

Whilst occupying this privileged region in the chemical space, peptides have a number of recognised disadvantages which have limited their use in the clinic. These are primarily associated with their poor bioavailability, unsatisfactory membrane permeability and ADMET properties including rapid renal clearance resulting from short half-lives. Shorter sequences typically have enhanced pharmacokinetic properties but exhibit poorer binding affinity to their targets, whilst larger peptides have improved potency but reduced stability and cell permeability, limiting them to extracellular targets. As a result, significant efforts to optimise the drug-like properties of peptides for use as therapeutics such as through use of unnatural amino acids, amino-terminal capping, macrocyclisation and conjugation of small molecule tags have led to continued improvements to limiting short metabolic half-lives in recent years.[171]

1.4.2 Cyclic peptides

Cyclic peptides are attracting growing attention for their favourable pharmacological characteristics which make them promising candidates in drug development.[172] The cyclisation of the linear peptide precursor gives them reduced conformational flexibility, enhancing their degree of preorganisation for binding to their molecular targets such that their binding affinity is significantly higher due to a decreased entropic penalty.[166, 173] In addition, macrocyclic peptides demonstrate increased metabolic stability, lower toxicity and enhanced cell-penetrating activity.[174, 175] The increased target affinity, selectivity, stability and membrane permeability offered by cyclic peptides means they represent a central class of peptides that tackle conventional challenges associated with the use of peptides as therapeutics. As such, they account for nearly half of peptide drug approvals by the FDA between 2017 and 2023 including terlipressin **44** and rezafungin **45** (**Fig. 1.15**), during which time approximately 10% of all drugs approved were peptides.[174]

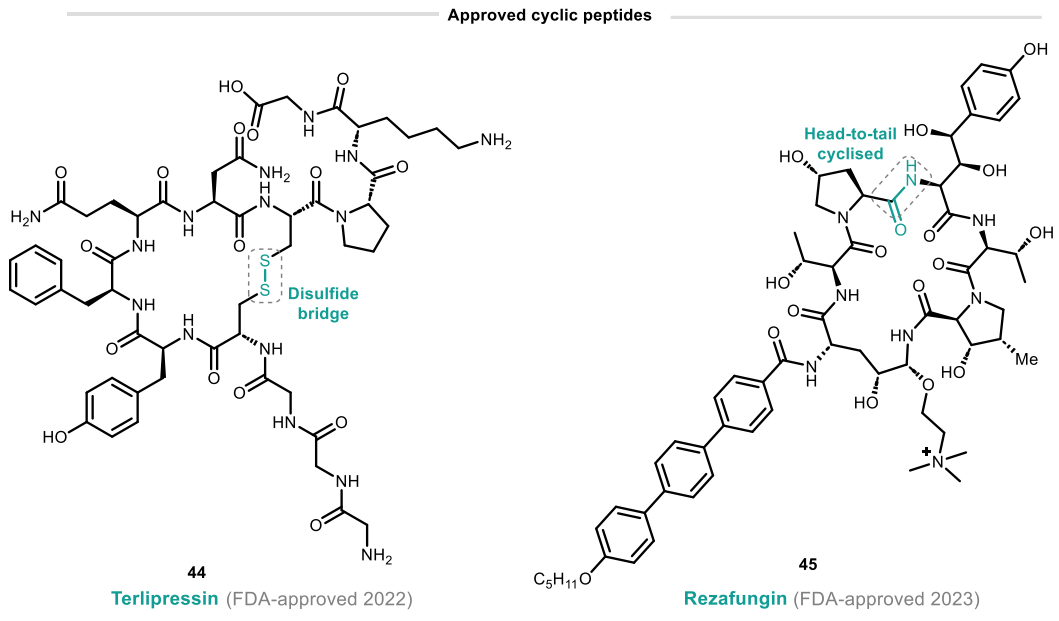

Figure 1.15 Structures of Terlipressin and Rezafungin, FDA-approved cyclic peptide therapeutics, and their cyclisations methods highlighted.

1.4.3 Somatostatin and its analogues as therapeutics in the clinic

Somatostatin (SST) **46** is a cyclic peptide hormone which inhibits the secretion of growth hormone, insulin, glucagon, gastrin, secretin and thyroid-stimulating hormone, and many tumours overexpress at least one of its five G-protein coupled receptor (GPCR) subtypes. Its use as a therapeutic has been precluded by its prohibitively short half-life of less than 3 minutes, which has resulted in the generation of hundreds of somatostatin analogues.[176-178] Crucially, it was necessary to establish the minimum structural requirements of the peptide for its biological activity, which began with the work of Guillemin and co-workers in the 1970s, methodically shortening the peptide, deleting single residues, replacing residues with alanine and substituting residues with their corresponding D-amino acids.[179-182] The first analogue to be reported with increased potency featured a substitution of Trp with *D*-Trp by Vale and co-workers in 1975, featuring in all subsequent reported analogues.[183]

In 1979, Nutt and co-workers generated analogue **47** (**Fig. 1.16A**),[184] proposing a type II β-turn about the Phe-Trp-Lys-Thr sequence from NMR studies that was subsequently determined to be the biologically-active of the peptide for receptor-recognition.[185, 186] Systematic Ala substitutions by Vale *et al.* and subsequent determination of inhibitory activity against growth hormone (GH) revealed the smallest peptide motif required to inhibit GH secretion as Cys-Phe-Trp-Lys-Thr-Cys in **48** (**Fig. 1.16A**).[187] Following these seminal works, ensuing somatostatin analogue development for improved pharmacokinetic and pharmacodynamic properties were based on the incorporation of this tetrapeptide pharmacophore as a lead sequence.

Arguably the most consequential somatostatin analogue development came in 1982 with the work of Pless and co-workers (**Fig. 1.16B**), who took hexapeptide **49** and applied a series of modifications to find a peptide that would impart increased stability whilst also increasing the potency of the agent. A series of peptides resulted in the generation of octreotide **50**, which exhibited a 70-fold increase in growth hormone (GH) inhibition *in vivo*, as well as achieving higher stability and enhanced selectivity.[188] Featuring a *D*-Phe residue on the *N*-

terminus, the *D*-Trp residue that early studies linked to potency and a Thr-ol amino alcohol at the *C*-terminus, this octapeptide was approved for clinical use by the FDA in 1988 and continues to be used by clinicians today, with a significantly increased half-life of 12 h compared to less than 3 minutes for the native somatostatin.[189] The particular overexpression of SSTR2 and SSTR5 receptors in breast, lung and neuroendocrine tumours means peptide anticancer agents such as these have a degree on inherent specificity.[190, 191]

Beyond analogue development based on the Phe-Trp-Lys-Thr lead sequence, the rational design of nonpeptide mimetics is an alternative approach. For example, nonpeptide scaffolding using carbohydrates has been carried out with the aim of improving oral bioavailability and stability, such as the incorporation of glycoamino acid **50** into peptide **51** (**Fig. 1.16C**), imparting conformational stability with the rigid pyranose ring.[192, 193] The carbohydrate moiety was found to induce a β-turn, whilst still exhibiting an IC_{50} of 0.15 uM for the inhibition of glutathione and representing an analogue for superior oral bioavailability. Increasingly, more innovative analogues for peptide therapeutic development are being generated through the incorporation of small-molecule components into peptides which can improve their potency, stability and cell permeability, including conjugation to lipids, steroids and sugars.[171]

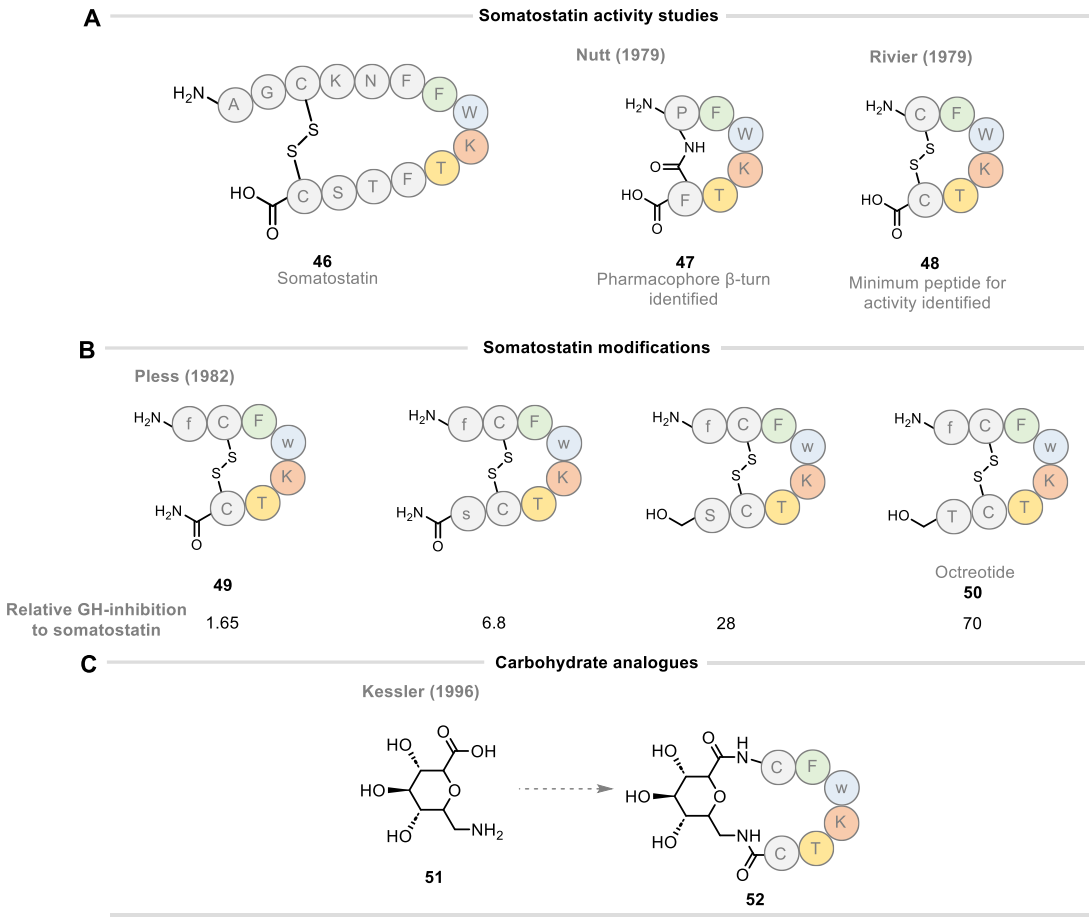

Figure 1.16 Somatostatin analogues. A) The structure of somatostatin **46**, hexapeptide **47** that was used to determine the Phe-Trp-Lys-Thr β-turn pharmacophore (Nutt and co-workers, 1979) and hexapeptide **48** that was found to be the minimum sequence for biological activity (Rivier and co-workers, 1979); B) Somatostatin analogue generation and activity relative to somatostatin, generating octreotide (Pless and co-workers, 1982); C) Incorporation of glycoamino acid **51** into hexapeptide mimetic **52** (Kessler and co-workers, 1996). *D*-amino acids are denoted in lower case and the Phe-Trp-Lys-Thr pharmacophore is highlighted in colour.

1.4.4 Tumour-targeting peptides and peptide-drug conjugates

The utilisation of functional targeting ligands that bind specifically with receptors or antigens overexpressed in cancer cells has emerged as a promising approach to improving the efficacy of anticancer drug delivery through the generation of peptide-drug conjugates (PDCs) consisting of a targeting peptide linked via a cleavable linker to a therapeutic payload[194, 195] As described previously in **Section 1.2.3**, a suite of cleavable linkers activated by various intracellular processes (e.g. upregulated enzymes, low intracellular pH, elevated ROS and GSH levels) which further enhance targeting proficiency have now been developed for use in

systems such as these.[196, 197] A diverse range of ligands for tumour targeting has emerged in recent years including folic acid,[198] carbohydrates,[199, 200] aptamers,[201] antibodies[202] and peptides[203], each possessing advantages and disadvantages.[204]

Owing to their exceptional specificity and affinity for their targets when compared to small molecules, antibodies and peptides have become two central classes of targeting ligands. In contrast to antibodies, peptides offer enhanced cell penetration, ease of synthesis, lower immunogenicity, toxicity and cost whilst retaining superior specificity in comparison to small molecule ligands.[205] As such, tumour-homing peptides have emerged as a distinct class of targeting ligand (**Table 1.1**), following identification either from natural peptide derivatives or through large-scale screening of peptide libraries including phage display.[206, 207]

Table 1.1 Tumour-homing peptides and their associated tumour targets.

Peptide	Sequence	Cancer type	Ref.
Octreotide	fCFwKTCT-ol	Neuroendocrine, breast, lung	189
iRGD	CRGDKGPDC	Pancreatic, lung, colon	208
PL3	AGRGRLVR	Gliomas, prostate, carcinoma	209
Lin TT1	AKRGARSTA	Breast	210
Lyp-1	CGNKRTRGC	Breast, osteosarcoma	211
CREKA	CREKA	Gliomas, lung	212
NGR	CNGRC	Pancreatic, angiogenic islets	213
REA	CREAGRKAC	Prostate, breast, cervical	214
$(KLAKLAK)_2$	KLAKLAKKLAKLAK	Breast, lung, bladder	215
AGR	CAGRRSAYC	Prostatic intraepithelial neoplasia	216

Somatostatin and its rationally-designed synthetic analogue octreotide bind specifically to five subtypes of somatostatin receptors (SSTR) which are upregulated in many cancers, making them suitable targeting ligands for tumour-homing peptides.[191] Moreover, of the five receptor subtypes, SSTR2 exhibits the highest expression levels and is overexpressed in the largest number of tumour types; it is to this receptor subtype that octreotide demonstrates its highest affinity, with this affinity being directly associated with the therapeutic's clinical success.[217-219]

For example, Single-Photon Emission Computed Tomography (SPECT) and positron emission tomography (PET) are imaging techniques used in nuclear medicine for diagnostic and therapeutic purposes, based on radiolabelled target-specific ligands and appropriate radionuclides such as ^{68}Ga, ^{111}In and ^{177}Lu.[220] In 1994, ^{111}In-diethylenetriaminopentaacetic acid (DPTA)-octreotide or OctreoScan **53** (**Fig. 1.17A**) made it to market as a radiolabelled diagnostic agent in the first clinical approval of a peptide-drug conjugate.[221, 222] Since then, the conjugation of tumour-homing peptides has transformed the radiopharmaceutical field, with numerous peptide analogues consisting of a radiolabelled chelating agent conjugated to a targeting peptide (predominantly based on somatostatin and octreotide), being developed.[223]

Since the early radiopharmaceutical peptide conjugates which were designed for the diagnostic detection of primarily neuroendocrine tumours, later examples developed this class of agent into therapeutics, now known as peptide receptor radionuclide therapy (PRRT).[224] The two main examples of these are octreotide conjugates ^{68}Ga-DOTA-TOC **54** and ^{117}Lu DOTA-TATE **55**.[225]

Conjugates of tumour-homing peptides including somatostatin and its analogues have also been developed with small molecule anticancer agents described in **Section 1.2** to facilitate targeted delivery to cancer cells.[226, 227] In 2018, Gellerman and co-workers reported peptide-drug conjugates (**56**) between somatostatin analogues and three major drugs used to treat pancreatic cancer, camptothecin, combrestatin-4A and azatoxin, and were able to demonstrate specific accumulation in tumours in an animal xenograft model as well as significant toxicity towards pancreatic cancer cell lines.[228]

Enzymatic activation of cleavable linkers for self-immolative drug release using tumour-homing peptides has received significant interest in chemical biology in recent years.[229, 230] In 2019, Sewald and co-workers designed conjugate **57** featuring tumour-homing peptide octreotide, cryptophycin-55 glycinate and a cathepsin-B-cleavable dipeptide sequence, Val-Cit, for selective cleavage in tumours (**Fig. 1.17B**).[59, 231] The cryptophycin-55 payload was conjugated to the Val-Cit cleavable sequence via a Gly-Pro dipeptide designed to self-immolatively form a diketopiperazine (DKP) upon enzymatic activation, releasing the drug in its active form. The conjugate was demonstrated to be selectively accumulated and

internalised in cells overexpressing SSTR2, exhibiting high stability and cytotoxicity comparable to the free drug.

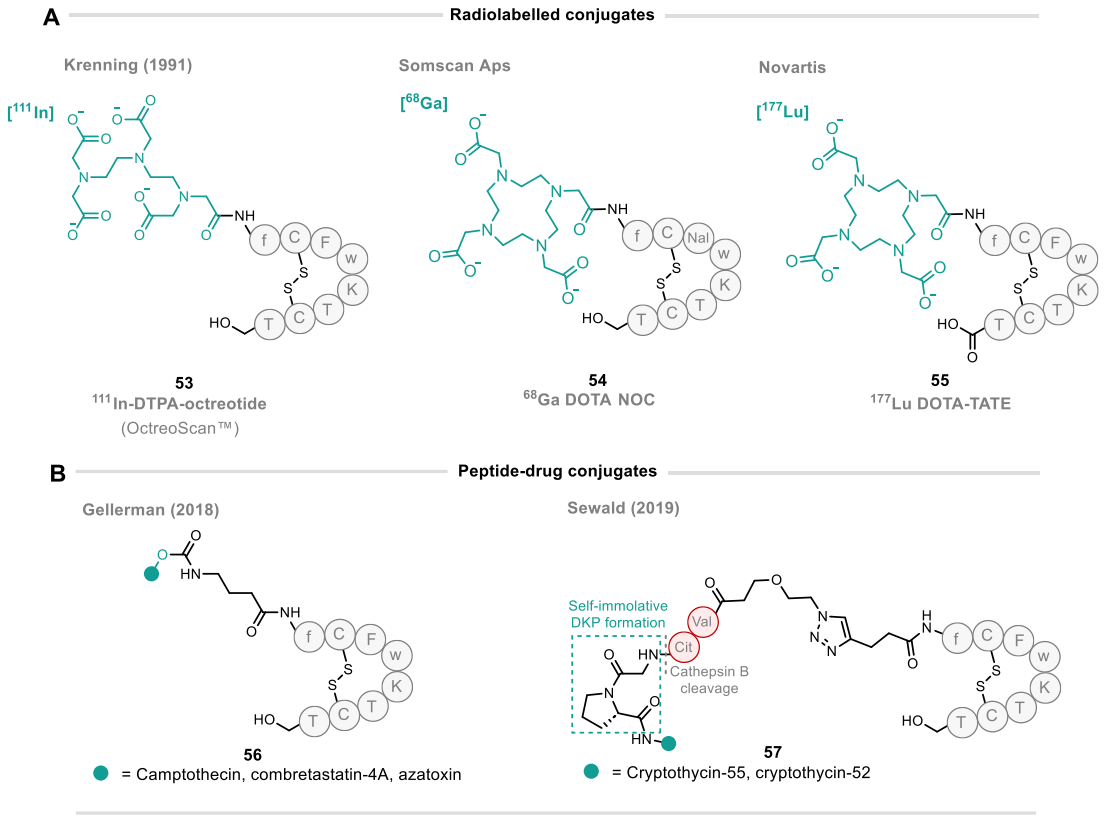

Figure 1.17 Application of somatostatin analogues as tumour-homing peptides for targeted drug delivery. A) Radiolabelled somatostatin-analogue conjugates, designed for scintigraphic diagnostic imaging (^{111}In-DTPA-octreotide and ^{68}Ga-DOTA-NOTA) and PRRT (^{177}Lu-DOTA-TATE; FDA approved 2018); B) Examples of peptide-drug conjugates using octreotide and cleavable linkers.

1.5 Responsive polymers for biotechnology and drug delivery

The development of polymeric materials for useful purposes can be traced back to the economic impetus of the rubber boom in the late 19th century following Goodyear's discovery of the vulcanisation process.[232, 233] The late 1950s saw the inception of 'smart polymers', a class of polymers which change their physical and/or chemical properties in response to external stimuli such as pH,[234] temperature,[235] redox activity,[236] mechanical force,[237] chemical[238] and enzymatic stimuli.[232, 239]

A class of stimuli-responsive polymers which has garnered particular attention in recent years is degradable self-immolative polymers (SIPs), initially pioneered by Shabat and co-workers building upon their work on small molecule dendritic scaffolds for payload release for prodrug chemistry in 2003.[240-243] Whereas conventional biodegradable polymers consist of hydrolysable bonds which result in a diffusion-limited degradation profile,[244, 245] SIPs are designed to disassemble and depolymerise through a domino-like fragmentation event which is initiated upon specific cleavage of a masking group, analogous to the prodrug activation strategies described in **Section 1.2.** Various SIPs based on a range of masking groups and stimuli have been designed for applications in sensing,[246] diagnostics,[247, 248] materials science[249, 250] and drug delivery.[251]

Several self-immolative polymers have been designed using enzyme-cleavable masking groups that can be specifically activated by a chosen enzyme to induce polymer disassembly and degradation. In 2008, Shabat and co-workers reported the first example of a SIP which also represented the first enzyme-activated SIP (**Fig 1.18**). The researchers generated a polymer **58** with a polybenzylcarbamate backbone capped with a 4-hydroxy-2-butanone trigger for activation by bovine serum albumin (BSA) to initiate a β-elimination reaction, subsequently triggering 1,6-elimination and carboxylation reactions. Polymer disassembly released monomeric aniline units **59** which produce green fluorescent emission suitable for use in molecular sensing.[252]

Shabat and co-workers extended their work in 2009 to the incorporation side reporters in each monomer unit with a penicillin-amidase(PGA)-cleavable masking group trigger in a comb polymer **60 (Fig 1.18)**.[253] Enzymatic activation initiates 1,6-elimination and decarboxylation reactions leading to polymer disassembly and the release of 4-nitroaniline groups suitable for use in diagnostic applications, whilst incorporation of suitable monomer units bearing small-molecule therapeutics may represent potential as a targeted drug delivery strategy.

The manipulation of hydrophilicity properties of polymers has been exploited in the development of stimuli-responsive SIPs. In 2013, Philips and co-workers applied a pinacol-boronate trigger to hydrophobic polymer **61** which would depolymerise to release a series of

hydrophilic products in response to H_2O_2 generated from a target enzyme (**Fig. 1.18**).[254] These products are then able to pass through a point-of-care assay paper-based device for enzyme analyte quantification. In the absence of H_2O_2, the sample can only travel slowly through the hydrophobic polymer, whereas polymer degradation into hydrophilic products switches the wetting properties of the paper to hydrophilic allowing the sample to pass through the device at a rate which depends on the concentration of peroxide and therefore enzyme analyte.

Matson and co-workers produced a further example of a system for use as in diagnostics in 2019, reporting a self-immolative polymer **62** with a poly(benzylthiourethane) backbone with an aryl-azide masking group for activation by H_2S (**Fig 1.18**). This is designed to trigger polymeric disassembly to release carbonyl sulfide which is efficiently converted into H_2S by carbonic anhydrase, generating an amplification of the self-immolative polymer degradation.[255] Reductions in endogenous H_2S production in the body have been linked to a variety of disease states, making the development small-molecule and polymeric H_2S donors a recent research endeavour.[256] This work represents an SIP capable of releasing multiple equivalents of H_2S in response to low concentrations of H_2S through a signal-amplified enzymatically-catalysed response.

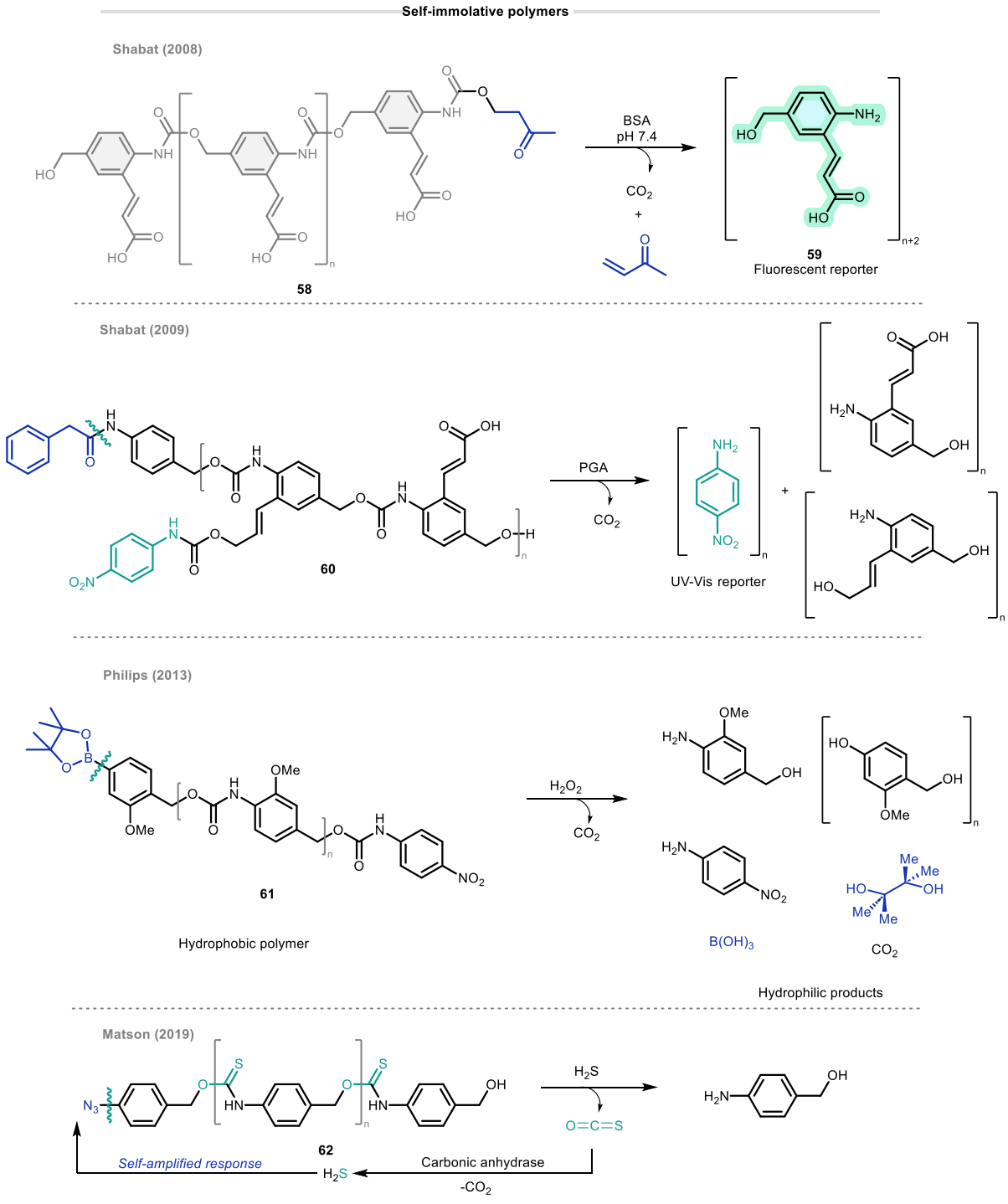

Figure 1.18 Degradable self-immolative polymers (SIPs).

1.5.1 Polymer-based drug delivery systems

As masking group cleavage by a chemical or biological trigger initiates a cascade of irreversible, intramolecular fragmentation reactions which disassemble the SIP into small molecule fragments, they are able to provide a high degree of amplification. This amplified

response to a low concentration of a range of stimuli gives SIPs a unique advantage in the design of increasingly creative drug delivery platforms.[257, 258] There are two general classes of SIP drug delivery strategies: polymeric prodrugs,[259-261] through covalent linkage of drug molecules, and the formulation of SIPs into higher-order assemblies such as capsules, micelles and vesicles for the encapsulation of drug molecules.[262-264]

In 2014, Liu and co-workers produced amphilphilic block copolymers using a poly(benzylcarbamate) self-immolative polymer linked to a hydrophilic poly(N,N-dimethylacrylamide) polymer (**Fig. 1.19**; **63-65**), which then self-assembled into self-immolative polymersome copolymer vesicles and disintegrate into water-soluble small molecule fragments upon activation.[265] The self-immolative polymer was capped with perylen-3-yl, 2-nitrobenzyl or disulfide masking groups which are activated by visible light, UV light or reductive conditions respectively. Triggered drug release via cascade depolymerisation with both hydrophobic and hydrophilic anticancer therapeutics doxorubicin and camptothecin was demonstrated, whilst cell viability assays confirmed negligible cytotoxicity for the vesicles.

The Liu group went on to extend this work to a hyperbranched SIP polymeric prodrug system also utilising a poly(benzylcarbamate) backbone (**66-68**).[251] Spatiotemporally-controlled release of drugs conjugated at the dendritic end sites of the polymer branches following depolymerisation via a series of quinone-methide eliminations in response to visible light was demonstrated, as well as mitochondria-targeted fluorescent sensing of H_2O_2 using suitable conjugated fluorophores. Integrin-targeting cRGD and mitochondrion-targeting CGKRK peptides were employed for targeted drug delivery and mitochondria sensing applications respectively, analogous those described in **Section 1.4**.

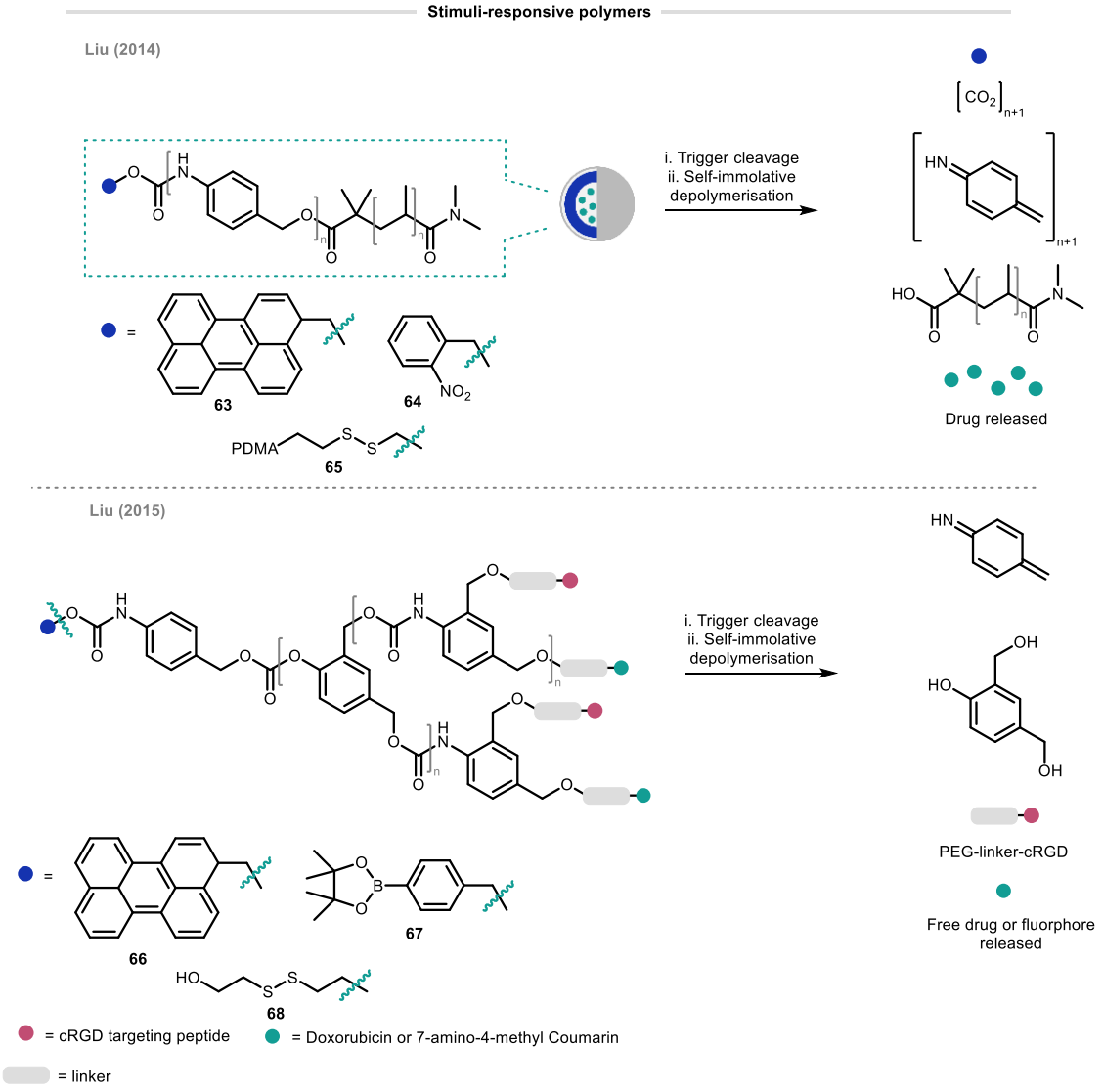

Figure 1.19 Polymer-based drug delivery systems. A) Amphiphilic block copolymer self-immolative vesicles which release encapsulated drug molecules upon activation (Liu and co-workers, 2014); B) Polymeric prodrug design featuring a hyperbranched self-immolative polymer network with covalently linked drug molecules and targeting peptides (Liu and co-workers, 2015).

1.5.2 Two-photon polymerisation (TPP)

Two-photon polymerisation (TPP) is a modern lithographic polymerisation technique that employs direct laser writing (DLW) for the fabrication of three-dimensional micro- and nanostructures.[266, 267] First demonstrated by Maruo *et al.* in 1997 in a seminal study which combined the concepts of two-photon absorption and photopolymerisation-based additive manufacturing to fabricate 3D microstructures via TPP,[268] the technology has since found applications in micro-optics,[269] biomedical devices,[270] scaffolds for tissue engineering[271] and

plasmonic components,[272] particularly following its commercialisation by Nanoscribe GmbH in 2007.

A photosensitive material suitable for photopolymerisation via UV, visible or near infra-red (NIR) light is referred to as a photoresist, typically consisting of a reactive monomeric compound, a crosslinking agent and a suitable photoinitiator, capable of generating reactive species, as well as a small volume of organic solvent if required. Either radical or cationic polymerisation may take place depending on the photoresist; radical polymerisation is achieved through the generation of reactive species through a growing chain, commonly used in acrylic, styrene and other alkene-based monomers, whereas cationic polymerisation features ring-opening polymerisation typically with epoxides, lactones and cyclic ethers.[273]

Two classes of photoresists are available for photopolymerisation: positive- and negative-tone. For postive-tone photoresists, the region which is exposed to the laser is soluble to and washed away by the developer, leaving a complimentary structure to the exposed region, which is desirable for printing microholes or microfluidic channels. Negative tone is much more popular for microstructure fabrication, as the unexposed photoresist is washed away using an appropriate developer, whilst the fabricated structures remain adhered to the glass surface. Crucially, only when the concentration of the generated active photoinitiator is above a characteristic threshold, does a change in the phase of the photoresist resin from liquid to solid become irreversible, with peripheral parts of the focal volume where the intensity is below the polymerisation threshold resulting in incomplete polymerisation, removed in the developing step.[267]

Two-photon absorption is defined as the simultaneous absorption of two photons in order to excite a molecule to a higher state; the sum of the photon energies matches the electronic transition of the photoinitiator.[274] TPA was first described theoretically in Marie Göppert-Mayer's thesis in 1931[275] before being first experimentally observed by Kaiser *et al.* in 1961 following the invention of the laser in 1960.[276]

In TPP, polymerisation is started by two-photon absorption by the photoinitiator triggered by a femtosecond laser pulse from a NIR laser beam, generating radical species to initiate

photopolymerisation. A femtosecond laser pulse is employed due to the second transition from the virtual state of the photoinitiator occurring within 1 fs of the initial transition.[267] Absorption in femtolitre-volume regions termed polymerisation voxels provides the building blocks for microstructure fabrication, extending in the z-axis.[273, 277] Following radical formation in the photoinitiator via two-photon absorption, chain growth propagation takes place, followed by polymerisation termination resulting in polymerized voxels.

The line width and therefore fabrication resolution may be quantitatively expressed in the form of the following equation (**Eq. 1.1**), derived by Shukla *et al.*[278]:

$$w = r_0 \left[ln \left(\frac{\sigma \left(\frac{\eta \rho_0}{\rho_{th}} \right) \left(\frac{T\boldsymbol{P}}{\hbar \omega_L} \right)}{\pi^{\frac{3}{2}} \boldsymbol{v_b} \boldsymbol{\upsilon} \boldsymbol{\tau}_L r_0^3} \right) \right]^{\frac{1}{2}} \quad \textbf{(Eq. 1.1)}$$

where r_0 is the laser beam radius, σ is the two-photon absorption of the photoinitiator, η is the two-photon quantum efficiency of the photoresist, ρ_0 is the concentration of generated photoacid, ρ_{th} is the concentration of photoacid required for polymerisation initiation, T is the fraction of light transmitted through the microscope objective, P is the average laser power, v_b is the scan speed, υ is the pulse repetition rate, and τ_L is the pulse width. Crucially, the average laser power (in mW) and the scan speed (in μm s^{-1}), proportional and inversely proportional to the fabrication resolution respectively, are the two central user-controllable parameters which determine TPP fabrication.

Recently, there have been increased efforts to develop stimuli-responsive microstructures using TPP, including hydrogels containing hydrophilic moieties in the polymer network, making them capable of water absorption and exhibit a change in physical properties. The composition of the photoresist can be designed to produce a polymeric hydrogel structure fabricated via TPP which can respond to a range of stimuli such as light, temperature, pH and chemical stimuli.

In 2020, Chu and co-workers reported a pH-responsive hydrogen biomimetic printed by TPP, exhibiting expansion and contraction in response to pH above and below 9.0 respectively (**Fig. 1.20A**).[279] Through the incorporation of acrylic acid to the photoresist, polymers with pendant carboxylic acid groups were produced which were deprotonated and ionised above

the ionisation threshold at pH 9, resulting in electrostatic repulsion and polymer expansion, with subsecond response times. Additionally, the hydrogel demonstrated strong and weak swelling in alkaline and acidic solution respectively.

Selhuber-Unkel and co-workers generated the first thermoresponsive poly(*N*-isopropylacrylamide) (pNIPAM) hydrogels printed using TPP at the micrometre scale (**Fig. 1.20B**).[280, 281] pNIPAM is is a known thermoresponsive material due to a reversible phase transition at its lower critical solution temperature (LCST), being hydrophilic below the LCST and hydrophobic above, exhibiting significantly higher volume of the material in the hydrated, swollen state below the LCST. Microvalves which open at higher temperature were printed from a photoresist featuring *N*-isopropylacrylamide monomer, *N*,*N*`-methylenebis(acrylamide) comonomer and lithium phenyl(2,4,6-trimethylbenzoyl)phosphinate (LAP) photoinitiator, manipulating hydration-dependent volume changes in the design of temperature-dependent microactuators. Furthermore, the researchers were able to enhance the extent of shrinking and opening with a low writing speed at the base, resulting in a greater degree of crosslinking, and a high writing speed at the lid, associated with a less crosslinked polymer network.

Degradable structures have also been demonstrated, such as by Mattoli and co-workers in 2022, who used a 2-methylene-1,3-dioxepane (MDO) and pentaerylthritol tetraacrylate photoresist to produce polymers susceptible to degradation in basic conditions (**Fig. 1.20C**).[282] Using the MDO monomer and tetracrylate crosslinker results in the formation of polyester-crosslinked networks which are sensitive to nucleophiles and aqueous base/acid treatment. Hydroxide-triggered structure degradation with KOH was demonstrated with various acrylate (tetra-, tri- and difunctional) crosslinkers, as well as use of a photobase (4-amino-quinoline) which upon excitation produces a high concentration of methoxide ions.

A pH-responsive microstructures

Chu (2020)

Photoinitiator

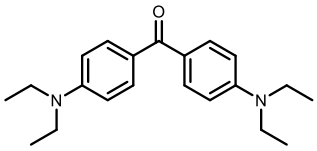

4,4,bis (diethylamino) benzophenone

Monomer(s)

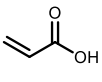

Acrylic acid

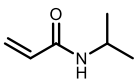

NIPAAM

Crosslinker

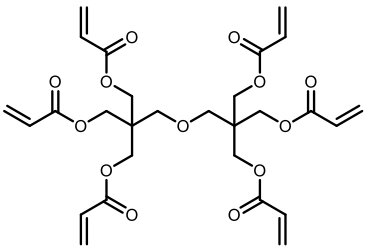

Dipentaerythritol hexaacrylate

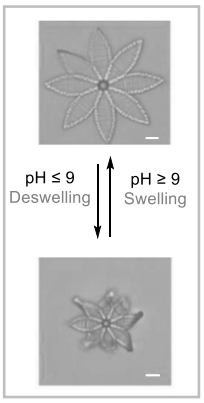

Hydrogen contraction and expansion in response to pH

B Temperature-responsive microstructures

Selhuber-Unkel (2023)

Photoinitiator

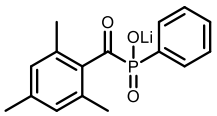

Lithium phenyl(2,4,6-trimethyl benzoyl) phosphinate

Monomer(s)

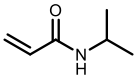

NIPAAM

Crosslinker

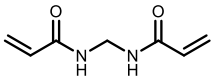

N,N'-methylenebis(acrylamide)

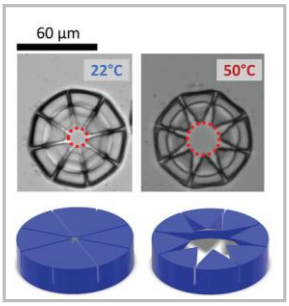

Hydrogel microvalve opening upon heating from 22 °C to 50 °C

C Base-responsive microstructures

Mattoli (2022)

Photoinitiator

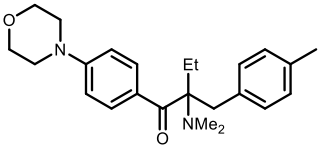

Irgacure 379

Monomer(s)

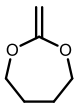

2-Methylene-1,3-dioxepane

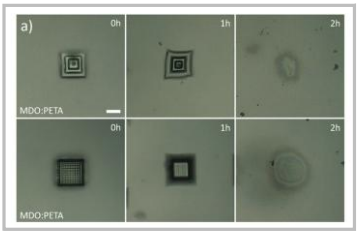

Polymer degradation observed upon treatment with KOH (0.5 M) at 50 °C

Crosslinker

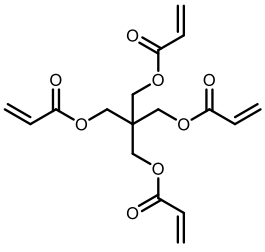

Pentaerythritol tetraacrylate (PETA)

Figure 1.20 Selected examples of stimuli-responsive microstructures printed using TPP DLW. A) pH-responsive microstructures (Chu and co-workers, 2020); B) Temperature-responsive microstructures (Selhuber-Unkel and co-workers, 2022); C) Base/nucleophile-responsive microstructures (Mattoli and co-workers, 2022).

The porous properties of fabricated hydrogels have attracted attention for application in drug delivery devices, via their ability to swell and absorb small molecules.[283] Salem and co-workers reported a controlled drug delivery strategy via TPP-fabricated devices in 2018, modulating the release of fluorophore rhodamine B via porosity and morphology tuning with printing parameter variation (**Fig. 1.21A**).[284] Photopolymerisation of poly(ethylene glycol) dimethacrylate (PEGDMA) woodpile structures successfully encapsulated rhodamine B and demonstrated a positive correlation between the pore size and release rate, also exhibiting no cytotoxicity to a range of cell lines and therefore representing a potential drug delivery methodology.

In 2019, Sitti and co-workers reported a enzymatically-degradable hydrogel microswimmer for controlled cargo delivery, using a double-helical 3D microswimmer, magnetically powered under rotational magnetic fields (**Fig. 1.21B)**.[285] By using a photoresist featuring a gelatin methacryloyl and superparamagnetic iron oxide nanoparticle photoresist suspension, the researchers demonstrated full degradation of the microswimmer mediated by metalloproteinase-2 (MMP-2), a disease-marker enzyme associated with tumour metastasis, in 118 h to nontoxic products. Exposure to pathological concentrations of MMP-2 resulted in swelling of the fabricated hydrogel and release of embedded small molecule cargo. As gelatin is cleavable by MMP-2, using iron oxide nanoparticles dispersed in galatin methacryloyl enabled the printing of a polymer suitable for enzymatic breakdown to trigger cargo release.

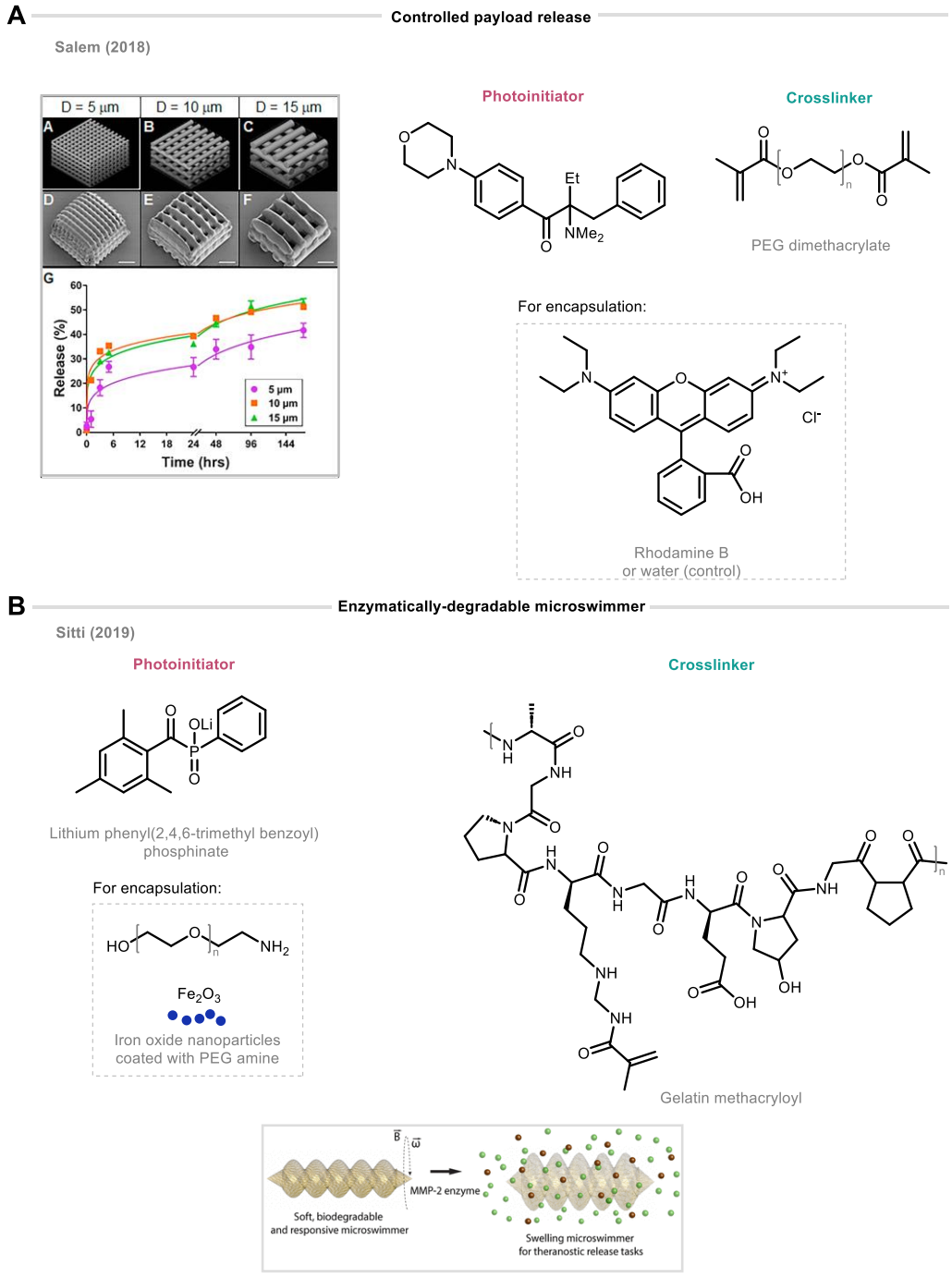

Figure 1.21 TPP-fabricated microstructures for drug-delivery applications. A) Demonstration of controlled payload release and tuning of printing parameters (Salem and co-workers, 2018); B) Enzyme-activated degradable microswimmer for controlled cargo delivery (Sitti and co-workers, 2019).

1.6 Work described in this thesis

This chapter has described the development of various strategies designed to improve the targeting of therapeutics and reduce systemic drug release. Prodrugs with masking groups that are selectively cleaved at a tumour site (**Section 1.2.1**), the use of somatostatin analogues as tumour-targeting agents (**Section 1.4.3**, **1.4.4**) and degradable polymeric systems (**Section 1.5**) have been highlighted.

To date, research on targeted therapeutics of this type has focused primarily on developing proof-of-concept studies aiming to alleviate medicinal chemistry shortcomings associated with small molecule drugs. The application of modern prodrug strategies which seek to exploit the endogenous overexpression of enzymes in the tumour microenvironment to peptide-based therapeutics and to polymer systems remains an underexplored area.

Chapter 2 details efforts to develop responsive polymers which bear pendant β-glucuronic acid and β-galactose carbohydrate moieties, aiming to expand existing glycopolymers (**Section 1.3**). A range of glycomonomer conjugates and their associated control compounds were synthesised and subsequently polymerised using two-photon polymerisation (TPP) and bulk methods, using various crosslinkers and demonstrated to be highly tuneable to parameter adjustment in TPP. Their enzymatic response is investigated and future directions for application to substrate binding outlined.

Chapter 3 describes the multistep synthesis of various self-immolative crosslinkers, building upon the application of similar scaffolds to β-glycosidase-activated prodrug design for multidrug release (**Section 1.2.1**). These were subsequently polymerised by TPP and bulk methods, designed to depolymerise upon enzymatic activation. Their enzymatic response is investigated.

Chapter 4 outlines the development of a glycopeptide prodrug analogue, applying somatostatin and its analogues (**Section 1.4.3**) as model systems through pharmacophore modification with a β-galactoside unnatural glycoamino acid. The glycoamino acid synthesis, peptide synthesis and biological evaluation of the prodrug are reported.

Chapter 5 lays out attempts to develop hypoxia-activated prodrug analogues of somatostatin and its analogues, building upon work by Conway and co-workers (**Section 1.2.1**). The synthesis of a hypoxia-activated unnatural amino acid is described.

Chapter 2

Glycosidase Responsive Glycopolymers

Chapter 2: Glycosidase Responsive Glycopolymers

2.1 Introduction and Aims

A variety of glycosidases including β-glucuronidase and β-galactosidase are upregulated across a range of tumour types compared to significantly lower expression levels in healthy cells.[107] This has previously been exploited in the development of glycosidase-activated prodrugs, which consist of a cytotoxic anticancer drug conjugated to a sugar via a self-immolative linker, such that enzymatic cleavage of the glycosidic bond liberates the active drug.

Glycopolymers may be defined as polymers bearing pendant saccharide groups, which exhibit multivalent interactions and large amplification effects in molecular recognition.[146] For example, lectins on the cell surface have been demonstrated to exhibit a strong affinity to carbohydrate pendant moieties on glycopolymers, making them suitable for use in lectin recognition.

This project aims to develop synthetic routes to β-glucuronic acid and β-galactose monomers suitable for subsequent polymerisation via two-photon polymerisation (TPP). The generated polymers are designed for enzyme-responsive applications which take advantage of activated polymer physical property manipulation, similar to solvent-activated polymeric hydrogel drug delivery systems which load a therapeutic cargo into a dehydrated hydrophilic polymer for release upon swelling changes in aqueous environment.

In addition, the glycopolymers generated would be suitable for use in molecular recognition through carbohydrate-binding lectins and boronic acids, utilising the carbohydrate backbone as opposed to exploiting enzymatic activity in biological contexts. Building upon previous work which exploits the overexpression of glycosidases for prodrug activation[286] (**Fig 2.1A**) and for fluorescent probe design (**Fig. 2.1B**),[287] this project would provide the first examples of applying carbohydrate scaffolds of this type to polymeric microstructures (**Fig. 2.1C**).

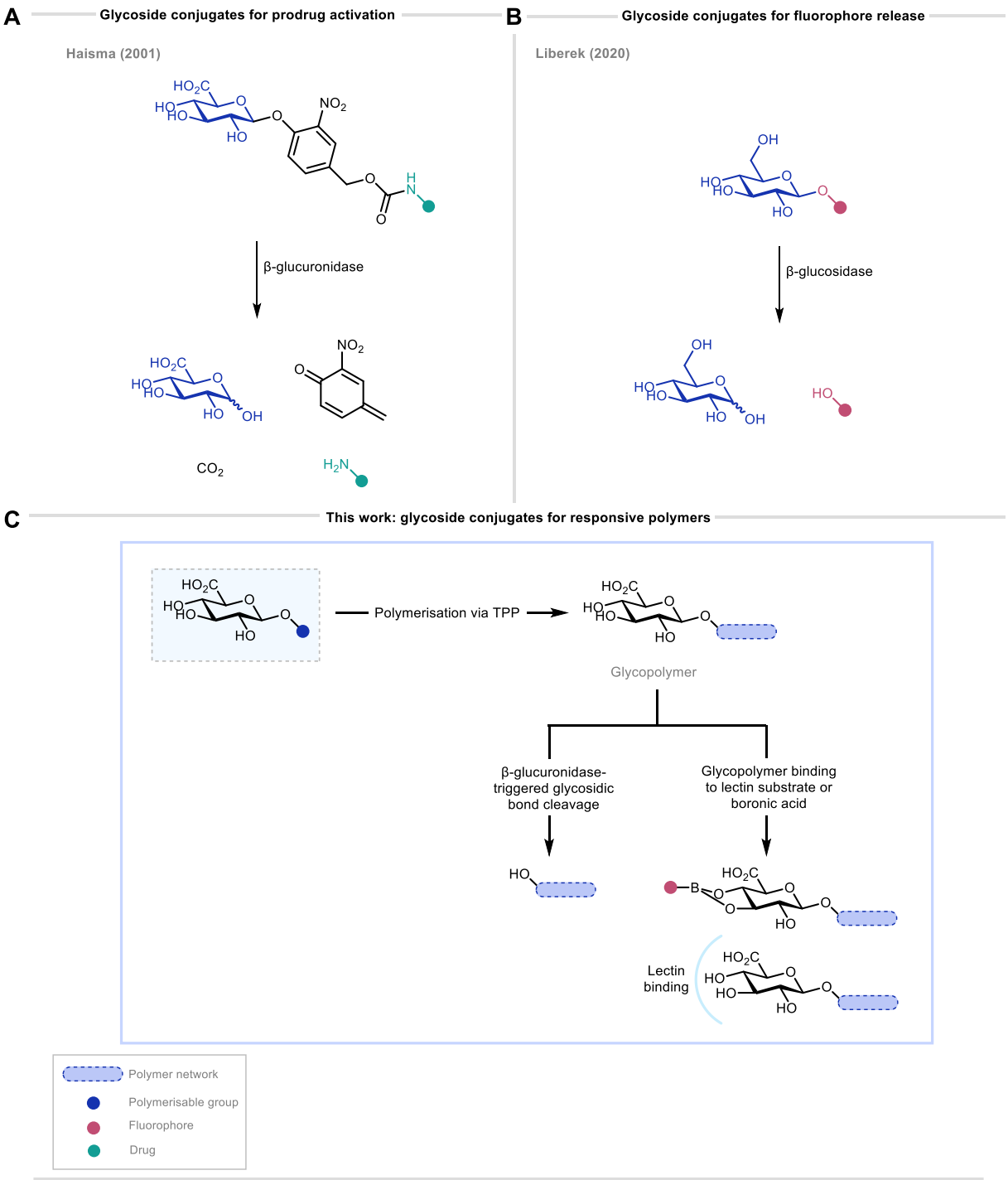

Figure 2.1 Applications of glycopolymers. A) Previous work on glycosidase-activated prodrugs (Haisma and co-workers, 2001); B) Previous work on glycosidase-activated fluorescent probes (Liberek and co-workers, 2020); C) This work on glycopolymers for glycosidase-activated materials response and for binding to lectin or boronic acid substrates.

2.2 Results and Discussion

2.2.1 Synthesis

In order to generate glycopolymers, molecules which contain a carbohydrate moiety and a polymerisable group were required. Glycomonomer conjugates bearing polymerisable groups and β-glucuronic acid or β-galactose carbohydrate moieties were prepared through derivatisation of vinylbenzyl and acrylamide functional groups commonly used in polymer synthesis with different physical properties as polymers.

2.2.1 β-glucuronide monomer synthesis

It was intended to form glycomonomer conjugates via glycosylation of suitable acceptors bearing polymerisable groups with an appropriate glycosyl donor. Firstly, glucuronolactone **69** was ring-opened and protecting groups installed (**Scheme 2.1**).

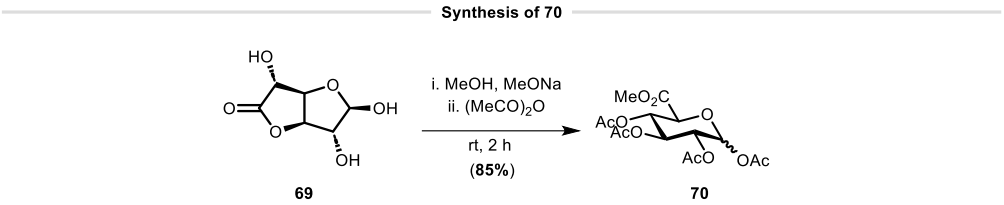

Scheme 2.1 Synthesis of **70**.

Ring-opening and methyl ester formation using sodium methoxide followed by peracetylation with acetic anhydride in one pot provided peracetylated glucuronic acid derivative **70** in 85% yield.

Often in the synthesis of glycosylated conjugates, a more reactive glycosyl donor is generated. However, in some instances, typically dependent on the reactivity of the glycosyl acceptor as well as the extent to which the protecting groups on the donor deactivate the compound towards the reaction, glycosylation can be carried out directly in the presence of Lewis acid and a suitable acceptor without requiring a more reactive donor. Test reactions of percacetylated **70** were carried out (**Scheme 2.2**).

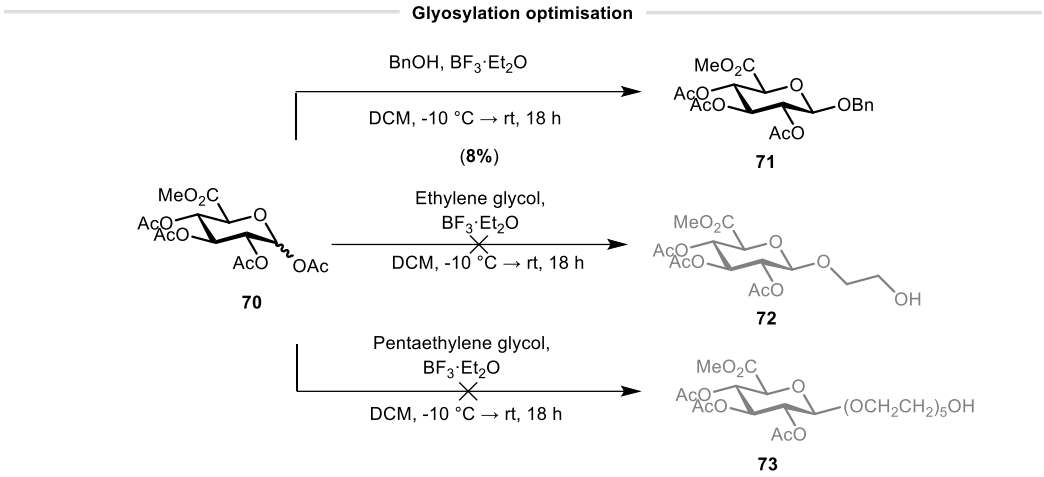

Scheme 2.2 Test glycosylations with glycosyl donor **70**.

Firstly, a test reaction with glycosyl acceptor benzyl alcohol using $BF_3 \cdot Et_2O$ as a Lewis acid catalyst furnished glucuronide target molecule **71** in a low yield of 8%. Subsequent reactions using acceptors ethylene glycol and pentaethylene glycol, intended for further functionalisation, were not successful under the same conditions, resulting in recovery of unreacted glycosyl donor and the hydrolysis product. Target molecules **72** and **73** were not isolated.

In order to develop reliable access to desired glucuronides, α-bromo and trichloroacetimidate glycosyl donors were synthesised for further test reactions (**Scheme 2.3**).

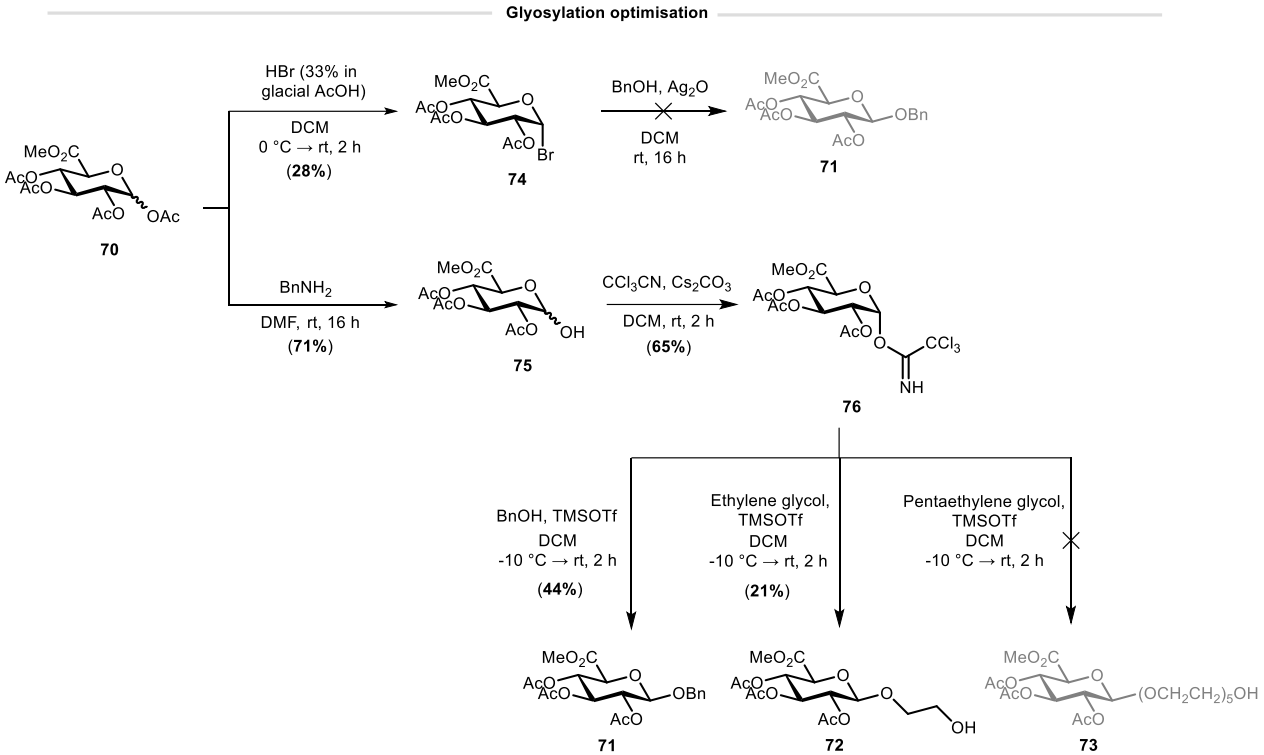

Scheme 2.3 Optimisation of glycosylation conditions using α-bromo and trichloroacetimidate glycosyl donors.

Firstly, the α-bromo glycosyl donor **74** was synthesised in 28% yield using a 33% solution of HBr in acetic acid; longer reaction times than 2 hours led to substantial formation of the hydrolysis product, owing to the instability of **74**. Glycosylation using BnOH as a test substrate glycosyl acceptor and Ag_2O as a halogen-selective Lewis acid did not yield target molecule **71**, with the hydrolysis product exclusively recovered. Alternative glycosyl donor trichloracetimidate **76** was next synthesised across two steps; hemiacetal **75** was first furnished in a 71% yield upon reaction with benzyl amine and subsequent reaction with trichloroacetonitrile provided desired trichloroacetimidate **76** in a 65% yield. Glycosylation with BnOH was successfully carried out, with Lewis acid TMSOTf being found to give the best results to yield glucuronide **71** in 44% yield. Glycosylation with ethylene glycol as a

glycosyl acceptor gave glucuronide **72** in 21% yield, whereas reaction with pentaethylene glycol yielded the hydrolysis product only.

With an optimised route to glucuronides established, it was next necessary to synthesise appropriate glycosyl donors bearing polymerisable groups. Using commercially available 4-vinyl benzylchloride (**77**), two were synthesised (**Scheme 2.4**).

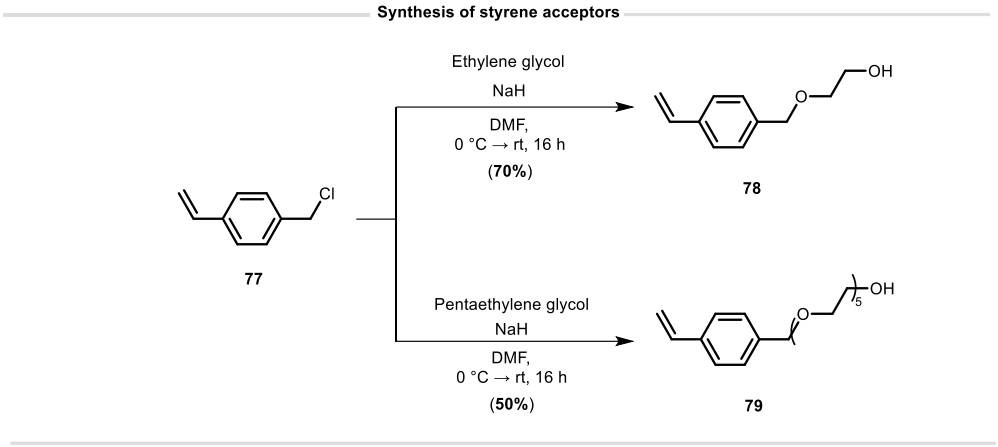

Scheme 2.4 Synthesis of styrene glycosyl acceptors **78** and **79.**

4-vinyl benzylchloride (**77**) was derivatised via Williamson ether syntheses. Using sodium hydride for alkoxide generation, reaction with ethylene glycol provided derivative **78** in 70% yield, whilst use of pentaethylene glycol furnished **79** in 50% yield.

These glycosyl acceptors were taken forward for test glycosylations (**Scheme 2.5**).

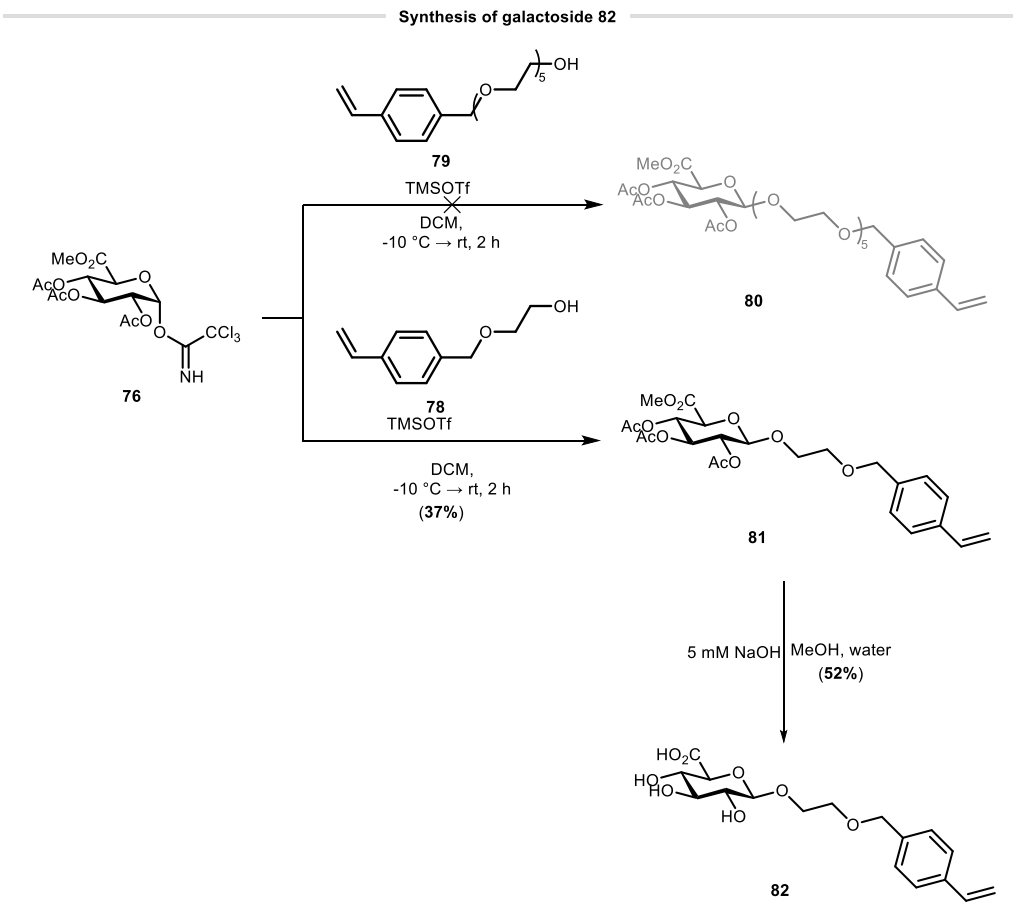

Scheme 2.5 Glycosylations of glycosyl acceptors **78** and **79** with trichloroacetimidate **76**.

Glycosylation of pentaethylene-glycol-functionalised acceptor **79** with trichloroacetimidate **76** using TMSOTf as a Lewis acid catalyst was unsuccessful. However, glycosylation with acceptor **79** under the same conditions gave glucuronide **81** in 37% yield. This was subsequently deprotected using sodium hydroxide to furnish target molecule **82** in a yield of 52%.

Glucuronide conjugates with different polymerisable groups such as acrylamide-based functional groups which have been used for hydrogel polymer formation were next required.[288] The glycosylation of *N*-hydroxyethyl acrylamide (**Scheme 2.6**) was attempted using different glycosyl donors and Lewis acid catalysts.

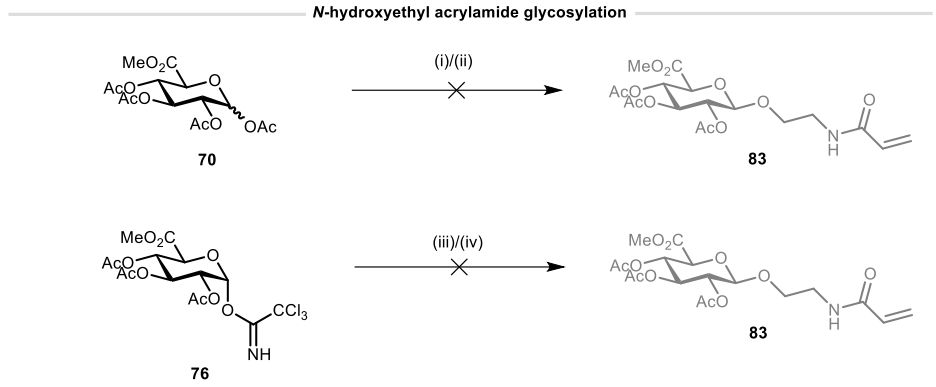

Scheme 2.6 Attempted glycosylation of *N*-hydroxylethyl acrylamide with glycosyl donors **70** and **76**; (i) *N*-hydroxyethyl acrylamide, $BF_3 \cdot Et_2O$, (ii) *N*-hydroxyethyl acrylamide, TMSOTf, (iii) *N*-hydroxyethyl acrylamide, $BF_3 \cdot Et_2O$, (iii) *N*-hydroxyethyl acrylamide, TMSOTf.

Reaction of peracetylated donor **70** with *N*-hydroxyethyl acrylamide acceptor was attempted both with $BF_3 \cdot Et_2O$ and TMSOTf as the Lewis acid catalyst, which led to the recovery of the hydrolysis product and side products. Reaction of trichloroacetmidate **76** with the same conditions resulted in no formation of target molecule glucuronide **83** and only the hydrolysis product. Increasing the equivalents of acceptor and catalyst had no effect.

As attempts to use *N*-hydroxyethyl acrylamide as an acceptor were not fruitful, alternative synthetic strategies were explored. This involved utilising the versatile click chemistry approach to conjugate the polymerisable group to the glucuronic acid moiety. A target molecule **86** derivatised from *N*-hydroxyethyl acrylamide was devised, selecting the alkyne click handle which would allow use of the copper-catalysed alkyne-azide cycloaddition (CuAAC) for the conjugation to the glucuronic acid moiety. **Scheme 2.7** describes the synthesis of **86**.

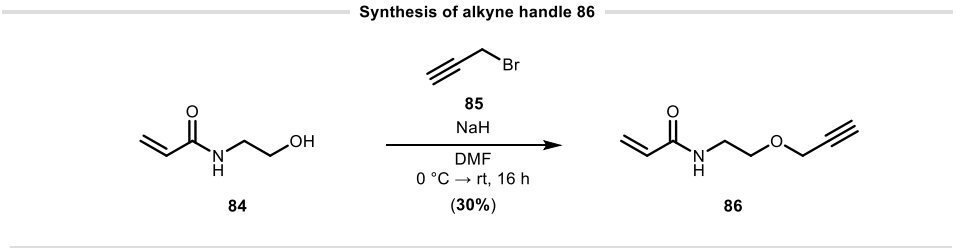

Scheme 2.7 Propargylation of *N*-hydroxyethyl acrylamide **84** to alkyne **86**.

Activation of *N*-hydroxyethyl acrylamide **84** with sodium hydride and subsequent propargylation with propargyl bromide **85** furnished alkyne click handle **86** in 30% yield. A

minimum of one hour was found to be necessary to facilitate alkoxide generation with sodium hydride prior to propargyl bromide addition, with lower yields obtained following reduced reaction times for this step.

A glucuronide azide handle was synthesised for conjugation to the acrylamide alkyne **86** (**Scheme 2.8**).

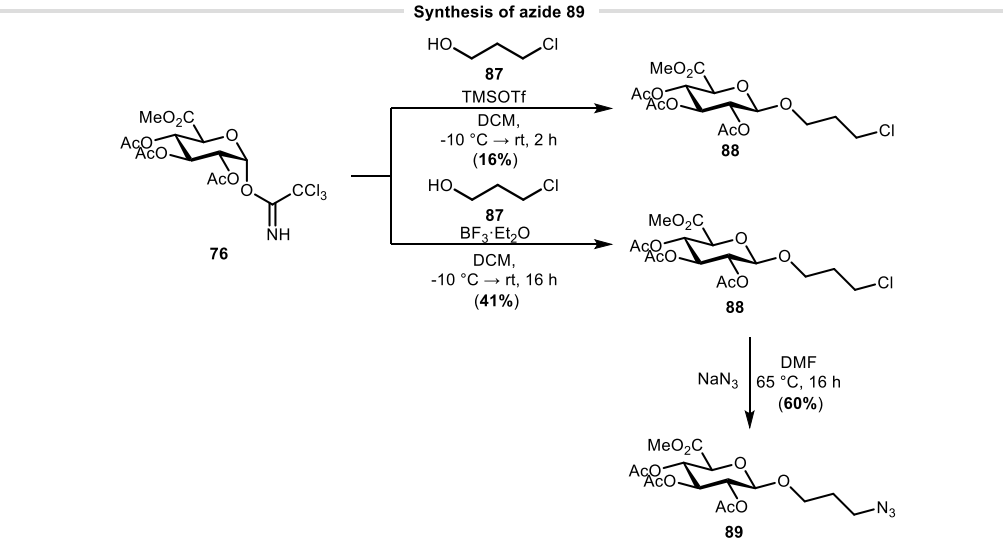

Scheme 2.8 Synthesis of azide **89**.

Trichloroacetimidate **76** was glycosylated with acceptor 3-chloro-propan-1-ol **87** using TMSOTf to give glucuronide **88** in a low yield of 16%. Switching Lewis acid catalyst to $BF_3{\cdot}Et_2O$ successfully increased the yield to 41%. Subsequent azidation with sodium azide at 65 °C gave azide-substituted product **89** in 60% yield.

The click Cu(I)-catalysed alkyne-azide 1,3-dipolar cycloaddition (CuAAC) between alkyne **86** and glucuronide azide **89** required optimisation described in **Table 2.1**.

Table 2.1 Optimisation table for the synthesis of **90**.

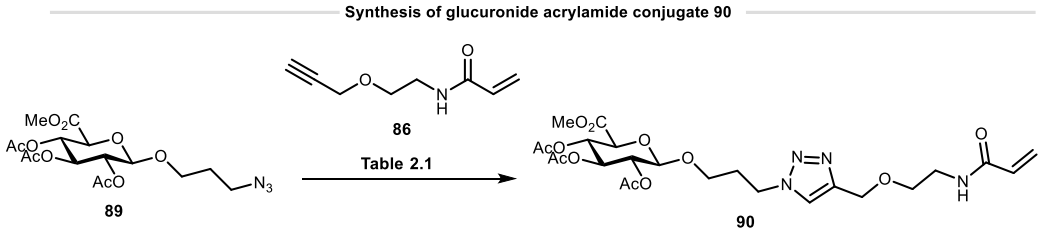

Entry	$CuSO_4.5H_2O$ eq.	Sodium ascorbate eq.	Solvent	Yield
1	2.0	4.0	DCM/water (3:1 v/v), 0.01 M	24%
2	1.0	2.0	THF/water (1:1 v/v) 0.02 M	45%
3	1.0	2.0	THF/water (1:1 v/v), 0.01 M	13%
4	10 mol%	20 mol%	DCM/MeOH/water (1:1:0.1 v/v), 0.1 M	64%

Reaction of alkyne **86** with azide **89** using 2.0 equivalents of $CuSO_4 \cdot 5H_2O$, 4.0 equivalents of sodium ascorbate and DCM/water (3:1 v/v) as a solvent mixture yielded **90** in a low yield of 24% (entry 1). Reduction of equivalents to 1.0 and 2.0 respectively and use of THF/water (1:1 v/v) and an increased concentration to 0.02 M (entry 2) gave an improved yield of 45%, however reducing this concentration to 0.01 M (entry 3) furnished **90** in a low yield of 13%. The best results were found using catalytic amounts of $CuSO_4 \cdot 5H_2O$ and sodium ascorbate with a DCM/MeOH/water (1:1:0.1 v/v) at 0.1 M using 5% v/v water, resulting in a yield of 64%.

Base-mediated deprotection was finally carried out (**Scheme 2.9**).

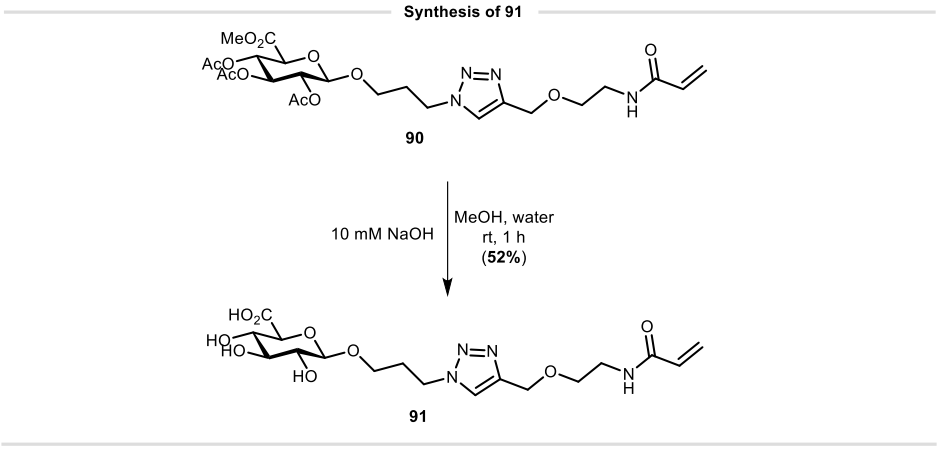

Scheme 2.9 Deprotection of **90**.

Glucuronide **90** was deprotected using sodium hydroxide to give target molecule **91** in 52% yield.

2.2.1.1 Polymerisation and enzymatic testing of glucuronide monomers

TPP is an established multiphoton photolithographic polymerisation technique for the generation of high-resolution microstructures. The incorporation of the synthesised glucuronide monomers into a suitable photoresist would therefore allow for the printing of well-defined microstructures in a controlled fashion, subsequently allowing for the monitoring of changes to the polymers' physical properties upon enzymatic treatment by using microscopy. This technique has been successfully commercialised by Nanoscribe GmbH in the form of their GT Photonic printers, which were used in this project for polymer microfabrication. The polymerisation work was carried out in collaboration with Dr Alexa Ennis and Prof. Larisa Florea.

There are three essential components to the polymerisation cocktail used to form these polymers: the monomer, crosslinker and photoinitiator. As the component with the β-glucuronidase-responsive moiety is in this case the monomer, it was important to ensure a sufficient mole percentage of monomer was used for an enzymatic response to be observable, whilst also using enough crosslinker to have a sufficiently crosslinked system and a minimum volume of solvent required for polymer printing. The monomers (glucuronide-styrene **82**, glucuronide-acrylamide **91**, acrylamide **92** and styrene control

monomer **78**), crosslinkers (Sartomer® **93** and PEG-DA-700 **94)** and photoinitiators (DEATC **95** and LAP **96**) used in this section are shown in **Fig 2.2.**

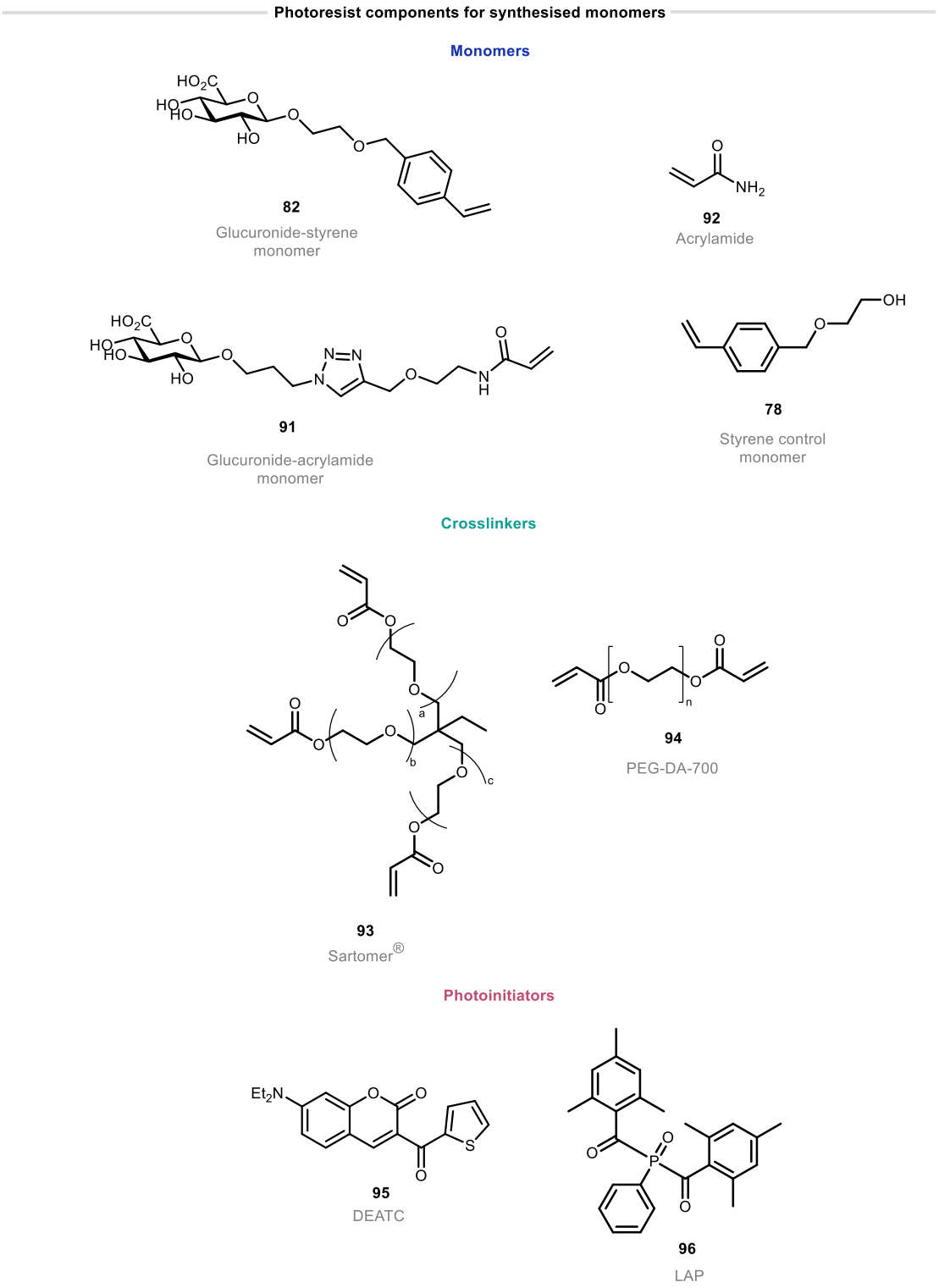

Figure 2.2 Components of photoresists incorporating synthesised monomers **82**, **91** and **78.**

The workflow for TPP employed in this work is described in **Fig. 2.3**. A concentrated solution, typically in the order of 1 g/mL or 50 wt% of solvent as an upper limit, of a photoresist containing crosslinker, monomer and photoinitiator is transferred to a silanised glass slide and polymerised via the TPP process described in **Section 1.5.1**.

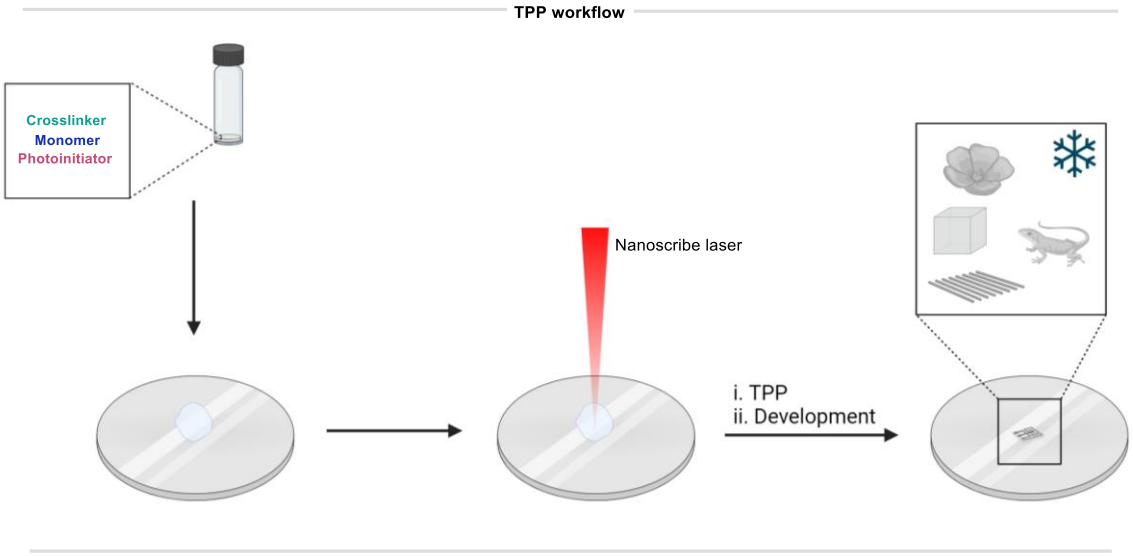

Figure 2.3 A schematic describing the workflow for TPP, from photoresist preparation to printing. A drop of a concentrated (approx. 1 M, 1 g/mL) photoresist solution is transferred to a silanised glass slide and then polymerised by TPP and developed using propylene glycol methyl ether and isopropanol.

Glucuronide-styrene monomer **82** synthesised in **Section 2.2.1** was initially incorporated into photoresist cocktails with acrylamide **92** as a comonomer, Sartomer® **93** and PEG-DA-700 **94** crosslinkers, using DEATC **95** and LAP **96** as photoinitiators. **Table 2.2** describes the optimisation of photoresists incorporating these components.

Table 2.2 Photoresist compositions for the optimisation of glucuronide-styrene monomer **82** printing.

Entry	Monomer mol %	Comonomer	Crosslinker	Photoinitator	Solvent (wt%)	Outcome
1	20	Acrylamide	PEG-DA-700	LAP	H_2O (20 %)	Poorly defined structures
2	20	Acrylamide	PEG-DA-700	LAP	H_2O (35 %)	Poorly defined structures
3	20	Acrylamide	PEG-DA-700	LAP	H_2O (49 %)	Poorly defined structures
4	20	Acrylamide	Sartomer®	LAP	H_2O (30 %)	No printing
5	22	-	Sartomer®	DEATC	H_2O (28%)	Poorly defined structures
6	25	-	PEG-DA-700	DEATC	DMSO:H_2O (1:1 v/v, 37%)	No printing

7	25	-	PEG-DA-700	DEATC	DMSO:H_2O (2:1 v/v, 37%)	Printed well

As glucuronide-styrene monomer **153** is most soluble in water, initial photoresists used water as a solvent, beginning with 20 weight% (entry 1) and increasing up to 49 weight % following limited solubility of reagents (entries 2-4). Using acrylamide as a comonomer and both PEG-DA-700 (entries 1-3) and Sartomer® (entry 4) crosslinkers, only limited printing of typically poorly-defined structures (entries 1-3) was achieved, with no printing for entry 4. For each, the solubility of the photoresist cocktails was not optimal, prompting a change to the DEATC **166** photoinitiator (entry 5), which led to some successful printing but structures of low definition. Switching solvent to a 2:1 v/v mixture of DMSO:water at increased solvent weight% resulted in successful printing (entry 6). Reducing DMSO to 1:1 v/v DMSO:water was unsuccessful (entry 7).

Images of selected structures acquired from photoresists described in entries 1-3 and entry 5, which generated some printing but mostly of poorly defined structures at higher laser powers, are shown below in **Fig. 2.4**.

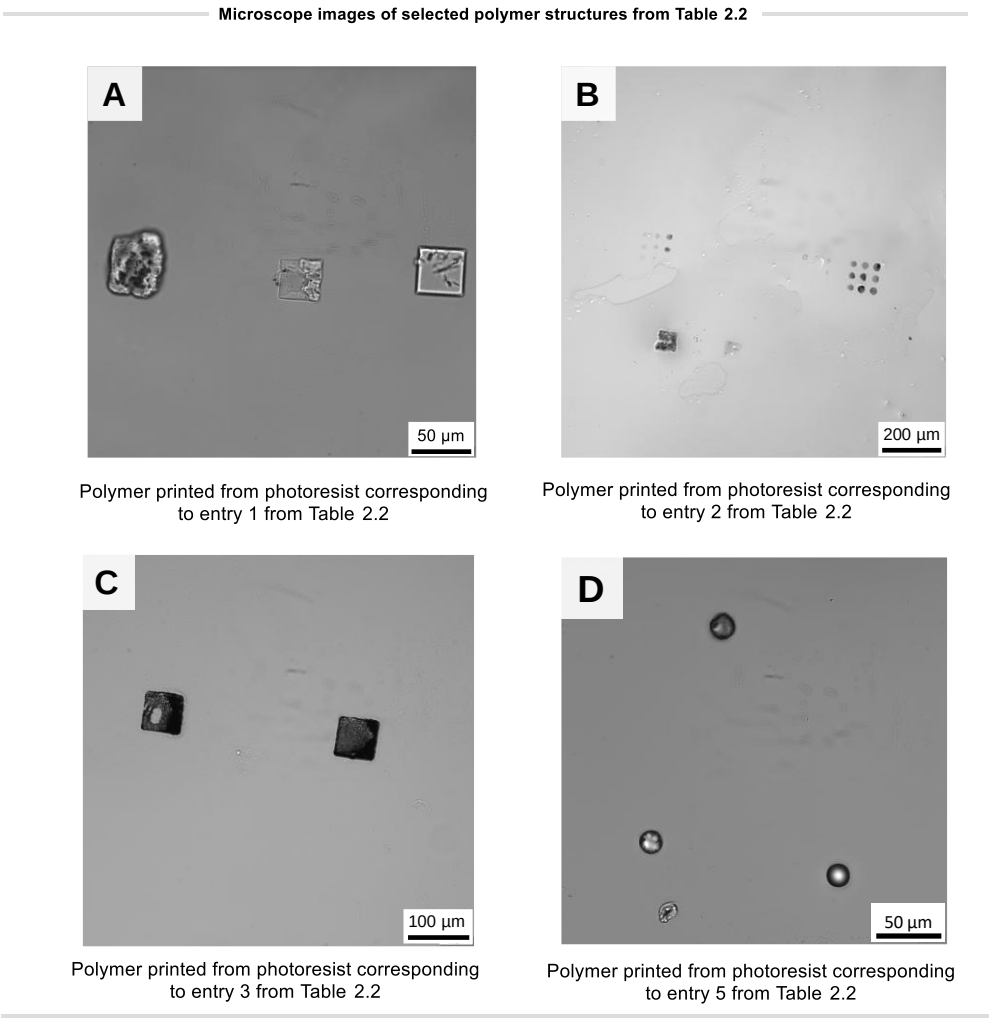

Figure 2.4 Selected polymer structures corresponding to photoresists described in Table 2.2. A) Entry 1; B) Entry 2; Entry 3; Entry 5.

Photoresists described in entry 2 and entry 3 required high laser powers and resulted in limited printing (**Fig 2.4B** and **Fig. 2.4C**), whereas the photoresists in entry 1 and entry 5 gave more promising results and more well-defined structures (**Fig. 2.4A** and **Fig. 2.4D**). However, many of the structures were not well defined with defects and the limited solubility of the photoresist cocktails meant the composition of the polymer network was not sufficiently unambiguous.

Images of structures printed from the photoresist described in entry 6 are shown below in **Fig. 2.5**.

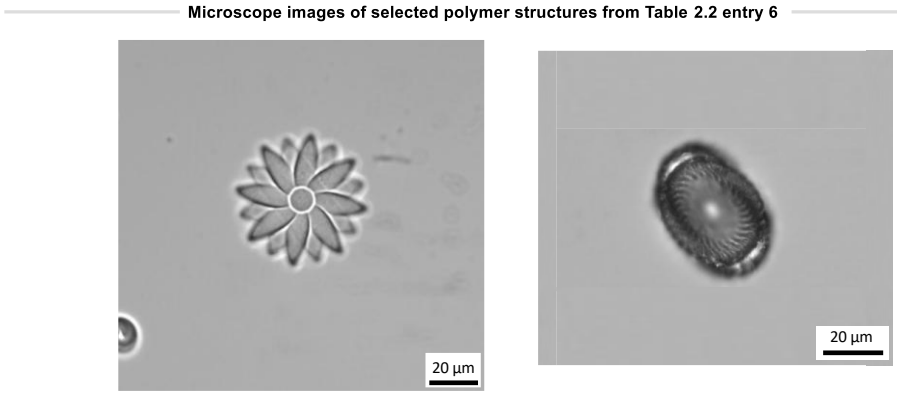

Figure 2.5 Microscope images of selected polymer structures (fabricated floral structure and origami vase) corresponding to the photoresist described in entry 6 in **Table 2.2.**

Well-defined microstructures including floral structures and an origami vase (**Fig. 2.5**) were printed with this photoresist. The full photoresist composition is shown below in **Table 2.3.**

Table 2.3 Photoresist corresponding to entry 6 in **Table 2.2.**

Compound	Mass / mg	Mol %	Weight %
Glucuronide-styrene monomer **82**	12	27	7%
PEG diacrylate 700 crosslinker	87	100	54%
7-Diethylamino-3-thenoylcoumarin (DEATC)	4	10	2%
DMSO	40	-	25%
Water	20	-	12%

Following this, SEM images were taken by Dr Alexa Ennis of the floral and origami vase structures (**Fig. 2.6**).

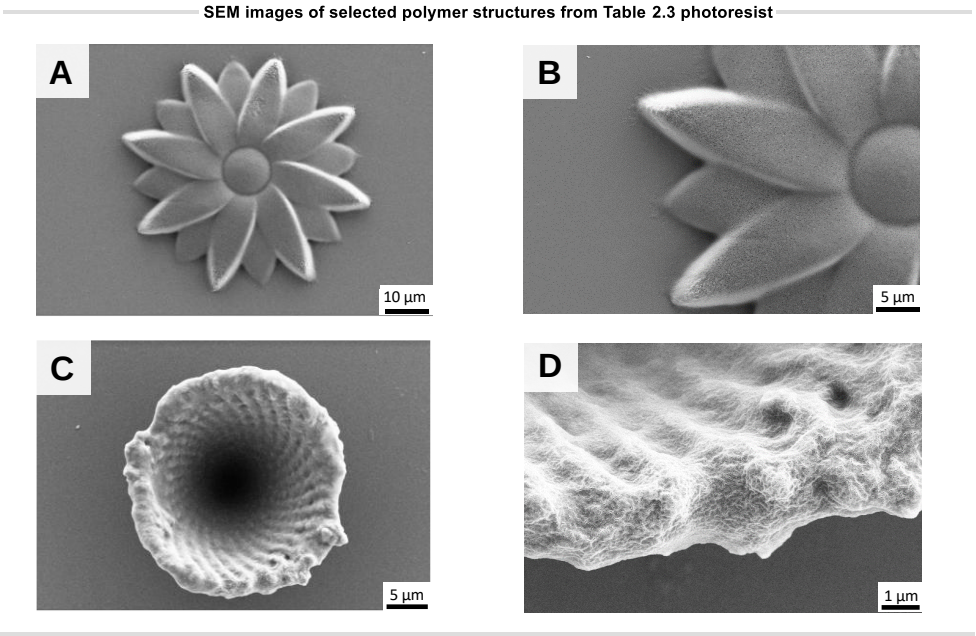

Figure 2.6 SEM images of selected structures printed using the photoresist described in Table 2.3. A) Floral structure at 10 µm scale; B) Floral structure at 5 µm scale; C) Origami vase structure at 5 µm scale; D) Origami vase structure at 1 µm scale.

SEM confirmed sub-micrometre structure resolution of these printed polymers. Styrene control monomer **78** was next polymerised via TPP using the photoresist described in **Table 2.4** below.

Table 2.4 Photoresist composition used for the polymerisation of control monomer **78**.

Compound	Mass / mg	Mol %	Weight %
Styrene control monomer **78**	6	28%	4%
PEG diacrylate 700 crosslinker	88	100%	55%
7-Diethylamino-3-thenoylcoumarin (DEATC)	5	12%	3%
Ethyl acetate	40	-	25%
DMSO	20	-	13%

This photoresist was successfully used to print a variety of structures via TPP (**Fig. 2.7**).

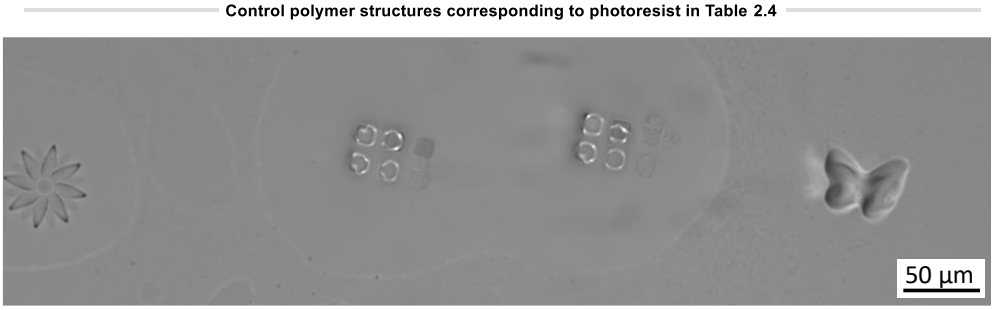

Figure 2.7 Selected structures corresponding to polymers printed using the photoresist described in **Table 2.4** with the styrene control monomer **78**.

Gratifyingly, the structures printed of the styrene control monomer **78** were noticeably softer than the polymers printed from the glucuronide-styrene monomer **82**. As this confirms a distinct differentiation in the physical properties of the polymer compared to the glycopolymers which feature the glucuronic acid moieties, enzymatic cleavage of the glycosidic bond would be expected to trigger a materials response as the polymer's physical properties are altered.

Following the printing of glucuronide-styrene monomer **82** with the photoresist described in **Table 2.3**, subsequent attempts to reproduce well-defined structures were typically not successful, resulting in inconsistent results. The primary challenge encountered was the solubility of the components of the polymerisation cocktail at the high concentrations required for 2PP. Whilst the glucuronide-styrene monomer **82** had good solubility in water but limited solubility in DMSO, the crosslinkers and photoinitiator were soluble at high concentrations in DMSO but had limited solubility in water. Tests with different organic solvents, use of neat crosslinker and mixtures of water and DMSO were not able to produce a reliable solvent for this photoresist. Moreover, high solubility of all components of the cocktail was essential to ensure the composition of the final printed polymer was able to be determined and subsequently tested accurately.

Photoresists were also prepared using the glucuronide-acrylamide monomer **91**, such as the one described below in **Table 2.5**.

Table 2.5 Photoresist composition used for the polymerisation of glucuronide-acrylamide monomer **91**.

Compound	Mass / mg	Mol %	Weight %
Glucuronide-acrylamide monomer **91**	11	28%	7%
PEG-DA-700 crosslinker	87	100%	53%
DEATC photoinitiator	5	12%	3%
Water	30	-	19%
DMSO	30	-	19%

Unfortunately, developing a fully soluble photoresist cocktail also proved challenging for this glucuronide monomer. Although some printing was achieved, as the photoresist was not fully dissolved the composition of the polymer could not be known with confidence and TPP printing was not consistent.

Due to challenges encountered in reproducibly forming a well-dissolved photoresist cocktail containing glucuronide monomers **82** and **91**, the precursor of **82** with acetyl protecting groups installed, **81**, was instead incorporated into a photoresist cocktail, which could then be deprotected following polymerisation. As compound **81** has very good solubility in a range of organic solvents, forming a well-dissolved cocktail in a low volume of DMSO was straightforward.

Peracetylated glucuronide monomer **81** was polymerised via TPP using the photoresist described in **Table 2.6**.

Table 2.6 Photoresist composition used for the polymerisation of peracetylated glucuronide-styrene monomer **81**.

Compound	Mass / mg	Mol %	Weight %
Peracetylated glucuronide-styrene monomer **81**	11	37%	4%
Sartomer® crosslinker	57	100%	55%
7-Diethylamino-3-thenoylcoumarin (DEATC)	6	30%	3%
DMSO	20	-	21%

This photoresist was used to fabricate a range of microstructures at high resolution using TPP (**Fig. 2.8**).

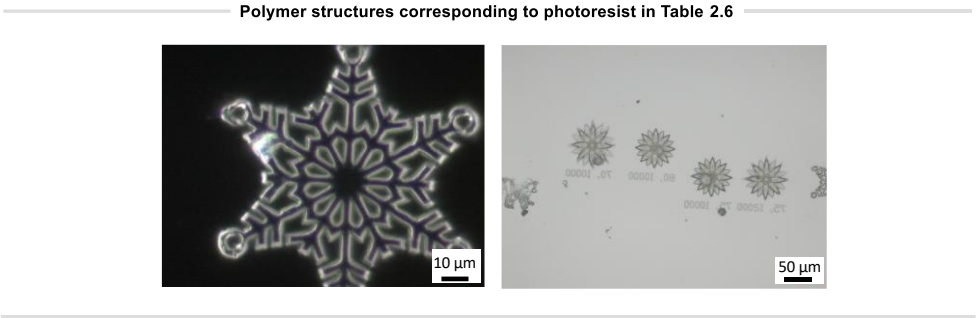

Figure 2.8 Selected structures printed from photoresist in **Table 2.6**.

The range of structures printed were well-defined and suitable for enzymatic testing. Following the printing of the polymer, it was important to next confirm the polymer's stability to water and base treatment as acetyl and methyl ester deprotection under basic conditions was required to generate the deprotected glycopolymer (**Fig. 2.9**).

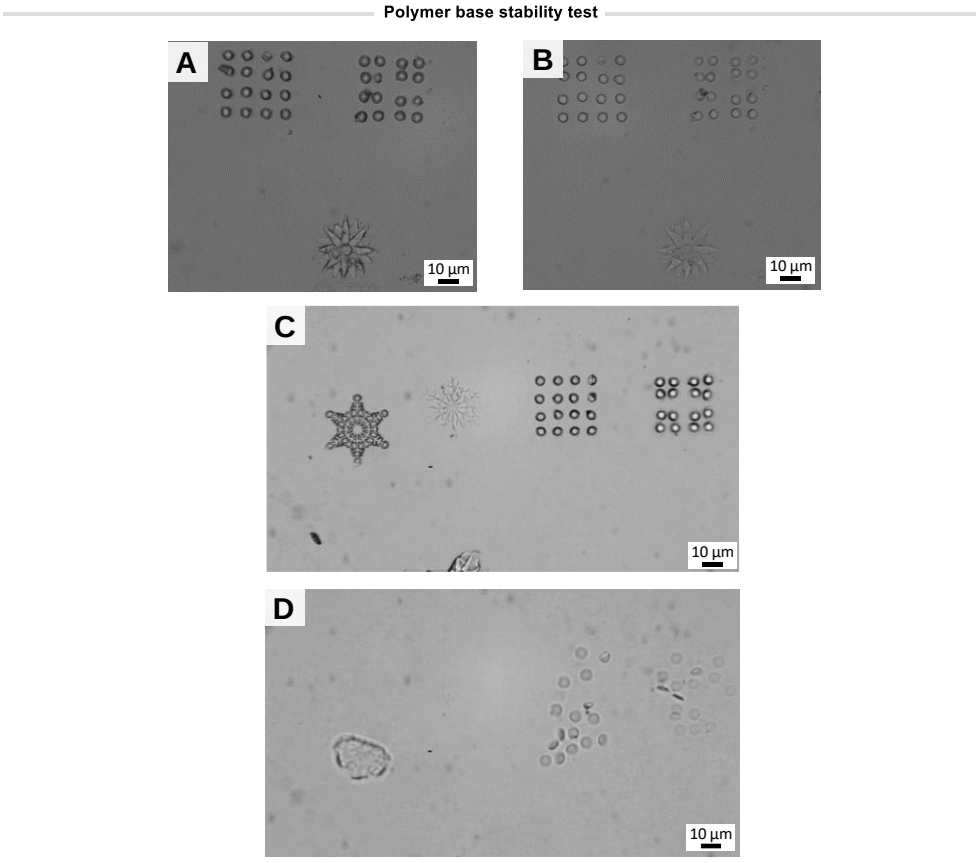

Figure 2.9 Selected structures monitored to validate base stability. A) Before any treatment; B) After water treatment; C) Before 0.1 M NaOH treatment; D) After 0.1 M NaOH treatment.

The structures were stable in aqueous solution (**Fig. 2.9A** and **Fig. 2.9B**), but treatment with 0.1 M NaOH resulted in structure delamination from the surface of the slide and degradation. This occurred rapidly and was observed in real time upon addition of the basic solution. UV polymerisation was used as a bulk polymerisation technique with a scaled up photoresist corresponding to the one described in **Table 2.6**. This successfully formed polymer beads at mm scale, which were subsequently treated with basic solution in an experiment analogous to the one described above (**Fig. 2.10**).

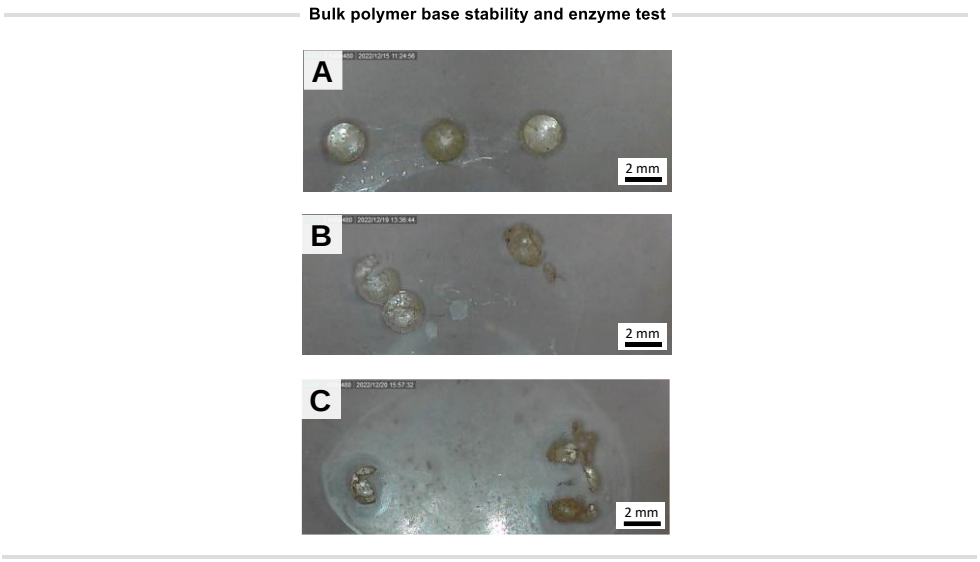

Figure 2.10 Base stability and enzymatic degradation experiment for bulk polymer beads. A) Image before treatment; B) Image after 0.1 M NaOH treatment; C) Image after β-glucuronidase treatment (50 U).

Degradation of the polymer beads was observed following treatment with a 0.1M NaOH solution (**Fig. 2.10B**), confirming the incompatibility of these photoresists for these experiments as the polymer would need to be stable under the basic conditions required for deacetylation. Treatment with β-glucuronidase (**Fig. 2.10C**) appeared to trigger additional degradation, although the confidence of this result is limited due to the significant degradation caused by the sodium hydroxide.

The instability of these polymers to base was accounted for by the use of the Sartomer® **93** crosslinker (**Fig. 2.2**) used, which contains ester linkages. Control polymers printed by 2PP using the photoresist described in **Table 2.7** were tested to confirm any observable degradation under microscopy under basic conditions (**Fig. 2.11**).

Table 2.7 Photoresist composition for a control polymer without glucuronide-styrene monomer **81**.

Compound	Mass / mg	Mol %	Weight %
Sartomer® crosslinker	57	100%	73%
7-Diethylamino-3-thenoylcoumarin (DEATC)	6	31%	8%
DMSO	15	-	19%

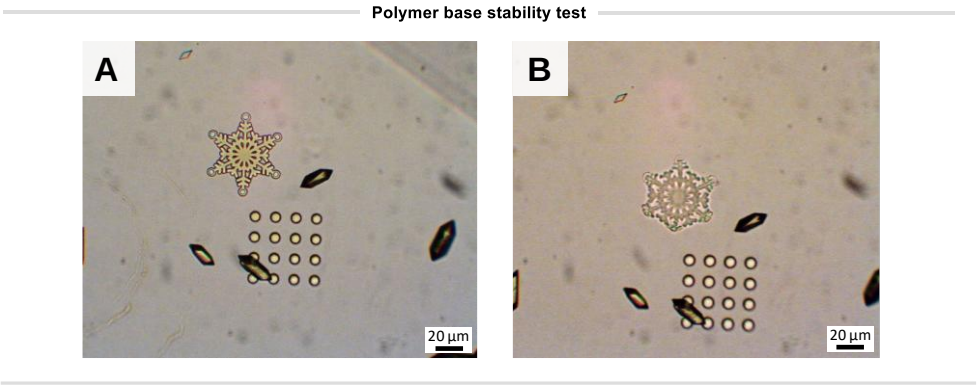

Figure 2.11 Images of selected polymer structures printed from the photoresist described in Table 2.7. A) Before treatment; B) After 0.1 M NaOH treatment.

These experiments confirmed instability of the crosslinker to basic conditions, with real-time delamination of printed structures observed, with full delamination noted upon gentle drying of the glass slide.

As the crosslinkers so far explored were not compatible with base treatment, crosslinkers with compatible functional groups were explored. For example, it was sought to use amide-based crosslinkers which should have sufficient stability to the conditions required. Commercially available *N*,*N*'-methylene bisacrylamide was used in the first instance.

Control polymers were first planned to be made so that the stability of the crosslinker to base could be tested prior to incorporation into a cocktail with the glucuronide-styrene monomer **81**. After successive attempts to polymerise *N*,*N*'-methylenebisacrylamide by TPP, printing could not be achieved. It was hypothesised that this could be accounted for by the lack of

functionality on the molecule and that trifunctional acrylamide monomers which would allow for more extensive crosslinking would achieve better results. As such, a trifunctional analogue of *N*,*N*'-methylene bisacrylamide with three acrylamide groups was synthesised (**Scheme 2.10**).

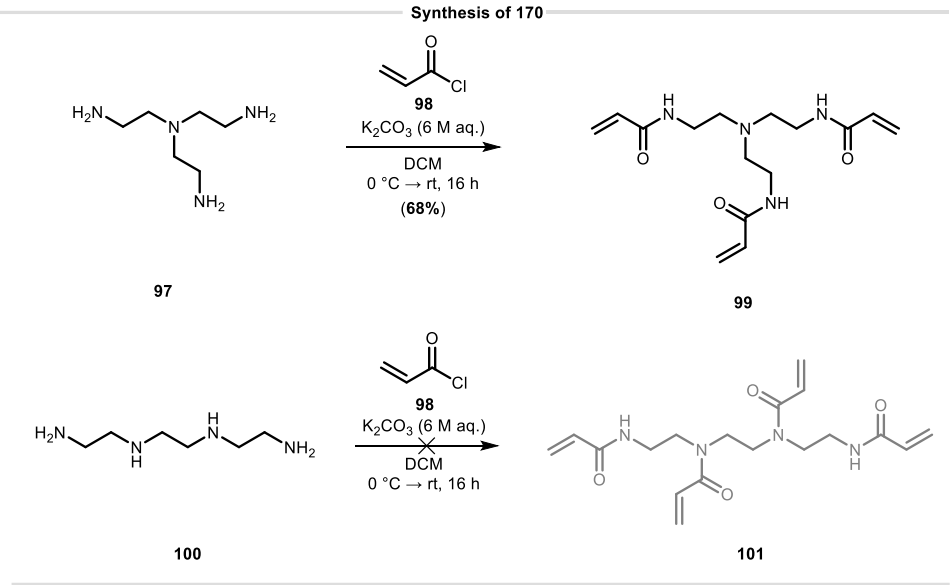

Scheme 2.10 Synthesis of trifunctional acrylamide crosslinker **99** and attempted synthesis of **101**.

Reaction of triamine **97** with acryloyl chloride **98** furnished trifunctional acrylamide crosslinker **99** in a 68% yield. Reaction of tetramine **100** with acryloyl chloride under the same conditions formed **101** confirmed by HRMS, however the purity and stability of this compound was not sufficient for use. Trifunctional acrylamide crosslinker **99** was then incorporated into a photoresist cocktail for TPP (**Table 2.8**).

Table 2.8 Photoresist composition for the trifunctional acrylamide crosslinker **99**.

Compound	Mass / mg	Mol %	Weight %
Crosslinker **99**	15	100%	48%
7-Diethylamino-3-thenoylcoumarin (DEATC)	1	6%	4%
DMSO	15	-	48%

This photoresist was successfully used to print a range of structures using TPP which could then be used to confirm the stability of the polymers to base treatment (**Fig. 2.12**).

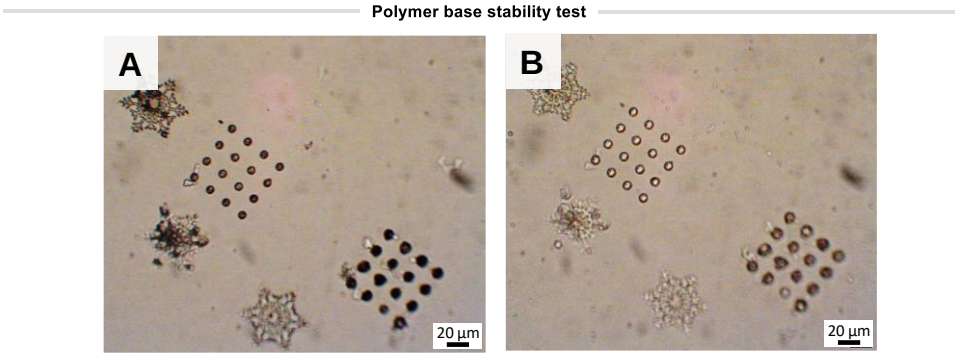

Figure 2.12 Base stability test of polymer structures printed from photoresist in Table 2.8. A) Image before treatment; B) Image after 0.1 M NaOH treatment).

Images of the polymers containing crosslinker **99** before and after treatment in **Fig. 2.12** confirm the stability of crosslinker **99** to base and therefore was suitable for incorporation into a photoresist cocktail containing peracetylated glucuronide styrene monomer **81**. However, it was found that following successive attempts to polymerise various cocktails which contained trifunctional acrylamide crosslinker **99** and peracetylated glucuronide styrene monomer **81**, printing could not be achieved. Only cocktails without the glucuronide monomer could be printed.

As D-galactose has a reported solubility of 50 mg/mL in DMSO compared to 33 mg/mL for D-glucuronic acid,[289, 290] β-galactoside analogues were synthesised for the generation of alternative glycopolymers which were expected to have enhanced solubility in DMSO to aid photoresist cocktail preparation. β-galactosidase is also overexpressed across a range of

tumour types, making it suitable for incorporation into a tumour-targeting responsive application.[107]

2.2.2 β-Galactoside Monomer Synthesis

In addition to β-glucuronide monomers, β-galactoside monomers were also synthesised, which were anticipated to have significantly improves solubility in DMSO. A β-galactoside-styrene monomer **106** was synthesised as described in **Scheme 2.11**.

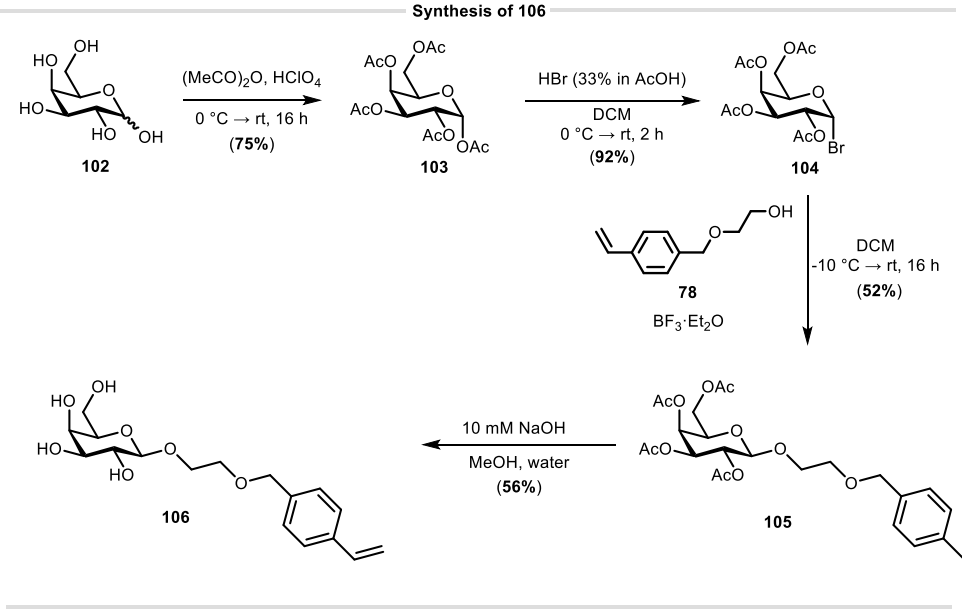

Scheme 2.11 Synthesis of galactoside **106**.

Peracetylation of galactose **102** with acetic anhydride and perchloric acid gave peracetylated **103** in a yield of 75%, after which bromination using a 33% solution of HBr in acetic acid furnished α-bromo galactosyl donor **104** in 92% yield. Glycosylation of α-bromo donor **104** with acceptor **78** provided galactoside **105** in 52% yield, which was subsequently deprotected using a 10 mM sodium hydroxide solution to give target molecule **106** in a yield of 56%.

Next, a galactoside derivative bearing an acrylamide polymerisable group was synthesised (**Scheme 2.12**).

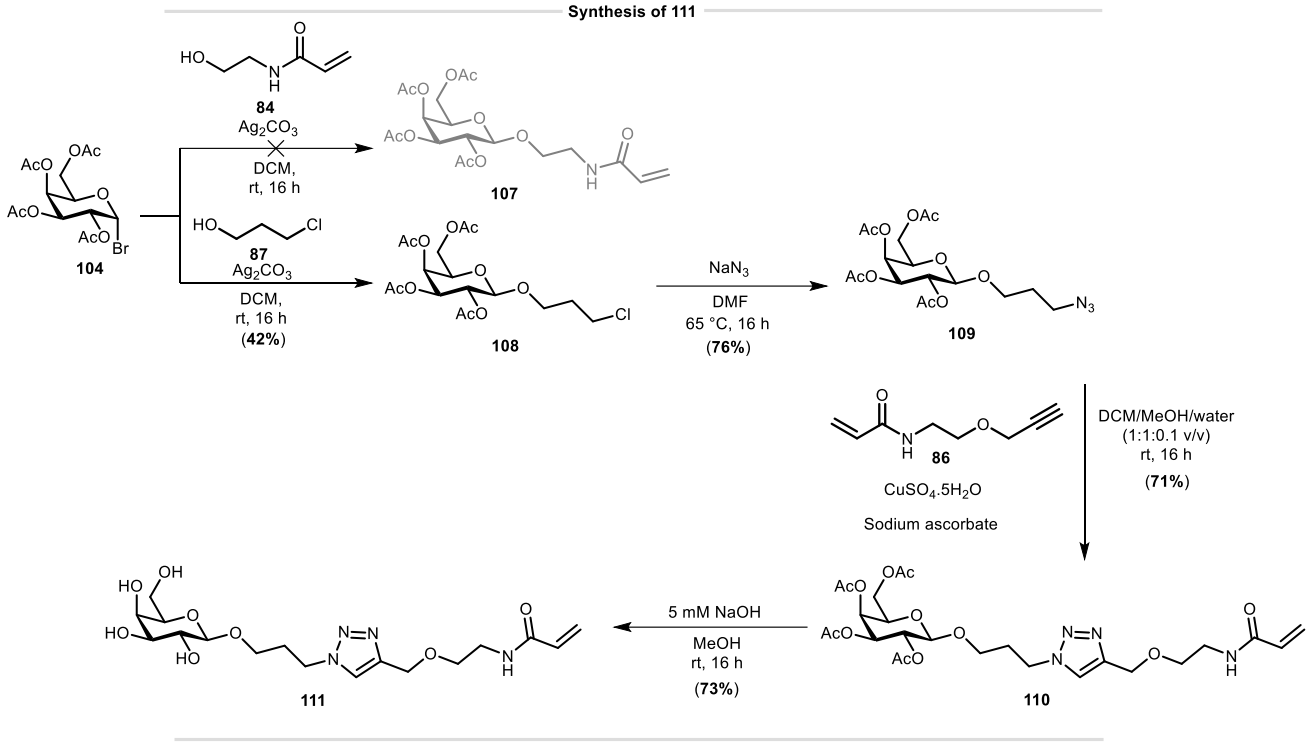

Scheme 2.12 Synthesis of galactoside **111**.

Initially, glycosylation of α-bromo galactosyl donor **104** with commercially-available *N*-hydroxyethyl acrylamide was attempted, however only hydrolysed donor was recovered. Following this, a similar route as described for the synthesis of glucuronide conjugate **91** was carried out. Glycosylation of α-bromo galactosyl donor **104** with 3-chloropropan-1-ol using Ag_2CO_3 furnished galactoside chloride **108** in a yield of 42%. Subsequent azidation with NaN_3 at 65 °C gave galactoside azide **109** in 76% yield, which was followed by Cu(I)-catalysed alkyne-azide cycloaddition to provide **110** in 71% yield. Finally, deprotection using 5 mM sodium hydroxide furnished target molecule **111** in 73% yield.

It was next necessary to synthesise a control compound consisting of the same structure without the carbohydrate moieties, which would correspond to the compound released upon glycosidase-mediated glycosidic bond cleavage. To allow for safe handling of the small

molecule azide intermediate required in this synthetic route, the hydroxyl group of three-carbon compound 3-chloropropan-1-ol was first protected (**Scheme 2.13**).

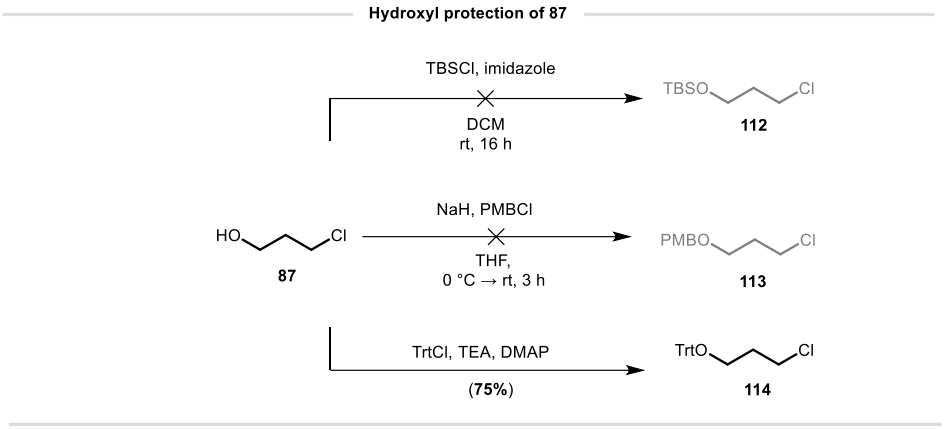

Scheme 2.13 Test reactions for protecting group installation on the hydroxyl group of 3-chloropropan-1-ol

Reaction of 3-chloropropan-1-ol **87** with TBSCl and PMBCl to give **112** and **113** were unsuccessful, however use of trityl chloride successfully furnished trityl-protected **114** in 75% yield.

114 was then functionalised to synthesise control compound **117**, described in **Scheme 2.14**.

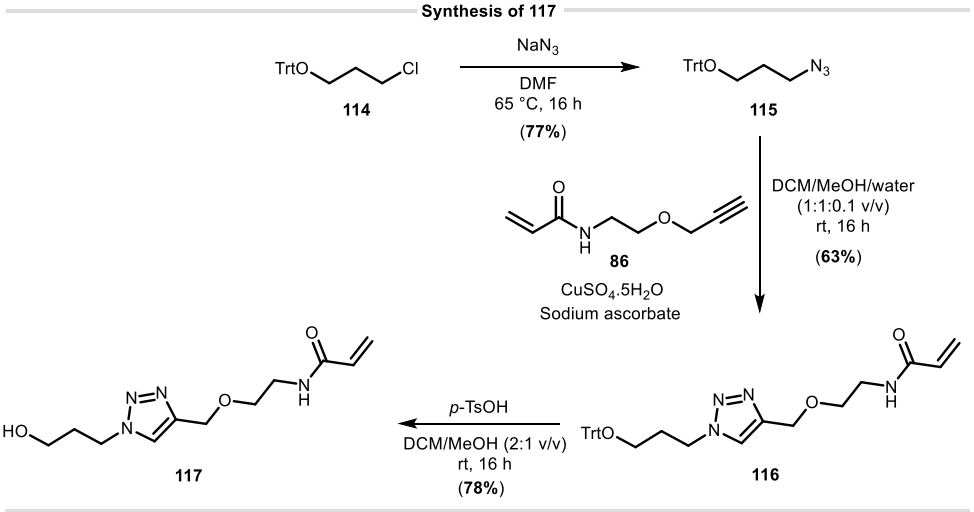

Scheme 2.14 Synthesis of triazole-acrylamide control compound **117**.

Azidation of **114** with NaN_3 at 65 °C gave azide **115** in 77% yield, which was then reacted with alkyne **86** in a Cu(I)-catalysed alkyne-azide cycloaddition with $CuSO_4.5H_2O$ and sodium ascorbate to furnish triazole **116** in a yield of 63%. Finally, trityl deprotection using *para*-toluenesulfonic acid provided target molecule **117** in 78% yield.

2.2.2.1 Polymerisation and Enzymatic Testing of Galactoside Monomers

Following the successful synthesis of galactoside monomers **107** and **111** incorporating the styrene and acrylamide polymerisable groups respectively, as well as their associated control compounds **78** and **117** which correspond to the compounds excluding the galactose moiety, these compounds were incorporated into various photoresists seeking to optimise TPP conditions to reliably generate polymer microstructures. The monomer (galactoside styrene **106**, galactoside acrylamide **111** and acrylamide control monomer **117**), crosslinker (Sartomer® **93** and PEG-DA-700 **94**) and photoinitiator (DEATC **95**) photoresist components used in this section are described in **Fig. 2.11.**

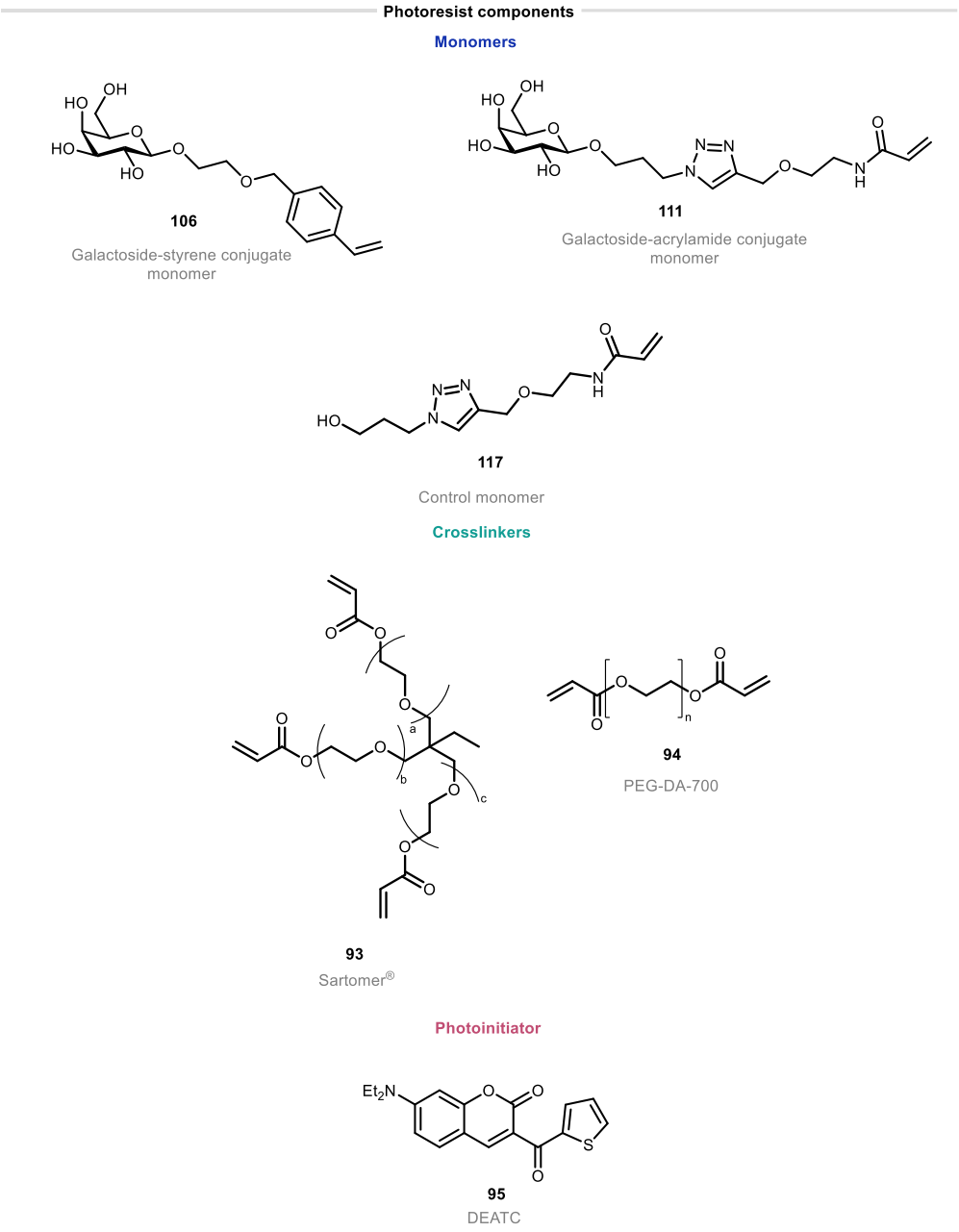

Figure 2.11 Monomer, crosslinker and photoinitiator photoresist components used in this section.

Galactoside-styrene conjugate **106**, galactoside-acrylamide conjugate **111** and triazole acrylamide control compound **117** were polymerised using Sartomer® **93** and PEG-DA-700 **94** as crosslinkers and DEATC **95** as the photoinitiator. Polymerisation of the control compound corresponding to galactoside-styrene conjugate **106** was described in **Section 2.2.1.1.**

Firstly, galactoside-styrene conjugate **106** was polymerised using Sartomer® **94** as the crosslinker and DEATC **95** as the photoinitiator with varying mol% of monomer **106** relative

to the crosslinker. **Table 2.9** describes the monomer mol% and DMSO weight% used for these photoresists.

Table 2.9 Galactoside-styrene monomer **106** mol% and DMSO weight % corresponding to photoresists A-D used for its polymerisation, using Sartomer® **93** as the crosslinker and DEATC **95** as the photoinitiator.

Photoresist	Monomer 177 mol%	DMSO weight %
Photoresist A	35%	25%
Photoresist B	50%	22%
Photoresist C	54%	33%
Photoresist D	62%	26%

Whereas glucuronic acid analogues proved to be stubbornly insoluble in a range of solvents at the concentrations required for TPP, the galactoside-styrene monomer **106** had high solubility in DMSO as anticipated, resulting in well-dissolved photoresist cocktails suitable for TPP. When using a limited solvent weight percentage between 22% and 33%, each photoresist printed well-defined polymer structures. Polymerisation of photoresists with up to 62 mol% of monomer **106** successfully allowed for the generation of polymers with a significant amount of **106** in the polymer backbone and therefore increasing the amount of galactose moieties for responsive applications. Selected structures polymerised from these photoresists are shown below in **Fig 2.13**.

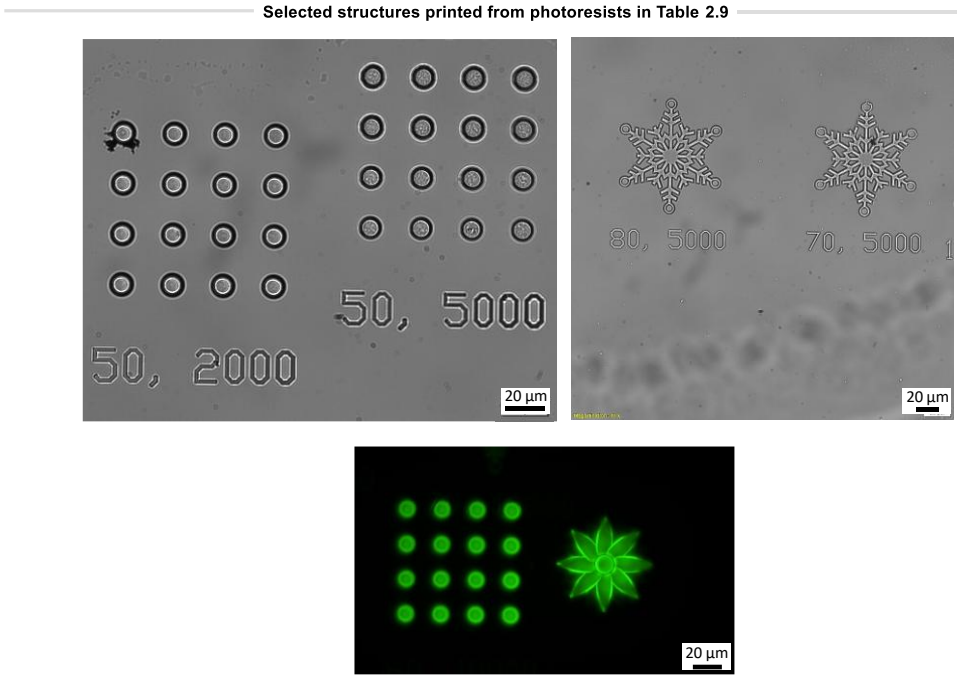

Figure 2.13 Images of selected microstructures printed from photoresists A-D in **Table 2.9**, all with Sartomer® crosslinker and DEATC photonitiator. The bottom image shows fluorescence from the fluorescent DEATC **95** photoinitiator when excited at 555 nm under an epifluorescent microscope.

A range of different microstructures with different shapes and dimensions were printed at different laser powers and scan speeds. The arrays of pillars demonstrates printing at 50% laser power at scan speeds of both 2,000 and 5,000 µm s^{-1}. Minimising the laser power and using faster scan speeds results in polymers with a lower degree of crosslinking, thereby increasing their susceptibility to induced degradation.

Next, enzymatic degradation studies applying the protocol described in **Fig. 2.14** were carried out to validate a change in physical properties of the polymers (**Fig. 2.15**).

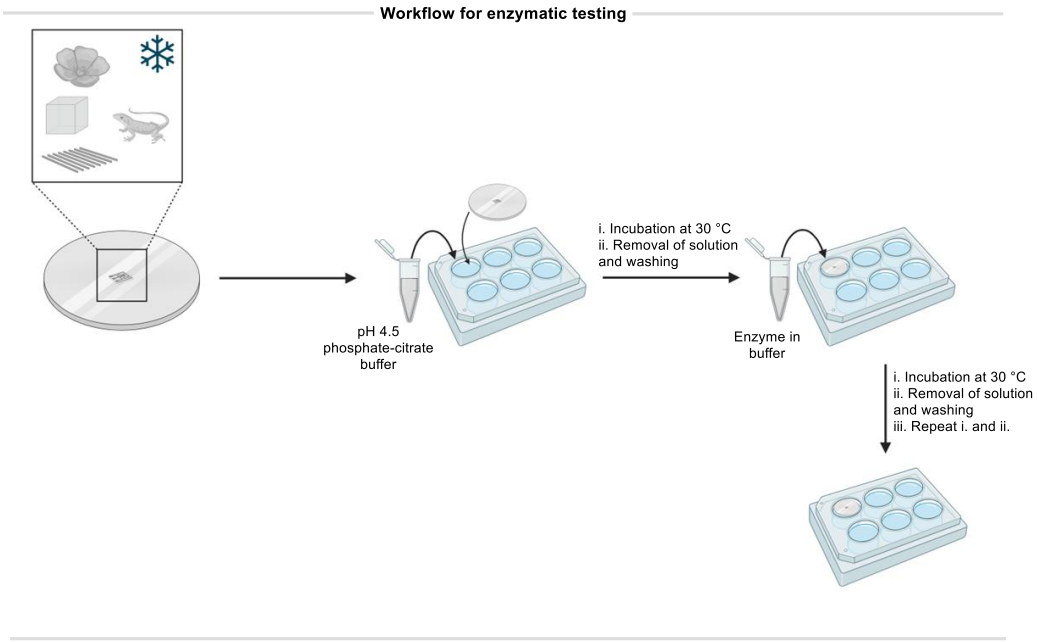

Figure 2.14 A schematic describing the workflow for enzymatic testing of the printed β-galactosidase-responsive microstructures. 230U/mL enzyme concentration, treated for 10 x 10 h and washed three times with water between each repetition.

Following TPP fabrication of microstructures and imaging using microscopy, the glass slide is transferred to a well plate and incubated with pH 4.5 phosphate-citrate buffer at 30 °C overnight as a control experiment. Following this, the slide is reimaged, washed three times with water and then β-galactosidase added (230 U/mL in pH 4.5 phosphate-citrate buffer) and incubated at 30 °C overnight, followed by washing with water. This is carried out twice each day over a five-day period and then reimaged.

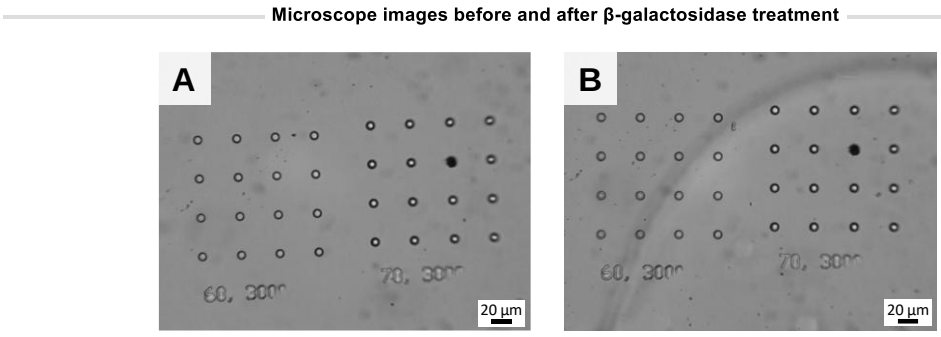

Figure 2.15 Images of selected microstructures before and after β-galactosidase treatment (230 U/mL), following the protocol described in Fig. 2.13. A) Before treatment; B) After treatment (ten additions over a course of five days).

Experiments carried out to validate a change in physical properties in response to enzymatic activation were unable to confirm an observable difference between the monitored structures. Swelling in aqueous environment appeared minimal.

Due to these results, the development of galactoside polymers for application to lectin recognition and boronic acid binding was selected as an alternative utilisation of glycopolymers of this type. Galactoside-acrylamide monomer **111** was polymerised at varying mol% relative to the crosslinker and using both Sartomer® and PEG-DA-700 crosslinkers, starting with Sartomer® (**Table 2.10** and **Table 2.11**).

Table 2.10 Photoresist used to print polymer structures of galactoside-acrylamide monomer **111** with the Sartomer® crosslinker, using 20 mol% of monomer **111** relative to the crosslinker.

Compound	Mass / mg	Mol %	Weight %
Galactose-acrylamide monomer **111**	9.8	20%	5%
Sartomer® crosslinker	112	100%	61%
DEATC photoinitiator	2	5%	1%
DMSO	50	-	27%
Water	10	-	5%

Table 2.11 Photoresist used to print polymer structures of galactoside-acrylamide monomer **111** with the Sartomer® crosslinker, using 44 mol% of monomer **111** relative to the crosslinker.

Compound	Mass / mg	Mol %	Weight %
Galactose-acrylamide monomer **111**	14	44%	9%
Sartomer® crosslinker	73	100%	46%
DEATC photoinitiator	1.3	5%	1%
DMSO	53	-	33%
Water	17	-	10%

These photoresists were successfully used to print polymer microstructures using TPP (**Fig. 2.16**).

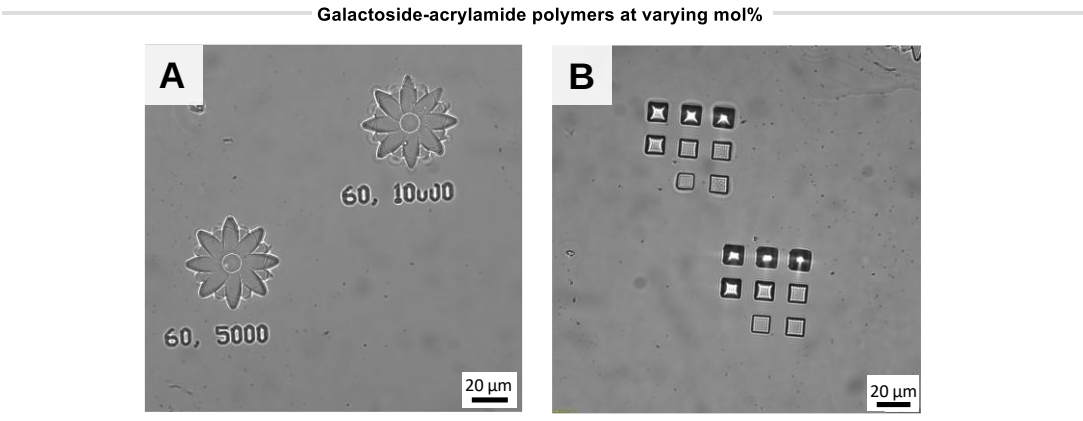

Figure 2.16 Images of selected structures printed from photoresists incorporating galactoside-acrylamide monomer 111 and the Sartomer® crosslinker. A) Floral microstructures printed from photoresist in **Table 2.10** with 20 mol% of monomer **182**; B) Two arrays of cube structures with increasing laser powers printed from photoresist in **Table 2.11** with 44 mol% of monomer **182**.

A range of microstructure were printed, including at low laser powers. **Fig. 2.16A** shows two floral structures printed at 60% laser power at scan speeds of both 5,000 µm s^{-1} and 10,000 µm

s^{-1} and **Fig. 2.16B** shows two arrays of cube structures printed at increasing laser power, from 20% to 100%, showing proficient polymerisation from 30% upwards. These results demonstrate the efficiency of the photoresists used at both 20 mol% and 44 mol% of galactoside-acrylamide monomer **111**, producing well-defined polymer structures under highly tuneable conditions.

Following these promising results, photoresists which use the PEG-DA-700 crosslinker were developed to polymerise galactoside-acrylamide monomer **111** (**Table 2.12** and **Table 2.13**) with an alternative crosslinker.

Table 2.12 Photoresist used to print polymer structures of galactoside-acrylamide monomer **111** with the PEG-DA-700 crosslinker, using 20 mol% of monomer **111** relative to the crosslinker.

Compound	Mass / mg	Mol %	Weight %
Galactoside-acrylamide monomer **111**	11	20%	6%
PEG-DA-700 crosslinker	86.5	100%	50%
DEATC photoinitiator	2.4	6%	1%
DMSO	50	-	27%
Water	10	-	5%

Table 2.13 Photoresist used to print polymer structures of galactoside-acrylamide monomer **111** with the PEG-DA-700 crosslinker, using 44 mol% of monomer **111** relative to the crosslinker.

Compound	Mass / mg	Mol %	Weight %
Galactoside-acrylamide monomer **111**	14	44%	8%
PEG-DA-700 crosslinker	54	100%	29%

DEATC photoinitiator	1.5	6%	1%
DMSO	51	-	28%
Water	16	-	9%

These photoresists were successfully used for TPP of galactoside-acrylamide monomer **111**, using limited solvent at 27-28 weight% of DMSO and varying mol% of monomer. Selected structures are shown in **Fig 2.17**.

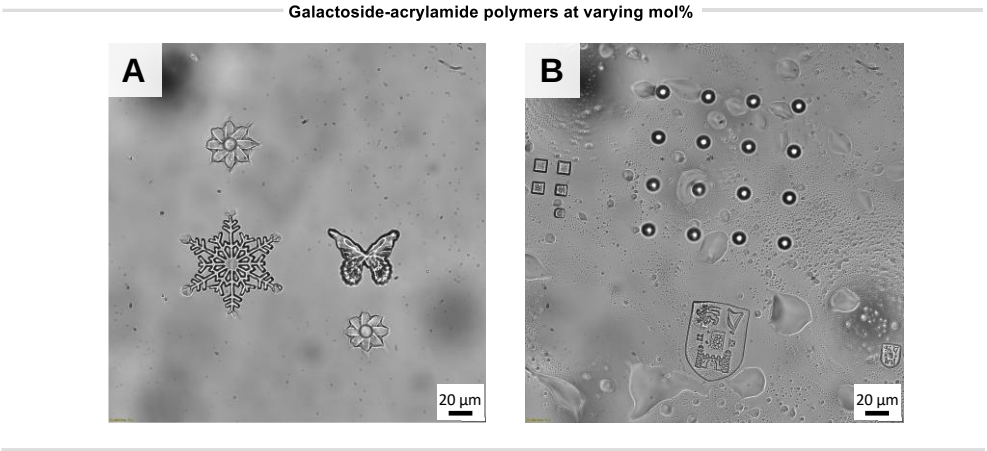

Figure 2.17 Images of selected structures printed from photoresists incorporating galactoside-acrylamide monomer 111 and the PEG-DA-700 crosslinker. A) Floral, snowflake and butterfly microstructures printed from photoresist in **Table 2.12** with 20 mol% of monomer **111**; B) An array of pillars and the Trinity College Dublin university crest printed from photoresist in **Table 2.13** with 44 mol% of monomer **111**.

A variety of structure types were successfully printed with both photoresists including floral, snowflake, butterfly, pillar and Trinity College Dublin crest structures using both 20 mol% and 40 mol% of galactoside-acrylamide monomer **111**. These results demonstrate the successful polymerisation of photoresists which incorporate significant amounts of carbohydrate-containing monomers and with different crosslinkers.

Next, control polymers were produced for use in future experiments seeking to validate a polymer response results from the carbohydrate moieties. Triazole-acrylamide control monomer **117** was polymerised using photoresists in **Table 2.14** and **Table 2.15**.

Table 2.14 Photoresist used to print polymer structures of triazole control monomer **117** with the Sartomer® crosslinker, using 20 mol% of monomer **117** relative to the crosslinker.

Compound	Mass / mg	Mol %	Weight %
Triazole-acrylamide control monomer **117**	8.5	40%	5%
Sartomer® crosslinker	79	100%	57%
DEATC photoinitiator	1.5	6%	1%
DMSO	40	-	29%
Water	10	-	7%

Table 2.15 Photoresist used to print polymer structures of triazole control monomer **117** with the PEG-DA-700 crosslinker, using 45 mol% of monomer **117** relative to the crosslinker.

Compound	Mass / mg	Mol %	Weight %
Triazole-acrylamide control monomer **117**	8.8	45%	8%
PEG-DA-700 crosslinker	54	100%	47%
DEATC photoinitiator	1.3	5%	1%
DMSO	40	-	35%
Water	10	-	9%

Triazole-acrylamide control monomer **117** was successfully incorporated into these photoresists with good solubility in DMSO using both Sartomer® and PEG-DA-700

crosslinkers. These photoresists were used to print microstructure polymers shown in **Fig 2.18.**

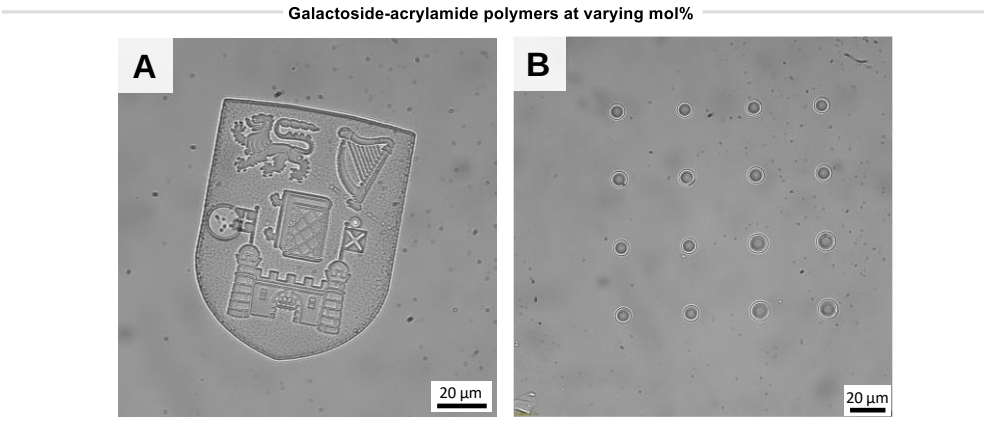

Figure 2.18 Images of selected microstructures printed from photoresists incorporating the triazole-acrylamide control compound 117. A) Trinity College Dublin university crest printed from photoresist in **Table 2.14** with Sartomer® crosslinker; B) An array of pillars printed from photoresist in **Table 2.15** with PEG-DA-700 crosslinker.

The photoresist described in **Table 2.14** with Sartomer® crosslinker and 40 mol% of triazole-acrylamide monomer **117** was found to successfully print a variety of structures including the Trinity College Dublin university crest at high resolution (**Fig. 2.18A**). Gratifyingly, the photoresist described in **Table 2.15** with the PEG-DA-700 crosslinker and 45 mol% of monomer **117** was also proficient for the polymerisation of microstructures (**Fig. 2.18B**).

2.3 Conclusions and Future Work

This project has demonstrated the successful synthetic development of routes to a range of glycomonomer conjugates which were subsequently incorporated into various photoresists for polymerisation via TPP. The galactose-styrene and galactose-acrylamide monomers **106** and **111** were most successful, forming well-dissolved photoresist cocktails and a range of microstructures being printed via TPP (**Fig. 2.19**). The control monomer analogues of these conjugates were also polymerised via TPP to form well-defined microstructures. Enzymatic testing with β-galactosidase was not able to validate an observable physical property change or degradation via microscopy. The lack of observable changes in the physical properties of

the polymers by microscopy is rationalised by the restricted access to the glycosidic bond of the glycopolymers through the dense polymer network.

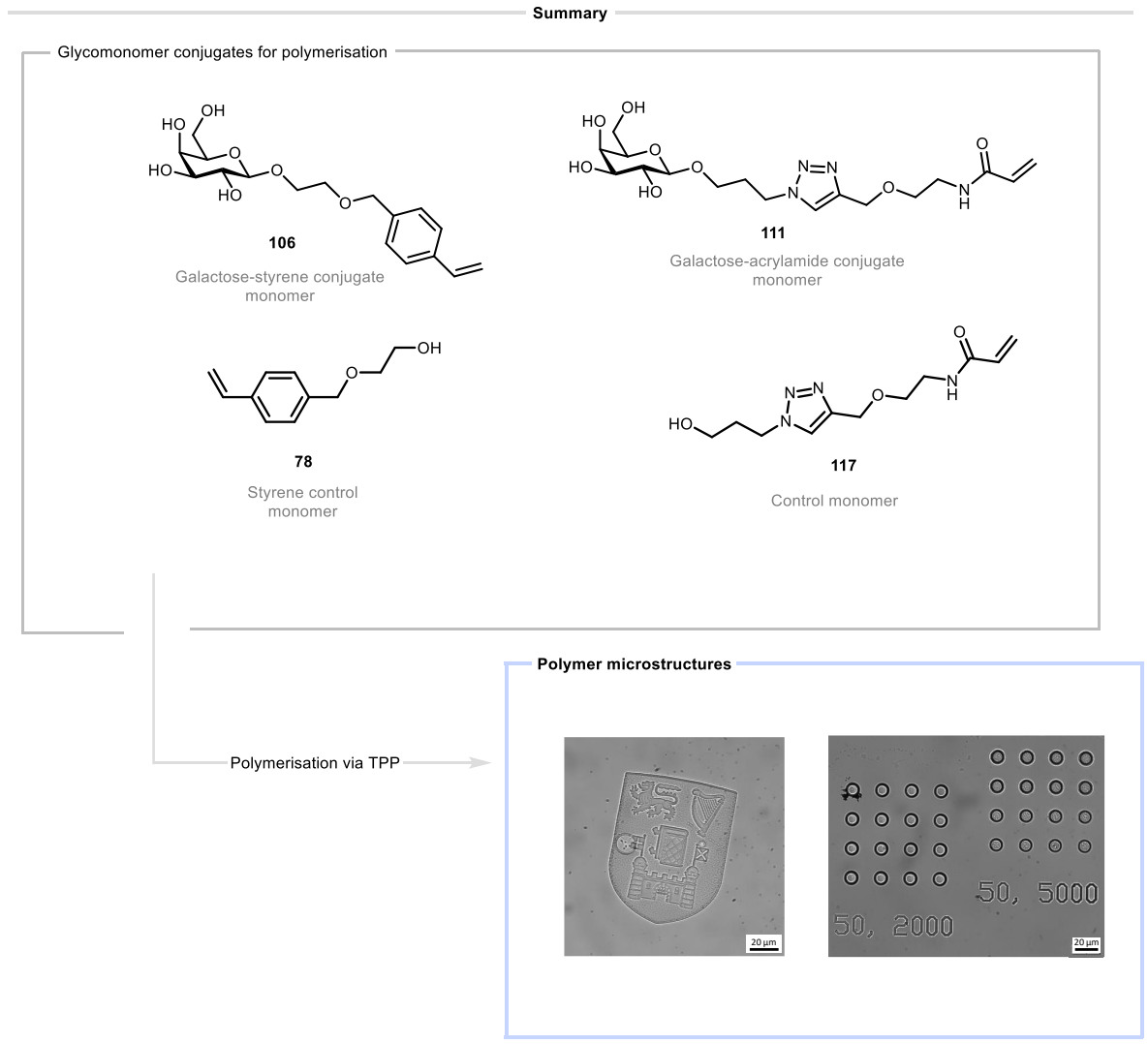

Figure 2.19 Summary of glycomonomer conjugates synthesised and polymerised via TPP.

Following unsuccessful enzymatic testing, future work using these high-resolution polymer microstructures could involve applying the glycopolymers to alternative applications such as lectin recognition for cell-surface adhesion and binding to boronic acid conjugates bearing fluorophores to demonstrate selective binding via microscopy (**Fig. 2.20**).

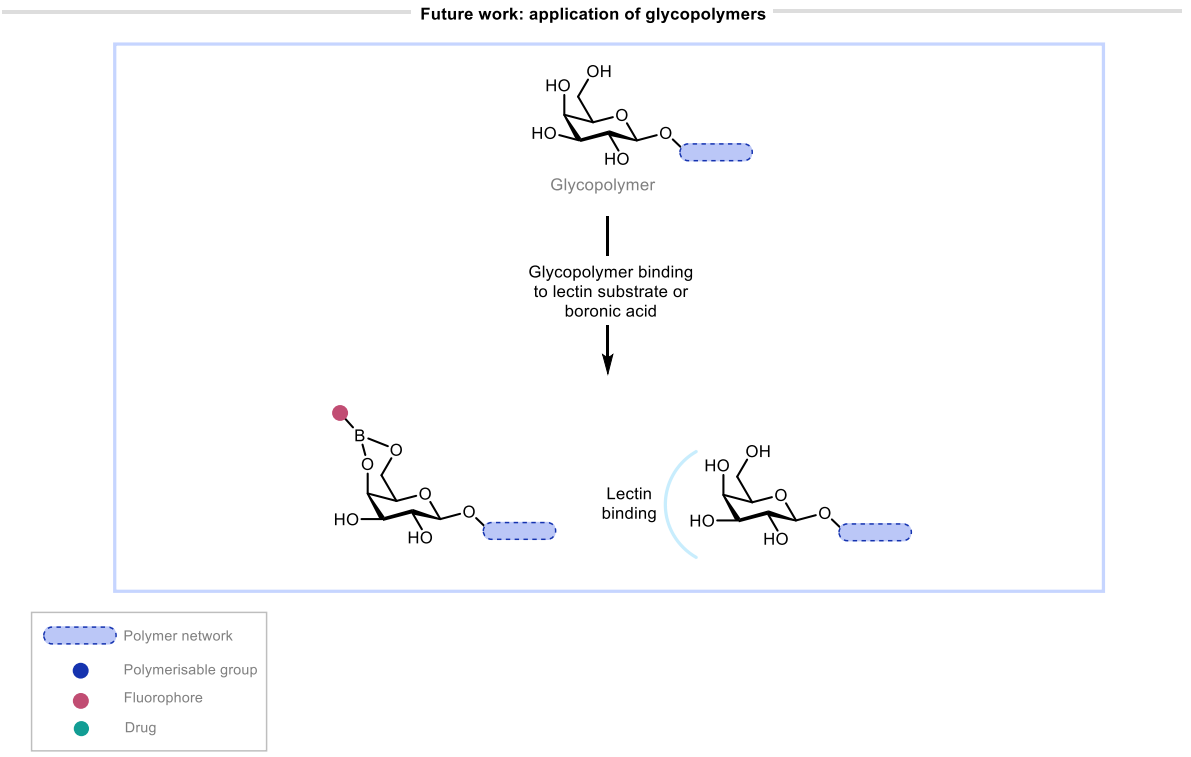

Figure 2.20 Future work on applying the galactose glycopolymers to boronic acid or lectin binding.

Chapter 3

Development of Self-Immolative Glycosidase-Responsive Crosslinkers for Degradable Polymers

Chapter 3: Development of Self-Immolative Glycosidase-Responsive Crosslinkers for Degradable Polymers

3.1 Introduction

Self-immolative polymers (SIPs) which undergo depolymerisation and degradation in response to external stimuli constitute an emerging class of polymers which have been applied to an increasing diverse range of uses spanning from materials science to diagnostics and drug delivery.[241] Analogous to prodrug strategies which mask selected functional groups associated with the biological activity of the drug, SIPs use masking groups which can be specifically cleaved to initiate depolymerisation of the polymer backbone upon activation.

Currently, SIPs which are enzymatically activated remains an underexplored field with limited examples. The development of enzymatically activated SIPs offers the potential to expand this class of responsive polymer to more biological contexts and complement existing polymeric drug delivery strategies.

Glycosidases such as β-glucuronidase and β-galactosidase are upregulated in a range of tumour types, with their level of activity being implicated throughout the cancer development stages, which has made them promising targets in the development of prodrugs by using cleavable carbohydrate triggers. Despite their application in antibody-directed enzyme prodrug therapy and prodrug monotherapy,[107] the use of carbohydrates in activatable polymeric systems has not been studied.

Moreover, despite being utilised for the development of an increasingly extensive range of stimuli-responsive systems, examples of enzyme-responsive polymers printed using two-photon polymerisation (TPP) remains limited to one example which requires magnetic nanoparticles and rotational magnetic fields for its design.[285] Therefore, the expansion of the use of TPP, which occupies a privileged space in polymer science due to its purpose of printing microstructures at exceptional resolution in a highly controlled manner, to enzyme-

responsive applications which require only endogenous upregulation in a biological context presents a promising research challenge.

3.2 Aims

The aim of this project was to develop glycosidase-activated degradable self-immolative polymers which could be applied in a range of responsive applications including sensing and drug delivery, exploiting the overexpression of glycosidases in various tumours. This required activatable carbohydrate-conjugate crosslinkers which are held together by self-immolative chains, which were designed based on scaffolds developed for dual drug delivery reported by Papot and co-workers (**Fig. 3.1A**); the conjugation of polymerisable groups instead of therapeutic payloads would generate compounds suitable for polymerisation.

Optimisation of the polymerisation cocktail and two-photon polymerisation parameters was required to generate glycosidase-responsive SIPs suitable for degradation studies (**Fig. 3.1B**) to present a proof-of-concept study to demonstrate the first glycosidase-responsive polymeric system. This responsive polymeric system would be designed to depolymerise in response to glycosidase-triggered enzymatic activation and as such this study sought to demonstrate polymeric degradation in the first instance, and subsequently develop applications in biological contexts. A drug delivery system which encapsulates a therapeutic payload for release upon enzymatically-triggered depolymerisation in the tumour microenvironment may offer an innovative addition to the strategies hitherto developed in the fields of chemical biology and materials science.

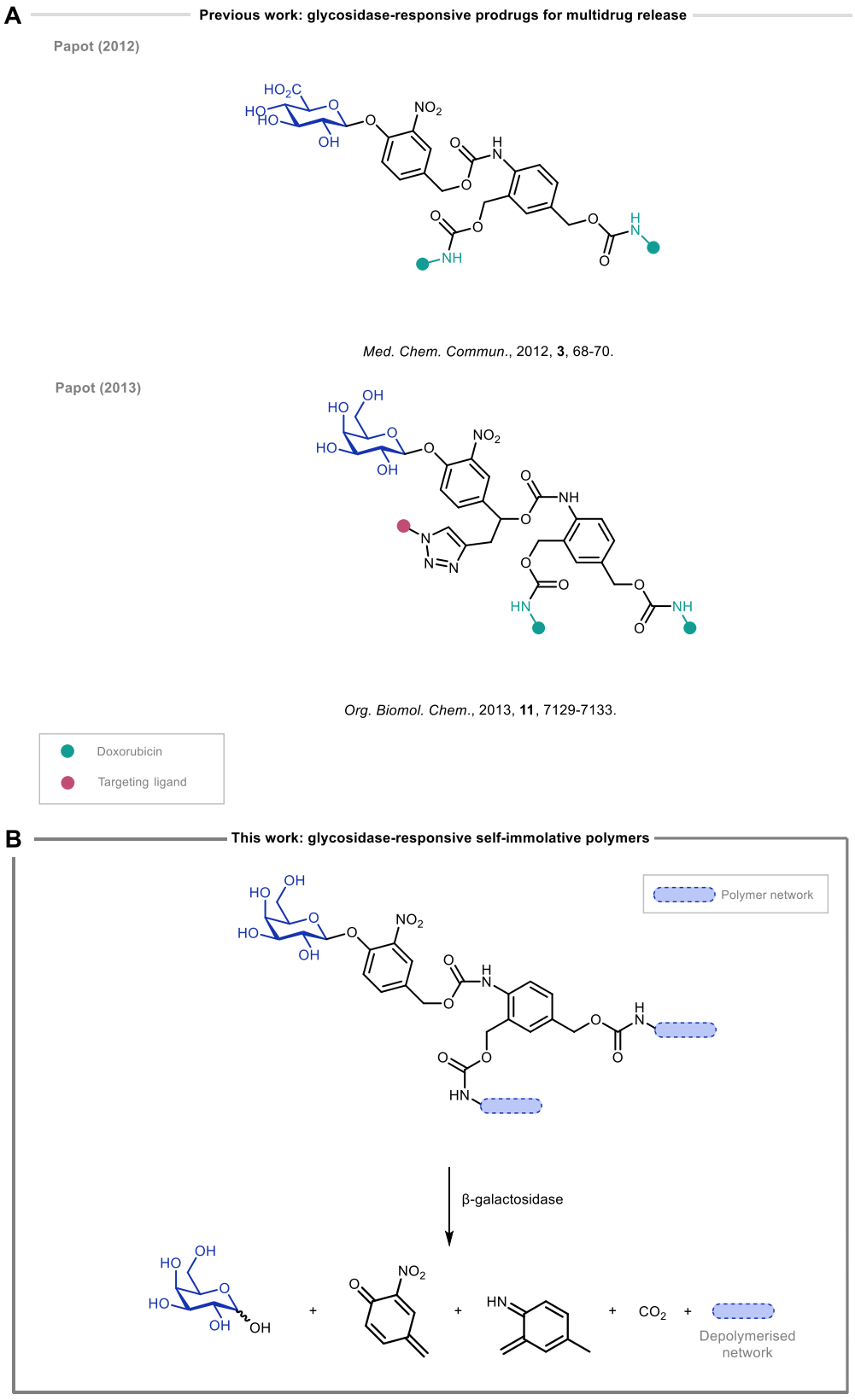

Figure 3.1 Development of glycosidase-responsive self-immolative scaffolds. A) Previous work: the application of self-immolative scaffolds to glycosidase prodrugs for multidrug release (Papot and co-workers, 2012 and 2013); B) This work: the application of self-immolative scaffolds to glycosidase-responsive degradable polymers.

3.3 Synthesis of carbohydrate-conjugate crosslinkers

In order to prepare polymers that would depolymerise upon activation by a desired trigger and stimuli, it was necessary to design crosslinkers bearing masking groups such that the final polymer network would be held together by cleavable groups. For glycosidase-responsive polymers, this would require bi- or trifunctional carbohydrate-conjugates bearing a minimum of two polymerisable groups which, upon activation, would lead to the separate release of both groups in a self-immolative fashion, disrupting the polymer network in a single self-amplified cleavage event. The design of suitable crosslinkers in this chapter was influenced by the 2'-bis(2-acetoxyethoxy)methyl (ACE) orthoester protecting group,[291] bis-acetal-based substrate design in fluorescence probes[292] and self-immolative scaffolds synthesised for multidrug release in prodrugs.[133]

3.3.1 Crosslinker design based on ACE nucleotide protecting group

Originally reported by Scaringe *et al.* in 1998,[291] the ACE 2`-hydroxyl protecting group has become an established choice for RNA nucleoside and oligonucleotide synthesis, facilitating final 2`-*O*-deprotection under mildly acidic aqueous conditions whilst being orthogonal to silyl ether protecting groups used for the 5`-hydroxyl group (**Fig. 3.2A**).[293] Crucially, installation of an orthoester type functionality on a glycosidic bond would, upon cleavage, give an unstable intermediate which would separately decompose, making for a potential degradable crosslinker. A retrosynthetic analysis of target molecule **118** (**Fig. 3.2B**) was carried out to identify the building blocks required to make this crosslinker. Transesterification of triethyl orthoformate (**120**) with **78** to give orthoformate **119** which could then be reacted with glucuronic acid hemiacetal **75** following a reported procedure described for RNA synthesis.[294]

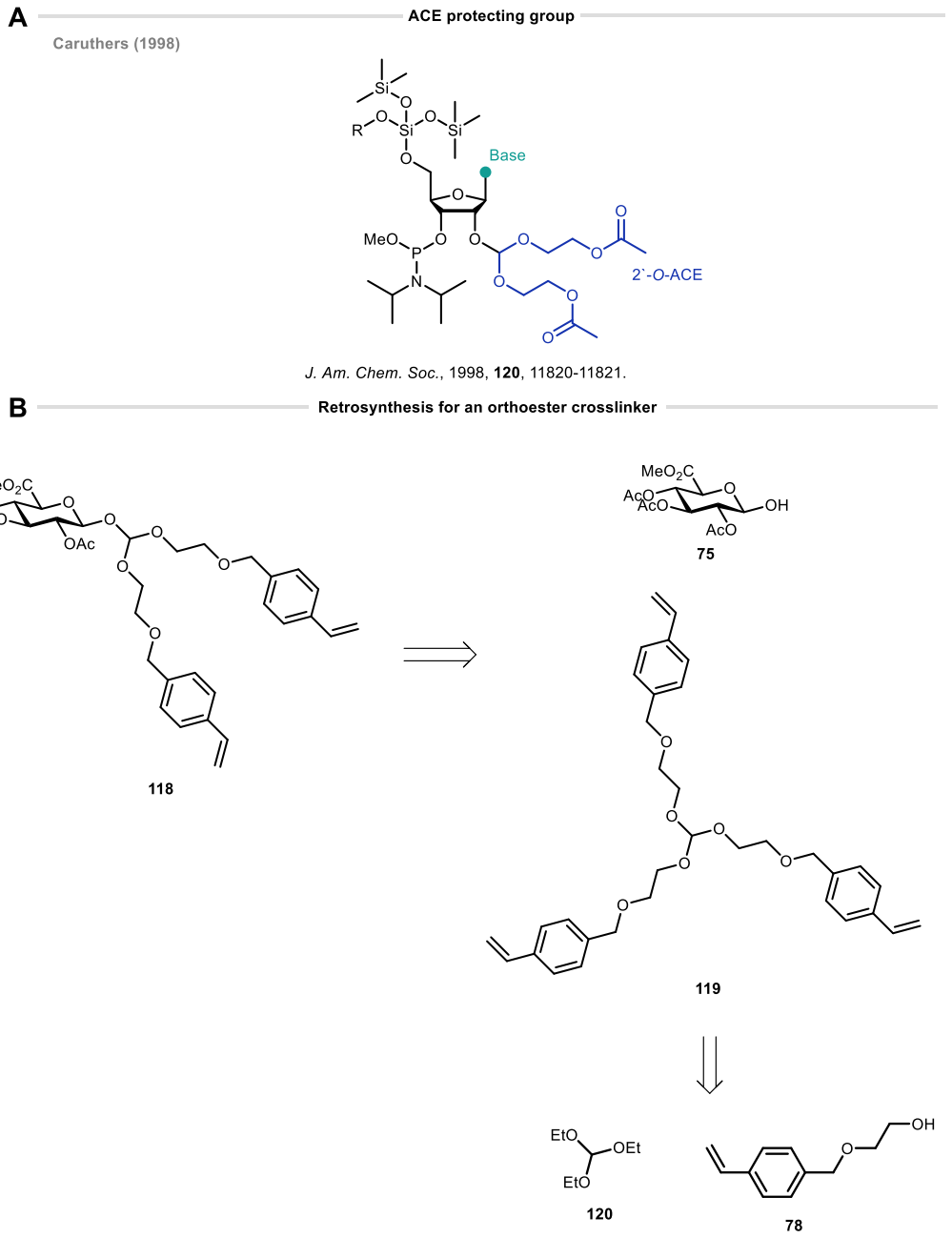

Figure 3.2 Orthoester crosslinker design. A) Acid-labile orthoester protecting group on the 2`-hydroxyl (2`-ACE) for RNA synthesis; B) Retrosynthetic analysis for **118** to give synthetic equivalent building blocks.

First, hydroxyl styrene derivative **78** was synthesised (**Scheme 3.1**).

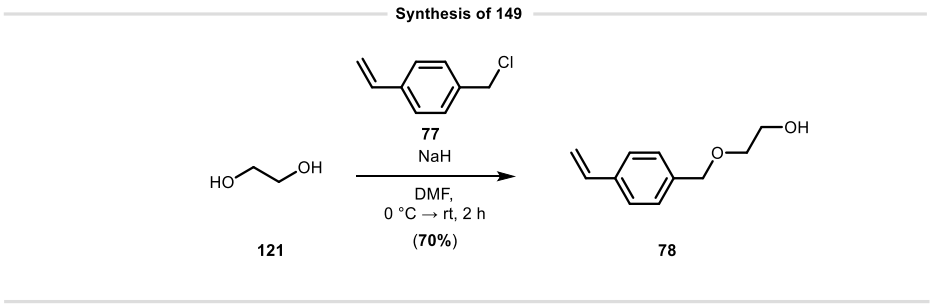

Scheme 3.1 Synthesis of **78.**

Williamson ether synthesis using ethylene glycol (**121**) and 4-vinylbenzyl chloride (**77**) with NaH gave **78** in 70% yield. Test reactions for the synthesis of orthoesters **119** and **122** required for coupling to a glucuronic acid derivative were then carried out (**Scheme 3.2**).

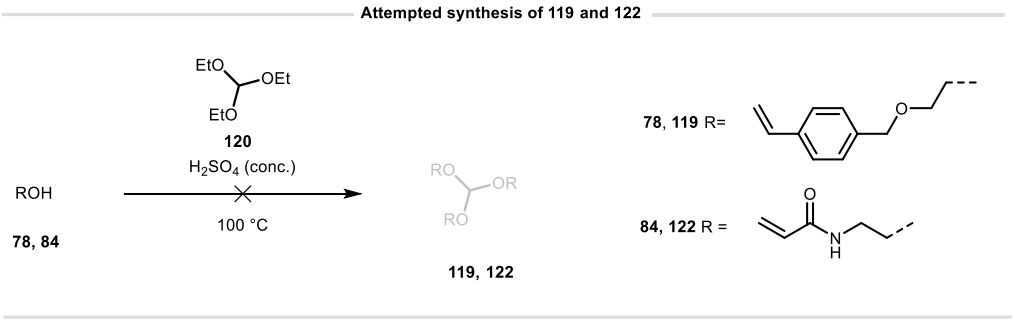

Scheme 3.2 Attempted synthesis of **119** and **122.**

These reactions were carried out using hydroxyl styrene **78** and *N*-hydroxyethyl acrylamide (**84**), reacting with triethyl orthoformate at 100 °C, using distillation apparatus to distil across liberated ethanol to drive the equilibrium to favour the target molecule. However, these high temperature conditions instead led to polymerisation of **78** and **84** and it was not possible to isolate the target molecules.

3.3.2 Crosslinker design based on bis-acetal-based substrates (BABS)

In 2017, Cecioni *et al.* reported Förster resonance energy transfer (FRET)-quenched bis-acetal based substrates (BABS) for glycosidases incorporating a hemiacetal leaving group which facilitates separation of a fluorophore and quencher upon glycosidic cleavage (**Fig. 3.3A**).[292] The structure of a crosslinker **123** bearing two polymerisable groups for separate release upon enzymatic activation, based on BABS, is shown in **Fig. 3.3B**.

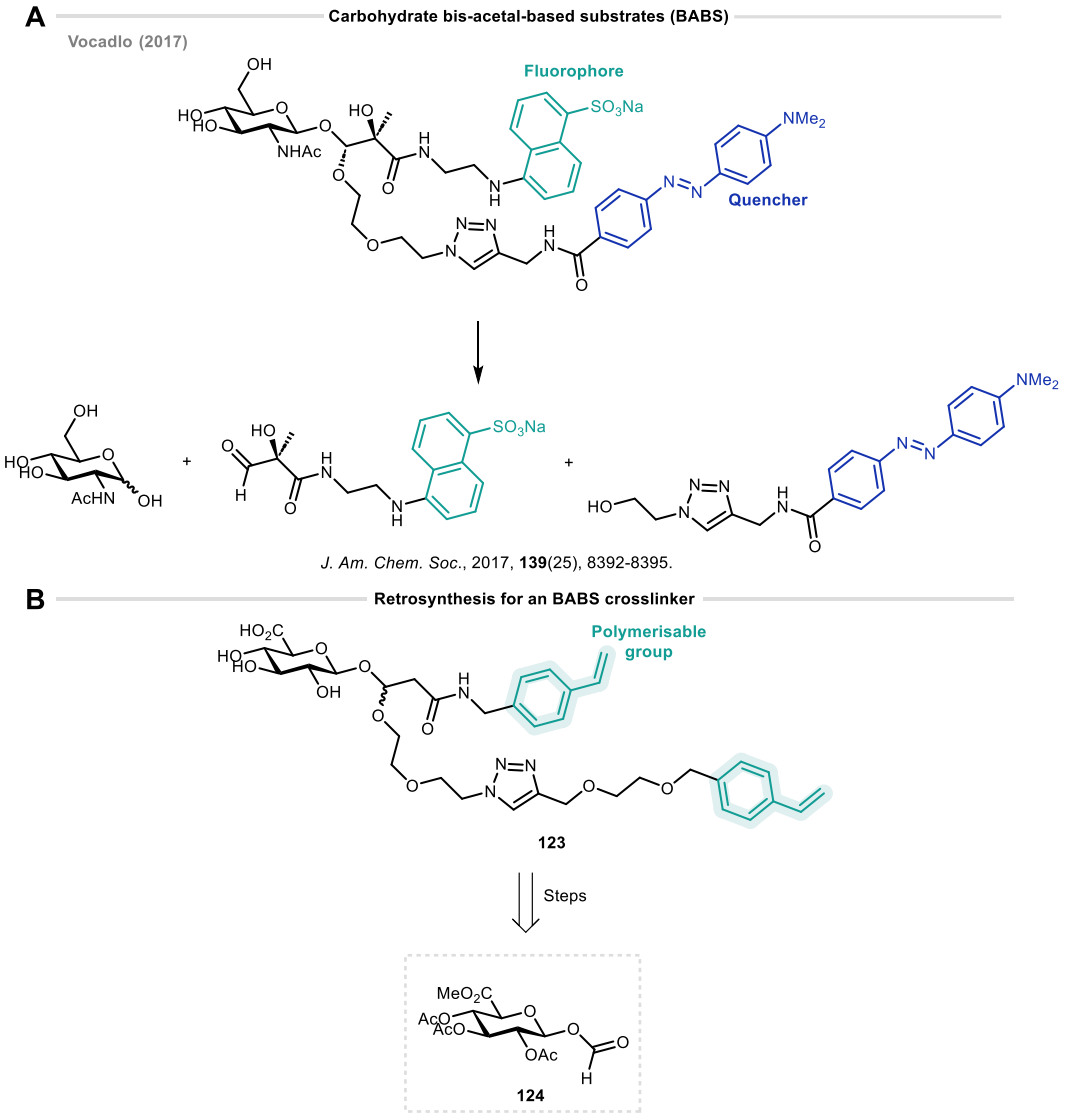

Figure 3.3 Bis-acetal-based substrates (BABS). A) BABS fluorescence-quenched probe design (Vocadlo and co-workers, 2017); B) The design for a potential BABS-based degradable crosslinker and identification of formyl glucuronide **124** as an early-stage intermediate for its synthesis.

The BABS-based degradable crosslinker **123** design incorporates the finding by Cecioni *et al.* in 2022 that reduction in steric congestion at the quaternary carbon proximal to the glycosidic bond enhanced enzymatic substrate processing; the target molecule therefore is an analogue of the least hindered BABS published in this study.[295] Formyl glucuronide **124** was identified as an essential early-stage intermediate required for this synthesis. Breakdown of the hemiacetal which is released upon enzymatic activation would be expected to be further enhanced by the acidic environment characteristic of malignant tumours if applied to a targeted drug delivery system.

For the preparation of a BABS crosslinker, it was first necessary to optimise the synthesis of formyl glucuronide **124** (**Scheme 3.3**).

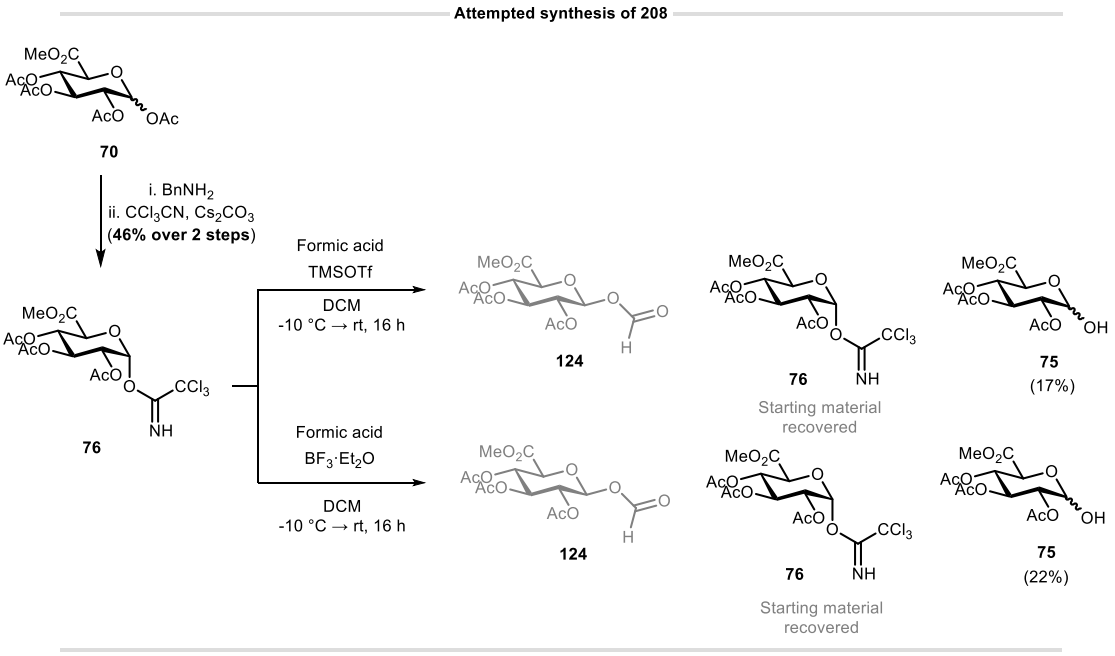

Scheme 3.3 Attempted synthesis of **124** via standard glycosylation conditions from trichloroacetimidate **76.**

Trichloroacetimidate **76** was formed in a 46% yield over two steps from acetylated glucuronic acid **70** via reaction with benzylamine, followed by reaction with CCl_3CN and Cs_2CO_3. Trichloroacetimidate glycosyl donor **76** was reacted with formic acid using either Lewis acid catalysts TMSOTf or $BF_3{\cdot}Et_2O$, however the target molecule was not isolated from either reaction, instead recovering trichloroacetimidate **76** and the hydrolysis product **75**. Recovery of the trichloroacetimidate **76**, a reactive intermediate, indicates that the Lewis acid catalysts were being quenched by the formic acid glycosyl donor, not forming the oxocarbenium intermediate, and therefore not allowing the reaction to proceed as desired.

In order to explore an alternative route, the use of a thioglycoside glycosyl donor was explored (**Scheme 3.4**), which was used by Cecioni *et al.* to generate a formylated galactose derivative.[295]

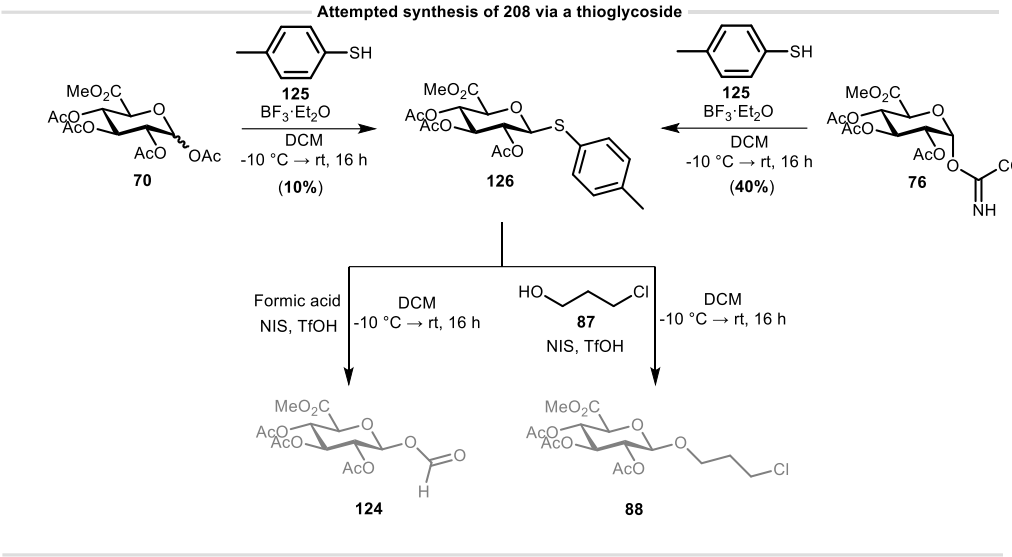

Scheme 3.4 Attempted synthesis of **124** via a thioglycoside glycosyl donor.

S-glycosylation of donors peracetylated glucuronic acid **70** and trichloroacetimidate **76** with 4-methylbenzenethiol (**125**) gave thioglycoside **126** in 10% and 40% yield respectively. Test *O*-glycosylations promoted by *N*-iodosuccinimide (NIS) and catalytic TfOH with acceptors formic acid and 3-chloropropan-1-ol **87** did not yield target glycosides **124** and **88** respectively, primarily recovering unreacted starting material. Due to this, this route was not taken forward.

3.3.3 Crosslinker design based on glycosidase-responsive prodrugs for multidrug release

The use of dendritic linkers for the preparation of self-immolative scaffolds for use in drug delivery, sensing and polymeric applications has been developed extensively by Shabat and co-workers. A design plan for a degradable self-immolative crosslinker using a dendritic linker **127**, building upon its initial incorporation into a dual-functionalised fluorescent reporter **128** (Shabat and co-workers, 2008) and subsequent expansion to a glycosidase-activated prodrug **129** for dual drug release (Papot and co-workers, 2012), is described in **Fig. 3.3**.

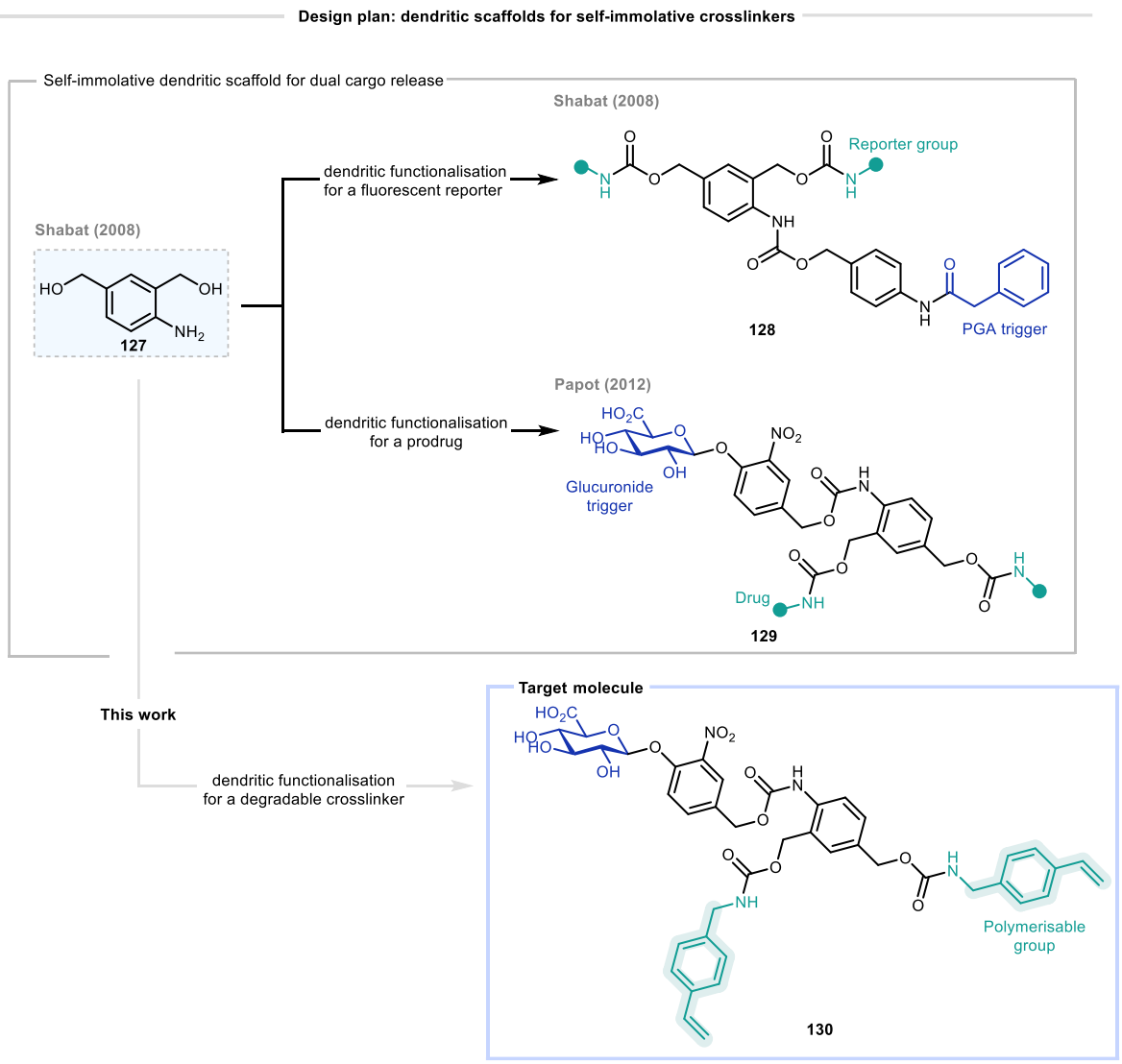

Figure 3.3 The design of a self-immolative dual-functionalised crosslinker based on previous work reported by Shabat and co-workers on dendritic scaffolds for dual cargo release.

Target molecule **130** was designed to employ a carbohydrate trigger group and have two coupled polymerisable groups such that, following polymerisation, enzymatic cleavage of the glycosidic bond would initiate the separate release and therefore breakdown of the crosslinked polymer network in a self-immolative fashion.

A series of test reactions were carried out to optimise the essential glycosylation step in the early part of the route (**Scheme 3.5**).

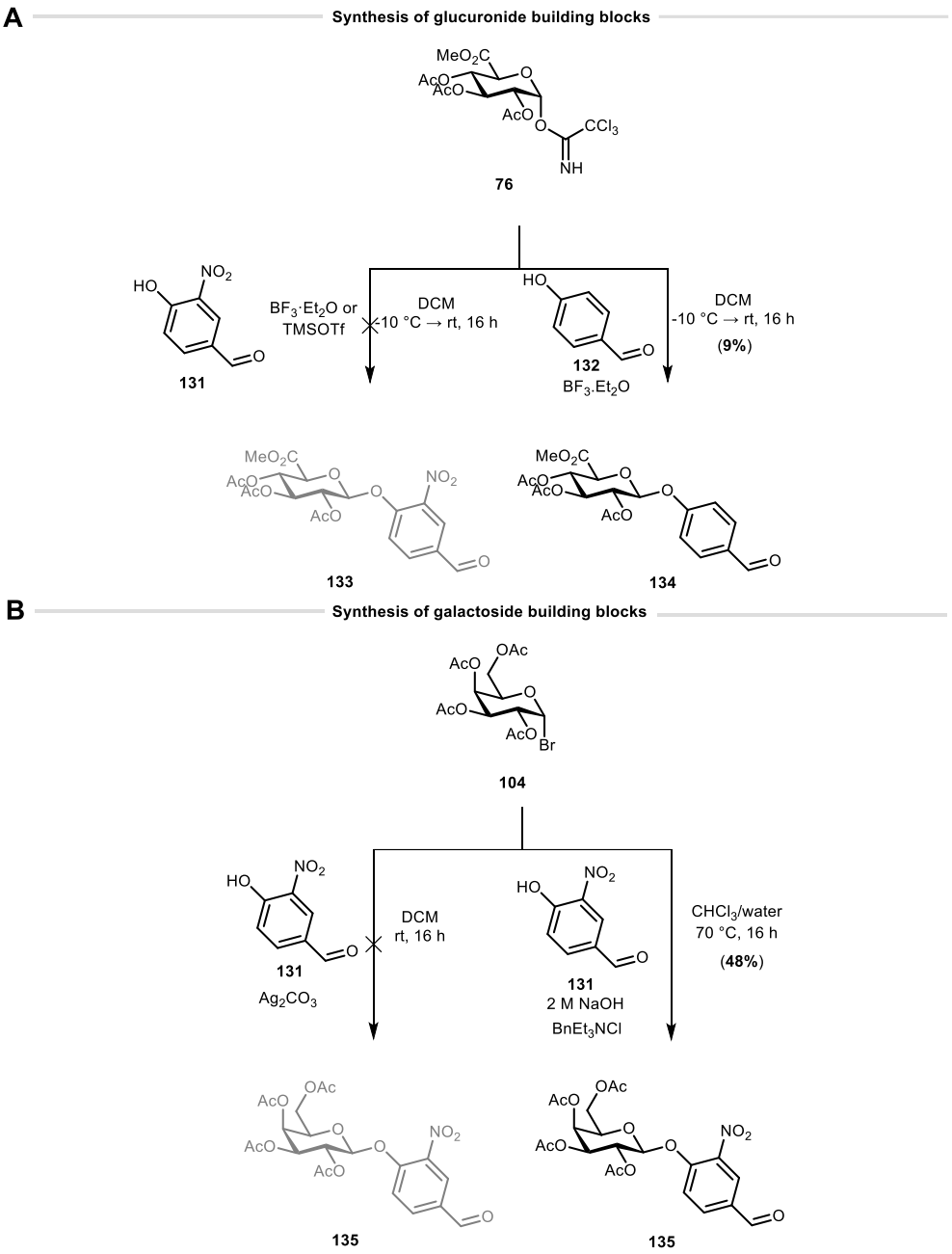

Scheme 3.5 Test glycosylations with 4-hydroxy-3-nitrobenzaldehyde and 4-hydroxybenzaldehyde. A) Glucuronic acid test reactions; B) Galactose test reactions.

Glucuronic acid trichloroacetimidate **76** was first reacted with 4-hydroxy-3-nitro-benzaldehyde (**131**) under standard glycosylation conditions using either $BF_3{\cdot}Et_2O$ and TMSOTf, recovering only the hydrolysis product with no isolation of glucuronide **133**. A test glycosylation with the more reactive 4-hydroxy-benzaldehyde (**132**) yielded the glycoside **134** in only 9% yield. Galactose bromide **104** was next explored as a donor for glycosylation with

4-hydroxy-3-nitro-benzaldehyde; the reaction using Königs-Knorr conditions did not proceed.

Glycosylations using phenolic acceptors have been reported to be challenging due to their weakened nucleophilicity under acidic conditions,[296] further enhanced in the case of acceptor **131** due to the presence of the electron-withdrawing nitro group on the aromatic ring. The reaction is made further challenging due to the combination of the highly disarmed nature of the glucuronic acid glycosyl donor **76** with the deactivated nature of the electron-poor glycosyl acceptor **131**. *C*-glycosylation also competes with the desired *O*-glycosylation reaction in the presence of a conventional Lewis acid catalyst when using phenolic acceptors.[297]

Kleine *et al.*[298] and Morelli *et al.*[299] have sought to circumvent these challenges through the optimisation of glycosylation by glycosyl halide donors under basic conditions, deprotonating the phenolic donor and activating it towards *O*-glycosylation. These researchers have found phase transfer catalysis conditions to be the most promising approach, with later work optimising these conditions further at elevated temperature using sodium hydroxide.[300] After applying these conditions and minimising the amount of phenolic acceptor **131** to 1.8 equivalents to aid the challenging chromatographic separation of phenol **131** from the product, using $BnEt_3NCl$ as the phase transfer catalyst, reproducible yields of 48% were obtained to give glucuronide **135**, which was found to be stable at room temperature after several months of storage.

Following glycosylation with 4-hydroxy-3-nitrobenzaldehyde (**131**), a reduction of the aldehyde was required to allow for further functionalisation (**Scheme 3.6**).

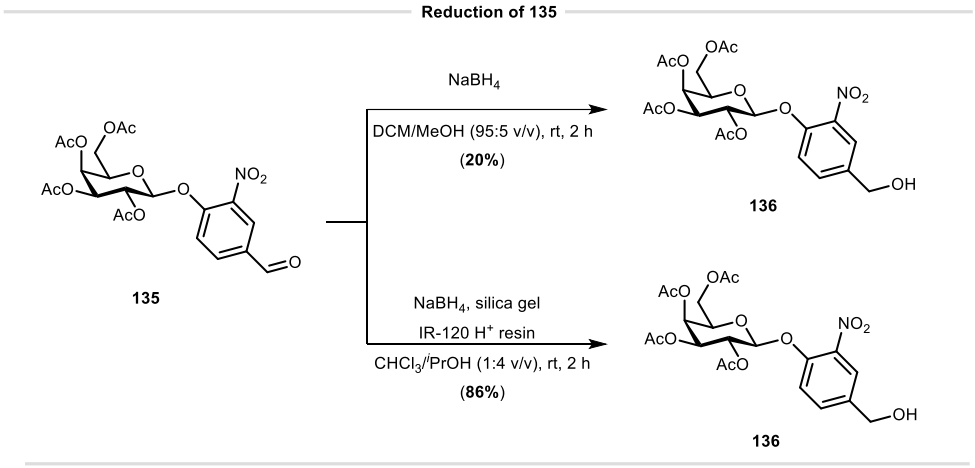

Scheme 3.6 Optimisation of reduction of aldehyde **135**.

The use of conventional reduction conditions in $NaBH_4$ to reduce **135** initially produced **136** in a low yield of 20%. This was rationalised by the reported propensity of the intermediate alkoxy species to induce acetyl group migration in this reaction. However, the addition of silica gel and an acidic ion exchange resin (IR-120 H^+ form) reported by Schuster *et al.*,[300] led to substantially improved yields of 86% of **136**, with no chromatographic purification required.

The dendritic linker **127** previously described in **Fig. 3.3** was next required, which allows for dual functionalisation in a self-immolative scaffold. The synthesis of this compound requires a four-step route starting from commercially available starting material 1,3-phenylene dimethanol **137**. **Scheme 3.7** describes the synthesis of nitrophenyl intermediate **139**.

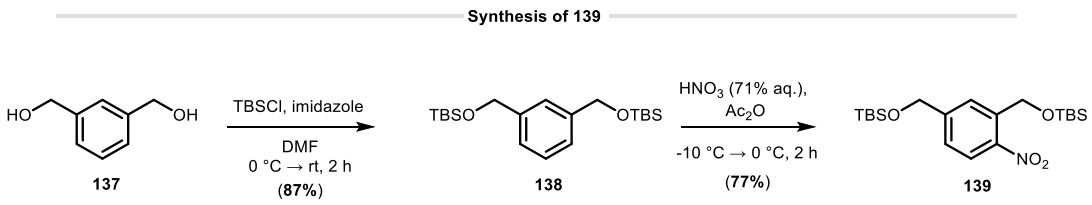

Scheme 3.7 Synthesis of nitrophenyl derivative **139**.

Tert-butyldimethylsilyl(TBS)-TBS-protection of the hydroxyl groups using TBSCl and imidazole gave **138** in 87% yield. Subsequent nitration in a mixture of 71% aq. HNO_3 and Ac_2O furnished nitrophenyl **139** in 77% yield.

The reduction of the nitro group proved more challenging and required optimisation (**Table 3.1**).

Table 3.1 Optimisation table for the Reduction of nitrophenyl **139** to aniline **140**.

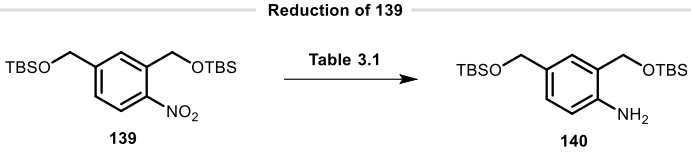

Entry	Reagents	Temperature	Yield
1	Pd/C, H_2	rt	18%
2	$Pd(OH)_2$, H_2	rt	16%
3	Fe, NH_4Cl	rt	No reaction
4	Pd/C, ammonium formate	rt	No reaction
5	Pd/C, ammonium formate	65 °C	58%

Hydrogenation with Pd/C (entry 1) and $Pd(OH)_2$ (entry 2) produced **140** in low yields of 18% and 16%, with TBS-deprotection being observed. No reaction took place with iron-promoted reducing metal reduction with Fe/NH_4Cl (entry 3) or Pd/C and ammonium formate (entry 4). However, Pd/C with ammonium formate at overnight reflux (entry 5) gave **140** in a good yield of 58% with no TBS deprotection observed.

Finally, fluoride-mediated TBS-deprotection was carried out **(Scheme 3.8)**. Providing a source of fluoride ions, this reaction typically proceeds efficiently with TBAF owing to the formation of the Si-F bond which is 30 kcal mol^{-1} stronger than the Si-O bond.[301, 302]

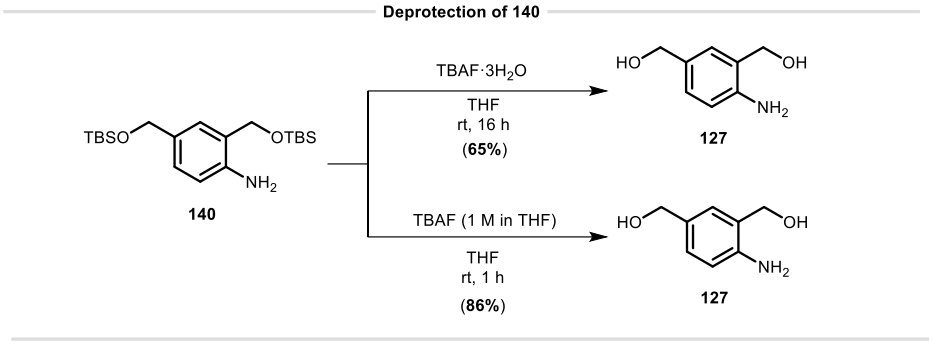

Scheme 3.8 TBS-deprotection of **140**.

A 1 M solution of TBAF in anhydrous THF was successfully used to deprotect from silyl protecting groups to form aniline **127** with two free hydroxyl groups in a yield of 86%. Yields were found to be superior when using an anhydrous solution of TBAF in THF in comparison to TBAF trihydrate, which gave yields of 65%, resulted in more challenging chromatographic purification and required longer reaction times. Next, activation of galactoside **136**, subsequent coupling to the dendritic linker and further activation was investigated (**Scheme 3.9**).

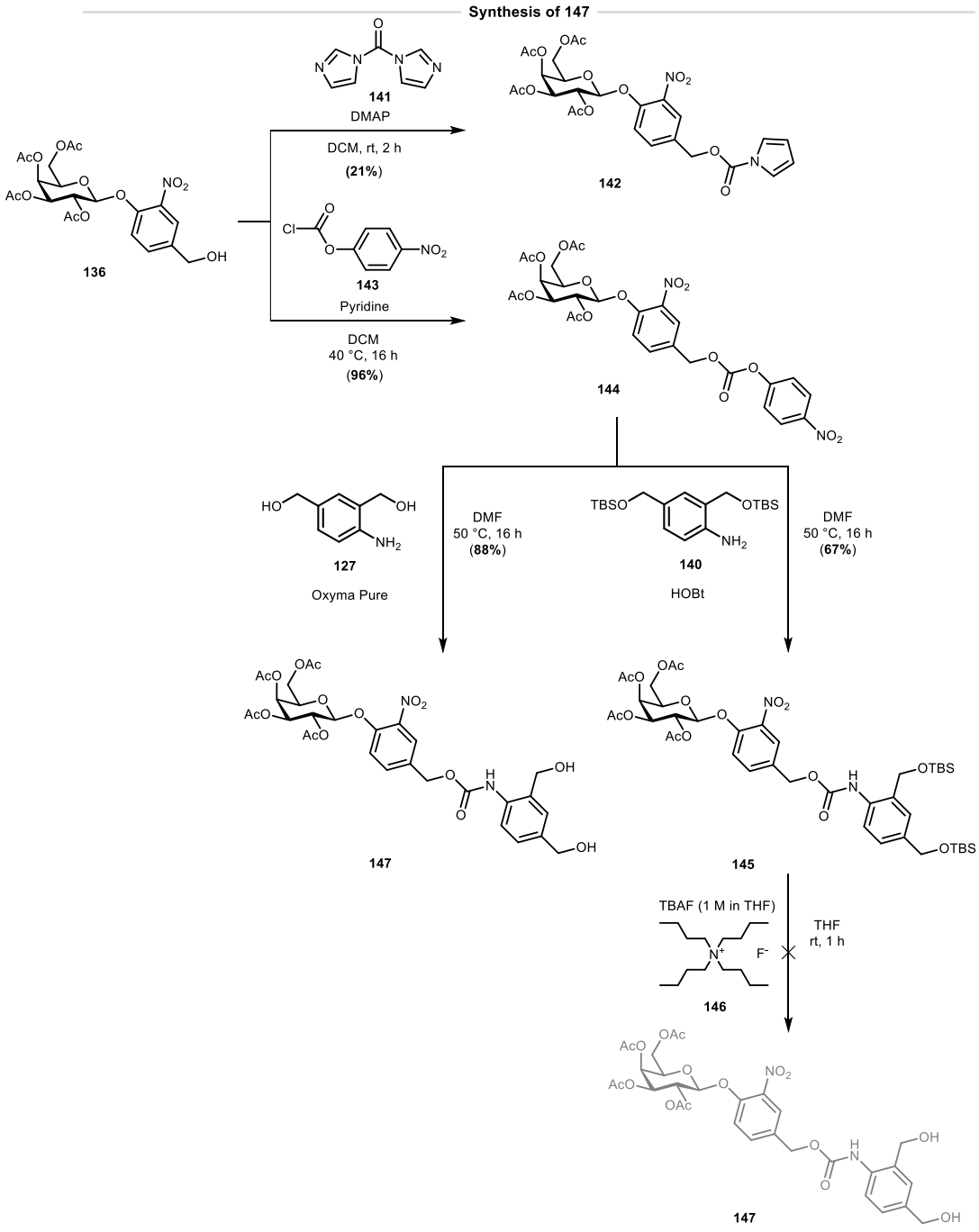

Scheme 3.9 Optimised synthetic route to galactoside diol **147**.

Activation of galactoside **136** was initially carried out using 1,1`-carbonyldiimidazole (CDI) (**141**), which furnished carbamate **142** in an unsatisfactory yield of 21%. Reaction with 4-nitrophenyl chloroformate (**143**) under reflux gave a dramatically improved yield of 96% in the preparation of activated carbonate **144**. This intermediate is reported to be room-temperature-stable and in our hands remained stable after several months under cold storage at -20 °C.[300] Carbonate **144** was then reacted with TBS-protected aniline **144** using HOBt to

give galactoside **145** in a 67% yield. However, the subsequent attempted TBS-deprotection using a 1 M solution of TBAF in THF produced an intractable complex mixture. Reports of TBAF-catalysed deacylation in the literature may elucidate the challenges associated with using this reagent with an acetylated galactose moiety in the molecule.[303, 304] Following this, coupling carbonate **144** with the deprotected aniline analogue **127** in the same conditions gave galactoside carbamate **147** at 88% yield with Oxyma Pure without the requirement of a subsequent TBAF(**146**)-mediated deprotection step. The dual activation of intermediate **147** was next investigated (**Scheme 3.10**).

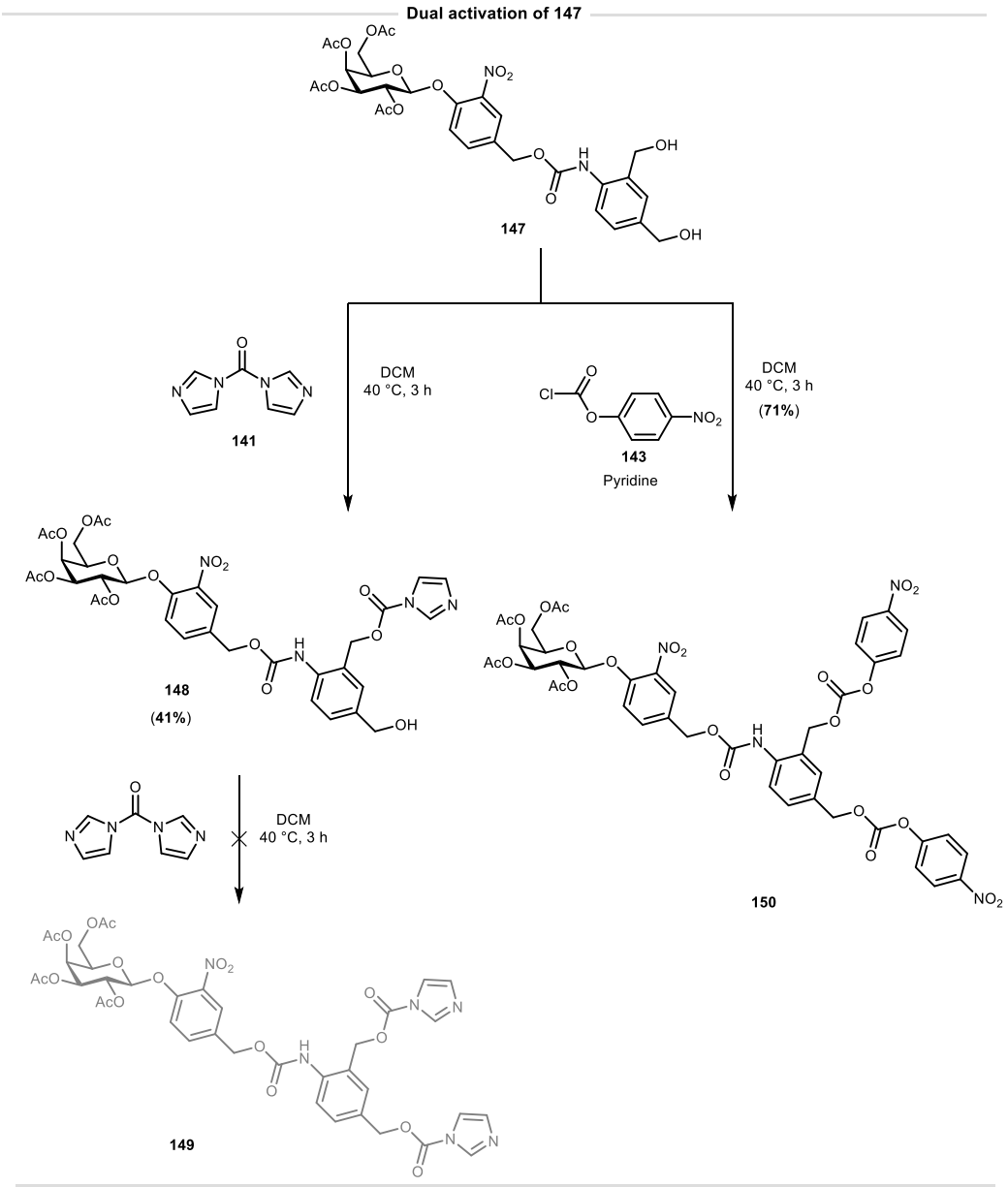

Scheme 3.10 Optimisation of the dual activation of intermediate diol **147** using CDI (**141**) and 4-nitrophenyl chloroformate (**143**).

Activation with CDI **141** was found to afford the monofunctionalised derivative **148** in 41% yield when the reaction was carried out under reflux for 3 hours; the difunctionalised target molecule **149** was not isolated. A subsequent attempt to install the additional imidazole unit through further reaction of monofunctionalised derivative **148** was unsuccessful, with minimal consumption of the starting material after 3 hours and degradation to diol **147** observed following overnight reaction.

Applying the same conditions used for the formation of activated carbonate **136** in **Scheme 3.9** to diol **147** produced difunctionalised carbonate **150** in 71% yield using 4-nitrophenyl chloroformate (**143**) under reflux for 3 hours.

With galactoside dicarbonate **150** in hand, it was next necessary to synthesise amines bearing polymerisable groups for coupling to the decarbonate, in order to generate the final β-galactosidase-responsive self-immolative crosslinker molecules. **Scheme 3.11** describes the synthesis of these amines.

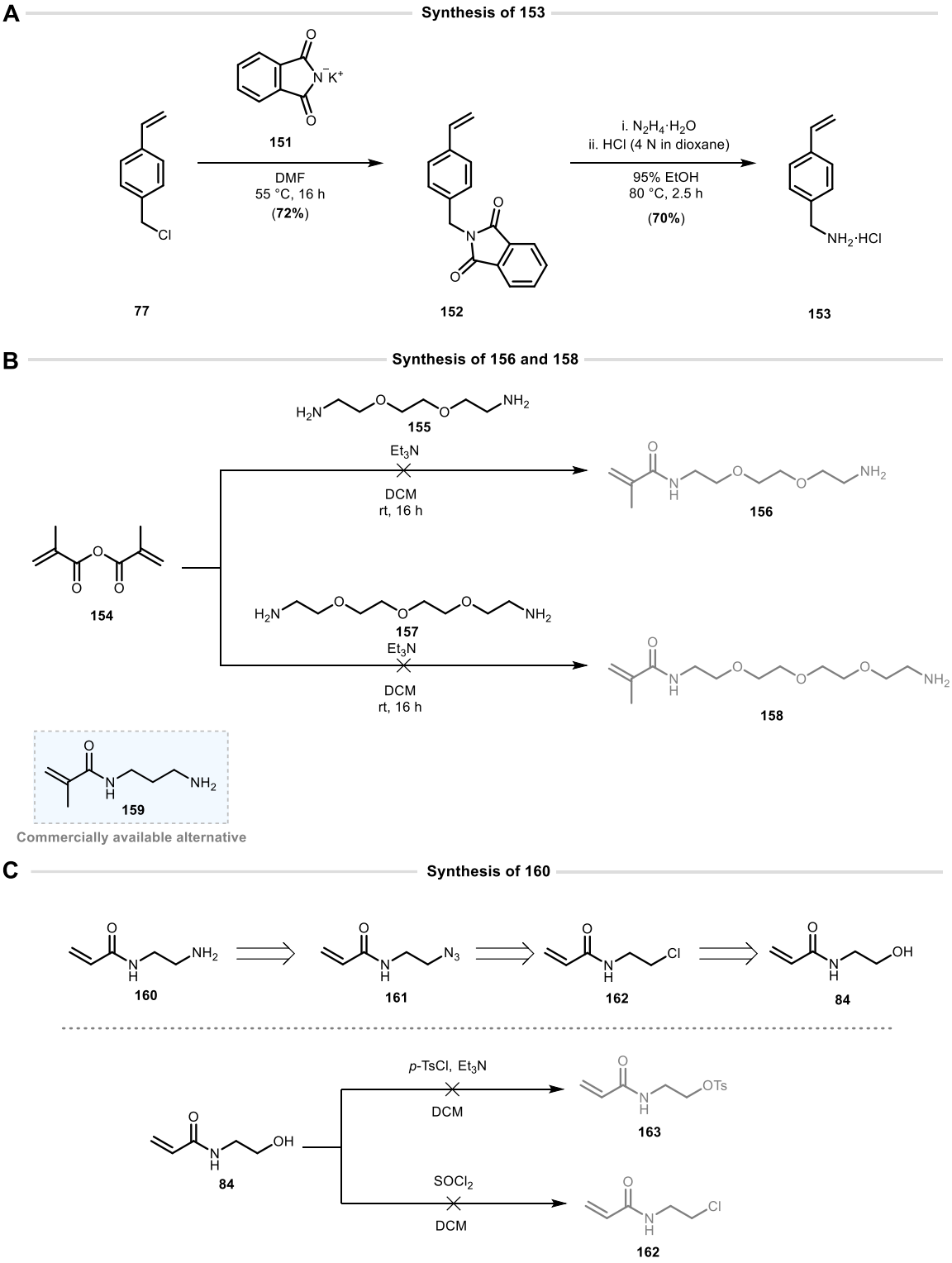

Scheme 3.11 Synthesis of amine-functionalised polymerisable groups. A) Styrene derivative **153**; B) Methacrylamide derivatives **156** and **158**, with commercially-available alternative **159**; C) Retrosynthesis of target amine and attempted synthesis of acrylamide derivative **160**.

A Gabriel amine synthesis was used to synthesise styrene amine derivative **153** (**Scheme 3.11A**). Reaction of 4-vinylbenzyl chloride **77** with potassium phthalamide **151** at 55 °C

furnished intermediate phthalimide **152** in 72% yield. Amine **153** was liberated following treatment with hydrazine at reflux in 70% yield, which was then converted into its corresponding hydrochloride salt via addition of a 4 N solution of HCl in dioxane for storage purposes.

In addition to using the styrene polymerisable group, other polymerisable groups were investigated with the aim of a suite of polymers with varying properties. The inclusion of more hydrophilic groups such as the amide in acrylamide and methacrylamide derivatives contributes to the polymer network's hydrophilicity and aids swelling, allowing the formation of hydrogels that can absorb significant volumes of water.[305] For this purpose, PEGylated methacrylamide derivatives of varying lengths were conceived, with the additional objective of enhancing enzyme accessibility to the polymer network.

Test reactions of anhydride **154** with 2,2`-(ethane-1,2-diylbis(oxy))diethanamine (**155**) and 1,11`-diamino-3,6,9-trioxaundecane (**157**) (**Scheme 3.11B**) did not yield target molecules **156** and **158** due to the formation of complex mixtures and challenging chromatographic purification regarding the separation of the starting material from the product. As an alternative, methacrylamide **159** was identified as a commercially available amine.

Scheme 3.11C describes a retrosynthetic analysis of acrylamide-based amine **160**, identifying building blocks for its synthesis via a Staudinger reduction, requiring azide **161**, or a Gabriel amine synthesis as an alternative. Firstly, it was necessary to functionalise *N*-hydroxyethyl acrylamide (**84**) with a suitable leaving group. Reactions with both *para*-toluenesulfonyl chloride (*p*-TsCl) and thionyl chloride ($SOCl_2$), to give the tosylated **163** and chlorinated **162** derivatives respectively, were attempted, however these target molecules were not isolated.

Therefore, styrene-based amine **153** and methacrylamide-based amine **159** were identified as appropriate amines bearing polymerisable groups for coupling to the activated scaffold **150**. These couplings are described below in **Scheme 3.12**.

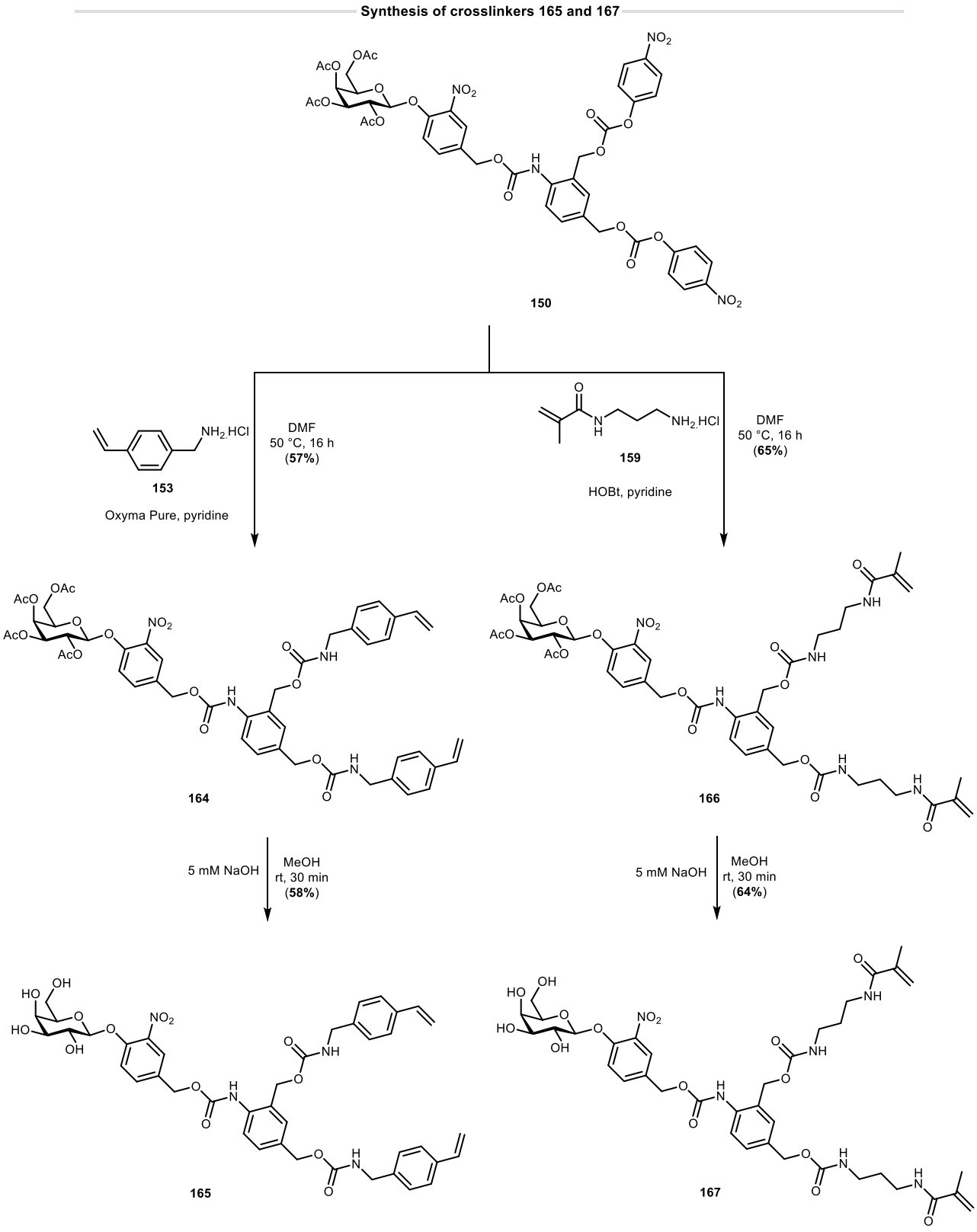

Scheme 3.12 Final steps of the synthesis of β-galactosidase-responsive self-immolative crosslinkers **165** and **167**.

Coupling of activated carbonate **150** with styrene amine derivative **153** using Oxyma Pure furnished carbamate **164** in 57% yield, with subsequent deprotection using a 5 mM NaOH

solution in MeOH produced the final target compound **165**. In the case of the methacrylamide **159**, use of HOBt for the coupling was found to be most effective, with the monosubstituted by-product being primarily isolated when using Oxyma Pure. With HOBt, the disubstituted target molecule **166** was isolated 65% yield. Deprotection using 5 mM NaOH gave the final target compound **167** in 64% yield. The monosubstituted product **168** is shown below in **Fig 3.4**.

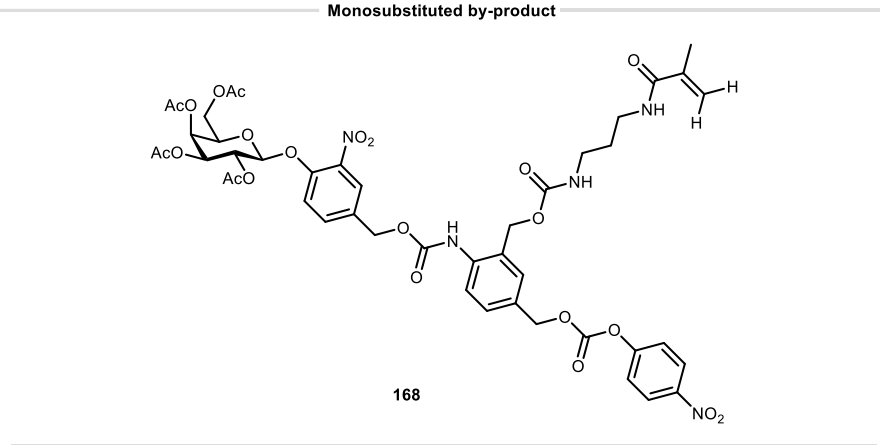

Figure 3.4 Monosubstituted by-product **168**.

In addition to dual-functionalised crosslinkers, it was sought to develop tri-functionalised crosslinkers for enhanced polymer crosslinking and to allow for the investigation of the generated polymers for their response to enzymatic activation. The design plan for a target molecule which extends work by Scheeren and co-workers to incorporate a dendritic linker that would release three end groups separately upon enzymatic activation and is outlined in **Fig. 3.5**.

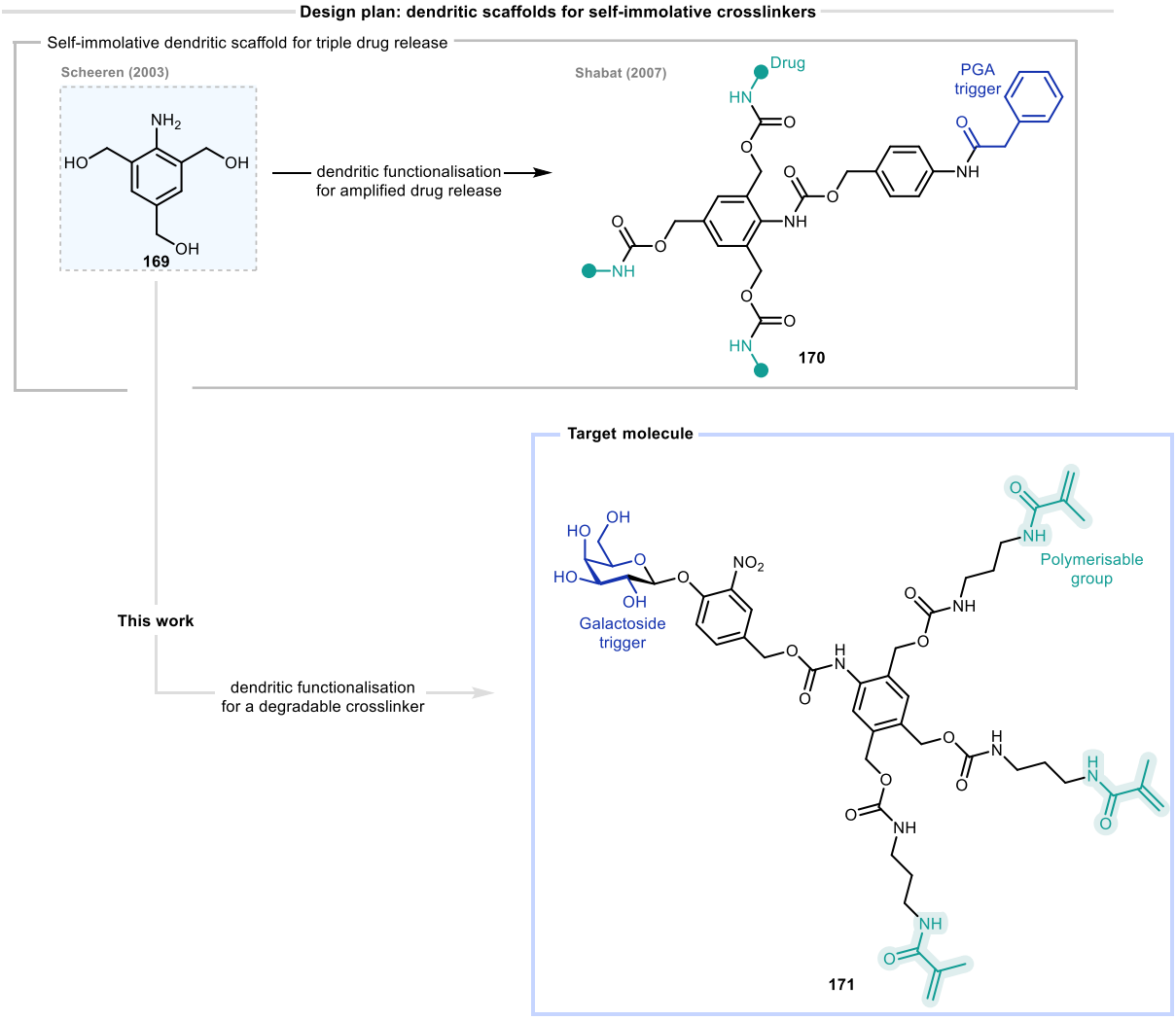

Figure 3.5 The design of a self-immolative tri-functionalised crosslinker based on previous work reported by Shabat and co-workers on dendritic scaffolds for triple cargo release.[134]

In 2003, de Groot *et al.* reported the design of "cascade-release dendrimers" such as **170** for the multiple release of the end groups of the dendrimers' termini upon a single triggering event.[243] The end of this study highlighted a dendritic core design which may be applied to more advanced systems, suitable for trifunctionalisation and demonstrated the lack of toxicity of this core. This is a promising result for its use in biological contexts, as non-toxic degradation properties are an important requirement for biocompatible polymeric systems. This triple-release linker **169** provided the essential core for the design of trifunctionalised target molecule crosslinker **171** and this would represent its first application in an activatable system.

Application of the optimised synthesis for the diol analogue to benzene-1,3,5-trityltrimethanol starting material **172** successfully generated dendritic core **169** (**Scheme 3.13**).

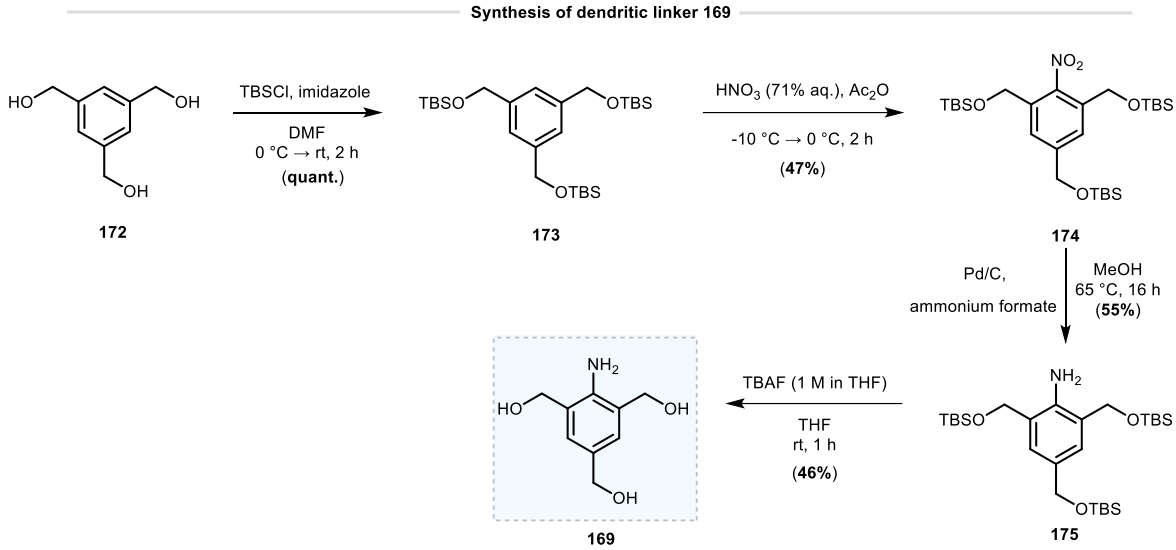

Scheme 3.13 Synthesis of dendritic linker **169**.

TBS protection of 1,3,5-trityltrimethanol **172** gave phenyl derivative **173** in quantitative yield, which was subsequently nitrated to furnish nitrophenyl derivative **174** in 47% yield. Reduction of this compound using Pd/C and ammonium formate under reflux gave **175** in 55% yield, which was finally TBS-deprotected using a 1 M solution of TBAF in anhydrous THF to provide triol **169** in 46% yield. Chromatographic purification of the final target compound proved challenging due to coelution of unreacted TBAF. Switching flash column chromatography mobile phase from a 2% → 5% MeOH in MeOH gradient to an isocratic run using 5% MeOH in EtOAc proved successful in negating these issues.

The coupling of this dendritic linker to glycoside **144** and the following steps in this route are described in **Scheme 3.14** below.

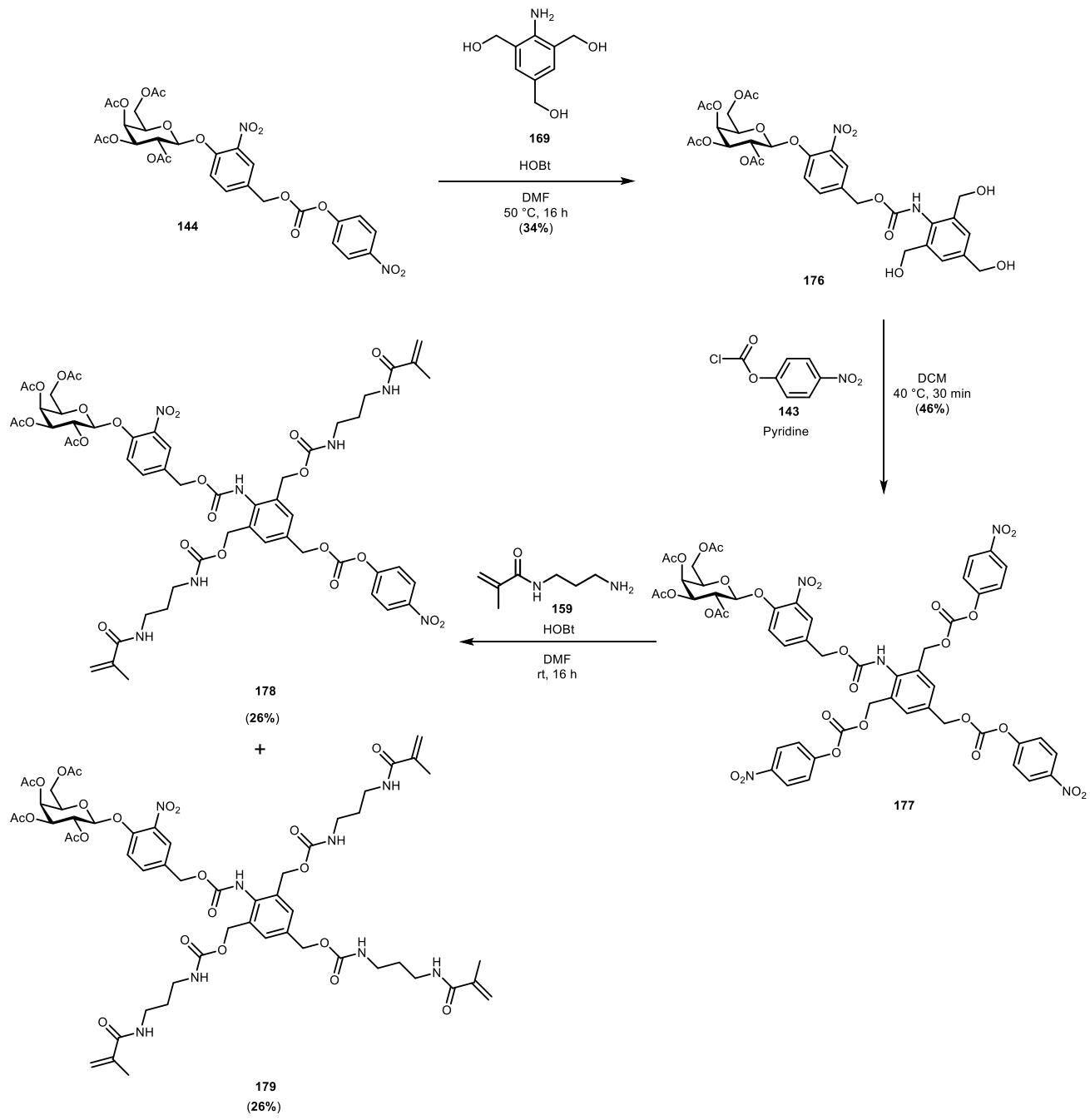

Scheme 3.14 Synthesis of trifunctionalised galactoside **179**.

Coupling of linker **169** to galactoside **144** using HOBt at 50 °C gave galactoside triol **176** in 34% yield. Subsequent activation using 4-nitrophenyl chloroformate **143** under reflux was achieved in 46% yield to provide activated tricarbonate **177**. Coupling with methacrylamide amine **159** using HOBt at room temperature furnished both disubstituted side-product **178** and the desired trifunctionalised derivative **179** both in 26% yield.

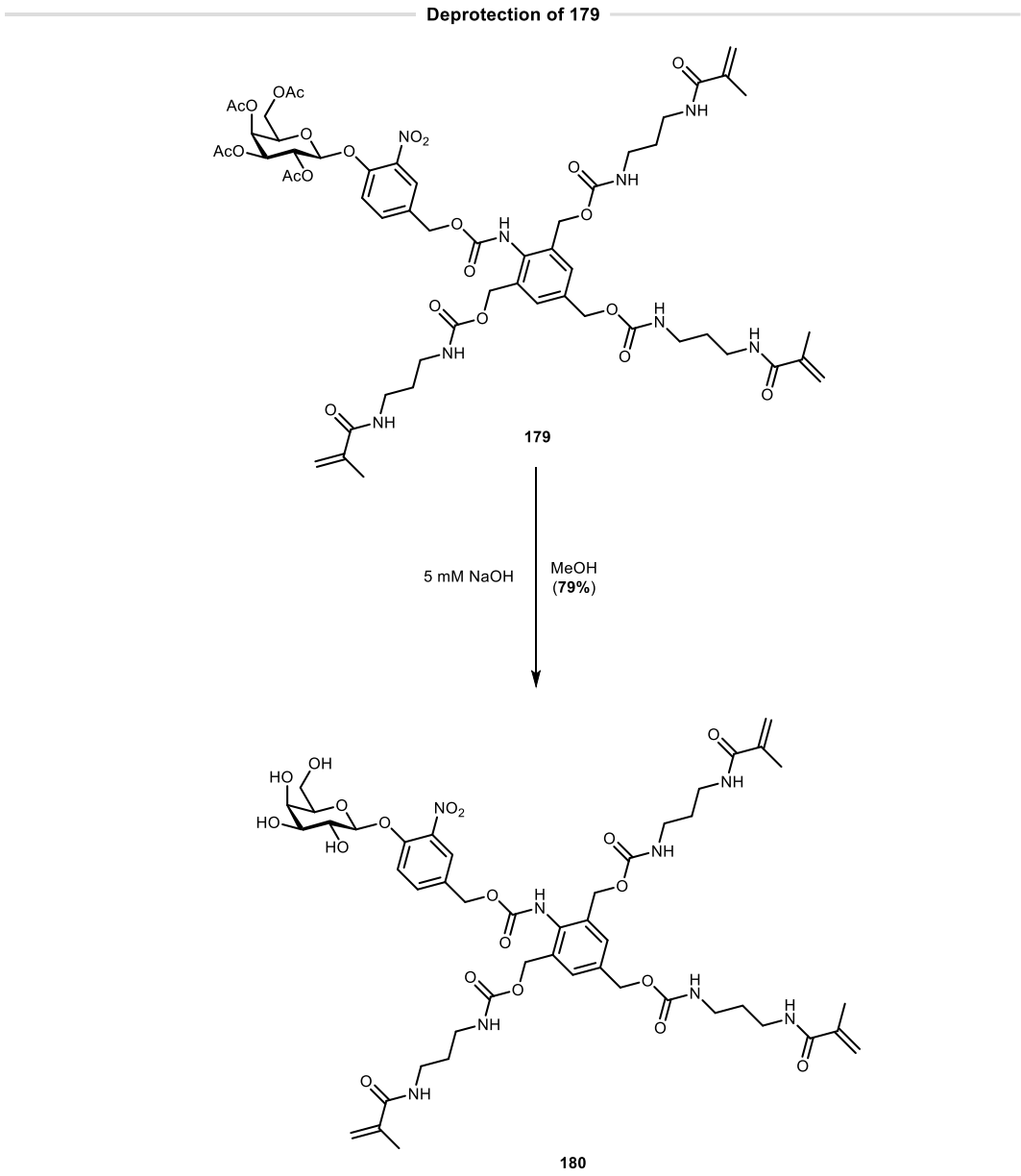

Scheme 3.15 Deprotection of galactoside **179**.

Deprotection of galactoside **179** in 5 mM NaOH in MeOH provided final target compound **180** in a yield of 79%.

3.4 Polymerisation of β-galactosidase-responsive self-immolative crosslinkers

With a series of self-immolative crosslinkers synthesised, it was next sought to develop suitable photoresists and optimise the polymerisation conditions via two-photon polymerisation (TPP). This work was carried out in collaboration with Dr Alexa Ennis and Prof. Larisa Florea. The general TPP protocol and experiments designed to validate a response of the β-galactosidase-responsive polymers are described in **Section 2.1.1.1** and **2.2.1.1** respectively.

3.4.1 Polymerisation of difunctional styrene crosslinker 165

Dual-functionalised styrene crosslinker **247** was incorporated into a series of photoresists in efforts to optimise the TPP printing to generate polymers crosslinked with a β-galactosidase-labile network. The crosslinker (galactoside **180**), photoinitiator (DEATC **95**) and monomer (HEAA **84**, acrylamide **92**, PEG-PEA **181** and styrene **182**) components of these photoresists are shown in **Fig 3.6**. In addition, a maximum of 50 wt% of DMSO was used as a solvent.

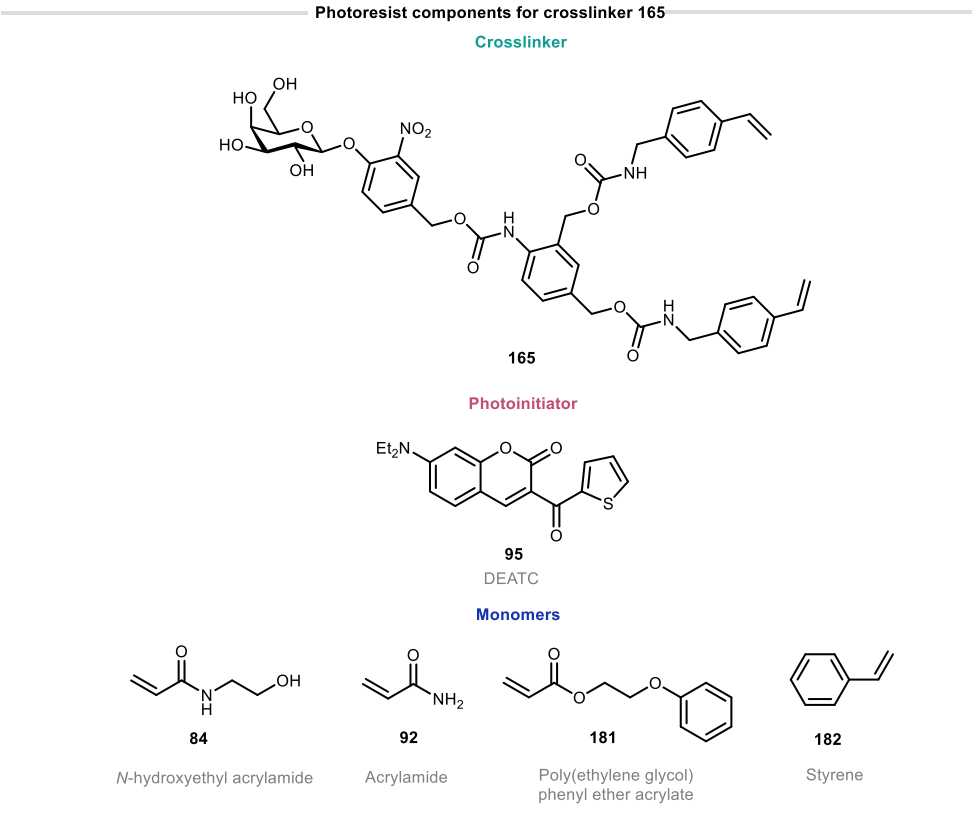

Figure 3.6 The different components used for photoresists for polymerisation of crosslinker **165**.

These components were incorporated into the photoresists described below in **Table 3.2.**

Table 3.2 Optimisation table for the development of a photoresist for the TPP of crosslinker **165**. Crosslinker mol % relative to the amount of monomer used, DEATC used as the photoinitiator.

Entry	Crosslinker mol%	Monomer	Solvent weight%	Outcome
1	100	-	40	No printing
2	40	HEAA	50	No printing
3	50	PEG-PEA	50	No printing
4	40	PEG-PEA	40	Printing
5	25	PEG-PEA	5	No printing
6	35	Acrylamide	50	No printing
7	15	Acrylamide	50	No printing
8	25	Styrene	50	No printing

Attempts to polymerise crosslinker **165** without a comonomer (entry 1) were not successful, so comonomer HEAA was added (entry 2) to the photoresist composition. In this case, poor solubility and an observed emulsion precluded printing. Changing the monomer to PEG-PEA (entries 3 to 5) formed photoresist with much improved solubility, however printing polymer structures through the optimisation of various TPP parameters including the laser power, scan speed and slicing proved challenging. Under forcing conditions at high laser powers (150%), some printing was observed (entry 4). Use of acrylamide (entries 6, 7) and styrene did not aid polymerisation, with no printing observed and poor solubility in these photoresist cocktails respectively.

The full table describing the composition of the photoresist which resulted in the successful polymerisation at high laser powers is described in **Table 3.3.**

Table 3.3 Composition of the photoresist successfully used to polymerise crosslinker **165**, composed of crosslinker **165**, monomer PEG-PEA, photoinitiator DEATC and DMSO as solvent. Mol% is the molar ratio relative to the amount of crosslinker **165** used.

Compound	Mass / mg	Mol%	Weight %
Crosslinker **165**	5	100	35
PEG-PEA	2	102	14
DEATC	0.4	20	3
DMSO	7	-	49

These polymer microstructures were next treated with β-galactosidase to investigate their response to enzymatic activation. The images taken of selected microstructures before the experiment, following incubation with buffer and following ten repeated incubations with β-galactosidase are shown in **Fig. 3.7**.

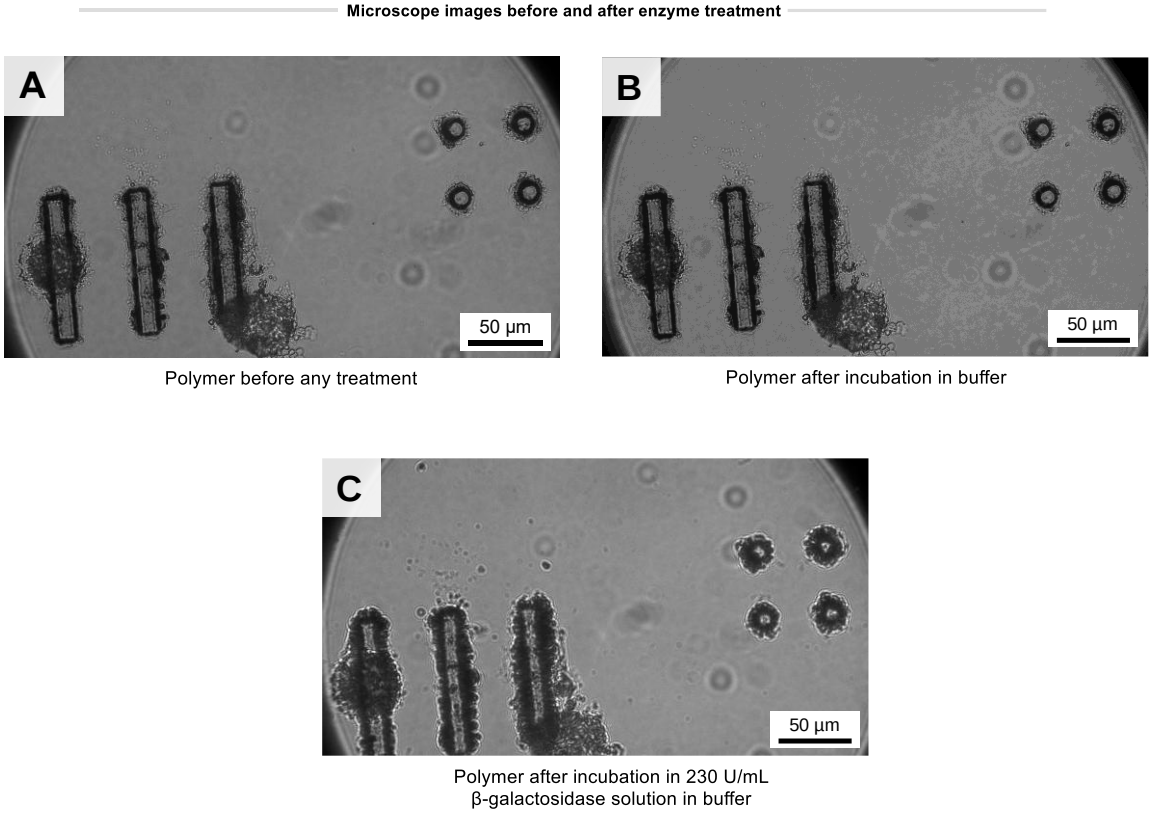

Figure 3.7 Images of the polymer associated with the photoresist from Table 3.3. A) Image of selected microstructures of the polymer prior to any treatment. B) Image of microstructures following incubation with pH 4.5 phosphate-citrate buffer at 30 °C overnight. C) Image of microstructures

following incubation with a 230 U/mL β-galactosidase in pH 4.5 phosphate-citrate buffer at 30 °C after 5 days (2 fresh additions of enzyme per day as per **Fig. 2.14**).

The stability of the structures at 30 °C in pH 4.5 phosphate-citrate buffer was confirmed (**Fig. 3.7B**), however little to no noticeable degradation was observed following repeated enzyme treatment under these conditions (**Fig. 3.7C**). The high laser powers required for polymerisation and consequent high degree of crosslinking may contribute to more challenging degradation of the polymer network.

Following this, polymerisation of crosslinker **165** was carried out using bulk UV polymerisation using the photoresist described in **Table 3.4**.

Table 3.4 Composition of the photoresist successfully used to polymerise crosslinker **247** via bulk UV polymerisation, composed of crosslinker **165**, monomer PEG-PEA, photoinitiator phenylbis(2,4,6-trimethylbenzoyl)phosphine oxide (PBPO) and DMSO as solvent. Mol % is the molar ratio relative to the amount of PEG-PEA used.

Compound	Mass / mg	Moles / mmol	Mol%	Weight %
Crosslinker **165**	5	0.006	50	35
PEG-PEA	4	0.006	100	40
PBPO initiator	0.6	0.001	12.5	6
DMSO	5	-	-	51

This photoresist was successfully used to form polymers which incorporate the β-galactosidase-responsive crosslinker **165**. A selected polymer was removed from the silicone mould and an enzyme degradation test carried out (**Fig 3.8**).

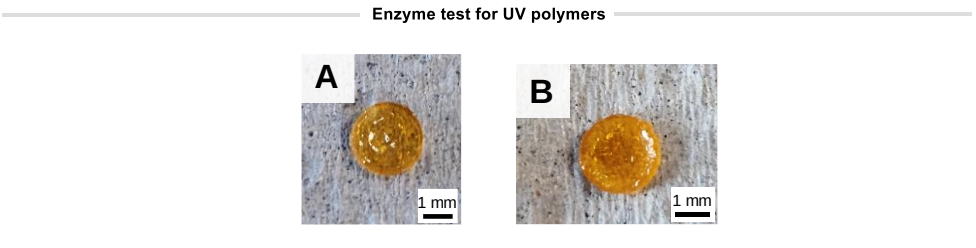

Figure 3.8 β-galactosidase test for UV polymers from photoresist in Table 3.4. A) Image before enzyme treatment; B) Image after enzyme treatment (100 U/mL, 30 °C, repeated ten times).

No observable degradation was observed from this experiment.

3.4.2 Polymerisation of difunctional methacrylamide crosslinker 167

Dual-functionalised methacrylamide crosslinker **167** was next incorporated into a series of photoresists in efforts to optimise the TPP printing to generate polymers crosslinked with a β-galactosidase-labile network for this crosslinker. The increased hydrophilicity of the methacrylamide groups was anticipated to improve the hydrogel properties of the polymers. The components of these photoresists are shown in **Fig 3.9.**

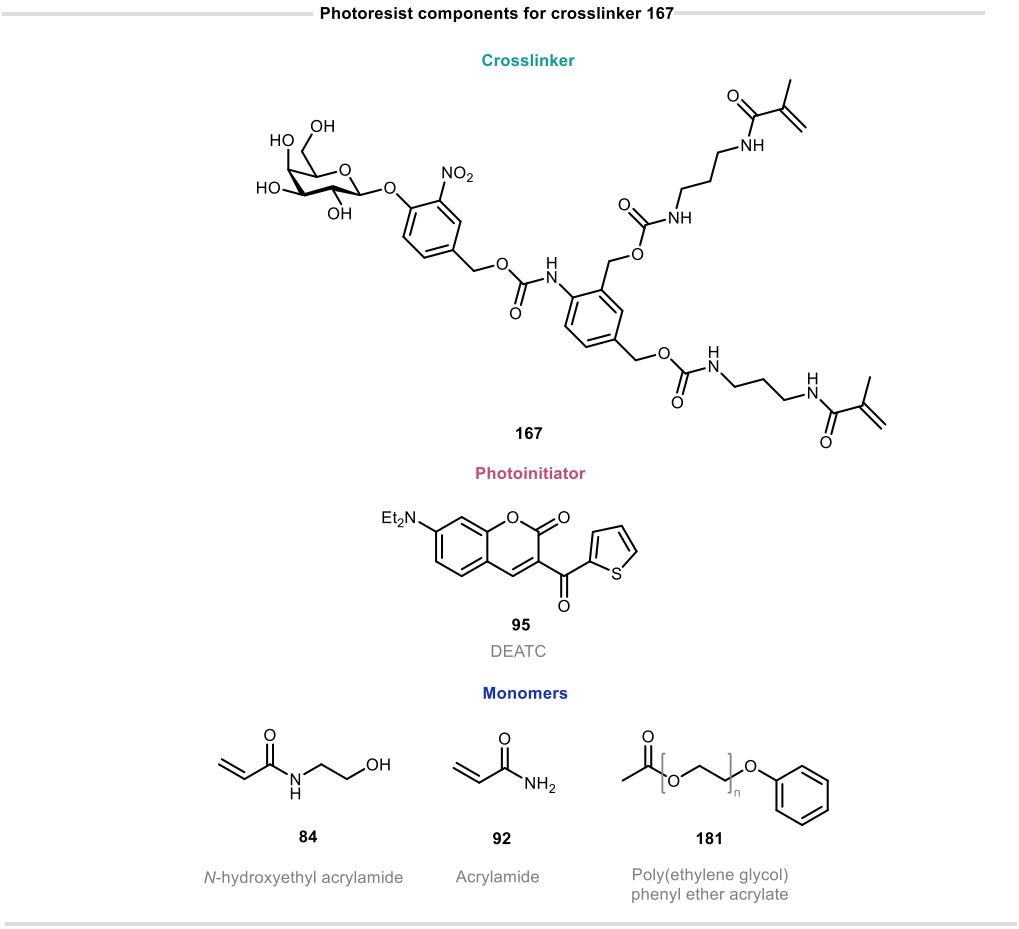

Figure 3.9 The components used to develop photoresist compositions for crosslinker **167**.

These components were incorporated into the photoresists described below in **Table 3.5** aiming to optimise the polymerisation of crosslinker **167** using TPP.

Table 3.5 Optimisation table for the development of a photoresist for the TPP of crosslinker **167**. Crosslinker mol % relative to the amount of monomer used, DEATC used as the photoinitiator.

Entry	Crosslinker mol%	Monomer	Solvent weight%	Outcome
1	25	PEG-PEA	20	-
2	40	PEG-PEA	50	-
3	40	PEG-PEA	40	-
4	25	HEAA	40	-
5	20	Acrylamide	40	-

Unfortunately, no appreciable polymerisation via TPP was observed under the conditions attempted.

3.4.3 Polymerisation of trifunctional methacrylamide crosslinker 180

Following challenges encountered in forming polymers from the dual-functionalised crosslinkers **165** and 167, a trifunctionalised derivative **180** was designed and synthesised as described previously in **Scheme 3.14.** This crosslinker **180** was then incorporated into a series of photoresists using components described in **Fig 3.10**. The PEG-PEA monomer was selected as it displayed the most promising results from the previous crosslinkers.

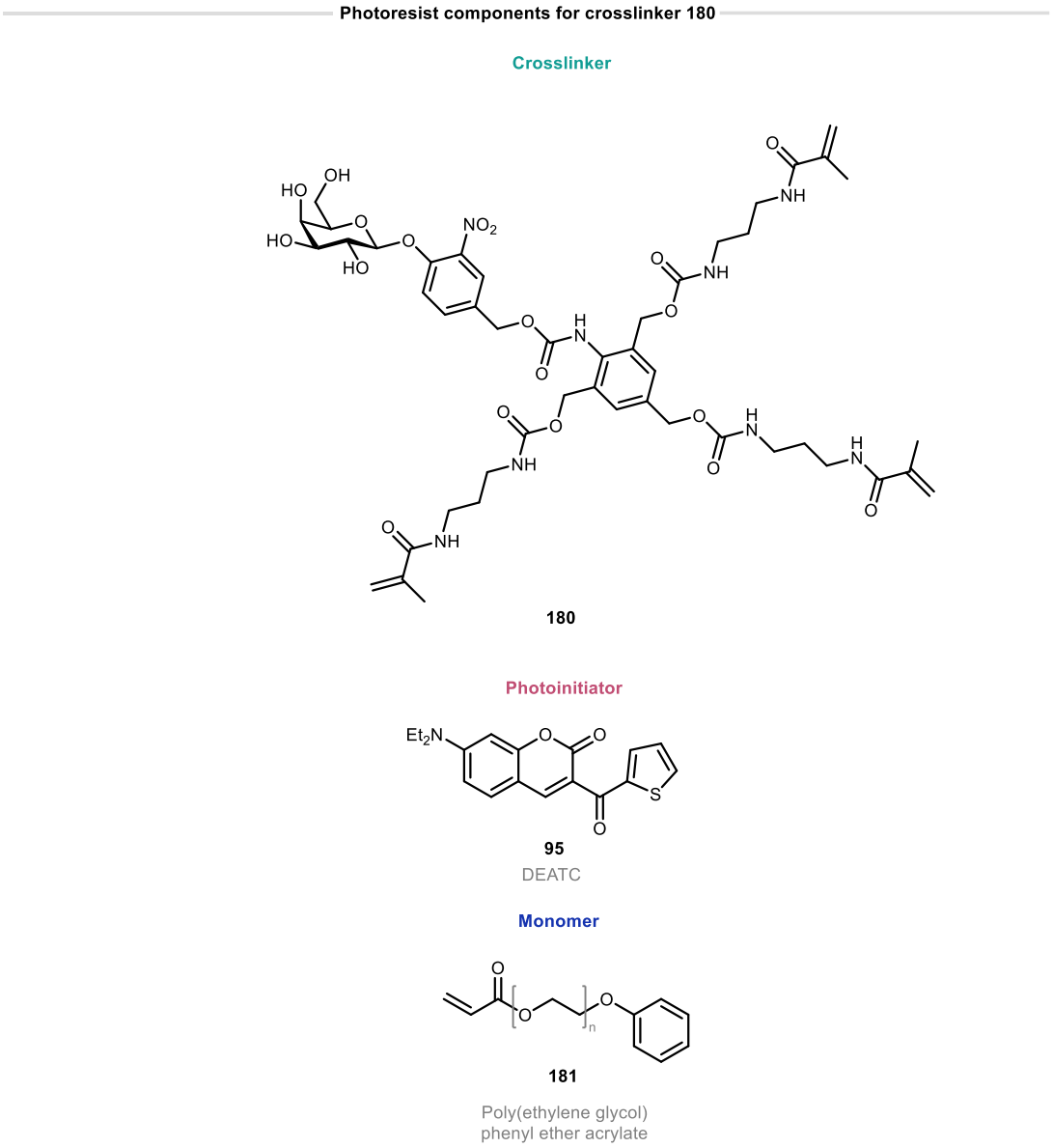

Figure 3.10 The components used to develop photoresist compositions for crosslinker **180**.

The photoresist with the most success is outlined in **Table 3.6**.

Table 3.6 Composition of the photoresist successfully used to polymerise crosslinker **180**, composed of crosslinker **180**, monomer PEG-PEA, photoinitiator DEATC and DMSO as solvent. Mol % is the molar ratio relative to the amount of PEG-PEA monomer used.

Compound	Mass / mg	Moles / mmol	Mol%	Weight %
Crosslinker 180	5.8	0.006	39	39
PEG-PEA	4.6	0.014	100	31
DEATC	0.5	0.002	11	3
DMSO	4	-	-	27

Printing was achieved with this photoresist, although structure resolution was not optimal. Selected structures are shown in **Fig 3.11.**

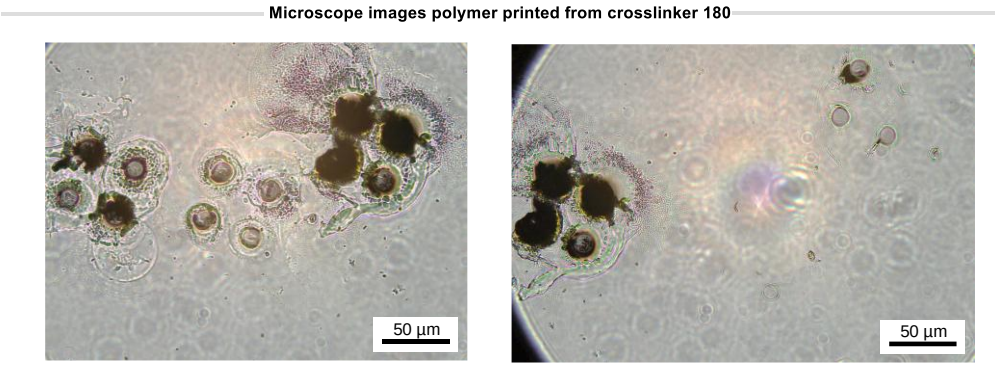

Figure 3.11 Images of selected microstructures printed using photoresist in **Table 3.6**

Polymerisation typically required high laser powers, resulting in burn-in of resulting structures to the slide. The most well-defined structures were chosen to be monitored for enzyme degradation studies, with images shown in **Fig. 3.12.**

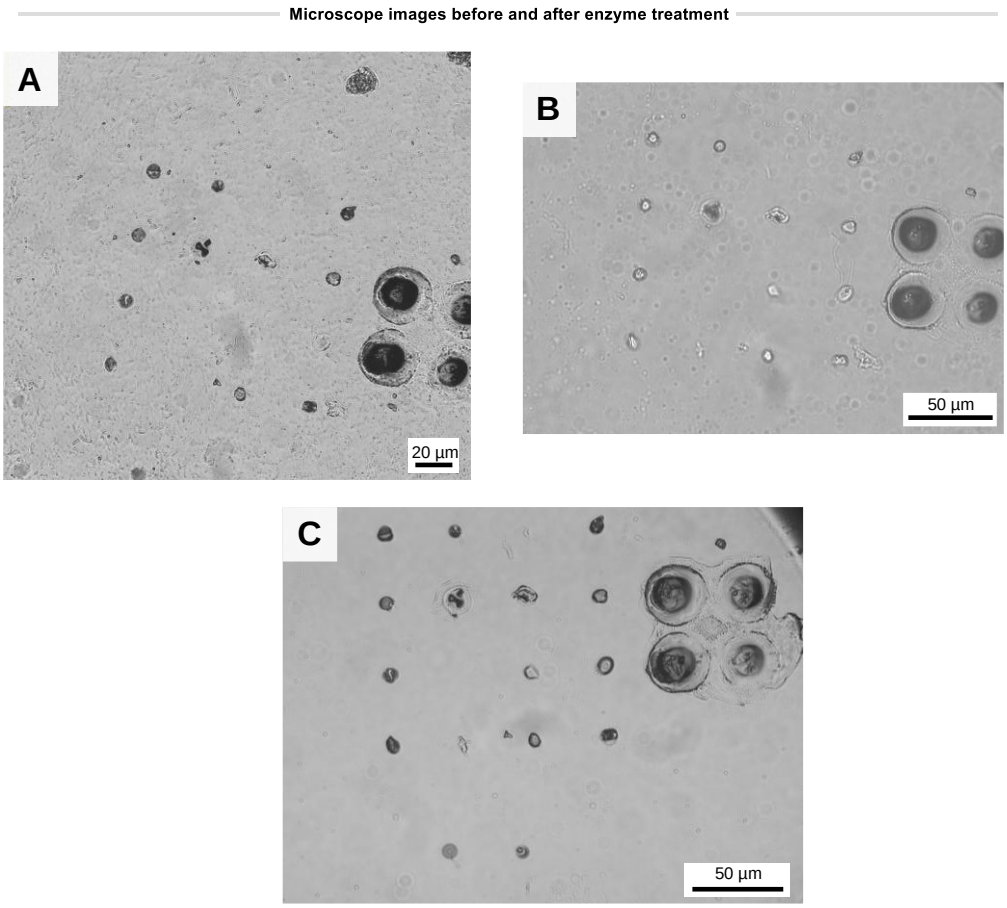

Figure 3.12 Images of the polymer associated with the photoresist from Table 3.6. A) Image of selected microstructures of the polymer prior to any treatment. B) Image of microstructures following incubation with pH 4.5 phosphate-citrate buffer at 30 °C overnight. C) Image of microstructures following incubation with a 230 U/mL β-galactosidase in pH 4.5 phosphate-citrate buffer at 30 °C after 5 days (2 fresh additions of enzyme per day as per **Fig. 2.14**).

Similar observations were observed with trifunctional crosslinker **180**, with stability in pH 4.5 phosphate-citrate buffer at 30 °C confirmed (**Fig. 3.12B**) but no observable degradation following incubation with β-galactosidase (**Fix. 3.12C**). Due to difficulties achieving appreciable polymerisation using TPP, less harsh conditions including lower laser powers and faster scan speeds which would reduce the degree of crosslinking to generate polymers more susceptible to degradation was not possible. As such, the polymers successfully generated using high laser powers had densely crosslinked networks, making degradation more challenging.

3.5 Conclusions and Future Work

The work described in this chapter has successfully demonstrated the first examples of self-immolative scaffolds applied to crosslinkers designed for glycosidase-activated polymeric degradable systems (**Fig. 3.13**). Subsequent to successful synthetic optimization, β-galactosidase-activatable crosslinkers **165** and **180** were polymerised by both TPP and bulk UV polymerisation. Unfortunately, the resolution of microstructures printed by TPP was suboptimal and required forcing conditions, resulting in a higher degree of crosslinking than planned. Enzymatic testing was not able to validate an observable materials response using microscopy.

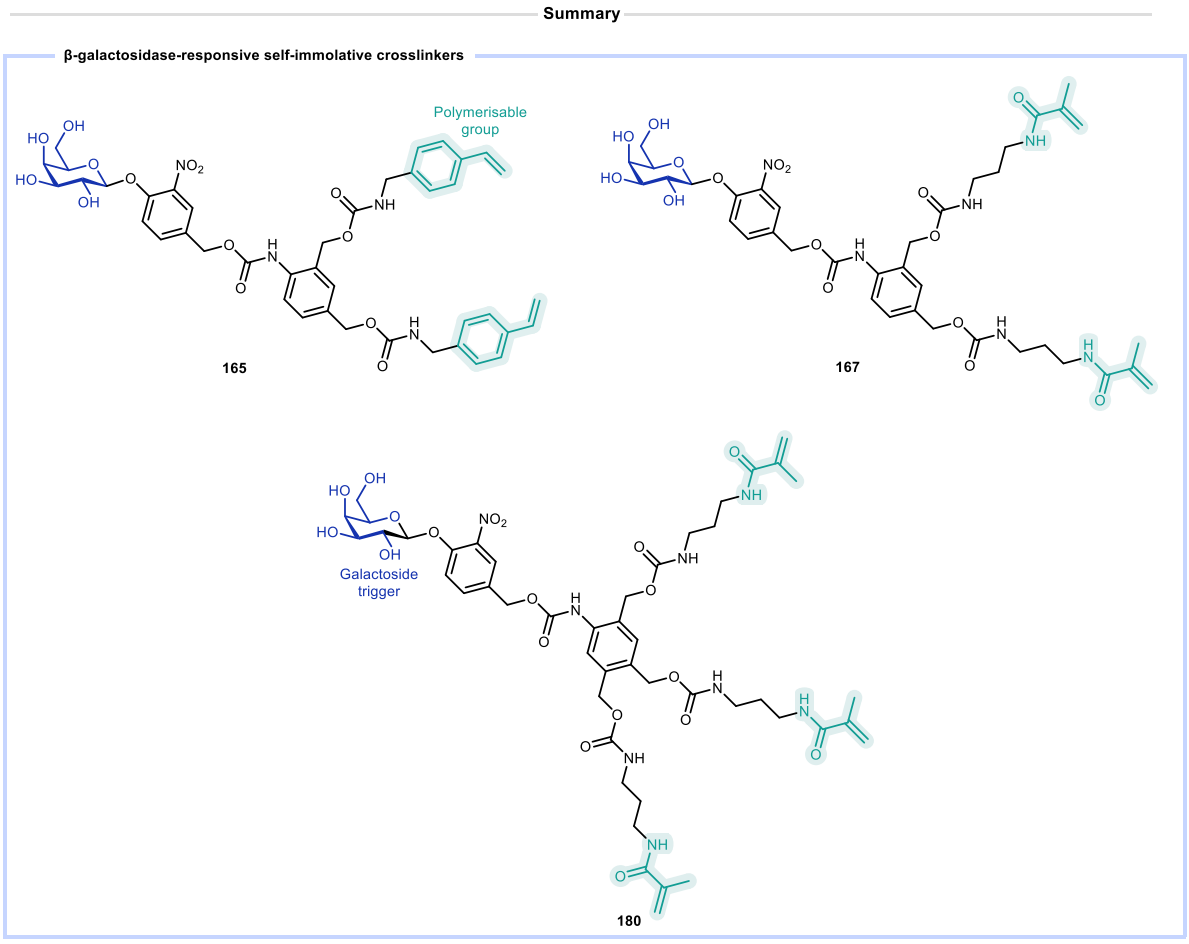

Figure 3.13 Dual-functionalised crosslinkers **165** and **167** and tri-functionalised crosslinker **180**.

Chapter 4

Development of a β-Galactosidase-Activated Glycopeptide Prodrug Analogue

Chapter 4: Development of a β-Galactosidase-Activated Glycopeptide Prodrug Analogue

4.1 Introduction

In recent years, rational prodrug design has become an integrated and increasingly innovative part of drug discovery efforts, facilitating improved targeting of therapeutics through the generation of inactive analogues which release the active drug upon specific activation at the tumour site. In particular, the incorporation of masking groups which block the reactivity of important functional groups and are cleavable upon activation by enzymes overexpressed in the tumour microenvironment are increasingly being used in prodrug strategies, offering rapid and specific release upon reaction.

Somatostatin and its synthetic analogue octreotide bind specifically to five subtypes of somatostatin receptors (SSTR) which are upregulated in many cancers, making them suitable targeting ligands as tumour-homing peptides.[191] The application of these analogues to peptide-drug conjugates with small molecule anticancer agents such as **183** and radiolabelled chelating agents such as **55** has facilitated targeted delivery to cancer cells by exploiting the binding of the peptide to these receptors (**Fig. 4.1**).[226, 227] In recent years, enzymatic activation of cleavable linkers for self-immolative drug release using tumour-homing peptides has been explored, offering a dual-targeting approach by exploiting the overexpression of the peptide receptors and the enzyme.[229, 230] However, the development therapeutic peptides as inactive prodrugs which are released in a targeted manner remains an underexplored field.

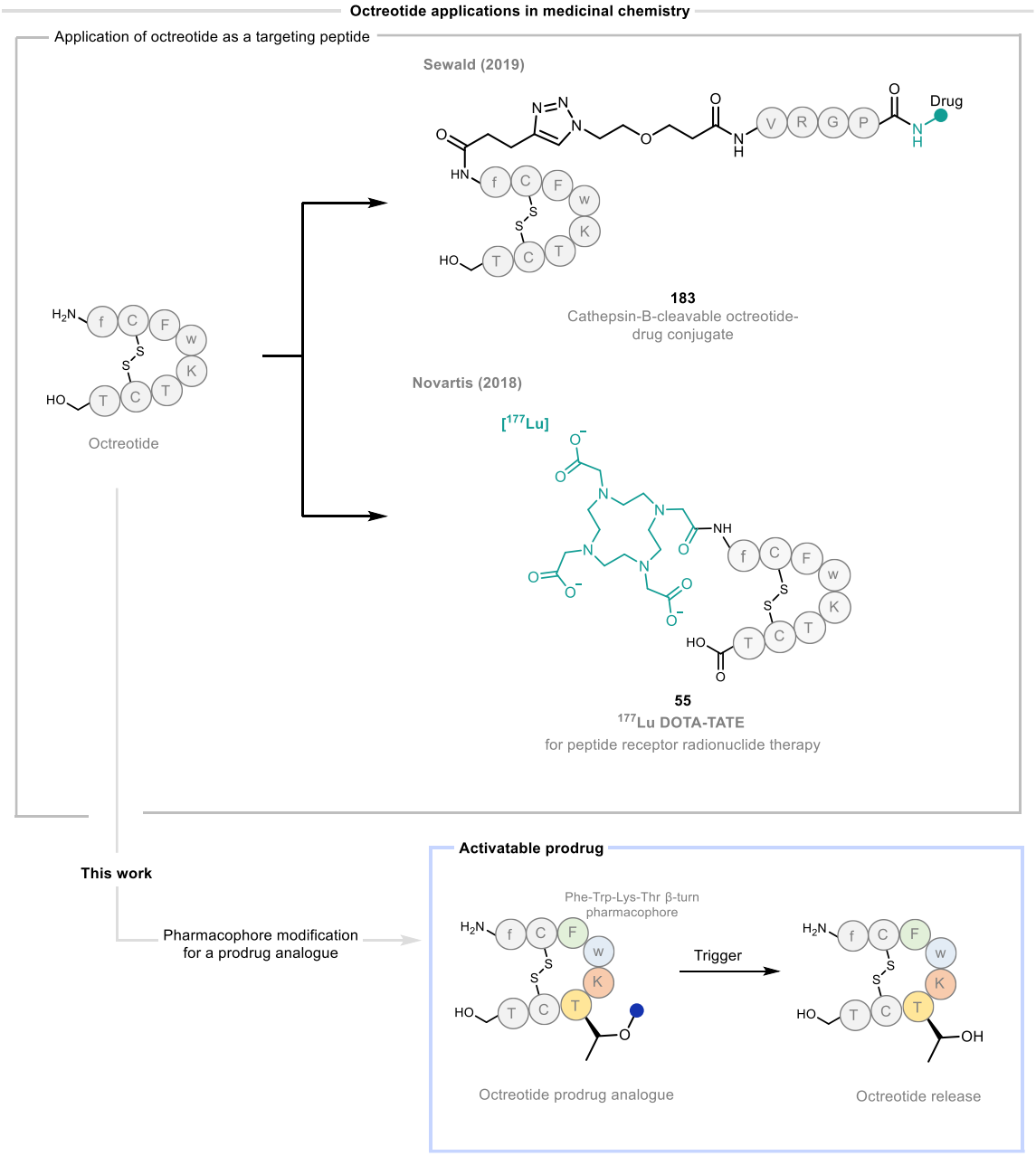

Figure 4.1 The application of octreotide as a tumour-homing peptide to peptide-drug conjugates (previous work) and directly to an activatable prodrug strategy as a model system via pharmacophore modification (this work).

This project aimed to use somatostatin and octreotide as model peptides for the development of an enzymatically-activated prodrug strategy which would exploit the overexpression of somatostatin receptors and those of the enzyme. In this chapter, β-galactosidase was selected as the targeted enzyme, which is overexpressed in a range of cancer types including gastric cancers which also exhibit upregulation of somatostatin receptors.[306, 307] The pharmacophore of somatostatin and octreotide which is constituted by the Phe-Trp-Lys-Thr β-turn was

planned to be modified to generate inactive prodrug analogues by blocking the part of the peptide which binds to its receptors. This would be achieved through the synthesis of glycoside analogues of the threonine and lysine amino acids which, upon enzymatic activation, would release their unmodified form to release the active peptide therapeutic (**Fig. 4.2**).

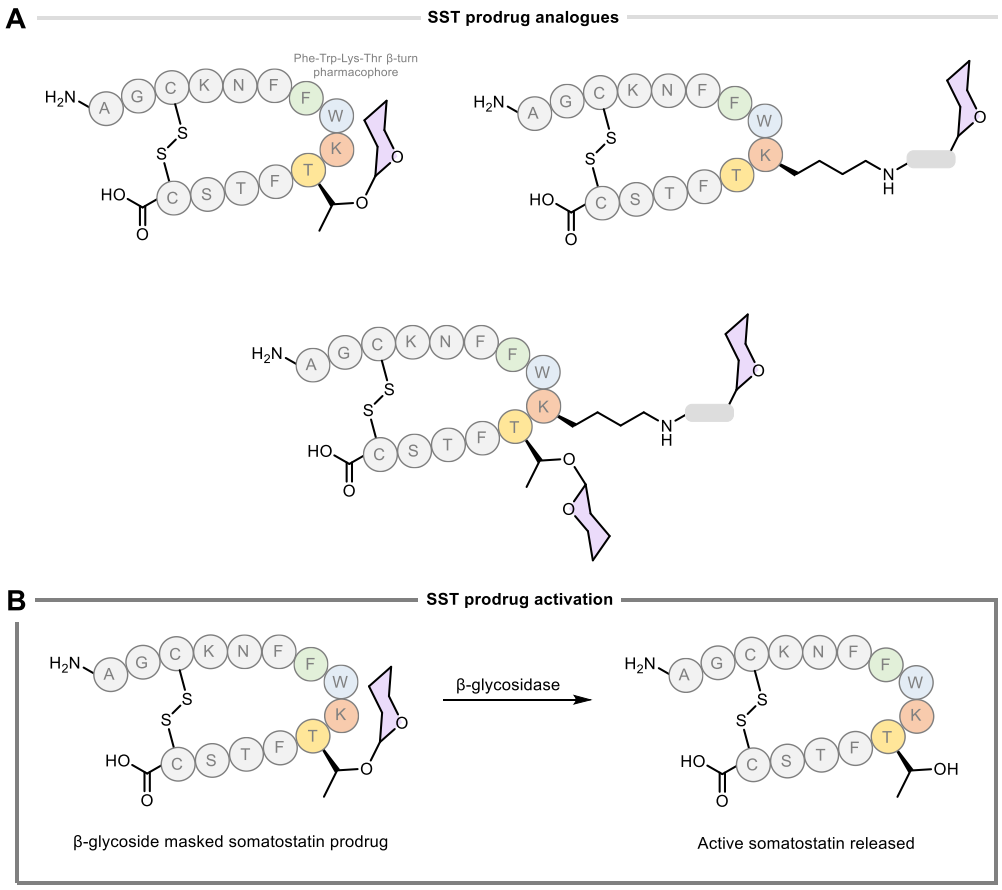

Figure 4.2 Somatostatin prodrug analogues. A) Glycoside analogues with modified threonine and lysine residues; B) Prodrug activation by β-glycosidase.

4.2 Results and Discussion

4.2.1 Glycoamino acid synthesis

In order to generate prodrug analogues of somatostatin and octreotide through modification of the peptide pharmacophore, it was necessary to synthesise unnatural amino acid analogues of one or more of the four essential amino acids in this motif. Lysine and threonine were selected due to the synthetic versatility of the amine and hydroxyl functional groups, which was expected to allow for the formation of cleavable glycoside conjugates. In the first instance, the synthesis of galactoside threonine analogues was explored, enabling direct glycosylation of the side chain to galactose derivatives, identifying target molecules **184** and **185** (**Fig. 4.3**).

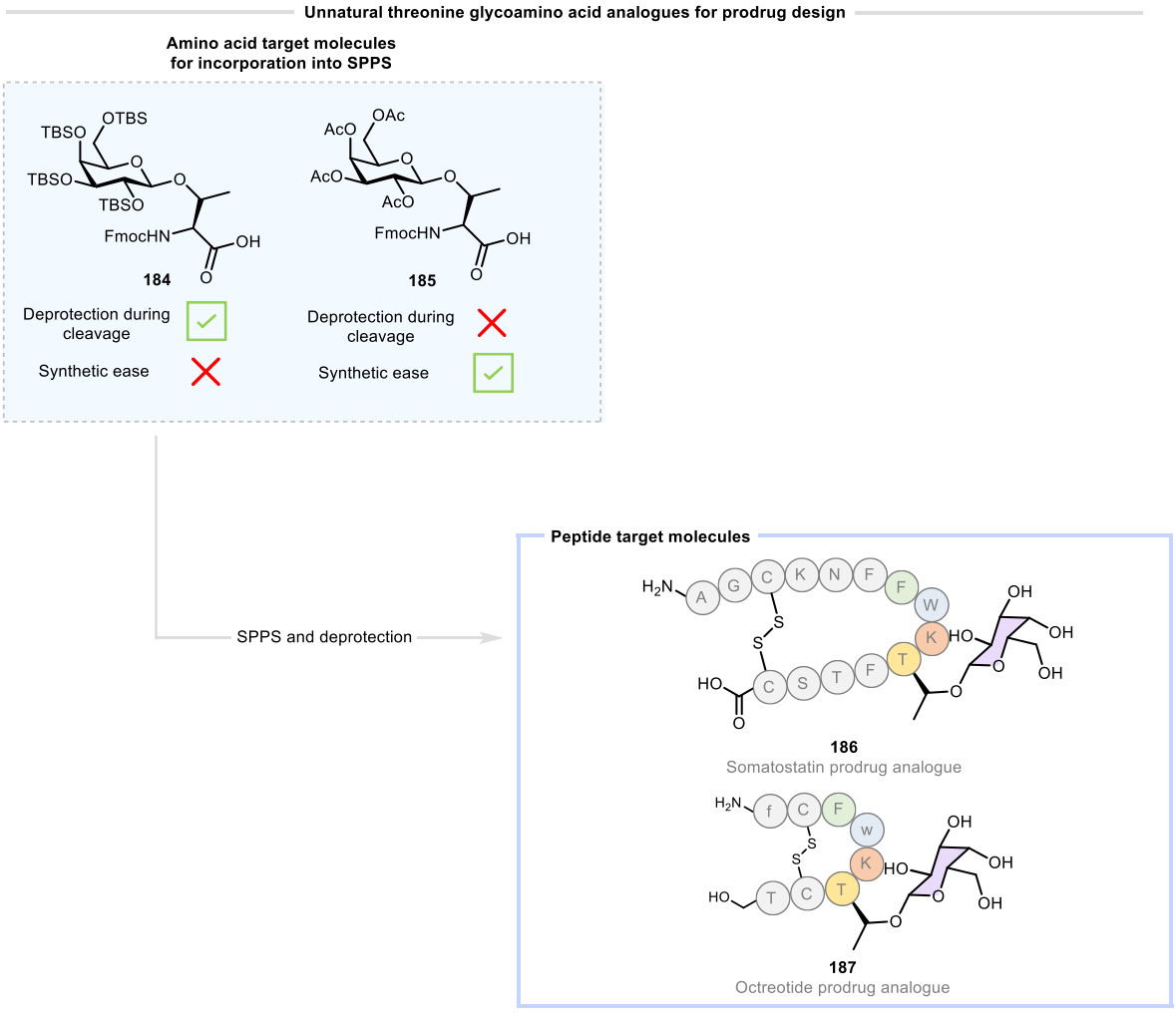

Figure 4.3 Unnatural amino acid threonine analogues **184** and **185** for incorporation into SPPS to generate prodrugs **186** and **187**.

Galactoside threonine analogues **184** and **185** are both suitable for incorporation into SPPS to generate peptide prodrug analogues **186** and **187**. TBS-protected analogue **184** was

selected as an initial target molecule following a glycopeptide synthetic strategy reported by Yan, Li *et al.* which uses silyl-ether-protected glycoamino acid building blocks.[308] As these protecting groups are removed under TFA-mediated peptide cleavage conditions, it avoids the requirement of base-mediated acetyl deprotection following peptide cleavage, which may cause side reactions such as β-elimination and necessitate further purification.[309, 310] To this end, it was first attempted to apply a route to glycoamino acids developed by Yan, Li *et al.* which uses a peracetylated glycosyl donor for β-selectivity in the glycosylation step through neighbouring group participation followed by protecting group manipulations to afford TBS-protected glycoamino acid **184**. Firstly, the synthesis of glycoamino acid **185** was explored which could subsequently be deprotected and reprotected with TBS groups (**Scheme. 4.1**).

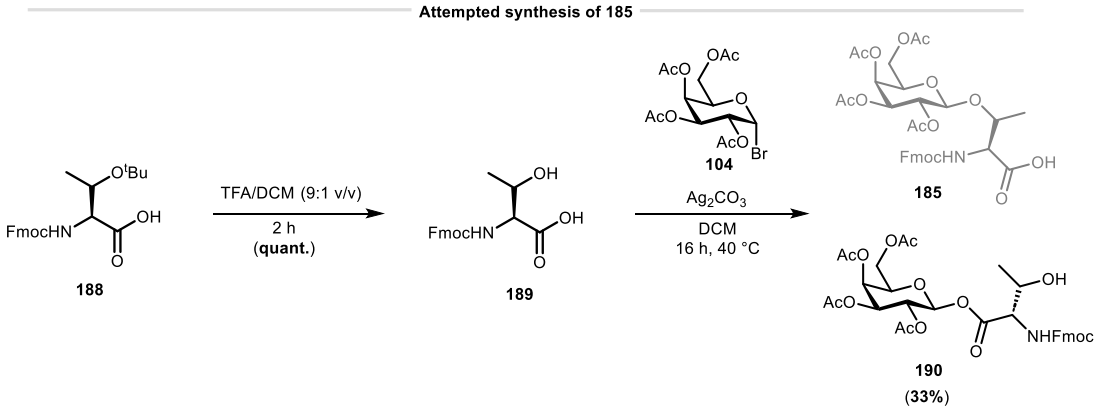

Scheme 4.1 Attempted synthesis of peracetylated glycoside threonine analogue **185** required prior to conversion to TBS-protected analogue **184**.

Tert-butyl deprotection of Fmoc-Thr(^{t}Bu)-OH (**188**) using TFA gave **189** in a quantitative yield, which was followed by attempted glycosylation with galactosyl donor **104**. Instead of providing galactoside glycoamino acid **185**, this reaction was found to be fully selective for the free carboxylic acid to form galactoside **190** in 33% yield, with no reaction of the more nucleophilic alcohol. This was rationalised by silver-carbonate-mediataed deprotonation of the Fmoc-Thr-OH carboxylic acid, generating the carboxylate derivative with significantly increased nucleophilicity.

In order to prevent undesired reaction at the carboxylic acid and to allow for a selective route to glycoamino acid **185**, the free acid was protected and a synthetic route using this as an acceptor developed (**Scheme 4.2**).

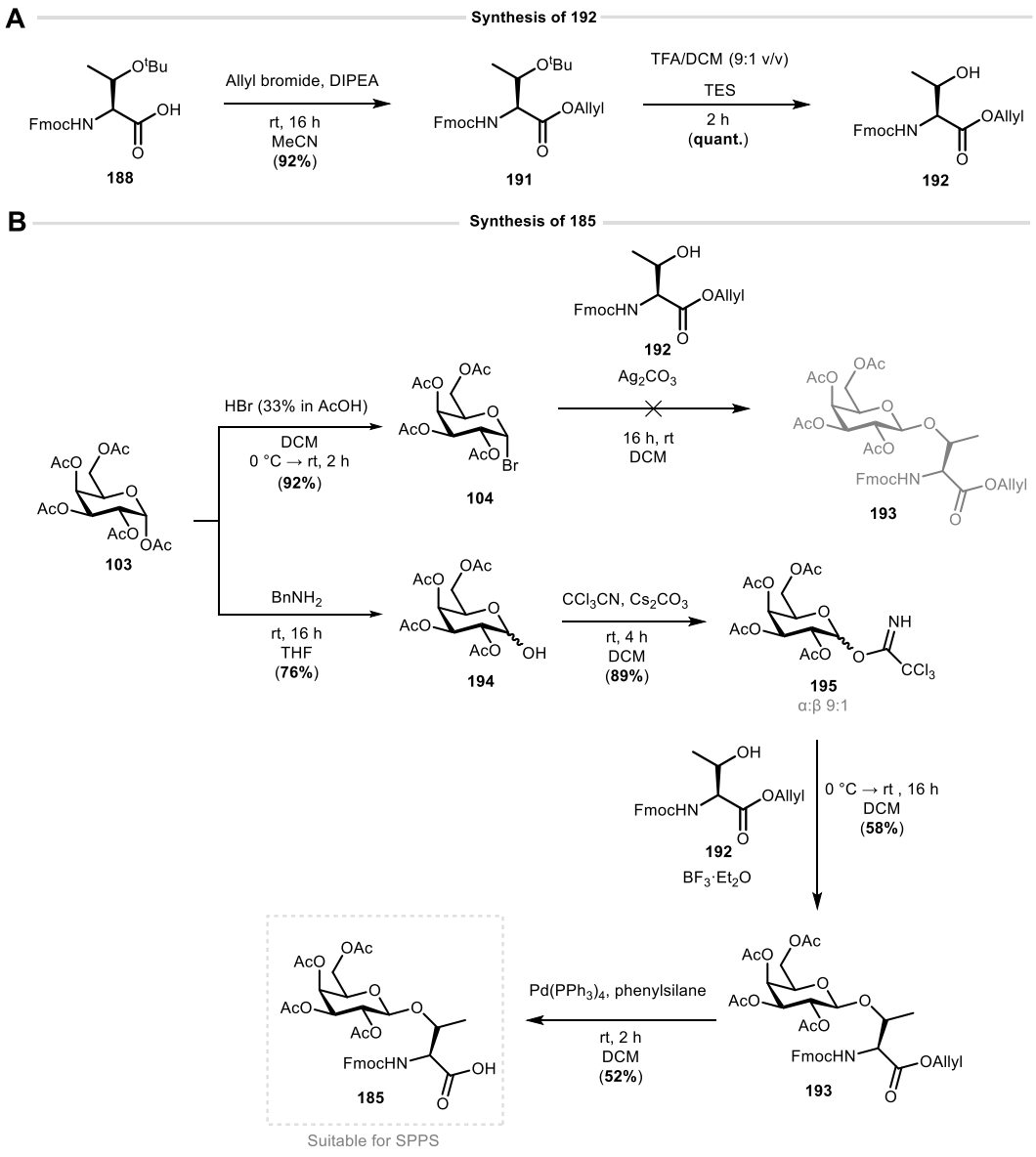

Scheme 4.2 Synthesis of building blocks for glycoamino acid threonine analogue. A) Allylation and deprotection to synthesise acceptor **192** for glycosylation; B) Synthetic route to glycoamino acid **185**.

Firstly, the acceptor for glycosylation was synthesised (**Scheme 4.2A**) starting with allylation of Fmoc-Thr(ᵗBu)-OH (**188**) using allyl bromide to give Fmoc-Thr(ᵗBu)-OAllyl **191** in a 92% yield. This was followed by *tert*-butyl deprotection using TFA and TES as a cation scavenger to provide acceptor Fmoc-Thr-OAllyl **192** in a quantitative yield.

Next, suitable glycosyl donors and the subsequent glycoamino acid synthesis was investigated (**Scheme 4.2B**). Bromination of peracetylated galactose **103** provided α-bromo galactosyl donor **104** in a 92% yield, however no reaction took place in the attempted Königs-Knorr glycosylation with Fmoc-Thr-OAllyl **192** and Ag_2CO_3. The synthesis of alternative

trichloroacetimidate donor **195** was successful, starting from formation of hemiacetal **194** using benzylamine in 76% yield followed by reaction with CCl_3CN to give trichloroacetimidate **195** in 89% yield. This intermediate was isolated in a 2:3 α:β ratio when the reaction was carried out for 2 hours and a 9:1 α:β ratio when the reaction was carried out for 4 hours; the anomers were easily separable via chromatography and were combined for subsequent glycosylation. Glycosylation with Fmoc-Thr-OAllyl acceptor **192** using $BF_3 \cdot Et_2O$ as a Lewis acid catalyst furnished galactoside **193** in a 58% yield. Finally, allyl deprotection using $Pd(PPh_3)_3$ and phenylsilane provided glycoamino acid **185** in a yield of 52%. When triethylsilane was used instead of phenylsilane, no reaction took place.

The synthesis of silyl-protected glycoamino acids was attempted, as the silyl protecting groups could be removed during peptide cleavage (**Scheme 4.3**).

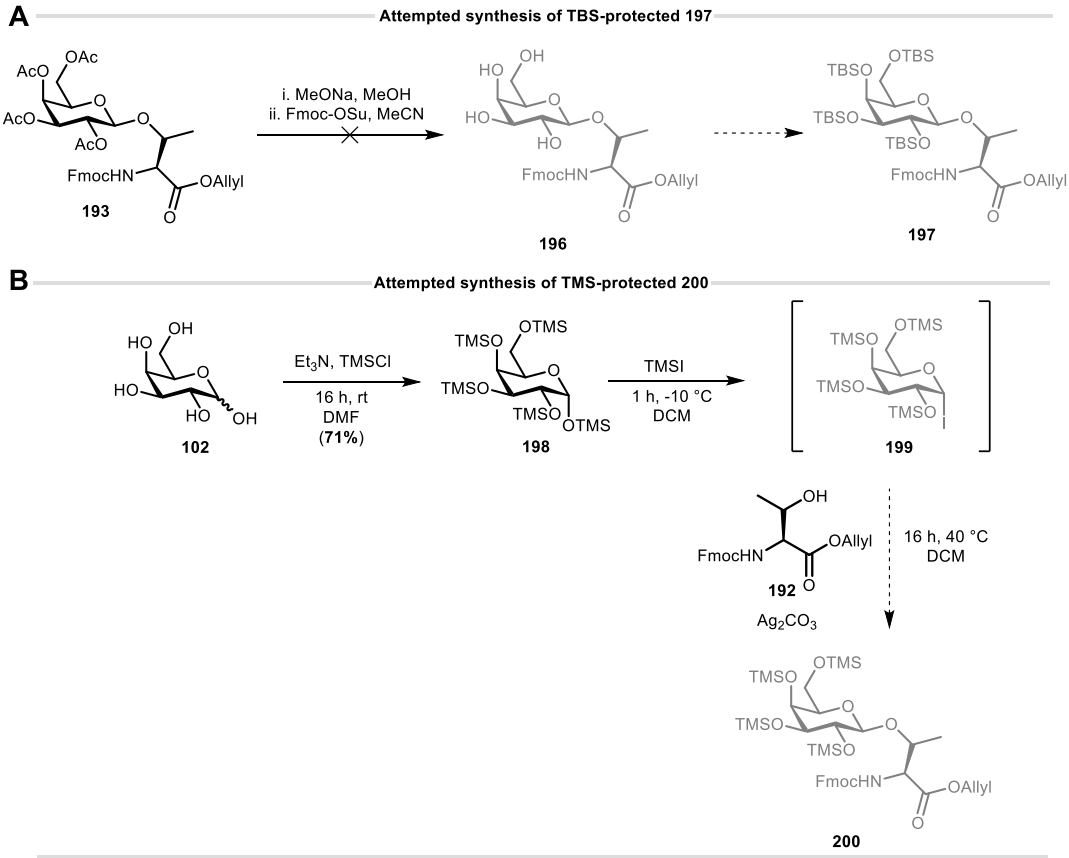

Scheme 4.3 Attempted syntheses of silyl-protected glycoamino acids. A) TBS-protected **197**; B) TMS-protected **200**.

Initially, a synthetic route developed by Yan, Li *et al.*[308] which manipulates the carbohydrate hydroxyl protecting groups, was attempted aiming to synthesise a TBS-protected unnatural

amino acid. One-pot acetyl deprotection using sodium methoxide and Fmoc-reprotection of **193** (**Scheme 4.3A**), which could be reprotected with TBSCl to provide **197**, did not yield free galactose derivative **196**, instead resulting in a complex mixture.

Next, an alternative route which uses glycosylation conditions to favour β-selectivity via an α-iodo donor was investigated (**Scheme 4.3B**). Kulkarni *et al.* reported a fully β-selective glycosylation using per-TMS galactosyl iodide donor, with Ag_2CO_3 as a heterogeneous catalyst and under reflux.[311] Per-TMS protection of galactose **102** was carried out with TMSCl to provide **198** in 71% yield. Next, galactosyl iodide **199** formation was attempted, which would allow for the subsequent formation of 200, however TMS deprotection and donor hydrolysis was instead observed under these conditions.

Following these results, peracetylated glycoamino acid **185** was instead selected for use in SPPS to form the glycopeptide octreotide analogue. The acetyl protecting groups could be deacetylated either on-resin or following cleavage.

With a reliable synthetic route to an unnatural threonine glycoamino acid analogue in hand, the synthesis of a lysine glycoamino acid was next investigated. As lysine also features in the pharmacophore of the peptide, this would allow for the synthesis of additional prodrug analogues. The synthesis of appropriate galactoside aldehydes and alkyl chlorides are described in **Scheme 4.4**.

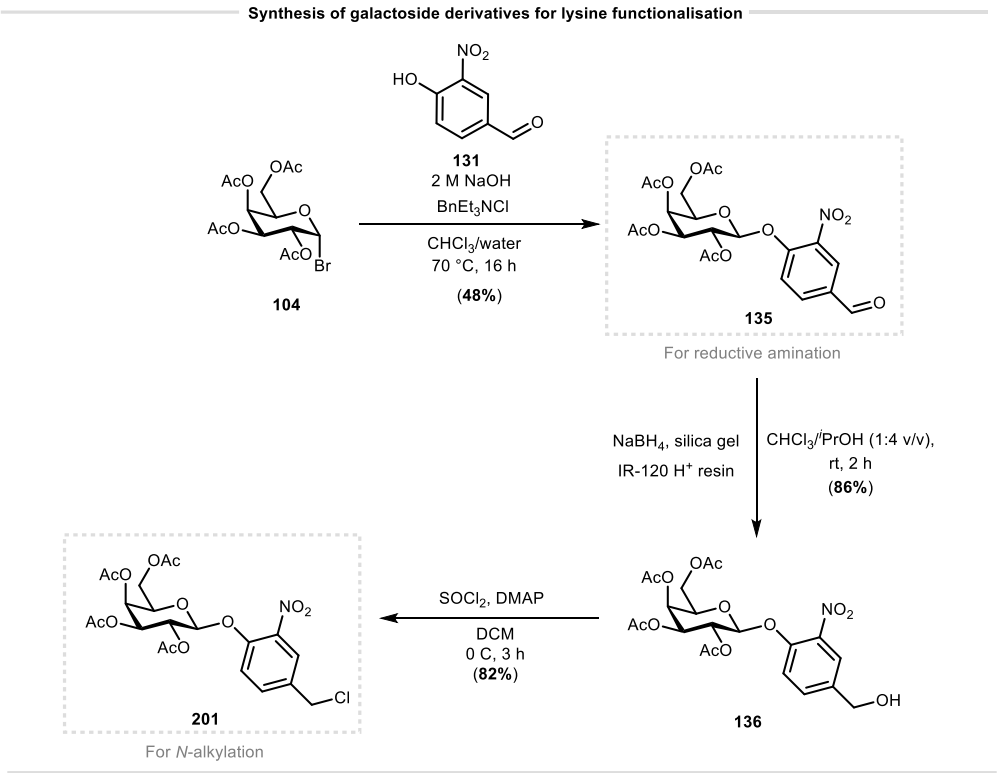

Scheme 4.4 Synthesis of aldehyde **135** and alkyl chloride **201** for reaction with lysine derivatives.

Glycosylation of α-bromo galactosyl donor **104** with 4-hydroxy-3-nitrobenzaldehyde (**131**) under basic conditions with $BnEt_3NCl$ as a phase-transfer catalyst provided galactoside **135** in a 48% yield, which was suitable as a substrate for reductive amination with lysine derivatives. Reduction of galactoside **135** using $NaBH_4$ and silica gel to prevent acetyl group migration gave galactoside **136** in an 86% yield. The hydroxyl functional group was chlorinated using $SOCl_2$ to furnish galactoside **201** in a yield of 82%, suitable for *N*-alkylation.

Aldehyde galactoside **135** and chloride galactoside **201** were then investigated for lysine derivative functionalisation to give β-galactose-masked unnatural amino acids for prodrug generation (**Scheme 4.5**).

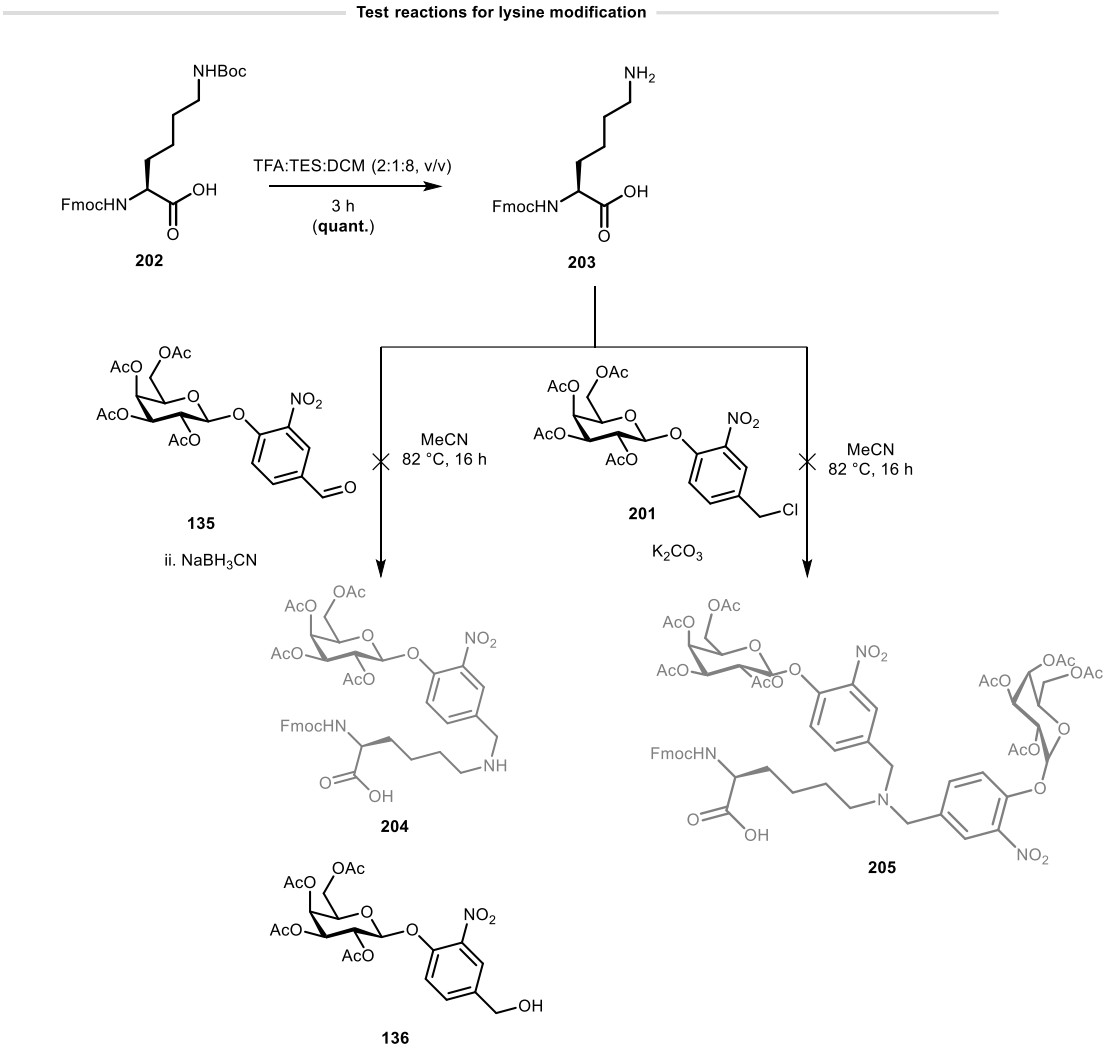

Scheme 4.5 Test reactions for lysine modification.

The Boc amine protecting group on Fmoc-Lys(Boc)-OH (**202**) was first deprotected using TFA to give Fmoc-Lys-OH (**203**) in a quantitative yield. Reductive amination with galactoside **135** and $NaBH_3CN$ did not yield target molecule **204**, with only the aldehyde reduction product **136** being isolated. In addition, *N*-alkylation with galactoside **201** did not yield the target compound **205**.

As octreotide is a peptide alcohol with a reduced threoninol at the C-terminus, careful consideration of the synthetic strategy to access octreotide analogues was required. There are several reported synthetic routes to peptide alcohols which use a modified resin or coupling of a protected threoninol to a conventional resin followed by late-stage peptide modification (**Fig. 4.4**).

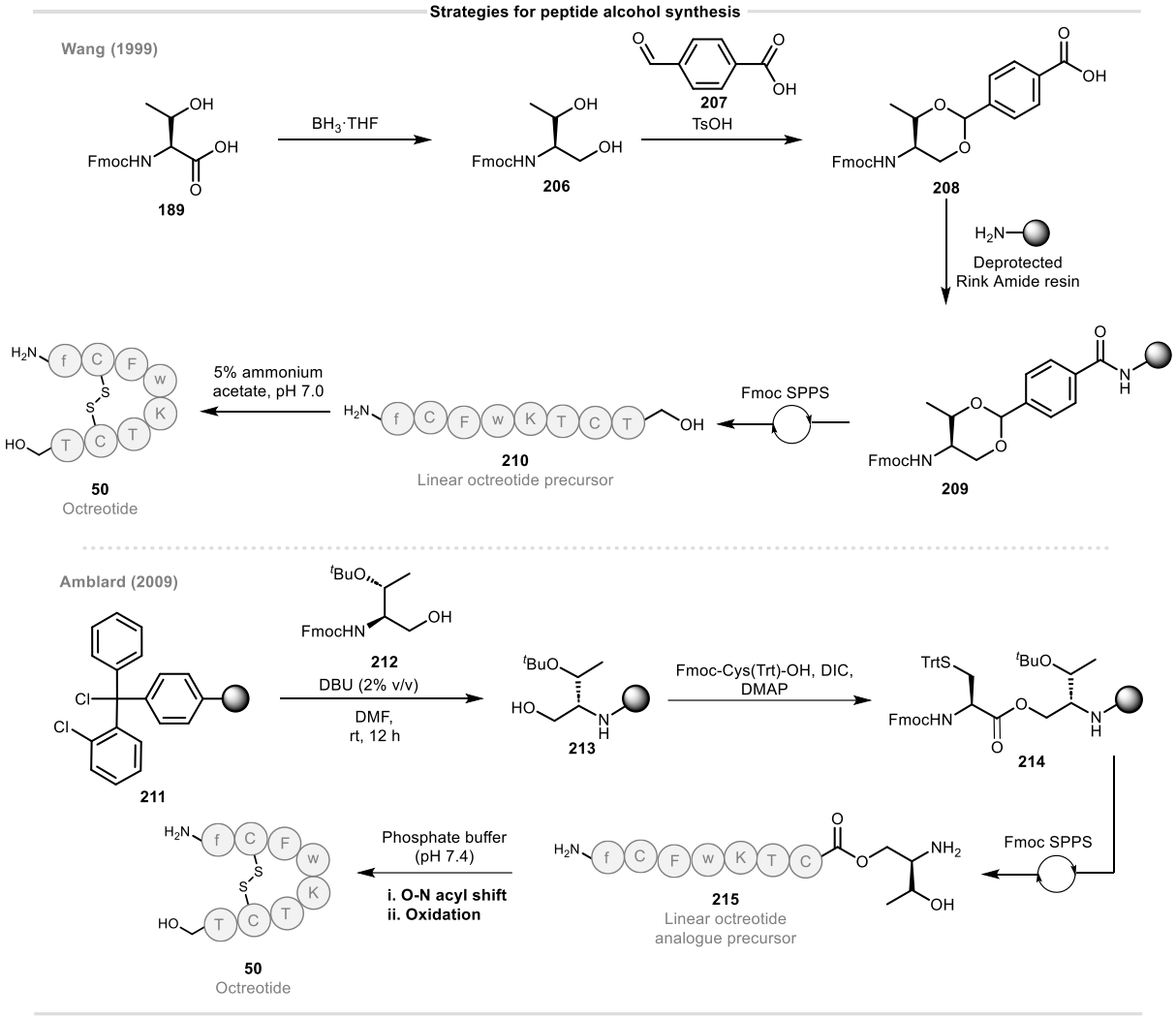

Figure 4.4 Strategies for peptide alcohol synthesis applied to octreotide: resin modification (Wang and co-workers, 1999) and a route using an esterification followed by an O-N acyl shift following peptide cleavage (Amblard and co-workers, 2009).

The route developed by Wang and co-workers reduces Fmoc-Thr-OH (**189**) to Fmoc-Thr-ol (**206**), followed by reaction with 4-carboxybenzaldehyde (**207**) to form **208.** Subsequent coupling to Rink amide resin provides modified resin **209**, and finally standard Fmoc/^{t}Bu SPPS and cleavage to form linear peptide **210** yields octreotide **50** following oxidation. The route described by Amblard and co-workers applies a one-pot DBU-mediated Fmoc-deprotection and coupling of Fmoc-Thr(^{t}Bu)-ol (**212**) to **213** to overcome difficult anchoring of the hydroxyl function, which is then subjected to a Steglich esterification with Fmoc-Cys(Trt)-OH to provide **214**. Standard Fmoc/^{t}Bu SPPS and cleavage gives linear precursor **215** which is then subjected to an O-N acyl shift and finally oxidation to form octreotide **50**.

The route described by Wang and co-workers was initially selected, requiring the synthesis of cyclic acetal **208** starting from the reduced Fmoc-Thr-ol **206**. Reaction conditions explored for the reduction of Fmoc-Thr-OH (**189**) are described in **Table 4.1.**

Table 4.1 Attempted optimisation of the reduction of Fmoc-Thr-OH (**189**).

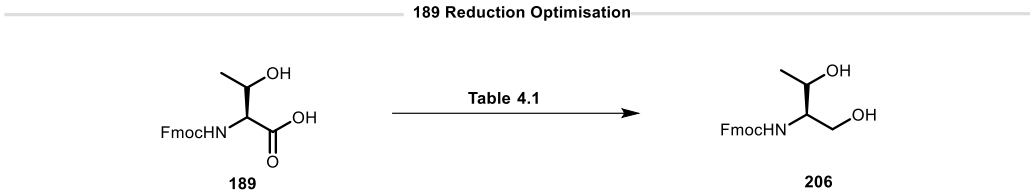

Entry	Reagents	Outcome
1	i. CDI ii. $NaBH_4$	No reaction
2	i. Isobutyl chloroformate ii. $NaBH_4$	Complex mixture formed; unreacted starting material recovered
3	BH_3·THF	No reaction

CDI activation followed by reduction with $NaBH_4$ (entry 1) led to no reaction, whilst using isobutyl chloroformate as the activating agent led to a complex mixture with no isolation of the target molecule (entry 2). Finally, no reaction was observed when using BH_3·THF for direct reduction (entry 3).

Following this, the route developed by Amblard and co-workers (**Fig. 4.4**) was focused on, which requires only a one-step synthesis prior to SPPS and can use the ^{t}Bu-protected Fmoc-Thr(^{t}Bu)-OH (**188**).

Instead, reduction of Fmoc-Thr(^{t}Bu)-OH (**188**) was carried out (**Scheme 4.6**).

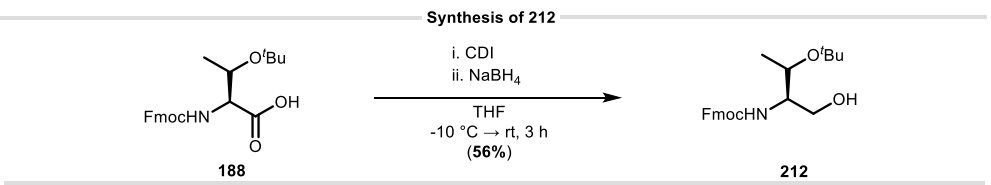

Scheme 4.6 Synthesis of **212**.

Fmoc-Thr(^{t}Bu)-OH (**188**) was first activated with CDI and then reduced using $NaBH_4$ in one pot to furnish Fmoc-Thr(^{t}Bu)-ol (**212**) in a 56% yield.

Threoninol derivative **212** was then applied to the octreotide synthetic strategy described by Amblard and co-workers (**Scheme 4.7**).

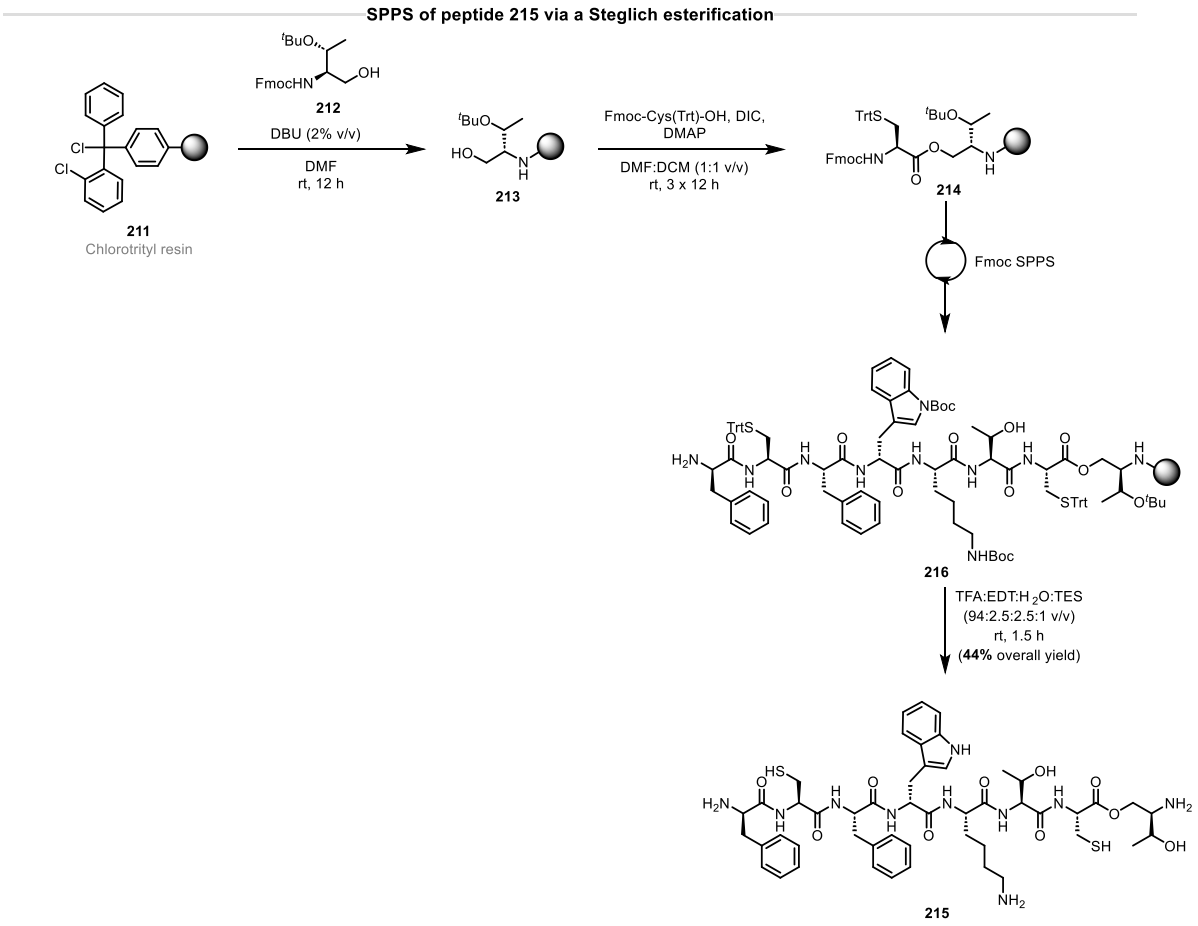

Scheme 4.7 SPPS of linear peptide **215** via a Steglich esterification for the first Fmoc-Cys(Trt)-OH coupling.

Threoninol derivative **212** was Fmoc-deprotected and loaded onto the 2-chlorotrityl resin **211** via the alpha amino group in one pot using a 2% DBU solution in anhydrous DMF to give **213**. Next, a Steglich esterification with Fmoc-Cys(Trt)-OH was carried out using DIC and DMAP to provide **214** suitable for standard Fmoc/^{t}Bu SPPS. Fmoc/^{t}Bu SPPS and cleavage using TFA:EDT:H_2O:TES (94:2.5:2.5:1 v/v) gave linear octreotide precursor **215** in an overall yield of 44%.

The linear peptide was then subjected to one-pot O-N acyl transfer and oxidation using aqueous phosphate buffer at pH 7.2 for 48 hours (**Fig. 4.5**).

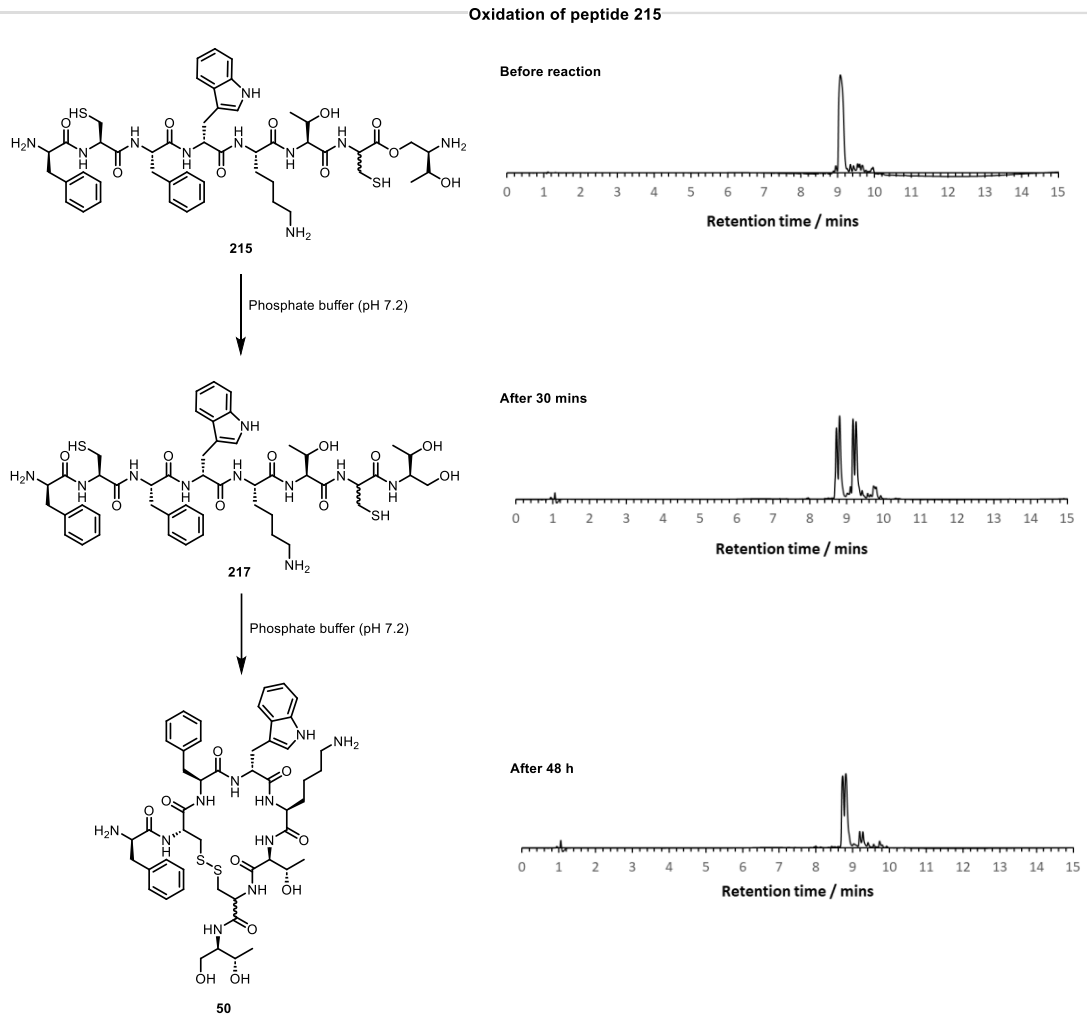

Figure 4.5 O-N acyl shift followed by oxidation to form octreotide **50** and the corresponding HPLC trace for each peptide (5-95% MeCN in H_2O + 0.1% TFA, 220 nm).

After 30 mins, RP HPLC analysis showed consumption of the linear peptide starting material and the formation of four new peaks corresponding to the linear peptide following acyl transfer to **217** (R_T = 9.17, 9.25 min) and the oxidised peptide **50** (R_T = 8.72, 8.81 min). Following 48 hours, the oxidised peptide was present in a 9:1 ratio to the non-oxidised peptide following acyl migration. Despite the apparent single peak observed for the linear peptide starting material **215,** the two sets of double peaks of roughly equal intensity following the reaction indicated full epimerisation had taken place.

With the epimerisation rationalised by the overnight base treatment required for the Steglich esterification of Fmoc-Cys(Trt)-OH, an amino acid susceptible to base-mediated racemisation, a Mitsunobu reaction was attempted instead (**Scheme 4.8**)

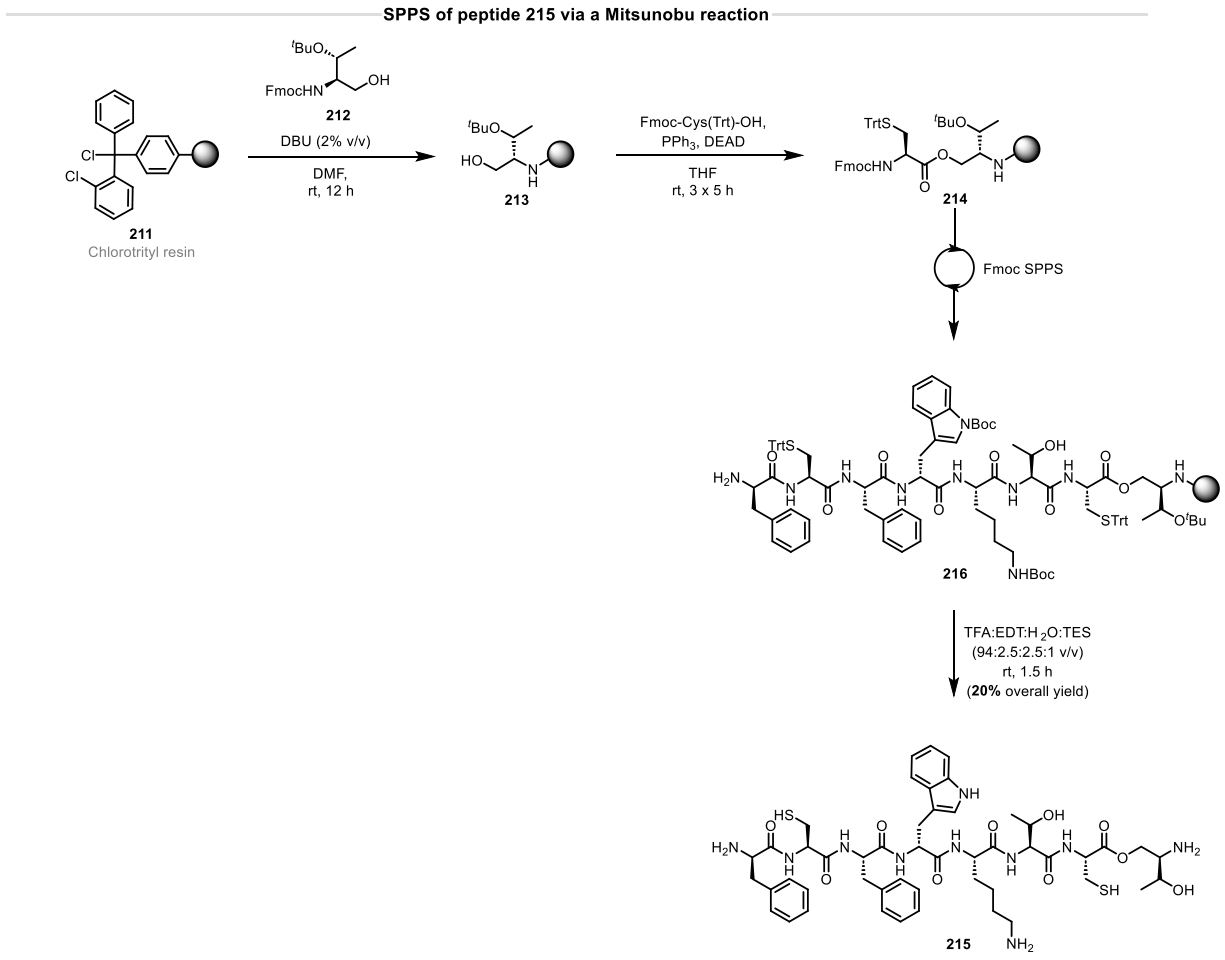

Scheme 4.8 SPPS of linear peptide **215** via a Mitsunobu reaction for the first Fmoc-Cys(Trt)-OH coupling.

As in **Scheme 4.7**, Fmoc-Thr(ᵗBu)-ol (**212**) was Fmoc-deprotected and loaded onto the 2-chlorotrityl resin **211** in one pot using a 2% DBU solution in anhydrous DMF to give **213.** Mitsunobu reaction with Fmoc-Cys(Trt)-OH using PPh_3 and diethyl azodicarboxylate (DEAD) provided **214** which was subjected to standard Fmoc/ᵗBu SPPS to give resin-bound peptide **216**. Cleavage using TFA:EDT:H_2O:TES (94:2.5:2.5:1 v/v) furnished peptide **215** in an overall yield of 20%.

O-N acryl transfer and oxidation using aqueous phosphate buffer at pH 7.2 was then carried out and followed using RP HPLC (**Fig. 4.6**).

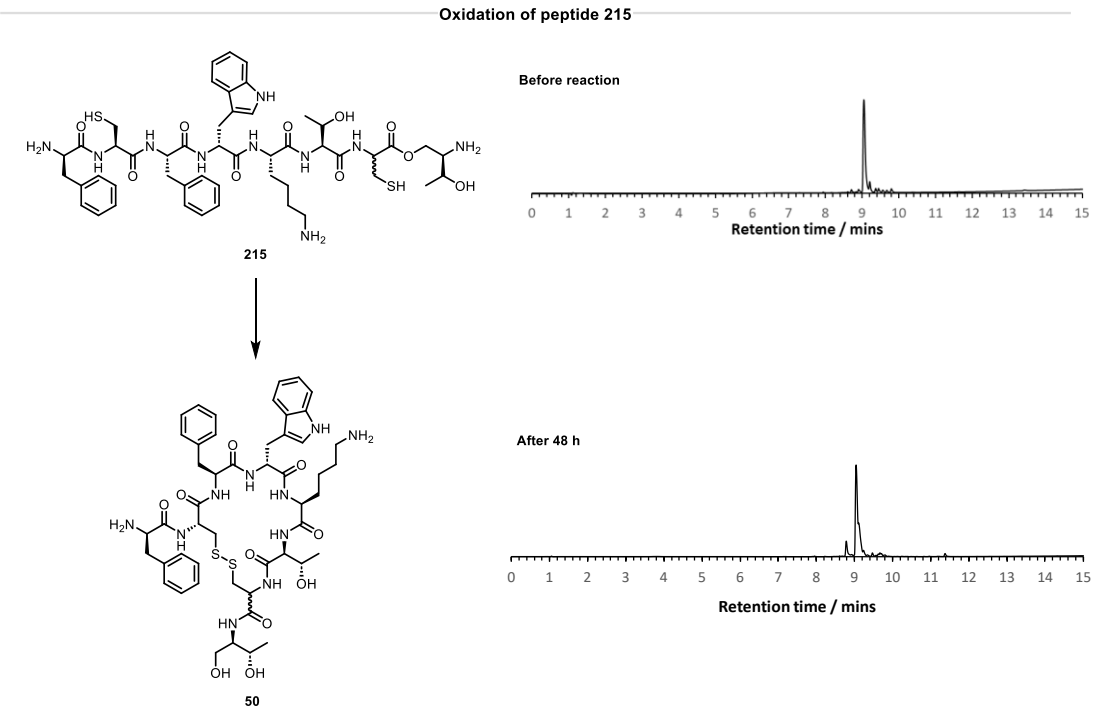

Figure 4.6 O-N acyl shift and oxidation to form octreotide **50** and the corresponding HPLC trace for each peptide (5-95% MeCN in H_2O + 0.1% TFA, 220 nm).

After 48 hours, the starting material linear peptide was consumed (R_T = 9.43 min) and a new peak formed (R_T = 9.04 min). Although the linear peptide had a noticeably sharper peak compared to the synthesis which used the Steglich esterification, following O-N acyl migration and oxidation, the final product appeared as a broad double peak and therefore was not purified.

As a result, focus was shifted to the synthesis of somatostatin analogues which could be achieved using conventional Fmoc/^{t}Bu SPPS. Somatostatin linear analogue **218** was synthesised using Fmoc/^{t}Bu SPPS in an overall yield of 65% and oxidised (**Scheme 4.9**).

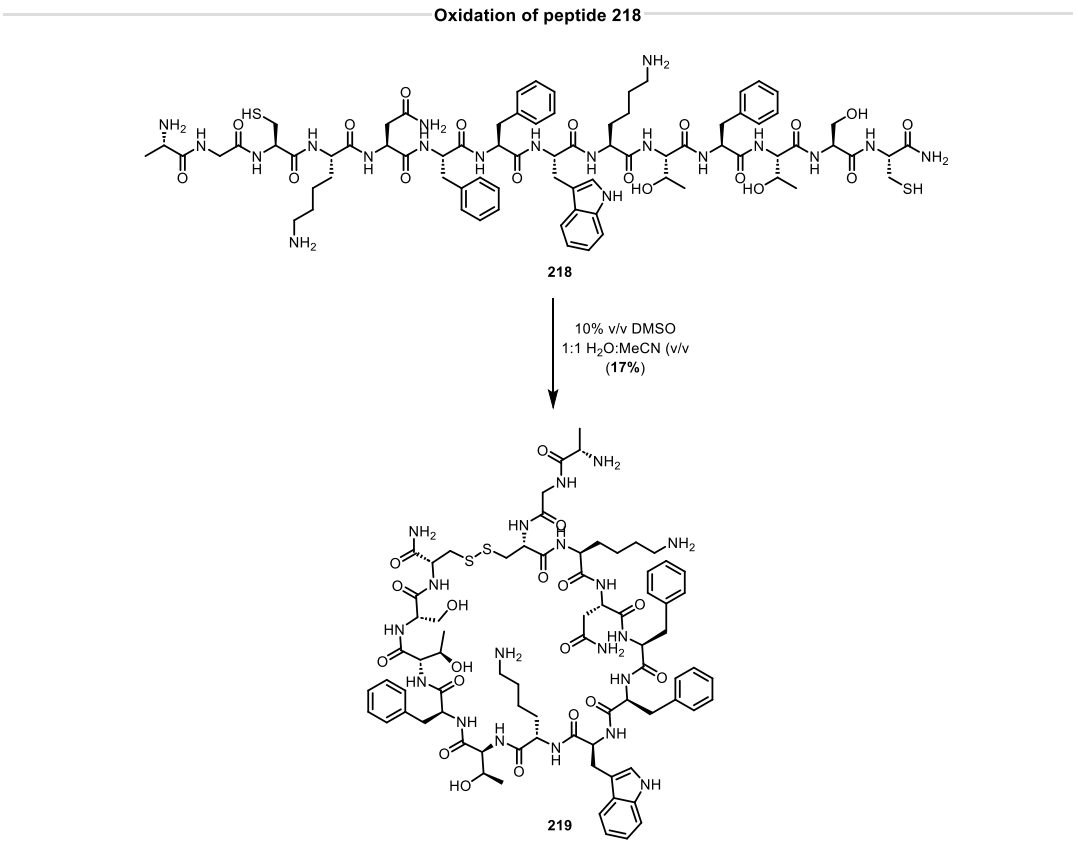

Scheme 4.9 Oxidation of linear somatostatin analogue **218** to cyclised peptide **219**.

The linear precursor was oxidised with 10% v/v DMSO in 1:1 v/v H_2O:MeCN to give cyclised somatostatin analogue **219** in a yield of 17% following semi-preparative HPLC purification. Glycoamino acid **185** was next incorporated into SPPS for the synthesis of glycopeptide **308** (**Scheme 4.10**).

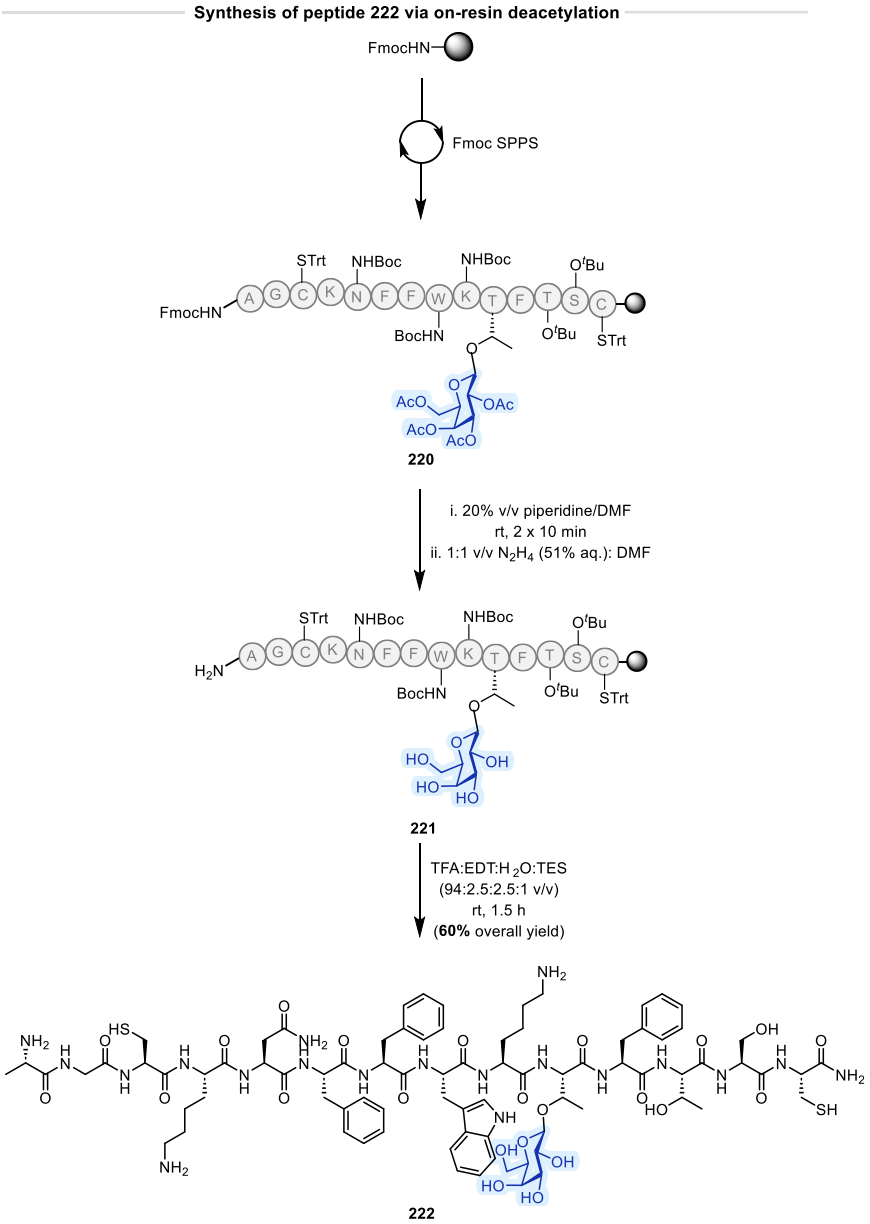

Scheme 4.10 Synthetic route to glycopeptide somatostatin analogue linear precursor **222** via Fmoc/^{t}Bu SPPS and on-resin deacetylation.

Standard Fmoc/^{t}Bu SPPS substituting glycoamino acid **185** for the threonine residue in the pharmacophore of the somatostatin 14-mer peptide sequence gave resin-bound glycopeptide **220**. Final piperidine-mediated Fmoc-deprotection and on-resin deacetylation using a 1:1 v/v solution of hydrazine hydrate (51% aq.) in DMF furnished the deacetylated glycopeptide **221** prior to cleavage from the resin. Peptide cleavage using TFA:EDT:H_2O:TES (94:2.5:2.5:1 v/v) provided linear glycopeptide **222** in an overall yield of 60%.

The linear glycopeptide **222** was next cyclised (**Scheme 4.11**).

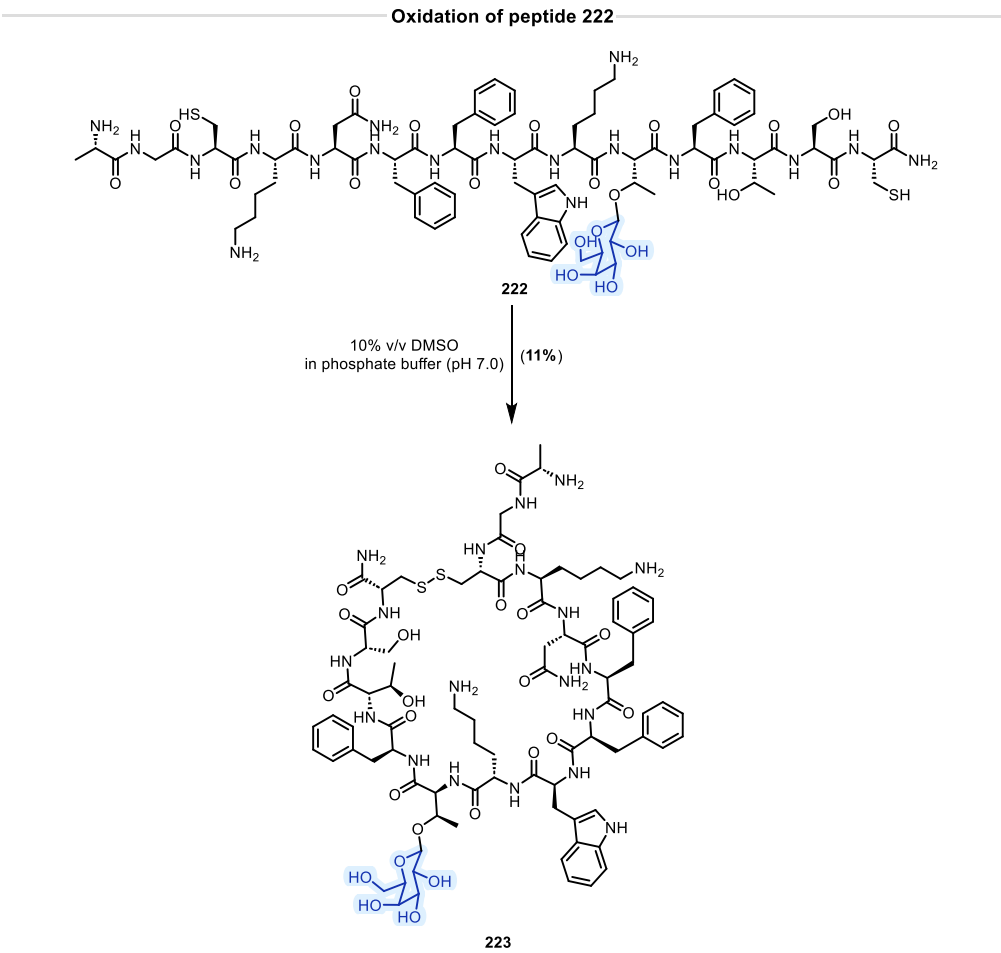

Scheme 4.11 Oxidation of linear glycopeptide **222** to glycopeptide somatostatin analogue **223**.

Glycopeptide **222** was oxidised using a 10% v/v DMSO solution in aqueous phosphate buffer at pH 7.0 to give glycopeptide somatostatin analogue **223** in a yield of 11% following semi-preparative RP HPLC purification.

4.2.2 Biological evaluation

Glycopeptide somatostatin analogue **223** was next taken forward for biological evaluation, which was carried out in collaboration with Sara Corbezzolo and Prof. Michael Monaghan. A cell viability MTT assay was planned, aiming to validate a reduction in cytotoxicity of the inactive glycopeptide prodrug and then the β-galactosidase-mediated release of somatostatin to trigger an increase in cytotoxicity.

HeLa cells were used for this cytotoxicity study due to their high expression levels of SSTR2,[312] which is the receptor type that is overexpressed in the largest number of tumour types and to

which somatostatin and its analogues demonstrate their highest affinity.[218] Firstly, an MTT assay using somatostatin was performed after 48 and 72 hours and across a concentration range (10 μM, 33 μM and 100 μM) (**Fig 4.7**). Gratifyingly, after 72 hours there was a reduction in cell viability in all tested concentrations caused by the cytotoxicity of the somatostatin peptide, with no reduction observed in absence of the peptide, making this assay suitable for validating the prodrug behaviour of glycopeptide **223**.

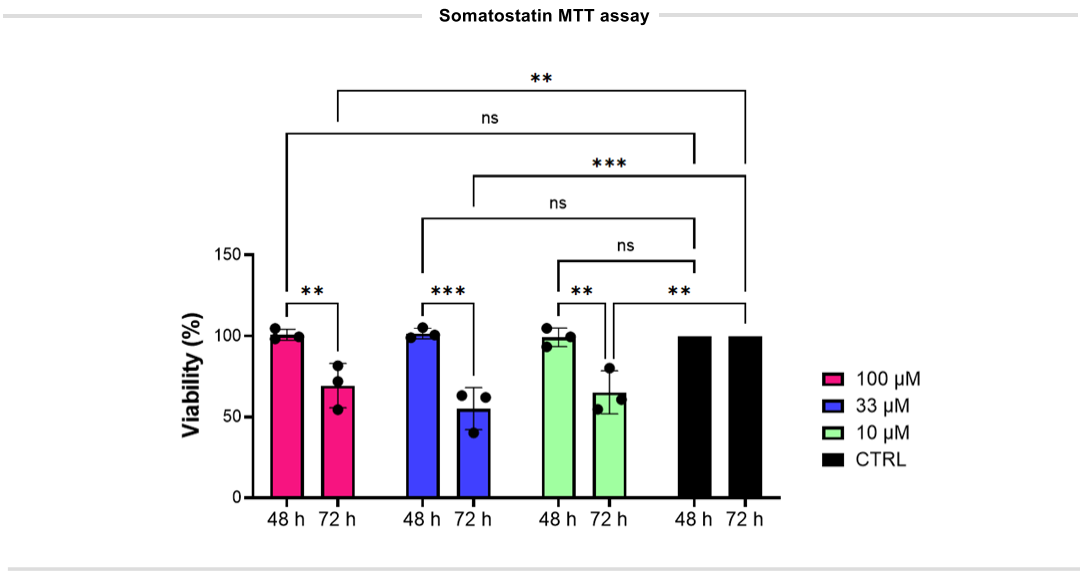

Figure 4.7 HeLa cells MTT assay after 48 and 72 hours using somatostatin at 10 μM, 33 μM and 100 μM.

With a suitable assay in hand, glycopeptide somatostatin analogue **223** was applied to this MTT assay with some additional controls. Firstly, the HeLa cells were treated with the peptide on its own, as well as with the addition of β-galactosidase to trigger release of the active peptide. For controls, a separate group used β-galactosidase and isopropyl β-D-1-thiogalactopyranoside (IPTG) as a competitive β-galactosidase inhibitor to validate any observed enzyme response, and a final control group used IPTG without any enzyme. All groups, including controls, would be applied to the native somatostatin analogue **219** synthesised in **Scheme 4.9**.

The results of this MTT assay are described below in **Fig 4.8**.

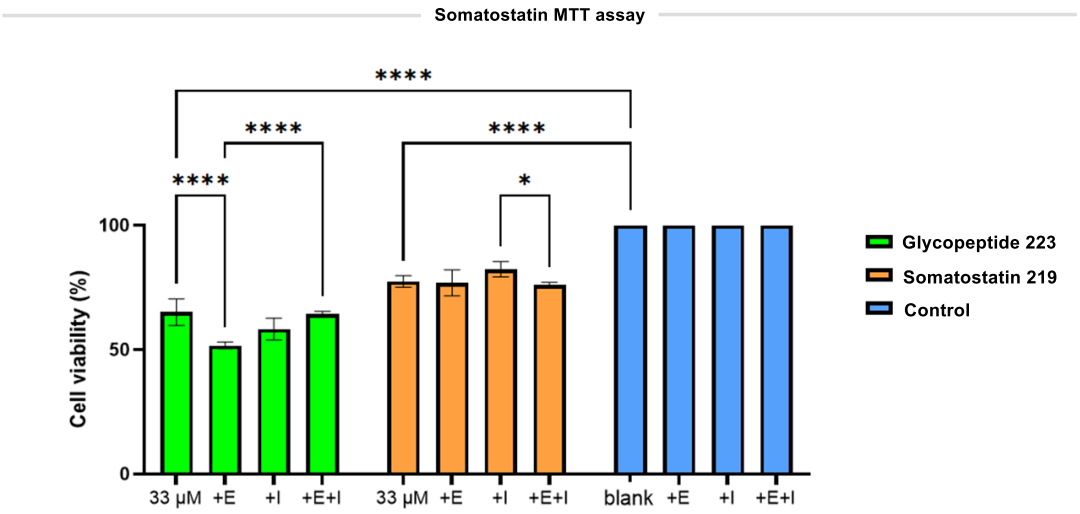

Figure 4.8 HeLa cells MTT assay after 72 hours using glycopeptide **223** and somatostatin analogue **219** at 33 µM. E = Enzyme (β-galactosidase, 100 U/mL), I = IPTG β-galactosidase inhibitor (0.2 mM), E+I = Enzyme and inhibitor.

Gratifyingly, for the glycopeptide 223, addition of β-galactosidase resulted in a significant reduction in cell viability and this effect was dramatically reduced when using IPTG as a competitive inhibitor. This demonstrates an increase in cytotoxicity mediated by β-galactosidase-triggered glycosidic bond cleavage as the pharmacophore becomes unmodified and the active peptide is released. These effects were not observed for the unmodified somatostatin **219**, which was unaffected by enzyme treatment with no glycosidic bond for the enzyme to cleave. However, for glycopeptide **223** to function as a prodrug, it would be expected for this peptide to have a significant increase in cell viability in comparison to the unmodified somatostatin **219** due to the masked pharmacophore, preventing somatostatin receptor binding. On the contrary, this assay indicates slightly higher cytotoxicity of the glycopeptide **223** when compared to the cell viability of the unmodified somatostatin **219**. It is possible that β-galactosidase activity in the HeLa cells[313] could be giving rise to this observation and additional experiments will be required to validate the result.

4.3 Conclusions and Future Work

In this chapter, various synthetic routes to unnatural amino acid galactoside analogues of threonine and lysine which feature in the pharmacophore associated with the biological activity of therapeutic peptide somatostatin are explored. The first example of a synthetic route to a galactoside threonine analogue is described, which was subsequently incorporated into SPPS to synthesise a prodrug glycopeptide analogue of somatostatin (**Fig. 4.9A**). Following the synthesis of the unmodified somatostatin analogue, both peptides were tested in an MTT assay which successfully validated the β-galactosidase-triggered cytotoxicity increase of the glycopeptide as the pharmacophore was unmasked, however the current results have not demonstrated a reduction in cytotoxicity of the glycopeptide prodrug (**Fig. 4.9B**)

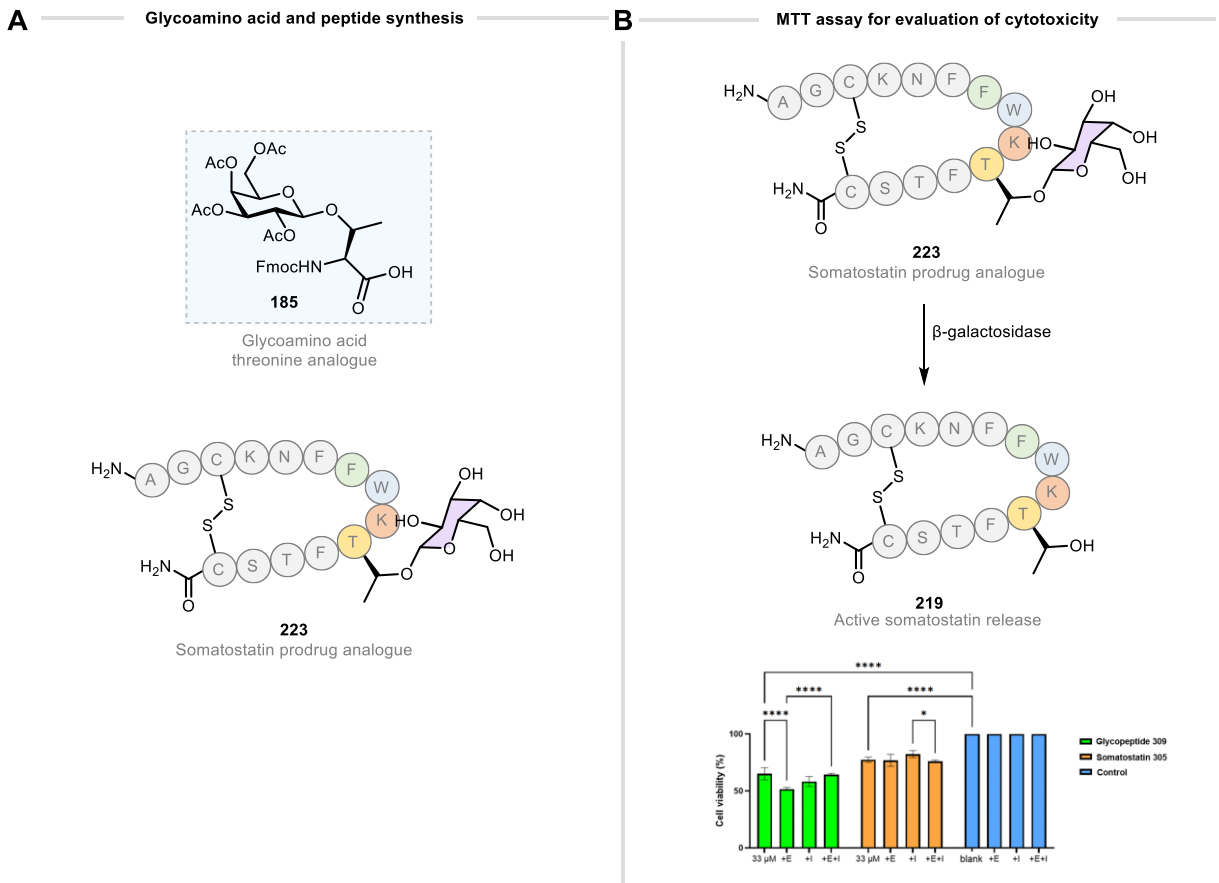

Figure 4.9 Summary of work described in this chapter. A) Glycoamino acid **185** and glycopeptide somatostatin prodrug analogue **223** synthesised using this amino acid; B) Biological evaluation of the glycopeptide via an MTT assay.

Future work on this project will require further MTT assays to investigate the prodrug behaviour of the glycopeptide. In terms of developing the medicinal chemistry aspects of this work, synthetic somatostatin analogue octreotate, which features in the clinically-approved ^{177}Lu DOTATATE therapeutic used in peptide receptor radionuclide therapy, could be used as an additional model peptide (**Fig 4.10**). As this analogue does not feature a C-terminal alcohol like octreotide, it would be easily accessible via standard SPPS. Finally, a disulfide rebridging strategy such as via a functionalised maleimide could allow for the generation of a peptide-drug conjugate prodrug utilising a somatostatin analogue as a tumour-homing peptide, a β-galactoside as a masking group and a drug for more effacious delivery.

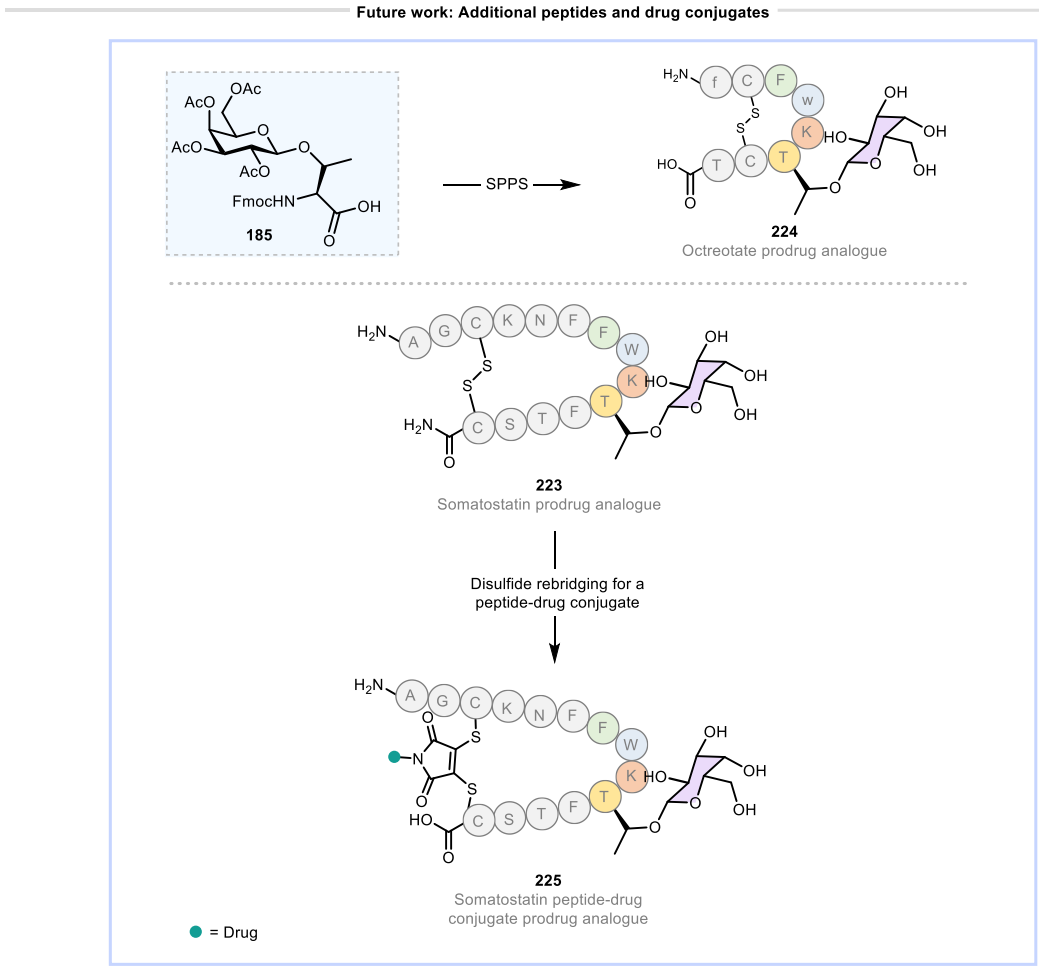

Figure 4.10 Future work to synthesise additional peptide examples for this prodrug strategy and generate peptide-drug prodrug conjugates via disulfide rebridging.

Chapter 5

Efforts Towards the Development of a Hypoxia-Activated Peptide Prodrug Analogue

Chapter 5: Efforts Towards the Development of a Hypoxia-Activated Peptide Prodrug Analogue

5.1 Introduction

In recent years, rational prodrug design has become an integrated and increasingly innovative part of cancer drug discovery efforts, facilitating improved targeting of therapeutics through the generation of inactive analogues which release the active drug upon specific activation at the tumour site. In particular, the incorporation of masking groups which block the reactivity of important functional groups and are cleavable upon activation by enzymes overexpressed in the tumour microenvironment are increasingly being used in prodrug strategies, offering rapid and specific release upon reaction.

As the level of hypoxia, which is a pathological hallmark of solid tumours, is directly correlated with the nitroreductase activity in the tumour microenvironment, nitroaromatic masking groups which are readily reduced by nitroreductases have been developed for use in hypoxia-activated prodrugs. Conway and co-workers in collaboration with Ester Hammond have pioneered recent efforts to apply nitroaromatic hypoxia-activated protecting groups to various inhibitors including checkpoint kinase 1 (Chk1) inhibitor CH-01[314] and lysine deacetylase (KDAC) inhibitors SAHA[315] and Panobinostat.[91]

As described in **Section 1.4.3**, cyclic peptide hormone somatostatin (SST) and its analogues, such as octreotide, have demonstrated use clinically for treatment of carcinoid syndrome and neuroendocrine tumours. In addition, they have also been applied to peptide-drug conjugates as tumour-homing peptides due to their specific binding to somatostatin receptors (SSTRs), which are overexpressed in various tumour types.[189]

5.2 Aims

The overall objective of this project was to apply nitroaromatic bioreductive protecting groups to SST as a model peptide to generate hypoxia-activated prodrug SST analogues, through modification of the threonine and/or lysine residues of the Phe-Trp-Lys-Thr β-turn pharmacophore. Initially, the functionalisation of Thr and Lys amino acids with nitroaromatic hypoxia-activated protecting groups would be explored, followed by the incorporation of the appropriate unnatural amino acids into solid-phase peptide synthesis (SPPS) (**Fig. 5.1A**). Following this, biological evaluation was planned to confirm the release of the active SST peptide in a hypoxia-dependent manner (**Fig. 5.1B**) and confirm the cytotoxicity level of the prodrug analogues to verify a significant reduction in toxicity, a prerequisite of a suitable prodrug. Beyond this, it was envisaged that disulfide rebridging reactions could produce peptide-drug conjugates of the prodrugs.

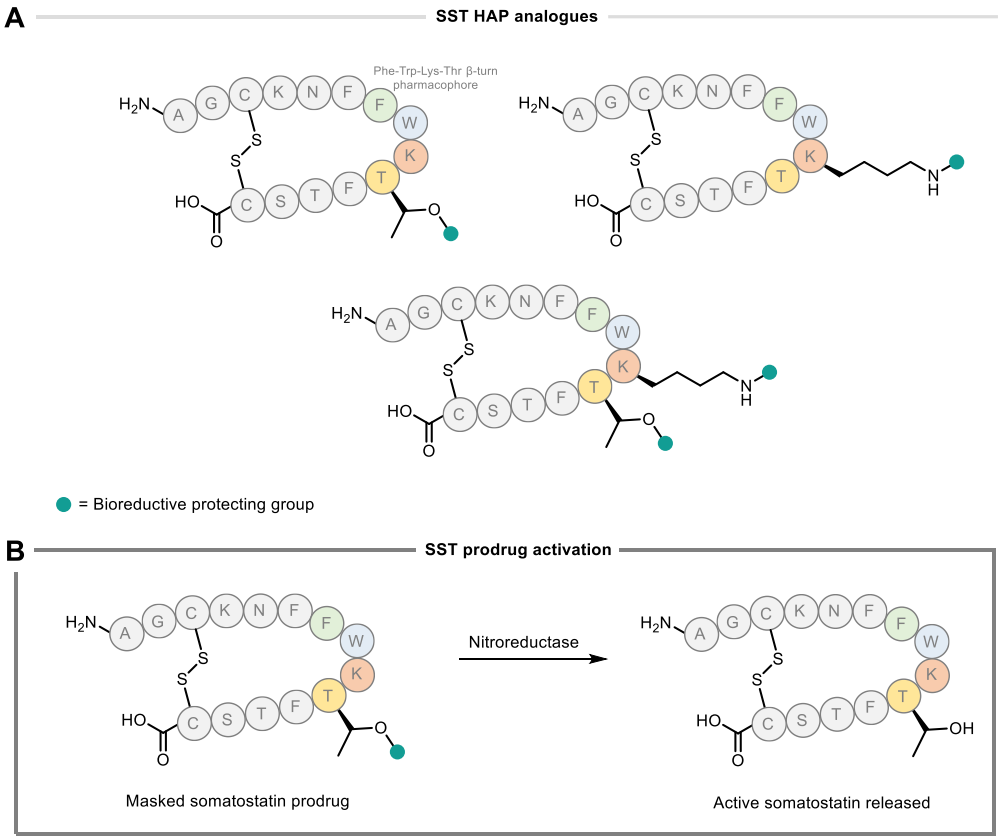

Figure 5.1 Project aims summary. A) SST HAP analogues bearing nitroaromatic bioreductive protecting groups on the Thr and/or Lys side chains. The Phe-Trp-Lys-Thr pharmacophore is highlighted in colour. B) Nitroreductase-mediated prodrug activation in a hypoxic environment.

5.3 Results and Discussion

For the synthesis of unnatural amino acids functionalised with bioreductive protecting groups, the associated reduction potentials of different nitroaromatic groups previously applied to hypoxia-activated prodrugs were considered. As described in section 1.2.4, a smaller negative reduction potential indicates more facile reduction; a suitable prodrug will require a bioreductive group that is sufficiently stable in normoxic conditions whilst being efficiently cleaved in hypoxic conditions. Two widely used groups are the 4-nitrobenzyl group (-0.49 V) and the more easily reduced 1-methyl-2-nitroimidazole group (-0.39 V), which were selected for the first unnatural amino acid target molecules. Recently, the nitrobenzyl group has been reported to require elevated enzyme concentrations above levels associated with cellular reduction for cleavage to take place, making it less suitable than other bioreductive groups for *in vivo* studies.[315]

5.3.1 Nitrobenzyl bioreductive group

The *para*-nitrobenzyl bioreductive protecting group was selected as the first group to generate hypoxia-activatable unnatural amino acids due to its literature precedence and synthetic versatility, with suitable commercially available *para*-nitrobenzyl reagents. Various routes to modification of lysine, one of the essential SST amino acids in the Phe-Trp-Lys-Thr pharmacophore, were explored aiming to produce a Lys analogue that could be incorporated into SPPS and release the cleavable protecting group upon reduction by nitroreductases (**Scheme 5.1**)

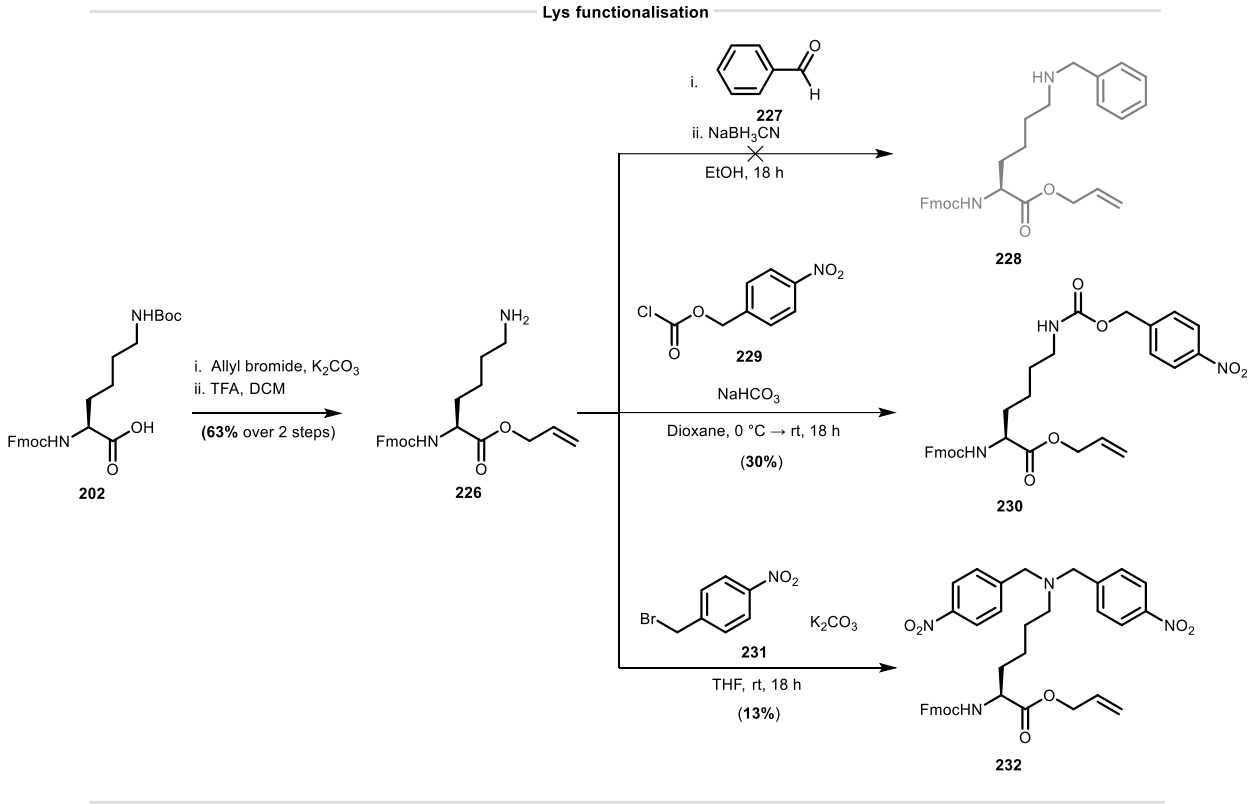

Scheme 5.1 Lys functionalisation attempts to install the *p*-nitrobenzyl group.

Fmoc-Lys(Boc)-OH (**202**) was first allyl-protected using allyl bromide followed by Boc deprotection using TFA to yield **226** in a 63% yield over two steps, which was then used as a substrate for a series of test reactions. A reductive amination was attempted using benzaldehyde **227** and sodium cyanoborohydride, although no reaction was observed and **228** was not isolated. Functionalisation using *para*-nitrobenzyl chloroformate (**229**) via a carbamate linkage gave **230** in 30% yield, however the chloroformate may not be stable to the conditions required for peptide cleavage. Reaction with *para*-nitrobenzyl bromide (**231**) afforded disubstituted product **232** in a prohibitively low yield of 13%.

Following challenges to generate suitable lysine analogues in appreciable yields, it was sought to install the *para*-nitrobenzyl group on the threonine amino acid hydroxyl side chain (**Scheme 5.2**).

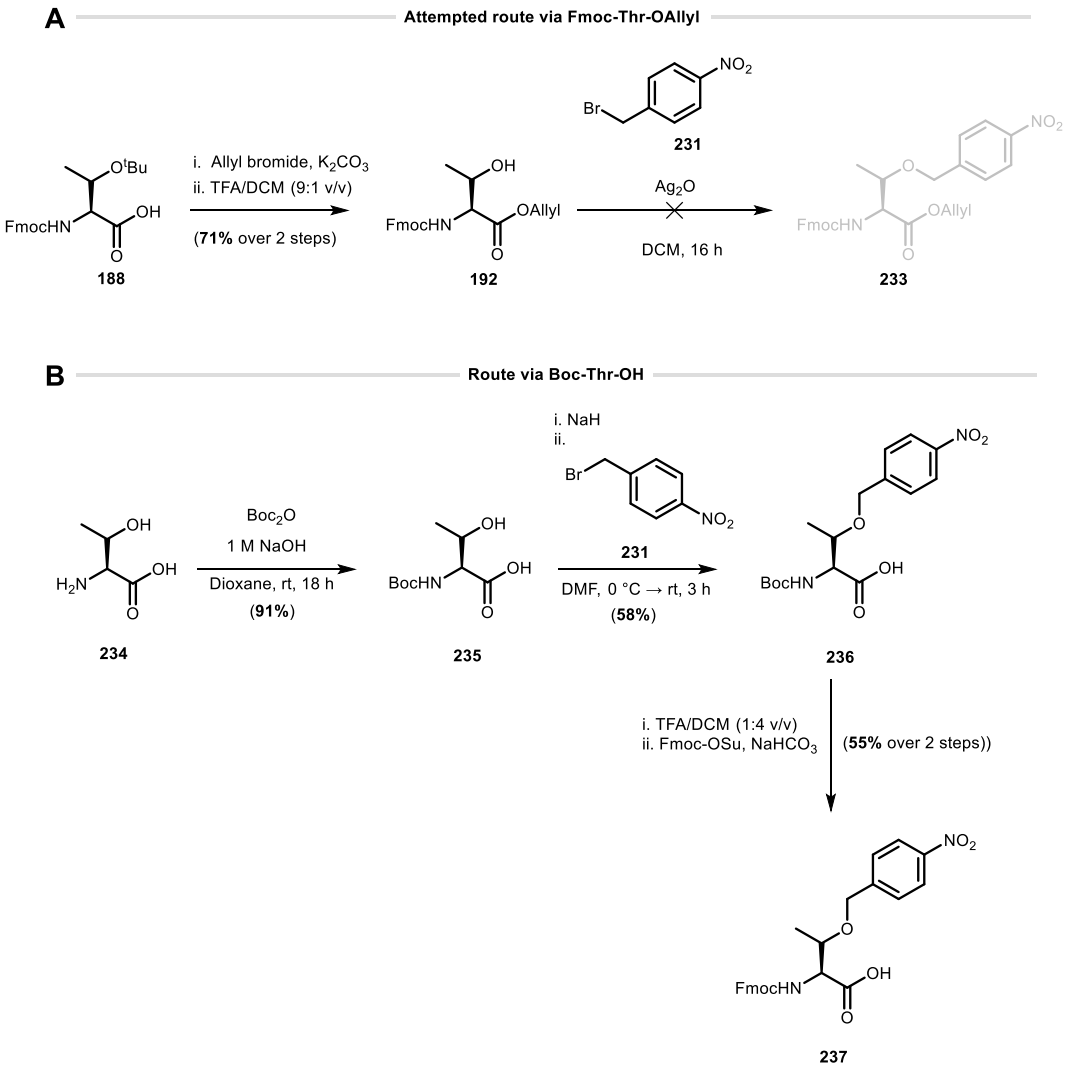

Scheme 5.2 Functionalisation of Thr with *para*-nitrobenzyl bioreductive group. A) Attempted reaction of Fmoc-Thr-O(allyl) with *para*-nitrobenzyl bromide; B) Synthetic route to unnatural amino acid **237** via Boc-Thr-OH.

It was initially attempted to functionalise Fmoc-Thr(^{t}Bu)-OH (**188**) using conditions which would not deprotect the base-labile Fmoc protecting group (**Scheme 5.2A**). Allylation of the carboxylic acid followed by ^{t}Bu-deprotection in TFA gave **192** in 71% yield over two steps. However, reaction with *para*-nitrobenzyl bromide (**231**) using halogen-selective Lewis acid Ag_2O did not provide **233**.

In order to facilitate use of a sufficiently strong base to generate the nucleophilic alkoxide, *L*-threonine (**234**) was protected with the acid-labile *tert*-butyloxycarbonyl (Boc) protecting group using Boc_2O to give **235** in 91% yield. *In situ* formation of the alkoxide using sodium hydride (NaH) followed by reaction with *para*-nitrobenzyl bromide (**231**) furnished **236** in

58% yield via a Williamson ether synthesis. Finally, Boc-deprotection using TFA followed by Fmoc-protection with Fmoc-OSu gave amino acid **237** in 55% yield across two steps, suitable for incorporation into Fmoc/^{t}Bu SPPS.

5.3.2 Nitroimidazole bioreductive group

The 1-methyl-2-nitroimidazole bioreductive group is the most widely used protecting group for hypoxia-activated responsive molecules, exhibiting promising release profiles including at enzymatic concentrations corresponding to those in the tumour microenvironment. Due to this, efforts were applied to generating lysine and threonine analogues bearing the 1-methyl-2-nitroimidazole group on the amine and hydroxyl side chains. Retrosynthetic analysis of target molecules **238** and **242** supported synthetic routes starting from 1-methyl-2-nitroimidazole derivative **241** (**Figure 5.2**).

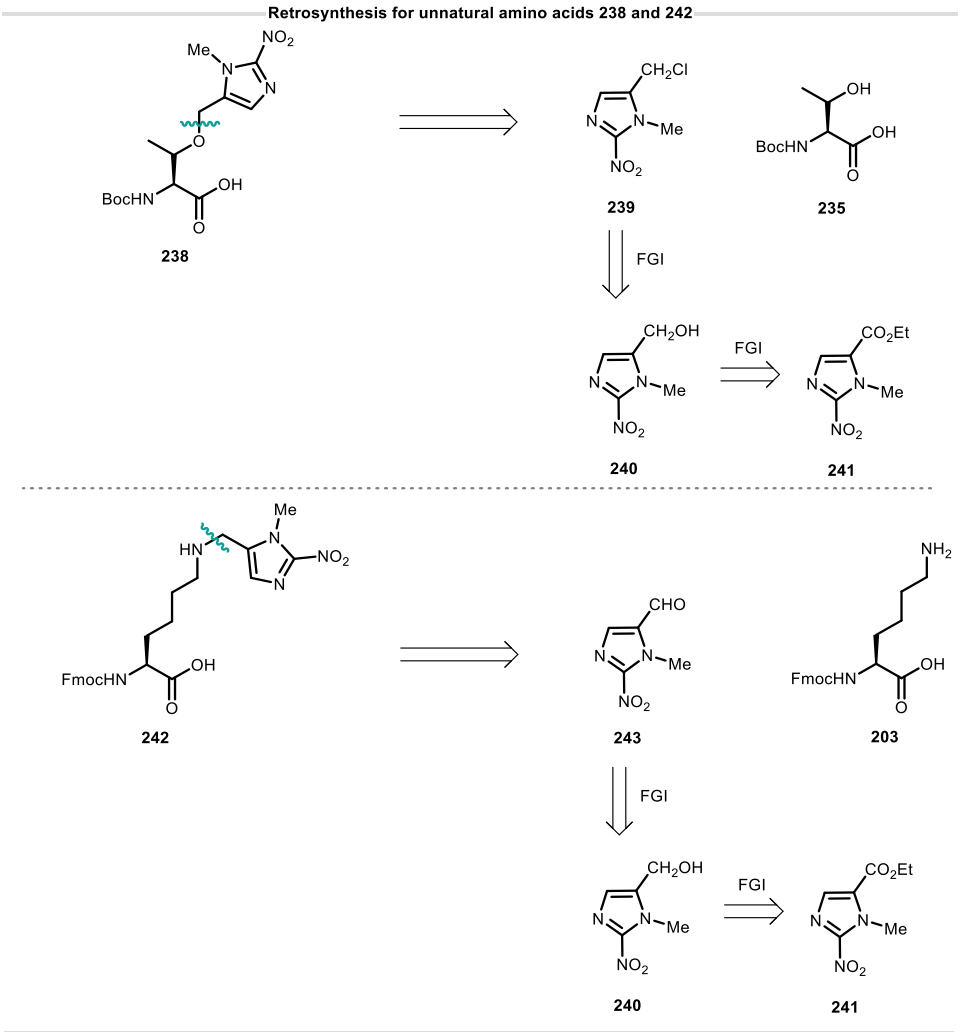

Figure 5.2 Retrosynthetic analysis of target unnatural amino acids **238** and **242.**

For threonine, alkyl chloride 1-methyl-2-nitroimidazole derivative **239** was required for reaction with Boc-Thr-OH (**235**) to furnish **238** via a Williamson ether synthesis, which may subsequently be converted into the Fmoc-protected analogue. Reduction of ethyl ester **241** would provide alcohol **240** as a precursor. For lysine, aldehyde **243** was needed for reaction with Fmoc-Lys-OH (**203**) via a reductive amination to give target molecule **242**. The aldehyde could be accessed via oxidation of **240**.

Unlike the *para*-nitrobenzyl bioreductive group, the synthetic precursors available for forming conjugates with the 1-methyl-2-nitroimidazole group are significantly less accessible, requiring a multistep route that has been the subject of several optimisation studies attempting to develop scalable conditions.[90, 316, 317] The synthesis of aminoimidazole building block **247**, based on the most established route to-date,[318] is described in **Scheme 5.3**.

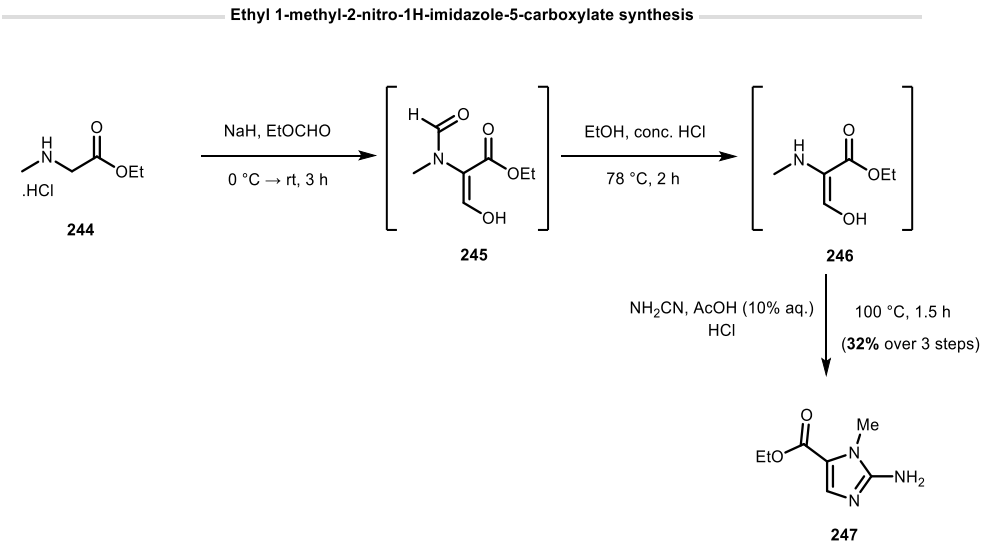

Scheme 5.3 Synthesis of aminoimidazole **247**.

This is a 3-step one-pot route which starts with the treatment of sarcosine ethyl ester (**244**) with sodium hydride and ethyl formate to give **245**, followed by *N*-deformylation under acidic conditions to provide intermediate **246** and finally a Markwald cyclisation with cyanamide at acidic pH to generate aminoimidazole **247**, which was obtained in a maximum yield of 32% over three steps.

As had been reported,[318-320] the scalability of this route was found to be challenging, precluded by prohibitively low yields in the region of 3-10% when scaled up. Various conditions were

attempted aiming to develop a reliable one-pot multistep synthesis to the key aminoimidazole building block **336**, including amore concentrated solution for the formylation step without THF[321] and pH adjustment to 4-5 instead of to 3 for the cyclisation step.[322, 323] A recent protocol reported by Skwarska *et al.*[315] was also attempted, which uses 4.0 equivalents of NaH instead of 10.0 and a small amount of EtOH to aid solubility in the first step and carrying out the *N*-formyl hydrolysis at room temperature

Despite these efforts, a reliable protocol remained elusive, with low yields of **247** precluding the required scalability for the synthesis of appropriate 1-methyl-2-nitroimidazole derivatives. Obstacles widely reported include the insolubility of reagents in the α-C-formylation step often resulting in the failure of this step to proceed[316] and the susceptibility of the ethyl ester group to hydrolyse[90] which contributed to the challenges encountered in carrying out this synthesis.

247 was taken forward for subsequent reaction for the generation of intermediates identified in the retrosynthetic analysis from **Fig. 5.2** (**Scheme 5.4**).

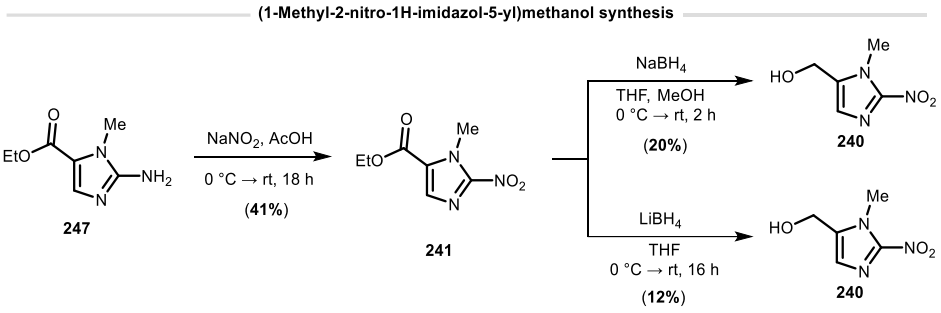

Scheme 5.4 Synthesis of **240**.

Reaction of aminoimidazole **247** with sodium nitrite in acetic acid gave nitroimidazole **241** in 41% yield. The instability of **241**, spontaneously forming tetrahydroimidazo pyrimidine derivatives, has been reported to necessitate prompt reaction following purification.[317] Ester reduction attempts using $NaBH_4$ and $LiBH_4$ yielded **240** successfully although in low yields of 20% and 12% respectively. The low yields of these steps further hindered scaling up this route. Due to the quantities of unnatural amino acids required for SPPS, this lack of scalability of this synthetic route precluded further work towards the target molecules described in **Fig. 5.2.**

5.3.3 Nitroquinoline bioreductive group

Conway and co-workers have recently explored the use of the nitroquinoline group as a bioreductive hypoxia-activated protecting group for prodrugs.[91] They predict a similar reduction potential to the nitroimidazole group, making it a promising alternative with more facile synthetic accessibility. Retrosynthetic analysis identified suitable building blocks for ligation of this group to threonine and lysine (**Fig. 5.3**).

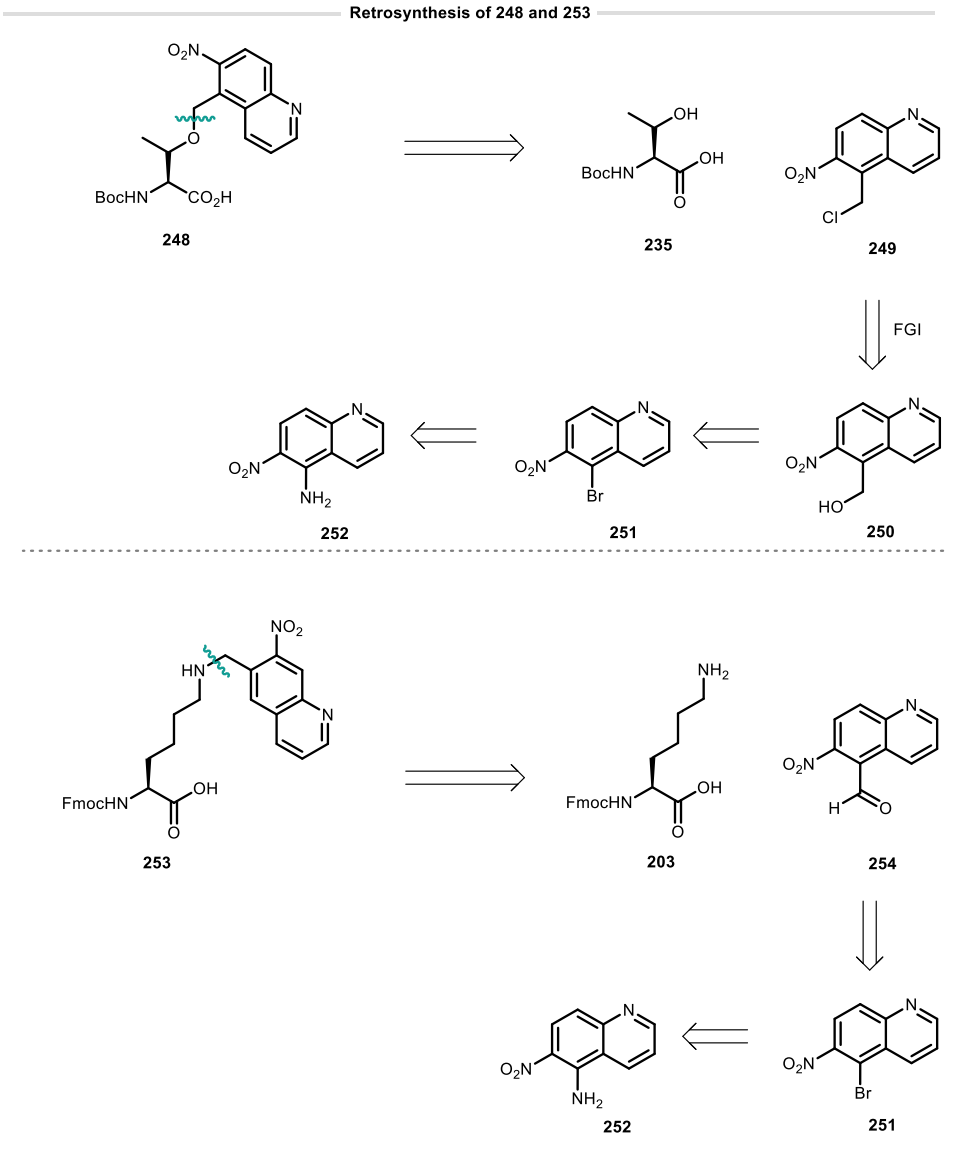

Figure 5.3 Retrosynthetic analysis of unnatural amino acids **248** and **253**.

For threonine, a Williamson ether synthesis using Boc-Thr-OH (**235**) and nitroquinoline alkyl chloride **249** would generate a suitable threonine analogue **248**, requiring a protecting

group manipulation to install the Fmoc amine protecting group. **249** could be generated starting from a Sandmeyer bromination of aniline **252** to give bromide **251**, followed by a lithium-halogen exchange and further functionalisation to give alcohol **250** and finally reaction with thionyl chloride to provide alkyl chloride **249**. In the case of lysine, a reductive amination via Fmoc-Lys-OH **203** and aldehyde nitroquinoline **254** would give the desired unnatural amino acid. Aldehyde **254** could be generated via lithium-halogen exchange and formylation of **251**. Appropriate nitroquinoline derivatives in both cases could be synthesised from commercially available 5-amino-6-nitroquinoline **252**.

It was first necessary to generate the nitroquinoline analogues required for these reactions. The synthetic routes explored, following similar reactions used for nitroquinoline derivatives reported by Conway and co-workers,[91, 324] for this are described in **Scheme 5.4**.

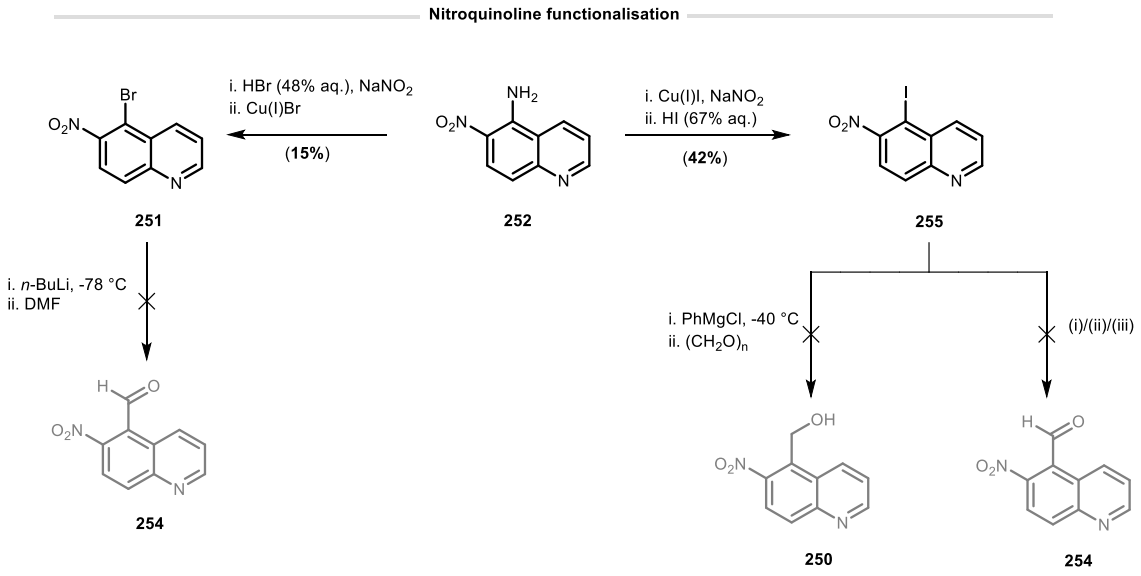

Scheme 5.4 Attempted synthesis of nitroquinoline derivatives **254** and **250**; (i) *n*-BuLi, N-formyl piperidine, -78 °C, (ii) PhLi, EtOCHO, -78 °C, (iii) *n*-BuLi, DMF, -78 °C.

Sandmeyer iodination of 5-amino-6-nitroquinlone (**252**) provided 5-iodo-6-nitroquinoline (**255**) in 42% yield. Lithium-halogen exchange reactions with nitroarene derivatives are known to be challenging due to the high electrophilciity of the nitro group, leading to nucleophilic attack or electron-transfer reactions triggered by organometallic species.[325] Therefore the generation of a nitroarylmagnesium halide via an iodine-magnesium exchange proposed by Knochel and co-workers to overcome this was explored.[326] This was attempted

followed by reaction with paraformaldehyde in one pot for the generation of (6-nitroquinolin-5-yl)methanol (**250**), however only unreacted starting material and quenched intermediate. Following this, formylation reactions were carried out for the generation of **254**, suitable for reductive amination with Fmoc-Lys-OH **203** and also for the formation of **250** via aldehyde reduction. This was attempted via lithium-iodine exchange using *n*-BuLi and PhLi lithiating agents, as well as DMF and EtOCHO formylating reactants. These attempts yielded unreacted starting material, quenched intermediate and side-product 2-butyl-6-nitroquinoline only. Finally, 5-amino-6-nitroquinoline (**252**) was brominated to give **251** in 15% yield, followed by a formylation attempt using *n*-BuLi and DMF, which did not yield the target molecule **254**.

5.4 Conclusions and Future Work

In this project, a number of approaches were explored for the synthesis of unnatural threonine and lysine analogues which bear suitable bioreductive protecting groups, for the generation of somatostatin prodrug analogues. Synthetic routes to nitroimidazole and nitroquinoline bioreductive groups with suitable reactive handles for ligation to threonine and lysine lacked reliability and scalability, precluding their further use in this work. Threonine analogue **237** was successfully synthesised across four steps. Due to the large negative reduction potential of the nitrobenzyl group, it is significantly more stable and more difficult to reduce compared to e other bioreductive groups, with higher concentrations of nitroreductase being required, therefore making it unsuitable for *in vivo* studies.[91, 318] As a result of this and the challenges in the synthesis of alternative bioreductive groups, **237** was not taken forward for integration into SPPS.

However, despite reduced prospects for *in vivo* assays, the nitrobenzyl group has previously been applied to hypoxia-activated prodrugs successfully.[314] Therefore, unnatural amino acid **237** and a control benzyl analogue **256** which should not be susceptible to nitroreductase-mediated reduction could be taken forward into the production of model somatostatin and octreotide peptides via SPPS (**Fig. 5.4**). An inhibition assay or MTT assay would confirm

reduced cytotoxicity of the prodrug. Treatment with reductases such as human NADPH-cytochrome P450 (CYP), which reduce nitroaryl groups in an oxygen-dependent manner, under hypoxic conditions as described by O'Connor *et al.*[318] would allow the determination of active-peptide release under these conditions for peptide analogues which incorporate **237**.

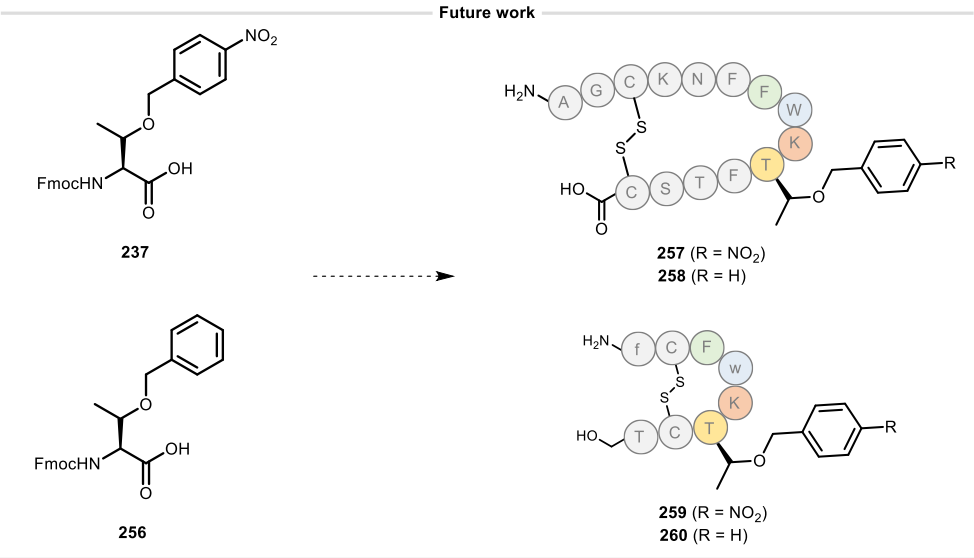

Figure 5.4 Incorporation of unnatural amino acids **237** and **256** into SPPS to give hypoxia-activated prodrug analogues of somatostatin **257** and octreotide **259**, as well as their associated controls **258** and **260** using the benzyl unnatural amino acid analogue **256**..

Chapter 6

Summary and Conclusions

Chapter 6: Conclusions and Summary

6 Conclusions and Summary

The work discussed in this thesis explores the extension of existing enzyme-activated prodrug strategies to tumour-homing model peptides and also to the development of responsive polymeric systems.

In Chapter 2, synthetic routes to a range of glycomonomer conjugates based on the β-glucuronic acid and β-galactose carbohydrate moieties and styrene and acrylamide polymerisable groups were outlined. The associated control compounds corresponding to the degradation products following glycosidase-mediated glycosidic bond cleavage were synthesised. The polymerisation of these compounds via two-photon polymerisation was investigated and optimised to generate microstructures of sub-micrometre resolution for all of the β-galactoside monomers and all control compounds. Unfortunately, it was not possible to validate a change in the physical properties of the polymers upon treatment with β-galactosidase. Future work could focus on applying these highly defined polymer microstructures to galectin and boronic acid binding, whereby fluorophore conjugates would facilitate validation of specific binding via microscopy.

In Chapter 3, various strategies to glycosides suitable for use as glycosidase-responsive crosslinkers which may be activated by the overexpression of endogenous glycosidases were explored. Synthetic routes to self-immolative scaffolds for dual- and tri-functionalised crosslinkers were successfully developed. The application of these crosslinkers to polymerisation via two-photon polymerisation was investigated, resulting in limited success. The microstructures that were generated, as well as polymers produced via bulk methods, were tested for a response to β-galactosidase-mediated activation via microscopy, although any observable degradation was minimal.

In Chapter 4, various synthetic routes to unnatural amino acid galactoside analogues of threonine and lysine which feature in the pharmacophore associated with the biological activity of therapeutic peptide somatostatin were explored. The first example of a synthetic route to a galactoside threonine analogue is described, which was subsequently incorporated

into SPPS to synthesise a prodrug glycopeptide analogue of somatostatin. An MTT assay successfully validated the β-galactosidase-triggered cytotoxicity increase of the glycopeptide as the pharmacophore was unmasked, however the current results have not demonstrated a reduction in cytotoxicity of the glycopeptide prodrug in comparison to the native peptide. Future work could focus on the optimisation of this assay and if promising results are obtained, a further somatostatin analogue of octreotate could be synthesised using standard Fmoc/^{t}Bu SPPS.

Finally, in Chapter 5, several approaches were explored for the synthesis of unnatural threonine and lysine analogues which bear suitable bioreductive protecting groups, for the generation of hypoxia-activated somatostatin prodrug analogues. Synthetic routes to nitroimidazole and nitroquinoline bioreductive groups with suitable reactive handles for ligation to threonine and lysine lacked scalability, precluding their further use in this work. A *p*-nitrobenzyl threonine analogue was successfully synthesised; although the *p*-nitrobenzyl bioreductive group has been reported to require higher nitroreductase concentrations due to its larger, negative reduction potential, future work could use this unnatural amino acid to generate a prodrug analogue of somatostatin.

Chapter 7

Experimental

Chapter 7: Experimental

7.1 General Methods

Chemical Synthesis

Reagents used were purchased from Sigma Aldrich, Fisher Scientific, Fluorochem and Tokyo Chemical Industry (TCI) and used without further purification. All moisture-sensitive reactions were carried out in oven-dried round bottom-flasks under an argon atmosphere in anhydrous solvents. Anhydrous DCM, THF and MeCN were dried using a PureSolv MD solvent purification system and anhydrous DMF, MeOH and EtOH were purchased from Sigma Aldrich and dried over molecular sieves. Petroleum ether refers to the fraction of petroleum ether that boils at 40 – 60 °C. Room temperature (rt) reactions were carried out between 18 – 21 °C. Melting points were measured using a Griffin melting point apparatus and are uncorrected with solvents of crystallisation listed along with the observed melting point range.

Flash Column Chromatography and Thin Layer Chromatography (TLC)

Flash column chromatography was performed with 60 Å (230-400 mesh particle size) silica gel from Sigma Aldrich. TLC was conducted using aluminium backed plates coated with silica matrix (0.2 mm) and fluorescent indicator (254 nm) from Sigma Aldrich. Visualisation was carried out using a UV lamp and/or appropriate staining with ninhydrin (1.5 g ninhydrin, 5 mL AcOH, 500 mL 95% EtOH), anisaldehyde (9.2 mL *p*-methoxybenzaldehyde, 3.75 mL AcOH, 338 mL 95% EtOH) and $KMnO_4$ (3 g $KMnO_4$, 20 g K_2CO_3, 300 mL water).

High-Resolution Mass Spectrometry (HRMS)

High resolution mass spectra were acquired by ESI and APCI using a Bruker microTOF-Q III mass spectrometer (set to EI^+ or EI^- mode where appropriate). ESI mass spectra were acquired using a Bruker micrOTOF-Q III spectrometer interfaced to a Dionex UltiMate 3000 LC in positive and negative modes as required. Agilent ESI-L Low Concentration Tuning Mix

was used to calibrate the system, and this was also used as an internal lock mass. Masses were recorded over the range 100 – 2000 m/z. Operating conditions were as follows: end-plate offset 500 V, capillary 4500 V, nebulizer 2.0 bar, dry gas 8.0 L min^{-1}, and dry temperature 180 °C.

APCI experiments were carried out on a Bruker micrOTOF-Q III spectrometer interfaced to a Dionex UltiMate 3000 LC or direct insertion probe in positive or negative mode as required. Agilent APCI-TOF Tuning Mix was used to calibrate the system. Masses were recorded over a range of 100 – 2000 *m/z*. Operating conditions were as follows: capillary voltage 4000 V, corona 4000 nA, nebulizer gas 2.0 bar, dry gas 3.0 L min^{-1}, dry gas temperature 100 – 200 °C, vap. temperature 100 – 400 °C. Compass HyStar version 3.2 and micrOTOF Control version 3.2 software were used to analyse the data.

Nuclear Magnetic Resonance (NMR) Spectroscopy

NMR spectra were recorded on either an Agilent MR 400 spectrometer with operating frequencies of 399.84 MHz for ^{1}H and 100.55 MHz for ^{13}C, a Bruker Avance III 400 spectrometer with operating frequencies of 400.23 MHz for ^{1}H and 100.63 MHz for ^{13}C, or a Bruker Avance II 600 spectrometer with operating frequencies of 600.13 MHz for ^{1}H and 150.90 MHz for ^{13}C. NMR spectra were processed using MestReNova (version 14.2.2). ^{1}H NMR chemical shifts were referenced to residual non-deuterated solvent peaks within the NMR solvent; $CHCl_3$ (δ_H = 7.26 ppm), DMSO (δ_H = 2.50 ppm) and MeOH (δ_H = 3.31 ppm). The chemical shifts (δ) are reported in parts per million (ppm) and signal multiplicity as s = singlet, d = doublet, t = triplet, q = quartet, m = multiplet and combinations thereof. Coupling constant (*J*) are quoted in Hertz (Hz) and reported to the nearest 0.1 Hz. ^{13}C NMR spectra are proton-decoupled with chemical shifts referenced to residual deuterated solvent peaks in the NMR solvent; $CDCl_3$ (δ_C = 77.16 ppm), DMSO-d_6 (δ_C = 39.52 ppm) and methanol-d_4 (δ_C = 49.10 ppm). Product identification and peak assignments were carried out using additional 1D experiments (TOCSY), 2D experiments (HSQC, HMBC) and pulse experiments (DEPT-135) where appropriate.

Infra-red (IR) Spectroscopy

Infra-red spectra were acquired using a Perkin Elmer FT-IR Spectrum 100 spectrometer equipped with an ATR attachment. Absorbance shape and intensity are described as w = weak; m = medium; s = strong; sh = sharp; br = broad.

High-Performance Liquid Chromatography (HPLC)

Reverse phase (RP) high performance liquid chromatography (HPLC) was performed on a Shimadzu Nexera lite Low Pressure Gradient system with an SPD-M40 photodiode array (PDA) detector at 220 nm. For analytical HPLC, an Ascentis Express 90 Å C18, 100 mm x 4.6 mm; 5 µm column with a flow rate of 1 mL min^{-1}. A gradient of 5% solvent B to 95% was used (solvent A: 0.1% TFA in H_2O; solvent B: 0.1% TFA in MeCN).

For semi-preparative HPLC purification, an Ascentis C18 250 x 10 mm, 5 µm column at a flow rate of 4 mL min^{-1} and eluted using a gradient of 5% solvent B to 95% over 30 min followed by 95% solvent B for 10 min. Fractions were collected, lyophilised, and analysed by RP-HPLC and HRMS.

7.2 Synthetic Methods for Chapter 2

Methyl 1,2,3,4-tetra-O-acetyl-D-glucopyranuronate (70)

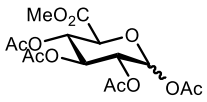

70

Following a procedure described by Leu *et al.*,[327] a mixture of D-(+)-glucurono-3,6-lactone (2.00 g, 11.3 mmol) and MeONa (20 mg, 0.36 mmol) in MeOH (20 mL) was stirred at rt under argon for 2 h. The reaction mixture was concentrated under reduced pressure to give a yellow-orange oily residue. The residue was then suspended in acetic anhydride (7.70 mL, 71.8 mmol), perchloric acid (36 µL) was added to the mixture dropwise in an ice bath and stirred under argon for 2 h at rt. After this time TLC analysis (10% MeOH/DCM) showed conversion of starting material (R_F = 0.1) to product (R_F = 0.9); analysis in 30% EtOAc/hexane confirmed consumption of the starting material (R_F = 0.0) and the formation of a product (R_F = 0.3). The reaction mixture was concentrated under reduced pressure to give a brown residue which was purified by flash column chromatography (30% EtOAc/hexane) to produce **70** (1.94 g, 5.19 mmol, 45%, 2:1 α:β anomers) as an off-white syrup.

^{1}H NMR (600 MHz, $CDCl_3$) δ_H α-anomer: 6.39 (d, J_{H1H2} 3.6 Hz, 1H, H1), 5.51 (m, 1H, H_4), 5.20 – 5.26 (m, 1H, H3), 5.10 – 5.16 (m, 1H, H2), 4.41 (d, J_{H5H4} 10.2 Hz, 1H, H5), 3.75 (s, 3H, COOC$\underline{H}_3$), 1.99 – 2.25 (m, 15H, OCOC$\underline{H}_3$).

β-anomer: 5.76 (d, J_{H1H2} 7.7 Hz, 1H, H1), 5.28 – 5.33 (m, 1H, H4), 5.20 – 5.26 (m, 1H, H3), 5.10 – 5.16 (m, 2H, H2), 4.18 (d, *J* 9.6 Hz, 1H, H5), 3.75 (s, 3H, COOC$\underline{H}_3$), 1.99 – 2.25 (m, 15H, OCOC$\underline{H}_3$) ppm.

HRMS (ESI$^+$) *m/z* calc. for $C_{15}H_{20}O_{11}Na$ $[M+Na]^+$ 399.0904; found 399.0897.

The spectral data are in agreement with the literature.[328]

2,3,4-tri-O-acetyl-1-O-benzyl-β-D-glucopyranuronate (71)

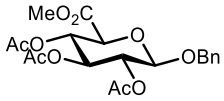

71

Following a modified procedure reported by Harnor *et al.*,[329] BnOH (0.10 mL, 1.10 mmol) was added to a mixture of **76** (100 mg, 0.21 mmol) in anhydrous DCM (2 mL) over molecular sieves (4 Å) and stirred at rt for 30 min. The reaction mixture was then cooled to 0 °C and $BF_3 \cdot Et_2O$ (30 µL, 0.21 mmol) was added dropwise, then allowed to warm to rt and stirred for 16 h under argon. After this time TLC analysis (30% EtOAc/hexane) showed partial conversion of starting material (R_F = 0.3) to product (R_F = 0.5). The mixture was filtered through Celite® and the filtrate was washed with saturated $NaHCO_3$ (3 x 5 mL). The organic phase was dried over $MgSO_4$, filtered and concentrated under reduced pressure. The crude product was purified by flash column chromatography (30% EtOAc/hexane) to give **71** (39 mg, 0.09 mmol, 44%) as a clear oil.

^{1}H NMR (400 MHz, $CDCl_3$) δ_H 7.40 – 7.26 (m, 5H, ArH), 5.19 – 5.31 (m, 2H, H3, H4), 5.07 – 5.13 (m, 1H, H5), 4.94 (d, J_{H1H2} 12.3 Hz,1H, H1), 4.62 (br s, 2H, Ph-C$\underline{H}_2$), 4.02 – 4.06 (m, 1H, H2), 3.79 (s, 3H, COOC$\underline{H}_3$), 1.99 – 2.04 (m, 9H, OCOC$\underline{H}_3$) ppm.

^{13}C NMR (100 MHz, $CDCl_3$) δ_C 170.1 (O$\underline{C}$OCH$_3$), 169.4 (O$\underline{C}$OCH$_3$), 169.0 (O$\underline{C}$OCH$_3$), 167.3 ($\underline{C}$OOCH$_3$), 136.5 (ArC), 128.5 (ArC), 128.1 (ArC), 127.8 (ArC), 99.2 (C1), 72.6 (C2), 72.1 (C3), 71.2 (C5), 70.9 (Ph-$\underline{C}$H$_2$), 69.4 (C4), 52.9 (COO$\underline{C}$H$_3$), 20.6 (OCO$\underline{C}$H$_3$), 20.5 (OCO$\underline{C}$H$_3$) ppm.

HRMS (ESI$^+$) *m/z* calc. for $C_{20}H_{24}O_{10}Na$ $[M+Na]^+$ 467.1267; found 467.1262.

The spectral data are in agreement with the literature.[330]

1-*O*-[(pentaethylene glycol)-β-D-glucopyran]uronic acid (73) (attempted)

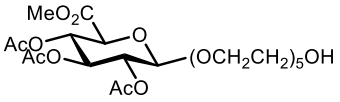

73

Pentaethylene glycol (0.27 mL, 1.25 mmol) was added to a mixture of trichloracetimidate **76** (119 mg, 0.25 mmol) in anhydrous DCM (5 mL) over molecular sieves (3 Å). The reaction

mixture was stirred for 30 min at rt under argon, then cooled to 0 °C and $BF_3 \cdot Et_2O$ (30 µL, 0.28 mmol) added dropwise. The reaction allowed to warm to rt and stirred for 18 h under argon. After this time TLC analysis (30% EtOAc/hexane) showed consumption of the material ($R_f = 0.5$) and the formation of a new spot ($R_f = 0.2$). The reaction mixture was quenched with Et_3N (0.18 mL, 1.30 mmol), then filtered through Celite® and the filtrate concentrated under reduced pressure. The crude product was purified by flash column chromatography (30% EtOAc/hexane) to recover the hydrolysis product only.

Methyl tetra-*O*-acetyl-β-D-glucopyranuronate (74)

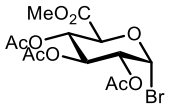

74

Following a modified procedure described by Perez *et al.*,[331] **70** (200 mg, 0.53 mmol) was dissolved in anhydrous DCM (2 mL) under argon and cooled to 0 °C. HBr (33% in glacial AcOH; 0.55 mL) was added to this solution dropwise. The mixture was slowly warmed to rt and stirred for 18 h. After this time TLC analysis (30% EtOAc/hexane) showed partial conversion of starting material ($R_F = 0.3$) to product ($R_F = 0.5$). The reaction mixture was then diluted with DCM (10 mL) and poured onto iced $NaHCO_3$ (10 mL). The organic phase was washed with water (10 mL) and brine (10 mL). The combined organic phases were dried ($MgSO_4$), filtered, concentrated under reduced pressure and the crude product purified by flash column chromatography (30% EtOAc/hexane) to give methyl tetra-*O*-acetyl-β-D-glucopyranuronate (**74**) (58 mg, 0.15 mmol, 28%) as a clear oil.

^{1}H NMR (400 MHz, $CDCl_3$) δ_H 6.62 (d, J_{H1H2} 4.0 Hz, 1H, H_1), 5.59 (app. t, J 10.0 Hz, 1H, H_3), 5.22 (m, 1H, H_4), 4.84 (dd, J_{H2H3} 10.0 Hz, J_{H2H1} 4.0 Hz, 1H, H_2), 4.56 (d, J_{H5H4} 10.4 Hz, 1H, H_5), 3.75 (3H, s, COOC$\underline{H}_3$), 2.08 (s, 3H, OCOC$\underline{H}_3$), 2.04 (m, 6H, 2x OCOC$\underline{H}_3$) ppm.

^{13}C NMR (100 MHz, $CDCl_3$) δ_C 169.7 (O$\underline{C}$OCH$_3$), 169.6 (O$\underline{C}$OCH$_3$), 169.4 (O$\underline{C}$OCH$_3$), 168.8 ($\underline{C}$OOCH$_3$), 85.4 (C1), 72.0 (C5), 70.3 (C2), 69.3 (C3), 68.5 (C4), 53.1 (COO$\underline{C}$H$_3$), 20.6 (2x OCOO$\underline{C}$H$_3$), 20.4 (OCOO$\underline{C}$H$_3$) ppm.

The spectral data are in agreement with the literature.[332]

Methyl 2,3,4-tri-O-acetyl-D-glucopyranuronate (75)

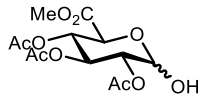

75

Following a procedure described by Oliva *et al.*,[333] **140** (500 mg, 1.33 mmol) was dissolved in anhydrous DMF (5 mL) under argon. Benzylamine (0.175 mL, 1.60 mmol) was added to the solution and the mixture was stirred at rt for 18 h. After this time TLC analysis (40% EtOAc/hexane) showed conversion of the starting material (R_F = 0.5) to product (R_F = 0.4). The solvent was removed under reduced pressure and the residue was purified by flash column chromatography (40% EtOAc/hexane) to give hemiacetal **75** (211 mg, 0.63 mmol, 48%, 10:9 α:β anomers) as a clear oil.

^{1}H NMR (400 MHz, $CDCl_3$) δ_H α-anomer: 6.38 (d, J_{H1H2} 3.7 Hz, 1H, H1), 5.50 (app. t, J 9.6 Hz, 1H, H3), 5.07 – 5.29 (m, 2H, H2, H4), 4.40 (d, J_{H5H4} 10.3 Hz, 1H, H5), 3.73 (s, 3H, COOC$\underline{H}_3$), 2.17 (s, 3H, OCOC$\underline{H}_3$), 1.99 – 2.03 (m, 6H, 2x OCOC$\underline{H}_3$) ppm.

β-anomer: 5.75 (d, J_{H1H2} 7.8 Hz, 1H, H1), 5.07 – 5.29 (m, 3H, H2, H3, H4), 4.17 (d, J_{H5H4} 9.5 Hz, 1H, H5), 3.73 (s, 3H, COOC$\underline{H}_3$), 2.10 (s, 3H, OCOC$\underline{H}_3$), 1.99 – 2.03 (m, 6H, 2x OCOC$\underline{H}_3$) ppm.

^{13}C NMR (100 MHz, $CDCl_3$) δ_C 170.2 (O$\underline{C}$OCH$_3$), 170.0 (O$\underline{C}$OCH$_3$), 169.7 (O$\underline{C}$OCH$_3$), 168.5 ($\underline{C}$OOCH$_3$), 90.2 (β-C1), 88.8 (α-C1), 70.8 (C5), 69.5 (C4), 69.1 (C3), 68.0 (C2), 52.9 (COO$\underline{C}$H$_3$), 20.7 (OCO$\underline{C}$H$_3$), 20.5 (OCO$\underline{C}$H$_3$), 20.4 (OOO$\underline{C}$H$_3$) ppm.

HRMS (ESI$^+$) *m/z* calc. for $C_{23}H_{38}O_{15}Na$ $[M+Na]^+$ 357.0798; found 357.0784.

The spectral data are in agreement with the literature.[333]

2,3,4-tri-*O*-acetyl-1-*O*-trichloroacetimidoyl-α-D-glucopyranuronate (76)

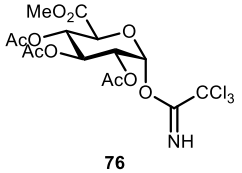

76

Following a procedure described by Oliva *et al.*,[333] Cs_2CO_3 (78 mg, 0.24 mmol) and CCl_3CN (0.96 mL, 9.60 mmol) were added to a solution of **75** (320 mg, 0.96 mmol) in anhydrous DCM (10 mL). The mixture was stirred at rt for 2 h under argon, after which time TLC analysis (30% EtOAc/hexane) showed conversion of starting material (R_F = 0.1) to product (R_F = 0.5). The reaction mixture was then concentrated under reduced pressure and the crude product purified by flash column chromatography (30% EtOAc/hexane) to give **76** (250 mg, 54%, α-anomer) as an off-white crystalline solid.

^{1}H NMR (400 MHz, $CDCl_3$) δ_H 8.72 (s, 1H, NH), 6.62 (d, J_{H1H2} 3.6 Hz, 1H, H1), 5.62 (app. t, J 9.9 Hz, 1H, H3), 5.26 (app. t, J 10.2 Hz, 1H, H4), 5.15 (dd, J_{H2H3} 10.2 J_{H2H1} 3.6 Hz, 1H, H2), 4.49 (d, J_{H5H4} 10.2 Hz, 1H, H5), 3.75 (s, 3H, $COOC\underline{H}_3$), 2.05-2.02 (m, 6H, 2x $OCOC\underline{H}_3$), 2.01 (s, 3H, $OCOC\underline{H}_3$) ppm.

^{13}C NMR (100 MHz, $CDCl_3$) δ_C 169.8 ($O\underline{C}OCH_3$), 169.7 ($O\underline{C}OCH_3$), 169.4 ($O\underline{C}OCH_3$), 167.1 ($\underline{C}OOCH_3$), 160.5 ($O\underline{C}NH$), 92.6 (C1), 90.5 ($\underline{C}Cl_3$), 70.4 (C5), 69.4 (C2), 69.1 (C4), 68.9 (C3), 53.0 ($OCO\underline{C}H_3$), 20.6 ($OCO\underline{C}H_3$), 20.5 ($OCO\underline{C}H_3$), 20.4 ($OCO\underline{C}H_3$) ppm.

HRMS (ESI^+) *m/z* calc. for $C_{15}H_{18}Cl_3NO_{10}Na$ $[M+Na]^+$ 499.9894; found 499.9899.

mp 108 – 109 °C (lit. 108 – 110 °C)[329] from EtOAc/hexane.

The spectral data are in agreement with the literature.[329]

2,3,4-tri-O-acetyl-1-O-ethoxy-β-D-glucopyranuronate (72)

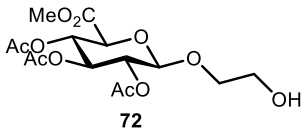

72

Following a modified procedure reported by Harnor *et al.*,[329] ethylene glycol (0.36 mL, 6.50 mmol) was added to a mixture of **76** (619 mg, 1.30 mmol) in anhydrous DCM (5 mL) over molecular sieves (3 Å). The reaction mixture was stirred for 30 min at rt under argon, then cooled to 0 °C and $BF_3 \cdot Et_2O$ (0.16 mL, 1.30 mmol) added dropwise. The reaction allowed to warm to rt and stirred for 18 h under argon. After this time TLC analysis (30% EtOAc/hexane)

showed consumption of the material (R_f = 0.5) and the formation of a product (R_f = 0.2). The reaction mixture was quenched with Et_3N (0.18 mL, 1.30 mmol), then filtered through Celite® and the filtrate concentrated under reduced pressure. The crude product was purified by flash column chromatography (30% EtOAc/hexane) to give **72** (97 mg, 0.26 mmol, 20%) as a clear oil.

^{1}H NMR (400 MHz, $CDCl_3$) δ_H 5.31 – 5.18 (m, 2H, H3, H4), 5.01 (app. t, *J* 10.0 Hz, 1H, H2), 4.61 (d, J_{H1H2} 7.6 Hz, 1H, H1), 4.07 (d, J_{H5H4} 9.6 Hz, 1H, H5), 3.89 – 3.80 (m, 2H, CHOC$\underline{H}_2$), 3.75 (s, 3H, COOC$\underline{H}_3$), 3.73 – 3.69 (2H, m, C$\underline{H}_2$OH), 2.05 (3H, s, OCOC$\underline{H}_3$), 2.01 – 2.04 (6H, m, OCOC$\underline{H}_3$) ppm.

^{13}C NMR (100 MHz, $CDCl_3$) δ_C 170.1 (O$\underline{C}$OCH$_3$), 169.5 (O$\underline{C}$OCH$_3$), 169.4 (O$\underline{C}$OCH$_3$), 167.1 ($\underline{C}$OOCH$_3$), 101.2 (C1), 73.0 (CHO*C*H$_2$), 72.2 (C5), 71.9 (C3), 71.3 (C2), 69.1 (C4), 61.9 ($\underline{C}$H$_2$OH), 53.1 (COO$\underline{C}$H$_3$), 20.7 (OCO$\underline{C}$H$_3$), 20.6 (OCO$\underline{C}$H$_3$), 20.5 (OCO$\underline{C}$H$_3$) ppm.

HRMS (ESI$^+$) *m/z* calc. for $C_{15}H_{22}O_{11}Na$ $[M+Na]^+$ 401.1060; found 401.1048.

The spectral data are in agreement with the literature.[334]

2-((4-vinylbenzyl)oxy)ethan-1-ol (78)

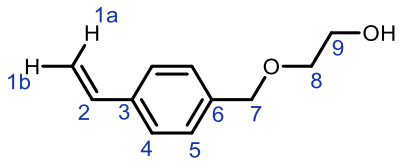

78

Following a procedure described by Lee *et al.*,[335] ethylene glycol (0.11 mL, 2.0 mmol) was added dropwise to a stirred solution of NaH (60% dispersion in mineral oil; 32 mg, 0.80 mmol) in anhydrous DMF (3 mL) at 0 °C. After the solution was stirred over 1 h, 4-vinylbenzyl chloride (0.10 mL, 0.70 mmol) was added dropwise to the suspension at 0 °C and stirred at rt for 18 h. After this time TLC analysis (30% EtOAc/hexane) showed complete conversion of starting material (R_F = 0.9) to product (R_F = 0.2) and water (5 mL) was poured into the solution. The aqueous phase was extracted with EtOAc (3 × 5 mL) and combined organic phases dried over $MgSO_4$, filtered and concentrated under reduced pressure. The product was further purified by a flash column chromatography (30% EtOAc/hexane) to yield **78** (78 mg, 0.44 mmol, 63%) as a pale yellow oil.

^{1}H NMR (400 MHz, $CDCl_3$) δ_H 7.40 (d, J_{H4H5} 8.0 Hz, 2H, H4), 7.31 (d, J_{H5H4} 8.2 Hz, 2H, H5), 6.72 (1H, m, H2), 5.75 (d, J_{H1aH2} 17.6 Hz, 1H, H1a), 5.25 (d, J_{H1bH2} 10.9 Hz, 1H, H1b), 4.54 (s, 2H, H7), 3.74 (m, 2H, H9), 3.57 (m, 2H, H8), 2.54 (s, 1H, OH) ppm.

^{13}C NMR (100 MHz, $CDCl_3$) δ_C 137.6 (ArC), 137.2 (ArC), 136.5 (C2), 128.1 (C5), 126.3 (C4), 114.0 (C1), 73.0 (C7), 71.4 (C8), 61.9 (C9) ppm.

HRMS (ESI$^+$) *m/z* calc. for $C_{11}H_{14}O_2Na$ $[M+Na]^+$ 201.0892; found 201.0885.

The spectral data are in agreement with the literature.[335]

1-(4-vinylphenyl)-2,5,8,11,14-pentaoxahexadecan-16-ol (79)

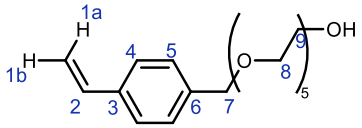

79

Following a procedure described by Lee *et al.*,[335] pentaethylene glycol (0.21 mL, 1.0 mmol) was added dropwise to a stirred solution of NaH (60% dispersion in mineral oil; 15 mg, 0.40 mmol) in anhydrous DMF (3 mL) at 0 °C. After the solution was stirred over 1 h, 4-vinylbenzyl chloride (0.05 mL, 0.35 mmol) was added dropwise to the suspension at 0 °C and stirred at rt for 18 h. After this time TLC analysis (2% MeOH/DCM) showed complete conversion of starting material (R_F = 0.9) to product (R_F = 0.4) and water (5 mL) was poured into the solution. The aqueous phase was extracted with EtOAc (3 × 5 mL) and combined organic phases dried over $MgSO_4$, filtered and concentrated under reduced pressure. The product was further purified by a flash column chromatography (2% MeOH/DCM) to yield **79** (177 mg, 0.50 mmol, 50%) as a clear oil.

^{1}H NMR (400 MHz, $CDCl_3$) δ_H 7.37 (d, J_{H4H5} 8.0 Hz, 2H, H4), 7.29 (d, J_{H5H4} 8.0 Hz, 2H, H5), 6.70 (dd, J_{H2H1a} 17.6 Hz J_{H2H1b} 10.9 Hz, 1H, H2), 5.73 (d, J_{H1aH2} 17.6 Hz, 1H, H1a), 5.22 (d, J_{H1bH2} 10.9 Hz, 1H, H1b), 4.54 (s, 2H, H7), 3.52 – 3.73 (m, 20H, H8, H9), 2.95 (s, 1H, OH) ppm.

HRMS (ESI$^+$) *m/z* calc. for $C_{19}H_{31}O_6$ $[M+H]^+$ 354.2042; found 354.2049.

The spectral data are in agreement with the literature.[336]

1-*O*-[(1-(4-vinylphenyl)-2,5,8,11,14-pentaoxahexadecane)-β-D-glucopyran]uronic acid (80) (attempted)

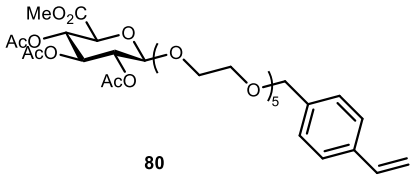

80

79 (138 mg, 0.39 mmol) in anhydrous DCM (1 mL) was added to suspension of trichloroacetimidate **76** (124 mg, 0.26 mmol) in anhydrous DCM (1 mL) and molecular sieves (4Å) under argon. The reaction mixture was stirred for 10 min at room temperature and then cooled to -10 °C. TMSOTf (8 µL, 0.040 mmol) was added dropwise to the reaction mixture and stirred at -10 °C for 30 min and then at rt for 3 h under argon. After this time, TLC analysis (2% MeOH/DCM) showed complete consumption of starting material (R_F = 0.4) and the formation of two spots (R_F = 0.2, 0.5) and the reaction mixture was quenched with Et_3N (5 µL), filtered through Celite® and concentrated under reduced pressure. The crude product was purified by flash column chromatography (30% EtOAc/hexane) to recover the hydrolysis product and a by-product.

Methyl 1-*O*-[(2-((4-vinylbenzyl)oxy)ethane)-2,3,4-tri-*O*-acetyl-β-D-glucopyran]uronate (81)

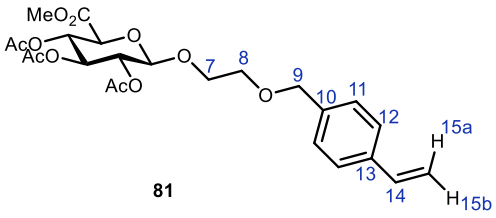

81

78 (420 mg, 2.36 mmol) was added to suspension of trichloroacetimidate **76** (747 mg, 1.57 mmol) in anhydrous DCM (10 mL) and molecular sieves (4Å) under argon. The reaction mixture was stirred for 10 min at room temperature and then cooled to -10 °C. TMSOTf (14 µL, 0.079 mmol) was added dropwise to the reaction mixture and stirred at -10 °C for 30 min and then at rt for 1 h under argon. After this time, TLC analysis (7:3 hexane:EtOAc) showed complete conversion of starting material (R_F = 0.5) to a product (R_F = 0.2) and the reaction mixture was quenched with Et_3N, filtered through Celite® and concentrated under reduced

pressure. The product was purified by flash column chromatography (30% EtOAc/hexane) to give compound **81** (266 mg, 0.54 mmol, 34%) as a clear oil.

^{1}H NMR (400 MHz, $CDCl_3$) δ_H 7.32 – 7.39 (m, 2H, H12), 7.24 – 7.29 (m, 2H, H11), 6.70 (dd, $J_{H14H15a}$17.6 Hz $J_{H14H15b}$ 10.9 Hz, 1H, H14), 5.70 (dd, $J_{H15aH14}$ 17.6 Hz $J_{H15aH15b}$ 1.0 Hz, 1H, H15a), 5.19 – 5.27 (m, 3H, H15b, H3, H5), 4.98 – 5.06 (m, 1H, H2), 4.67 (d, 1H, J_{H1H2} 7.7 Hz, 1H, H1), 4.47 – 4.54 (m, 2H, H9), 3.96 – 4.04 (m, 2H, H4, H7a), 3.75 – 3.79 (m, 1H, H7b), 3.73 (s, 3H, $COOCH_3$), 3.59 – 3.64 (m, 2H, H7), 2.01 (s, 6H, 2x $OCOCH_3$), 1.98 (s, 3H, $OCOCH_3$) ppm.

^{13}C NMR (100 MHz, $CDCl_3$) δ_C 170.2 ($OCOCH_3$), 169.44 ($OCOCH_3$), 169.36 ($OCOCH_3$), 167.3 ($COOCH_3$), 137.7 (ArC), 137.0 (ArC), 136.5 (C14), 127.8 (C11), 126.3 (C12), 113.9 (C15), 100.9 (C1), 73.1 (C9), 72.1 (C8), 70.6 (C7), 53.2 ($COOCH_3$), 20.7 ($OCOCH_3$), 20.6 ($OCOCH_3$), 20.5 ($OCOCH_3$) ppm.

HRMS (ESI^+) *m/z* calc. for $C_{24}H_{30}O_{11}Na$ $[M+Na]^+$ 517.1686; found 517.1680.

ν_{max}/cm^{-1} (neat) 2956 (aromatic stretch), 1748 (CO).

1-*O*-[(2-((4-vinylbenzyl)oxy)ethane)-β-D-glucopyran]uronic acid (82)

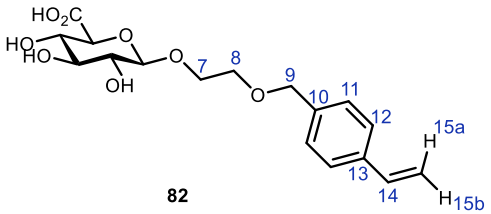

82

81 (640 mg, 1.30 mmol) was dissolved in MeOH (15 mL), then 1 M NaOH (5 mL) and water (10 mL) were added and the reaction mixture was stirred for 3 h at rt. After TLC analysis (10% water, 40% isopropanol/EtOAc) showed consumption of the starting material (R_F = 0.9) and formation of the product (R_F = 0.3), the reaction was then quenched by adding Amberlite™ until the pH of the solution was neutral. The solution was filtered and concentrated under reduced pressure to yield **82** as an off-white amorphous solid (249 mg, 0.68 mmol, 52%).

^{1}H NMR (400 MHz, DMSO-d_6) δ_H 7.47-7.42 (m, 2H, H12), 7.35-7.30 (m, 2H, H11), 6.77-6.68 (dd, $J_{H14H15b}$ 17.6 $J_{H14H15a}$ 10.9 Hz, 1H, H14), 5.81 (dd, J_{15aH14} 17.6 $J_{15aH15b}$ 1.1 Hz, 1H, H15a), 5.24 (dd, J_{15bH14} 10.9 $J_{15bH15a}$ 1.1 Hz, 1H, H15b), 4.50 (s, 2H, H9), 4.13 (d, J_{H1H2} 7.8 Hz, 1H, H1),

3.94-3.83 (m, 1H, H5), 3.67-3.58 (m, 3H, H4, H7), 3.19-3.00 (m, 3H, H2, H8), 2.90-2.98 (t, *J* 8.3 Hz, 1H, H3) ppm.

^{13}C NMR (100 MHz, DMSO-d_6) δ_C 172.7 (C6), 136.9 (C13), 128.3 (C10), 126.5 (C11), 114.5 (C14), 103.4 (C1), 72.2 (C8), 68.3 (C5), 77.3 (C2), 74.1 (C7), 73.8 (C3), 72.7 (C5), 72.2 (C8), 69.5 (C4), 68.3 (C6) ppm.

HRMS (ESI^-) *m/z* calc. for $C_{17}H_{21}O_8$ $[M]^-$ 353.1242; found 353.1243.

ν_{max}/cm^{-1} (neat) 3314 (OH), 2915 (aromatic stretch), 1739 (CO).

mp 101 – 102 °C.

Methyl 1-*O*-[(*N*-ethylacrylamide)-2,3,4-tri-*O*-acetyl-β-D-glucopyran]uronate (83) (attempted)

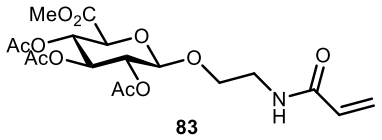

83

Method A:

N-hydroxyethyl acrylamide (76 µL, 0.73 mmol) was added to suspension of trichloroacetimidate **76** (140 mg, 0.29 mmol) in anhydrous DCM (3 mL) and molecular sieves (4 Å) under argon. The reaction mixture was stirred for 10 min at room temperature and then cooled to -10 °C. TMSOTf (8 µL, 0.040 mmol) was added dropwise to the reaction mixture and stirred at -10 °C for 30 min and then at rt for 3 h under argon. After this time, TLC analysis (30% EtOAc/hexane) showed partial consumption of starting material (R_F = 0.4) and the formation of a new spot (R_F = 0.3) and the reaction mixture was quenched with Et_3N (5 µL), filtered through Celite® and concentrated under reduced pressure. The crude product was purified by flash column chromatography (30% EtOAc/hexane) to recover unreacted trichloroacetimidate starting material and the hydrolysis product.

Method B:

N-hydroxyethyl acrylamide (73 µL, 0.70 mmol) was added to suspension of trichloroacetimidate **76** (132 mg, 0.28 mmol) in anhydrous DCM (3 mL) and molecular sieves (4 Å) under argon. The reaction mixture was stirred for 10 min at room temperature and then cooled to -10 °C. $BF_3.Et_2O$ (35 µL, 0.28 mmol) was added dropwise to the reaction

mixture and stirred at -10 °C for 30 min and then at rt for 3 h under argon. After this time, TLC analysis (30% EtOAc/hexane) showed partial consumption of starting material (R_F = 0.4) and the formation of two spots (R_F = 0.1, 0.3) and the reaction mixture was quenched with Et_3N (40 µL), filtered through Celite® and concentrated under reduced pressure. The crude product was purified by flash column chromatography (30% EtOAc/hexane) to recover the hydrolysis product and a by-product.

_N_-(2-(prop-2-yn-1-yloxy)ethyl)acrylamide (86)

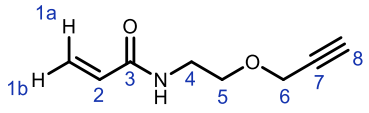

86

N-hydroxyethyl acrylamide (0.18 mL, 1.07 mmol) was added dropwise to a suspension of NaH (60% in mineral oil; 37 mg, 0.92 mmol) in anhydrous DMF (5 mL) at 0 °C and the mixture was stirred at this temperature for 30 min under argon. Propargyl bromide (70 µL, 9.81 mmol) was then added dropwise at 0°C and the reaction mixture was stirred at rt for 16 h under argon. After this time, TLC analysis (50% EtOAc/hexane) showed consumption of the starting material (R_F = 0.0) and the formation of a product (R_F = 0.3). The resulting mixture was diluted with water (10 mL) and extracted with EtOAc (3 x 5 mL). The combined organic layers were washed with brine (10 mL), dried over anhydrous Na_2SO_4, filtered and concentrated under reduced pressure. The crude product was purified by flash column chromatography (30% → 50% EtOAc/hexane) as eluent to give compound **86** (60 mg, 37%) as a clear oil.

^{1}H NMR (400 MHz, $CDCl_3$) δ_H 6.29 (br s, 1H, NH), 6.23 (dd, J_{H1aH2} 17.0, J_{H1aH1b} 1.6 Hz, 1H, H1a), 6.09 (dd, J_{H2H1a} 17.0, J_{H2H1b} 10.1 Hz, 1H, H2), 5.59 (dd, J_{H1bH2} 10.2, J_{H1bH1a} 1.6 Hz, 1H, H1b), 4.12 (d, J_{H6H8} 2.4 Hz, 2H, H6), 3.56-3.61 (m, 2H, H5), 3.48 – 3.53 (m, 2H, H4), 2.43 (t, J_{H8H6} 2.4 Hz, 1H, H8) ppm.

^{13}C NMR (100 MHz, $CDCl_3$) δ_C 165.7 (C3), 130.8 (C2), 126.4 (C1), 79.3 (C7), 74.9 (C8), 68.6 (C5), 58.4 (C6), 39.1 (C4) ppm.

HRMS (ESI$^+$) *m/z* calc. for $C_8H_{11}NNaO_2$ $[M+Na]^+$ 176.0682; found 176.0686.

ν_{max}/cm^{-1} (neat) 3287 (alkene stretch), 1656 (CO).

Methyl 1-*O*-[(3-chloropropyl)-2,3,4-tri-*O*-acetyl-β-D-glucopyran]uronate (88)

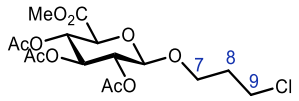

88

3-chloro-1-propanol (0.81 mL, 9.75 mmol) was added to a mixture of acetimidate **76** (930 mg, 1.95 mmol) in anhydrous DCM (10 mL) over molecular sieves and the reaction was stirred for 30 min at rt under argon. The reaction mixture was then cooled to -10 °C and $BF_3{\cdot}Et_2O$ (248 µL, 2.15 mmol) was added dropwise and stirred at rt for 16 h under argon. After this time, TLC analysis (30% EtOAc/hexane) showed complete consumption of the starting material (R_F = 0.5) and the formation of a new spot (R_F = 0.3). The reaction mixture was quenched with Et_3N (0.30 mL, 2.15 mmol), filtered through Celite® and concentrated under reduced pressure. The crude product was purified by flash column chromatography (30% EtOAc/hexane) to give **88** (393 mg, 0.96 mmol, 49%) as a white powder.

^{1}H NMR (400 MHz, $CDCl_3$) δ_H 5.17 – 5.30 (m, 2H, H3, H4), 4.96 – 5.04 (m, 1H, H2), 4.55 (d, J_{H1H2} 7.7 Hz, 1H, H1), 3.97 – 4.07 (m, 2H, H5, H7a), 3.76 (s, 3H, COOC$\underline{H}_3$), 3.66 – 3.73 (m, 1H, H7b), 3.60 (d, J_{H9H8} 5.3 Hz, 2H, H9), 2.05 (s, 3H, OCOC$\underline{H}_3$), 2.02 (m, 6H, OCOC$\underline{H}_3$), 1.90-1.97 (m, 1H, H8) ppm.

^{13}C NMR (100 MHz, $CDCl_3$) δ_C 172.0 (C6), 170.1 (O$\underline{C}$OCH$_3$), 169.4 (O$\underline{C}$OCH$_3$), 169.3 (O$\underline{C}$OCH$_3$), 167.2 (O$\underline{C}$OCH$_3$), 101.1 (C1), 72.6 (C5), 72.0 (C3), 71.2 (C2), 69.4 (C4), 66.6 (C7), 52.9 (COO$\underline{C}$H$_3$), 41.3 (C9), 32.1 (C8), 20.6 (OCO$\underline{C}$H$_3$), 20.5 (OCO$\underline{C}$H$_3$) ppm.

HRMS (ESI$^+$) *m/z* calc. for $C_{16}H_{23}ClNaO_{10}$ $[M+Na]^+$ 433.0871; found 433.0885.

mp 130 – 131 °C (lit. 129 – 130 °C)[337] from EtOAc/hexane.

The spectral data is in agreement with the literature.[338]

Methyl 1-*O*-[(3-azidopropyl)-2,3,4-tri-*O*-acetyl-β-D-glucopyran]uronate (89)

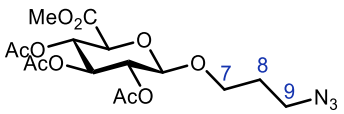

89

NaN_3 (59 mg, 0.90 mmol) was added to a solution of **88** (75 mg, 0.18 mmol) in anhydrous DMF (2 mL) and the reaction mixture was stirred at 65 °C for 16 h under argon. After this time, TLC analysis (30% EtOAc/hexane) showed no change in R_F (0.3) from the starting

material. The solvent was evaporated under reduced pressure and the residue was dissolved in DCM (10 mL) and washed with distilled water (3 x 5 mL). The organic phase was dried ($MgSO_4$), filtered and concentrated under reduced pressure. The crude product was purified by flash column chromatography (30% EtOAc/hexane) to give **89** (25 mg, 0.06 mmol, 33%) as a clear oil.

^{1}H NMR (400 MHz, $CDCl_3$) δ_H 5.14 – 5.34 (m, 2H, H3, H4), 4.96-5.04 (m, 1H, H2), 4.55 (d, J_{H1H2} 7.7 Hz, 1H, H1), 4.01 – 4.07 (m, 1H, H5), 3.93-4.00 (s, 1H, H7), 3.75 (s, 3H, COOC$\underline{H}_3$), 3.57 – 3.64 (m, 1H, H7), 3.29-3.40 (m, 2H, H9), 2.05 (s, 3H, OCOC$\underline{H}_3$), 1.99-2.03 (m, 6H, OCOC$\underline{H}_3$), 1.76-1.91 (m, 2H, H_8) ppm.

^{13}C NMR (100 MHz, $CDCl_3$) δ_C 170.1 (O$\underline{C}$OCH$_3$), 169.4 (O$\underline{C}$OCH$_3$), 169.3 (O$\underline{C}$OCH$_3$), 167.2 ($\underline{C}$OOCH$_3$), 101.8 (C_1), 71.2 (C2), 72.6 (C5), 72.0(C3), 69.4 (C4), 66.7 (C7), 52.9 (COO$\underline{C}$H$_3$), 28.9 (C8), 20.6 (2x OCO$\underline{C}$H$_3$), 20.5 (OCO$\underline{C}$H$_3$) ppm.

HRMS (ESI$^+$) *m/z* calc. for $C_{16}H_{23}N_3NaO_{10}$ $[M+Na]^+$ 440.1276; found 440.1263.

ν_{max}/cm^{-1} (neat) 2095 (azide stretch), 1738 (CO).

The spectral data are in agreement with the literature.[338]

Methyl 1-*O*-[(*N*-(2-((1-(3-(l1-oxidaneyl)propyl)-1H-1,2,3-triazol-4-yl)methoxy)ethyl)acrylamide)-2,3,4-tri-*O*-acetyl-β-D-glucopyran]uronate (90)

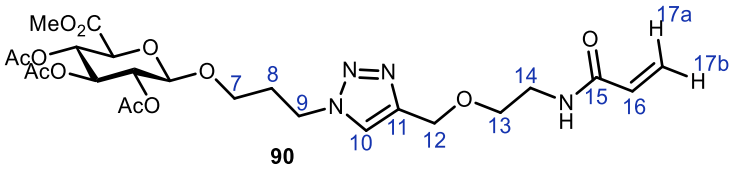

90

$CuSO_4 \cdot 5H_2O$ (5 mg, 0.0019 mmol) in water (0.1 mL) and *L*-ascorbic acid sodium salt (8 mg, 0.38 mmol) were added to a solution of alkyne **86** (29 mg, 0.19 mmol) and azide **89** (80 mg, 0.19 mmol) in degassed DCM/MeOH (1:1 v/v; 2 mL) and the resulting mixture stirred at rt for 16 h under argon. After this time TLC analysis (30% EtOAc/hexane) showed consumption of the starting material (R_F = 0.3) and the formation of a product (R_F = 0.0); analysis in EtOAc confirmed consumption of the starting material (R_F = 0.9) and formation of a product (R_F = 0.2). The reaction was diluted with DCM (10 mL) and water (10 mL) added and the aqueous layer was extracted with DCM (3×10 mL). The combined organic layers were washed with EDTA (sat. aq.; 2×10 mL), dried ($MgSO_4$) and concentrated under reduced pressure. The

crude product was purified via flash column chromatography (50% EtOAc/hexane → EtOAc) to give **90** (69 mg, 0.12 mmol, 64%) as a clear oil.

^{1}H NMR (400 MHz, $CDCl_3$) δ_H 7.67 (s, 1H, H10), 6.41 (br s, 1H, NH), 6.28 (dd, $J_{H17aH16}$ 17.0 $J_{H17aH17b}$ 1.6 Hz, 1H, H17a), 6.08 – 6.17 (m, 1H, H16), 5.63 (dd, $J_{H17bH16}$ 10.2 $J_{H17bH17a}$ 1.6 Hz, 1H, H17b), 5.26 (app. t, J_{H3H2} 9.2 Hz, 1H, H3), 5.17 – 5.23 (m, 1H, H4), 5.03 (dd, J_{H2H3} 9.2 J_{H2H1} 7.7 Hz, 1H, H2), 4.63 (s, 2H, H12), 4.56 (d, J_{H1H2} 7.7 Hz, 1H, H1), 4.36 – 4.50 (m, 2H, H9), 4.04 (d, J_{H5H4} 9.6 Hz, 1H, H5), 3.76 – 3.81 (m, 1H, H7a), 3.75 (s, 3H, $COOC\underline{H}_3$), 3.62 – 3.67 (m, 2H, H13), 3.50 – 3.58 (m, 3H, H7b, H14), 2.13 – 2.19 (m, 2H, H8), 2.07 (s, 3H, $OCOC\underline{H}_3$), 2.04 (s, 3H, $OCOC\underline{H}_3$), 2.02 (s, 3H, $OCOC\underline{H}_3$).

^{13}C NMR (100 MHz, $CDCl_3$) δ_C 170.0 ($O\underline{C}OCH_3$), 169.48 ($O\underline{C}OCH_3$), 167.44 ($O\underline{C}OCH_3$), 167.3 ($\underline{C}OOCH_3$), 165.6 ($NH\underline{C}O$), 144.5 (C11), 130.9 (C16), 126.4 (C17), 123.6 (C10), 100.5 (C1), 72.4 (C5), 71.9 (C3), 71.2 (C2), 69.4 (C4), 69.2 (C13), 65.8 (C7), 64.2 (C12), 53.0 ($COO\underline{C}H_3$), 46.5 (C9), 39.4 (C14), 30.1 (C8), 20.7 ($OCO\underline{C}H_3$), 20.6 ($OCO\underline{C}H_3$), 20.5 ($OCO\underline{C}H_3$).

HRMS (ESI$^+$) *m/z* calc. for $C_{24}H_{34}N_4NaO_{12}$ $[M+Na]^+$ 593.2065; found 593.2076.

ν_{max}/cm^{-1} (neat) 2955 (alkene stretch), 1752 (CO).

1-*O*-[(*N*-(2-((1-(3-(l1-oxidaneyl)propyl)-1H-1,2,3-triazol-4-yl)methoxy)ethyl)acrylamide)-β-D-glucopyran]uronic acid (91)

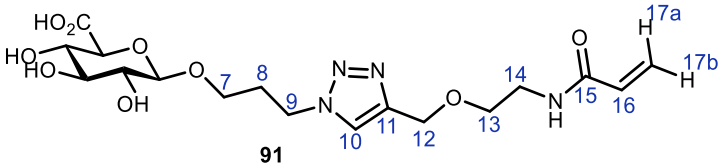

91

NaOH (0.4 M; 3 mL) was slowly added to a solution of **90** (157 mg, 0.28 mmol) in MeOH (3 mL) and the reaction was stirred at rt for 3h. After this time, TLC analysis (3% MeOH/DCM) showed complete consumption of the starting material (R_F = 0.4) and the formation of a new spot (R_F = 0.0); analysis in 20% water, 30% IPA/EtOAc confirmed consumption of the starting material (R_F = 1.0) and the formation of a product (R_F = 0.3). The reaction was quenched by adding Amberlite until the pH of the solution was neutral, filtered and concentrated under

reduced pressure. The crude product was purified by flash column chromatography (20% water, 30% IPA/EtOAc) to give **91** (42 mg, 0.10 mmol, 36%) as a pale grey solid.

^{1}H NMR (400 MHz, D_2O) δ_H 8.07 (s, 1H, H10), 6.25 (dd, $J_{H16H17a}$ 17.2 Hz $J_{H16H17b}$ 9.9 Hz, 1H, H16), 6.16 (dd, 1H, $J_{H17aH16}$ 17.2 Hz $J_{H17aH17b}$ 1.7 Hz, H17a), 5.76 (dd, 1H, $J_{H17bH16}$ 9.8 Hz $J_{H17bH17a}$ 1.7 Hz, H17b), 4.68 (s, 2H, H12), 4.56 (t, 2H, J_{H9H8} 6.8 Hz, H9), 4.43 (d, 1H, J_{H1H2} 7.9 Hz, H1), 3.84 – 3.91 (m, 1H, H7), 3.64 – 3.76 (m, 3H, H5, H13), 3.58-3.65 (m, 1H, H7), 3.50 – 3.55 (m, 2H, H3, H14), 3.44-3.48 (m, 2H, H4, H14), 3.30 – 3.36 (m, 1H, H2, H12), 2.17 – 2.26 (2H, m, H8) ppm.

^{13}C NMR (100 MHz, D_2O) δ_C 175.7 (C6), 168.5 (C15), 144.4 (C11), 129.8 (C16), 127.3 (C17), 123.1 (C10), 102.1 (C1), 76.2 (C5), 73.0 (C2), 72.1 (C3), 71.8 (C13), 68.0 (C14), 66.4 (C7), 62.8 (C12), 47.1 (C9), 39.0 (C4), 29.5 (C8) ppm.

HRMS (ESI$^+$) *m/z* calc. for $C_{17}H_{25}N_4O_9Na$ $[M+Na]^+$ 429.1627; found 429.1630.

ν_{max}/cm^{-1} (neat) 2956 (alkene stretch), 1752 (CO).

mp 112 – 114 °C.

N,*N*',*N*''-(nitrilotris(ethane-2,1-diyl))triacrylamide (99)

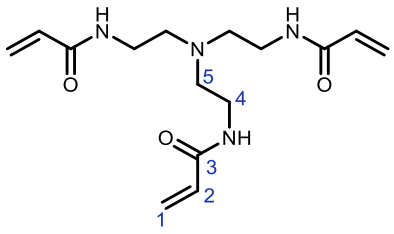

99

Acryloyl chloride (0.37 mL, 4.52 mmol) was added dropwise to a mixture of K_2CO_3 (6M aq.; 1.14 mL, 6.85 mmol,) and tris(2-aminoethyl)amine (0.21 mL, 1.37 mmol) in DCM (1.4 mL) at 0 °C and the mixture was allowed to stir at room temperature for 16 h. After this time, TLC analysis (5% MeOH/DCM) showed consumption of the acryloyl chloride (R_F = 0.9) and the formation of a product (R_F = 0.1). The reaction mixture was diluted with water (10 mL) and extracted with DCM (3 x 10 mL). The combined organic extracts were washed with brine (10 mL), dried ($MgSO_4$), filtered and concentrated under reduced pressure. The crude product was purified by flash column chromatography (5 → 10% MeOH/DCM) to give **99** (287 mg, 0.93 mmol, 68%) as an off-white solid.

^{1}H NMR (400 MHz, $CDCl_3$) δ_H 7.30 – 7.41 (m, 3H, NH), 6.17 – 6.26 (m, 6H, H1a, H2), 5.45 – 5.59 (m, 3H, H1b), 3.26 – 3.35 (m, 6H, H5), 2.51 – 2.61 (m, 6H, H4) ppm.

^{13}C NMR (100 MHz, $CDCl_3$) δ_C 166.4 (C3), 131.0 (C2), 126.3 (C1), 53.8 (C4), 37.6 (C5) ppm.

HRMS (ESI^+) *m/z* calc. for $C_{15}H_{25}N_4O_3$ $[M+H]^+$ 309.1921; found 309.1921.

mp 116 – 118 °C (lit. 118 – 120 °C)[339] from DCM.

The spectral data are in agreement with the literature.[339]

β-D-Galactose pentaacetate (103)

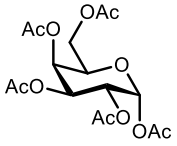

103

Perchloric acid (144 µL) was added dropwise to a suspension of D-galactose (8.00 g, 44.43 mmol) in acetic anhydride (42.0 mL, 420 mmol) at 0 °C and stirred for 1 h at this temperature. After this time, TLC analysis (30% EtOAc/hexane) showed complete consumption of *D*-galactose (R_F = 0.0) and the formation of a new product (R_F = 0.4). The reaction mixture was diluted with EtOAc (150 mL) and washed with $NaHCO_3$ (sat. aq.; 3 x 50 mL). The combined organic phases were washed with brine (sat. aq.; 50 mL), dried ($MgSO_4$) and concentrated under reduced pressure. The crude product was recrystallised from hot ethanol to give **103** (11.87 g, 30.42 mmol, 68%, α-anomer) as a white syrup.

^{1}H NMR (400 MHz, $CDCl_3$) δ_H 6.36-6.38 (m, 1H, H1), 5.48-5.51 (m, 1H, H3), 5.31-5.33 (m, 2H, H2, H4), 4.31-4.36 (m, 1H, H5), 4.03-4.15 (m, 2H, H6), 2.08-2.24 (s, 6H, $OCOCH_3$), 1.96-2.06 (m, 9H, $OCOCH_3$).

^{13}C NMR (100 MHz, $CDCl_3$) δ_C 170.4 ($OCOCH_3$), 170.1 ($OCOCH_3$), 169.9 ($OCOCH_3$), 168.9 ($OCOCH_3$), 89.8 (C1), 68.7 (C5), 67.4 (C3), 67.3 (C2), 66.4 (C4), 61.2 (C6), 20.9 ($OCOCH_3$), 20.7 ($OCOCH_3$), 20.63 ($OCOCH_3$), 20.60 ($OCOCH_3$), 20.5 ($OCOCH_3$).

HRMS (ESI^+) *m/z* calc. for $C_{16}H_{22}NaO_{11}$ $[M+Na]^+$ 413.1054; found 413.1050.

The spectral data are in agreement with the literature.[340]

1-bromo-1-deoxy-2,3,4,6-tetra-*O*-acetyl-α-D-galactopyranoside (104)

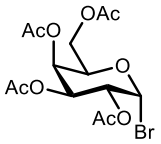

104

HBr (33% in AcOH; 24.6 mL, 138.42 mmol) was added dropwise to **103** (9.00 g, 23.1 mmol) at 0 °C and the reaction was slowly warmed to rt and stirred for 2 h. After this time, TLC analysis (30% EtOAc/hexane) showed the complete consumption of starting material (R_F = 0.2) and the formation of a new product spot (R_F = 0.4). The reaction mixture was then poured onto ice, water (100 mL) was added and extracted with DCM (3x 100 mL). The organic layer was washed with $NaHCO_3$ (sat. aq.; 3 x 100 mL), brine (100 mL), dried ($MgSO_4$), filtered and concentrated under reduced pressure to give **104** (8.60 g, 20.97 mmol, 91%, α-anomer) as a pale yellow oil.

^{1}H NMR (400 MHz, $CDCl_3$) δ_H 6.69 (d, 1H, J_{H1H2} 3.9 Hz, H_1), 5.51 (dd, 1H, J_{H4H3} 3.4 Hz, J_{H4H5} 1.4 Hz, H4), 5.40 (dd, 1H, J_{H3H2} 10.6 Hz, J_{H3H4} 3.4 Hz, H3), 5.04 (dd, 1H, J_{H2H3} 10.6 Hz J_{H2H1} 4.0 Hz, 1H, H2), 4.48 (m, 1H, H5), 4.07 – 4.19 (m, 2H, H6), 2.15 (s, 3H, OCOC$\underline{H}_3$), 2.11 (s, 3H, OCOC$\underline{H}_3$), 2.05 (s, 3H, OCOC$\underline{H}_3$), 2.01 (s, 3H, OCOC$\underline{H}_3$) ppm.

^{13}C NMR (100 MHz, $CDCl_3$) δ_C 170.3 (O$\underline{C}$OCH$_3$), 170.1 (O$\underline{C}$OCH$_3$), 169.9 (O$\underline{C}$OCH$_3$), 169.8 (O$\underline{C}$OCH$_3$), 88.1 (C1), 71.1 (C5), 68.0 (C3), 67.8 (C2), 67.0 (C4), 60.8 (C6), 20.8 (OCO$\underline{C}$H$_3$), 20.64 (OCO$\underline{C}$H$_3$), 20.59 (OCO$\underline{C}$H$_3$), 20.56 (OCO$\underline{C}$H$_3$) ppm.

HRMS (ESI$^+$) *m/z* calc. for $C_{14}H_{19}BrNaO_9$ $[M+Na]^+$ 433.0105; found 433.0111.

The spectral data are in agreement with the literature.[341]

(2-((4-vinylbenzyl)oxy)ethane)-2,3,4,6-tetra-*O*-acetyl-β-D-galactopyranoside (105)

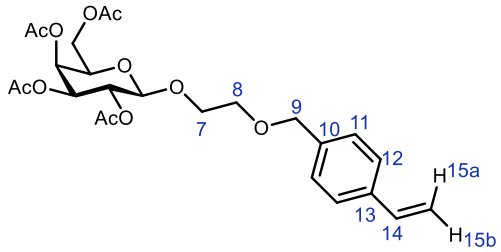

105

78 (64 mg, 0.36 mmol) and silver carbonate (99 mg, 0.12 mmol) were added to a mixture of galactosyl bromide **104** (75 mg, 0.18 mmol) in anhydrous DCM (10 mL) over molecular sieves. The mixture was stirred at room temperature in the dark for 16 h under argon. After this time, TLC (30% EtOAc/hexane) showed consumption of the starting material (R_F = 0.4) and formation of a product (R_F = 0.2). The reaction mixture was then filtered through Celite® and concentrated under reduced pressure and the crude product purified by flash column chromatography (30% EtOAc/hexane) to give **105** (48 mg, 0.95 mmol, 52%) as a clear oil.

^{1}H NMR (400 MHz, $CDCl_3$) δ_H 7.35 – 7.42 (m, 2H, H12), 7.24 – 7.31 (m, 2H, H11), 6.70 (dd, 1H, $J_{H14H15a}$ 17.6 Hz $J_{H14H15b}$ 10.9 Hz, H14), 5.73 (dd, $J_{H15aH14}$ 17.6 Hz $J_{H15aH15b}$ 1.2 Hz, H15a), 5.38 (m, 1H, H15b), 5.19 – 5.25 (m, 2H, H2, H4), 5.01 (dd, 1H, J_{H3H2} 10.1 Hz J_{H3H4} 3.4 Hz, H3), 4.57 (d, 1H, J_{H1H2} 8.0 Hz, H1), 4.50 – 4.53 (m, 2H, H9), 4.06 – 4.20 (m, 2H, H6), 3.94 – 4.03 (m, 1H, H7), 3.89 (t, 1H, J_{H5H6} 6.7 J_{H5H4} 1.2 Hz, H5), 3.72 – 3.79 (m, 1H, H7), 3.59 – 3.63 (m, 2H, H8), 2.14 (s, 3H, OCOC$\underline{H}_3$), 2.02 (s, 3H, OCOC$\underline{H}_3$), 1.95 – 2.00 (m, 6H, OCOC$\underline{H}_3$) ppm.

^{13}C NMR (100 MHz, $CDCl_3$) δ_C 170.4 (O$\underline{C}$OCH$_3$), 170.3 (O$\underline{C}$OCH$_3$), 170.2 (O$\underline{C}$OCH$_3$), 169.5 (O$\underline{C}$OCH$_3$), 137.7 (C13), 137.0 (C10), 136.5 (C14), 127.8 (C11), 126.3 (C12), 113.9 (C15), 101.4 (C1), 73.0 (C9), 70.9 (C2), 70.7 (C5), 69.2 (C7), 69.1 (C8), 68.8 (C3), 67.1 (C4), 61.3 (C6), 20.74 (OCO$\underline{C}$H$_3$), 20.68 (OCO$\underline{C}$H$_3$), 20.60 (OCO$\underline{C}$H$_3$) ppm.

HRMS (ESI$^+$) *m/z* calc. for $C_{25}H_{36}NO_{11}$ $[M+H]^+$ 526.2283; found 526.2289.

ν_{max}/cm^{-1} (neat) 1742s (CO), 2980 (C=CH$_2$ vinyl).

(2-((4-vinylbenzyl)oxy)ethane)-β-D-galactoside (106)

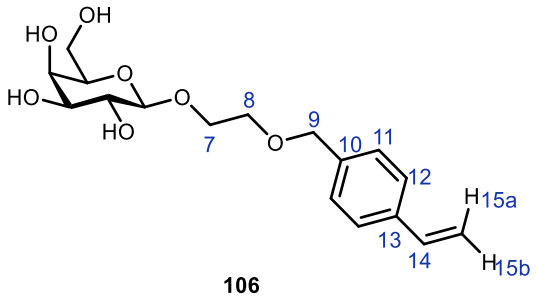

106

1 M NaOH (0.5 mL) and water (1 mL) were added to a solution of **76** (80 mg, 0.16 mmol) in MeOH (1.5 mL) and the reaction mixture was stirred for 3 h at rt. After this time, TLC analysis (30% EtOAc/hexane) showed consumption of the starting material (R_F = 0.2) and the formation of a product (R_F = 0.0); analysis in 10% MeOH/DCM confirmed consumption of the starting material (R_F = 0.9) and the formation of a product (R_F = 0.3). The reaction was then quenched by adding Amberlite acidic ion exchange resin until the pH of the solution was neutral. The solution was filtered, concentrated under reduced pressure and purified by flash column chromatography (10% MeOH/DCM), followed by lyophilisation to give **106** (30 mg, 0.09 mmol, 55%) as an off-white amorphous solid.

^{1}H NMR (600 MHz, DMSO-d_6) δ_H 7.42 – 7.47 (m, 2H, H12), 7.29 – 7.33 (d, 2H, H11), 6.72 (dd, $J_{H14H15b}$ 17.6 Hz $J_{H14H15a}$ 10.9 Hz, H14), 5.81 (dd, 1H, $J_{H15bH14}$ 17.6 Hz $J_{H15bH15a}$ 1.2 Hz, H15), 5.24 (dd, 1H, $J_{H15bH14}$ 10.9 Hz $J_{H15bH15a}$ 1.2 Hz, H15b), 4.84 (d, 1H, J_{C2OHH3} 4.6 Hz, C2-OH), 4.69 (d, 1H, J_{C3OHH3} 5.4 Hz, C3-OH), 4.56 (t, 1H, J_{C6OHH6} 5.6 Hz, C6-OH), 4.49 (s, 2H, H9), 4.35 (d, 1H, J_{C4OHH4} 4.6 Hz, C4-OH), 4.12 (d, 1H, J_{H1H2} 7.4 Hz, H1), 3.86 – 3.90 (m, 1H, H7a), 3.55 – 3.65 (m, 4H, H4, H6, H7b) 3.44 – 3.54 (m, 2H, H8), 3.22 – 3.30 (m, 3H, H2, H3, H5) ppm.

^{13}C NMR (100 MHz, DMSO-d_6) δ_C 137.2 (C13), 136.4 (C14), 136.2 (C10), 127.8 (C11), 126.0 (C12), 114.0 (C15), 103.6 (C1), 75.2 (C2), 73.4 (C3), 71.7 (C9), 70.5 (C5), 69.0 (C7), 68.0 (C4), 67.7 (C6), 60.4 (C8) ppm.

HRMS (ESI$^+$) *m/z* calc. for $C_{17}H_{24}NaO_7$ $[M+Na]^+$ 363.1414; found 363.1419.

ν_{max}/cm^{-1} (neat) 3345br (OH), 2919 (C=CH_2 vinyl), 1041 (C-OH).

mp 120 – 121 °C.

(*N*-ethylacrylamide)-2,3,4,6-tetra-*O*-acetyl-β-D-galactopyranoside (107) (attempted)

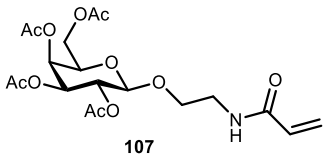

107

N-hydroxyethyl acrylamide (0.10 mL, 0.98 mmol) and silver carbonate (270 mg, 0.98 mmol) were added to a mixture of galactosyl bromide **104** (200 mg, 0.49 mmol) in anhydrous DCM (5 mL) over molecular sieves (3 Å). The mixture was stirred at room temperature for 16 h in the dark under argon. After this time, TLC analysis (30% EtOAc/hexane) showed consumption of the starting material (R_F = 0.4) and formation of the product (R_F = 0.2), and the reaction mixture was filtered through Celite® and concentrated under reduced pressure. The crude product was then purified by flash column chromatography (20% → 30% EtOAc/hexane) to recover the hydrolysis product only.

(3-chloropropyl)-2,3,4,6-tetra-*O*-acetyl-β-D-galactopyranoside (108)

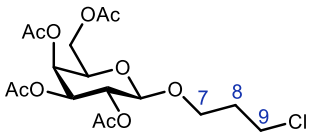

108

3-chloropropan-1-ol (1.96 mL, 23.4 mmol) and silver carbonate (6.46 g, 23.4 mmol) were added to a mixture of galactosyl bromide **104** (4.80 g, 11.7 mmol) in anhydrous DCM (30 mL) over molecular sieves (3Å). The mixture was stirred at room temperature for 16 h in the dark under argon. After this time, TLC analysis (30% EtOAc/hexane) showed consumption of the starting material (R_F = 0.4) and formation of the product (R_F = 0.3), and the reaction mixture was filtered and concentrated under reduced pressure. The crude product was then purified by flash column chromatography (20% → 30% EtOAc/hexane) to give **108** (2.01 g, 4.90 mmol, 42%) as a white solid.

^{1}H NMR (400 MHz, $CDCl_3$) δ_H 5.39 (dd, J_{H4H3} 3.4 J_{H4H5} 1.2 Hz, 1H, H4), 5.20 (dd, J_{H2H3} 10.5 J_{H2H1} 7.9 Hz, 1H, H2), 5.02 (dd, J_{H3H2} 10.5 J_{H3H4} 3.4 Hz, 1H, H3), 4.47 (d, J_{H1H2} 7.9 Hz, 1H, H1), 4.09 – 4.22 (m, 2H, H6), 4.01 (dt, J_{H7aH7b} 9.9 Hz J_{H7aH8} 5.1 Hz, 1H, H7a), 3.91 (td, J_{H5H6} 6.7 J_{H5H4} 1.2 Hz, 1H, H5), 3.66 – 3.74 (m, 1H, H7b), 3.61 (dd, J_{H9H8a} 7.2 J_{H9H8b} 5.2 Hz, 2H, H9), 2.15 (s, 3H, OCOC$\underline{H}_3$), 2.08 (s, 3H, OCOC$\underline{H}_3$), 2.06 – 2.08 (m, 1H, H8a), 2.05 (s, 3H, OCOC$\underline{H}_3$), 1.99 (s, 3H, OCOC$\underline{H}_3$), 1.92 – 2.03 (m, 1H, H8b).

^{13}C NMR (100 MHz, $CDCl_3$) δ_C 170.4 (O<u>C</u>OCH_3), 170.3 (O<u>C</u>OCH_3), 170.2 (O<u>C</u>OCH_3), 170.0 (O<u>C</u>OCH_3),101.6 (C1), 70.9 (C3), 70.7 (C5), 68.9 (C2), 67.0 (C4), 66.4 (C7), 61.3 (C6), 41.4 (C9), 32.2 (C8), 20.8 (OCO<u>C</u>H_3), 20.69 (OCO<u>C</u>H_3), 20.68 (OCO<u>C</u>H_3), 20.6 (OCO<u>C</u>H_3).

HRMS (ESI$^+$) *m/z* calc. for $C_{33}H_{36}NO_{14}$ $[M+H]^+$ 447.1028; found 447.1028.

mp 73 – 75 °C (lit. 78 °C)[342] from EtOAc/hexane.

The spectral data are consistent with the literature.[343]

(3-azidopropyl)-2,3,4,6-tetra-*O*-acetyl-β-D-galactopyranoside (109)

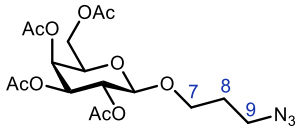

109

NaN_3 (1.54 g, 23.7 mmol) was added to a solution of **108** (2.01 g, 4.74 mmol) in anhydrous DMF (10 mL), then heated to 65 °C and stirred for 16 h under argon. After this time, TLC analysis (30% EtOAc/hexane) showed one spot with similar R_F to the starting material (R_F = 0.3). Water (20 mL) was added to the reaction mixture and the organic product then extracted with EtOAc (5 x 20 mL). The combined organic extracts were washed with brine (10 x 20 mL), dried ($MgSO_4$), filtered and concentrated under reduced pressure to give **109** (1.85 g, 4.29 mmol, 91%) as a clear oil.

^{1}H NMR (400 MHz, $CDCl_3$) δ_H 5.39 (dd, J_{H4H3} 3.4 J_{H4H5} 1.2 Hz, 1H, H4), 5.20 (dd, J_{H2H3} 10.5 Hz J_{H2H1} 7.9 Hz, 1H, H2), 5.01 (dd, J_{H3H2} 10.5 Hz J_{H3H4} 3.4 Hz, 1H, H3), 4.47 (d, J_{H1H2} 7.9 Hz, 1H, H1), 4.15 (qd, J_{H6aH6b} 11.2 Hz J_{H6H5} 6.7 Hz, 2H, H6), 3.96 (dt, J_{H7aH7b} 9.8 Hz J_{H7aH8} 5.4 Hz, 1H, H7a), 3.91 (td, J_{H5H6} 6.7 Hz J_{H5H4} 1.2 Hz, 1H, H5), 3.56 – 3.64 (m, 1H, H7b), 3.33 – 3.41 (m, 2H, H9), 2.15 (s, 3H, OCOC<u>H</u>$_3$), 2.08 (s, 3H, OCOC<u>H</u>$_3$), 2.05 (s, 3H, OCOC<u>H</u>$_3$), 1.99 (s, 3H, OCOC<u>H</u>$_3$), 1.75 – 1.93 (m, 2H, H8) ppm.

^{13}C NMR (100 MHz, $CDCl_3$) δ_C 170.4 (O<u>C</u>OCH_3), 170.3 (O<u>C</u>OCH_3), 170.2 (O<u>C</u>OCH_3), 169.5 (O<u>C</u>OCH_3),101.4 (C1), 70.9 (C3), 70.7 (C5), 68.8 (C2), 67.0 (C4), 66.5 (C7), 61.3 (C6), 47.9 (C9), 29.0 (C8), 20.8 (OCO<u>C</u>H_3), 20.7 (2x OCO<u>C</u>H_3), 20.6 (OCO<u>C</u>H_3) ppm.

HRMS (ESI$^+$) *m/z* calc. for $C_{17}H_{25}N_3NaO_{10}$ $[M+Na]^+$ 454.1432; found 454.1439.

ν_{max}/cm^{-1} (neat) 2097 (N=N), 1745 (CO).

The spectral data are consistent with the literature.[343]

(*N*-(2-((1-propyl-1H-1,2,3-triazol-4-yl)methoxy)ethyl)acrylamide)-2,3,4,6-tetra-*O*-acetyl-β-D-galactopyranoside (110)

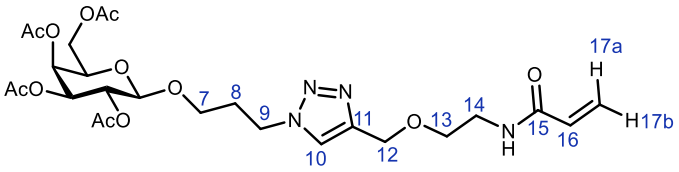

110

A solution of $CuSO_4 \cdot 5H_2O$ (0.065 mmol, 18 mg) and sodium ascorbate (0.13 mmol, 26 mg) in water (0.4 mL) was added to a solution of azide **109** (280 mg, 0.65 mmol) and alkyne **86** (100 mg, 0.65 mmol) in degassed DCM:MeOH (1:1 v/v; 8 mL) and stirred at rt for 16 h under argon. After this time, TLC analysis (30% EtOAc/hexane) showed consumption of the azide starting material (R_F = 0.3) and the formation of a product (R_F = 0.1). Water (10 mL) was added to the reaction mixture and the organic product extracted with DCM (3 x 10 mL). The combined organic extracts were washed with EDTA (sat. aq.; 3 x 10 mL) and brine (1 x 20 mL), then dried ($MgSO_4$), filtered and concentrated under reduced pressure. The crude material was purified by flash column chromatography (2% → 5% MeOH/DCM) to give **110** (225 mg, 0.39 mmol, 60%) as a clear oil.

^{1}H NMR (400 MHz, $CDCl_3$) δ_H 7.54 (s, 1H, H10), 6.24 – 6.36 (m, 2H, NH, H17a), 6.12 (dd, $J_{H16H17a}$ 16.9 $J_{H16H17b}$ 10.2 Hz, 1H, H16), 5.63 (dd, $J_{H17bH16}$ 10.2 $J_{H17bH17a}$ 1.6 Hz, 1H, H17b), 5.40 (dd, J_{H4H3} 3.6 J_{H4H5} 1.2 Hz, 1H, H4), 5.21 (dd, J_{H2H3} 10.5 J_{H2H1} 7.9 Hz, 1H, H2), 5.02 (dd, J_{H3H2} 10.5 J_{H3H4} 3.4 Hz, 1H, H3), 4.64 (s, 2H, H12), 4.45 – 4.53 (m, 2H, H1, H9a), 4.35 – 4.44 (m, 1H, H9b), 4.14 (qd, J_{H6aH6b} 11.3 J_{H6H5} 6.7 Hz, 1H, H6), 3.83 – 3.93 (m, 2H, H5, H7a), 3.66 (t, J_{H13H14} 5.0 Hz, 2H, H13), 3.52 – 3.58 (m, 2H, H14), 3.45 – 3.51 (m, 1H, H7b), 2.10 – 2.25 (m, 1H, H8), 2.16 (s, 3H, OCOC$\underline{H}_3$), 2.09 (s, 3H, OCOC$\underline{H}_3$), 2.03 (s, 3H, OCOC$\underline{H}_3$), 1.99 (s, 3H, OCOC$\underline{H}_3$) ppm.

^{13}C NMR (100 MHz, CDCl3) δ_C 170.5 (O$\underline{C}$OCH$_3$), 170.2 (O$\underline{C}$OCH$_3$), 170.1 (O$\underline{C}$OCH$_3$), 170.0 (O$\underline{C}$OCH$_3$), 165.6 (C15), 144.6 (C11), 130.9 (C16), 126.4 (C17), 122.9 (C10), 101.3 (C1), 70.8 (C3, C5), 69.3 (C13), 68.8 (C2), 67.0 (C4), 65.8 (C7), 64.3 (C12), 61.2 (C6), 46.7 (C9), 39.4 (C14), 30.2 (C8), 20.9 (OCO$\underline{C}$H$_3$), 20.7 (2x OCO$\underline{C}$H$_3$), 20.6 (OCO$\underline{C}$H$_3$) ppm.

HRMS (ESI$^+$) *m/z* calc. for $C_{25}H_{36}N_4NaO_{12}$ $[M+Na]^+$ 607.2222; found 607.2228.

ν_{max}/cm^{-1} (neat) 2938 (aromatic stretch), 1744 (CO).

(*N*-(2-((1-propyl-1H-1,2,3-triazol-4-yl)methoxy)ethyl)acrylamide)-β-D-galactopyranoside (111)

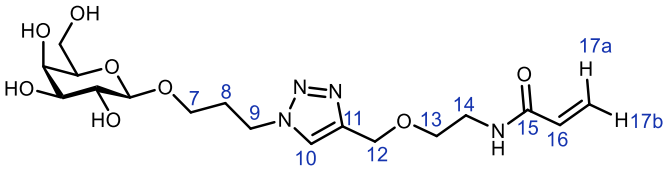

111

NaOH (1 M, 0.10 mL, 0.10 mmol) was added to a solution of **110** (150 mg, 0.26 mmol) in MeOH (4 mL) and stirred for 30 min at rt. After this time, TLC analysis (5% MeOH/DCM) showed complete consumption of the starting material (R_F = 0.4) and the formation of a product (R_F = 0.0); analysis in 10% MeOH/DCM confirmed consumption of the starting material (R_F = 0.8) and the formation of a product (R_F = 0.3). The reaction mixture was then neutralised with Amberlite IRC-120 H^+ resin, filtered and concentrated under reduced pressure to give **111** (79 mg, 0.19 mmol, 73%) as a pale red oil.

^{1}H NMR (400 MHz, D_2O) δ_H 8.06 (s, 1H, H10), 6.25 (dd, $J_{H16H17a}$ 17.2 Hz $J_{H16H17b}$ 9.7 Hz, 1H, H16), 6.17 (dd, $J_{H17aH16}$ 17.2 Hz $J_{H17aH17b}$ 1.9 Hz, 1H, H17a), 5.76 (dd, $J_{H17bH16}$ 9.8 Hz $J_{H17bH17a}$ 1.9 Hz, 1H, H17a), 4.68 (s, 2H, H12), 4.57 (t, J_{H9H8} 6.8 Hz, 2H, H9), 4.36 (d, J_{H1H2} 7.8 Hz, 1H, H1), 3.93 (dd, J_{H4H3} 3.6 J_{H4H5} 1.0 Hz, 1H, H4), 3.86 – 3.90 (m, 1H, H7a), 3.74 – 3.80 (m, 2H, H6), 3.68 – 3.72 (t, J_{H13H14} 5.7 Hz, 2H, H13), 3.65 – 3.68 (m, 1H, H3), 3.62 – 3.65 (m, 1H, H5), 3.58 – 3.61 (m, 1H, H7b), 3.53 (dd, J_{H2H3} 10.0 Hz J_{H2H1} 7.8 Hz, 1H, H2), 3.47 (t, J_{H14H13} 5.7 Hz, 2H, H14), 2.23 (app. dq, J_{H8H7} 7.6 J_{H8H9} 6.8 Hz, 2H, H8) ppm.

^{13}C NMR (100 MHz, D_2O) δ_C 168.6 (C15), 143.8 (C11), 129.8 (C16), 127.3 (C17), 125.3 (C10), 102.8 (C1), 75.1 (C3), 72.7 (C5), 70.7 (C2), 68.0 (C13), 66.3 (C7), 62.8 (C12), 61.0 (C6), 47.1 (C9), 39.0 (C14), 29.5 (C8) ppm.

HRMS (ESI$^+$) *m/z* calc. for $C_{25}H_{36}N_4NaO_{12}$ $[M+Na]^+$ 455.1539; found 455.1537.

ν_{max}/cm^{-1} (neat) 3314 (OH), 2877 (aromatic stretch), 1656 (CO).

tert-butyl(3-chloropropoxy)dimethylsilane (112) (attempted)

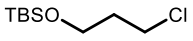

112

Imidazole (0.22 mL, 3.89 mmol) was added to a solution of 3-chloro-propan-1-ol (0.25 mL, 2.99 mmol) in DCM (10 mL) and stirred for 10 min. The reaction was then cooled to 0 °C and TBSCl (0.54 g, 3.59 mmol) was added and then stirred at rt for 18 h. After this time, TLC analysis (10% EtOAc/hexane) showed partial consumption of the starting material (R_F = 0.0) and the formation of a product (R_F = 0.4). The reaction mixture was then diluted with DCM (10 mL) and washed with NH_4Cl (sat. aq.; 15 mL). The aqueous phase was extracted with DCM (3 x 10 mL) and the combined organic extracts were washed with brine (sat aq.; 20 mL), then dried ($MgSO_4$), filtered and concentrated under reduced pressure. The crude product was purified via flash column chromatography (10% EtOAc/hexane → EtOAc) which did not yield the target molecule.

1-((3-chloropropoxy)methyl)-4-methoxybenzene (113) (attempted)

113

Sodium hydride (60% dispersion in mineral oil; 179 mg, 4.49 mmol) was added to a solution of 3-chloro-propan-1-ol (0.25 mL, 2.99 mmol) in anhydrous THF (10 mL) at 0 °C and stirred for 1 h at this temperature. Tetrabutylammonium iodide (44 mg, 0.12 mmol) and PMBCl (0.61 mL, 4.49 mmol) were then added at 0 °C and the reaction left to warm to rt and stirred for 16 h. After this time, TLC analysis (10% EtOAc/hexane) showed partial consumption of the hydroxyl starting material (R_F = 0.0), little consumption of PMBCl (R_F = 0.2) and the formation of a complex mixture The reaction mixture was then cooled to 0 °C and quenched with NH_4Cl (sat. aq.; 10 mL). The aqueous phase was extracted with Et_2O (2 x 20 mL) and the combined organic extracts were washed with brine (10 mL), dried ($MgSO_4$), filtered and concentrated under reduced pressure. The target molecule was not isolated.

((3-chloropropoxy)methanetriyl)tribenzene (114)

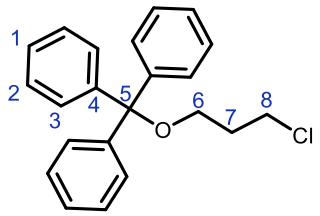

114

Triethylamine (0.18 mL, 1.28 mmol), chlorotriphenylmethane (357 mg, 1.28 mmol), and DMAP (37 mg, 0.30 mmol) were added to a solution of 3-chloro-propan-1-ol (0.10 mL, 1.16 mmol) in anhydrous DCM (5 mL) and this stirred for 16 h at rt under argon. After this time, TLC analysis (5% EtOAc/hexane) showed consumption of the starting material (R_F = 0.3) and the formation of a product (R_F = 0.8); analysis in hexane confirmed consumption of the starting material (R_F = 0.0) and the formation of a product (R_F = 0.2). The reaction mixture was diluted with DCM (15 mL) and washed with $NaHCO_3$ (sat. aq.; 2 x 10 mL). The combined organic phases were washed with brine (10 mL), dried ($MgSO_4$), filtered and concentrated under reduced pressure. The crude product was purified by flash column chromatography (hexane → 5% EtOAc/hexane) to give **114** (277 mg, 0.82 mmol, 71%) as a white crystalline powder.

^{1}H NMR (400 MHz, $CDCl_3$) δ_H 7.41 – 7.51 (m, 6H, H3), 7.29 – 7.37 (m, 6H, H2), 7.22 – 7.33 (m, 3H, H1), 3.73 (t, J_{H6H7} 7.6 Hz, 2H, H6), 3.26 (t, J_{H8H7} 5.9 Hz, 2H, H8), 2.01 – 2.12 (m, 2H, H7) ppm.

^{13}C NMR (100 MHz, $CDCl_3$) δ_C 144.1 (C4), 128.7 (C3), 127.8 (C2), 127.0 (C1), 88.6 (C5), 60.3 (C8), 42.2 (C6), 33.4 (C7) ppm.

HRMS (ESI$^+$) *m/z* calc. for $C_{22}H_{21}ClNaO$ $[M+Na]^+$ 359.1173; found 359.1169.

ν_{max}/cm^{-1} (neat) 699 (C-Cl).

mp 73 – 75 °C (lit. 73 – 75 °C)[344] from EtOAc/hexane.

The spectral data are in agreement with the literature.[345]

((3-azidopropoxy)methanetriyl)tribenzene (115)

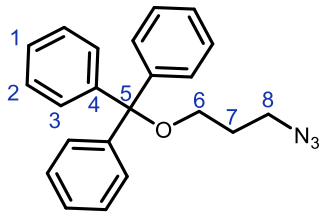

115

NaN_3 (258 mg, 3.97 mmol) was added to a solution of **114** (267 mg, 0.79 mmol) in anhydrous DMF (3 mL) and stirred at 65 °C for 16 h under argon. After this time, TLC analysis (2% EtOAc/hexane) showed partial consumption of the starting material (R_F = 0.7) and the formation of a product (R_F = 0.6). The reaction mixture was diluted in DCM (10 mL) and washed with brine (3 x 10 mL). The combined organic phases were dried ($MgSO_4$), filtered and concentrated under reduced pressure. The crude product was purified by flash column chromatography (hexane ⟶ 2% EtOAc/hexane) to give **115** (145 mg, 0.42 mmol, 55%) as a white powder.

^{1}H NMR (400 MHz, $CDCl_3$) δ_H 7.40-7.48 (m, 6H, H3), 7.27-7.34 (m, 6H, H2), 7.20-7.26 (m, 3H, H1), 3.44 (t, J_{H6H7} 6.9 Hz, 2H, H6), 3.18 (t, J_{H8H7} 6.0 Hz, 2H, H8), 1.80-1.91 (m, 2H, H7).

^{13}C NMR (100 MHz, $CDCl_3$) δ_C 144.1 (C4), 128.8 (C3), 127.8 (C2), 127.0 (C1), 86.6 (C5), 60.4 (C8), 48.8 (C6), 29.5 (C7).

HRMS (ESI$^+$) *m/z* calc. for $C_{22}H_{21}N_3NaO$ $[M+Na]^+$ 366.1577; found 366.1577.

mp 78 – 80 °C.

The spectral data are in agreement with the literature.[346]

N-(2-((1-(3-(trityloxy)propyl)-1H-1,2,3-triazol-4-yl)methoxy)ethyl)acrylamide (116)

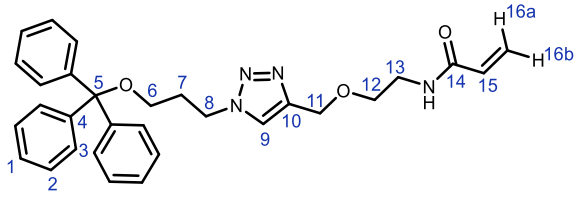

116

A solution of $CuSO_4 \cdot 5H_2O$ (0.033 mmol, 8 mg) and sodium ascorbate (0.066 mmol, 13 mg) in water (0.4 mL) was added to a solution of azide **115** (0.33 mmol, 112 mg) and alkyne **86** (0.33 mmol, 51 mg) in degassed DCM/MeOH (1:1 v/v, 4 mL) and stirred for 16 h under argon. After this time, TLC analysis (EtOAc) showed consumption of alkyne **86** (R_F = 0.8)

and the formation of a product (R_F = 0.4). The reaction mixture was diluted with DCM (10 mL) and water (10 mL), extracted with DCM (2 x 10 mL). The combined organic phases were washed with EDTA (sat. aq.; 2 x 10 mL), dried ($MgSO_4$), filtered and concentrated under reduced pressure. The crude residue was purified via a silica plug (EtOAc) to give **116** (103 mg, 0.21 mmol, 63%) as a pale grey solid.

^{1}H NMR (400 MHz, $CDCl_3$) δ_H 7.40 – 7.47 (m, 6H, H3), 7.23 – 7.38 (m, 10H, H1, H2, H9), 6.30 (dd, $J_{H16bH15}$ 17.0 $J_{H16bH16a}$ 1.5 Hz, 1H, H16b), 6.28 (m, 1H, NH), 6.11 (dd, $J_{H15H16b}$ 17.0 $J_{H15H16a}$ 10.3 Hz, 1H, H15), 5.65 (dd, $J_{H16aH15}$ 10.3 $J_{H16aH16b}$ 1.5 Hz, 1H, H16a), 4.51 – 4.59 (m, 4H, H11, H6), 3.60 – 3.67 (m, 2H, H12), 3.53 – 3.59 (m, 2H, H13), 3.15 (t, 2H, J_{H8H7} 5.7 Hz, H8), 2.15 – 2.26 (m, 2H, H7) ppm.

^{13}C NMR (100 MHz, $CDCl_3$) δ_C 165.6 (C14), 144.2 (C10), 143.8 (C4), 130.8 (C15), 128.6 (ArC), 127.9 (ArC), 126.5 (C16), 122.9 (ArC), 86.7 (C5), 69.1 (C12), 64.1 (C6, C11), 59.4 (C8), 47.5 (C6, C11), 39.4 (C13), 30.6 (C7) ppm.

ν_{max}/cm^{-1} (neat) 1620s (CO), 1444 (C=C, aromatic).

mp 120-121 °C.

N-(2-((1-(3-hydroxypropyl)-1H-1,2,3-triazol-4-yl)methoxy)ethyl)acrylamide (117)

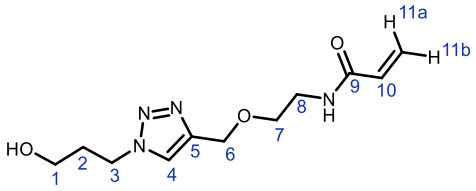

117

p-toluenesulfonic acid monohydrate (76 mg, 0.40 mmol) was added to a solution of **116** (100 mg, 0.20 mmol) in MeOH/DCM (2:1 v/v, 4 mL) and stirred at rt for 2 h. After this time, TLC analysis (EtOAc) showed consumption of the starting material (R_F= 0.3) and the formation of a new spot (R_F = 0.1). The reaction was quenched with $NaHCO_3$ (sat. aq.; 5 mL), diluted with DCM (10 mL) and extracted with DCM (2 x 10 mL). The combined organic phases were washed with brine (10 mL), dried ($MgSO_4$), filtered and concentrated under reduced pressure. The crude product was purified by flash column chromatography (10% MeOH/DCM) to give **117** (40 mg, 0.16 mmol, 79%) as a clear oil.

^{1}H NMR (400 MHz, $CDCl_3$) δ_H 7.59 (s, 1H, H4), 6.58 (br s, 1H, NH), 6.26 (dd, $J_{H11aH10}$ 17.0 $J_{H11aH11b}$ 1.6 Hz, 1H, H11a), 6.12 (dd, $J_{H10H11a}$ 17.0 $J_{H10H11b}$ 10.2 Hz, 1H, H10), 5.62 (dd, $J_{H11bH10}$ 10.2 $J_{H11bH11a}$ 1.6 Hz, 1H, H11b), 4.62 (s, 2H, H6), 4.51 (t, J_{H1H2} 6.8 Hz, 2H, H1), 3.58 – 3.68 (m, 4H, H3, H7), 3.52 (app. q, J_{H8H7} 5.1 Hz, 2H, H8), 2.12 (app. p, J_{H2H1} 6.4 Hz, 2H, H2) ppm.

^{13}C NMR (100 MHz, $CDCl_3$) δ_C 165.9 (C9), 144.5 (C5), 130.8 (C10), 126.5 (C11), 123.2 (C4), 69.0 (C7), 64.1 (C6), 58.5 (C3), 47.0 (C1), 39.4 (C8), 32.5 (C2) ppm.

HRMS (ESI^+) *m/z* calc. for $C_{11}H_{19}N_4O_3$ $[M+H]^+$ 255.1452; found 255.1457.

ν_{max}/cm^{-1} (neat) 3310 (OH), 2923 (C=CH_2), 1634 (CO).

7.2.2 General Polymerisation Methods

Two-Photon Polymerisation (TPP)

TPP was carried out using the commercial Nanoscribe GT Photonic Professional system (Nanoscribe GmbH). This system uses a near IR Erbium-doped, pulsed laser that operates at a wavelength of 780 nm. An oil immersion configuration was employed for all fabrication processes using a 63x immersion objective (NA = 1.4, WD = 190 μm) (Zeiss, Plan Apochromat).

To ensure covalent attachment of the fabricated 3D microstructure to the glass substate, the glass cover slips were treated with a silanisation procedure: glass cover slips (high precision round cover slips, 30 mm, thickness 170 ± 5 μm; No 1.5; acquired from Gerhard Menzel GMBH) were first rinsed with acetone, IPA, ethanol, methanol and deionised water. The washed slides were then dried under N_2 before being placed in a UV ozone cleaner for 20 minutes (Osssila, United Kingdom). The slides were submerged in a mixture of the silanising agent 3-(trimethoxysilyl)propyl methacrylate (3 vol %) in ethanol and a weak acid activator (acetic acid, 0.1 vol %). The slides were rinsed with ethanol, dried under N_2 and left to bake in an oven at 60 ˚C for 3 h.

For the fabrication setup, the slides substrates were placed in a holder and a drop of oil (Zeiss Immersol 518F) was placed in the centre of the unsilanised side of the slide. On the opposite side of the slide (silanised side) a drop of the unpolymerised photoresist was placed. A range of microstructures were then fabricated by focusing the laser with the help of a 63x immersion

objective (NA = 1.4, WD = 190 μm) (Zeiss, Plan Apochromat). Unless otherwise stated, post fabrication all samples were developed in propylene glycol methyl ether acetate (PGMEA) for 20 minutes followed by a 5 minute submersion in isopropanol (IPA) and dried under a mild stream of clean dry air.

Scanning electron microscopy (SEM)

For each resist a grid structure with a designed line width of 0.4 μm and pore size of 2.8 μm was fabricated at a range of laser powers. Each grid had a designed width of 60 μm and a designed height of 3 μm. All structures were characterised *via* SEM microscopy performed using a Zeiss ULTRA plus microscope with a GEMINI® FESEM column (Zeiss, Germany). Cryo SEM was also used to characterise the hydrogel microstructures in their hydrated state. In this process, a drop of deionised water was placed on the top side of the slide before the slide was submerged in liquid N_2 and placed into the Cryo Zeiss ULTRA SEM for imaging.

7.3 Synthetic Methods for Chapter 3

6-(2-((4-vinylbenzyl)oxy)ethoxy)-1,11-bis(4-vinylphenyl)-2,5,7,10-tetraoxaundecane (119) (attempted)

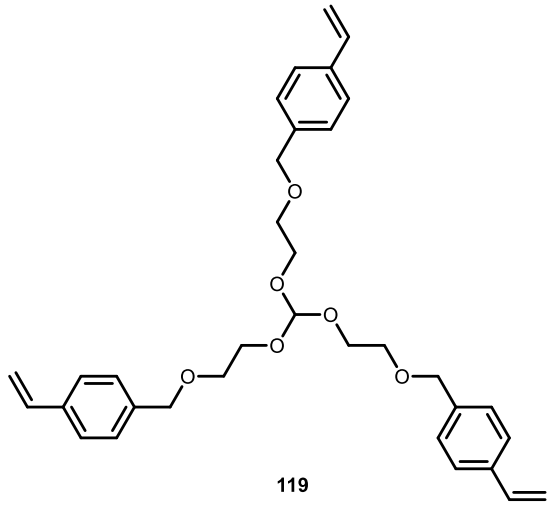

119

H_2SO_4 (conc.; 5 μL) was added to **78** (250 mg, 1.40 mmol) and triethyl orthoformate (78 μL, 0.47 mmol) and the reaction was distilled at 100 °C under argon. After 1 h, TLC analysis (20% EtOAc/hexane) showed partial consumption of the starting material (R_F = 0.3) and the formation of a product (R_F = 0.0) and the reaction mixture had become highly viscous. It was

not possible to dissolve the reaction mixture in organic solvent and the reaction was abandoned.

N,N',N''-((methanetriyltris(oxy))tris(ethane-2,1-diyl))triacrylamide (122) (attempted)

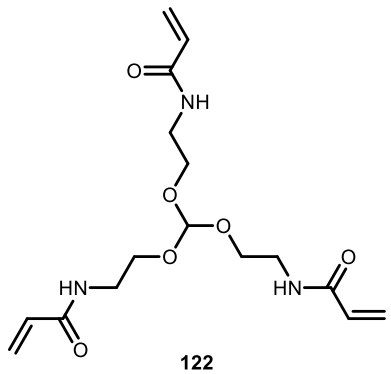

122

H_2SO_4 (conc.; 5 µL) was added to *N*-hydroxyethyl acrylamide (0.44 mL, 4.35 mmol) and triethyl orthoformate (0.24 mL, 1.45 mmol) and the reaction was distilled at 100 °C under argon. After 1 h, the reaction mixture had become highly viscous. It was not possible to dissolve the reaction mixture in organic solvent and the reaction was abandoned.

Methyl 1-*O*-[(formaldehyde)-2,3,4-tri-*O*-acetyl-β-D-glucopyran]uronate (124) (attempted)

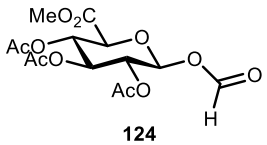

124

Method A:

Formic acid (46 µL, 1.21 mmol) was added to a solution of trichloroacetimidate **76** (115 mg, 0.24 mmol) in anhydrous DCM (2 mL) over molecular sieves at -10 °C under argon and stirred for 10 min at rt. The reaction mixture was then cooled to -10 °C and TMSOTf (5 µL, 0.025 mmol) was added dropwise to and stirred at -10 °C for 30 min and then at rt for 16 h. After this time, TLC analysis (30% EtOAc/hexane) showed partial consumption of acetimidate **76** (R_F = 0.5) and the formation of a new spot (R_F = 0.2.) The reaction mixture was quenched with Et_3N (35 µL, 0.25 mmol), filtered through Celite®, concentrated under reduced pressure and purified by flash column chromatography (10 → 30% EtOAc/hexane) to recover unreacted trichloroacetimidate **76** and the hydrolysis product.

Method B:

Formic acid (49 µL, 1.31 mmol) was added to a solution of trichloroacetimidate **76** (125 mg, 0.26 mmol) in anhydrous DCM (2 mL) over molecular sieves at -10 °C under argon and stirred for 10 min at rt. The reaction mixture was then cooled to -10 °C and $BF_3 \cdot Et_2O$ (34 µL, 0.29 mmol) was added dropwise to and stirred at -10 °C for 30 min and then at rt for 16 h. After this time, TLC analysis (30% EtOAc/hexane) showed partial consumption of acetimidate **76** (R_F = 0.5) and the formation of a new spot (R_F = 0.2.) The reaction mixture was quenched with Et_3N (35 µL, 0.25 mmol), filtered through Celite®, concentrated under reduced pressure and purified by flash column chromatography (10 → 30% EtOAc/hexane) to recover unreacted trichloroacetimidate **76** and the hydrolysis product.

Method C:

Formic acid (14 µL, 0.38 mmol), TfOH (16 µL, 0.18 mmol), and NIS (61 mg, 0.27 mmol) were added to thioglycoside **126** (96 mg, 0.22 mmol) in anhydrous DCM (3 mL) at to 0 °C, then allowed to warm to rt and stirred for 16 h under argon. After this time, TLC analysis (40% EtOAc/hexane) showed partial consumption of the starting material (R_F = 0.4) and the formation of two spots (R_F = 0.1, 0.2). The reaction mixture was diluted with DCM (10 mL), then washed with water (2 x 10 mL), $NaHCO_3$ (sat. aq.; 2 x 10 mL) and brine (20 mL). The organic phase was dried ($MgSO_4$), filtered and concentrated under reduced pressure. The crude product was purified by flash column chromatography (40% EtOAc/hexane) to recover the hydrolysis product and a by-product.

Methyl 1-*S*-[toluene]uronate (126)

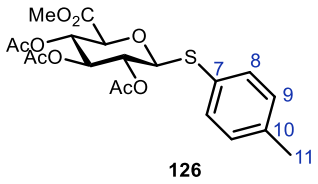

126

4-methyl-benzenthiol (275 mg, 2.22 mmol) was added to a solution of trichloroacetamide **76** (530 mg, 1.11 mmol) in anhydrous DCM (10 mL) over molecular sieves and stirred at rt for 10 min under argon The reaction mixture was then cooled to -10 °C and $BF_3 \cdot Et_2O$ (175 µL, 1.23 mmol) was added dropwise, slowly allowed to warm to rt and stirred for 16 h under argon. After this time, TLC analysis (30% EtOAc/hexane) showed consumption of the acetamide (R_F = 0.3) and the formation of a new product spot (R_F = 0.3). The reaction mixture was quenched with Et_3N (0.17 mL, 1.23 mmol, filtered and concentrated under reduced pressure. The crude product was purified by flash column chromatography to give a **126** (192 mg, 0.44 mmol, 40%) as a clear oil.

^{1}H NMR (400 MHz, $CDCl_3$) δ_H 7.35-7.41 (m, 2H, H9), 7.10-7.15 (m, 2H, H8), 5.25 (app. t, J_{H3H2} 9.4 Hz, 1H, H3), 5.14 (app. t, J_{H4H5} 9.8 Hz, 1H, H4), 4.92 (app. t, J_{H2H1} 10.0 Hz, 1H, H2), 4.66 (t, J_{H1H2} 10.0, 1H, H1), 4.01 (app. d, J_{H5H4} 9.8, 1H, H5), 3.75 (s, 3H, $COOCH_3$), 2.34 (s, 3H, H11), 2.08 (s, 3H, $OCOCH_3$), 1.99 (s, 6H, 2x $OCOCH_3$) ppm.

^{13}C NMR (100 MHz, $CDCl_3$) δ_C 170.1 ($COCH_3$), 169.4 ($COCH_3$), 169.1 ($COCH_3$), 166.9 ($COOCH_3$), 139.0 (C10), 134.0 (C9), 129.8 (C8), 127.1 (C7), 86.2 (C1), 76.1 (C5), 73.3 (C3), 69.6 (C2), 69.2 (C4), 52.9 ($COOCH_3$), 21.2 ($OCOCH_3$), 20.8 ($OCOCH_3$), 20.6 ($OCOCH_3$), 20.5 ($OCOCH_3$) ppm.

HRMS (ESI$^+$) *m/z* calc. for $C_{20}H_{24}NaO_9S$ $[M+Na]^+$ 463.1033; found 463.1040.

ν_{max}/cm^{-1} (neat) 1740s (CO), 1494 (C=C, aromatic).

The spectral data are in agreement with the literature.[347]

Methyl 1-*O*-[(benzaldehyde)-2,3,4-tri-*O*-acetyl-β-D-glucopyran]uronate (133)

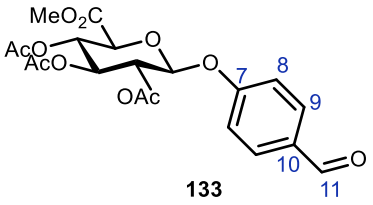

133

4-hydroxybenzaldehyde (28 mg, 0.23 mmol) was added to a solution of trichloroacetimidate **76** (110 mg, 0.23 mmol) in anhydrous DCM (2 mL) over molecular sieves at -10 °C under argon and stirred for 10 min at rt. The reaction mixture was then cooled to -10 °C and $BF_3 \cdot Et_2O$ (30 µL, 0.25 mmol) was added dropwise to and stirred at -10 °C for 30 min and then at rt for 16 h. After this time, TLC analysis (30% EtOAc/hexane) showed complete consumption of acetimidate **76** (R_F = 0.5), partial consumption of 4-hydroxybenzaldehyde (R_F = 0.4) and the formation of a new spot (R_F = 0.3.) The reaction mixture was quenched with Et_3N (35 µL, 0.25 mmol), filtered through Celite®, concentrated under reduced pressure and purified by flash column chromatography (10 → 30% EtOAc/hexane) to give **133** (9 mg, 0.021 mmol, 9%) as a white crystalline solid.

^{1}H NMR (400 MHz, $CDCl_3$) δ_H 9.92 (s, 1H, H11), 7.74-7.97 (m, 2H, H9), 7.06-7.15 (m, 2H, H8), 5.17-5.47 (m, 4H, H1, H2, H3, H4), 4.22 – 4.28 (m, 1H, H5), 3.72 (s, 3H, $COOCH_3$), 2.04 – 2.08 (m, 9H, $OCOCH_3$) ppm.

^{13}C NMR (100 MHz, $CDCl_3$) δ_C 190.7 (C11), 170.1 ($OCOCH_3$), 169.3 ($OCOCH_3$), 169.2 ($OCOCH_3$), 166.7 ($COOCH_3$), 161.1 (C7), 132.0 (C10), 131.9 (C9), 116.9 (C8), 98.1 (C1), 72.8 (C5), 71.6 (C2-4), 71.0 (C2), 68.9 (C4), 53.1 ($COOCH_3$), 20.6 ($OCOCH_3$), 20.5 ($OCOCH_3$) ppm.

HRMS (ESI^+) *m/z* calc. for $C_{20}H_{22}NaO_{11}$ $[M+Na]^+$ 461.1054; found 461.1051.

mp 167 – 169 °C (lit. 170 – 171 °C)[348] from EtOAc/hexane).

The spectral data are in agreement with the literature.[349]

1-*O*-[(3-nitrobenzaldehyde)-2,3,4,6-tetra-*O*-acetyl-β-D-galactopyran]uronate (135)

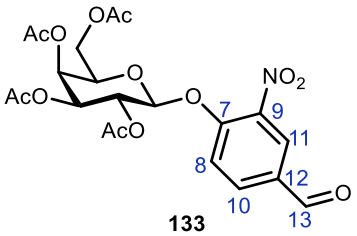

133

$BnEt_3NCl$ (184 mg, 0.81 mmol) and 2 M NaOH (0.91 mL, 1.82 mmol) were added to galactosyl bromide **104** (414 mg, 1.01 mmol) and 4-hydroxy-3-nitrobenzaldehyde (304 mg, 1.82 mmol) in $CHCl_3$ (4 mL) and stirred at 70 °C for 16 h. After this time, TLC analysis (50% EtOAc/hexane) showed complete consumption of glycosyl bromide **104** (R_F = 0.6), partial consumption of 4-hydroxy-3-nitrobenzaldehyde (R_F = 0.4) and the formation of a new spot (R_F = 0.3). The reaction mixture was diluted with $CHCl_3$ (10 mL), the organic layer washed with sodium bicarbonate (sat aq.; 10 mL), brine (10 mL), dried ($MgSO_4$), filtered and concentrated under reduced pressure. The crude product was purified by flash column chromatography (5% → 10% acetone/toluene) to give **135** (239 mg, 0.48 mmol, 48%) as an off-white solid.

^{1}H NMR (400 MHz, $CDCl_3$) δ_H 9.97 (s, 1H, H13), 8.29 (d, 1H, J_{H10H11} 1.6 Hz, H10), 8.06 (dt, 1H, J_{H11H9} 8.6 Hz J_{H11H10} 1.6 Hz, H11), 7.48 (d, 1H, J_{H9H11} 8.6 Hz, H9), 5.53 – 5.62 (m, 1H, H2), 5.48 (d, 1H, J_{H4H3} 3.3 Hz, H4), 5.21 (d, 1H, J_{H1H2} 7.9 Hz, H1), 5.09 – 5.16 (m, 1H, H3), 4.21 – 4.30 (m, 1H, H5), 4.09 – 4.21 (m, 2H, H6), 2.18 (s, 3H, OCOC$\underline{H}_3$), 2.04 – 2.13 (m, 6H, OCOC$\underline{H}_3$), 2.01 (s, 3H, OCOC$\underline{H}_3$) ppm.

^{13}C NMR (100 MHz, $CDCl_3$) δ_C 188.7 (C13), 170.3 (O$\underline{C}$OCH$_3$), 170.1 (2x O$\underline{C}$OCH$_3$), 169.2 (O$\underline{C}$OCH$_3$), 153.5 (C7), 141.2 (C12), 134.0 (C11), 131.5 (C8), 126.9 (C10), 118.8 (C9), 100.06 (C1), 71.8 (C6), 70.4 (C3), 67.6 (C2), 66.6 (C4), 61.4 (C5), 20.67 (OCO$\underline{C}$H$_3$), 20.62 (OCO$\underline{C}$H$_3$), 20.59 (OCO$\underline{C}$H$_3$), 20.56 (OCO$\underline{C}$H$_3$) ppm.

HRMS (ESI$^+$) *m/z* calc. for $C_{21}H_{23}NNaO_{13}$ $[M+Na]^+$ 520.1062; found 520.1063.

mp 191 – 193 °C (lit. 191 – 192 °C)[350] from acetone/toluene.

The spectral data are in agreement with the literature.[331]

1-*O*-[((3-nitrophenyl)methanol)-2,3,4,6-tetra-*O*-acetyl-β-D-galactopyran]uronate (136)

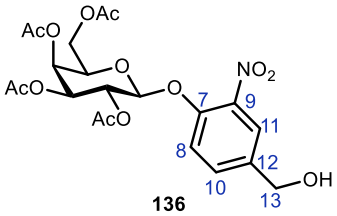

136

135 (985 mg, 1.98 mmol) was dissolved in degassed $CHCl_3$ (16 mL) and ^{i}PrOH (4 mL), silica gel (42–60 mesh, 2 g) and Amberlite IR-120 H^+form (50 mg) added and the mixture cooled to 0 °C. Within 30 min freshly powdered $NaBH_4$ (150 mg, 3.96 mmol) was added portionwise and stirring continued at 0 °C for further 1.5 h. After this time, TLC analysis (50% EtOAc/hexane) showed consumption of the starting material (R_F = 0.2) and the formation of a product (R_F = 0.5). The reaction was quenched by addition of ice-cold NH_4Cl (sat. aq.; 10 mL) and the product was extracted with DCM (3 x 10 mL). The combined organic phases were washed with brine (10 mL), dried ($MgSO_4$), filtered and concentrated under reduced pressure to give **136** (851 mg, 1.70 mmol, 86%) as a white powder.

^{1}H NMR (400 MHz, $CDCl_3$) δ_H 7.80 (d, J_{H11H10} 2.1 Hz, 1H, H11), 7.52 (dd, J_{H10H8} 8.6 Hz J_{H10H11} 2.1 Hz, 1H, H10), 7.35 (d, J_{H8H10} 8.6 Hz, 1H, H8), 5.54 (dd, J_{H2H3} 10.5 Hz J_{H2H1} 7.9 Hz, 1H, H2), 5.47 (dd, J_{H4H3} 3.4 Hz J_{H4H5} 1.2 Hz, 1H, H4), 5.10 (dd, J_{H3H2} 10.5 Hz J_{H3H4} 3.4 Hz, 1H, H3), 4.73 (d, J_{H13OH} 5.4 Hz, 2H, H13), 4.13 – 4.19 (m, 1H, H6), 4.22 – 4.28 (m, 1H, H6), 4.03 – 4.08 (m, 1H, H5), 2.19 (s, 3H, OCOC$\underline{H}_3$), 2.13 (s, 3H, OCOC$\underline{H}_3$), 2.07 (s, 3H, OCOC$\underline{H}_3$), 2.01 (s, 3H, OCOC$\underline{H}_3$) ppm.

^{13}C NMR (100 MHz, $CDCl_3$) δ_C 170.3 (O$\underline{C}$OCH$_3$), 170.2 (O$\underline{C}$OCH$_3$), 170.1 (O$\underline{C}$OCH$_3$), 169.4 (O$\underline{C}$OCH$_3$), 148.5 (C7), 141.4 (C9), 137.1 (C12), 131.7 (C10), 123.3 (C11), 120.2 (C8), 100.9 (C1), 71.4 (C5), 70.6 (C3), 67.9 (C2), 66.7 (C4), 63.5 (C13), 61.3 (C6), 20.7 (3 x OCO$\underline{C}$H$_3$), 20.6 (OCO$\underline{C}$H$_3$) ppm.

HRMS (ESI$^+$) *m/z* calc. $C_{21}H_{25}NNaO_{13}$ $[M+Na]^+$ 522.1218; found 522.1214.

ν_{max}/cm^{-1} (neat) 3578 (OH), 1741 (CO), 1530 (NO).

mp 193 – 194 °C (lit. 195 – 196 °C)[350] from DCM.

The spectral data are in agreement with the literature.[331]

1,3-bis(((tert-butyldimethylsilyl)oxy)methyl)benzene (138)

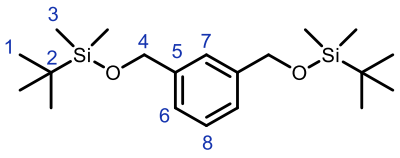

138

Imidazole (147 mg, 2.16 mmol) and TBSCl (326 mg, 2.16 mmol) were added to a solution of 1,3-dimethanolbenzene (100 mg, 0.72 mmol) in anhydrous DMF (2 mL) at 0° C. The reaction mixture was allowed to warm to room temperature and stirred for 2 h under argon. After TLC analysis (hexane) showed consumption of the starting material (R_F = 0.0) and the formation of a new spot (R_F = 0.2), the reaction was diluted with water (10 mL), extracted with EtOAc (3 x 10 mL) and washed with brine (5 x 10 mL). The combined organic phases were dried ($MgSO_4$), filtered, concentrated under reduced pressure and the crude product was purified by flash column chromatography (hexane → 3% EtOAc/hexane) to give **138** (228 mg, 0.62 mmol, 86%) as a clear oil.

^{1}H NMR (600 MHz, $CDCl_3$) δ_H 7.27 – 7.35 (m, 2H, H7, H8), 7.19 – 7.24 (m, 2H, H6), 4.77 (s, 4H, H4), 0.97 (br s, 12H, H3), 0.13 (br s, 18H, H1).

^{13}C NMR (100 MHz, $CDCl_3$) δ_C 141.3 (C5), 128.1 (C7), 124.6 (C6), 123.8 (C8), 65.0 (C4), 25.9 (C1), 18.4 (C2), -5.3 (C3).

HRMS (ESI$^+$) *m/z* calc. for $C_{20}H_{39}O_2Si_2$ $[M+H]^+$ 367.2483; found 367.2481.

The spectral data are in agreement with literature.[351]

(((4-nitro-1,3-phenylene)bis(methylene))bis(oxy))bis(tert-butyldimethylsilane) (139)

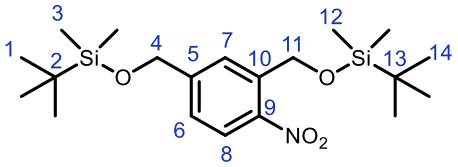

139

Nitric acid (71% aq.; 3 mL) was added dropwise to acetic anhydride (15 mL) at 0°C and the mixture was stirred for 15 minutes at rt under argon. A solution of compound **138** (5.90 g, 16.11 mmol) in acetic anhydride (10 mL) was added dropwise at -10 °C, the reaction mixture was allowed to warm to 0° C and was stirred for 1 h. After this time, TLC analysis (2% EtOAc/hexane) showed consumption of the starting material (R_F = 0.3) and the formation of a new product spot (R_F = 0.5). The reaction mixture was diluted with EtOAc (100 mL) and

was washed with sat. aq. $NaHCO_3$ (5 x 50 mL). The combined organic phases were washed with brine (100 mL), dried ($MgSO_4$) and the solvent was removed under reduced pressure. The crude product was purified by flash column chromatography (hexane → 5% EtOAc/hexane) to give **139** (4.82 g, 73%) as a pale yellow oil.

^{1}H NMR (400 MHz, $CDCl_3$) δ_H 8.11 (d, 1H, J_{H8H6} 8.4 Hz, H8), 7.88 – 7.91 (m, 1H, H7), 7.35 – 7.39 (m, 1H, H6), 5.13 (s, 2H, H11), 4.85 (s, 2H, H4), 0.92 – 1.03 (m, 18H, H1, H14), 0.08 – 0.20 (m, 12H, H3, H12) ppm.

^{13}C NMR (100 MHz, $CDCl_3$) δ_C 148.1 (C10), 138.5 (C5), 125.0 (C7), 124.8 (C8), 124.5 (C6), 64.4 (C4), 62.3 (C11), 26.0 (C14), 25.9 (C1), 18.45 (C13), 18.42 (C2), -5.3 (C12), -5.4 (C3) ppm.

HRMS (ESI$^+$) *m/z* calc. for $C_{20}H_{37}NNaO_4Si_2$ $[M+Na]^+$ 434.2153; found 434.2154.

ν_{max}/cm^{-1} (neat) 1521 (N-O).

The spectral data are in agreement with the literature.[351]

2,4-bis(((tert-butyldimethylsilyl)oxy)methyl)aniline (140)

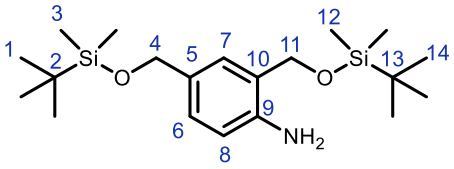

140

Pd/C (79 mg, 10 wt%) and ammonium formate (606 mg, 9.61 mmol) were added to a solution of **139** (791 mg, 1.92 mmol) in anhydrous MeOH and the reaction mixture was heated to reflux for 16 h under argon. After this time, TLC analysis (2% EtOAc/hexane) showed complete consumption of **139** (R_F = 0.7) and the formation of a new product (R_F = 0.3). The reaction mixture was then filtered through Celite®, concentrated under reduced pressure and the crude product purified by flash column chromatography (1% → 2% EtOAc/hexane) to give **140** (421 mg, 1.10 mmol, 58%) as an off-white oil.

^{1}H NMR (600 MHz, $CDCl_3$) δ_H 7.05 (dd, 1H, J_{H6H8} 8.0 J_{H6H7} 2.1 Hz, H6), 7.00 (d, 1H, J_{H7H6} 2.1 Hz, H7), 6.63 (d, 1H, J_{H8H6} 8.0 Hz, H8), 4.68 (s, 2H, H11), 4.61 (s, 2H, H4), 0.87 – 0.94 (m, 18H, H1, H14), 0.05 – 0.08 (m, 12H, H3, H12) ppm.

^{13}C NMR (100 MHz, $CDCl_3$) δ_C 145.1 (C9), 130.8 (C10), 127.1 (C7), 127.0 (C6), 115.6 (C8), 65.1 (C4), 65.0 (C11), 26.0 (C1, C14), 25.9 (C1, C14), 18.5 (C2, C13), 18.3 (C2, C13), -5.1 (C3, C12), -5.2 (C3, C12) ppm.

HRMS (ESI^+) *m/z* calc. for $C_{20}H_{39}NNaO_2Si_2$ $[M+Na]^+$ 404.2412; found 404.2410.

The spectral data are in agreement with the literature.[351]

(4-amino-1,3-phenylene)dimethanol (127)

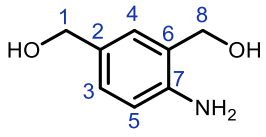

127

TBAF (1 M in THF; 1.26 mL, 1.26 mmol) was added to **140** (160 mg, 0.42 mmol) in anhydrous THF (2 mL) and the reaction was stirred at rt for 30 min under argon. After this time, TLC analysis (5% EtOAc/hexane) showed complete consumption of the starting material (R_F = 0.3) and the formation of a new spot (R_F = 0.0). The solvent was then removed under reduced pressure and the crude product was purified by flash column chromatography (5% MeOH/DCM) to give **127** (60 mg, 0.39 mmol, 93%) as a pale brown oil.

R_F = 0.3 (5% MeOH/DCM).

^{1}H NMR (400 MHz, MeOD) δ_H 7.06 – 7.16 (m, 2H, H3, H4), 6.76 (d, 1H, J_{H5H3} 8.0 Hz, H5), 4.61 (s, 2H, H8), 4.49 (s, 2H, H1) ppm.

^{13}C NMR (100 MHz, MeOD) δ_C 145.3 (C7), 130.6 (C6), 127.9 (C4), 127.7 (C3), 125.5 (C2), 115.7 (C5), 63.9 (C1), 62.2 (C8) ppm.

HRMS (ESI^-) *m/z* calc. for $C_8H_{11}NO_2$ $[M-H]^-$ 152.0717; found 152.0712.

The spectral data are in agreement with the literature.[351]

(3-nitrobenzyl 1H-imidazole-1-carboxylate)-2,3,4,6-tetra-*O*-acetyl-β-D-galactopyranoside (142)

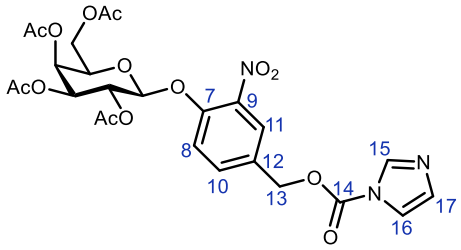

142

DMAP (3 mg, 0.024 mmol) was added to a solution of alcohol **140** (61 mg, 0.12 mmol) and CDI (39 mg, 0.24 mmol) in anhydrous DCM (2 mL). The reaction mixture was stirred at rt for 4 h under argon. After this time, TLC analysis (30% EtOAc/hexane) showed consumption of the starting material (R_F = 0.5) and the formation of a product (R_F = 0.2). The reaction was then quenched with ice-cold water (10 mL) and extracted with DCM (3 x 10 mL). The combined organic extracts were washed with $NaHCO_3$ (sat. aq.; 10 mL) and brine (sat. aq.; 10 mL), then dried ($MgSO_4$), filtered and concentrated under reduced pressure. The crude product was purified by flash column chromatography (50% EtOAc/hexane → 70% EtOAc/hexane) to give **142** (15 mg, 0.025 mmol, 21%) as a clear oil.

^{1}H NMR (400 MHz, DMSO-d_6) δ_H 8.32 (s, 1H, H15), 8.10 (d, J_{H11H10} 2.1 Hz, 1H, H11), 7.87 (dd, J_{H10H8} 8.7 Hz J_{H10H11} 2.1 Hz, 1H, H10), 7.61 – 7.65 (m, 1H, H16), 7.44 (d, J_{H8H10} 8.7 Hz, 1H, H8), 7.08 (d, J_{H17H16} 1.7 Hz, 1H, H17), 5.61 (d, J_{H1H2} 7.4 Hz, 1H, H1), 5.46 (s, 2H, H13), 5.34 – 5.38 (m, 1H, H4), 5.20 – 5.28 (m, 2H, H2, H3), 4.44 – 4.52 (m, 2H, H5, H6a), 4.08 – 4.15 (m, 1H, H6b), 2.15 (s, 3H, OCOC$\underline{H}_3$), 2.03 (s, 6H, OCOC$\underline{H}_3$), 1.95 (s, 3H, OCOC$\underline{H}_3$) ppm.

^{13}C NMR (100 MHz, DMSO-d_6) δ_C 170.4 (O$\underline{C}$OCH$_3$), 170.3 (O$\underline{C}$OCH$_3$), 170.0 (O$\underline{C}$OCH$_3$), 169.3 (O$\underline{C}$OCH$_3$), 148.8 (C7), 148.6 (C14), 137.8 (C15), 134.5 (C10), 130.8 (C17), 130.6 (C9), 125.2 (C11), 122.7 (C12), 118.2 (C8), 118.1 (C16), 99.0 (C1), 71.3 (C5), 70.4 (C2), 68.1 (C3), 67.6 (C4), 61.7 (C6), 21.0 (OCO$\underline{C}$H$_3$), 20.9 (OCO$\underline{C}$H$_3$), 20.79 (OCO$\underline{C}$H$_3$), 20.77 (OCO$\underline{C}$H$_3$) ppm.

HRMS (ESI$^+$) *m/z* calc. for $C_{25}H_{27}N_3NaO_{14}$ $[M+Na]^+$ 616.1385; found 616.1405.

The spectral data are in agreement with the literature.[352]

(3-nitrobenzyl (4-nitrophenyl) carbonate)-2,3,4,6-tetra-*O*-acetyl-β-D-galactopyranoside (144)

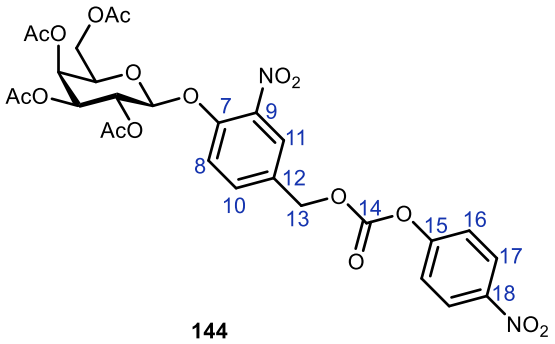

144

Pyridine (284 µL, 3.52 mmol) was added to a solution of alcohol **136** (703 mg, 1.41 mmol) and 4-nitrophenyl chloroformate (653 mg, 3.24 mmol) in anhydrous DCM (20 mL). The reaction mixture was heated to reflux for 16 h under argon. After this time, TLC analysis (50% EtOAc/hexane) showed conversion of alcohol **136** (R_F = 0.1) to a new product (R_F = 0.3). The reaction mixture was diluted with water (20 mL) and extracted with DCM (3 x 20 mL). The combined organic phases were washed with brine (sat. aq.; 20 mL), dried ($MgSO_4$) and concentrated under reduced pressure. The crude product was purified by flash column chromatography (10% EtOAc/hexane → 50% EtOAc/hexane) to give **144** (591 mg, 0.86 mmol, 61%) as a white powder.

^{1}H NMR (400 MHz, $CDCl_3$) δ_H 8.21 – 8.29 (m, 2H, H17), 7.88 (d, J_{H11H10} 2.2 Hz, 1H, H11), 7.60 (dd, J_{H10H8} 8.6 Hz J_{H10H11} 2.2 Hz, 1H, H10), 7.34 – 7.41 (m, 3H, H16, H8), 5.53 (dd, J_{H2H3} 10.5 Hz J_{H2H1} 7.9 Hz, 1H, H2), 5.46 (dd, J_{H4H3} 3.4 Hz J_{H4H5} 1.2 Hz, 1H, H4), 5.27 (s, 2H, H13), 5.06 – 5.13 (m, 2H, H1, H3), 4.20 – 4.27 (m, 1H, H6), 4.05 – 4.18 (m, 2H, H5, H6), 2.17 (s, 3H, OCOC$\underline{H}_3$), 2.05 (s, 3H, OCOC$\underline{H}_3$), 1.96 – 2.03 (m, 6H, OCOC$\underline{H}_3$) ppm.

^{13}C NMR (100 MHz, $CDCl_3$) δ_C 171.2 (O$\underline{C}$OCH$_3$), 170.14 (O$\underline{C}$OCH$_3$), 170.10 (O$\underline{C}$OCH$_3$), 169.3 (O$\underline{C}$OCH$_3$), 155.3 (C18), 152.3 (C14), 149.7 (C9), 145.5 (C15), 141.2 (C7), 133.8 (C10), 130.2 (C12), 125.42 (C11), 125.36 (C17), 121.7 (C16), 119.8 (C8), 100.6 (C1), 71.5 (C5), 70.5 (C3), 68.9 (C13), 67.8 (C2), 66.7 (C4), 61.3 (C7), 21.03 (OCO$\underline{C}$H$_3$), 20.7 (OCO$\underline{C}$H$_3$), 20.6 (OCO$\underline{C}$H$_3$), 20.5 (OCO$\underline{C}$H$_3$) ppm.

HRMS (ESI$^+$) *m/z* calc. for $C_{28}H_{28}N_2NaO_{17}$ $[M+Na]^+$ 687.1280; found 687.1282.

ν_{max}/cm^{-1} (neat) 1743 (CO), 1533 (N-O).

mp 70 – 72 °C (lit. 77 – 79 °C)[353] from EtOAc/hexane.

The spectral data are in agreement with the literature.[353]

(3-nitrobenzyl (2,4-bis(((tert-butyldimethylsilyl)oxy)methyl)phenyl)carbamate)-2,3,4,6-tetra-*O*-acetyl-β-D-galactopyranoside (145)

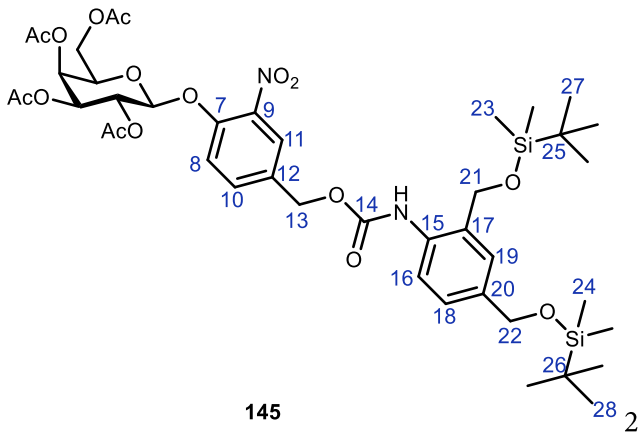

145

HOBt (26 mg, 0.17 mmol) was added to a solution of aniline **140** (114 mg, 0.30 mmol) and carbonate **144** (100 mg, 0.15 mmol) in anhydrous DMF (2 mL). The reaction mixture was heated to 50 °C and stirred for 16 h under argon. After this time, TLC analysis (40% EtOAc/hexane) showed consumption of carbonate **144** (R_F = 0.2) and the formation of a new product (R_F = 0.5). The solution was concentrated under reduced pressure and the crude material was purified by flash column chromatography (10% EtOAc/hexane → 40% EtOAc/hexane) to give **145** (91 mg, 0.10 mmol, 67%) as a pale yellow oil.

^{1}H NMR (400 MHz, $CDCl_3$) δ_H 8.51 (s, 1H, NH), 7.93 – 7.99 (m, 1H, H16), 7.85 (d, J_{H11H10} 2.2 Hz, 1H, H11), 7.57 (dd, J_{H10H8} 8.6 Hz J_{H10H11} 2.2 Hz, 1H, H10), 7.37 (d, J_{H8H10} 8.6 Hz, 1H, H8), 7.24 (dd, J_{H18H16} 8.4 Hz J_{H18H19} 2.0 Hz, 1H, H18), 7.05 – 7.08 (m, 1H, H19), 5.56 (dd, J_{H2H3} 10.5 J_{H2H1} 7.9 Hz, 1H, H2), 5.48 (dd, J_{H4H3} 3.5 Hz J_{H4H5} 1.2 Hz, 1H, H4), 5.18 – 5.21 (m, 2H, H13), 5.12 (dd, J_{H3H2} 10.5 Hz J_{H3H4} 3.5 Hz, 1H, H3), 5.09 (d, J_{H1H2} 7.9 Hz, 1H, H1), 4.74 (s, 2H, H21), 4.68 (s, 2H, H22), 4.23 – 4.27 (m, 1H, H6), 4.07 – 4.11 (m, 1H, H5), 2.20 (s, 3H, OCOC$\underline{H}_3$), 2.14 (s, 3H, OCOC$\underline{H}_3$), 2.08 (s, 3H, OCOC$\underline{H}_3$), 2.03 (s, 3H, OCOC$\underline{H}_3$), 0.93 (s, 9H, H27, H28), 0.90 (s, 9H, H27, H28), 0.06 – 0.11 (m, 12H, H23, H24) ppm.

^{13}C NMR (100 MHz, $CDCl_3$) δ_C 171.1 (O$\underline{C}$OCH$_3$), 170.2 (O$\underline{C}$OCH$_3$), 170.1 (O$\underline{C}$OCH$_3$), 169.4 (O$\underline{C}$OCH$_3$), 153.1 (C14), 149.0 (C9), 141.3 (C7), 136.5 (C17), 136.2 (C20), 133.2 (C10), 132.9 (C12), 126.5 (C18), 125.9 (C19), 124.6 (C11), 119.9 (C8), 119.6 (C16), 100.8 (C1), 71.5 (C5), 70.6 (C3), 67.8 (C2), 66.7 (C4), 65.5 (C21), 64.8 (C13), 64.5 (C22), 61.4 (C6), 25.9 (C27, C28),

25.7 (C27, C28), 20.7 (3x OCO<u>C</u>H$_3$), 20.6 (OCO<u>C</u>H$_3$), 18.4 (C25, C26), 18.1 (C25, C26), -5.2 (C23, C24), -5.4 (C23, C24) ppm.

HRMS (ESI$^+$) *m/z* calc. for $C_{42}H_{62}N_2NaO_{17}Si_2$ [M+Na]$^+$ 929.3530; found 929.3522.

ν_{max}/cm^{-1} (neat) 2954 (Aromatic CH), 1751 (CO), 1536 (NO).

(3-nitrobenzyl (2,4-bis(hydroxymethyl)phenyl)carbamate)-2,3,4,6-tetra-*O*-acetyl-β-D-galactopyranoside (147)

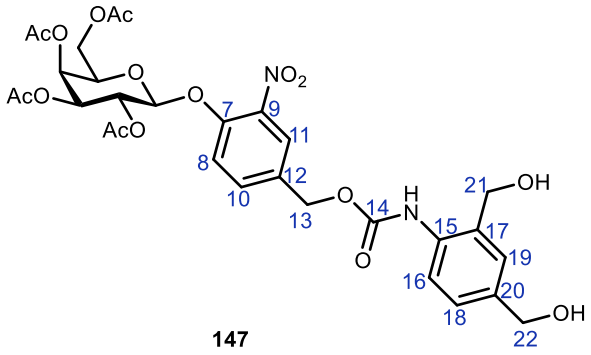

147

Method A (attempted):

TBAF (1 M in THF; 0.5 mL, 0.5 mmol) was added to a solution of **144** (70 mg, 0.08 mmol) in anhydrous THF (2 mL) and stirred at rt for 6 h under argon. After this time, TLC analysis (40% EtOAc/hexane) showed consumption of the starting material (R_F = 0.5) and the formation of a complex mixture. The reaction mixture was concentrated under reduced pressure and purified by flash column chromatography (30% EtOAc → 70% EtOAc/hexane) which did not yield the target molecule.

Method B:

Aniline **127** (46 mg, 0.15 mmol) in anhydrous DMF (1 mL) and HOBt (26 mg, 0.17 mmol) were added to solution of carbonate **144** (100 mg, 0.15 mmol) in anhydrous DMF (1 mL). The mixture was stirred at 50 °C for 3 h under argon. After this time, TLC analysis (50% EtOAc/hexane) showed consumption of the starting material (R_F = 0.3) and the formation of a product (R_F = 0.0); analysis in 2% MeOH/DCM confirmed consumption of the starting material (R_F = 0.9) and the formation of a product (R_F = 0.2). The solution was concentrated under reduced pressure and the crude material was purified by flash column chromatography (1% → 2% MeOH/DCM) to afford **147** (47 mg, 0.069 mmol, 46%) as a clear oil.

^{1}H NMR (400 MHz, methanol-d_4) δ_H 7.90 (s, 1H, H11), 7.60 – 7.74 (m, 2H, H8, H16), 7.49 (d, J_{H10H8} 8.7 Hz, 1H, H10), 7.35 (s, 1H, H19), 7.29 (d, J_{H18H16} 8.3 Hz, 1H, H18), 5.46 – 5.54 (m, 1H, H4), 5.35 – 5.46 (m, 2H, H1, H2), 5.27 (dd, J_{H3H2} 9.4 Hz J_{H3H4} 3.3 Hz, 1H, H3), 5.22 (s, 2H, H13), 4.66 (s, 2H, H21), 4.59 (s, 2H, H22), 4.31 – 4.41 (m, 1H, H5), 4.18 – 4.38 (m, 2H, H6), 2.21 (s, 3H, OCOC$\underline{H}_3$), 2.04 – 2.15 (m, 6H, OCOC$\underline{H}_3$), 2.00 (s, 3H, OCOC$\underline{H}_3$) ppm.

^{13}C NMR (100 MHz, methanol-d_4) δ_C 171.0 (O$\underline{C}$OCH$_3$), 170.9 (O$\underline{C}$OCH$_3$), 170.4 (O$\underline{C}$OCH$_3$), 170.2 (O$\underline{C}$OCH$_3$), 154.8 (C14), 149.1 (C9), 141.4 (C7), 138.0 (C20), 135.5 (C17), 133.4 (C8), 133.0 (C12), 127.1 (C18), 126.8 (C15), 124.4 (C11), 118.8 (C10), 100.1 (C1), 71.6 (C5), 71.0 (C3), 68.6 (C2), 67.6 (C4), 65.1 (C13), 63.8 (C22), 62.0 (C21), 19.7 (OCO$\underline{C}$H$_3$), 19.6 (OCO$\underline{C}$H$_3$), 19.5 (2x OCO$\underline{C}$H$_3$) ppm.

HRMS (ESI$^+$) *m/z* calc. for $C_{30}H_{34}N_2NaO_{16}$ $[M+Na]^+$ 701.1801; found 701.1801.

ν_{max}/cm^{-1} (neat) 3341 (OH), 1735 (CO), 1531 (NO).

(3-nitrobenzyl (2,4-bis((((4-nitrophenoxy)carbonyl)oxy)methyl)phenyl)carbamate)-2,3,4,6-tetra-*O*-acetyl-β-D-galactopyranoside (150)

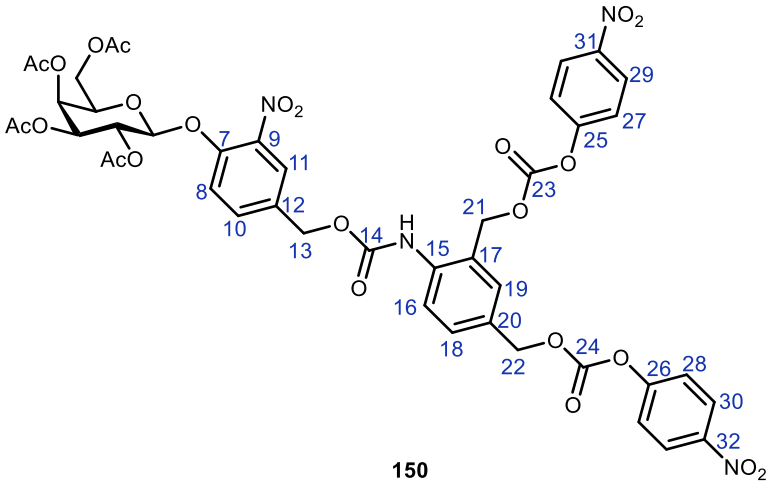

150

Pyridine (0.77 mL, 9.73 mmol) was added dropwise to a solution of **147** (1.10 g, 1.62 mmol) and 4-nitrophenyl chloroformate (1.96 g, 9.73 mmol) in anhydrous DCM (15 mL) at rt and the reaction mixture was heated under reflux for 3 h under argon. After this time, TLC analysis (60% EtOAc/hexane) showed consumption of the starting material (R_F = 0.2) and the formation of a product (R_F = 0.5). The reaction mixture was then diluted with DCM (20 mL), washed with water (3 x 20 mL), the organic fraction dried ($MgSO_4$), filtered and concentrated

under reduced pressure. The crude product was purified by flash column chromatography (40% → 60% EtOAc/hexane) to give **150** (1.16 g, 1.15 mmol, 71%) as a pale yellow oil.

^{1}H NMR (400 MHz, $CDCl_3$) δ_H 8.18 – 8.33 (m, 4H, H29, H30), 7.89 (d, J_{H16H18} 8.1 Hz, 1H, H16), 7.83 – 7.87 (m, 1H, H11), 7.62 (br s, 1H, NH), 7.56 (dd, J_{H10H8} 8.6 Hz J_{H10H11} 2.2 Hz, H10), 7.48 – 7.53 (m, 2H, H18, H19), 7.31 – 7.40 (m, 4H, H27, H28), 5.53 (dd, J_{H2H3} 10.5 Hz J_{H2H1} 7.9 Hz, 1H, H2), 5.41 – 5.49 (m, 1H, H4), 5.31 (s, 2H, H21), 5.27 (s, 2H, H22), 5.20 (s, 2H, H13), 5.05 – 5.13 (m, 2H, H1, H3), 4.21 – 4.28 (m, 1H, H6), 4.04 – 4.17 (m, 2H, H5, H6), 2.18 (s, 3H, OCOC$\underline{H}_3$), 2.05 (s, 3H, OCOC$\underline{H}_3$), 2.03 (s, 3H, OCOC$\underline{H}_3$), 2.01 (s, 3H, OCOC$\underline{H}_3$) ppm.

^{13}C NMR (100 MHz, $CDCl_3$) δ_C 170.3 (O$\underline{C}$OCH$_3$), 170.2 (O$\underline{C}$OCH$_3$), 170.1 (O$\underline{C}$OCH$_3$), 169.4 (O$\underline{C}$OCH$_3$), 155.4 (C32), 155.1 (C31), 153.4 (C14), 153.0 (C24), 152.4 (C23), 149.2 (C7), 145.7 (C25), 145.5 (C26), 141.3 (C9), 137.4 (C17), 133.5 (C10), 132.1 (C12), 132.0 (C19), 131.1 (C18), 130.8 (C15), 125.4 (C30), 125.3 (C29), 125.0 (C11), 121.8 (C27), 121.7 (C28), 119.8 (C8), 100.7 (C1), 71.5 (C5), 70.5 (C3), 70.0 (C22), 67.8 (C2), 67.6 (C21), 66.7 (C4), 65.5 (C13), 61.3 (C6), 20.7 (OCO$\underline{C}$H$_3$), 20.6 (2x OCO$\underline{C}$H$_3$), 20.5 (OCO$\underline{C}$H$_3$) ppm.

HRMS (ESI$^+$) *m/z* calc. for $C_{44}H_{40}N_4NaO_{24}$ $[M+Na]^+$ 1031.1925; found 1031.1918.

ν_{max}/cm^{-1} (neat) 2979 (Ar CH), 1751 (CO), 1532 (NO).

2-(4-vinylbenzyl)isoindoline-1,3-dione (152)

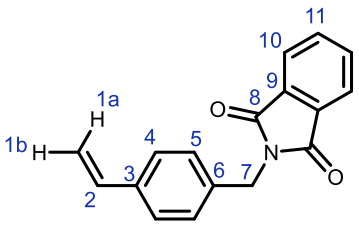

152

Potassium phthalimide (128 mg, 0.69 mmol) was added to a solution of 4-vinylbenzyl chloride (92 µL, 0.66 mmol) in anhydrous DMF (5 mL) under argon. The reaction mixture was then heated to 55 °C and stirred for 16 h, after which time TLC analysis (15% EtOAc/hexane) showed consumption of the starting material (R_F = 0.9) and the formation of a product (R_F = 0.3). Water (50 mL) was then added and the organic product was extracted with EtOAc (3 x 50 mL). The combined organic extracts were washed with brine (sat. aq.; 5 x

50 mL), dried ($MgSO_4$), filtered and concentrated under reduced pressure. The crude product was purified by flash column chromatography (5 → 15% EtOAc/hexane) to give **152** (125 mg, 0.48 mmol, 72%) as a white crystalline powder.

^{1}H NMR (400 MHz, $CDCl_3$) δ_H 7.80 – 7.87 (m, 2H, H10), 7.65 – 7.73 (m, 2H, H11), 7.32 – 7.43 (m, 4H, H4, H5), 6.67 (dd, J_{H2H1b} 17.6 Hz J_{H2H1a} 10.8 Hz, 1H, H2), 5.71 (d, J_{H1aH2} 17.6 Hz, 1H, H1a), 5.22 (d, J_{H1bH2} 10.8 Hz, 1H, H1b), 4.82 (s, 2H, H7) ppm.

^{13}C NMR (100 MHz, $CDCl_3$) δ_C 168.0 (C8), 137.2 (C3), 136.3 (C2), 135.9 (C6), 134.0 (C11), 132.1 (C9), 128.9 (C5), 126.5 (C4), 123.4 (C10), 114.2 (C1), 41.4 (C7) ppm.

HRMS (ESI$^+$) *m/z* calc. for $C_{17}H_{13}NNaO_2$ $[M+Na]^+$ 286.0838; found 286.0841.

mp 96-98 °C (lit. 97 – 98 °C)[354] from EtOAc/hexane).

The spectral data are in agreement with the literature.[354]

(4-vinylphenyl)methanamine hydrochloride (153)

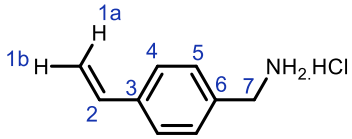

153

Hydrazine monohydrate (51% w/w hydrazine; 66 µL, 1.09 mmol) was added to a suspension of **152** (200 mg, 0.76 mmol) in EtOH (2 mL) and then the reaction mixture was heated to reflux for 2 h. After this time, TLC analysis (15% EtOAc/hexane) showed the consumption of the starting material (R_F = 0.3) and the formation of a product (R_F = 0.0); analysis in 15% MeOH/DCM confirmed consumption of the starting material (R_F = 1.0) and the formation of a product (R_F = 0.4). The reaction mixture was then allowed to cool to rt, NaOH (1 M aq.; 10 mL) added and the organic product extracted with DCM (3 x 10 mL). The combined organic extracts were washed with brine (sat. aq.; 20 mL), dried ($MgSO_4$) and filtered. HCl (4N in dioxane; 0.4 mL, 1.52 mmol) was added to precipitate the hydrochloride salt which was obtained following solvent removal under reduced pressure to give **153** (78 mg, 0.46 mmol, 61%) as a white powder.

^{1}H NMR (400 MHz, DMSO-d_6) δ_H 8.53 (s, 3H, N$\underline{H}_3^+$), 7.45 – 7.53 (m, 4H, H4, H5), 6.74 (dd, J_{H2H1a} 17.7 Hz J_{H2H1b} 10.9 Hz, 1H, H2), 5.87 (dd, J_{H1aH2} 17.7 Hz J_{H1aH1b} 1.0 Hz, 1H, H1a), 5.29 (dd, J_{H1bH2} 10.9 Hz J_{H1bH1a} 1.0 Hz, 1H, H1b), 3.99 (s, 2H, H7).

^{13}C NMR (100 MHz, DMSO-d_6) δ_C 137.6 (C3), 136.6 (C2), 134.1 (C6), 129.7 (C5), 126.7 (C3), 115.4 (C1), 42.3 (C7).

The spectral data are in agreement with the literature.[355]

N-(2-(2-(2-aminoethoxy)ethoxy)ethyl)methacrylamide (156) (attempted)

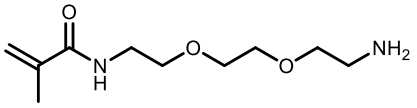

156

Methacrylic anhydride (0.75 mL, 5.06 mmol) was added to a solution of 2,2'-(ethane-1,2-diylbis(oxy))diethanamine (4.95 mL, 33.8 mmol) was in anhydrous DCM (20 mL) at 0 °C and stirred for 16 h under argon. After this time, TLC analysis (10% MeOH/DCM) showed partial consumption of the starting material (R_F = 0.1) and the formation of a product spot (R_F = 0.2); both spots exhibited significantly smearing on the TLC plate. The reaction mixture was concentrated under reduced pressure and the crude product purified by flash column chromatography (5% → 10% MeOH/DCM) to yield an inseparable mixture of starting material and product.

N-(2-(2-(2-(2-aminoethoxy)ethoxy)ethoxy)ethyl)methacrylamide (158) (attempted)

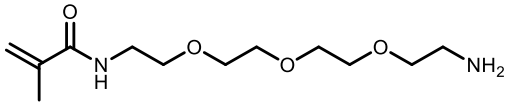

158

Methacrylic anhydride (116 uL, 0.78 mmol) was added to a solution of 1,11-diamino-3,6,9-trioxaundecane (233 µL, 1.56 mmol) was in chloroform (5 mL) at 0 °C and stirred for 16 h. After this time, TLC analysis (10% MeOH/DCM) showed partial consumption of the starting material (R_F = 0.1) and the formation of a product spot (R_F = 0.2); both spots exhibited significantly smearing on the TLC plate. The reaction mixture was concentrated under reduced pressure and the crude product purified by flash column chromatography (5% → 10% MeOH/DCM) to yield an inseparable mixture of starting material and product.

N-(2-chloroethyl)acrylamide (162) (attempted)

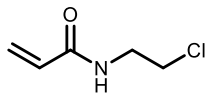

162

$SOCl_2$ (0.29 mL, 3.92 mmol) was added to a suspension of hydroxyethyl acrylamide (0.27 mL, 2.61 mmol) in anhydrous DCM (10 mL) and the reaction mixture was stirred at rt for 16 h under argon. After this time, TLC analysis (10% MeOH/DCM) showed partial consumption of the starting material (R_F = 0.3) and the formation of a complex mixture. The reaction mixture was diluted with DCM (10 mL), washed with $NaHCO_3$ (sat. aq.; 3 x 10 mL) and the organic phase was dried ($MgSO_4$), filtered and concentrated under reduced pressure. The crude product was purified by flash column chromatography (10% MeOH/DCM) which did not yield the target molecule.

2-acrylamidoethyl 4-methylbenzenesulfonate (163) (attempted)

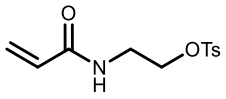

163

p-toluenesulfonyl chloride (547 mg, 2.87 mmol) was added to a solution of N-hydroxyethyl acrylamide (300 mg, 2.61 mmol) and triethylamine (728 µL, 5.22 mmol) in anhydrous DCM 10 mL) and stirred at rt for 16 h under argon. After this time, TLC analysis (50% EtOAc/hexane) showed partial consumption of the starting material (R_F = 0.1) and the formation of a new spot (R_F = 0.3). The reaction mixture was diluted with DCM (20 mL), washed with HCL (0.1 M aq.; 20 mL) and brine (sat. aq.; 20 mL). The organic phase was dried ($MgSO_4$), filtered, concentrated under reduced pressure and the crude product purified by flash column chromatography which did not yield the target molecule.

(3-nitrobenzyl (2,4-bis((((4-vinylbenzyl)carbamoyl)oxy)methyl)phenyl)carbamate)-2,3,4,6-tetra-*O*-acetyl-β-D-galactopyranoside (164)

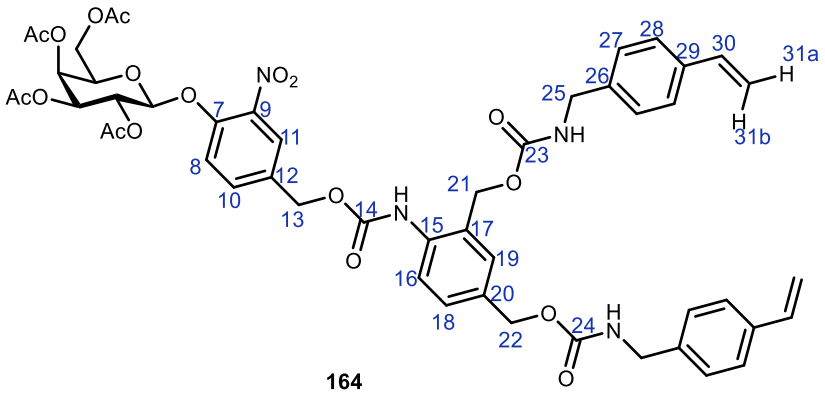

164

Amine **153** (46 mg, 0.34 mmol) and HOBt (28 mg, 0.18 mmol) were added to a solution of dicarbonate **150** (87 mg, 0.086 mmol) in anhydrous DMF (1 mL) and the reaction mixture was stirred at rt for 16 h under argon. After this time, TLC analysis (2% MeOH/DCM) showed complete consumption of the starting material (R_F = 0.5) and the formation of a product (R_F = 0.3). The reaction mixture was concentrated under reduced pressure and the crude product was purified by flash column chromatography (DCM → 2% MeOH/DCM) to give **164** (50 mg, 0.05 mmol, 59%) as a pale yellow oil.

^{1}H NMR (400 MHz, DMSO-d$_6$) δ_H 9.26 (s, 1H, NH), 7.96 (m, 1H, H11), 7.88 (app. t, *J* 6.1 Hz, 1H, H16), 7.72 – 7.82 (m, 1H, H10), 7.35 – 7.49 (m, 7H, H8, H18, H19, H28), 7.22 (d, J_{H27H28} 7.8 Hz, 4H, H29, H27), 6.70 (ddd, $J_{H30H31a}$ 10.8 Hz $J_{H30H31b}$ 17.8 Hz J_{H30H28} 3.6 Hz, 2H, H30), 5.79 – 5.82 (m, 1H, H31a, H31b), 5.73 – 5.77 (m, 1H, H31a, H31b), 5.59 (d, J_{H1H2} 7.3 Hz, 1H, H1), 5.35 – 5.38 (m, 1H, H4), 5.20 – 5.29 (m, 4H, H2, H3, H31a, H31b), 5.16 (s, 2H, H13), 5.06 (s, 2H, H21), 5.00 (s, 2H, H22), 4.48 (app. t, *J* 6.3 Hz, 1H, H5), 4.18 (d, J_{H25H27} 6.2 Hz, 4H, H25), 4.13 (dd, J_{H6H5} 6.3 J_{H6aH6b} 4.4 Hz, 2H, H6), 2.15 (s, 3H, OCOC$\underline{H}_3$), 2.03 (s, 6H, 2x OCOC$\underline{H}_3$), 1.95 (s, 3H, OCOC$\underline{H}_3$) ppm.

^{13}C NMR (100 MHz, DMSO-d$_6$) δ_C 169.9 (O$\underline{C}$OCH$_3$), 169.8 (O$\underline{C}$OCH$_3$), 169.5 (O$\underline{C}$OCH$_3$), 168.8 (O$\underline{C}$OCH$_3$), 156.3 (C23), 156.3 (C24), 153.9 (C14), 147.9 (C7), 141.1 (C9), 140.2 (C29), 139.4 (C20), 139.3 (C15), 136.3 (C30), 135.7 (C26), 133.6 (C10), 132.2 (C12), 127.2 (C27), 126.0 (C28), 124.1 (C11), 117.8 (C8), 113.8 (C31), 98.5 (C1), 70.8 (C5), 69.9 (C2), 67.7 (C3), 67.0 (C4), 65.0 (C22), 64.4 (C13), 61.9 (C21), 61.2 (C6), 43.6 (C25), 20.5 (OCO$\underline{C}$H$_3$),20.4 (OCO$\underline{C}$H$_3$), 20.30 (OCO$\underline{C}$H$_3$), 20.27 (OCO$\underline{C}$H$_3$) ppm.

HRMS (ESI$^+$) *m/z* calc. for $C_{50}H_{52}N_4NaO_{18}$ $[M+Na]^+$ 1019.3169; found 1019.3178.

ν_{max}/cm^{-1} (neat) 2975 (Ar CH), 1746 (CO), 1533 (NO).

(3-nitrobenzyl (2,4-bis((((4-vinylbenzyl)carbamoyl)oxy)methyl)phenyl)carbamate)-β-D-galactopyranoside (165)

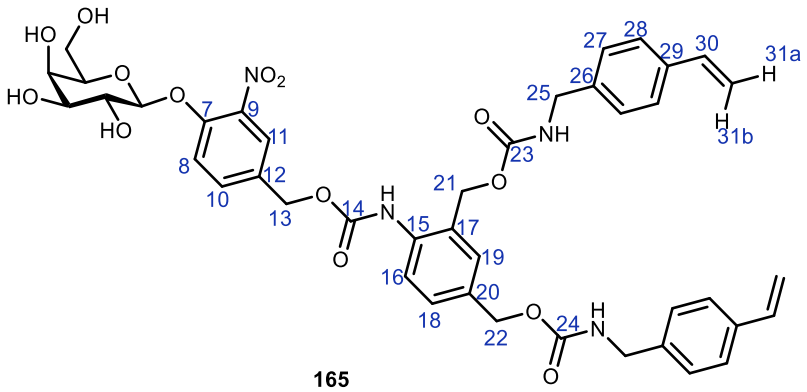

165

NaOH (1 M, 0.13 mL, 0.13 mmol) was added to **164** (65 mg, 0.065 mmol) in MeOH:DCM (5:1 v/v; 2 mL) and stirred for 30 min at rt. After this time, TLC analysis (2% MeOH/DCM) showed complete consumption of the starting material (R_F = 0.3) and the formation of a product (R_F = 0.0); analysis in 10% MeOH/DCM confirmed consumption of the starting material (R_F = 1.0) and the formation of a product (R_F = 0.2). The reaction mixture was then neutralised with Amberlite IRC-120 H^+ resin and filtered. The filtrate was concentrated under reduced pressure and the crude product purified by flash column chromatography (2% → 10% MeOH/DCM)) to give **165** (32 mg, 0.39 mmol, 59%) as an off-white powder.

^{1}H NMR (600 MHz, DMSO-d_6) δ_H 9.27 (s, 1H, NH), 7.93 (s, 1H, H11), 7.90 (t, J_{NHH25} 6.2 Hz, 1H, NH), 7.66 – 7.69 (m, 1H, H10), 7.47 (d, J_{H16H18} 8.2 Hz, 1H, H16), 7.44 (d, J_{H8H10} 8.8 Hz, 1H, H8), 7.38 – 7.42 (m, 4H, H28), 7.36 (br s, 1H, H19), 7.30 (d, J_{H18H16} 8.2 Hz, 1H, H18), 7.19 – 7.23 (m, 4H, H27), 6.69 (ddd, $J_{H30H31a}$ 17.8 Hz $J_{H30H31b}$ 10.8 J_{H30H28} 4.1 Hz, 2H, H30), 5.79 (dd, $J_{H31aH30}$ 17.8 Hz $J_{H31aH31b}$ 1.1 Hz, 2H, H31a), 5.22 (dd, $J_{H31bH30}$ 10.8 Hz $J_{H31aH31b}$ 1.1 Hz, 2H, H31a), 5.19 (d, J_{OHH2} 5.3 Hz, 1H, H2-OH), 5.13 (s, 2H, H13), 5.03 – 5.08 (m, 3H, H1, H21), 4.99 (s, 2H, H22), 4.93 (d, J_{OHH3} 5.9 Hz, 1H, H3-OH), 4.68 (t, J_{OHH6} 5.5 Hz, 1H, H6-OH), 4.62 (d, J_{OHH4} 4.6 Hz, 1H, H4-OH), 4.15 – 4.20 (m, 4H, H25), 3.68 – 3.70 (m, 1H, H3), 3.63 (t, J_{H5H6} 6.1 Hz, 1H, H5), 3.55 – 3.59 (m, 1H, H4), 3.52 – 3.55 (m, 1H, H6a), 3.47 – 3.50 (m, 1H, H6b), 3.39 – 3.41 (m, 1H, H2) ppm.

^{13}C NMR (100 MHz, DMSO-d_6) δ_C 156.4 (C23), 156.3 (C24), 149.3 (C7), 139.8 (C20), 139.7 (C15), 139.4 (C26), 136.3 (C30), 135.6 (C29), 133.7 (C17), 133.4 (C12), 130.2 (C9), 127.2

(C27), 126.1 (C28), 124.3 (C11), 117.1 (C8), 113.9 (C31), 100.9 (C1), 75.7 (C5), 73.3 (C2), 69.9 (C4), 67.9 (C3), 64.5 (C13), 61.9 (C21), 60.2 (C6), 43.5 (C25) ppm.

HRMS (ESI$^+$) *m/z* calc. for $C_{42}H_{44}N4NaO_{14}$ $[M+Na]^+$ 851.2746; found 851.2757.

ν_{max}/cm^{-1} (neat) 3296 (OH), 2922 (Ar CH), 1686 (CO), 1528 (NO).

mp 141 – 144 °C.

(3-nitrobenzyl (2,4-bis((((3-methacrylamidopropyl)carbamoyl)oxy)methyl)phenyl)carbamate)-2,3,4,6-tetra-*O*-acetyl-β-D-galactopyranoside (166)

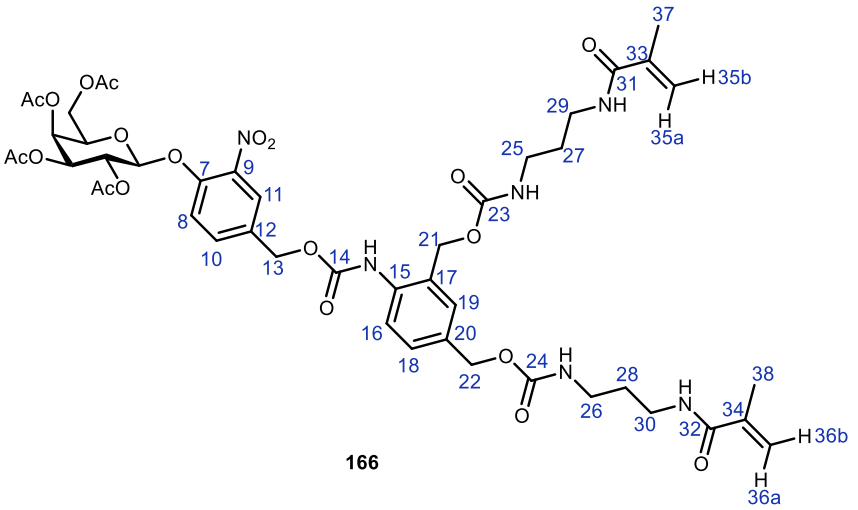

166

N-(3-aminopropyl)methacrylamidehydrochloride (64 mg, 0.36 mmol), HOBt (22 mg, 0.13 mmol) and pyridine (29 uL, 0.36 mmol) were added to a solution of dicarbonate **150** (60 mg, 0.06 mmol) in anhydrous DMF (1 mL) and the reaction mixture was stirred 16 hours at rt under argon. After this time, TLC analysis (2% MeOH/DCM) showed complete consumption of the starting material (R_F = 0.5) and the formation of a product (R_F = 0.2). The reaction mixture was concentrated under reduced pressure and the crude product was purified by flash column chromatography (0.5% → 2% MeOH/DCM) to give **166** (40 mg, 0.039 mmol, 65%).

^{1}H NMR (400 MHz, $CDCl_3$) δ_H 8.96 (s, 1H, NH), 7.81 – 7.89 (m, 2H, H11, H16), 7.57 (d, J_{H10H8} 8.7 Hz J_{H10H11} 2.2 Hz, 1H, H10), 7.30 – 7.37 (m, 3H, H8, H18, H19), 6.74 (s, 1H, NH), 6.48 (s, 1H, NH), 5.88 (t, *J* 6.2 Hz, 1H, NH), 5.74 (s, 1H, H35a/H36a), 5.71 (s, 1H, H35a/H36a), 5.53 (dd, J_{H2H3} 10.5 Hz J_{H2H1} 7.9 Hz, 1H, H2), 5.46 (dd, J_{H4H3} 3.4 Hz J_{H4H5} 1.2 Hz, 1H, H4), 5.27 – 5.36 (m, 4H, H35, H36), 5.19 (s, 2H, H13), 5.06 – 5.12 (m, 2H, H1, H3), 5.04

(s, 2H, H22), 5.02 (s, 2H, H21), 4.24 (dd, J_{H6aH6b} 11.3 Hz J_{H6H5} 6.1 Hz, 1H, H6a), 4.16 (dd, J_{H6bH6a} 11.3 Hz J_{H6H5} 6.1 Hz, 1H, H6b), 4.08 (dd, J_{H5H4} 7.1 Hz, J_{H5H6} 6.1 Hz, 1H, H5), 3.14 – 3.34 (m, 8H, H25, H26, H29, H30), 2.18 (s, 3H, OCOC$\underline{H}_3$), 2.11 (s, 3H, OCOC$\underline{H}_3$), 2.06 (s, 3H, OCOC$\underline{H}_3$), 2.00 (s, 3H, OCOC$\underline{H}_3$), 1.97 (s, 3H, H37/H38), 1.93 (s, 3H, H37/H38), 1.58 – 1.68 (m, 4H, H27, H28) ppm.

^{13}C NMR (100 MHz, $CDCl_3$) δ_C 170.2 (O$\underline{C}$OCH$_3$), 170.1 (O$\underline{C}$OCH$_3$), 169.4 (O$\underline{C}$OCH$_3$), 168.8 (O$\underline{C}$OCH$_3$), 157.8 (C23), 157.2 (C24), 153.7 (C14), 149.0 (C9), 141.2 (C7), 139.8 (C33/C34), 139.7 (C33/C34), 136.8 (C20), 133.4 (C10), 132.8 (C12), 132.3 (C19), 131.9 (C8), 130.0 (C18), 124.8 (C11), 119.9 (C35/C36), 119.7 (C35/C36), 100.7 (C1), 71.4 (C5), 70.5 (C3), 67.8 (C2), 66.7 (C4), 66.0 (C22), 64.9 (C13), 63.4 (C21), 61.3 (C6), 53.4 (C13), 37.6 (C25, C29), 37.4 (C25, C29), 36.0 (C26, C30), 35.5 (C26, C30), 30.0 (C27, C28), 29.7 (C27, C28), 20.7 (OCO$\underline{C}$H$_3$), 20.6 (2 x OCO$\underline{C}$H$_3$), 20.5 (OCO$\underline{C}$H$_3$), 18.63 (C37, C38), 18.59 (C37, C38) ppm.

HRMS (ESI$^+$) *m/z* calc. for $C_{46}H_{58}N_6NaO_6$ $[M+Na]^+$ 1037.3598; found 1037.3589.

ν_{max}/cm^{-1} (neat) 1749 (CO), 1535 (NO).

(3-nitrobenzyl (2,4-bis((((3-methacrylamidopropyl)carbamoyl)oxy)methyl)phenyl)carbamate)-β-D-galactopyranoside (167)

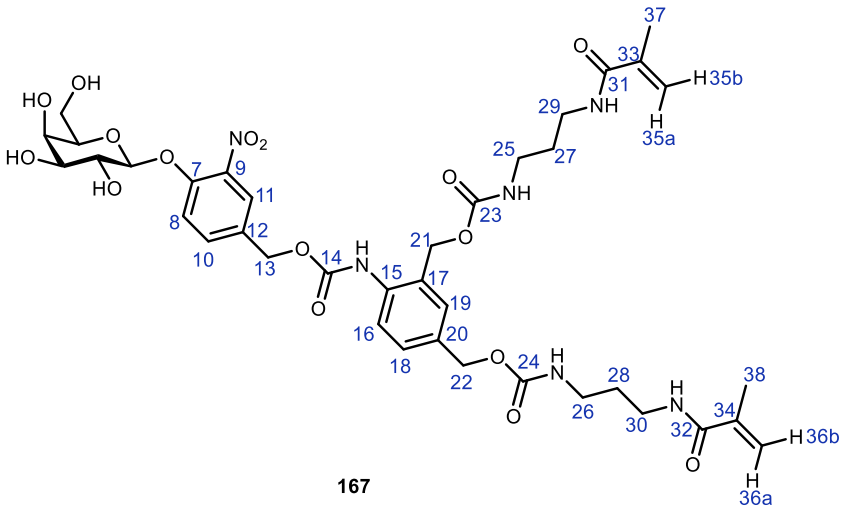

167

NaOH (1 M, 0.05 mL, 0.05 mmol) was added to a solution of **166** (101 mg, 0.10 mmol) in MeOH:DCM (5:1 v/v; 2 mL) and stirred for 30 min at rt. After this time, TLC analysis (6% MeOH/DCM) showed complete consumption of the starting material (R_F = 0.6) and the

formation of a product (R_F = 0.0); analysis in 10% MeOH/DCM confirmed consumption of the starting material (R_F = 0.9) and the formation of a product (R_F = 0.2). The reaction mixture was then neutralised with Amberlite IRC-120 H^+ resin and filtered. After removing the solvent under reduced pressure, the crude material was purified by flash column chromatography (2% → 10% MeOH/DCM) to give **167** (54 mg, 0.06 mmol, 64%) as a pale red solid.

R_F = 0.2 (10% MeOH/DCM).

^{1}H NMR (400 MHz, DMSO-d_6) δ_H 8.96 (s, 1H, NH), 7.93 (d, J_{H11H10} 2.2 Hz, 1H, H11), 7.84 – 7.89 (m, 1H, NH), 7.65 – 7.71 (m, 1H, H10), 7.41 – 7.48 (m, 2H, H8, H16), 7.26 – 7.33 (m, 3H, H18, H19, NH), 7.21 (t, *J* 5.8 Hz, 1H, NH), 7.13 – 7.17 (m, 1H, NH), 5.62 (s, 2H, H35a, H36a), 5.30 (2H, H35b, H36b), 5.14 (s, 2H, H13), 5.03 – 5.08 (m, 3H, H1, H1, H21), 4.96 (s, 2H, H22), 3.70 (br s, 1H, H4), 3.64 (app. t, J_{H5H6} 6.2 Hz, H5), 3.55 – 3.59 (m, 1H, H3), 3.54 (app. t, J_{H6aH5} 6.2 Hz, 1H, H6a), 3.48 (dd, J_{H6bH6a} 10.9 J_{H6bH5} 6.2 Hz, 1H, H6b), 3.39-3.43 (m, 1H, H2), 3.06 – 3.13 (m, 4H, H25, H26), 2.95 – 3.03 (m, 4H, H29, H30), 1.84 (6H, H37, H38), 1.57 (p, *J* 7.0 Hz, 4H, H27, H28) ppm.

^{13}C NMR (100 MHz, DMSO-d_6) δ_C 167.4 (C31, C32), 156.2 (C23), 156.0 (C24), 154.0 (C14), 149.3 (C7), 140.0 (C33), 139.9 (C34), 135.2 (C15), 133.7 (C10), 130.3 (C12), 128.5 (C18), 128.0 (C19), 124.2 (C11, C17), 124.1 (C18), 122.7 (C16), 118.8 (C35, C36), 117.1 (C8), 101.0 (C1), 75.8 (C5), 73.3 (C2), 70.0 (C3), 67.9 (C4), 64.8 (C22), 64.5 (C13), 61.7 (C21), 60.2 (C6), 36.5 (C25, C26), 38.1 (C29, C30), 29.42 (C27/C28), 29.35 (C27/C28), 18.6 (C37, C38) ppm.

HRMS (ESI^+) *m/z* calc. for $C_{38}H_{51}N_6O_{16}$ $[M+H]^+$ 847.3356; found 847.3355.

ν_{max}/cm^{-1} (neat) 3316 (OH), 2934 (aromatic stretch), 1697 (CO), 1529 (NO).

mp 89 – 91 °C.

(3-nitrobenzyl (2-((((3-methacrylamidopropyl)carbamoyl)oxy)methyl)-4-((((4-nitrophenoxy)carbonyl)oxy)methyl)phenyl)carbamate)-2,3,4,6-tetra-*O*-acetyl-β-D-galactopyranoside (168)

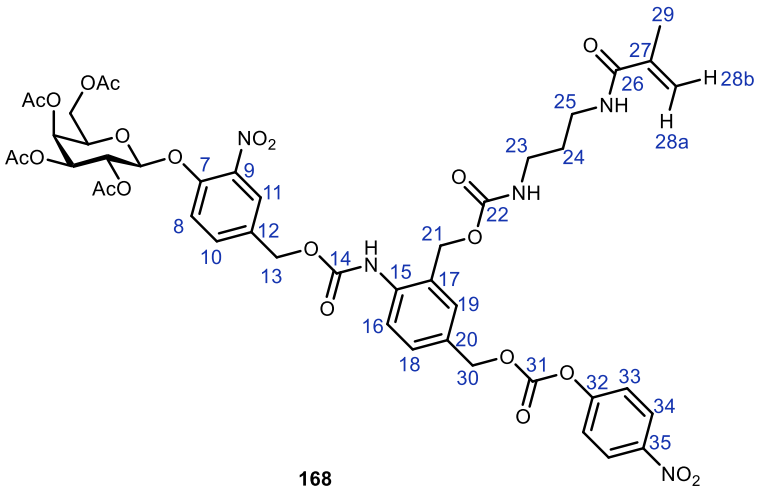

168

N-(3-aminopropyl)methacrylamidehydrochloride (71 mg, 0.40 mmol), Oxyma Pure (30 mg, 0.21 mmol) and pyridine (33 uL, 0.40 mmol) were added to a solution of dicarbonate **150** (100 mg, 0.099 mmol) in anhydrous DMF (1 mL) and the reaction mixture was stirred 16 hours at rt under argon. After this time, TLC analysis (2% MeOH/DCM) showed complete consumption of the starting material (R_F = 0.5) and the formation of a product (R_F = 0.3). The reaction mixture was concentrated under reduced pressure and the crude product was purified by flash column chromatography (0.5% → 2% MeOH/DCM) to give side-product **168** (28 mg, 0.028 mmol, 28%) as a pale yellow oil.

R_F = 0.3 (2% MeOH/DCM).

^{1}H NMR (400 MHz, $CDCl_3$) δ_H 8.99 (s, 1H, NH), 8.24 – 8.28 (m, 2H, H34), 7.95 (d, J_{H16H18} 8.4 Hz, 1H, H16), 7.88 (m, 1H, H11), 7.58 (dd, J_{H10H8} 8.6 Hz J_{H10H11} 2.2 Hz, 1H, H10), 7.39 – 7.45 (m, 2H, H18, H19), 7.32 – 7.38 (m, 3H, H8, H33), 6.29 (t, *J* 6.5 Hz, 1H, NH), 5.69 – 5.75 (m, 2H, NH, H28a), 5.53 (dd, J_{H2H3} 10.5 Hz J_{H2H1} 7.9 Hz, 1H, H2), 5.46 (dd, J_{H4H3} 3.4 Hz J_{H4H5} 1.2 Hz, 1H, H4), 5.31 (m, 1H, H28b), 5.24 (s, 2H, H30), 5.20 (s, 2H, H13), 5.11 (app. d, J_{H3H4} 3.4 Hz, 1H, H3), 5.04 – 5.10 (m, 3H, H1, H21), 4.24 (dd, J_{H6aH6b} 11.3 Hz J_{H6aH5} 6.9 Hz, 1H, H6a), 4.11 – 4.18 (m, 1H, H6b), 4.05 – 4.10 (m, 1H, H5), 3.34 (app. q, J_{H25H24} 6.3 Hz, 2H, H25), 3.19 (app. q, J_{H23H24} 6.3 Hz, 2H, H23), 2.18 (s, 3H, OCOC$\underline{H}_3$), 2.16 (s, 3H, OCOC$\underline{H}_3$), 2.11 (s, 3H, OCOC$\underline{H}_3$), 2.06 (s, 3H, OCOC$\underline{H}_3$), 2.01 (s, 3H, OCOC$\underline{H}_3$), 1.93 (s, 3H, H29), 1.61 – 1.68 (m, 3H, H24) ppm.

^{13}C NMR (100 MHz, $CDCl_3$) δ_C 170.3 (O$\underline{C}$OCH$_3$), 170.2 (O$\underline{C}$OCH$_3$), 170.1 (O$\underline{C}$OCH$_3$), 169.4 (O$\underline{C}$OCH$_3$), 169.1 (C26), 157.6 (C22), 155.5 (C35), 153.6 (C14), 152.4 (C31), 149.0 (C9),

145.4 (C32), 141.3 (C7), 139.6 (C27), 137.8 (C17), 133.4 (C10), 132.7 (C15), 132.5 (C19), 130.6 (C18), 129.7 (C20), 126.1 (C17), 125.3 (C34), 124.8 (C11), 122.0 (C16), 121.8 (C33), 120.0 (C28), 119.7 (C8), 100.7 (C1), 71.4 (C5), 70.5 (C3), 70.3 (C30), 67.8 (C2), 66.7 (C4), 65.0 (C13), 63.5 (C21), 61.3 (C6), 37.6 (C23), 35.9 (C25), 29.9 (C24), 20.68 (OCO$\underline{C}H_3$), 20.65 (2x OCO$\underline{C}H_3$), 20.6 (OCO$\underline{C}H_3$), 18.6 (C29) ppm.

HRMS (ESI$^+$) *m/z* calc. for $C_{45}H_{50}N_5O_{22}$ $[M+H]^+$ 1012.2942; found 1012.2930.

ν_{max}/cm^{-1} (neat) 2955 (Ar CH), 1748 (CO), 1529 (NO).

1,3,5-tris(((tert-butyldimethylsilyl)oxy)methyl)benzene (173)

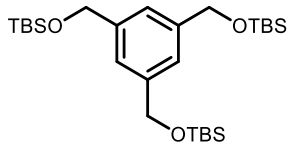

173

Imidazole (5.47 g, 80.33 mmol) and TBSCl (12.11 g, 80.33 mmol) were added to a solution of benzene-1,3,5-trityltrimethanol (3.00 g, 17.85 mmol) in anhydrous DMF (30 mL) at 0 °C and the reaction was allowed to warm to rt and stirred for 2 h under argon. After this time, TLC analysis (5% MeOH/DCM) showed consumption of the starting material (R_F = 0.3) and the formation of a product (R_F = 1.0); analysis in hexane showed the formation of a product (R_F = 0.3). Water (100 mL) was added to the reaction mixture and the organic product was extracted with Et_2O (3 x 50 mL). The combined organic extracts were washed with brine (10 x 50 mL), then dried ($MgSO_4$), filtered and concentrated under reduced pressure. The crude material was filtered through a silica plug (hexane) to give **173** (9.10 g, 17.85 mmol, quant.) as a pale yellow oil.

^{1}H NMR (400 MHz, $CDCl_3$) δ_H 7.19 (s, 1H, ArH), 4.76 (s, 6H, OC$\underline{H}_2$), 0.97 (s, 27H, TBS-^{t}Bu-$\underline{H}$), 0.13 (s, 15H, TBS-C$\underline{H}_3$) ppm.

^{13}C NMR (100 MHz, CDCl3) δ_C 141.3 (q ArC), 122.4 (Ar$\underline{C}$H), 65.1 (O$\underline{C}H_2$), 26.0 (TBS-^{t}Bu-$\underline{C}$), -3.6 (q TBS-^{t}Bu-$\underline{C}$), -5.2 (TBS-$\underline{C}H_3$) ppm.

HRMS (ESI$^+$) *m/z* calc. for $C_{27}H_{54}NaO_3Si_3$ $[M+Na]^+$ 533.3273; found 533.3277.

The spectral data are in agreement with the literature.[134]

1,3,5-tris(((tert-butyldimethylsilyl)oxy)methyl)benzene (174)

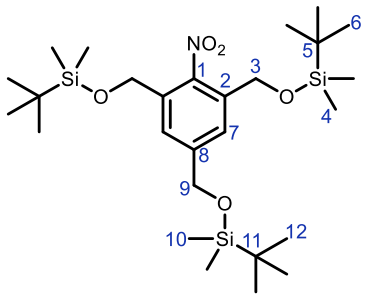

174

Nitric acid (71% aq.;, 3mL) was added dropwise to acetic anhydride (20 mL) at 0 °C and then warmed to rt and stirred for 15 min. After this time, the reaction was cooled to -10 °C and a solution of **173** (6.00 g, 11.76 mmol) in acetic anhydride (7 mL) was added dropwise, then warmed to rt and stirred for 2 h. After this time, TLC analysis (hexane) showed consumption of the starting material (R_F = 0.3) and the formation of a product (R_F = 0.0); analysis in 2% EtOAc/hexane confirmed consumption of the starting material (R_F = 0.8) and the formation of a product (R_F = 0.3).. The reaction mixture was diluted with EtOAc (100 mL) and washed with $NaHCO_3$ (5 x 100 mL) and brine (100 mL). The organic layer was dried ($MgSO_4$), filtered, concentrated under reduced pressure and the crude product purified by flash column chromatography (hexane → 2% EtOAc/hexane) to give **174** (2.80 g, 5.04 mmol, 43%) as a clear oil.

^{1}H NMR (400 MHz, $CDCl_3$) δ_H 7.52 (s, 2H, H7), 4.79 (s, 4H, H3), 4.78 (s, 2H, H9), 0.95 (s, 9H, H12), 0.93 (s, 18H, H6), 0.12 (s, 6H, H10), 0.10 (s, 12H, H4) ppm.

^{13}C NMR (100 MHz, CDCl3) δ_C 145.2 (C2), 144.8 (C1), 134.6 (C8), 124.0 (C7), 64.5 (C9), 61.5 (C3), 26.0 (C12), 25.9 (C6), 18.43 (C11), 18.36 (C5), -5.3 (C10), -5.5 (C4) ppm.

HRMS (ESI^+) *m/z* calc. for $C_{27}H_{53}KO_5Si_3$ $[M+K]^+$ 594.2863; found 594.2867.

The spectral data are in agreement with the literature.[134]

2,4,6-tris(((tert-butyldimethylsilyl)oxy)methyl)aniline (175)

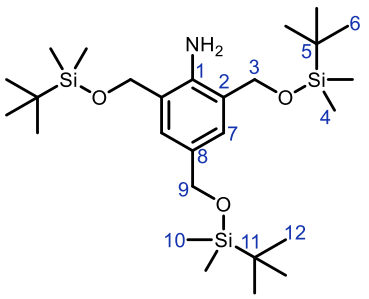

175

Pd/C (450 mg, 10 wt%) and ammonium formate (2.55 g, 40.5 mmol) were added to a solution of **174** (4.50 g, 8.10 mmol) in anhydrous MeOH (30 mL), then heated to reflux and stirred for 3 h under argon. After this time, TLC analysis (2% EtOAc/hexane) showed consumption of the starting material (R_F = 0.3) and the formation of a product (R_F = 0.2). The reaction mixture was cooled to rt, filtered through Celite® and concentrated under reduced pressure. The crude material was purified by flash column chromatography (1 → 4% EtOAc/hexane) to give **175** (2.35 g, 4.47 mmol, 55%) as a clear oil.

^{1}H NMR (400 MHz, $CDCl_3$) δ_H 6.94 (s, 2H, H7), 4.75 (br s, 2H, NH_2), 4.70 (s, 4H, H3), 4.60 (s, 2H, H9), 0.92 (s, 9H, H12), 0.89 (s, 18H, H6), 0.07 (s, 6H, H10), 0.06 (s, 12H, H4) ppm.

^{13}C NMR (100 MHz, CDCl3) δ_C 144.9 (C1), 129.5 (C8), 126.6 (C7), 125.1 (C2), 65.1 (C9), 64.9 (C3), 26.0 (C12), 25.8 (C6), 18.5 (C11), 18.2 (C5), -5.2 (C10), -5.1 (C4) ppm.

HRMS (ESI^+) *m/z* calc. for $C_{27}H_{56}NO_3Si_3$ $[M+H]^+$ 526.3563; found 526.3567.

The spectral data are in agreement with the literature.[134]

(2-aminobenzene-1,3,5-triyl)trimethanol (169)

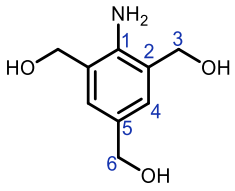

169

TBAF (1 M in THF; 18.1 mL) was added to a solution of **175** (2.30 g, 6.03 mmol) in anhydrous THF (20 mL) and stirred at rt for 3 h. After this time, TLC analysis (4% EtOAc/hexane) showed consumption of the starting material (R_F = 0.4) and the formation of a product (R_F = 0.0); analysis in 8% MeOH/DCM confirmed the formation of a product (R_F = 0.3). The reaction mixture was concentrated under reduced pressure and the crude product purified by

flash column chromatography (5% MeOH/EtOAc) to give **169** (550 mg, 3.0 mmol, 50%) as a clear oil.

^{1}H NMR (400 MHz, DMSO-d_6) δ_H 6.96 (s, 2H, H4), 5.01 (t, J_{OHH3} 5.3 Hz, 2H, H3-O<u>H</u>), 4.80 (t, J_{OHH6} 5.6 Hz, 1H, H6-O<u>H</u>), 4.72 (s, 2H, NH_2), 4.41 (d, J_{H3OH} 5.3 Hz, 4H, H3), 4.31 (d, J_{H6OH} 5.6 Hz, 2H, H6) ppm.

^{13}C NMR (100 MHz, DMSO-d_6) δ_C 143.5 (C1), 129.7 (C5), 126.4 (C4), 125.6 (C2), 63.7 (C6), 61.9 (C3) ppm.

HRMS (ESI$^+$) *m/z* calc. for $C_9H_{12}NO_3$ $[M+H]^+$ 182.0823; found 182.0818.

ν_{max}/cm^{-1} (neat) 3315 (OH), 2955 (aromatic stretch).

(3-nitrobenzyl (2,4,6-tris(hydroxymethyl)phenyl)carbamate)-2,3,4,6-tetra-*O*-acetyl-β-D-galactopyranoside (176)

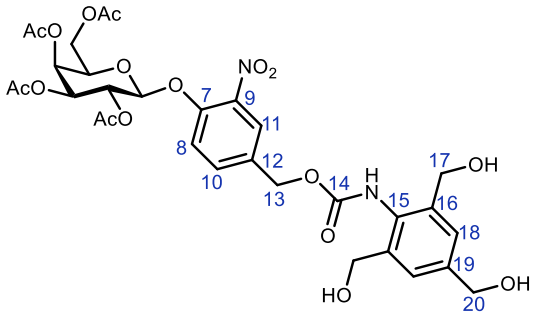

176

Aniline **169** (500 mg, 2.73 mmol) in dry DMF (1 mL) and HOBt (80 wt%; 507 mg, 3.0 mmol) were added to solution of carbonate **144** (1.81 g, 2.73 mmol) in anhydrous DMF (1 mL), then heated to 50 °C and stirred for 16 h under argon. After this time TLC analysis (50% EtOAc/hexane) showed consumption of the carbonate starting material (R_F = 0.3) and the formation of a product (R_F = 0.0); analysis in 4% MeOH/DCM confirmed the formation of a product (R_F = 0.4). The reaction mixture was concentrated under reduced pressure and the crude material purified by flash column chromatography (2 → 4% MeOH/DCM) to give **176** (659 mg, 0.93 mmol, 34%) as an off-white crystalline solid.

^{1}H NMR (400 MHz, methanol-d_4) δ_H 7.90 (s, 1H, H11), 7.69 (d, J_{H10H8} 8.7 Hz, 1H, H10), 7.48 (d, J_{H8H10} 8.7 Hz, 1H, H8), 7.44 (s, 2H, H18), 5.47 (dd, J_{H4H3} 3.5 Hz J_{H4H5} 1.1 Hz, 1H, H4), 5.35 – 5.42 (m, 2H, H1, H2), 5.26 (app. tt, J_{H3H2} 7.3 Hz J_{H3H4} 3.5 Hz, 1H, H3), 5.20 (s, 2H, H13), 4.63 (s, 2H, H20), 4.59 (s, 4H, H17), 4.36 (t, J_{H5H6} 6.5 Hz, 1H, H5), 4.22 (d, J_{H6H5} 6.5 Hz, 2H,

H6), 2.19 (s, 3H, OCOC<u>H</u>$_3$), 2.09 (s, 3H, OCOC<u>H</u>$_3$), 2.01 (s, 3H, OCOC<u>H</u>$_3$), 1.97 (s, 3H, OCOC<u>H</u>$_3$) ppm.

^{13}C NMR (100 MHz, methanol-d$_4$) δ_C 170.6 (O<u>C</u>OCH$_3$), 170.5 (O<u>C</u>OCH$_3$), 170.0 (O<u>C</u>OCH$_3$), 169.9 (O<u>C</u>OCH$_3$), 155.6 (C14), 148.7 (C7), 141.0 (C9), 140.5 (C19), 138.5 (C16), 132.8 (C10), 130.5 (C15), 125.0 (C18), 123.9 (C11), 118.4 (C8), 99.7 (C1), 71.2 (C5), 70.6 (C3), 68.2 (C2), 67.2 (C4), 64.9 (C13), 63.5 (C20), 61.2 (C6), 60.2 (C17), 19.5 (OCO<u>C</u>H$_3$), 19.3 (OCO<u>C</u>H$_3$), 19.2 (OCO<u>C</u>H$_3$), 19.1 (OCO<u>C</u>H$_3$) ppm.

HRMS (ESI$^-$) *m/z* calc. for $C_{31}H_{35}N_2O_{17}$ $[M\text{-}H]^+$ 707.1941; found 707.1941.

ν_{max}/cm^{-1} (neat) 3337 (OH), 1746 (CO), 1535 (NO).

mp 91 – 93 °C.

(3-nitrobenzyl (2,4,6-tris((((4-nitrophenoxy)carbonyl)oxy)methyl)phenyl)carbamate)-2,3,4,6-tetra-*O*-acetyl-β-D-galactopyranoside (177)

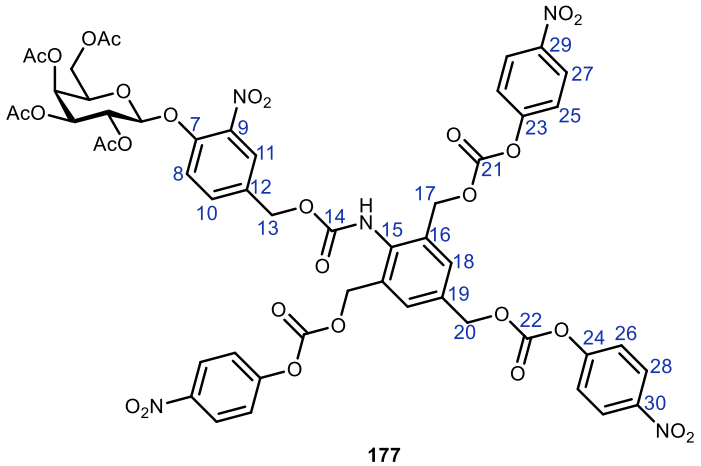

Pyridine (0.32 mL, 3.95 mmol) was added to a solution of **176** (350 mg, 0.49 mmol) and 4-nitrophenyl chloroformate (797 mg, 3.95 mmol) in anhydrous DCM (5 mL), then heated to reflux and stirred for 30 min under argon. After this time, TLC analysis (5% MeOH/DCM) showed consumption of the starting material (R_F = 0.3) and the formation of a product (R_F = 0.9); analysis in 50% EtOAc/hexane confirmed the formation of a product (R_F = 0.3). Water (50 mL) was then added to the reaction mixture and the organic product was extracted with DCM (3 x 50 mL). The combined organic extracts were dried ($MgSO_4$), filtered, concentrated and the crude product purified by flash column chromatography (40 → 60% EtOAc/hexane) to give **177** (330 mg, 0.27 mmol, 56%) as a clear oil.

^{1}H NMR (400 MHz, $CDCl_3$) δ_H 8.23 – 8.29 (m, 6H, H27, H28), 7.87 (s, 1H, H11), 7.67 (s, 2H, H18), 7.53 (d, J_{H10H8} 8.6 Hz, 1H, H10), 7.30 – 7.42 (m, 7H, H8, H25, H26), 5.53 (dd, J_{H2H3} 10.5 Hz J_{H2H1} 7.9 Hz, 1H, H2), 5.45 (dd, J_{H4H3} 3.4 Hz J_{H4H5} 1.2 Hz, 1H, H4), 5.34 (s, 2H, H20), 5.33 (s, 4H, H17), 5.19 (s, 2H, H13), 5.03 – 5.10 (m, 2H, H1, H3), 4.24 (dd, J_{H6aH6b} 11.3 Hz J_{H6H5} 6.8 Hz, 1H, H6a), 4.10 – 4.17 (m, 1H, H6b), 4.05 (t, J_{H5H6} 6.8 Hz, 1H, H5), 2.19 (s, 3H, OCOC$\underline{H}_3$), 2.11 (s, 3H, OCOC$\underline{H}_3$), 2.05 (s, 3H, OCOC$\underline{H}_3$), 2.01 (s, 3H, OCOC$\underline{H}_3$) ppm.

^{13}C NMR (100 MHz, $CDCl_3$) δ_C 170.3 (O$\underline{C}$OCH$_3$), 170.2 (O$\underline{C}$OCH$_3$), 170.1 (O$\underline{C}$OCH$_3$), 169.4 (O$\underline{C}$OCH$_3$), 155.3 (C30), 155.2 (C29), 154.2 (C14), 152.6 (C21), 152.4 (C22), 149.2 (C7), 145.63 (C23), 145.57 (C24), 141.4 (C12), 134.3 (C19), 133.3 (C10), 132.8 (C16), 132.0 (C15), 131.1 (C18), 125.4 (C27), 124.8 (C11), 121.78 (C25/C26), 122.7 (C25/C26), 120.0 (C8), 100.7 (C1), 71.4 (C5), 70.5 (C3), 69.5 (C20), 67.8 (C2), 67.0 (C17), 66.6 (C4), 65.9 (C13), 61.2 (C6), 20.7 (OCO$\underline{C}$H$_3$), 20.63 (2x OCO$\underline{C}$H$_3$), 20.56 (OCO$\underline{C}$H$_3$) ppm.

HRMS (ESI$^+$) *m/z* calc. for $C_{52}H_{45}N_5NaO_{29}$ $[M+Na]^+$ 1226.2092; found 1226.2086.

ν_{max}/cm^{-1} (neat) 1751 (CO), 1524 (NO).

(3-nitrobenzyl (2,6-bis((((3-methacrylamidopropyl)carbamoyl)oxy)methyl)-4-((((4-nitrophenoxy)carbonyl)oxy)methyl)phenyl)carbamate)-2,3,4,6-tetra-*O*-acetyl-β-D-galactopyranoside (178)

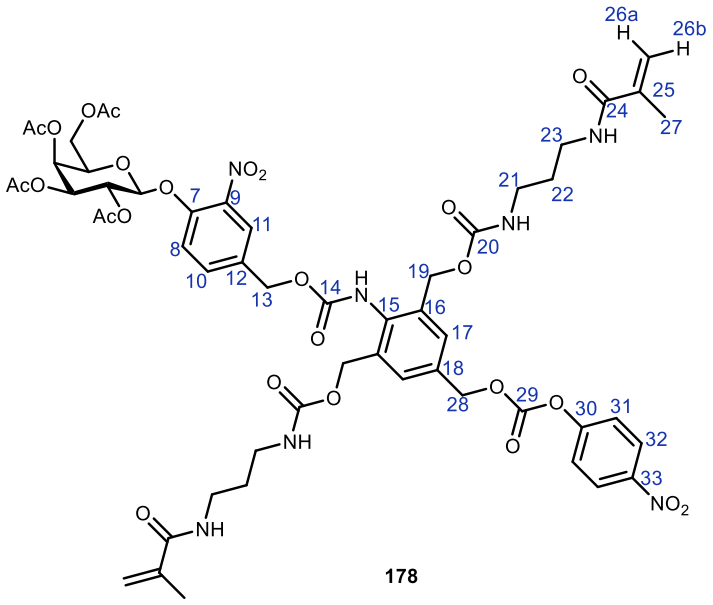

178

Amine **159** (295 mg, 1.65 mmol) and HOBt (153 mg, 0.91 mmol) were added to a solution of tricarbonate **177** (330 mg, 0.27 mmol) in anhydrous DMF (2 mL) and the reaction mixture was stirred for 16 hours at rt under argon. After this time, TLC analysis (50% EtOAc/hexane) showed complete consumption of the carbonate starting material (R_F = 0.3) and the formation of a product (R_F = 0.0); analysis in 5% MeOH/DCM confirmed the formation of a product (R_F = 0.4). The solution was concentrated under reduced pressure and the crude material was purified by flash column chromatography (2% MeOH → 15% MeOH/DCM) to give side-product **178** (85 mg, 0.07 mmol, 26%) as a clear oil.

^{1}H NMR (400 MHz, $CDCl_3$) δ_H 8.24 – 8.29 (m, 2H, H32), 7.88 (s, 1H, H11), 7.57 (d, J_{H10H8} 8.7 Hz, 1H, H10), 7.48 (s, 2H, H17), 7.32 – 7.41 (m, 3H, H8, H31), 6.38 (t, J_{NHH23} 6.3 Hz, 2H, NH), 5.70 (s, 2H, H26a), 5.54 (dd, J_{H2H3} 10.5 Hz J_{H2H1} 7.9 Hz, 1H, H2), 5.47 (dd, J_{H4H3} 3.4 J_{H4H5} 1.1 Hz, 1H, H4), 5.31 (s, 2H, H26b), 5.27 (s, 2H, H28), 5.18 (s, 2H, H13), 5.06 – 5.13 (m, 6H, H1, H3, H19), 4.25 (dd, J_{H6aH6b} 11.2 Hz J_{H6H5} 6.3 Hz, 1H, H6a), 4.17 (dd, J_{H6bH6a} 11.2 Hz J_{H6bH5} 6.3 Hz, 1H, H6b), 4.10 (t, J_{H5H6} 6.3 Hz, 1H, H5), 3.32 (app. q, J_{H23H22} 6.3 Hz, 4H, H23), 3.18 (app. q, *J* 6.2 Hz, 4H, H21), 2.18 (s, 3H, $OCOC\underline{H}_3$), 2.12 (s, 3H, $OCOC\underline{H}_3$), 2.07 (s, 3H, $OCOC\underline{H}_3$), 2.01 (s, 3H, $OCOC\underline{H}_3$), 1.94 (s, 6H, H27), 1.59 – 1.67 (m, 4H, H22) ppm.

^{13}C NMR (100 MHz, $CDCl_3$) δ_C 170.4 ($O\underline{C}OCH_3$), 170.19 ($O\underline{C}OCH_3$), 170.15 ($O\underline{C}OCH_3$), 169.4 ($O\underline{C}OCH_3$), 169.0 (C24), 156.9 (C20), 155.5 (C33), 154.3 (C14), 152.4 (C29), 149.1 (C7), 145.5 (C30), 141.2 (C12), 139.7 (C25), 134.1 (C16), 134.0 (C18), 133.3 (C10), 130.3 (C17), 125.3 (C32), 124.7 (C11), 121.9 (C31), 119.9 (C8), 119.8 (C15), 100.7 (C1), 71.4 (C5),

70.6 (C3), 70.0 (C28), 67.9 (C2), 66.7 (C4), 65.4 (C13), 63.2 (C19), 61.3 (C6), 37.6 (C21), 36.0 (C23), 29.9 (C22), 20.67 (2x OCO<u>C</u>H$_3$), 20.65 (OCO<u>C</u>H$_3$), 20.6 (OCO<u>C</u>H$_3$), 18.6 (C27) ppm.

HRMS (ESI$^+$) *m/z* calc. for $C_{54}H_{63}N_7NaO_{25}$ $[M+Na]^+$ 1232.3766; found 1232.3769.

ν_{max}/cm^{-1} (neat) 1753 (CO), 1527 (NO).

(3-nitrobenzyl (2,4,6-tris((((3-methacrylamidopropyl)carbamoyl)oxy)methyl) phenyl)carbamate)-2,3,4,6-tetra-*O*-acetyl-β-D-galactopyranoside (179)

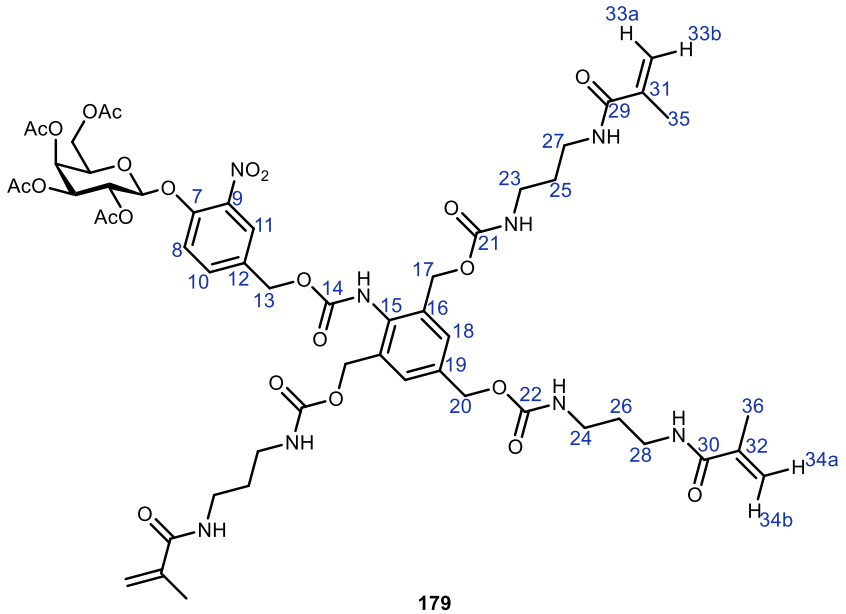

179

Amine **159** (295 mg, 1.65 mmol) and HOBt (153 mg, 0.91 mmol) were added to a solution of tricarbonate **178** (330 mg, 0.27 mmol) in anhydrous DMF (2 mL) and the reaction mixture was stirred for 16 hours at rt under argon. After this time, TLC analysis (50% EtOAc/hexane) showed complete consumption of the carbonate starting material (R_F = 0.3) and the formation of a product (R_F = 0.0); analysis in 5% MeOH/DCM confirmed the formation of a product (R_F = 0.3). The solution was concentrated under reduced pressure and the crude product was purified by flash column chromatography (2% MeOH → 15% MeOH/DCM) to give **179** (86 mg, 0.07 mmol, 26%) as an off-white crystalline solid.

^{1}H NMR (400 MHz, $CDCl_3$) δ_H 8.44 (s, 1H, NH), 7.86 (s, 1H, H11), 7.56 (d, J_{H10H8} 8.5 Hz, 1H, H10), 7.31 – 7.40 (m, 3H, H18, H8), 6.60 (s, 2H, NH), 5.66 – 5.80 (m, 5H, 33a, 34a, NH), 5.53 (dd, J_{H2H3} 10.5 J_{H2H1} 7.9 Hz, 1H, H2), 5.47 (app. d, J_{H4H3} 3.4 Hz, 1H, H4), 5.33 (s, 1H, H34b), 5.30 (s, 2H, H33b), 5.16 (s, 2H, H13), 5.08 – 5.13 (m, 2H, H1, H3), 5.05 (s, 6H, H17, H20),

4.21 – 4.27 (m, 1H, H6a), 4.17 (dd, J_{H6bH6a} 11.2 J_{H6bH5} 6.8 Hz, 1H, H6b), 4.11 (app. t, *J* 6.8 Hz, 1H, H5), 3.11 – 3.33 (m, 12H, H25, H27, H24, H28), 2.18 (s, 3H, OCOC$\underline{H}_3$), 2.12 (s, 3H, OCOC$\underline{H}_3$), 2.06 (s, 3H, OCOC$\underline{H}_3$), 2.01 (s, 3H, OCOC$\underline{H}_3$), 1.96 (s, 3H, H36), 1.93 (s, 6H, H35) ppm.

^{13}C NMR (100 MHz, $CDCl_3$) δ_C 170.4 (O$\underline{C}$OCH$_3$), 170.2 (O$\underline{C}$OCH$_3$), 170.1 (O$\underline{C}$OCH$_3$), 169.4 (O$\underline{C}$OCH$_3$), 169.0 (C29, C30), 157.2 (C21, C22), 154.4 (C14), 149.1 (C7), 139.8 (C31/C32), 139.7 (C31/C32), 133.8 (C16, C19), 133.3 (C10), 129.7 (C18), 124.7 (C11), 119.9 (C8), 119.9 (C13), 100.7 (C1), 71.4 (C5), 70.6 (C3), 67.9 (C2), 66.8 (C4), 65.7 (C20), 65.3 (C13), 63.2 (C17), 61.3 (C6), 37.6 (C23, C24), 35.9 (C27, C28), 29.8 (C25, C26), 20.69 (OCO$\underline{C}$H$_3$), 20.67 (OCO$\underline{C}$H$_3$), 20.65 (OCO$\underline{C}$H$_3$), 20.6 (OCO$\underline{C}$H$_3$), 18.63 (C36), 18.59 (C35) ppm.

HRMS (ESI$^+$) *m/z* calc. for $C_{55}H_{72}N_8NaO_{23}$[M+Na]$^+$ 1235.4603; found 1235.4627.

ν_{max}/cm^{-1} (neat) 1755 (CO), 1529 (NO).

mp 78 – 80 °C from MeOH/DCM.

(3-nitrobenzyl (2,4,6-tris((((3-methacrylamidopropyl)carbamoyl)oxy)methyl)phenyl)carbamate)-β-D-galactopyranoside (180)

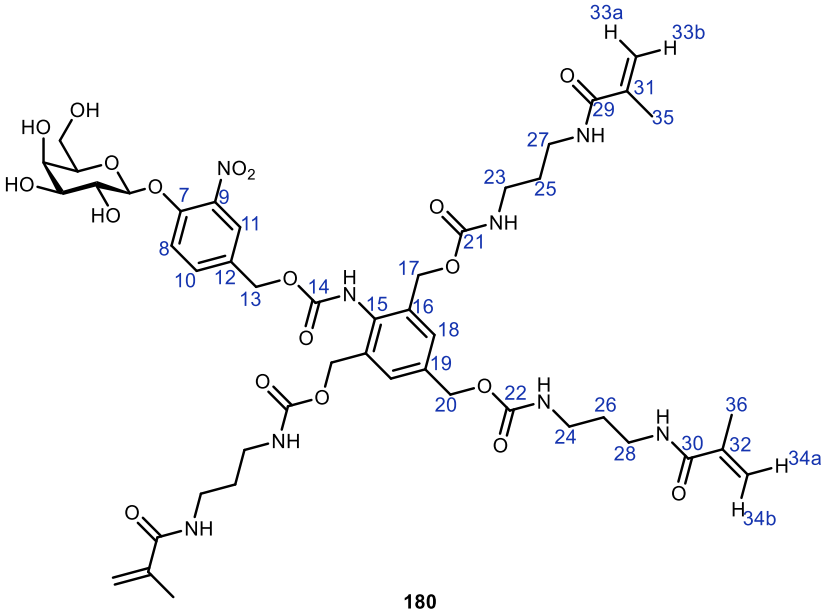

180

NaOH (1 M, 0.03 mL, 0.03 mmol) was added to a solution of **179** (75 mg, 0.06 mmol) in MeOH (2 mL) and stirred for 30 min at rt. After this time, TLC analysis (5% MeOH/DCM) showed complete consumption of the starting material (R_F = 0.3) and the formation of a product (R_F = 0.0). The reaction mixture was then neutralised with Amberlite IRC-120 H^+ resin, filtered and concentrated under reduced pressure to give **180** (51 mg, 0.049 mmol, 79%) as a pale red solid.

$\boldsymbol{R_F}$ = 0.1 (10% MeOH/DCM).

^{1}H NMR (400 MHz, methanol-d_4) δ_H 7.87 – 7.99 (m, 2H, H11, NH), 7.66 (d, J_{H10H8} 8.7 Hz, 1H, H8), 7.49 (d, J_{H8H10} 8.7 Hz, 1H, H8), 7.43 (s, 2H, H18), 5.69 (s, 3H, H33a, H34a), 5.32 – 5.37 (m, 3H, H33b, H34b), 5.19 (s, 2H, H13), 5.04 – 5.13 (m, 6H, H1, H17, H20, NH), 3.91 (app. d, J_{H4H3} 3.3 Hz, 1H, H4), 3.85 – 3.88 (m, 1H, H2), 3.71 – 3.80 (m, 3H, H3, H6), 3.56 – 3.62 (m, 1H, H5), 3.21 – 3.29 (m, 6H, H27, H28), 3.09 – 3.18 (m, 6H, H23, H24), 1.93 (s, 9H, H35, H36), 1.64 – 1.74 (m, 6H, H25, H26) ppm.

^{13}C NMR (100 MHz, methanol-d_4) δ_C 171.4 (C29, C30), 158.7 (C21, C22), 154.1 (C14), 151.2 (C7), 141.4 (C31/C32), 141.3 (C31/C32), 137.8 (C16), 136.5 (C19),134.4 (C10), 129.0 (C18), 127.1 (C15), 125.5 (C11), 124.1 (C12), 120.5 (C33, C34), 119.0 (C8), 103.1 (C1), 77.4 (C3), 74.9 (C5), 72.0 (C2), 10.2 (C4), 66.8 (C20), 63.8 (C17), 62.4 (C6), 39.2 (C23, C24), 37.9 (C27/C28), 37.8 (C27/C28), 18.8 (C35, C36) ppm.

HRMS (ESI$^+$) *m/z* calc. for $C_{47}H_{64}N_8NaO_{19}$ $[M+Na]^+$ 1067.4180; found 1067.4187.

ν_{max}/cm^{-1} (neat) 3314 (OH), 1698 (CO), 1528 (NO).

mp 61 – 64 °C.

7.4 Synthetic Methods for Chapter 4

Fmoc-Thr-OH (189)

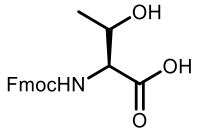

189

A solution of Fmoc-Thr(^{t}Bu)-OH (1.50 g, 3.78 mmol) in TFA:TES:DCM(2:1:8, v/v, 10 mL) was stirred at rt for 2 h. After this time, TLC analysis (30% EtOAc/hexane) showed consumption of the starting material (R_F = 0.3) and the formation of a new product spot (R_F = 0.0); analysis in 10% MeOH/DCM confirmed the consumption of the starting material (R_F = 1.0) and the formation of a product (R_F = 0.3). The reaction mixture was concentrated under reduced pressure and coevaporated with MeOH (3 x 10 mL) to give Fmoc-Thr-OH **189** (1.28 g, 3.78 mmol, quant.) as white powder.

^{1}H NMR (400 MHz, DMSO-d_6) δ_H 7.89 (d, *J* 7.5 Hz, 2H, ArH), 7.74 (d, *J* 7.5 Hz, 2H, ArH), 7.42 (t, *J* 7.5 Hz, 2H, ArH), 7.33 (t, *J* 7.5 Hz, 2H, ArH), 7.07 (d, $J_{NHC\alpha H}$ 9.0 Hz, 1H, NH), 4.27 – 4.33 (m, 2H, Fmoc-CH_2), 4.19 – 4.26 (m, 1H, Fmoc-CH), 4.10 (qd, $J_{\beta CH\gamma CH3}$ 6.4 Hz $J_{\beta CH\alpha CH}$ 3.5 Hz, 1H, βCH), 3.96 (dd, $J_{\alpha CHNH}$ 9.0 Hz $J_{\alpha CH\beta CH}$ 3.5 Hz, 1H, αCH), 1.10 (d, $J_{\gamma CH3\beta CH}$ 6.4 Hz, 3H, γ-CH_3) ppm.

^{13}C NMR (100 MHz, $CDCl_3$) δ_C 172.8 (COOH), 156.9 (NHCO), 144.3 (Fmoc qC), 144.2 (Fmoc qC), 141.2 (2x Fmoc qC), 128.2 (Fmoc Ar CH), 127.6 (Fmoc Ar CH), 125.8 (Fmoc Ar CH), 125.7 (Fmoc Ar CH), 120.57 (Fmoc Ar CH), 66.9 (βCH), 66.3 (Fmoc-CH_2), 57.6 (α-CH), 47.1 (Fmoc-CH), 20.8 (γ-CH_3) ppm.

HRMS (ESI$^+$) *m/z* calc. for $C_{19}H_{18}NO_5$ $[M+H]^+$ 340.1190; found 340.1197.

mp 114-115 °C (lit.[356] 98 – 105 °C) from MeOH.

The spectral data are in agreement with the literature.[356]

((9H-fluoren-9-yl)methyl ((2R,3S)-3-hydroxy-1-oxobutan-2-yl)carbamate)-2,3,4,6-tetra-*O*-acetyl-β-D-galactopyranoside (190)

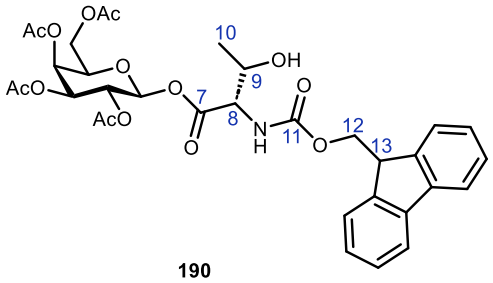

190

Fmoc-Thr-OH (4.37 g, 12.8 mmol) and silver carbonate (4.71 g, 17.08 mmol) were added to a mixture of galactosyl bromide **104** (3.50 g, 8.54 mmol) in anhydrous DCM (10 mL) over molecular sieves. The mixture was stirred at room temperature for 16 h under argon in the dark. After this time, TLC analysis (30% EtOAc/hexane) showed consumption of the starting material (R_F = 0.4) and formation of the product (R_F = 0.2), and the reaction mixture was filtered and concentrated under reduced pressure. The crude residue was then purified by flash column chromatography (30% → 50% EtOAc/hexane) to give **190** (1.89 g, 2.81 mmol, 33%) as a white solid.

^{1}H NMR (400 MHz,$CDCl_3$) δ_H 7.77 (d, *J* 7.5 Hz, 2H, ArH), 7.63 (t, *J* 7.2 Hz, 2H, ArH), 7.40 (t, *J* 7.4 Hz, 2H, ArH), 7.32 (m, 2H, ArH), 5.74 (d, J_{H1H2} 8.2 Hz, 1H, H1), 5.66 (d, J_{NHH8} 9.3 Hz, 1H, NH), 5.43 (d, J_{H4H3} 3.4 Hz, 1H, H4), 5.36 (dd, J_{H2H3} 10.4 J_{H2H1} 8.2 Hz, 1H, H2), 5.10 (dd, J_{H3H2} 10.4 J_{H3H4} 3.4 Hz, 1H, H3), 4.31 – 4.48 (m, 4H, H8, H9, H12), 4.26 (t, J_{H13H12} 7.2 Hz, 1H, H13), 4.18 (dq, J_{H6aH6b} 11.0 J_{H6H5} 5.4 Hz, 1H, H6a), 4.00 – 4.10 (m, 2H, H5, H6), 2.15 (s, 3H, OCOC$\underline{H}_3$), 2.05 (s, 3H, OCOC$\underline{H}_3$), 2.02 (s, 3H, OCOC$\underline{H}_3$), 2.00 (s, 3H, OCOC$\underline{H}_3$), 1.27 (d, $_JH10H9$ 6.4 Hz, 3H, H10) ppm.

^{13}C NMR (100 MHz, $CDCl_3$) δ_C 170.6 (O$\underline{C}$OCH$_3$), 170.1 (O$\underline{C}$OCH$_3$), 170.0 (O$\underline{C}$OCH$_3$), 169.9 (O$\underline{C}$OCH$_3$), 169.6 (O$\underline{C}$O-C8), 156.7 (NH$\underline{C}$OO), 143.9 (Fmoc qC), 143.7 (Fmoc qC), 141.3 (2x Fmoc qC), 127.8 (Fmoc ArC), 127.13 (Fmoc ArC), 127.09 (Fmoc ArC), 125.21 (Fmoc ArC), 125.17 (Fmoc ArC), 120.0 (Fmoc Ar $\underline{C}$H), 93.1 (C1), 72.2 (C5), 70.6 (C3), 67.7 (C9), 67.5 (C2), 67.4 (C12), 66.8 (C4), 61.0 (C6), 59.3 (C8), 47.1 (C13), 20.73 (OCO$\underline{C}$H$_3$), 20.66 (OCO$\underline{C}$H$_3$), 20.6 (OCO$\underline{C}$H$_3$), 20.5 (OCO$\underline{C}$H$_3$), 20.0 (C10) ppm.

HRMS (ESI$^+$) *m/z* calc. for $C_{33}H_{37}NNaO_{11}$ $[M+Na]^+$ 694.2106; found 694.2089.

ν_{max}/cm^{-1} (neat) 3406 (COOH), 2981 (Ar CH), 1746 (CO).

mp 101-103 °C.

Fmoc-Thr(ᵗBu)-O(Allyl) (191)

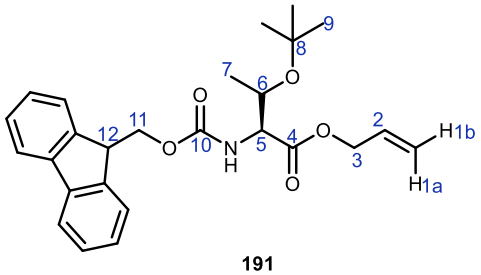

191

Allyl bromide (0.98 mL, 11.3 mmol) was added dropwise to a solution of Fmoc-Thr(ᵗBu)-OH (3.00 g, 7.55 mmol) and DIPEA (1.97 mL, 11.3 mmol) in anhydrous MeCN (10 mL) and stirred at rt for 16 h under argon. After this time, TLC analysis (10% EtOAc/hexane) showed consumption of the starting material (R_F = 0.0) and the formation of a product (R_F = 0.3). The reaction mixture was then concentrated under reduced pressure and filtered through a silica plug (10% EtOAc/hexane) to give **191** (3.09 g, 7.07 mmol, 94%) as a clear oil.

^{1}H NMR (400 MHz, $CDCl_3$) δ_H 7.79 (dq, *J* 7.6 1.0 Hz, 2H, ArH), 7.66 (tq, *J* 7.6 1.0 Hz, 2H, ArH), 7.43 (tt, *J* 7.5 1.3 Hz, 2H, ArH), 7.35 (tt, *J* 7.5 1.3 Hz, 2H, ArH), 5.95 (ddt, *J* 17.2 10.4 5.8 Hz, 1H, H2), 5.64 (d, *J* 9.6 Hz, 1H, NH), 5.38 (app. dq, *J* 17.2 1.5 Hz, 1H, H1a), 5.29 (app. dp, *J* 10.3 1.3 Hz, 1H, H1b), 4.71 (ddt, *J* 13.1 5.8 1.5 Hz, 1H, H3a), 4.58 (ddt, *J* 13.1 5.8 1.5 Hz, 1H, H3b), 4.35 – 4.48 (m, 2H, H11), 4.24 – 4.33 (m, 3H, H5, H6, H12), 1.27 (d, *J* 6.2 Hz, 3H, H7), 1.17 (s, 9H, H9) ppm.

^{13}C NMR (100 MHz, $CDCl_3$) δ_C 170.9 (C4), 156.8 (C10), 144.1 (Fmoc qC), 143.9 (Fmoc qC), 141.3 (2x Fmoc qC), 131.6 (C2), 127.7 (Fmoc ArC), 127.10 (Fmoc ArC), 127.08 (Fmoc ArC), 125.3 (Fmoc ArC), 125.2 (Fmoc ArC), 120.0 (Fmoc ArC), 119.9 (C1), 74.1 (C8), 67.4 (C6), 67.3 (C11), 66.0 (C3), 60.0 (C5), 47.2 (C12), 28.4 (C9), 21.0 (C7) ppm.

HRMS (ESI^+) *m/z* calc. for $C_{26}H_{31}NNaO_5$ $[M+Na]^+$ 460.2094; found 460.2097.

The spectral data are in agreement with the literature.[357]

Fmoc-Thr-O(Allyl) (192)

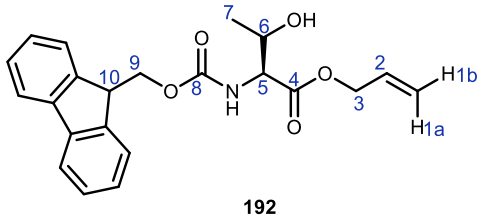

192

A solution of **191** (3.10 g, 7.09 mmol) in TFA:TES:DCM(2:1:8, v/v, 20 mL) at rt for 2 h. After this time, TLC analysis (10% EtOAc/hexane) showed consumption of the starting material (R_F = 0.3) and the formation of a new product spot (R_F = 0.0); analysis in 40% EtOAc/hexane confirmed consumption of the starting material (R_F = 0.9) and the formation of a product (R_F = 0.3). The solvent was removed under reduced pressure, coevaporated with MeOH (3 x 20 mL) and filtered through a silica plug (40% EtOAc/hexane) to give **192** (2.67 g, 3.78 mmol, 99%) as a clear oil.

^{1}H NMR (400 MHz, DMSO-d_6) δ_H 7.90 (d, *J* 7.5 Hz, 2H, ArH), 7.75 (ddd, *J* 7.5 2.1 1.0 Hz, 2H, ArH), 7.42 (t, *J* 7.5 Hz, 2H, ArH), 7.39 – 7.45 (m, 2H, ArH), 5.90 (ddt, *J* 17.4 10.5 5.2 Hz, 1H, H2), 5.34 (app. dq, *J* 17.4 1.7 Hz, 1H, H1a), 5.20 (app. dq, *J* 10.5 1.5 Hz, 1H, H1b), 4.83 (d, *J* 6.9 Hz, 1H, OH), 4.58 – 4.61 (m, 2H, H3), 4.29 – 4.33 (m, 2H, H9), 4.24 (t, *J* 7.0 Hz, 1H, H10), 4.07 – 4.14 (m, 2H, H5, H6), 1.11 (d, *J* 6.0 Hz, H7).

^{13}C NMR (100 MHz, DMSO-d_6) δ_C 170.5 (C4), 156.4 (C8), 143.8 (Fmoc qC), 143.7 (Fmoc qC), 140.7 (Fmoc qC), 132.4 (C2), 127.6 (Fmoc ArC), 127.0 (Fmoc ArC), 125.3 (Fmoc ArC), 120.1 (Fmoc ArC), 117.5 (C1), 66.4 (C6), 65.8 (C9), 64.8 (O$\underline{C}H_2$CH), 60.2 (C5), 46.6 (C10), 20.1 (C7).

HRMS (ESI$^+$) *m/z* calc. for $C_{22}H_{24}NO_5$ $[M+H]^+$ 382.1649; found 382.1649.

The spectral data are in agreement with the literature.[357]

2,3,4,6-tetra-*O*-acetyl-α/β-D-galactopyranose (194)

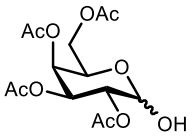

194

Benzylamine (0.21 mL, 1.92 mmol) was added to a solution of acetylated galactose **103** (500 mg, 1.28 mmol) in anhydrous THF (10 mL) and the reaction mixture was stirred for 16 h at rt under argon. After this time, TLC analysis (50% EtOAc/hexane) showed consumption of the starting material (R_F = 0.6) and the formation of a product (R_F = 0.3). The reaction mixture was concentrated under reduced pressure and the crude material purified by flash column chromatography (30 → 50% EtOAc/hexane) to give **194** (337 mg, 0.97 mmol, 55%, 2:1 ratio α:β anomers) as a brown oil.

^{1}H NMR (400 MHz, $CDCl_3$) δ_H 5.53 (d, $J_{\alpha\text{-}H1H2}$ 3.6 Hz, 1H, α-H1), 5.48 (dd, $J_{\alpha\text{-}H4H3}$ 3.4 $J_{\alpha\text{-}H4H5}$ 1.4 Hz, 1H, α-H4), 5.42 – 5.44 (m, 1H, β-H3), 5.39 – 5.41 (m, 1H, α-H3), 5.17 (dd, $J_{\alpha\text{-}H2H3}$ 10.8 Hz $J_{\alpha\text{-}H2H1}$ 3.6 Hz, 1H, α-H2), 5.06 – 5.09 (m, 2H, β-H2, β-H4), 4.70 – 4.73 (m, 1H, β-H1), 4.47 (td, $J_{\alpha\text{-}H5H6}$ 6.6 Hz $J_{\alpha\text{-}H5H4}$ 1.4 Hz, 1H, α-H5), 4.05 – 4.16 (m, 4H, α-H6, β-H6), 3.95 (td, $J_{\beta\text{-}H5H6}$ 6.6 $J_{\beta\text{-}H5H4}$ 1.2 Hz, 1H, β-H5), 2.16 (s, 3H, OCOC$\underline{H}_3$), 2.15 (s, 3H, OCOC$\underline{H}_3$), 2.11 (s, 3H, OCOC$\underline{H}_3$), 2.10 (s, 3H, OCOC$\underline{H}_3$), 2.07 (s, 3H, OCOC$\underline{H}_3$), 2.05 (s, 3H, OCOC$\underline{H}_3$), 2.01 (s, 3H, OCOC$\underline{H}_3$), 2.00 (s, 3H, OCOC$\underline{H}_3$) ppm.

^{13}C NMR (100 MHz, $CDCl_3$) δ_C 171.4 (O$\underline{C}$OCH$_3$),170.52 (O$\underline{C}$OCH$_3$), 170.48 (O$\underline{C}$OCH$_3$), 170.4 (O$\underline{C}$OCH$_3$), 170.24 (O$\underline{C}$OCH$_3$),170.16 (O$\underline{C}$OCH$_3$), 170.1 (O$\underline{C}$OCH$_3$), 170.0 (O$\underline{C}$OCH$_3$), 96.1 (β-C1), 90.7 (α-C1), 71.13 (β-C5), 71.06 (β-C4), 70.3 (β-C2), 68.3 (α-C2), 68.2 (α-C4), 67.2 (β-C3), 67.1 (α-C3), 66.3 (α-C5), 61.8 (α-C6), 61.5 (β-C6), 20.8 (OCO$\underline{C}$H$_3$), 20.74 (OCO$\underline{C}$H$_3$), 20.72 (OCO$\underline{C}$H$_3$), 20.67 (OCO$\underline{C}$H$_3$), 20.65 (OCO$\underline{C}$H$_3$), 20.63 (OCO$\underline{C}$H$_3$), 20.57 (OCO$\underline{C}$H$_3$), 20.4 (OCO$\underline{C}$H$_3$) ppm.

HRMS (ESI$^+$) *m/z* calc. for $C_{14}H_{20}NaO_{10}$ $[M+K]^+$ 371.0949; found 371.0951.

The spectral data are in agreement with the literature.[358]

1-*O*-(2,3,4,6-tetra-O-acetyl-α-D-galactopyranosyl)trichloroacetimidate (195α)

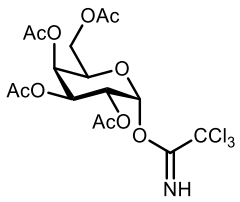

195

CCl_3CN (11.52 mL, 114.9 mmol) and Cs_2CO_3 (936 mg, 2.87 mmol) were added to a solution of **194** (4.00 g, 11.49 mmol) in anhydrous DCM (30 mL) and stirred for 3 h at rt under argon. After this time, TLC analysis (30% EtOAc/hexane) showed partial consumption of the starting material (R_F = 0.1) and the formation of two new products (R_F = 0.5). The reaction mixture was concentrated under reduced pressure and the crude product purified by flash column chromatography (20% → 30% EtOAc/hexane) to give **195** (5.03 g, 10.25 mmol, 89%) as an off-white crystalline solid.

^{1}H NMR (400 MHz, $CDCl_3$) δ_H 8.66 (s, 1H, NH), 6.60 (d, J_{H1H2} 3.5 Hz, 1H, H1), 5.56 (dd, J_{H4H3} 3.1 Hz J_{H4H5} 1.3 Hz, 1H, H4), 5.43 (dd, J_{H3H2} 10.9 J_{H3H4} 3.1 Hz, 1H, H3), 5.36 (dd, J_{H3H2} 10.9 J_{H2H1} 3.5 Hz, 1H, H2), 4.44 (dt, J_{H5H6} 6.6 J_{H5H4} 1.3 Hz, 1H, H5), 4.17 (dd, J_{H6aH6b} 11.3 J_{H6aH5} 6.6 Hz, 1H, H6a), 4.08 (dd, J_{H6bH6a} 11.3 J_{H6bH5} 6.6 Hz, 1H, H6b), 2.17 (s, 3H, OCOC$\underline{H}_3$), 2.03 (s, 3H, OCOC$\underline{H}_3$), 2.02 (s, 3H, OCOC$\underline{H}_3$), 2.01 (s, 3H, OCOC$\underline{H}_3$) ppm.

^{13}C NMR (100 MHz, $CDCl_3$) δ_C 170.3 (O$\underline{C}$OCH$_3$),170.12 (O$\underline{C}$OCH$_3$), 170.09 (O$\underline{C}$OCH$_3$), 170.0 (O$\underline{C}$OCH$_3$), 161.0 (O$\underline{C}$NH), 93.6 (C1), 90.8 ($\underline{C}Cl_3$), 69.0 (C5), 67.5 (C4), 67.4 (C3), 66.9 (C2), 61.3 (C6), 20.7 (OCO$\underline{C}$H$_3$), 20.64 (OCO$\underline{C}$H$_3$), 20.62 (OCO$\underline{C}$H$_3$), 20.55 (OCO$\underline{C}$H$_3$) ppm.

HRMS (ESI$^+$) *m/z* calc. for $C_{16}H_{20}Cl_3KNO_{10}$ $[M+K]^+$ 529.9784; found 529.9788.

mp 121-122 °C (lit.[359] 122 – 123 °C) from EtOAc/hexane.

The spectral data are in agreement with the literature.[360]

1-*O*-(2,3,4,6-tetra-O-acetyl-α-D-galactopyranosyl)trichloroacetimidate (195β)

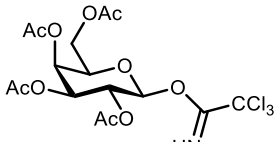

195

CCl_3CN (11.52 mL, 114.9 mmol) and Cs_2CO_3 (936 mg, 2.87 mmol) were added to a solution of **194** (4.00 g, 11.49 mmol) in anhydrous DCM (30 mL) and stirred for 3 h at rt under argon. After this time, TLC analysis (30% EtOAc/hexane) showed partial consumption of the starting material (R_F = 0.1) and the formation of two new products (R_F = 0.3). The reaction mixture was concentrated under reduced pressure and the crude product purified by flash column chromatography (20% → 30% EtOAc/hexane) to give **195** (621 mg, 1.26 mmol, 11%) as an off-white foam.

^{1}H NMR (400 MHz, $CDCl_3$) δ_H 8.71 (s, 1H, NH), 5.84 (d, J_{H1H2} 8.2 Hz, 1H, H1), 5.48 – 5.51 (m, 1H, H2), 5.44 – 5.47 (m, 1H, H4), 5.12 (dd, J_{H3H2} 10.4 J_{H3H4} 3.5 Hz, 1H, H3), 4.17 – 4.21 (m, 2H, H6), 4.08 – 4.13 (m, 1H, H5), 2.18 (s, 3H, OCOC$\underline{H}_3$), 2.04 (s, 3H, OCOC$\underline{H}_3$), 2.02 (s, 3H, OCOC$\underline{H}_3$), 2.01 (s, 3H, OCOC$\underline{H}_3$) ppm.

^{13}C NMR (100 MHz, $CDCl_3$) δ_C 170.3 (O$\underline{C}$OCH$_3$), 170.2 (O$\underline{C}$OCH$_3$), 170.1 (O$\underline{C}$OCH$_3$), 169.1 (O$\underline{C}$OCH$_3$), 161.1 (O$\underline{C}$NH), 96.1 (C1), 90.4 ($\underline{C}Cl_3$), 71.8 (C5), 70.7 (C3), 67.7 (C2), 66.7 (C4), 60.9 (C6), 20.7 (3x OCO$\underline{C}$H$_3$), 20.6 (OCO$\underline{C}$H$_3$) ppm.

HRMS (ESI$^+$) *m/z* calc. for $C_{16}H_{20}Cl_3NNaO_{10}$ $[M+Na]^+$ 514.0045; found 514.0048.

The spectral data are consistent with the literature.[361]

(allyl(((9H-fluoren-9-yl)methoxy)carbonyl)-L-threoninate)-2,3,4,6-tetra-*O*-acetyl-β-D-galactopyranoside (193)

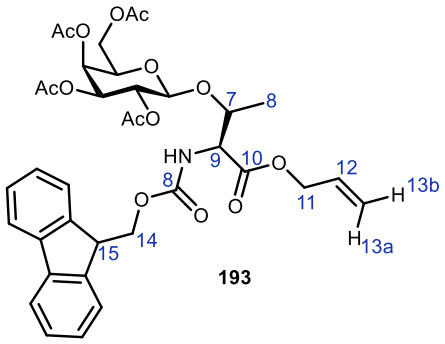

193

$BF_3{\cdot}Et_2O$ (0.41 mL, 3.40 mmol) was added dropwise to a solution of trichloroacetimidate **195** (1.50 g, 3.10 mmol) and **192** (1.74 g, 4.58 mmol) in anhydrous DCM (10 mL) at 0 °C, allowed to warm to rt and stirred for 16 h under argon. After this time, TLC analysis (30% EtOAc/hexane) showed consumption of the starting material (R_F = 0.5) and formation of a product (R_F = 0.2), and the reaction was quenched with Et_3N (0.47 mL, 3.40 mmol) and concentrated under reduced pressure. The crude material was then purified by flash column chromatography (30% → 50% EtOAc/hexane) to give **193** (1.10 g, 1.55 mmol, 51%) as an off-white crystalline solid.

^{1}H NMR (400 MHz, $CDCl_3$) δ_H 7.78 (d, *J* 7.5 Hz, 2H, ArH), 7.67 (t, *J* 8.2 Hz, 2H, ArH), 7.42 (tt, *J* 7.6 1.3 Hz, 2H, ArH), 7.34 (td, *J* 7.5 1.3 Hz, 2H, ArH), 5.87 – 6.00 (m, 1H, H12), 5.63 (d, *J* 9.3 Hz, 1H, NH), 5.33 – 5.42 (m, 2H, H4, H13a), 5.27 (app. dq, *J* 10.5 1.4 Hz, 1H, H13b), 5.15 (d, *J* 10.5 7.8 Hz, 1H, H2), 5.03 (dd, *J* 10.5 3.5 Hz, 1H, H3), 4.63 – 4.74 (m, 2H, H11), 4.35 – 4.51 (m, 5H, H14, H9, H7, H1), 4.28 (t, *J* 7.4 Hz, 1H, H15), 4.08 – 4.14 (m, 2H, H6), 3.88 (dt, *J* 6.8 1.3 Hz, 1H, H5), 2.17 (s, 3H, OCOC$\underline{H}_3$), 2.07 (s, 3H, OCOC$\underline{H}_3$), 2.06 (s, 3H, OCOC$\underline{H}_3$), 2.01 (s, 3H, OCOC$\underline{H}_3$) ppm.

^{13}C NMR (100 MHz, $CDCl_3$) δ_C 170.4 (O$\underline{C}$OCH$_3$), 170.2 (O$\underline{C}$OCH$_3$), 170.1 (O$\underline{C}$OCH$_3$), 169.7 (O$\underline{C}$OCH$_3$), 169.4 (O$\underline{C}$OCH$_3$), 161.1 (C10), 156.8 (C8), 144.0 (Fmoc qC), 143.7 (Fmoc qC), 141.3 (Fmoc qC), 131.7 (Fmoc qC), 127.7 (Fmoc ArC), 127.12 (Fmoc ArC), 127.09 (Fmoc ArC), 125.3 (Fmoc ArC), 125.2 (Fmoc ArC), 120.0 (Fmoc ArC), 118.6 (C13), 99.5 (C1), 75.0 (C7), 70.7 (C3), 70.6 (C5), 68.8 (C2), 67.3 (C14), 66.8 (C4), 66.2 (C11), 60.9 (C6), 58.6 (C9), 47.2 (C15), 21.1 (OCO$\underline{C}$H$_3$), 20.8 (OCO$\underline{C}$H$_3$), 20.7 (OCO$\underline{C}$H$_3$), 20.6 (OCO$\underline{C}$H$_3$) ppm.

HRMS (ESI$^+$) *m/z* calc. for $C_{36}H_{41}KNO_{14}$ $[M+K]^+$ 750.2159; found 750.2158.

ν_{max}/cm^{-1} (neat) 2981 (ArC), 1745 (CO).

mp 62-64 °C from EtOAc/hexane.

((((9H-fluoren-9-yl)methoxy)carbonyl)-L-threonine

)-2,3,4,6-tetra-*O*-acetyl-β-D-galactopyranoside (185)

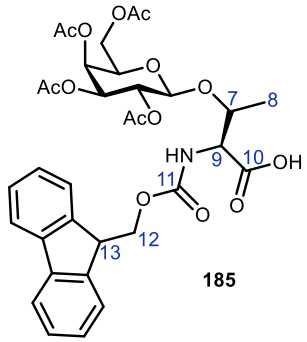

185

Phenylsilane (0.67 mL, 5.44 mmol) and $Pd(PPh_3)_4$ (5.00 g, 0.004 mmol) were added to a solution of **193** (968 mg, 1.36 mmol) in anhydrous DCM (10 mL) and stirred for 30 min at rt under argon. After this time, TLC analysis (40% EtOAc/hexane) showed complete consumption of the starting material (R_F = 0.3) and the formation of a product (R_F = 0.0); analysis in 5% MeOH/DCM confirmed consumption of the starting material (R_F = 1.0) and formation of a product (R_F = 0.3). The reaction mixture was concentrated under reduced pressure and the crude material purified by flash column chromatography (5% MeOH/DCM) to give **185** (830 mg, 1.24 mmol, 92%) as a pale brown crystalline solid.

^{1}H NMR (400 MHz, $CDCl_3$) δ_H 7.89 (d, *J* 7.5 Hz, 2H, ArH), 7.72 (dd, *J* 7.5 2.2 Hz, 2H, ArH), 7.42 (t, *J* 7.5 Hz, 2H, ArH), 7.33 (dd, *J* 8.3 6.4 Hz, 2H, ArH), 5.24 (d, J_{H4H3} 3.6 Hz, 1H, H4), 5.15 (dd, J_{H3H2} 10.3 J_{H3H4} 3.6 Hz, 1H, H3), 4.88 (dd, J_{H2H3} 10.3 J_{H2H3} 8.0 Hz, 1H, H2), 4.78 (d, J_{H1H2} 8.0 Hz, 1H, H1), 4.20 – 4.33 (m, 4H, H13, H12, H7), 4.16 (app. t, *J* 6.7 Hz, 1H, H5), 4.03 (d, J_{H6H5} 6.7 Hz, 2H, H6), 3.85 – 3.95 (m, 1H, H9), 2.09 (s, 3H, $OCOCH_3$), 1.98 (s, 6H, $OCOCH_3$), 1.92 (s, 3H, $OCOCH_3$) ppm.

^{13}C NMR (100 MHz, $CDCl_3$) δ_C 170.40 ($OCOCH_3$), 170.35 ($OCOCH_3$), 170.0 ($OCOCH_3$), 169.7 ($OCOCH_3$), 156.5 (C11), 144.4 (Fmoc qC), 144.2 (Fmoc qC), 141.2 (2x Fmoc qC), 128.1 (Fmoc ArC), 127.5 (Fmoc ArC), 125.7 (Fmoc ArC), 120.6 (Fmoc ArC), 98.4 (C1), 75.4 (C7), 70.7 (C3), 70.1 (C5), 69.2 (C2), 67.6 (C4), 66.3 (C12), 61.3 (C6), 59.6 (C9), 47.1 (C13), 21.0 ($OCOCH_3$), 20.93 ($OCOCH_3$), 20.86 ($OCOCH_3$), 20.8 ($OCOCH_3$) ppm.

HRMS (ESI^+) *m/z* calc. for $C_{33}H_{36}NO_{14}$ $[M+H]^+$ 670.2141; found 670.2144.

ν_{max}/cm^{-1} (neat) 2980 (ArC), 1748 (CO).

Mp 123-125 °C.

((((9H-fluoren-9-yl)methoxy)carbonyl)-L-threonine

)-β-D-galactopyranoside (196) (attempted)

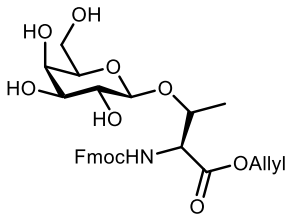

196

193 (100 mg, 0.15mmol) was dissolved in dry MeOH (1 mL) followed by the addition of sodium methoxide (138 mg, 2.55 mmol). The mixture was stirred for 30 min at rt and then acidified with HCl (1 M) to pH 2. After this time, TLC analysis (50% EtOAc/hexane) showed consumption of the starting material (R_F = 0.5) and the formation of a product (R_F = 0.0). The reaction mixture was concentrated under reduced pressure and redissolved in water (1 mL), then the pH was adjusted to 8-9 with Et_3N. Fmoc-OSu (51 mg, 0.15 mmol) in MeCN (1 mL) was added and then stirred at rt for 16 h. The reaction was quenched with HCl (1 M) and concentrated under reduced pressure. The crude product was purified by flash column chromatography (5% H_2O, 45% IPA/EtOAc) which did not yield the target molecule.

2,3,4,6-tetra-*O*-(trimethylsilyl)-α-D-Galactose (198)

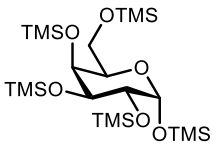

198

TMSCl (3.82 mL, 30.1 mmol) was added to a solution of triethylamine (4.26 mL, 30.1 mmol) and *D*-galactose (1.00 g, 5.60 mmol) in anhydrous DMF (5 mL) at 0 °C, the reaction mixture was allowed to warm to rt and stirred for 3 h under argon. After this time, TLC analysis (hexane) showed complete consumption of the starting material (R_F = 0.0) and formation of a product (R_F = 0.1). Water (20 mL) was added to the mixture and the product was extracted with hexane (3 x 20 mL). The combined organic extracts were washed with water (20 mL)

and brine (20 mL), then dried ($MgSO_4$), filtered and concentrated under reduced pressure to give **198** (2.11 g, 3.91 mmol, 71%) as a yellow oil.

^{1}H NMR (400 MHz, $CDCl_3$) δ_H 5.05 (d, J_{H1H2} 2.2 Hz, 1H, H1), 3.88 – 3.93 (m, 2H, H3, H5), 3.81 – 3.84 (m, 2H, H2, H4), 3.60 – 3.67 (m, 1H, H6a), 3.51 – 3.57 (m, 1H, H6b), 0.05 – 0.20 (m, 45H, TMS-C$\underline{H}_3$) ppm.

^{13}C NMR (100 MHz, $CDCl_3$) δ_C 94.6 (C1), 72.3 (C5), 71.1 (C3), 70.5 (C2), 70.0 (C4), 0.7 (TMS-$\underline{C}H_3$), 0.5 (TMS-$\underline{C}H_3$), 0.3 (TMS-$\underline{C}H_3$), 0.2 (TMS-$\underline{C}H_3$), -0.50 (TMS-$\underline{C}H_3$) ppm.

HRMS (ESI$^+$) *m/z* calc. for $C_{21}H_{52}NaO_6Si_5$ $[M+Na]^+$ 563.2502; found 563.2508.

The spectral data are in agreement with the literature.[362]

(1-(chloromethyl)-3-nitrobenzene

)-2,3,4,6-tetra-*O*-acetyl-β-D-galactopyranoside (201)

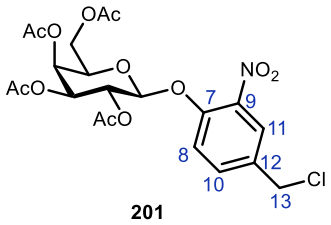

201

Thionyl chloride (79 µl, 1.08 mmol) and DMAP (6 mg, 0.05 mmol) were added to a solution of **136** (269 mg, 0.54 mmol) in anhydrous DCM (5 mL) at 0°C. The reaction mixture was then allowed to warm to room temperature and stirred for 3 h under argon. After this time, TLC analysis (60% EtOAc/hexane) showed complete consumption of the starting material (R_F = 0.2) and the formation of a product (R_F = 0.9); analysis in 40% EtOAc/hexane) confirmed consumption of the starting material (R_F = 0.8) and the formation of a product (R_F = 0.3). The reaction was quenched with water (10 mL) and extracted with DCM (3 x 10 mL). The combined organic extracts were washed with brine (20 mL), dried ($MgSO_4$), filtered and concentrated under reduced pressure to give **201** (228 mg, 0.44 mmol, 82%) as an off-white oil.

^{1}H NMR (400 MHz, $CDCl_3$) δ_H 7.83 (d, J_{H11H10} 2.3 Hz, 1H, H11), 7.55 (dd, J_{H10H8} 8.6 J_{H10H11} 2.3 Hz, 1H, H10), 7.35 (d, J_{H8H10} 8.6 Hz, 1H, H8), 5.54 (dd, J_{H2H3} 10.5 Hz J_{H2H1} 7.9 Hz, 1H, H2), 5.47 (dd, J_{H4H3} 3.4 Hz J_{H4H5} 1.2 Hz, 1H, H4), 5.05 – 5.13 (m, 2H, H1, H3), 4.57 (s, 2H, H13), 4.25 (dd, J_{H6aH6b} 11.3 J_{H6aH5} 7.0 Hz, 1H, H6a), 4.16 (dd, J_{H6bH6a} 11.3 J_{H6bH5} 6.1 Hz, 1H, H6b),

4.07 (ddd, J_{H5H6a} 7.0 J_{H5H6b} 6.1 J_{H5H4} 1.2 Hz, 1H, H5), 2.19 (s, 3H, OCOC$\underline{H}_3$), 2.12 (s, 3H, OCOC$\underline{H}_3$), 2.07 (s, 3H, OCOC$\underline{H}_3$), 2.01 (s, 3H, OCOC$\underline{H}_3$) ppm.

^{13}C NMR (100 MHz, $CDCl_3$) δ_C 170.3 (O$\underline{C}$OCH$_3$), 170.2 (O$\underline{C}$OCH$_3$), 170.1 (O$\underline{C}$OCH$_3$), 169.4 (O$\underline{C}$OCH$_3$), 149.2 (C7), 141.2 (C9), 133.7 (C10), 133.5 (C12), 125.2 (C11), 120.1 (C8), 100.7 (C1), 71.5 (C5), 70.5 (C3), 67.8 (C2), 66.7 (C4), 61.3 (C6), 44.2 (C13), 20.67 (OCO$\underline{C}$H$_3$), 20.65 (2x OCO$\underline{C}$H$_3$), 20.6 (OCO$\underline{C}$H$_3$) ppm.

HRMS (ESI$^+$) *m/z* calc. for $C_{21}H_{24}ClNNaO_{12}$ $[M+Na]^+$ 540.0879; found 540.0887.

ν_{max}/cm^{-1} (neat) 2967 (Ar CH), 1742 (CO), 1531 (NO).

The spectral data are in agreement with the literature.[363]

Fmoc-Lys-OH (203)

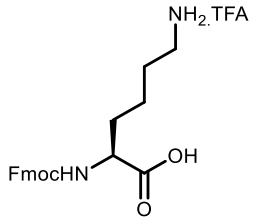

203

A solution of Fmoc-Lys(Boc)-OH (1.00 g, 2.14 mmol) in TFA:TES:DCM(2:1:8, v/v, 18 mL) at rt for 2 h. After this time, TLC analysis (5% MeOH/DCM) showed consumption of the starting material (R_F = 0.5) and the formation of a product (R_F = 0.1). The reaction mixture was concentrated under reduced pressure and azeotroped (3 x 20 mL MeOH) to give Fmoc-Lys-OH **203** (1.00 g, 2.14 mmol, quant.) as a TFA salt as a clear oil.

^{1}H NMR (400 MHz, DMSO-d_6) δ_H 7.90 (dd, *J* 7.5 1.1 Hz, 2H, ArH), 7.69 – 7.75 (m, 2H, ArH), 7.42 (td, *J* 7.5 1.1 Hz, 2H, ArH), 7.33 (td, *J* 7.5 1.1 Hz, 2H, ArH), 4.26 – 4.37 (m, 2H, Fmoc-C$\underline{H}_2$), 4.23 (app. q., *J* 6.1 Hz, 1H, Fmoc-C$\underline{H}$), 3.93 (ddd, *J* 9.8 8.0 4.6 Hz, 1H, α-C$\underline{H}$), 2.71 – 2.81 (m, 2H, ε-C$\underline{H}_2$), 1.47 – 1.78 (m, 4H, β-C$\underline{H}_2$, γ-C$\underline{H}_2$), 1.30 – 1.41 (m, 2H, δ-C$\underline{H}_2$).

^{13}C NMR (100 MHz, DMSO-d_6) δ_C 173.8 (C$\underline{O}$OH), 156.2 (NH$\underline{C}$O), 143.8 (Fmoc qC), 143.7 (Fmoc qC), 140.7 (Fmoc qC), 127.6 (Fmoc ArC), 127.0 (Fmoc ArC), 125.2 (Fmoc ArC), 120.1 (Fmoc ArC), 65.5 (Fmoc $\underline{C}H_2$), 53.6 (α-$\underline{C}$H), 46.6 (Fmoc $\underline{C}$H), 38.6 (ε-$\underline{C}H_2$), 30.1 (β-$\underline{C}H_2$), 26.5 (γ-$\underline{C}H_2$), 22.5 (δ-$\underline{C}H_2$).

HRMS (ESI$^+$) *m/z* calc. for $C_{21}H_{25}N_2O_4$ $[M+H]^+$ 369.1809; found 369.1815.

The spectral data are in agreement with the literature.[364]

N^2-(((9H-fluoren-9-yl)methoxy)carbonyl)-N6,N6-bis(3-nitrobenzyl)-L-lysine (205) (attempted)

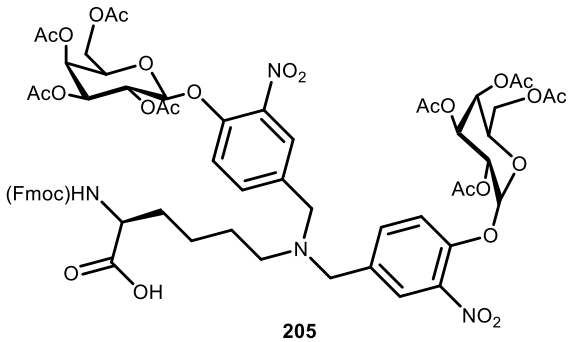

205

Potassium carbonate (21 mg, 0.15 mmol) and **203** (103 mg, 0.20 mmol) were added to a solution of Fmoc-Lys-OH (47 mg, 0.10 mmol) in acetonitrile (2 mL) and then heated to reflux for 16 h under argon. After this time, TLC analysis (5% MeOH/DCM) showed consumption of the starting material (R_F = 0.8) and the formation of a complex mixture. The reaction mixture was concentrated under reduced pressure and purified by flash column chromatography which yielded a complex mixture of products.

N_2-(((9H-fluoren-9-yl)methoxy)carbonyl)-N_6-(3-nitrobenzyl)-L-lysine-2,3,4,6-tetra-*O*-acetyl-β-D-galactopyranoside (204) (attempted)

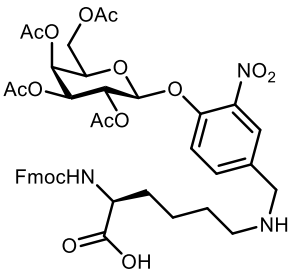

204

Fmoc-Lys-OH (140 mg, 0.30 mmol) was added to aldehyde **135** (150 mg, 0.30 mmol) in anhydrous MeCN and stirred at rt for 3 h under argon. After this time, $NaBH_3CN$ (19 mg, 0.30 mmol) was added and the reaction mixture was stirred at rt for 16 h under argon. After this time, TLC analysis (30% EtOAc/hexane) showed conversion of the starting material (R_F = 0.6) to a product (R_F = 0.3) and the crude product was purified by flash column chromatography (30% EtOAc/hexane) to yield the reduced aldehyde product only.

Fmoc-Thr(^{t}Bu)-ol (212)

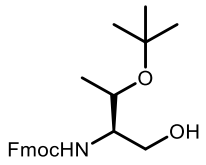

212

A solution of Fmoc-Thr-OH (3.00 g, 7.60 mmol) and 1,1'-carbonyldiimadazole (1.53 g, 9.40 mmol) in THF (20 mL) was stirred at rt for 30 min under argon. After this time, TLC analysis (30% EtOAc/hexane) showed consumption of the starting material (R_F = 0.1) and the formation of a product (R_F = 0.6). The solution was then cooled to 0 °C and a solution of sodium borohydride (430 mg, 1.14 mmol) in H_2O (10 mL) was added dropwise. The reaction mixture was warmed to rt and stirred for 1.5 h under argon. After this time TLC analysis (30% EtOAc/hexane) showed consumption of the starting material (R_F = 0.6) and formation of a product (R_F = 0.3). The reaction was neutralised with 0.1 M HCl and extracted with EtOAc (5 x 20 mL). The combined organic extracts were washed with $NaHCO_3$ (sat. aq.; 20 mL) and brine (20 mL), dried ($MgSO_4$), filtered and concentrated under reduced pressure. The crude product was purified by flash column chromatography (30% EtOAc/hexane) to give **212** (1.61 g, 4.21 mmol, 55%) as an off-white crystalline solid.

7.4.1 Standard Procedures for Solid-Phase Peptide Synthesis (SPPS)

General Methods

SPPS was performed manually in polypropylene syringe reaction vessels (10 mL; Torviq, MI, USA and 10 mL, 3 mL; Astech, Wicklow, Ireland) fitted with a polystyrene frit. All reactions were performed at room temperature under continuous agitation on an LBX Instruments Orb-B2 shaker set to 180 rpm. As all peptides synthesised contained Cys residues, the cleavage cocktail (TFA:EDT:H_2O:TES; 94:2.5:2.5:1 v/v) was exclusively used instead of the standard (TFA:TES:H_2O; 95:2.5:2.5 v/v) cocktail.

General Procedure 1: Resin Deprotection and Coupling of β-Amino Alcohol (2-ClTrt)

Following a protocol described by Tailhades *et al.*,[365] 2-chlorotrityl resin (0.125 g, 0.2 mmol, 100-200 mesh, 1.6 mmol/g, 1.0 equiv.) was swollen with agitation in anydrous DMF (4 mL) in a SPPS syringe for 20 min under argon and then drained. The Fmoc-β-amino alcohol (3.0 equiv.) was dissolved in a solution of DBU (2 %) in anhydrous DMF, and the resulting solution was added to the 2-chlorotrityl chloride resin. The reaction mixture was agitated at room temperature for 12 h under argon, and the resin was then removed by filtration and washed with DMF (3 x 5 mL), DMF (3 x 5 mL), and DCM (3 x 5 mL). To cap unreacted 2-ClTrt resin, a solution of DCM :DIPEA:MeOH (17:2:1 v/v/v; 5 mL) was added to the syringe for 2 x 10 min and then the resin was washed with two rounds of DCM (3 x 5 mL), DMF (3 x 5mL).

General Procedure 2: Steglich Esterification of Fmoc-Cys(Trt)-OH to Resin-Bound β-Amino Alcohol

Following a protocol described by Tailhades *et al.*,[365] DIC (3.0 equiv.) and DMAP (0.3 equiv) were added to a solution of Fmoc-AA-OH (6.0 equiv. relative to resin substitution) in a mixture of anhydrous DCM and DMF (1:1 v/v; 0.3 M). The resulting mixture was stirred with the β-amino alcohol functionalized resin for 6 h at rt. After this time, excess reagents were drained from the syringe and the resin was washed with DMF (3 x 5 mL), DCM (3 x 5 mL), DMF (3 x 5 mL).

General Procedure 3: Mitsunobu Coupling of Fmoc-Cys(Trt)-OH to Resin-Bound β-Amino Alcohol

Following a protocol described by Tailhades *et al*,[365] a solution of PPh_3 (3.0 equiv.) and Fmoc-Cys(Trt)-OH (3 equiv.) in anhydrous THF (20 mL per gram of resin) was added to the resin. A 40 % solution of DEAD in toluene (3 equiv) was then added, and the mixture was stirred for 6 h at room temperature. After this time, excess reagents were drained from the syringe and the resin was washed with anhydrous DMF (3 x 5 mL), DCM (3 x 5 mL) and (DMF (3 x 5 mL). This procedure was repeated twice.

General Procedure 4: Resin Deprotection and Coupling of First Amino Acid (Rink Amide)

Rink amide AM resin (0.26 g, 0.2 mmol, 0.78 mmol/g, 100 - 200 mesh, 1.0 equiv.) was swollen with agitation in DMF (4 mL) in a SPPS syringe for 20 min and then drained. The resin-bound Fmoc protecting group was removed using 20% (v/v) piperidine in DMF (4 mL; 2 x 10 min) and the resin was washed with DMF (3 x 5 mL), DCM (3 x 5 mL) and DMF (3 x 5 mL). Fmoc-protected amino acid (4.0 eq.) was pre-activated with HATU (3.9 eq.) and DIPEA (8.0 eq.) in DMF (0.2 M) for 30 seconds and then transferred to the syringe containing the resin and agitated for 45 min. After this time, excess reagents were drained from the syringe and the resin was washed with DMF (3 x 5 mL), DCM (3 x 5 mL), DMF (3 x 5 mL). The coupling reaction and washes were then repeated.

General Procedure 5: Bromophenol Blue (BPB Monitoring of Coupling and Deprotection Reactions)

Successful coupling was qualitatively monitored by treatment of a small resin sample with a solution of bromophenol blue (BPB) in DCM (0.15 mM; 0.1 mL). For the monitoring of Fmoc-deprotection reactions, the beads would turn blue upon BPB treatment in the presence of a free amine; for the monitoring of amino acid coupling reactions, the beads would turn yellow. In the case of an incomplete deprotection or coupling, the associated procedure for the reaction was repeated.

General Procedure 6: Coupling of Subsequent Amino Acids

The subsequent amino acid coupling cycles consisted of **(i)** Fmoc deprotection with 20% (v/v) piperidine in DMF (4 mL; 2 x 10 min). **(ii)** Resin washes with DMF (3 x 5 mL), DCM (3 x 5 mL) and DMF (3 x 5 mL). **(iii)** Pre-activation of Fmoc-AA-OH (4.0 eq) with HATU (3.9 equiv.)/DIPEA (8.0 equiv.) in DMF (0.2 M) for 30 seconds followed by addition to the peptide resin and agitation for 45 min. **(iv)** (iii) was repeated for all amino acid couplings followed by washes with DMF (3 x 5 mL) between the repeat couplings. **(v)** Resin washes with DMF (3 x 5 mL), DCM (3 x 5 mL) and DMF (3 x 5 mL). **(vi)** Qualitative BPB test as per **General Procedure 5**. Following the final coupling, the resin was treated with 20% (v/v) piperidine in

DMF (5 mL, 2 x 10 min) and the resin was washed with 2 rounds of DMF (3 x 5 mL), DCM (3 x 5 mL), followed by drying of the resin under reduced pressure.

General Procedure 7: Coupling of Cysteine

Coupling of Fmoc-Cys(Trt)-OH/Fmoc-Cys(Acm)-OH consisted of **(i)** Fmoc deprotection by the addition of 20% (v/v) piperidine in DMF (4 mL) to the resin for 2 x 10 min, **(ii)** resin washes with DMF (3 x 5 mL), DCM (3 x 5 mL) and DMF (3 x 5 mL), **(iii)** peptide coupling with addition of DIC (4.0 equiv.), Oxyma Pure (4.0 equiv.) and Fmoc-Cys(Trt)-OH (4.0 equiv., 0.2 M) in DMF:DCM (1:1, v/v) were preactivated for 30 seconds and then added to the peptide resin for 45 min, **(iv)** resin washes with DMF (3 x 5 mL), DCM (3 x 5 mL) and DMF (3 x 5 mL), **(v)** qualitative BPB test as per **General Procedure 5**.

General Procedure 8: N-Acetylation Capping

Following Fmoc deprotection, a solution of 20% acetic anhydride in pyridine was added to the peptide resin and agitated for 3 x 4 min. The acetylation solution was drained and resin washes with DMF (3 x 5 mL), DCM (3 x 5 mL) and DMF (3 x 5 mL).

General Procedure 9: On-resin Deacetylation of Glycopeptides

Following a protocol reported by Galashov *et al.*,[366] in the final step prior to peptide cleavage, the resin was treated with a mixture of N_2H_4 (51% aq.)/DMF (1:1, v/v) for 30 minutes. Liquid was drained from the syringe and resin was washed DMF (3 x 5 mL), DCM (3 x 5 mL) and DMF (3 x 5 mL).

General Procedure 10: Global Deprotection and Resin Cleavage

The dried resin was swollen in DCM (4 mL) for 20 min, then drained and immersed in the cleavage cocktail (TFA:EDT:H_2O:TES; 94:2.5:2.5:1 v/v/v; 3mL) unless otherwise stated, capped tightly and agitated for 90 min. The syringe was then drained, and the filtrate was collected. The resin was then washed with cleavage cocktail (3 x 2 mL) and the washings were combined with the initial filtrate. The combined filtrate was concentrated under a stream of N_2 to form an oily residue which was precipitated with ice-cold Et_2O (8 mL). The suspension

was centrifuged and the supernatant was decanted. The pellet was resuspended in ice-cold diethyl ether (10 mL), centrifuged and the supernatant was decanted twice. After the final wash, the pellet was dried under a stream of N_2 and the crude peptide dried under reduced pressure.

H_2N-D-Phe-Cys-Phe-D-Trp-Lys-Thr-Cys-OThr-$CONH_2$ (215)

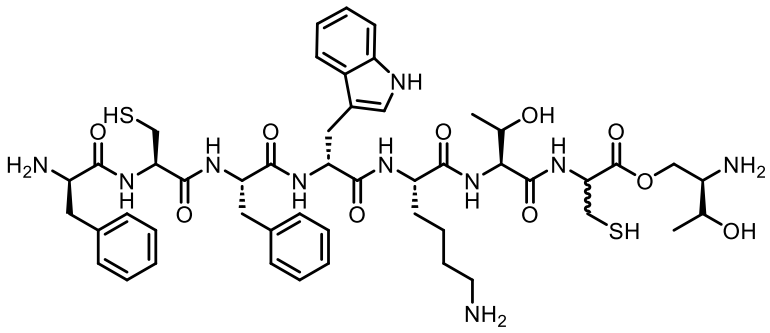

215

Peptide **215** was synthesised following two procedures:

Method A:

Fmoc-Thr(^{t}Bu)-ol **212** (307 mg, 0.8 mmol) was loaded to 2-ClTrt resin (125 mg, 0.2 mmol) as per **General Procedure 1**. Fmoc-Cys(Trt)-OH (703 mg, 1.2 mmol) was then coupled via Steglich esterification according to **General Procedure 2**. Fmoc-Thr(^{t}Bu)-OH (403 mg, 0.6 mmol), Fmoc- Lys(Boc)-OH (281 mg, 0.6 mmol), Fmoc-D-Trp(Boc)-OH (316 mg, 0.6 mmol), Fmoc-Phe-OH (232 mg, 0.6 mmol), Fmoc-Cys(Trt)-OH (351 mg, 0.6 mmol), Fmoc-D-Phe-OH (232 mg, 0.6 mmol) were coupled according to **General Procedures 6** and **7** . The resin was treated with 20% (v/v) piperidine in DMF (5 mL; 2 x 10 min) prior to cleavage. The peptide was cleaved from the resin using **General Procedure 10** yielding linear peptide **215** (90 mg, 0.087 mmol, 44%) as a white fluffy solid.

Method B:

Fmoc-Thr(^{t}Bu)-ol **212** (154 mg, 0.4 mmol) was loaded to 2-ClTrt resin (63 mg, 0.1 mmol) as per **General Procedure 1**. Fmoc-Cys(Trt)-OH (234 mg, 0.4 mmol) was then coupled via Mitsunobu reaction according to **General Procedure 2**. Fmoc-Thr(^{t}Bu)-OH (403 mg, 0.6 mmol), Fmoc- Lys(Boc)-OH (141 mg, 0.3 mmol), Fmoc-D-Trp(Boc)-OH (158 mg, 0.3

mmol), Fmoc-Phe-OH (116 mg, 0.3 mmol), Fmoc-Cys(Trt)-OH (176 mg, 0.3 mmol), Fmoc-D-Phe-OH (116 mg, 0.3 mmol) were coupled according to **General Procedures 6** and **7**. The resin was treated with 20% (v/v) piperidine in DMF (5 mL; 2 x 10 min) prior to cleavage. The peptide was cleaved from the resin using **General Procedure 10** yielding linear peptide **215** (41 mg, 0.040 mmol, 20%) as a white fluffy solid.

HRMS (ESI$^+$) *m/z* calc. for $C_{49}H_{68}N_{10}O_{10}S_2$ $[M+H]^+$ 1043.4454; found 1043.4433.

R_T = 9.07 min (5 – 95% MeCN in H_2O with 0.1% TFA over 12 min, 220 nm).

Octreotide (50)

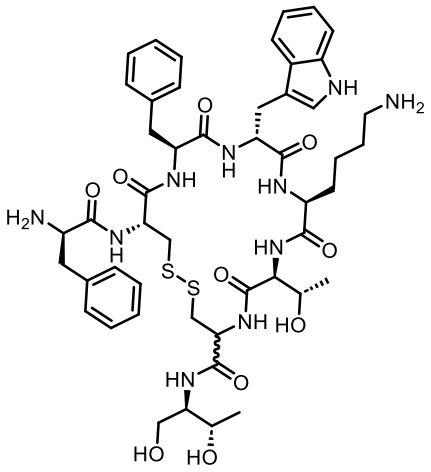

50

Peptide **215** was dissolved in phosphate buffer (pH 7.4) and the mixture was stirred at room temperature for 48 h. After this time, analytical HPLC analysis showed consumption of the starting material (R_T = 9.07 min) and formation of two new peaks (R_T = 8.72 min, 8.81 min). Due to two peaks of equal intensity forming, indicating racemisation of the growing peptide during SPPS, this peptide (**50**) was not purified.

HRMS (ESI$^+$) *m/z* calc. for $C_{49}H_{67}N_{10}O_{10}S_2$ $[M+H]^+$ 1019.4478; found 1019.4477.

R_T = 8.72 min (5 – 95% MeCN in H_2O with 0.1% TFA over 12 min, 220 nm).

H_2N-Ala-Gly-Cys-Lys-Asn-Phe-Phe-Trp-Lys-Thr-Phe-Thr-Ser-Cys-$CONH_2$ (218)

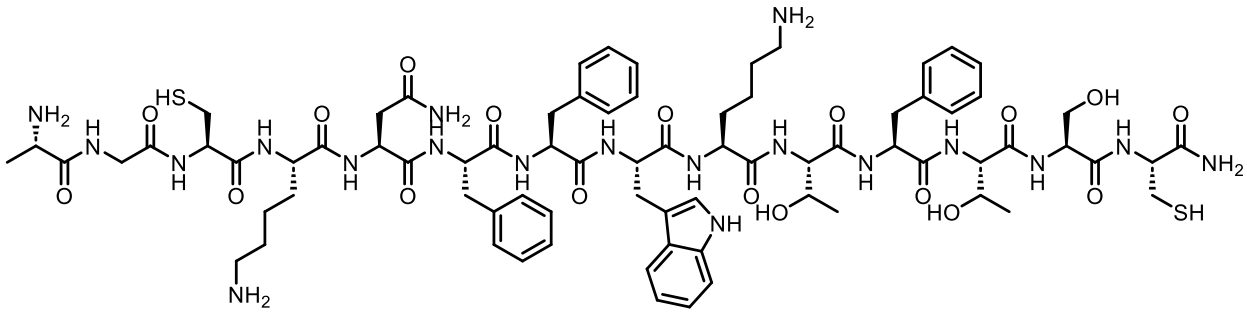

218

Fmoc-Cys(Trt)-OH (586 mg, 1.00 mmol) was loaded to Rink Amide AM resin (321 mg, 0.25 mmol) as per a modified **General Procedure 4** using **General Procedure 7** for Cys coupling. Fmoc-Ser(^{t}Bu)-OH (383 mg, 1.00 mmol), Fmoc-Thr(^{t}Bu)-OH (397 mg, 1.00 mmol), Fmoc-Phe-OH (387 mg, 1.00 mmol), Fmoc-Thr(^{t}Bu)-OH (397 mg, 1.00 mmol), Fmoc-Lys(Boc)-OH (469 mg, 1.00 mmol), Fmoc-Trp(Boc)-OH (527 mg, 1.00 mmol), Fmoc-Phe-OH (387 mg, 1.00 mmol), Fmoc-Phe-OH (387 mg, 1.00 mmol), Fmoc-Asn(Trt)-OH (597 mg, 1.00 mmol), Fmoc-Lys(Boc)-OH (469 mg, 1.00 mmol), Fmoc-Cys(Trt)-OH (586 mg, 1.00 mmol), Fmoc-Gly-OH (297 mg, 1.00 mmol), Fmoc-Ala-OH (370 mg, 1.00 mmol) were coupled according to **General Procedures 6** and **7** . The resin was treated with 20% (v/v) piperidine in DMF (5 mL; 2 x 10 min) followed by on-resin deacetylation according to **General Procedure 9** using N_2H_4 prior to cleavage. The peptide was cleaved from the resin using **General Procedure 10** yielding linear peptide **218** (249 mg, 0.15 mmol, 61%) as a white fluffy solid.

HRMS (ESI$^+$) *m/z* calc. for $C_{76}H_{109}N_{19}O_{18}S_2$ $[M+2H]^{2+}$ 819.8814; found 819.8835.

$\mathbf{R_T}$ = 9.14 min (5 – 95% MeCN in H_2O with 0.1% TFA over 12 min, 220 nm).

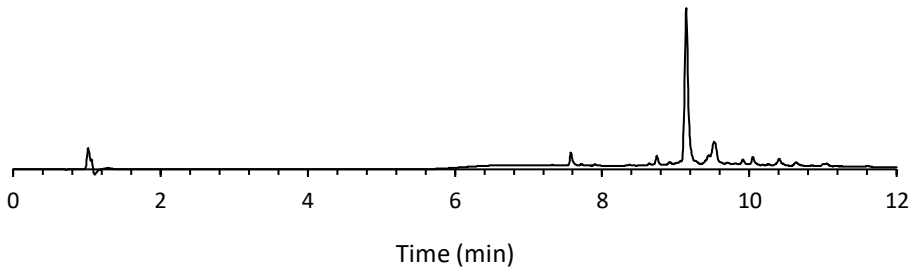

H_2N-cyclo(1,12)[Ala-Gly-Cys-Lys-Asn-Phe-Phe-Trp-Lys-Thr-Phe-Thr-Ser-Cys]-$CONH_2$ (219)

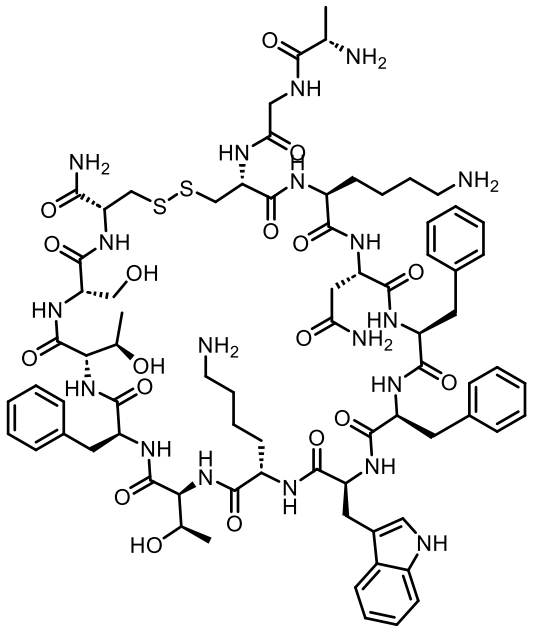

219

DMSO (1 mL) was added to a solution of linear peptide **218** (20 mg, 12 μmol) in 1:1 v/v water:MeCN (9 mL) and stirred at rt for 48 h. After this time, HPLC analysis showed consumption of the starting material (RT = 9.14 min) and the formation of a new peak (9.15 min). The crude material was purified by semi-preparative HPLC to give cyclic peptide **219** (1.7 mg, 1.04 μmol, 9%) as a white fluffy solid.

HRMS (ESI$^+$) *m/z* calc. for $C_{76}H_{107}N_{19}O_{18}S_2$ $[M+2H]^{2+}$ 818.8736; found 818.8748.

R_T = 9.15 min (5 – 95% MeCN in H_2O with 0.1% TFA over 12 min, 220 nm).

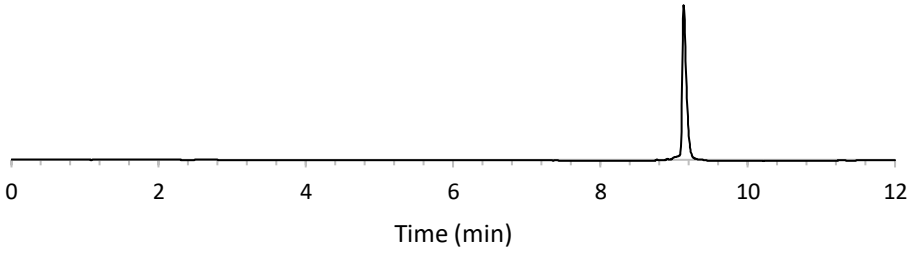

H_2N-Ala-Gly-Cys-Lys-Asn-Phe-Phe-Trp-Lys-Thr-Phe-Thr(β-Gal)-Ser-Cys-$CONH_2$ (222)

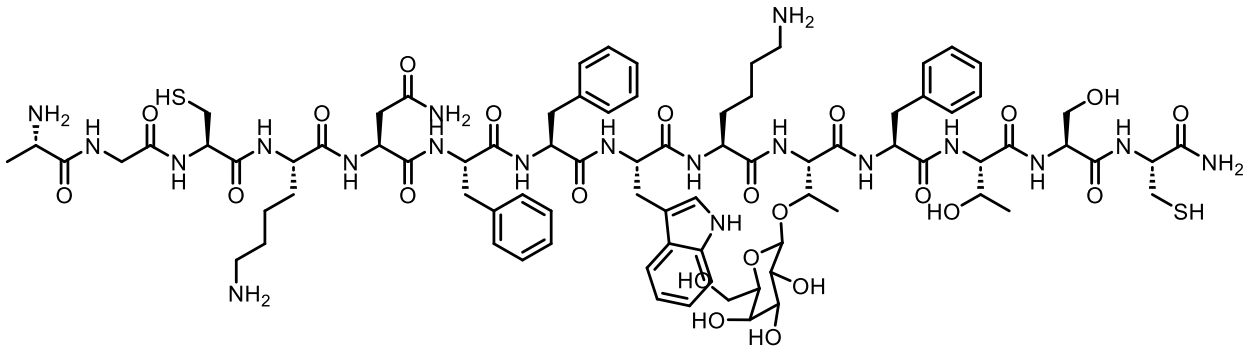

222

Fmoc-Cys(Trt)-OH (586 mg, 1.00 mmol) was loaded to Rink Amide AM resin (321 mg, 0.25 mmol) as per a modified **General Procedure 4** using **General Procedure 7** for Cys coupling. Fmoc-Ser(^{t}Bu)-OH (383 mg, 1.00 mmol), Fmoc-Thr(^{t}Bu)-OH (397 mg, 1.00 mmol), Fmoc-Phe-OH (387 mg, 1.00 mmol), unnatural amino acid **185** (671 mg, 1.00 mmol), Fmoc-Lys(Boc)-OH (469 mg, 1.00 mmol), Fmoc-Trp(Boc)-OH (527 mg, 1.00 mmol), Fmoc-Phe-OH (387 mg, 1.00 mmol), Fmoc-Phe-OH (387 mg, 1.00 mmol), Fmoc-Asn(Trt)-OH (597 mg, 1.00 mmol), Fmoc-Lys(Boc)-OH (469 mg, 1.00 mmol), Fmoc-Cys(Trt)-OH (586 mg, 1.00 mmol), Fmoc-Gly-OH (297 mg, 1.00 mmol), Fmoc-Ala-OH (370 mg, 1.00 mmol) were coupled according to **General Procedures 6** and **7**. The resin was split and a portion of the resin (0.1 mmol) was then treated with 20% (v/v) piperidine in DMF (5 mL; 2 x 10 min) followed by on-resin deacetylation according to **General Procedure 9** using N_2H_4 prior to cleavage. The peptide was cleaved from the resin using **General Procedure 10** yielding linear peptide **222** (54 mg, 0.030 mmol, 30%) as a white fluffy solid.

HRMS (ESI$^+$) m/z calc. for $C_{82}H_{119}N_{19}O_{23}S_2$ $[M+2H]^{2+}$ 900.9078; found 900.9100.

$\mathbf{R_T}$ = 9.34 min (5 – 95% MeCN in H_2O with 0.1% TFA over 12 min, 220 nm).

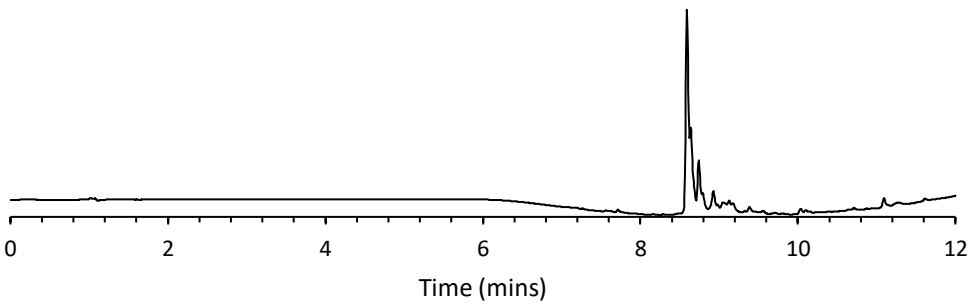

H_2N-cyclo(1,12)[Ala-Gly-Cys-Lys-Asn-Phe-Phe-Trp-Lys-Thr-Phe-Thr(β-Gal)-Ser-Cys]-$CONH_2$ (223)

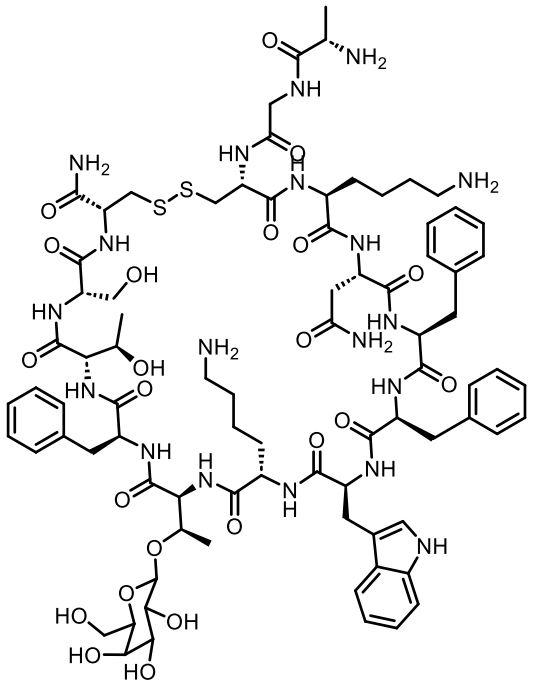

223

Linear peptide **222** (10 mg, 5.5 μmol) out in MeCN/pH 7.4 phosphate buffer (1:1 v/v) and 10% DMSO at rt for 48 h. After this time, HPLC analysis showed consumption of the starting material (R_T = 9.34 min) and the formation of a new peak (R_T = 8.68 min). The crude material was purified by semi-preparative HPLC to give cyclic peptide **223** (1.1 mg, 0.60 μmol, 11%) as a fully white solid.

HRMS (ESI$^+$) *m/z* calc. for $C_{82}H_{117}N_{19}O_{23}S_2$ $[M+2H]^{2+}$ 899.9000; found 899.9018.

R_T = 8.68 min (5 – 95% MeCN in H_2O with 0.1% TFA over 12 min, 220 nm).

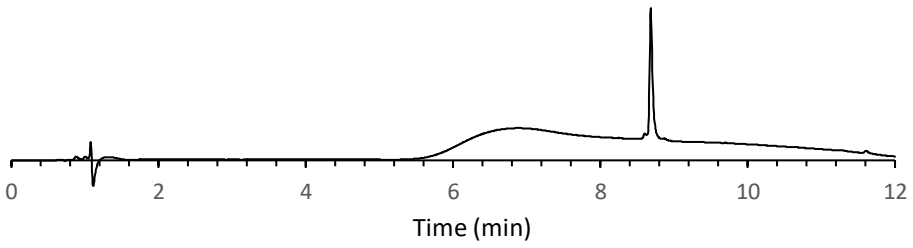

7.5 Synthetic Methods for Chapter 5

Allyl N^2-(((9H-fluoren-9-yl)methoxy)carbonyl)-N^6-(*tert*-butoxycarbonyl)-L-lysinate (226)

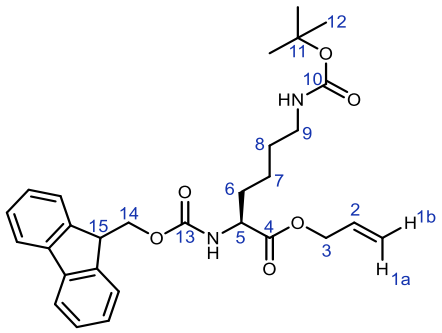

226

Following a modified procedure by Y. Lee *et al.*,[367] allyl bromide (0.11 mL, 1.25 mmol) was added to a suspension of Fmoc-Lys(Boc)-OH (500 mg, 1.04 mmol) and K_2CO_3 (290 mg, 2.08 mmol) in acetone (15 mL). The mixture was stirred at room temperature for 18 h, after which time TLC analysis (1% MeOH/DCM) showed consumption of the starting material (R_F = 0.1) and formation of a product (R_F = 0.9); TLC analysis (40% EtOAc/hexane) confirmed consumption of the starting material (R_F = 0.0) and the formation of a product (R_F = 0.4). The reaction mixture was then filtered through Celite® and the filtrate concentrated under reduced pressure. The crude residue purified by flash column chromatography (40% EtOAc/hexane) to yield **226** (343 mg, 0.67 mmol, 64%) as a white crystalline solid.

^{1}H NMR (400 MHz, $CDCl_3$) δ_H 7.79 (d, *J* 7.6 Hz, 2H, ArH), 7.60 – 7.65 (m, 2H, ArH), 7.43 (t, *J* 7.3 Hz, 2H, ArH), 7.34 (t, *J* 7.4 Hz, 2H, ArH), 5.99-5.88 (m, 1H, H2), 5.34 – 5.44 (m, 2H, H1a, NH), 5.29 (dd, J_{H1bH2} 10.4 Hz, J_{H1bH1a} 1.2 Hz, 1H, H1b), 4.67 (d, J_{H3H2} 5.6 Hz, 2H, H3), 4.37 – 4.48 (m, 3H, H5, H14), 4.25 (t, J_{H15H14} 7.0 Hz, 1H, H15), 3.14 (br s, 2H, H9), 1.58-1.36 (m, 13H, H6, H7, H8, H12) ppm.

^{13}C NMR (100 MHz, $CDCl_3$) δ_C 172.2 (C4), 156.1 (C13), 143.9 (ArC), 141.5 (ArC), 131.7 (C2), 127.7 (ArC), 127.1 (ArC), 125.1 (ArC), 120.0 (ArC), 119.1 (C1), 67.1 (C14), 66.0 (CH_2CHCH), 53.8 (C5), 47.2 (C15), 40.1 (C9), 32.2 (C6), 29.6 (C8), 28.5 (C12), 22.4 (C7) ppm.

HRMS (ESI$^+$) *m/z* calc. for $C_{29}H_{36}N_2NaO_6$ $[M+Na]^+$ 531.2471, found 531.2464.

mp 121 – 123 °C (lit.[368] 123 °C) from EtOAc/hexane).

Spectral data in agreement with the literature.[368]

Allyl N^2-(((9H-fluoren-9-yl)methoxy)carbonyl)-N^6-(((4-nitrobenzyl)oxy)carbonyl)-L-lysinate (230)

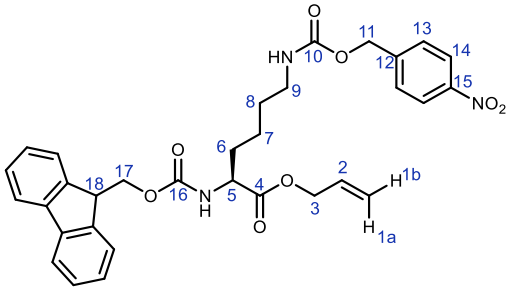

230

TFA (1 mL) was added to a solution of **202** (343 mg, 0.68 mmol) in DCM (3 mL) and stirred at rt for 2 h. After this time TLC analysis (2% MeOH/DCM) showed complete consumption of starting material (R_f = 0.9) and formation of a single product (R_F = 0.1), after which reaction mixture was concentrated under reduced pressure. **226** (108 mg, 0.32 mmol) was dissolved in water (5 mL) and dioxane (3 mL) at 0 °C. $NaHCO_3$ (23 mg, 0.32 mmol) was added followed by nitrobenzyl chloroformate (65 mg, 0.36 mmol). The reaction mixture was stirred at 0 °C for 2 h, after which time TLC analysis (1% MeOH/DCM) showed consumption of starting material (R_F = 0.2) and formation of a product (R_F = 0.6), then warmed to rt and stirred for 18 h. The reaction mixture was washed with Et_2O (3 x 10 mL) and the combined aqueous layers acidified to pH 2 (HCl, 1 M) and extracted with EtOAc (3 x 10 mL). The combined organic layers were dried over Na_2SO_4, filtered and the solvent removed under reduced pressure. The crude residue was purified by flash column chromatography (40% EtOAc/hexane) to give **230** (47 mg, 30%) as a colourless oil.

^{1}H NMR (400 MHz, $CDCl_3$) δ_H 8.16 – 8.21 (m, 2H, H14), 7.74 (d, J 7.6 Hz, 2H, Fmoc ArH), 7.60-7.55 (m, 2H, Fmoc ArH), 7.52-7.48 (m, 2H, H13), 7.43-7.35 (m, 2H, Fmoc ArH), 7.27 – 7.32 (m, 2H, J 1.1 Hz, ArH), 5.84 – 5.95 (m, 1H, H2), 5.48 (d, J_{NHH5} 7.9 Hz, 1H, NH), 5.29 – 5.35 (m, 1H, H1a), 5.25 (dd, J_{H1bH2} 10.2 Hz, 1H, J_{H1bH1a} 1.1 Hz, H1b), 5.11 (d, J_{NHH9} 7.1 Hz,

1H, NH), 4.80 (s, 2H, H11), 4.64 (d, J_{H3H2} 5.4 Hz, 2H, H3), 4.33 – 4.44 (m, 3H, H5, H17), 4.19 (t, J_{H18H17} 6.8 Hz, 1H, H18), 3.15 – 3.22 (m, 2H, H9), 1.75-1.32 (m, 6H, H6, H7, H8) ppm.

^{13}C NMR (100 MHz, $CDCl_3$) δ_C 172.1 (C4), 156.1 (C10), 148.4 (C15), 144.0 (C12), 141.3 (Fmoc ArC), 131.4 (C2), 128.0 (Fmoc ArC), 127.8 (Fmoc ArC), 127.1 (Fmoc ArC), 127.0 (C13), 125.0 (Fmoc ArC), 123.7 (C14), 120.0 (Fmoc ArC), 119.1 (C1), 67.1 (C17), 66.1 (C3), 63.9 (C11), 53.6 (C5), 47.1 (C18), 40.7 (C9), 32.3 (C7), 29.1 (C8), 22.2 (C7) ppm.

HRMS (ESI^+) *m/z* calc. for $C_{32}H_{33}N_3O_8$ $[M+H]^+$ 587.2268; found 588.2340.

ν_{max}/cm^{-1} (neat) 1690 (CO), 1523 (NO_2).

(*tert*-butoxycarbonyl)-L-allothreonine (235)

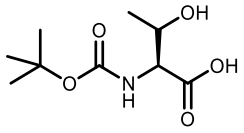

235

L-Threonine (200 mg, 1.68 mmol) was dissolved in 1 M NaOH (3.5 mL) and the resulting solution was cooled down to 0 °C. Boc anhydride (440 mg, 2.02 mmol) in dioxane (1.7 mL) was added and the reaction mixture was stirred at 0 °C for 30 min and then at rt overnight. After this time, TLC analysis (10% MeOH/DCM) showed consumption of the starting material (R_F = 0.1) and the formation of a product (R_F = 0.3). The solvents were evaporated to half of the volume and the reaction mixture was adjusted to pH 2 using 1 M HCl. The solution was extracted with EtOAc (3 x 5 mL), the combined organic phases was dried over $MgSO_4$ and the solvents removed under reduced pressure to obtain **235** (333 mg, 1.51 mmol, 90%) as a clear oil.

^{1}H NMR (400 MHz, $CDCl_3$) δ_H 5.72 (d, $J_{NHC\alpha H}$ 9.0 Hz, 1H, NH), 4.42 (m, 1H, β-CH), 4.30 (d, $J_{C\alpha HNH}$ 9.0 Hz, 1H, α-CH), 1.46 (s, 9H, $C(C\underline{H}_3)_3$), 1.26 (m, 3H, γ-CH_3) ppm.

^{13}C NMR (100 MHz, $CDCl_3$) δ_C 174.6 ($\underline{C}O_2H$), 156.7 ($\underline{C}ONH$), 80.5 ($\underline{C}(CH_3)_3$), 68.0 (β-C), 58.7 (α-C), 28.4 ($C(\underline{C}H_3)_3$), 19.3 (γ-C) ppm.

HRMS (ESI^-) *m/z* calc. for $C_9H_{16}NO_5$ $[M-H]^+$ 218.1027; found 218.1036.

The spectral data are in agreement with the literature.[369]

N-(*tert*-butoxycarbonyl)-*O*-(4-nitrobenzyl)-L-allothreonine (236)

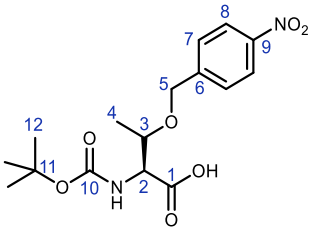

236

Following a modified procedure by M. Khan,[4] NaH (60% suspension in mineral oil; 46 mg, 1.15 mmol) was added portion-wise at -10 °C to a stirring solution of Boc-L-threonine (**235**) (100 mg, 0.46 mmol) in DMF (4 mL) and stirred for 2 h under argon. 4-nitrobenzyl bromide (0.15 g, 0.69 mmol) was added to this portion-wise and the reaction mixture was stirred at rt for 4 h. After this time TLC analysis (70% EtOAc/hexane) showed partial consumption of the starting material (R_F = 0.1) and formation of a product (R_F = 0.9); analysis in 30% EtOAc/hexane confirmed consumption of the starting material (R_F = 0.0) and the formation of a product (R_F = 0.3) The reaction mixture was quenched with ice cold water and washed with Et_2O (2 x 5 mL). The separated aqueous layer was acidified using citric acid (10% aq.) to pH 2 and extracted with EtOAc (2 x 5 mL). The combined organic layers were washed with water (5 x 10 mL) and then dried over Na_2SO_4, filtered and concentrated under reduced pressure. The crude residue was purified by flash column chromatography (30% EtOAc/hexane) to yield **236** (94 mg, 0.27 mmol, 58%) as a white powder.

^{1}H NMR (400 MHz, $CDCl_3$) δ_H 8.19 (d, J_{H8H7} 8.6 Hz, 2H, H8), 7.52 (d, J_{H7H8} 8.6 Hz, 2H, H7), 5.46 (d, J_{NHH2} 9.0 Hz, 1H, NH), 5.29 (dd, J 25.2 13.6 Hz, 2H, H5), 4.28 – 4.42 (m, 2H, H2, H3), 1.44 (s, 9H, H12), 1.24 – 1.30 (m, 3H,H4) ppm.

^{13}C NMR (100 MHz, $CDCl_3$) δ_C 171.3 (C1), 156.3 (C10), 147.8 (C9), 142.7 (C6), 128.3 (C8), 123.8 (C7), 80.3 (C11), 67.9 (C3), 65.5 (C5), 58.9 (C2), 28.4 (C12), 20.1 (C4) ppm.

HRMS (ESI^+) *m/z* calc. for $C_9H_{22}N_2NaO_5$ $[M+Na]^+$ 377.1327; found 377.1319.

ν_{max}/cm^{-1} (neat) 3476 (NH), 1703 (CO), 1520 (NO_2).

mp 100-102 °C from EtOAc/hexane

***N*-(((9*H*-fluoren-9-yl)methoxy)carbonyl)-*O*-(4-nitrobenzyl)-L-allothreonine (237)**

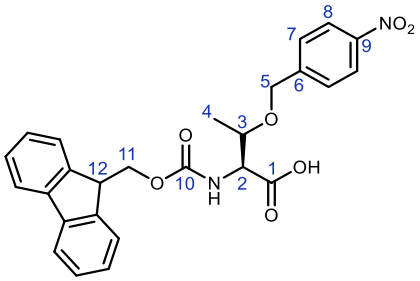

237

TFA (1 mL) was added to a solution of **325** (89 mg, 0.25 mmol) in DCM (3 mL) and stirred at rt for 2 h. The reaction mixture was then concentrated under reduced pressure and resuspended in dioxane (2 mL). Fmoc-OSu (90 mg, 0.27 mmol) in dioxane (5 mL) was added and the mixture was stirred for 2 h at rt. After this time TLC analysis (30% EtOAc/hexane) showed complete consumption of the starting material (R_F = 0.0) and the formation of a product (R_F = 0.3). The reaction mixture was added to water (20 mL), the pH adjusted to 2 with HCl (1 M aq.) and extracted with EtOAc (3 x 10 mL). The combined organic extracts were washed with brine (20 mL), dried over $MgSO_4$, filtered and concentrated under reduced pressure. The crude product was purified by flash column chromatography (30% EtOAc/hexane) to yield **237** (60 mg, 0.13 mmol, 50%) as a white crystalline solid.

^{1}H NMR (400 MHz, $CDCl_3$) δ_H 8.16 (d, J_{H8H7} 8.6 Hz, 2H, H8), 7.78 (d, J 8.0 Hz, 2H, Fmoc ArH), 7.58 – 7.62 (m, 2H, Fmoc ArH), 7.49 (d, J_{H7H8} 8.6 Hz, 2H, H7), 7.41 (t, J 8.0 Hz, 2H, Fmoc ArH), 7.30 (t, J 8.0, 2H, Fmoc ArH), 5.80 (d, J_{NHH2} 9.1 Hz, 1H, NH), 5.23 – 5.33 (m, 2H, H5), 4.40 – 4.48 (m, 4H, H2, H3, H11), 4.22 (t, J_{H12H11} 7.35 Hz, 1H, H12), 1.24 – 1.33 (m, 3H, H4) ppm.

^{13}C NMR (100 MHz, $CDCl_3$) δ_C 170.8 (C1), 156.9 (C10), 147.7 (C9), 143.6 (Fmoc ArC), 142.5 (Fmoc ArC), 141.3 (C6), 128.2 (C8), 127.8 (Fmoc ArC), 127.1 (Fmoc ArC), 125.0 (Fmoc ArC), 123.8 (C7), 120.1 (Fmoc ArC), 67.9 (C3), 67.3 (C11), 65.7 (C5), 59.3 (C2), 47.1 (C12), 20.1 (C4) ppm.

HRMS (ESI$^+$) *m/z* calc. for $C_{26}H_{24}N_2NaO_7$ $[M+Na]^+$ 499.1475; found 499.1477.

ν_{max}/cm^{-1} (neat) 3472 (NH), 1748 (CO), 1685 (CO), 1520 (NO_2), 1389 (NO_2).

mp 112-115 °C (from EtOAc/hexane).

Ethyl (Z)-3-hydroxy-2-(*N*-methylformamido)acrylate (245)

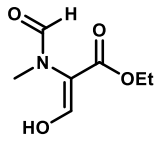

245

Following an adapted procedure by O'Connor *et al.*,[90] NaH (60% dispersion in mineral oil, 2.50 g, 65.0 mmol) was added slowly to a suspension of sarcosine ethyl ester hydrochloride (1.00 g, 6.50 mmol) in ethyl formate (24 mL) at 0 °C, and allowed to stir for 3 h. After this time, a yellow suspension had formed, and the mixture was concentrated and dried under reduced pressure. The mineral oil was removed from the resulting solid by washing with hexane (2 × 30 mL), the hexane decanted, and the remaining solid dried under reduced pressure to yield intermediate **245** which was used without further purification.

Ethyl 2-amino-1-methyl-1H-imidazole-5-carboxylate (247)

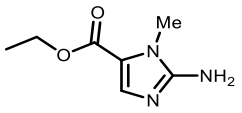

247

EtOH (20 mL) and conc. aq. HCl (4 mL) were added to the solid ethyl (Z)-3-hydroxy-2-(*N*-methylformamido)acrylate (**245**), and the suspension heated under reflux for 2 h. The reaction mixture was filtered while hot, and the resulting colourless solid washed with boiling EtOH (2 × 30 mL). The filtrate was concentrated under reduced pressure to leave an aqueous solution, which was diluted 10% aq. acetic acid (90 mL). The solution was adjusted to pH 4 with sodium acetate (1.04 g, 13 mmol) and cyanamide (0.56 g, 13 mmol) was added. The resulting solution was heated under reflux for 1.5 h. After this time the solution was cooled to ambient temperature and concentrated under reduced pressure to a volume of approximately 10 mL. The pH was adjusted to 8-9 with K_2CO_3, resulting in the formation of a precipitate. The solid was isolated by filtration, washed with aqueous K_2CO_3 solution (1 M, 1 × 10 mL), H_2O (2 × 5 mL), and dried under reduced pressure, to afford **247** (335 mg, 2.08 mmol, 32%) as a yellow solid.

R_F = 0.2 (5% MeOH/DCM).

^{1}H NMR (400 MHz, DMSO-d_6) δ_H 7.40 (s, 1H, ArH), 5.42 (s, 2H, NH_2), 4.25 (q, $J_{CH2,CH3}$ 7.1 Hz, 3H, C<u>H</u>$_2$CH$_3$), 3.66 (s, 3H, Im-C<u>H</u>$_3$), 1.33 (t, $J_{CH3,CH2}$ 7.1 Hz, 3H, CH$_2$C<u>H</u>$_3$) ppm.

^{13}C NMR (100 MHz, $CDCl_3$) δ_C 134.6 (ArC), 60.0 (<u>C</u>H$_2$CH$_3$), 30.6 (Im-<u>C</u>H$_3$), 14.4 (CH$_2$<u>C</u>H$_3$) ppm.

HRMS (ESI$^+$) *m/z* calc. for $C_8H_{12}NO_3$ $[M+H]^+$ 170.0812; found 170.0811.

ν_{max}/cm^{-1} (neat) 3397 (NH), 1648 (CO).

mp 133-135 °C (lit. 130-133 °C)[370] from water.

The spectral data are in agreement with the literature. [90]

Ethyl 1-methyl-2-nitro-1*H*-imidazole-5-carboxylate (241)

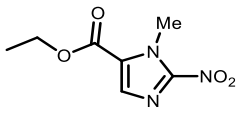

241

A solution of Ethyl (2-amino-1-methyl-imidazol-5-yl)carboxylate **247** (150 mg, 0.90 mmol) in glacial acetic acid (2 mL) was added, dropwise at 0 °C, to a solution of sodium nitrite (621 mg, 9.0 mmol) in water (1 mL). The solution was stirred at 0 °C for 1 h and then warmed to rt for 18 h, after which time TLC analysis (DCM) showed consumption of starting material (R_F = 0.1) and formation of a product (R_F = 0.3). The solution was extracted with DCM (3 x 5 mL). The combined organic fractions were washed with a saturated aqueous solution of sodium sulfite (10 mL), $NaHCO_3$ (10 mL), water (10 mL) and brine (10 mL) then dried over $MgSO_4$, filtered, and concentrated under reduced pressure. The residue was dissolved in DCM (10 mL) and filtered through a silica plug to yield ethyl (1- methyl-2-nitro-imidazol-5-yl)carboxylate **241** (71 mg, 0.37 mmol, 41%) as a white solid.

^{1}H NMR (400 MHz, DMSO-d_6) δ_H 7.78 (s, 1H, ArH), 4.34 (q, J_{CH2CH3} 7.2 Hz, 2H, C<u>H</u>$_2$CH$_3$), 4.18 (s, 3H, Im-C<u>H</u>$_3$), 1.32 (t, $J_{CH3,CH2}$ 7.0 Hz, 3H, CH$_2$C<u>H</u>$_3$) ppm.

^{13}C NMR (100 MHz, DMSO-d_6) δ_C 158.8 (ArC), 133.8 (ArC), 126.1 (ArC), 61.4 (<u>C</u>H$_2$CH$_3$), 35.2 (Im-<u>C</u>H$_3$), 14.0 (CH$_2$<u>C</u>H$_3$) ppm.

HRMS (ESI$^+$) *m/z* calc. for $C_7H_{10}N_3O_4$ $[M+H]^+$ 200.0665; found 200.0666.

ν_{max}/cm^{-1} (neat) 1644 (CO), 1544 (NO_2).

mp 59-61 °C (lit. 56-58 °C)[370] from DCM.

The spectral data are in agreement with the literature.[91]

(1-methyl-2-nitro-1H-imidazol-5-yl)methanol (240)

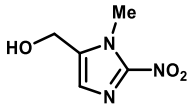

240

A solution of sodium borohydride (33 mg, 0.87 mmol) in anhydrous ethanol (1.3 mL) was added dropwise to a solution of **241** (57 mg, 0.29 mmol) in anhydrous THF (1.7 mL) with vigorous stirring at 0 °C. The reaction was stirred at 0 °C for 3 h then slowly added to a stirred mixture of Et_2O (20 mL) and wet methanol (20 mL) at 0 °C. The resulting solution was stirred at 0 °C for 30 min, after which time TLC analysis (DCM) showed partial consumption of starting material (R_F = 0.3) and formation of a product (R_F = 0.1), then gradually acidified to pH 5 with aqueous 2 M HCl. The solution was concentrated under reduced pressure and the residue was then extracted with EtOAc (5 x 10 mL), the combined organic components were dried over Na_2SO_4, filtered, and concentrated under reduced pressure to yield **240** (57 mg, 0.29 mmol, 32%) as a cream-white solid.

^{1}H NMR (600 MHz, DMSO-d_6) δ_H 7.11 (s, 1H, ArH), 5.49 (t, $J_{OH,CH2}$ 5.3 Hz, 1H, OH), 4.55 (d, $J_{CH2,OH}$ 5.5 Hz, 2H, C$\underline{H}_2$OH), 3.92 (s, 3H, Im-C$\underline{H}_3$) ppm.

^{13}C NMR (100 MHz, $CDCl_3$) δ_C 146.1 (ArC), 139.1 (ArC), 127.0 (ArC), 53.5 ($\underline{C}H_2OH$), 34.6 (Im-$\underline{C}H_3$) ppm.

HRMS (ESI$^+$) *m/z* calc. for $C_5H_7N_3NaO_3$ $[M+Na]^+$ 180.0379; found 180.0374.

ν_{max}/cm^{-1} (neat) 3228br (OH), 1540 (NO_2), 1331 (NO_2).

mp 139-141 °C (lit. 141-143 °C)[315] from EtOAc.

The spectral data are in agreement with the literature.[91]

5-iodo-6-nitroquinoline (255)

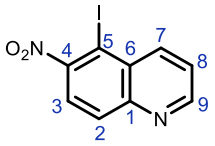

255

Following a procedure reported by Skwarska *et al.*,[91] 5-amino-6-nitroquinoline (200 mg, 1.06 mmol), CuI (202 mg, 1.06 mmol) and sodium nitrite (161 mg, 2.33 mmol) were dissolved in DMSO (10 mL) then heated to 60 °C. HI (67% aq.; 0.55 mL, 5.72 mmol) was added dropwise at 60 °C and heating was continued for 30 min. After this time TLC analysis (30% EtOAc/hexane) showed conversion of starting material (R_F = 0.1) to product (R_F = 0.4). The reaction mixture was cooled to 0 °C and quenched with potassium carbonate (sat. aq.; 20 mL). The quenched reaction mixture was extracted with EtOAc (5 x 20 mL) and the combined organic fractions were washed with brine (80 mL), dried over Na_2SO_4, filtered, and concentrated under reduced pressure. The crude product was purified by flash column chromatography (30% EtOAc/hexane) to yield **255** (106 mg, 0.35 mmol, 33%) as a yellow crystalline solid.

^{1}H NMR (400 MHz, $CDCl_3$) δ_H 9.01 (dd, $^3J_{H9H8}$ 4.2 Hz, $^4J_{H9H7}$ 1.6 Hz, 1H, H_9), 8.67 (ddd, $^3J_{H7H8}$ 8.7 Hz $^4J_{H7H9}$ 1.7 Hz $^5J_{H7H2}$ 0.8 Hz, 1H, H_7), 8.22 (dd, $^3J_{H2H3}$ 9.0 Hz $^5J_{H2H7}$ 0.84 Hz,1H, H_2), 7.93 (d, $^3J_{H3H2}$ 9.0 Hz, 1H, H_3), 7.63 (dd, $^3J_{H8H7}$ 8.7 Hz $^3J_{H8H9}$ 4.2 Hz, 1H, H_8) ppm.

^{13}C NMR (100 MHz, $CDCl_3$) δ_C 153.3 (C_9), 148.5 (C_1), 143.0 (C_7), 131.9 (C_2), 130.8 (C_6), 124.5 (C_8), 124.2 (C_3), 92.8 (C_5) ppm.

HRMS (ESI$^+$) *m/z* calc. for $C_9H_6IN_2O_2$ $[M+Na]^+$ 300.9476; found 300.9468.

ν_{max}/cm^{-1} (neat) 1560 (NO_2).

mp 162-164 °C (lit. 160 – 162 °C)[326] from EtOAc/hexane.

The spectral data are in agreement with the literature.[326]

5-bromo-6-nitroquinoline (251)

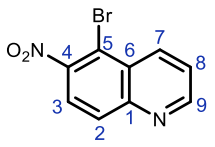

251

Following a procedure reported by Son *et al.*,[371] $NaNO_2$ (84 mg, 1.21 mmol, 1.14 eq) dissolved in H_2O (3 mL) was added to a solution of 5-amino-6-nitroquinoline (200 mg, 1.06 mmol) in HBr (48% aq.; 2 mL) and cooled to -10 °C. The mixture was stirred at -10 °C for 10 min and CuBr (176 mg, 1.23 mmol) dissolved in H_2O (4 mL) and HBr (48% aq.; 1.3 mL) was added. The mixture was heated at 60 °C for 30 min, after which time TLC analysis (30% EtOAc/hexane) showed conversion of starting material (R_F = 0.1) to product (R_F = 0.3). The mixture was poured into ice-water, basified with NaOH (4 M aq.) to pH 10, and extracted with EtOAc (5 x 50 mL). The combined organic fractions were washed with brine (200 mL), dried over $MgSO_4$, filtered and concentrated under reduced pressure. The crude product was purified by flash column chromatography (30% EtOAc/hexane) to yield **251** (40 mg, 0.16 mmol, 15%) as a white powder.

^{1}H NMR (400 MHz, $CDCl_3$) δ_H 9.07 (d, J_{H9H8} 4.3 Hz, 1H, H_9), 8.78 (ddd, $^3J_{H7H8}$ 8.7 Hz $^4J_{H7H9}$ 1.6 Hz $^5J_{H7H2}$ 0.8 Hz, 1H, H_7), 8.23 (dd, $^3J_{H2H3}$ 9.0 Hz $^5J_{H2H7}$ 0.8 Hz,1H, H_2), 8.00 (d, J_{H3H2} 9.1 Hz, 1H, H_3), 7.68 (dd, $^3J_{H8H7}$ 8.7 $^3J_{H8H9}$ 4.2 Hz, 1H, H_8) ppm.

^{13}C NMR (100 MHz, $CDCl_3$) δ_C 153.1 (C_9), 148.6 (C_1), 137.5 (C_7), 130.7 (C_2), 130.8 (C_6), 124.3 (C_3), 123.9 (C_8), 115.2 (C_5) ppm.

HRMS (ESI$^+$) *m/z* calc. for $C_9H_6IN_2O_2$ $[M+Na]^+$ 252.9614; found 252.9607.

ν_{max}/cm^{-1} (neat) 1514 (NO_2).

mp 123 – 125 °C (lit. 184 – 185 °C)[372] from EtOAc/hexane.

The spectral data are in agreement with the literature.[91]

6-nitroquinoline-5-carbaldehyde (254) (attempted)

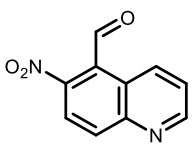

254

5-Iodo-6-nitroquinoline (90 mg, 0.30 mmol) in anhydrous THF (4 mL) was cooled to -78 °C. A 1.9 M solution of phenyl lithium (0.175 mL, 0.33 mmol) in Bu_2O was added to the solution dropwise, and the reaction stirred for 30 min. Ethyl formate (0.12 mL, 1.50 mmol) was added dropwise at -78 °C, the reaction left to gradually warm to rt, and stirred overnight. The reaction mixture was then concentrated under reduced pressure and purified by flash column chromatography (50% EtOAc/hexane), which did not isolate the desired product.

(6-nitroquinolin-5-yl)methanol (250) (attempted)

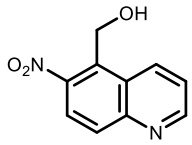

250

5-Iodo-6-nitroquinoline (100 mg, 0.33 mmol) was dissolved in anhydrous THF (2.5 mL) and cooled to -40 °C. A 2.0 M solution of phenyl magnesium chloride (0.20 mL, 0.37 mmol) in THF was added dropwise and the solution was stirred for 10 min. Paraformaldehyde (40 mg, 1.3 mmol) was added to the solution and the reaction mixture was warmed to rt then heated to 40 °C for 18 h. The reaction mixture was cooled to rt, quenched with water (15 mL) and extracted with EtOAc (3 x 15 mL). The combined organic fractions were washed with brine (40 mL), dried over Na_2SO_4, filtered, and concentrated under reduced pressure. The crude product was then purified by flash column chromatography, (50% EtOAc/hexane) which did not isolate the desired product.

Chapter 8

References

Chapter 8: References

1. A. Warnock, One million lives saved: How our research milestones mean more moments for people with cancer, https://news.cancerresearchuk.org/2023/09/01/one-million-lives-saved/, (accessed 24 July, 2024).
2. F. Bray, M. Laversanne, E. Weiderpass and I. Soerjomataram, The ever-increasing importance of cancer as a leading cause of premature death worldwide, *Cancer*, 2021, **127**, 3029-3030.

3. S. Chen, Z. Cao, K. Prettner, M. Kuhn, J. Yang, L. Jiao, Z. Wang, W. Li, P. Geldsetzer, T. Bärnighausen, D. E. Bloom and C. Wang, Estimates and Projections of the Global Economic Cost of 29 Cancers in 204 Countries and Territories From 2020 to 2050, *JAMA Oncology*, 2023, **9**, 465-472.
4. F. Guida, R. Kidman, J. Ferlay, J. Schüz, I. Soerjomataram, B. Kithaka, O. Ginsburg, R. B. Mailhot Vega, M. Galukande, G. Parham, S. Vaccarella, K. Canfell, A. M. Ilbawi, B. O. Anderson, F. Bray, I. dos-Santos-Silva and V. McCormack, Global and regional estimates of orphans attributed to maternal cancer mortality in 2020, *Nature Medicine*, 2022, **28**, 2563-2572.
5. I. Soerjomataram, C. Cabasag, A. Bardot, M. M. Fidler-Benaoudia, A. Miranda-Filho, J. Ferlay, D. M. Parkin, R. Ranganathan, M. Piñeros, A. Znaor, L. Mery, Y. W. Joko-Fru, R. Dikshit, R. Sankaranarayanan, R. Swaminathan and F. Bray, Cancer survival in Africa, central and south America, and Asia (SURVCAN-3): a population-based benchmarking study in 32 countries, *The Lancet Oncology*, 2023, **24**, 22-32.
6. C. Duggan, D. Trapani, A. M. Ilbawi, E. Fidarova, M. Laversanne, G. Curigliano, F. Bray and B. O. Anderson, National health system characteristics, breast cancer stage at diagnosis, and breast cancer mortality: a population-based analysis, *The Lancet Oncology*, 2021, **22**, 1632-1642.
7. L. Falzone, S. Salomone and M. Libra, Evolution of Cancer Pharmacological Treatments at the Turn of the Third Millennium, *Frontiers in Pharmacology*, 2018, **9**.
8. V. Malhotra and M. C. Perry, Classical Chemotherapy: Mechanisms, Toxicities and the Therapeutc Window, *Cancer Biology & Therapy*, 2003, **2**, 1-3.
9. O. Tacar, P. Sriamornsak and C. R. Dass, Doxorubicin: an update on anticancer molecular action, toxicity and novel drug delivery systems, *Journal of Pharmacy and Pharmacology*, 2013, **65**, 157-170.
10. M. Flynn, K. A. Heale and L. Alisaraie, Mechanism of Off-Target Interactions and Toxicity of Tamoxifen and Its Metabolites, *Chemical Research in Toxicology*, 2017, **30**, 1492-1507.
11. Z. N. Al-Mahayri, M. M. AlAhmad and B. R. Ali, Current opinion on the pharmacogenomics of paclitaxel-induced toxicity, *Expert Opinion on Drug Metabolism & Toxicology*, 2021, **17**, 785-801.
12. K. M. Hamed, I. M. Dighriri, A. F. Baomar, B. T. Alharthy, F. E. Alenazi, G. H. Alali, R. H. Alenazy, N. T. Alhumaidi, D. H. Alhulayfi, Y. B. Alotaibi, S. S. Alhumaidan, Z. A. Alhaddad, A. A. Humadi, S. A. Alzahrani and R. H. Alobaid, Overview of Methotrexate Toxicity: A Comprehensive Literature Review, *Cureus*, 2022, **14**, e29518.
13. J. Rautio, N. A. Meanwell, L. Di and M. J. Hageman, The expanding role of prodrugs in contemporary drug design and development, *Nature Reviews Drug Discovery*, 2018, **17**, 559-587.
14. A. Najjar, A. Najjar and R. Karaman, Newly Developed Prodrugs and Prodrugs in Development; an Insight of the Recent Years, *Molecules*, 2020, **25**.
15. V. Stella, R. Borchardt, M. Hageman, R. Oliyai, H. Maag and J. Tilley, *Prodrugs: Challenges and Rewards*, Springer New York, 2007.
16. K. M. Huttunen, H. Raunio and J. Rautio, Prodrugs—from Serendipity to Rational Design, *Pharmacological Reviews*, 2011, **63**, 750.
17. P. J. Davis, Hydrolysis in Drug and Prodrug Metabolism: Chemistry, Biochemistry, and Enzymology By Bernard Testa (University of Lausanne, Switzerland) and Joachim M. Mayer (deceased). Verlag Helvetica Chimica Acta: Zurich and Wiley-VCH GmbH

& Co. KGaA: Weinheim, Germany. 2003. xx + 780 pp. $215.00. ISBN 3-906390-25-X, *Journal of the American Chemical Society*, 2004, **126**, 16684-16684.
18. B. Testa, Prodrug research: futile or fertile?, *Biochemical Pharmacology*, 2004, **68**, 2097-2106.
19. X. Zhang, X. Li, Q. You and X. Zhang, Prodrug strategy for cancer cell-specific targeting: A recent overview, *European Journal of Medicinal Chemistry*, 2017, **139**, 542-563.
20. H.-H. Han, H.-M. Wang, P. Jangili, M. Li, L. Wu, Y. Zang, A. C. Sedgwick, J. Li, X.-P. He, T. D. James and J. S. Kim, The design of small-molecule prodrugs and activatable phototherapeutics for cancer therapy, *Chemical Society Reviews*, 2023, **52**, 879-920.
21. S. K. Sharma and K. D. Bagshawe, Antibody Directed Enzyme Prodrug Therapy (ADEPT): Trials and tribulations, *Advanced Drug Delivery Reviews*, 2017, **118**, 2-7.
22. R. Duncan and M. J. Vicent, Polymer therapeutics-prospects for 21st century: The end of the beginning, *Advanced Drug Delivery Reviews*, 2013, **65**, 60-70.
23. C. F. Riber and A. N. Zelikin, Recent advances in macromolecular prodrugs, *Current Opinion in Colloid & Interface Science*, 2017, **31**, 1-9.
24. J. R. McCombs and S. C. Owen, Antibody drug conjugates: design and selection of linker, payload and conjugation chemistry, *Aaps j*, 2015, **17**, 339-351.
25. G. Casi and D. Neri, Antibody–Drug Conjugates and Small Molecule–Drug Conjugates: Opportunities and Challenges for the Development of Selective Anticancer Cytotoxic Agents, *Journal of Medicinal Chemistry*, 2015, **58**, 8751-8761.
26. H. C. Hang, C. Yu, D. L. Kato and C. R. Bertozzi, A metabolic labeling approach toward proteomic analysis of mucin-type O-linked glycosylation, *Proceedings of the National Academy of Sciences*, 2003, **100**, 14846-14851.
27. N. J. Agard, J. A. Prescher and C. R. Bertozzi, A Strain-Promoted [3 + 2] Azide–Alkyne Cycloaddition for Covalent Modification of Biomolecules in Living Systems, *Journal of the American Chemical Society*, 2004, **126**, 15046-15047.
28. P. Thirumurugan, D. Matosiuk and K. Jozwiak, Click Chemistry for Drug Development and Diverse Chemical–Biology Applications, *Chemical Reviews*, 2013, **113**, 4905-4979.
29. R. Mahato, W. Tai and K. Cheng, Prodrugs for improving tumor targetability and efficiency, *Adv Drug Deliv Rev*, 2011, **63**, 659-670.
30. J. Li and P. R. Chen, Development and application of bond cleavage reactions in bioorthogonal chemistry, *Nature Chemical Biology*, 2016, **12**, 129-137.
31. S. S. Matikonda, D. L. Orsi, V. Staudacher, I. A. Jenkins, F. Fiedler, J. Chen and A. B. Gamble, Bioorthogonal prodrug activation driven by a strain-promoted 1,3-dipolar cycloaddition, *Chemical Science*, 2015, **6**, 1212-1218.
32. H. Lu, R. A. Forbes and A. Verma, Hypoxia-inducible Factor 1 Activation by Aerobic Glycolysis Implicates the Warburg Effect in Carcinogenesis*, *Journal of Biological Chemistry*, 2002, **277**, 23111-23115.
33. F. Kratz, S. Azab, R. Zeisig, I. Fichtner and A. Warnecke, Evaluation of combination therapy schedules of doxorubicin and an acid-sensitive albumin-binding prodrug of doxorubicin in the MIA PaCa-2 pancreatic xenograft model, *International Journal of Pharmaceutics*, 2013, **441**, 499-506.
34. Y. Jin, Y. Huang, H. Yang, G. Liu and R. Zhao, A peptide-based pH-sensitive drug delivery system for targeted ablation of cancer cells, *Chemical Communications*, 2015, **51**, 14454-14457.

35. M. Diehn, R. W. Cho, N. A. Lobo, T. Kalisky, M. J. Dorie, A. N. Kulp, D. Qian, J. S. Lam, L. E. Ailles, M. Wong, B. Joshua, M. J. Kaplan, I. Wapnir, F. M. Dirbas, G. Somlo, C. Garberoglio, B. Paz, J. Shen, S. K. Lau, S. R. Quake, J. M. Brown, I. L. Weissman and M. F. Clarke, Association of reactive oxygen species levels and radioresistance in cancer stem cells, *Nature*, 2009, **458**, 780-783.
36. H. Nakamura and K. Takada, Reactive oxygen species in cancer: Current findings and future directions, *Cancer Sci*, 2021, **112**, 3945-3952.
37. in *Essentials of Glycobiology*, eds. A. Varki, R. D. Cummings, J. D. Esko, H. H. Freeze, P. Stanley, C. R. Bertozzi, G. W. Hart and M. E. Etzler, Cold Spring Harbor Laboratory Press

Copyright © 2009, The Consortium of Glycobiology Editors, La Jolla, California., Cold Spring Harbor (NY), 2009.

38. G. A. Ellis, M. J. Palte and R. T. Raines, Boronate-Mediated Biologic Delivery, *Journal of the American Chemical Society*, 2012, **134**, 3631-3634.
39. L. Wang, S. Xie, L. Ma, Y. Chen and W. Lu, 10-Boronic acid substituted camptothecin as prodrug of SN-38, *European Journal of Medicinal Chemistry*, 2016, **116**, 84-89.
40. C. Perez, J.-P. Monserrat, Y. Chen and S. M. Cohen, Exploring hydrogen peroxide responsive thiazolidinone-based prodrugs, *Chemical Communications*, 2015, **51**, 7116-7119.
41. C. Lin, H. He, Y. Zhang, M. Xu, F. Tian, L. Li and Y. Wang, Acetaldehyde-modified-cystine functionalized Zr-MOFs for pH/GSH dual-responsive drug delivery and selective visualization of GSH in living cells, *RSC Advances*, 2020, **10**, 3084-3091.
42. A. Bansal and M. C. Simon, Glutathione metabolism in cancer progression and treatment resistance, *J Cell Biol*, 2018, **217**, 2291-2298.
43. S. Santra, C. Kaittanis, O. J. Santiesteban and J. M. Perez, Cell-Specific, Activatable, and Theranostic Prodrug for Dual-Targeted Cancer Imaging and Therapy, *Journal of the American Chemical Society*, 2011, **133**, 16680-16688.
44. H. Chen, J. Liu, H. Ü. Kaniskan, W. Wei and J. Jin, Folate-Guided Protein Degradation by Immunomodulatory Imide Drug-Based Molecular Glues and Proteolysis Targeting Chimeras, *Journal of Medicinal Chemistry*, 2021, **64**, 12273-12285.
45. M. Scaranti, E. Cojocaru, S. Banerjee and U. Banerji, Exploiting the folate receptor α in oncology, *Nature Reviews Clinical Oncology*, 2020, **17**, 349-359.
46. M. Vizovisek, D. Ristanovic, S. Menghini, M. G. Christiansen and S. Schuerle, The Tumor Proteolytic Landscape: A Challenging Frontier in Cancer Diagnosis and Therapy, *Int J Mol Sci*, 2021, **22**.
47. D. S. Vinay, E. P. Ryan, G. Pawelec, W. H. Talib, J. Stagg, E. Elkord, T. Lichtor, W. K. Decker, R. L. Whelan, H. M. C. S. Kumara, E. Signori, K. Honoki, A. G. Georgakilas, A. Amin, W. G. Helferich, C. S. Boosani, G. Guha, M. R. Ciriolo, S. Chen, S. I. Mohammed, A. S. Azmi, W. N. Keith, A. Bilsland, D. Bhakta, D. Halicka, H. Fujii, K. Aquilano, S. S. Ashraf, S. Nowsheen, X. Yang, B. K. Choi and B. S. Kwon, Immune evasion in cancer: Mechanistic basis and therapeutic strategies, *Seminars in Cancer Biology*, 2015, **35**, S185-S198.
48. M. Olsson and B. Zhivotovsky, Caspases and cancer, *Cell Death & Differentiation*, 2011, **18**, 1441-1449.
49. D. F. Quail and J. A. Joyce, Microenvironmental regulation of tumor progression and metastasis, *Nature Medicine*, 2013, **19**, 1423-1437.

50. W. Du, X. Xia, F. Hu and J. Yu, Extracellular matrix remodeling in the tumor immunity, *Frontiers in Immunology*, 2024, **14**.
51. J. Winkler, A. Abisoye-Ogunniyan, K. J. Metcalf and Z. Werb, Concepts of extracellular matrix remodelling in tumour progression and metastasis, *Nature Communications*, 2020, **11**, 5120.
52. M. Egeblad and Z. Werb, New functions for the matrix metalloproteinases in cancer progression, *Nature Reviews Cancer*, 2002, **2**, 161-174.
53. J. F. Woessner and H. Nagase, Matrix Metalloproteinases and TlMPs, *Journal*, 2000, DOI: 10.1093/oso/9780198502685.002.0001, 0.
54. C. F. Albright, N. Graciani, W. Han, E. Yue, R. Stein, Z. Lai, M. Diamond, R. Dowling, L. Grimminger, S.-Y. Zhang, D. Behrens, A. Musselman, R. Bruckner, M. Zhang, X. Jiang, D. Hu, A. Higley, S. DiMeo, M. Rafalski, S. Mandlekar, B. Car, S. Yeleswaram, A. Stern, R. A. Copeland, A. Combs, S. P. Seitz, G. L. Trainor, R. Taub, P. Huang and A. Oliff, Matrix metalloproteinase–activated doxorubicin prodrugs inhibit HT1080 xenograft growth better than doxorubicin with less toxicity, *Molecular Cancer Therapeutics*, 2005, **4**, 751-760.
55. Z. Hu, X. Jiang, C. F. Albright, N. Graciani, E. Yue, M. Zhang, S.-Y. Zhang, R. Bruckner, M. Diamond, R. Dowling, M. Rafalski, S. Yeleswaram, G. L. Trainor, S. P. Seitz and W. Han, Discovery of matrix metalloproteases selective and activated peptide–doxorubicin prodrugs as anti-tumor agents, *Bioorganic & Medicinal Chemistry Letters*, 2010, **20**, 853-856.
56. A. Sharma, M.-G. Lee, H. Shi, M. Won, J. F. Arambula, J. L. Sessler, J. Y. Lee, S.-G. Chi and J. S. Kim, Overcoming Drug Resistance by Targeting Cancer Bioenergetics with an Activatable Prodrug, *Chem*, 2018, **4**, 2370-2383.
57. M. G. Vander Heiden, L. C. Cantley and C. B. Thompson, Understanding the Warburg Effect: The Metabolic Requirements of Cell Proliferation, *Science*, 2009, **324**, 1029-1033.
58. R. Henning, pH gradient across the lysosomal membrane generated by selective cation permeability and donnan equilibrium, *Biochimica et Biophysica Acta (BBA) - Biomembranes*, 1975, **401**, 307-316.
59. C. S. Gondi and J. S. Rao, Cathepsin B as a cancer target, *Expert Opinion on Therapeutic Targets*, 2013, **17**, 281-291.
60. V. S. Egorova, E. P. Kolesova, M. Lopus, N. Yan, A. Parodi and A. A. Zamyatnin, Jr., Smart Delivery Systems Responsive to Cathepsin B Activity for Cancer Treatment, *Pharmaceutics*, 2023, **15**.
61. Y. Li, T. Mei, S. Han, T. Han, Y. Sun, H. Zhang and F. An, Cathepsin B-responsive nanodrug delivery systems for precise diagnosis and targeted therapy of malignant tumors, *Chinese Chemical Letters*, 2020, **31**, 3027-3040.
62. M. Kovář, J. Strohalm, T. Etrych, K. Ulbrich and B. Říhová, Star structure of antibody-targeted HPMA copolymer-bound doxorubicin: a novel type of polymeric conjugate for targeted drug delivery with potent antitumor effect, *Bioconjugate chemistry*, 2002, **13**, 206-215.
63. A. J. Versluis, E. T. Rump, P. C. Rensen, T. J. Van Berkel and M. K. Bijsterbosch, Synthesis of a lipophilic daunoruhicin derivative and its incorporation into lipidic carriers developed for LDL receptor-mediated tumor therapy, *Pharmaceutical research*, 1998, **15**, 531-537.

64. G. M. Dubowchik, R. A. Firestone, L. Padilla, D. Willner, S. J. Hofstead, K. Mosure, J. O. Knipe, S. J. Lasch and P. A. Trail, Cathepsin B-Labile Dipeptide Linkers for Lysosomal Release of Doxorubicin from Internalizing Immunoconjugates: Model Studies of Enzymatic Drug Release and Antigen-Specific In Vitro Anticancer Activity, *Bioconjugate Chemistry*, 2002, **13**, 855-869.
65. L. Dunsmore, C. D. Navo, J. Becher, E. G. de Montes, A. Guerreiro, E. Hoyt, L. Brown, V. Zelenay, S. Mikutis, J. Cooper, I. Barbieri, S. Lawrinowitz, E. Siouve, E. Martin, P. R. Ruivo, T. Rodrigues, F. P. da Cruz, O. Werz, G. Vassiliou, P. Ravn, G. Jiménez-Osés and G. J. L. Bernardes, Controlled masking and targeted release of redox-cycling ortho-quinones via a C–C bond-cleaving 1,6-elimination, *Nature Chemistry*, 2022, **14**, 754-765.
66. M. Ough, A. Lewis, E. A. Bey, J. Gao, J. M. Ritchie, W. Bornmann, D. A. Boothman, L. W. Oberley and J. J. Cullen, Efficacy of beta-lapachone in pancreatic cancer treatment: Exploiting the novel, therapeutic target NQO1, *Cancer Biology & Therapy*, 2005, **4**, 102-109.
67. J. L. Bolton and T. Dunlap, Formation and Biological Targets of Quinones: Cytotoxic versus Cytoprotective Effects, *Chemical Research in Toxicology*, 2017, **30**, 13-37.
68. J. J. Pink, S. M. Planchon, C. Tagliarino, M. E. Varnes, D. Siegel and D. A. Boothman, NAD(P)H:Quinone Oxidoreductase Activity Is the Principal Determinant of β-Lapachone Cytotoxicity *, *Journal of Biological Chemistry*, 2000, **275**, 5416-5424.
69. D. E. Gerber, M. S. Beg, F. Fattah, A. E. Frankel, O. Fatunde, Y. Arriaga, J. E. Dowell, A. Bisen, R. D. Leff, C. C. Meek, W. C. Putnam, R. R. Kallem, I. Subramaniyan, Y. Dong, J. Bolluyt, V. Sarode, X. Luo, Y. Xie, B. Schwartz and D. A. Boothman, Phase 1 study of ARQ 761, a β-lapachone analogue that promotes NQO1-mediated programmed cancer cell necrosis, *British Journal of Cancer*, 2018, **119**, 928-936.
70. A. Corti, M. Franzini, A. Paolicchi and A. Pompella, Gamma-glutamyltransferase of cancer cells at the crossroads of tumor progression, drug resistance and drug targeting, *Anticancer Res*, 2010, **30**, 1169-1181.
71. M. H. Hanigan, in *Advances in Cancer Research*, eds. D. M. Townsend and K. D. Tew, Academic Press, 2014, vol. 122, pp. 103-141.
72. M. Chiba, Y. Ichikawa, M. Kamiya, T. Komatsu, T. Ueno, K. Hanaoka, T. Nagano, N. Lange and Y. Urano, An Activatable Photosensitizer Targeted to γ-Glutamyltranspeptidase, *Angew Chem Int Ed Engl*, 2017, **56**, 10418-10422.
73. L. Wang, Z. Liu, S. He, S. He and Y. Wang, Fighting against drug-resistant tumors by the inhibition of γ-glutamyl transferase with supramolecular platinum prodrug nano-assemblies, *Journal of Materials Chemistry B*, 2021, **9**, 4587-4595.
74. S. Bakthavatsalam, M. L. Sleeper, A. Dharani, D. J. George, T. Zhang and K. J. Franz, Leveraging γ-Glutamyl Transferase To Direct Cytotoxicity of Copper Dithiocarbamates against Prostate Cancer Cells, *Angewandte Chemie International Edition*, 2018, **57**, 12780-12784.
75. R. H. Thomlinson and L. H. Gray, *British Journal of Cancer*, 1955, **9**, 539-549.
76. J. Folkman, *Journal of the National Cancer Institute*, 1990, **82**, 4-7.
77. K. Ruan, G. Song and G. Ouyang, *J. Cell Biochem.*, 2009, **107**, 1053-1062.
78. B. Muz, P. de la Puente, F. Azab and A. K. Azab, *Hypoxia*, 2015, **3**, 83-92.
79. J. Zhang, H.-W. Liu, X.-X. Hu, J. Li, L.-H. Liang, X.-B. Zhang and W. Tan, Efficient Two-Photon Fluorescent Probe for Nitroreductase Detection and Hypoxia Imaging in Tumor Cells and Tissues, *Analytical Chemistry*, 2015, **87**, 11832-11839.

80. R. J. Riley and P. Workman, DT-diaphorase and cancer chemotherapy, *Biochemical Pharmacology*, 1992, **43**, 1657-1669.
81. M. I. Uddin, S. M. Evans, J. R. Craft, L. J. Marnett, M. J. Uddin and A. Jayagopal, Applications of Azo-Based Probes for Imaging Retinal Hypoxia, *ACS Medicinal Chemistry Letters*, 2015, **6**, 445-449.
82. Z. Zhang, K. Tanabe, H. Hatta and S.-i. Nishimoto, Bioreduction activated prodrugs of camptothecin: molecular design, synthesis, activation mechanism and hypoxia selective cytotoxicity, *Organic & Biomolecular Chemistry*, 2005, **3**, 1905-1910.
83. A. Monge, J. A. Palop, A. L. de Cerain, V. Senador, F. J. Martinez, Y. Sainz, S. Narro, E. Garcia and C. de Miguel, Hypoxia-Selective Agents Derived from Quinoxaline 1,4-Di-N-oxides, *Journal of Medicinal Chemistry*, 1995, **38**, 1786-1792.
84. Y. Zhou, M. Maiti, A. Sharma, M. Won, L. Yu, L. X. Miao, J. Shin, A. Podder, K. N. Bobba, J. Han, S. Bhuniya and J. S. Kim, Azo-based small molecular hypoxia responsive theranostic for tumor-specific imaging and therapy, *Journal of Controlled Release*, 2018, **288**, 14-22.
85. M. V. Papadopoulou and W. D. Bloomer, NLCQ-1 (NSC 709257): Exploiting Hypoxia with a Weak DNA-Intercalating Bioreductive Drug, *Clinical Cancer Research*, 2003, **9**, 5714-5720.
86. F. W. Hunter, B. G. Wouters and W. R. Wilson, Hypoxia-activated prodrugs: paths forward in the era of personalised medicine, *British Journal of Cancer*, 2016, **114**, 1071-1077.
87. Y. Li, Y. Sun, J. Li, Q. Su, W. Yuan, Y. Dai, C. Han, Q. Wang, W. Feng and F. Li, Ultrasensitive Near-Infrared Fluorescence-Enhanced Probe for in Vivo Nitroreductase Imaging, *Journal of the American Chemical Society*, 2015, **137**, 6407-6416.
88. K. Okuda, Y. Okabe, T. Kadonosono, T. Ueno, B. G. Youssif, S. Kizaka-Kondoh and H. Nagasawa, 2-Nitroimidazole-tricarbocyanine conjugate as a near-infrared fluorescent probe for in vivo imaging of tumor hypoxia, *Bioconjug Chem*, 2012, **23**, 324-329.
89. P. Wardman, *Environmental Health Perspectives*, 1985, **64**, 309-320.
90. L. J. O'Connor, C. Cazares-Körner, J. Saha, C. N. G. Evans, M. R. L. Stratford, E. M. Hammond and S. J. Conway, Efficient synthesis of 2-nitroimidazole derivatives and the bioreductive clinical candidate Evofosfamide (TH-302), *Organic Chemistry Frontiers*, 2015, **2**, 1026-1029.
91. A. Skwarska, E. D. D. Calder, D. Sneddon, H. Bolland, M. L. Odyniec, I. N. Mistry, J. Martin, L. K. Folkes, S. J. Conway and E. M. Hammond, Development and pre-clinical testing of a novel hypoxia-activated KDAC inhibitor, *Cell Chemical Biology*, 2021, **28**, 1258-1270.e1213.
92. S. L. Collins, J. Saha, L. C. Bouchez, E. M. Hammond and S. J. Conway, Hypoxia-Activated, Small-Molecule-Induced Gene Expression, *ACS Chemical Biology*, 2018, **13**, 3354-3360.
93. B. L. Cantarel, P. M. Coutinho, C. Rancurel, T. Bernard, V. Lombard and B. Henrissat, The Carbohydrate-Active EnZymes database (CAZy): an expert resource for Glycogenomics, *Nucleic Acids Res*, 2009, **37**, D233-238.
94. R. Wolfenden, X. Lu and G. Young, Spontaneous Hydrolysis of Glycosides, *Journal of the American Chemical Society*, 1998, **120**, 6814-6815.
95. D. E. Koshland Jr, STEREOCHEMISTRY AND THE MECHANISM OF ENZYMATIC REACTIONS, *Biological Reviews*, 1953, **28**, 416-436.

96. J. Ati, P. Lafite and R. Daniellou, Enzymatic synthesis of glycosides: from natural O- and N-glycosides to rare C- and S-glycosides, *Beilstein Journal of Organic Chemistry*, 2017, **13**, 1857-1865.
97. G. Davies and B. Henrissat, Structures and mechanisms of glycosyl hydrolases, *Structure*, 1995, **3**, 853-859.
98. A. Varki and J. Marth, Oligosaccharides in vertebrate development, *Seminars in Developmental Biology*, 1995, **6**, 127-138.
99. Y. Kim, H. Li, J. Choi, J. Boo, H. Jo, J. Y. Hyun and I. Shin, Glycosidase-targeting small molecules for biological and therapeutic applications, *Chemical Society Reviews*, 2023, **52**, 7036-7070.
100. G. Speciale, A. J. Thompson, G. J. Davies and S. J. Williams, Dissecting conformational contributions to glycosidase catalysis and inhibition, *Current Opinion in Structural Biology*, 2014, **28**, 1-13.
101. H. Elferink, J. P. J. Bruekers, G. H. Veeneman and T. J. Boltje, A comprehensive overview of substrate specificity of glycoside hydrolases and transporters in the small intestine : "A gut feeling", *Cell Mol Life Sci*, 2020, **77**, 4799-4826.
102. E. M. Wright, M. n. G. Martín and E. Turk, Intestinal absorption in health and disease—sugars, *Best Practice & Research Clinical Gastroenterology*, 2003, **17**, 943-956.
103. D. Malm, H. M. F. R. Stensland and Ø. Nilssen, in *Lysosomal Storage Disorders*, 2022, DOI: https://doi.org/10.1002/9781119697312.ch18, pp. 203-210.
104. J. C. Michalski and A. Klein, Glycoprotein lysosomal storage disorders: alpha- and beta-mannosidosis, fucosidosis and alpha-N-acetylgalactosaminidase deficiency, *Biochim Biophys Acta*, 1999, **1455**, 69-84.
105. H. H. Freeze, H. Schachter and T. Kinoshita, Genetic Disorders of Glycosylation, *Journal*, 2015.
106. V. La Cognata, M. Guarnaccia, A. Polizzi, M. Ruggieri and S. Cavallaro, Highlights on Genomics Applications for Lysosomal Storage Diseases, *Journal*, 2020, **9**, E1902.
107. H. Martin, L. R. Lázaro, T. Gunnlaugsson and E. M. Scanlan, Glycosidase activated prodrugs for targeted cancer therapy, *Chemical Society Reviews*, 2022, **51**, 9694-9716.
108. B. N. Vajaria and P. S. Patel, Glycosylation: a hallmark of cancer?, *Glycoconj J*, 2017, **34**, 147-156.
109. E. Gil-Martín, S. Gil-Seijo, C. Nieto-Novoa and A. Fernández-Briera, Elevation of acid glycosidase activities in thyroid and gastric tumours, *The International Journal of Biochemistry & Cell Biology*, 1996, **28**, 651-657.
110. E. C. Calvaresi and P. J. Hergenrother, Glucose conjugation for the specific targeting and treatment of cancer, *Chemical Science*, 2013, **4**, 2319-2333.
111. J. F. Fisher, A. W. Harrison, G. L. Bundy, K. F. Wilkinson, B. D. Rush and M. J. Ruwart, Peptide to glycopeptide: glycosylated oligopeptide renin inhibitors with attenuated in vivo clearance properties, *Journal of Medicinal Chemistry*, 1991, **34**, 3140-3143.
112. Y. Henin, C. Gouyette, O. Schwartz, J. C. Debouzy, J. M. Neumann and T. Huynh Dinh, Lipophilic glycosyl phosphotriester derivatives of AZT: synthesis, NMR transmembrane transport study and antiviral activity, *Journal of Medicinal Chemistry*, 1991, **34**, 1830-1837.
113. A. Namane, C. Gouyette, M. P. Fillion, G. Fillion and T. Huynh Dinh, Improved brain delivery of AZT using a glycosyl phosphotriester prodrug, *Journal of Medicinal Chemistry*, 1992, **35**, 3039-3044.

114. S. G. Patching, Glucose Transporters at the Blood-Brain Barrier: Function, Regulation and Gateways for Drug Delivery, *Molecular Neurobiology*, 2017, **54**, 1046-1077.
115. T. Halmos, M. Santarromana, K. Antonakis and D. Scherman, Synthesis of glucose-chlorambucil derivatives and their recognition by the human GLUT1 glucose transporter, *European Journal of Pharmacology*, 1996, **318**, 477-484.
116. Y. Mao, Y. Zhang, Z. Luo, R. Zhan, H. Xu, W. Chen and H. Huang, Synthesis, Biological Evaluation and Low-Toxic Formulation Development of Glycosylated Paclitaxel Prodrugs, *Molecules*, 2018, **23**.
117. J. Pohl, B. Bertram, P. Hilgard, M. R. Nowrousian, J. Stüben and M. Wießler, D-19575—a sugar-linked isophosphoramide mustard derivative exploiting transmembrane glucose transport, *Cancer Chemotherapy and Pharmacology*, 1995, **35**, 364-370.
118. P. L. Carl, P. K. Chakravarty and J. A. Katzenellenbogen, A novel connector linkage applicable in prodrug design, *Journal of Medicinal Chemistry*, 1981, **24**, 479-480.
119. V. Edupuganti, J. Tyndall and A. B. Gamble, Self-immolative Linkers in Prodrugs and Antibody Drug Conjugates in Cancer Treatment, *Recent Pat Anticancer Drug Discov*, 2021, **16**, 479-497.
120. L. F. Tietze, T. Feuerstein, A. Fecher, F. Haunert, O. Panknin, U. Borchers, I. Schuberth and F. Alves, Proof of Principle in the Selective Treatment of Cancer by Antibody-Directed Enzyme Prodrug Therapy: The Development of a Highly Potent Prodrug, *Angewandte Chemie International Edition*, 2002, **41**, 759-761.
121. L. F. Tietze, F. Major and I. Schuberth, Antitumor Agents: Development of Highly Potent Glycosidic Duocarmycin Analogues for Selective Cancer Therapy, *Angewandte Chemie International Edition*, 2006, **45**, 6574-6577.
122. L. F. Tietze, F. Major, I. Schuberth, D. A. Spiegl, B. Krewer, K. Maksimenka, G. Bringmann and J. Magull, Selective Treatment of Cancer: Synthesis, Biological Evaluation and Structural Elucidation of Novel Analogues of the Antibiotic CC-1065 and the Duocarmycins, *Chemistry – A European Journal*, 2007, **13**, 4396-4409.
123. L. F. Tietze and B. Krewer, Antibody-Directed Enzyme Prodrug Therapy: A Promising Approach for a Selective Treatment of Cancer Based on Prodrugs and Monoclonal Antibodies, *Chemical Biology & Drug Design*, 2009, **74**, 205-211.
124. L. F. Tietze, J. M. von Hof, M. Müller, B. Krewer and I. Schuberth, Glycosidic Prodrugs of Highly Potent Bifunctional Duocarmycin Derivatives for Selective Treatment of Cancer, *Angewandte Chemie International Edition*, 2010, **49**, 7336-7339.
125. T. Wirth, K. Schmuck, L. F. Tietze and S. A. Sieber, Duocarmycin Analogues Target Aldehyde Dehydrogenase 1 in Lung Cancer Cells, *Angewandte Chemie International Edition*, 2012, **51**, 2874-2877.
126. I. Niculescu-Duvaz and C. J. Springer, Antibody-directed enzyme prodrug therapy (ADEPT): a review, *Advanced Drug Delivery Reviews*, 1997, **26**, 151-172.
127. L. F. Tietze, H. J. Schuster, K. Schmuck, I. Schuberth and F. Alves, Duocarmycin-based prodrugs for cancer prodrug monotherapy, *Bioorganic & Medicinal Chemistry*, 2008, **16**, 6312-6318.
128. T. Legigan, J. Clarhaut, I. Tranoy-Opalinski, A. Monvoisin, B. Renoux, M. Thomas, A. Le Pape, S. Lerondel and S. Papot, The First Generation of β-Galactosidase-Responsive Prodrugs Designed for the Selective Treatment of Solid Tumors in Prodrug Monotherapy, *Angewandte Chemie International Edition*, 2012, **51**, 11606-11610.

129. L. F. Tietze, R. Seele, B. Leiting and T. Krach, Stereoselective synthesis of (1-alkoxyalkyl) α- and β-d-glucopyranosiduronates (acetal-glucopyranosiduronates): A new approach to specific cytostatics for the treatment of cancer, *Carbohydrate Research*, 1988, **180**, 253-262.
130. K. Bosslet, R. Straub, M. Blumrich, J. Czech, M. Gerken, B. Sperker, H. K. Kroemer, J. P. Gesson, M. Koch and C. Monneret, Elucidation of the mechanism enabling tumor selective prodrug monotherapy, *Cancer Res*, 1998, **58**, 1195-1201.
131. J. Li, Y. Zhu, M. Xie, Q. Zhang and W. Du, Design, synthesis, and biological evaluation of target water-soluble hydroxamic acid-based HDACi derivatives as prodrugs, *Chemical Biology & Drug Design*, 2019, **94**, 1760-1767.
132. C. Spitz, N. Primas, T. Terme and P. Vanelle, Nitro-Containing Self-Immolative Systems for Biological Applications, *Journal*, 2022, **15**.
133. M. Grinda, J. Clarhaut, B. Renoux, I. Tranoy-Opalinski and S. Papot, A self-immolative dendritic glucuronide prodrug of doxorubicin, *MedChemComm*, 2012, **3**, 68-70.
134. A. Sagi, E. Segal, R. Satchi-Fainaro and D. Shabat, Remarkable drug-release enhancement with an elimination-based AB3 self-immolative dendritic amplifier, *Bioorganic & Medicinal Chemistry*, 2007, **15**, 3720-3727.
135. R. Erez, E. Segal, K. Miller, R. Satchi-Fainaro and D. Shabat, Enhanced cytotoxicity of a polymer–drug conjugate with triple payload of paclitaxel, *Bioorganic & Medicinal Chemistry*, 2009, **17**, 4327-4335.
136. J. Fang, H. Nakamura and H. Maeda, The EPR effect: Unique features of tumor blood vessels for drug delivery, factors involved, and limitations and augmentation of the effect, *Adv Drug Deliv Rev*, 2011, **63**, 136-151.
137. T. Legigan, J. Clarhaut, B. Renoux, I. Tranoy-Opalinski, A. Monvoisin, J.-M. Berjeaud, F. Guilhot and S. Papot, Synthesis and Antitumor Efficacy of a β-Glucuronidase-Responsive Albumin-Binding Prodrug of Doxorubicin, *Journal of Medicinal Chemistry*, 2012, **55**, 4516-4520.
138. M. Grinda, J. Clarhaut, I. Tranoy-Opalinski, B. Renoux, A. Monvoisin, L. Cronier and S. Papot, A heterodimeric glucuronide prodrug for cancer tritherapy: the double role of the chemical amplifier, *ChemMedChem*, 2011, **6**, 2137-2141.
139. M. Grinda, T. Legigan, J. Clarhaut, E. Peraudeau, I. Tranoy-Opalinski, B. Renoux, M. Thomas, F. Guilhot and S. Papot, An enzyme-responsive system programmed for the double release of bioactive molecules through an intracellular chemical amplification process, *Organic & Biomolecular Chemistry*, 2013, **11**, 7129-7133.
140. P. V. Murphy, A. Dhara, L. S. Fitzgerald, E. Hever, S. Konda and K. Mandal, Small lectin ligands as a basis for applications in glycoscience and glycomedicine, *Chemical Society Reviews*, 2024, DOI: 10.1039/D4CS00642A.
141. V. I. Teichberg, I. Silman, D. D. Beitsch and G. Resheff, A beta-D-galactoside binding protein from electric organ tissue of Electrophorus electricus, *Proc Natl Acad Sci U S A*, 1975, **72**, 1383-1387.
142. A. de Waard, S. Hickman and S. Kornfeld, Isolation and properties of beta-galactoside binding lectins of calf heart and lung, *J Biol Chem*, 1976, **251**, 7581-7587.
143. C. M. Arthur, M. D. Baruffi, R. D. Cummings and S. R. Stowell, Evolving mechanistic insights into galectin functions, *Methods Mol Biol*, 2015, **1207**, 1-35.
144. F.-T. Liu and S. R. Stowell, The role of galectins in immunity and infection, *Nature Reviews Immunology*, 2023, **23**, 479-494.

145. R.-Y. Yang, G. A. Rabinovich and F.-T. Liu, Galectins: structure, function and therapeutic potential, *Expert Reviews in Molecular Medicine*, 2008, **10**, e17.
146. Y. Miura, Y. Hoshino and H. Seto, Glycopolymer Nanobiotechnology, *Chemical Reviews*, 2016, **116**, 1673-1692.
147. J. J. Lundquist and E. J. Toone, The Cluster Glycoside Effect, *Chemical Reviews*, 2002, **102**, 555-578.
148. J. E. Gestwicki, L. E. Strong and L. L. Kiessling, Tuning chemotactic responses with synthetic multivalent ligands, *Chemistry & Biology*, 2000, **7**, 583-591.
149. R. Jelinek and S. Kolusheva, Carbohydrate Biosensors, *Chemical Reviews*, 2004, **104**, 5987-6016.
150. V. Ladmiral, M. Semsarilar, I. Canton and S. P. Armes, Polymerization-Induced Self-Assembly of Galactose-Functionalized Biocompatible Diblock Copolymers for Intracellular Delivery, *Journal of the American Chemical Society*, 2013, **135**, 13574-13581.
151. R. A. Hegele and G. M. Maltman, Insulin's centenary: the birth of an idea, *Lancet Diabetes Endocrinol*, 2020, **8**, 971-977.
152. M. Bergmann and L. Zervas, Über ein allgemeines Verfahren der Peptid-Synthese, *Berichte der deutschen chemischen Gesellschaft (A and B Series)*, 1932, **65**, 1192-1201.
153. R. H. Sifferd and V. du Vigneaud, A NEW SYNTHESIS OF CARNOSINE, WITH SOME OBSERVATIONS ON THE SPLITTING OF THE BENZYL GROUP FROM CARBOBENZOXY DERIVATIVES AND FROM BENZYLTHIO ETHERS, *Journal of Biological Chemistry*, 1935, **108**, 753-761.
154. C. R. Harington and T. H. Mead, Synthesis of glutathione, *Biochem J*, 1935, **29**, 1602-1611.
155. V. d. Vigneaud, C. Ressler, C. J. M. Swan, C. W. Roberts, P. G. Katsoyannis and S. Gordon, THE SYNTHESIS OF AN OCTAPEPTIDE AMIDE WITH THE HORMONAL ACTIVITY OF OXYTOCIN, *Journal of the American Chemical Society*, 1953, **75**, 4879-4880.
156. G. A. Grant and G. A. Grant, in *Synthetic Peptides: A User's Guide*, Oxford University Press, 2002, DOI: 10.1093/9780195132618.003.0001, p. 0.
157. R. B. Merrifield, Solid Phase Peptide Synthesis. I. The Synthesis of a Tetrapeptide, *Journal of the American Chemical Society*, 1963, **85**, 2149-2154.
158. S. Chandrudu, P. Simerska and I. Toth, Chemical methods for peptide and protein production, *Molecules*, 2013, **18**, 4373-4388.
159. M. Muttanthaler, G. F. King, D. J. Adams and P. F. Alewood, *Nature Reviews*, 2021, **20**, 309-325.
160. M. Muttenthaler, G. F. King, D. J. Adams and P. F. Alewood, Trends in peptide drug discovery, *Nature Reviews Drug Discovery*, 2021, **20**, 309-325.
161. B. K. Muralidhara and M. Wong, Critical considerations in the formulation development of parenteral biologic drugs, *Drug Discovery Today*, 2020, **25**, 574-581.
162. R. Mosch and H.-J. Guchelaar, Immunogenicity of Monoclonal Antibodies and the Potential Use of HLA Haplotypes to Predict Vulnerable Patients, *Frontiers in Immunology*, 2022, **13**.
163. A. Vaisman-Mentesh, S. Rosenstein, M. Yavzori, Y. Dror, E. Fudim, B. Ungar, U. Kopylov, O. Picard, A. Kigel, S. Ben-Horin, I. Benhar and Y. Wine, Molecular Landscape of Anti-Drug Antibodies Reveals the Mechanism of the Immune Response Following Treatment With TNFα Antagonists, *Front Immunol*, 2019, **10**, 2921.

164. N. Tsomaia, Peptide therapeutics: Targeting the undruggable space, *European Journal of Medicinal Chemistry*, 2015, **94**, 459-470.
165. P. Matsson and J. Kihlberg, How Big Is Too Big for Cell Permeability?, *Journal of Medicinal Chemistry*, 2017, **60**, 1662-1664.
166. P. G. Dougherty, A. Sahni and D. Pei, *Chem. Rev.*, 2019, **119**.
167. T. Rolland, M. Taşan, B. Charloteaux, S. J. Pevzner, Q. Zhong, N. Sahni, S. Yi, I. Lemmens, C. Fontanillo, R. Mosca, A. Kamburov, S. D. Ghiassian, X. Yang, L. Ghamsari, D. Balcha, B. E. Begg, P. Braun, M. Brehme, M. P. Broly, A. R. Carvunis, D. Convery-Zupan, R. Corominas, J. Coulombe-Huntington, E. Dann, M. Dreze, A. Dricot, C. Fan, E. Franzosa, F. Gebreab, B. J. Gutierrez, M. F. Hardy, M. Jin, S. Kang, R. Kiros, G. N. Lin, K. Luck, A. MacWilliams, J. Menche, R. R. Murray, A. Palagi, M. M. Poulin, X. Rambout, J. Rasla, P. Reichert, V. Romero, E. Ruyssinck, J. M. Sahalie, A. Scholz, A. A. Shah, A. Sharma, Y. Shen, K. Spirohn, S. Tam, A. O. Tejeda, S. A. Wanamaker, J. C. Twizere, K. Vega, J. Walsh, M. E. Cusick, Y. Xia, A. L. Barabási, L. M. Iakoucheva, P. Aloy, J. De Las Rivas, J. Tavernier, M. A. Calderwood, D. E. Hill, T. Hao, F. P. Roth and M. Vidal, A proteome-scale map of the human interactome network, *Cell*, 2014, **159**, 1212-1226.
168. X. Wang, D. Ni, Y. Liu and S. Lu, *Front. Chem.*, 2021, **9**.
169. N. Tsomaia, *Eur. J. Med. Chem.*, 2015, **13**, 459-470.
170. A. Chi-Lung Lee, J. L. Harris, K. K. Khanna and J.-H. Hong, *Int. J. Mol. Sci.*, 2019, **20**, 2383.
171. Y. Wu, J. Williams, E. D. D. Calder and L. J. Walport, Strategies to expand peptide functionality through hybridisation with a small molecule component, *RSC Chemical Biology*, 2021, **2**, 151-165.
172. A. A. Vinogradov, Y. Yin and H. Suga, Macrocyclic Peptides as Drug Candidates: Recent Progress and Remaining Challenges, *Journal of the American Chemical Society*, 2019, **141**, 4167-4181.
173. M. Empting, in *Cyclic Peptides: From Bioorganic Synthesis to Applications*, The Royal Society of Chemistry, 2018, DOI: 10.1039/9781788010153-00001, pp. 1-14.
174. J. He, P. Ghosh and C. Nitsche, Biocompatible strategies for peptide macrocyclisation, *Chemical Science*, 2024, **15**, 2300-2322.
175. F. Milletti, Cell-penetrating peptides: classes, origin, and current landscape, *Drug Discov Today*, 2012, **17**, 850-860.
176. M. Brown, J. Rivier and W. Vale, Somatostatin: Analogs with Selected Biological Activities, *Science*, 1977, **196**, 1467-1469.
177. E. Biron, J. Chatterjee, O. Ovadia, D. Langenegger, J. Brueggen, D. Hoyer, H. A. Schmid, R. Jelinek, C. Gilon, A. Hoffman and H. Kessler, Improving Oral Bioavailability of Peptides by Multiple N-Methylation: Somatostatin Analogues, *Angewandte Chemie International Edition*, 2008, **47**, 2595-2599.
178. A. Janecka, M. Zubrzycka and T. Janecki, Somatostatin analogs, *The Journal of Peptide Research*, 2001, **58**, 91-107.
179. J. Rivier, P. Brazeau, W. Vale and R. Guillemin, Somatostatin analogs. Relative importance of the disulfide bridge and of the Ala-Gly side chain for biological activity, *Journal of Medicinal Chemistry*, 1975, **18**, 123-126.
180. N. Ling, R. Burgus, J. Rivier, W. Vale and P. Brazeau, The use of mass spectrometry in deducing the sequence of somatostatin--a hypothalamic polypeptide that inhibits the secretion of growth hormone, *Biochem Biophys Res Commun*, 1973, **50**, 127-133.

181. W. Vale, P. Brazeau, G. Grant, A. Nussey, R. Burgus, J. Rivier, N. Ling and R. Guillemin, [Preliminary observations on the mechanism of action of somatostatin, a hypothalamic factor inhibiting the secretion of growth hormone], *C R Acad Hebd Seances Acad Sci D*, 1972, **275**, 2913-2916.
182. W. Vale, J. Rivier, N. Ling and M. Brown, Biologic and immunologic activities and applications of somatostatin analogs, *Metabolism*, 1978, **27**, 1391-1401.
183. J. Rivier, M. Brown and W. Vale, D-Trp8-somatostatin: an analog of somatostatin more potent than the native molecule, *Biochem Biophys Res Commun*, 1975, **65**, 746-751.
184. D. F. Veber, F. W. Holly, R. F. Nutt, S. J. Bergstrand, S. F. Brady, R. Hirschmann, M. S. Glitzer and R. Saperstein, Highly active cyclic and bicyclic somatostatin analogues of reduced ring size, *Nature*, 1979, **280**, 512-514.
185. R. F. Nutt, D. F. Veber, P. E. Curley, R. Saperstein and R. Hirschmann, Somatostatin analogs which define the role of the lysine-9 amino group, *Int J Pept Protein Res*, 1983, **21**, 66-73.
186. R. M. Freidinger, D. S. Perlow, W. C. Randall, R. Saperstein, B. H. Arison and D. F. Veber, Conformational modifications of cyclic hexapeptide somatostatin analogs, *Int J Pept Protein Res*, 1984, **23**, 142-150.
187. W. Vale, M. Brown, C. Rivier, M. Perrin and J. Rivier, Brain Peptides: A New Endocrinology, 1979.
188. W. Bauer, U. Briner, W. Doepfner, R. Haller, R. Huguenin, P. Marbach, T. J. Petcher and Pless, SMS 201-995: a very potent and selective octapeptide analogue of somatostatin with prolonged action, *Life Sci*, 1982, **31**, 1133-1140.
189. S. W. J. Lamberts and L. J. Hofland, ANNIVERSARY REVIEW: Octreotide, 40 years later, *European Journal of Endocrinology*, 2019, **181**, R173-R183.
190. D. Böhme and A. G. Beck-Sickinger, *J. Pept. Sci.*, 2015, **21**, 186-200.
191. L.-C. Sun and D. H. Coy, Somatostatin Receptor-Targeted Anti-Cancer Therapy, *Current Drug Delivery*, 2011, **8**, 2-10.
192. E. G. von Roedern and H. Kessler, A sugar amino acid as a novel peptidomimetic, *Angewandte Chemie International Edition in English*, 1994, **33**, 687-689.
193. E. Graf von Roedern, E. Lohof, G. Hessler, M. Hoffmann and H. Kessler, Synthesis and conformational analysis of linear and cyclic peptides containing sugar amino acids, *Journal of the American Chemical Society*, 1996, **118**, 10156-10167.
194. R. Bajracharya, J. G. Song, B. R. Patil, S. H. Lee, H. M. Noh, D. H. Kim, G. L. Kim, S. H. Seo, J. W. Park, S. H. Jeong, C. H. Lee and H. K. Han, Functional ligands for improving anticancer drug therapy: current status and applications to drug delivery systems, *Drug Deliv*, 2022, **29**, 1959-1970.
195. M. Srinivasarao and P. S. Low, Ligand-Targeted Drug Delivery, *Chemical Reviews*, 2017, **117**, 12133-12164.
196. S. F. A. Rizvi, L. Zhang, H. Zhang and Q. Fang, Peptide-Drug Conjugates: Design, Chemistry, and Drug Delivery System as a Novel Cancer Theranostic, *ACS Pharmacology & Translational Science*, 2024, **7**, 309-334.
197. Q. Zhang, N. Liu, J. Wang, Y. Liu, K. Wang, J. Zhang and X. Pan, The Recent Advance of Cell-Penetrating and Tumor-Targeting Peptides as Drug Delivery Systems Based on Tumor Microenvironment, *Molecular Pharmaceutics*, 2023, **20**, 789-809.
198. M. Ahmadi, C. A. Ritter, T. von Woedtke, S. Bekeschus and K. Wende, Package delivered: folate receptor-mediated transporters in cancer therapy and diagnosis, *Chemical Science*, 2024, **15**, 1966-2006.

199. C. W. Zhang, J. G. Zhang, X. Yang, W. L. Du, Z. L. Yu, Z. Y. Lv and X. Z. Mou, Carbohydrates based stimulus responsive nanocarriers for cancer-targeted chemotherapy: a review of current practices, *Expert Opin Drug Deliv*, 2022, **19**, 623-640.
200. Z. Luo, Y. Dai and H. Gao, Development and application of hyaluronic acid in tumor targeting drug delivery, *Acta Pharm Sin B*, 2019, **9**, 1099-1112.
201. F. Gao, J. Yin, Y. Chen, C. Guo, H. Hu and J. Su, Recent advances in aptamer-based targeted drug delivery systems for cancer therapy, *Frontiers in Bioengineering and Biotechnology*, 2022, **10**.
202. C. Dumontet, J. M. Reichert, P. D. Senter, J. M. Lambert and A. Beck, Antibody–drug conjugates come of age in oncology, *Nature Reviews Drug Discovery*, 2023, **22**, 641-661.
203. V. Le Joncour and P. Laakkonen, Seek & Destroy, use of targeting peptides for cancer detection and drug delivery, *Bioorganic & Medicinal Chemistry*, 2018, **26**, 2797-2806.
204. S. Yan, J. Na, X. Liu and P. Wu, Different Targeting Ligands-Mediated Drug Delivery Systems for Tumor Therapy, *Pharmaceutics*, 2024, **16**.
205. Z. Jiang, J. Guan, J. Qian and C. Zhan, Peptide ligand-mediated targeted drug delivery of nanomedicines, *Biomaterials Science*, 2019, **7**, 461-471.
206. P. E. Saw and E. W. Song, Phage display screening of therapeutic peptide for cancer targeting and therapy, *Protein Cell*, 2019, **10**, 787-807.
207. E. Kondo, H. Iioka and K. Saito, Tumor-homing peptide and its utility for advanced cancer medicine, *Cancer Science*, 2021, **112**, 2118-2125.
208. K. N. Sugahara, G. B. Braun, T. H. de Mendoza, V. R. Kotamraju, R. P. French, A. M. Lowy, T. Teesalu and E. Ruoslahti, Tumor-penetrating iRGD peptide inhibits metastasis, *Mol Cancer Ther*, 2015, **14**, 120-128.
209. P. Lingasamy, A. Tobi, K. Kurm, S. Kopanchuk, A. Sudakov, M. Salumäe, T. Rätsep, T. Asser, R. Bjerkvig and T. Teesalu, Tumor-penetrating peptide for systemic targeting of Tenascin-C, *Scientific Reports*, 2020, **10**, 5809.
210. S. Sharma, V. R. Kotamraju, T. Mölder, A. Tobi, T. Teesalu and E. Ruoslahti, Tumor-Penetrating Nanosystem Strongly Suppresses Breast Tumor Growth, *Nano Lett*, 2017, **17**, 1356-1364.
211. N. Song, L. Zhao, M. Zhu and J. Zhao, Recent progress in LyP-1-based strategies for targeted imaging and therapy, *Drug Deliv*, 2019, **26**, 363-375.
212. Y. Zhang, J. Wei, S. Liu, J. Wang, X. Han, H. Qin, J. Lang, K. Cheng, Y. Li, Y. Qi, G. J. Anderson, S. Sukumar, S. Li and G. Nie, Inhibition of platelet function using liposomal nanoparticles blocks tumor metastasis, *Theranostics*, 2017, **7**, 1062-1071.
213. G. Colombo, F. Curnis, G. M. S. De Mori, A. Gasparri, C. Longoni, A. Sacchi, R. Longhi and A. Corti, Structure-Activity Relationships of Linear and Cyclic Peptides Containing the NGR Tumor-homing Motif*, *Journal of Biological Chemistry*, 2002, **277**, 47891-47897.
214. L. Zhang, E. Giraudo, J. A. Hoffman, D. Hanahan and E. Ruoslahti, Lymphatic zip codes in premalignant lesions and tumors, *Cancer Res*, 2006, **66**, 5696-5706.
215. S. Dufort, L. Sancey, A. Hurbin, S. Foillard, D. Boturyn, P. Dumy and J.-L. Coll, Targeted delivery of a proapoptotic peptide to tumors in vivo, *Journal of Drug Targeting*, 2011, **19**, 582-588.

216. S. Mukhopadhyay, C. M. Barnés, A. Haskel, S. M. Short, K. R. Barnes and S. J. Lippard, Conjugated Platinum(IV)–Peptide Complexes for Targeting Angiogenic Tumor Vasculature, *Bioconjugate Chemistry*, 2008, **19**, 39-49.
217. M. Körner, Specific biology of neuroendocrine tumors: Peptide receptors as molecular targets, *Best Practice & Research Clinical Endocrinology & Metabolism*, 2016, **30**, 19-31.
218. J. Reubi, B. Waser, J.-C. Schaer and J. A. Laissue, Somatostatin receptor sst1–sst5 expression in normal and neoplastic human tissues using receptor autoradiography with subtype-selective ligands, *European Journal of Nuclear Medicine*, 2001, **28**, 836-846.
219. J. C. Reubi and B. Waser, Concomitant expression of several peptide receptors in neuroendocrine tumours: molecular basis for in vivo multireceptor tumour targeting, *Eur J Nucl Med Mol Imaging*, 2003, **30**, 781-793.
220. K. Kumar, Radiolabeled Compounds for Diagnosis and Treatment of Cancer, *Molecules*, 2021, **26**.
221. W. H. Bakker, R. Albert, C. Bruns, W. A. P. Breeman, L. J. Hofland, P. Marbach, J. Pless, D. Pralet, B. Stolz, J. W. Koper, S. W. J. Lamberts, T. J. Visser and E. P. Krenning, [111In-DTPA-D-Phe1]-octreotide, a potential radiopharmaceutical for imaging of somatostatin receptor-positive tumors: synthesis, radiolabeling and in vitro validation, *Life Sciences*, 1991, **49**, 1583-1591.
222. Y. S. Zhu, K. Tang and J. Lv, Peptide-drug conjugate-based novel molecular drug delivery system in cancer, *Trends Pharmacol Sci*, 2021, **42**, 857-869.
223. M. Fani, R. Mansi, G. P. Nicolas and D. Wild, Radiolabeled Somatostatin Analogs—A Continuously Evolving Class of Radiopharmaceuticals, *Journal*, 2022, **14**.
224. D. Feijtel, M. de Jong and J. Nonnekens, Peptide Receptor Radionuclide Therapy: Looking Back, Looking Forward, *Curr Top Med Chem*, 2020, **20**, 2959-2969.
225. G. Santo, G. Di Santo and I. Virgolini, Peptide Receptor Radionuclide Therapy of Neuroendocrine Tumors: Agonist, Antagonist and Alternatives, *Seminars in Nuclear Medicine*, 2024, **54**, 557-569.
226. S. M. P. Vadevoo, S. Gurung, H.-S. Lee, G. R. Gunassekaran, S.-M. Lee, J.-W. Yoon, Y.-K. Lee and B. Lee, Peptides as multifunctional players in cancer therapy, *Experimental & Molecular Medicine*, 2023, **55**, 1099-1109.
227. A. G. Cheetham, D. Keith, P. Zhang, R. Lin, H. Su and H. Cui, Targeting Tumors with Small Molecule Peptides, *Curr Cancer Drug Targets*, 2016, **16**, 489-508.
228. E. Ragozin, A. Hesin, A. Bazylevich, H. Tuchinsky, A. Bovina, T. Shekhter Zahavi, M. Oron-Herman, G. Kostenich, M. A. Firer, T. Rubinek, I. Wolf, G. Luboshits, M. Y. Sherman and G. Gellerman, New somatostatin-drug conjugates for effective targeting pancreatic cancer, *Bioorganic & Medicinal Chemistry*, 2018, **26**, 3825-3836.
229. M. Alas, A. Saghaeidehkordi and K. Kaur, Peptide-Drug Conjugates with Different Linkers for Cancer Therapy, *J Med Chem*, 2021, **64**, 216-232.
230. B. M. Cooper, J. Iegre, D. H. O' Donovan, M. Ölwegård Halvarsson and D. R. Spring, Peptides as a platform for targeted therapeutics for cancer: peptide–drug conjugates (PDCs), *Chemical Society Reviews*, 2021, **50**, 1480-1494.
231. E. Figueras, A. Martins, A. Borbély, V. Le Joncour, P. Cordella, R. Perego, D. Modena, P. Pagani, S. Esposito, G. Auciello, M. Frese, P. Gallinari, P. Laakkonen, C. Steinkühler and N. Sewald, Octreotide Conjugates for Tumor Targeting and Imaging, *Pharmaceutics*, 2019, **11**.

232. M. Wei, Y. Gao, X. Li and M. J. Serpe, Stimuli-responsive polymers and their applications, *Polymer Chemistry*, 2017, **8**, 127-143.
233. A. Y. Coran, in *The Science and Technology of Rubber (Fourth Edition)*, eds. J. E. Mark, B. Erman and C. M. Roland, Academic Press, Boston, 2013, DOI: https://doi.org/10.1016/B978-0-12-394584-6.00007-8, pp. 337-381.
234. G. Kocak, C. Tuncer and V. Bütün, pH-Responsive polymers, *Polymer Chemistry*, 2017, **8**, 144-176.
235. F. Doberenz, K. Zeng, C. Willems, K. Zhang and T. Groth, Thermoresponsive polymers and their biomedical application in tissue engineering – a review, *Journal of Materials Chemistry B*, 2020, **8**, 607-628.
236. M. Huo, J. Yuan, L. Tao and Y. Wei, Redox-responsive polymers for drug delivery: from molecular design to applications, *Polymer Chemistry*, 2014, **5**, 1519-1528.
237. D. A. Davis, A. Hamilton, J. Yang, L. D. Cremar, D. Van Gough, S. L. Potisek, M. T. Ong, P. V. Braun, T. J. Martínez, S. R. White, J. S. Moore and N. R. Sottos, Force-induced activation of covalent bonds in mechanoresponsive polymeric materials, *Nature*, 2009, **459**, 68-72.
238. J. H. Holtz and S. A. Asher, Polymerized colloidal crystal hydrogel films as intelligent chemical sensing materials, *Nature*, 1997, **389**, 829-832.
239. J. Hu, G. Zhang and S. Liu, Enzyme-responsive polymeric assemblies, nanoparticles and hydrogels, *Chemical Society Reviews*, 2012, **41**, 5933-5949.
240. M. Avital-Shmilovici and D. Shabat, Self-immolative dendrimers: A distinctive approach to molecular amplification, *Soft Matter*, 2010, **6**, 1073-1080.
241. O. Shelef, S. Gnaim and D. Shabat, Self-Immolative Polymers: An Emerging Class of Degradable Materials with Distinct Disassembly Profiles, *Journal of the American Chemical Society*, 2021, **143**, 21177-21188.
242. R. J. Amir, N. Pessah, M. Shamis and D. Shabat, Self-Immolative Dendrimers, *Angewandte Chemie International Edition*, 2003, **42**, 4494-4499.
243. F. M. H. de Groot, C. Albrecht, R. Koekkoek, P. H. Beusker and H. W. Scheeren, "Cascade-Release Dendrimers" Liberate All End Groups upon a Single Triggering Event in the Dendritic Core, *Angewandte Chemie International Edition*, 2003, **42**, 4490-4494.
244. M. Vert, Aliphatic Polyesters: Great Degradable Polymers That Cannot Do Everything, *Biomacromolecules*, 2005, **6**, 538-546.
245. F. Seidi, Y. Zhong, H. Xiao, Y. Jin and D. Crespy, Degradable polyprodrugs: design and therapeutic efficiency, *Chemical Society Reviews*, 2022, **51**, 6652-6703.
246. R. E. Wang, F. Costanza, Y. Niu, H. Wu, Y. Hu, W. Hang, Y. Sun and J. Cai, Development of self-immolative dendrimers for drug delivery and sensing, *Journal of Controlled Release*, 2012, **159**, 154-163.
247. S. Gnaim, O. Green and D. Shabat, The emergence of aqueous chemiluminescence: new promising class of phenoxy 1,2-dioxetane luminophores, *Chemical Communications*, 2018, **54**, 2073-2085.
248. N. Hananya and D. Shabat, A Glowing Trajectory between Bio- and Chemiluminescence: From Luciferin-Based Probes to Triggerable Dioxetanes, *Angewandte Chemie International Edition*, 2017, **56**, 16454-16463.
249. M. S. Baker, H. Kim, M. G. Olah, G. G. Lewis and S. T. Phillips, Depolymerizable poly(benzyl ether)-based materials for selective room temperature recycling, *Green Chemistry*, 2015, **17**, 4541-4545.

250. K. Yeung, H. Kim, H. Mohapatra and S. T. Phillips, Surface-Accessible Detection Units in Self-Immolative Polymers Enable Translation of Selective Molecular Detection Events into Amplified Responses in Macroscopic, Solid-State Plastics, *Journal of the American Chemical Society*, 2015, **137**, 5324-5327.
251. G. Liu, G. Zhang, J. Hu, X. Wang, M. Zhu and S. Liu, Hyperbranched Self-Immolative Polymers (hSIPs) for Programmed Payload Delivery and Ultrasensitive Detection, *Journal of the American Chemical Society*, 2015, **137**, 11645-11655.
252. A. Sagi, R. Weinstain, N. Karton and D. Shabat, Self-Immolative Polymers, *Journal of the American Chemical Society*, 2008, **130**, 5434-5435.
253. R. Weinstain, A. Sagi, N. Karton and D. Shabat, Self-Immolative Comb-Polymers: Multiple-Release of Side-Reporters by a Single Stimulus Event, *Chemistry – A European Journal*, 2008, **14**, 6857-6861.
254. G. G. Lewis, J. S. Robbins and S. T. Phillips, Phase-Switching Depolymerizable Poly(carbamate) Oligomers for Signal Amplification in Quantitative Time-Based Assays, *Macromolecules*, 2013, **46**, 5177-5183.
255. C. R. Powell, J. C. Foster, S. N. Swilley, K. Kaur, S. J. Scannelli, D. Troya and J. B. Matson, Self-amplified depolymerization of oligo(thiourethanes) for the release of COS/H2S, *Polymer Chemistry*, 2019, **10**, 2991-2995.
256. D. J. Lefer, A new gaseous signaling molecule emerges: cardioprotective role of hydrogen sulfide, *Proc Natl Acad Sci U S A*, 2007, **104**, 17907-17908.
257. Y. Xiao, X. Tan, Z. Li and K. Zhang, Self-immolative polymers in biomedicine, *Journal of Materials Chemistry B*, 2020, **8**, 6697-6709.
258. M. Gisbert-Garzarán, M. Manzano and M. Vallet-Regí, Self-immolative chemistry in nanomedicine, *Chemical Engineering Journal*, 2018, **340**, 24-31.
259. Y. Zhang, Q. Yin, L. Yin, L. Ma, L. Tang and J. Cheng, Chain-Shattering Polymeric Therapeutics with On-Demand Drug-Release Capability, *Angewandte Chemie International Edition*, 2013, **52**, 6435-6439.
260. K. Cai, J. Yen, Q. Yin, Y. Liu, Z. Song, S. Lezmi, Y. Zhang, X. Yang, W. G. Helferich and J. Cheng, Redox-responsive self-assembled chain-shattering polymeric therapeutics, *Biomaterials Science*, 2015, **3**, 1061-1065.
261. K. Neumann, S. Jain, A. Gambardella, S. E. Walker, E. Valero, A. Lilienkampf and M. Bradley, Tetrazine-Responsive Self-immolative Linkers, *Chembiochem*, 2017, **18**, 91-95.
262. A. P. Esser-Kahn, N. R. Sottos, S. R. White and J. S. Moore, Programmable Microcapsules from Self-Immolative Polymers, *Journal of the American Chemical Society*, 2010, **132**, 10266-10268.
263. A. P. Esser-Kahn, S. A. Odom, N. R. Sottos, S. R. White and J. S. Moore, Triggered Release from Polymer Capsules, *Macromolecules*, 2011, **44**, 5539-5553.
264. M. A. DeWit and E. R. Gillies, A Cascade Biodegradable Polymer Based on Alternating Cyclization and Elimination Reactions, *Journal of the American Chemical Society*, 2009, **131**, 18327-18334.
265. G. Liu, X. Wang, J. Hu, G. Zhang and S. Liu, Self-Immolative Polymersomes for High-Efficiency Triggered Release and Programmed Enzymatic Reactions, *Journal of the American Chemical Society*, 2014, **136**, 7492-7497.
266. Z. Faraji Rad, P. D. Prewett and G. J. Davies, High-resolution two-photon polymerization: the most versatile technique for the fabrication of microneedle arrays, *Microsystems & Nanoengineering*, 2021, **7**, 71.

267. T. Baldacchini, *Three-dimensional microfabrication using two-photon polymerization : fundamentals, technology, and applications*, William Andrew, Amsterdam, [Netherlands, 2016.
268. S. Maruo, O. Nakamura and S. Kawata, Three-dimensional microfabrication with two-photon-absorbed photopolymerization, *Opt. Lett.*, 1997, **22**, 132-134.
269. M. Malinauskas, A. Žukauskas, V. Purlys, K. Belazaras, A. Momot, D. Paipulas, R. Gadonas, A. Piskarskas, H. Gilbergs, A. Gaidukevičiūtė, I. Sakellari, M. Farsari and S. Juodkazis, Femtosecond laser polymerization of hybrid/integrated micro-optical elements and their characterization, *Journal of Optics*, 2010, **12**, 124010.
270. C. Liao, W. Anderson, F. Antaw and M. Trau, Two-Photon Nanolithography of Tailored Hollow three-dimensional Microdevices for Biosystems, *ACS Omega*, 2019, **4**, 1401-1409.
271. A. Koroleva, A. Deiwick, A. Nguyen, S. Schlie-Wolter, R. Narayan, P. Timashev, V. Popov, V. Bagratashvili and B. Chichkov, Osteogenic differentiation of human mesenchymal stem cells in 3-D Zr-Si organic-inorganic scaffolds produced by two-photon polymerization technique, *PLoS One*, 2015, **10**, e0118164.
272. C. Reinhardt, S. Passinger, B. N. Chichkov, C. Marquart, I. P. Radko and S. I. Bozhevolnyi, Laser-fabricated dielectric optical components for surface plasmon polaritons, *Opt. Lett.*, 2006, **31**, 1307-1309.
273. S. O'Halloran, A. Pandit, A. Heise and A. Kellett, Two-Photon Polymerization: Fundamentals, Materials, and Chemical Modification Strategies, *Advanced Science*, 2023, **10**, 2204072.
274. M. Rumi and J. W. Perry, Two-photon absorption: an overview of measurements and principles, *Adv. Opt. Photon.*, 2010, **2**, 451-518.
275. M. Göppert-Mayer, Über Elementarakte mit zwei Quantensprüngen, *Annalen der Physik*, 1931, **401**, 273-294.
276. W. Kaiser and C. G. B. Garrett, Two-Photon Excitation in CaF2: Eu2+, *Physical Review Letters*, 1961, **7**, 229-231.
277. A. Jaiswal, C. K. Rastogi, S. Rani, G. P. Singh, S. Saxena and S. Shukla, Two decades of two-photon lithography: Materials science perspective for additive manufacturing of 2D/3D nano-microstructures, *iScience*, 2023, **26**, 106374.
278. S. Shukla, X. Vidal, E. P. Furlani, M. T. Swihart, K.-T. Kim, Y.-K. Yoon, A. Urbas and P. N. Prasad, Subwavelength Direct Laser Patterning of Conductive Gold Nanostructures by Simultaneous Photopolymerization and Photoreduction, *ACS Nano*, 2011, **5**, 1947-1957.
279. Y. Hu, Z. Wang, D. Jin, C. Zhang, R. Sun, Z. Li, K. Hu, J. Ni, Z. Cai, D. Pan, X. Wang, W. Zhu, J. Li, D. Wu, L. Zhang and J. Chu, Botanical-Inspired 4D Printing of Hydrogel at the Microscale, *Advanced Functional Materials*, 2020, **30**, 1907377.
280. T. Spratte, S. Geiger, F. Colombo, A. Mishra, M. Taale, L.-Y. Hsu, E. Blasco and C. Selhuber-Unkel, Increasing the Efficiency of Thermoresponsive Actuation at the Microscale by Direct Laser Writing of pNIPAM, *Advanced Materials Technologies*, 2023, **8**, 2200714.
281. M. Hippler, E. Blasco, J. Qu, M. Tanaka, C. Barner-Kowollik, M. Wegener and M. Bastmeyer, Controlling the shape of 3D microstructures by temperature and light, *Nature Communications*, 2019, **10**, 232.

282. M. Carlotti, O. Tricinci and V. Mattoli, Novel, High-Resolution, Subtractive Photoresist Formulations for 3D Direct Laser Writing Based on Cyclic Ketene Acetals, *Advanced Materials Technologies*, 2022, **7**, 2101590.
283. B. Wu, W. Chassé, K. Zick, M. D. Mantle, A. Heise, D. F. Brougham and V. M. Litvinov, The effect of hydrogen bonding on diffusion and permeability in UV-cured Polyacrylate-based networks for controlled release, *Journal of Controlled Release*, 2020, **327**, 150-160.
284. A.-V. Do, K. S. Worthington, B. A. Tucker and A. K. Salem, Controlled drug delivery from 3D printed two-photon polymerized poly(ethylene glycol) dimethacrylate devices, *International Journal of Pharmaceutics*, 2018, **552**, 217-224.
285. H. Ceylan, I. C. Yasa, O. Yasa, A. F. Tabak, J. Giltinan and M. Sitti, 3D-Printed Biodegradable Microswimmer for Theranostic Cargo Delivery and Release, *ACS Nano*, 2019, **13**, 3353-3362.
286. P. H. Houba, E. Boven, I. H. van der Meulen-Muileman, R. G. Leenders, J. W. Scheeren, H. M. Pinedo and H. J. Haisma, A novel doxorubicin-glucuronide prodrug DOX-GA3 for tumour-selective chemotherapy: distribution and efficacy in experimental human ovarian cancer, *Br J Cancer*, 2001, **84**, 550-557.
287. M. Reszka, I. E. Serdiuk, K. Kozakiewicz, A. Nowacki, H. Myszka, P. Bojarski and B. Liberek, Influence of a 4′-substituent on the efficiency of flavonol-based fluorescent indicators of β-glycosidase activity, *Organic & Biomolecular Chemistry*, 2020, **18**, 7635-7648.
288. G. Sennakesavan, M. Mostakhdemin, L. K. Dkhar, A. Seyfoddin and S. J. Fatihhi, Acrylic acid/acrylamide based hydrogels and its properties - A review, *Polymer Degradation and Stability*, 2020, **180**, 109308.
289. D-Galactose, https://www.medchemexpress.com/D-Galactose.html?srsltid=AfmBOorCegO5uw-4lFjBlYK8jaYarmRyl0TJKXVgXWZevSgSds7y5G_f, (accessed October, 2024).
290. D-Glucuronic acid, https://www.medchemexpress.com/d-glucuronic-acid.html?srsltid=AfmBOoqV0vI1Ny8XdcCbLl6XxZtIDCiovTg6IsGRAxYhkEWx3Pp6Y23L, (accessed October, 2024).
291. S. A. Scaringe, F. E. Wincott and M. H. Caruthers, Novel RNA Synthesis Method Using 5'-O-Silyl-2'-O-orthoester Protecting Groups, *Journal of the American Chemical Society*, 1998, **120**, 11820-11821.
292. S. Cecioni and D. J. Vocadlo, Carbohydrate Bis-acetal-Based Substrates as Tunable Fluorescence-Quenched Probes for Monitoring exo-Glycosidase Activity, *Journal of the American Chemical Society*, 2017, **139**, 8392-8395.
293. S. A. Hartsel, D. E. Kitchen, S. A. Scaringe and W. S. Marshall, in *Oligonucleotide Synthesis*, ed. P. Herdewijn, Humana Press, Totowa, NJ, 2005, DOI: 10.1385/1-59259-823-4:033, pp. 33-49.
294. M. Zhong and S. A. Strobel, Synthesis of Isotopically Labeled P-Site Substrates for the Ribosomal Peptidyl Transferase Reaction, *The Journal of Organic Chemistry*, 2008, **73**, 603-611.
295. S. Cecioni, R. A. Ashmus, P.-A. Gilormini, S. Zhu, X. Chen, X. Shan, C. Gros, M. C. Deen, Y. Wang, R. Britton and D. J. Vocadlo, Quantifying lysosomal glycosidase activity within cells using bis-acetal substrates, *Nature Chemical Biology*, 2022, **18**, 332-341.

296. M. Jacobsson, J. Malmberg and U. Ellervik, Aromatic O-glycosylation, *Carbohydrate Research*, 2006, **341**, 1266-1281.
297. Y. Chong, S.-W. Lee and J.-H. Ahn, Phenolic C-glycoside synthesis using microbial systems, *Current Opinion in Biotechnology*, 2022, **78**, 102827.
298. H. P. Kleine, D. V. Weinberg, R. J. Kaufman and R. S. Sidhu, Phase-transfer-catalyzed synthesis of 2,3,4,6-tetra-O-acetyl-β-d-galactopyranosides, *Carbohydrate Research*, 1985, **142**, 333-337.
299. L. Morelli, A. Bernardi and S. Sattin, Synthesis of potential allosteric modulators of Hsp90 by chemical glycosylation of Eupomatenoid-6, *Carbohydrate Research*, 2014, **390**, 33-41.
300. H. J. Schuster, B. Krewer, J. M. von Hof, K. Schmuck, I. Schuberth, F. Alves and L. F. Tietze, Synthesis of the first spacer containing prodrug of a duocarmycin analogue and determination of its biological activity, *Organic & Biomolecular Chemistry*, 2010, **8**, 1833-1842.
301. in *Greene's Protective Groups in Organic Synthesis*, 2006, DOI: https://doi.org/10.1002/9780470053485.ch2, pp. 16-366.
302. R. D. Crouch, Selective deprotection of silyl ethers, *Tetrahedron*, 2013, **69**, 2383-2417.
303. X. Zheng, R. D. Gandour and K. J. Edgar, Probing the Mechanism of TBAF-Catalyzed Deacylation of Cellulose Esters, *Biomacromolecules*, 2013, **14**, 1388-1394.
304. D. Xu and K. J. Edgar, TBAF and Cellulose Esters: Unexpected Deacylation with Unexpected Regioselectivity, *Biomacromolecules*, 2012, **13**, 299-303.
305. Z. Ahmad, S. Salman, S. A. Khan, A. Amin, Z. U. Rahman, Y. O. Al-Ghamdi, K. Akhtar, E. M. Bakhsh and S. B. Khan, Versatility of Hydrogels: From Synthetic Strategies, Classification, and Properties to Biomedical Applications, *Gels*, 2022, **8**.
306. H. Kubo, Y. Murayama, S. Ogawa, T. Matsumoto, M. Yubakami, T. Ohashi, T. Kubota, K. Okamoto, M. Kamiya, Y. Urano and E. Otsuji, β-Galactosidase is a target enzyme for detecting peritoneal metastasis of gastric cancer, *Sci Rep*, 2021, **11**, 10664.
307. T. Takahashi, Y. Saikawa, T. Igarashi, S. Tsuwano, K. Kumagai, R. Nakamura, T. Ooyama, N. Wada, H. Takeuchi, H. Takaishi and Y. Kitagawa, Octreotide acetate enables the administration of chemoradiotherapy, including the oral anticancer drug S-1, in gastric cancer patients with malignant gastrointestinal obstruction, *Oncol Lett*, 2010, **1**, 673-677.
308. B. Yan, W. Li and C. P. R. Hackenberger, A silyl ether-protected building block for O-GlcNAcylated peptide synthesis to enable one-pot acidic deprotection, *Organic & Biomolecular Chemistry*, 2021, **19**, 8014-8017.
309. K. Wakabayashi and W. Pigman, Synthesis of some glycodipeptides containing hydroxyamino acids, and their stabilities to acids and bases, *Carbohydrate Research*, 1974, **35**, 3-14.
310. M. Meldal, T. I. M. Bielfeldt, S. Peters, K. J. Jensen, H. Paulsen and K. Bock, Susceptibility of glycans to β-elimination in Fmoc-based O-glycopeptide synthesis, *International Journal of Peptide and Protein Research*, 1994, **43**, 529-536.
311. S. S. Kulkarni and J. Gervay-Hague, Two-Step Synthesis of the Immunogenic Bacterial Glycolipid BbGL1, *Organic Letters*, 2008, **10**, 4739-4742.
312. V. Novohradsky, A. Zamora, A. Gandioso, V. Brabec, J. Ruiz and V. Marchán, Somatostatin receptor-targeted organometallic iridium(iii) complexes as novel theranostic agents, *Chemical Communications*, 2017, **53**, 5523-5526.

313. C. Redwood-Sawyerr and D. N. Nesbeth, Tetracycline-mediated fluorescence correlates with passage number and β-galactosidase activity in HeLa and HEK293T cells, *Biology Open*, 2023, **12**, bio059691.
314. C. Cazares-Körner, I. M. Pires, I. D. Swallow, S. C. Grayer, L. J. O'Connor, M. M. Olcina, M. Christlieb, S. J. Conway and E. M. Hammond, CH-01 is a Hypoxia-Activated Prodrug That Sensitizes Cells to Hypoxia/Reoxygenation Through Inhibition of Chk1 and Aurora A, *ACS Chemical Biology*, 2013, **8**, 1451-1459.
315. E. D. D. Calder, A. Skwarska, D. Sneddon, L. K. Folkes, I. N. Mistry, S. J. Conway and E. M. Hammond, Hypoxia-activated pro-drugs of the KDAC inhibitor vorinostat (SAHA), *Tetrahedron*, 2020, **76**, 131170.
316. C. Jin, Q. Zhang and W. Lu, Synthesis and biological evaluation of hypoxia-activated prodrugs of SN-38, *European Journal of Medicinal Chemistry*, 2017, **132**, 135-141.
317. Y. Gerard, A. Voissiere, C. Peyrode, M.-J. Galmier, E. Maubert, D. Ghedira, S. Tarrit, V. Gaumet, D. Canitrot, E. Miot-Noirault, J.-M. Chezal, J.-M. and V. Weber, Design, synthesis and evaluation of targeted hypoxia-activated prodrugs applied to chondrosarcoma chemotherapy, *Bioorganic Chemistry*, 2020, **98**, 103747.
318. L. J. O'Connor, C. Cazares-Körner, J. Saha, C. N. Evans, M. R. Stratford, E. M. Hammond and S. J. Conway, Design, synthesis and evaluation of molecularly targeted hypoxia-activated prodrugs, *Nat Protoc*, 2016, **11**, 781-794.
319. B. Cavalleri, R. Ballotta and G. C. Lancini, Synthesis of 1-alkyl-2-nitroimidazole-5-carboxaldehydes, *Journal of Heterocyclic Chemistry*, 1972, **9**, 979-984.
320. 2007.
321. M. Matteuci, J.-X. Duan, H. Jiao, J. Kaizerman and S. Ammons, PHOSPHORAMIDATE ALKYLATOR PRODRUGS *WO2006US25881 20060629*, 2007, US. pat.
322. C. Jasper, D. H. Hahn, A. M. Breuning, P. Krattiger and M. Debor, SYNTHESIS OF 1-ALKYL-2-AMINO-IMIDAZOL-5-CARBOXYLIC ACID ESTER VIA CALPHA-SUBSTITUTED N-ALKYL-GLYCINE ESTER DERIVATIVES *WO2014EP02751 20141010* 2015, US. pat.
323. M. X. Fan and J. J. Cen, PEPTIDE EPOXYKETONE COMPOUNDS *WO2013US52143 20130725* 2014, US. pat.
324. 2014.
325. P. Knochel, W. Dohle, N. Gommermann, F. F. Kneisel, F. Kopp, T. Korn, I. Sapountzis and V. A. Vu, Highly Functionalized Organomagnesium Reagents Prepared through Halogen–Metal Exchange, *Angewandte Chemie International Edition*, 2003, **42**, 4302-4320.
326. I. Sapountzis, H. Dube, R. Lewis, N. Gommermann and P. Knochel, Synthesis of Functionalized Nitroarylmagnesium Halides via an Iodine–Magnesium Exchange, *The Journal of Organic Chemistry*, 2005, **70**, 2445-2454.
327. Y.-L. Leu, C.-S. Chen, Y.-J. Wu and J.-W. Chern, Benzyl Ether-Linked Glucuronide Derivative of 10-Hydroxycamptothecin Designed for Selective Camptothecin-Based Anticancer Therapy, *Journal of Medicinal Chemistry*, 2008, **51**, 1740-1746.
328. W. Pilgrim and P. V. Murphy, SnCl4- and TiCl4-Catalyzed Anomerization of Acylated O- and S-Glycosides: Analysis of Factors That Lead to Higher α:β Anomer Ratios and Reaction Rates, *The Journal of Organic Chemistry*, 2010, **75**, 6747-6755.

329. S. J. Harnor, T. Rennison, M. Galler, C. Cano, R. J. Griffin, D. R. Newell and B. T. Golding, Synthesis of 3′-deoxy-3′-fluorothymidine (FLT) 5′-O-glucuronide: a reference standard for imaging studies with [18F]FLT, *MedChemComm*, 2014, **5**, 984-988.
330. A. Kirschning, M. Ries, S. Domann, W. Martin, W. Albrecht, P. Arnold and S. Laufer, Synthesis and biological identification of the acyl glucuronide of the antiinflammatory drug ML-3000, *Bioorganic & Medicinal Chemistry Letters*, 1997, **7**, 903-906.
331. E. Calatrava-Pérez, L. A. Marchetti, G. J. McManus, D. M. Lynch, R. B. P. Elmes, D. C. Williams, T. Gunnlaugsson and E. M. Scanlan, Real-Time Multi-Photon Tracking and Bioimaging of Glycosylated Theranostic Prodrugs upon Specific Enzyme Triggered Release, *Chemistry – A European Journal*, 2022, **28**, e202103858.
332. F. A. Alharthi, G. F. S. Whitehead, I. J. Vitórica-Yrezábal and J. M. Gardiner, Solid state structure of sodium β-1-thiophenyl glucuronate identifies 5-coordinate sodium with three independent glucoronates, *Carbohydrate Research*, 2021, **502**, 108281.
333. C. García-Oliva, A. H. Cabanillas, A. Perona, P. Hoyos, Á. Rumbero and M. J. Hernáiz, Efficient Synthesis of Muramic and Glucuronic Acid Glycodendrimers as Dengue Virus Antagonists, *Chemistry – A European Journal*, 2020, **26**, 1588-1596.
334. R. Lucas, P. Peñalver, I. Gómez-Pinto, E. Vengut-Climent, L. Mtashobya, J. Cousin, O. S. Maldonado, V. Perez, V. Reynes, A. Aviñó, R. Eritja, C. González, B. Linclau and J. C. Morales, Effects of Sugar Functional Groups, Hydrophobicity, and Fluorination on Carbohydrate–DNA Stacking Interactions in Water, *The Journal of Organic Chemistry*, 2014, **79**, 2419-2429.
335. S.-I. Lee, K.-H. Yoon, M. Song, H. Peng, K. A. Page, C. L. Soles and D. Y. Yoon, Structure and Properties of Polymer Electrolyte Membranes Containing Phosphonic Acids for Anhydrous Fuel Cells, *Chemistry of Materials*, 2012, **24**, 115-122.
336. J.-F. Soulé, H. Miyamura and S. Kobayashi, Powerful Amide Synthesis from Alcohols and Amines under Aerobic Conditions Catalyzed by Gold or Gold/Iron, -Nickel or -Cobalt Nanoparticles, *Journal of the American Chemical Society*, 2011, **133**, 18550-18553.
337. M. D. Saunders and T. E. Timell, The acid hydrolysis of glycosides: V. Effect of the nature of the aglycon on the hydrolysis of glycosiduronic acids (glycuronides), *Carbohydrate Research*, 1967, **5**, 453-460.
338. Y. Chen, Y. Li, H. Yu, G. Sugiarto, V. Thon, J. Hwang, L. Ding, L. Hie and X. Chen, Tailored Design and Synthesis of Heparan Sulfate Oligosaccharide Analogues Using Sequential One-Pot Multienzyme Systems, *Angewandte Chemie International Edition*, 2013, **52**, 11852-11856.
339. G. Patras, G. G. Qiao, D. H. Solomon and R. Koch, Synthesis, Characterization, and Modelling of Novel Multifunctional Acryloyl-Based Monomers: An Experimental and Computational Study, *Australian Journal of Chemistry*, 2002, **55**, 675-680.
340. S. Deng, U. Gangadharmath and C.-W. T. Chang, Sonochemistry: A Powerful Way of Enhancing the Efficiency of Carbohydrate Synthesis, *The Journal of Organic Chemistry*, 2006, **71**, 5179-5185.
341. C. Romanò, D. Bengtsson, A. S. Infantino and S. Oscarson, Synthesis of fluoro- and seleno-containing d-lactose and d-galactose analogues, *Organic & Biomolecular Chemistry*, 2023, **21**, 2545-2555.
342. H. W. Coles, M. L. Dodds and F. H. Bergeim, Halogeno-alkyl Glycosides. I. Monohalogeno-alkyl Derivatives, *Journal of the American Chemical Society*, 1938, **60**, 1020-1022.

343. E. Calatrava-Pérez, S. A. Bright, S. Achermann, C. Moylan, M. O. Senge, E. B. Veale, D. C. Williams, T. Gunnlaugsson and E. M. Scanlan, Glycosidase activated release of fluorescent 1,8-naphthalimide probes for tumor cell imaging from glycosylated 'pro-probes', *Chemical Communications*, 2016, **52**, 13086-13089.
344. G. Horváth and P. Huszthy, Chromatographic enantioseparation of racemic α-(1-naphthyl)ethylammonium perchlorate by a Merrifield resin-bound enantiomerically pure chiral dimethylpyridino-18-crown-6 ligand, *Tetrahedron: Asymmetry*, 1999, **10**, 4573-4583.
345. E. Biron, F. Otis, J.-C. Meillon, M. Robitaille, J. Lamothe, P. Van Hove, M.-E. Cormier and N. Voyer, Design, synthesis, and characterization of peptide nanostructures having ion channel activity, *Bioorganic & Medicinal Chemistry*, 2004, **12**, 1279-1290.
346. G. Qiu, Ecole Centrale Marseille, 2020.
347. L. Huang and X. Huang, Highly Efficient Syntheses of Hyaluronic Acid Oligosaccharides, *Chemistry – A European Journal*, 2007, **13**, 529-540.
348. A. K. Ghosh and D. Farquhar, A methyl glucuronate prodrug of phosphorodiamidic mustard, *Tetrahedron Letters*, 1997, **38**, 8795-8798.
349. Y. Peng, Z. Shi, Y. Liang, K. Ding and Y. Wang, Targeting the tumor microenvironment by an enzyme-responsive prodrug of tubulin destabilizer for triple-negative breast cancer therapy with high safety, *European Journal of Medicinal Chemistry*, 2022, **236**, 114344.
350. A. K. Ghosh, S. Khan, F. Marini, J. A. Nelson and D. Farquhar, A daunorubicin β-galactoside prodrug for use in conjunction with gene directed enzyme prodrug therapy, *Tetrahedron Letters*, 2000, **41**, 4871-4874.
351. R. Erez and D. Shabat, The azaquinone-methide elimination: comparison study of 1,6- and 1,4-eliminations under physiological conditions, *Organic & Biomolecular Chemistry*, 2008, **6**, 2669-2672.
352. 2011.
353. A. Fernandes, A. Viterisi, F. Coutrot, S. Potok, D. A. Leigh, V. Aucagne and S. Papot, Rotaxane-Based Propeptides: Protection and Enzymatic Release of a Bioactive Pentapeptide, *Angewandte Chemie International Edition*, 2009, **48**, 6443-6447.
354. P. Garibay, P. H. Toy, T. Hoeg-Jensen and K. D. Janda, Application of a New Solid-Phase Resin: Benzamide ortho-Lithiation and the Synthesis of a Phthalide Library, *Synlett*, 1999, **1999**, 1438-1440.
355. D. C. Lenstra, J. J. Wolf and J. Mecinović, Catalytic Staudinger Reduction at Room Temperature, *The Journal of Organic Chemistry*, 2019, **84**, 6536-6545.
356. S. Nowshuddin, M. N. A. Rao and A. R. Reddy, Efficient Procedure for the Preparation of Oligomer-Free N α -Fmoc Amino Acids, *Synthetic Communications*, 2009, **39**, 2022-2031.
357. L. Rizzi, K. Cendic, N. Vaiana and S. Romeo, Alcohols immobilization onto 2-chlorotritylchloride resin under microwave irradiation, *Tetrahedron Letters*, 2011, **52**, 2808-2811.
358. T. B. Cai, D. Lu, X. Tang, Y. Zhang, M. Landerholm and P. G. Wang, New Glycosidase Activated Nitric Oxide Donors: Glycose and 3-Morphorlinosydnonimine Conjugates, *The Journal of Organic Chemistry*, 2005, **70**, 3518-3524.
359. P. H. Amvam-Zollo and P. Sinaÿ, Streptococcus pneumoniae type XIV polysaccharide: synthesis of a repeating branched tetrasaccharide with dioxa-type spacer-arms, *Carbohydr Res*, 1986, **150**, 199-212.

360. S. M. Andersen, M. Heuckendorff and H. H. Jensen, 3-(Dimethylamino)-1-propylamine: A Cheap and Versatile Reagent for Removal of Byproducts in Carbohydrate Chemistry, *Organic Letters*, 2015, **17**, 944-947.
361. R. Daly, G. Vaz, A. M. Davies, M. O. Senge and E. M. Scanlan, Synthesis and Biological Evaluation of a Library of Glycoporphyrin Compounds, *Chemistry – A European Journal*, 2012, **18**, 14671-14679.
362. C. M. Sevrain, J.-P. Haelters, A. Chantôme, H. Couthon-Gourvès, M. Gueguinou, M. Potier-Cartereau, C. Vandier and P.-A. Jaffrès, DiGalactosyl-Glycero-Ether Lipid: synthetic approaches and evaluation as SK3 channel inhibitor, *Organic & Biomolecular Chemistry*, 2013, **11**, 4479-4487.
363. 2018.
364. P. Li, X. Fu, Q. Zhou, X. Fu, A. Wang, G. Zhang, W. Jiao and C. Wang, Mechanistic understanding and the rational design of a SiO2@CD catalyst for selective protection of l-lysine, *Organic & Biomolecular Chemistry*, 2023, **21**, 551-563.
365. J. Tailhades, M.-A. Gidel, B. Grossi, J. Lécaillon, L. Brunel, G. Subra, J. Martinez and M. Amblard, Synthesis of Peptide Alcohols on the Basis of an O–N Acyl-Transfer Reaction, *Angewandte Chemie International Edition*, 2010, **49**, 117-120.
366. A. Galashov, E. Kazakova, C. E. Stieger, C. P. R. Hackenberger and O. Seitz, Rapid building block-economic synthesis of long, multi-O-GalNAcylated MUC5AC tandem repeat peptides, *Chemical Science*, 2024, **15**, 1297-1305.
367. Y. Lee and R. B. Silverman, Rapid, High-Yield, Solid-Phase Synthesis of the Antitumor Antibiotic Sansalvamide A Using a Side-Chain-Tethered Phenylalanine Building Block, *Organic Letters*, 2000, **2**, 3743-3746.
368. S. Oriana, Y. Cai, J. W. Bode and Y. Yamakoshi, Synthesis of tri-functionalized MMP2 FRET probes using a chemo-selective and late-stage modification of unprotected peptides, *Organic & Biomolecular Chemistry*, 2017, **15**, 1792-1800.
369. Z.-Z. Han, T. Dong, X.-X. Ming, F. Kuang and C.-P. Zhang, Synthesis and Biological Evaluation of CF3Se-Substituted α-Amino Acid Derivatives, *ChemMedChem*, 2021, **16**, 3177-3180.
370. L. J. O'Connor, C. Cazares-Körner, J. Saha, C. N. G. Evans, M. R. L. Stratford, E. M. Hammond and S. J. Conway, Design, synthesis and evaluation of molecularly targeted hypoxia-activated prodrugs, *Nature Protocols*, 2016, **11**, 781-794.
371. M.-H. Son, J. Y. Kim, E. J. Lim, D.-J. Baek, K. Choi, J. K. Lee, A. N. Pae, S.-J. Min and Y. S. Cho, Synthesis and biological evaluation of 2-(arylethynyl)quinoline derivatives as mGluR5 antagonists for the treatment of neuropathic pain, *Bioorganic & Medicinal Chemistry Letters*, 2013, **23**, 1472-1476.
372. A. Claus and M. Posselt, XLVIII. Ueber o-Oxychinolin-ana-sulfonsäure, *Journal für Praktische Chemie*, 1890, **41**, 32-41.